UNIVERSITY OF SHEFFIELD

DEPARTMENT OF CIVIL AND STRUCTURAL

ENGINEERING

BUCKLING STRENGTH OF WELDED AND

NON-WELDED ALUMINIUM MEMBERS

BY

Yuk Fai, Willy LAI

(M.Eng)

A Thesis Submitted to the University of Sheffield for

the Degree of Doctor of Philosophy

October 1988

—To Shirley and my parents

CONTENTS

7   COMPARISON BETWEEN DRAFT BS 8118 WITH THE-ORETICAL RESULTS

ACKNOWLEDGEMENT

DECLARATION

The author wishes to declare that, except for commonly understood and accepted ideas, or where specific reference is made, the work reported in this thesis is his own. The work has not previously been submitted in part or in whole to any University for any degree, diploma or other qualification.

Y F W LAI

SUMMARY

High strength aluminium alloys when welded suffer a local loss of strength due to heat-affected zone (HAZ) effects. The influence of such localised strength loss on structural behaviour of columns, beams and beam-columns is studied using numerical technique. Two programs INSTAF and BIAXIAL, previously developed for the use of steel structures, have been modified to incorporate the special features of the aluminium problem. The general in-plane behaviour of aluminium frames or members is studied by using program INSTAF. The general 3-D behaviour of aluminium members is simulated by the program BIAXIAL. Attention is given to the representation of the non-linear stress-strain behaviour of aluminium, in particular, its representation in a form suitable for incorporation into numerical processes. Results are presented for a wide range of problems to illustrate the severity of the HAZ effect on the load carrying capacity of structural members.

An experimental program has been carried out to study the effect of local transverse welds on beams. Altogether 5 non-welded and 22 welded 7019 aluminium beams have been tested and the test results have been compared with the theoretical predictions obtained by program INSTAF. The reliability of the theoretical studies is strongly supported by the general good agreement between experimental and theoretical results of the aluminium beams.

Finally, the theoretical results have been used to assess the suitability of the procedures given in the draft British Standard for the use of structural aluminium BS 8118. As a result of the comparison some new proposals and design recommendations are suggested.

<u>NOTATION</u>

b_h	extent of heat-affected zone (see Figure 2.4)
b_r	extent of reduced strength zone (see Figure 2.4)
k	non-dimensional coefficient
$[k_T]$	element tangent stiffness matrix
m	non-dimensional coefficient (see Sections 2.25 and A.1.2)
n	knee factor of parent metal in Ramberg-Osgood formula
n^*	knee factor of heat-affected material in Ramberg-Osgood formula
$\{q\}$	local vector of nodal displacements
$\{q\}^T$	transpose matrix of $\{q\}$
$\{q^I\}, \{q^J\}$	local vector of nodal displacements at joints I and J respectively
$\{\delta_q\}$	virtual variation of nodal displacements
$\{\Delta_q\}$	vector of incremental nodal displacements
r	radius of gyration
r_x, r_y	radius of gyration about x and y axes respectively
$\{r_E\}_G$	global vector of element displacements
$\{r_E\}_G^T$	transpose matrix of $\{r_E\}_G$
$\{r_E^I\}, \{r_E^J\}$	global vector of element displacements at joint I and J respectively
$\{\Delta r\}$	global vector of incremental nodal displacements for the entire structure

$\{\Delta r_E\}$	global vector of incremental element displacements
u	horizontal displacement of point A in Figure 3.1
u_x, u_y, u_z	displacement in x, y and z directions respectively
u_o	horizontal displacement of point O in Figure 3.1
u^I	local displacement at joint I in the x-direction
v	vertical displacement of point A in Figure 3.1
v_o	vertical displacement of point O in Figure 3.1
v^I	local displacement at joint I in the y-direction
x, y, z	reference axes in local coordinate system
A	area of the cross-section
A^*	area of reduced-strength zone
A_w	area of weld deposit
E	Young's modulus of parent metal
E^*	Young's modulus of heat-affected material
E_t	tangent modulus
F_t	tendon force
F_x, F_y	shear force in x and y direction respectively
H	depth of cross-section
H_t	height of the centre of reduced-strength zone
I_x	moment of inertia about x-axis
$\{K_T\}$	tangent stiffness matrix for the entire structure
L	length of member

L^*	length of reduced-strength
L_c	length of column
L_{cr}	critical region is defined as a distance extending from $0.25L$ either side of the point of maximum curvature when flexural buckling takes place
L_w	the total length within the critical region over which reduced-strength zone softening occurs
$\tilde{M}_{ax}$	major axis factored resistance moment in the presence of compression
$\tilde{M}_{ay}$	minor axis factored resistance moment in the presence of compression
M_{cr}	elastic buckling moment
M^*_{max}	factored moment resistance of welded beam
M_p	full 'plastic' moment $(= \sigma Z_p)$
M_{sx}	basic moment capacity of non-welded member under major axis buckling
M^*_{sx}	basic moment capacity of welded member under major axis buckling
M_{sy}	basic moment capacity of non-welded member under minor axis buckling
M^*_{sy}	basic moment capacity of welded member under minor axis buckling
M_x, M_y, M_z	bending moment about x, y and z axes respectively

$\overline{M}_x, \overline{M}_y$ Non-dimensionalised maximum bending strength of member about x-axis $\left(= \frac{M_x}{M_{0.2x}}\right)$ and y-axis $\left(= \frac{M_y}{M_{0.2y}}\right)$ respectively

M_{ult} maximum bending strength of non-welded member

M_{ult}^* maximum bending strength of welded member

$M_{0.2x}$ $= Z_{px}\sigma_{0.2}$

$M_{0.2y}$ $= Z_{py}\sigma_{0.2}$

M_ω bimoment or warping moment

P axial load

$\overline{P}$ non-dimensionalised maximum compressive strength of member $\left(= \frac{P_{ult}}{\sigma_{0.2}A}\right)$

P_c^* factored resistance of an axially loaded and welded compression member

P_{cx} factored resistance in compression of non-welded member under major axis buckling

P_{cx}^* factored resistance in compression of welded member under major axis buckling

P_{cy} factored resistance in compression of non-welded member under minor axis buckling

P_{cy}^* factored resistance in compression of welded member under minor axis buckling

P_e^* $= A\sigma_e^*$

P_{ult} maximum compressive strength of non-welded member

P_{ult}^* maximum compressive strength of welded number

$P_{0.2}$ $= A\sigma_{0.2}$

Q lateral point load

$[Q]$ the local vector of nodal forces

$[\Delta Q]$ vector of incremental forces for an inelastic element

Q_{ult} ultimate strength of non-welded member under lateral point load

Q_{ult}^* ultimate strength of welded member under lateral point load

$Q_{0.2x}$ lateral point load corresponding to the achievement of $M_{0.2x}$ within the cross-section

Q_{30}, Q_{60} lateral point load corresponding to central deflection of 30 mm and 60 mm respectively

$\{R_E\}_G$ global vector of element forces

$\{\Delta R_E\}$ global vector of incremental element forces

$[T]$ transformation matrix

T_F thickness of flange

T_w thickness of web

U^I global displacement at joint I in X-direction

V volume

V^I global displacement at joint I in Y-direction

W   breadth

W work of external work

X, Y, Z	reference axes in global coordinate system
Z_e	elastic modulus of a section
Z_p	plastic modulus of a section
Z_{px}	plastic modulus of a section about x-axis
Z_{py}	plastic modulus of a section about y-axis
σ	normal stress
σ_c	compressive residual stress
σ_e	elastic limit stress of parent metal
σ_e^*	elastic limit stress of heat-affected material
σ_t	tensile residual stress
σ_Y	yield stress of steel
σ_{ult}	ultimate tensile strength of parent metal
σ_{ult}^*	ultimate tensile strength of heat-affected material
σ_z	stress in z-direction
$\sigma_{0.1}$	0.1% proof stress of parent metal
$\sigma_{0.1}^*$	0.1% proof stress of heat-affected material
$\sigma_{0.2}$	0.2% proof stress of parent metal
$\sigma_{0.2}^*$	0.2% proof stress of heat-affected material
ε	strain
ε_e	elastic limit strain corresponding to σ_e
ε_{max}	maximum strength
ε_{ult}	ultimate elongation corresponding to σ_{ult}
ε_t	elongation at rupture of parent metal
ε_t^*	elongation at rupture of heat-affected material

ε_z	strain in z-direction
$\varepsilon_{0.2}$	0.2% strain
$\varepsilon_{\sigma_{0.2}}$	elongation corresponding to $\sigma_{0.2}$
θ	slope or rotation
θ^I	rotation at joint I
$\theta_x, \theta_y, \theta_z$	rotation about x, y and z-axes respectively
θ_ω	angle of twist due to M_ω
Δ_C	deflection at mid-span
Δ_Q	deflection at quarter-span
$\overline{\lambda}_M$	non-dimensionalised modified slenderness of beam $\left(= \sqrt{\frac{M_{0.2x}}{M_{cr}}}\right)$
λ_x	slenderness $\left(= \frac{L}{r_x}\right)$
$\overline{\lambda}_x$	non-dimensionalised slenderness ratio $\left(= \frac{\lambda_x}{\Pi\sqrt{\frac{E}{\sigma_{0.2}}}}\right)$
λ_y	slenderness $\left(= \frac{L}{r_y}\right)$
$\overline{\lambda}_y$	non-dimensionalised slenderness ratio $\left(= \frac{\lambda_y}{\Pi\sqrt{\frac{E}{\sigma_{0.2}}}}\right)$
β_x, β_y	ratio smaller to larger end moment about x and y axes respectively
$\delta_{x(max)}, \delta_{y(max)}$	maximum initial imperfection in x and y direction respectively
ω	reduction factor for reduced-strength zone material properties

<u>ABBREVIATION</u>

HAZ heat-affected zone

RSZ reduced-strength zone

INTRODUCTION

Applications of Aluminium	Reasons to Use Aluminium	Example
Aircraft structures	Lightness, high strength, high fatigue resistance, high corrosion resistance	European Airbus, Concorde
Ship structures	Non-magnetic, lightness, high strength, high corrosion resistance	Famous passenger liners such as Oriana and Canberra
Bridge structures	Low cost of maintenance, saving in dead weight, good appearance, high strength, high flexibility of extruded profiles	Two bridges for the Anglian Water Authority [3], military bridges developed by the Royal Armament Research and Development Establishment (R.A.R.D.E.)
Building structures	Good appearance, high flexibility of extruded profiles, good durability, good heat, light and radio radio waves reflector	Mosque Dome in Sudan [3], swimming pool roof in Romford, Shah Alam in Malaysia, Parabolic antennas for receiving television transmission by satellite
Ground transportation structures	Lightness, low cost of maintenance, good durability	Monocoque trains in London Underground, Leyland Trucks TX 450
Power transmission tower	Good conductivity, lightness, high corrosion resistance	V-tower in 500 kV line Ontario Hydro
Hi-tech equipment	Lightness of aluminium can give great accuracy of moment, good conductivity, good appearance, high corrosion resistance, high strength	Robots by Schrader Bellows, cable connectors by Hepworths
Domestic and office equipment	Good conductivity, non-toxic, good durability, good appearance	Amplifier Housing by Arcam Alpha, Domestic Radiators by Alurad, Telephone Booths by British Telecom KX

Table 1.1: General Use of Aluminium Alloys

1.1   Use of Aluminium

The birth of aluminium was begun in 1808 by Sir Humphrey Davy of the Royal Institution of London when he was working on alumina salts. At that time, aluminium was a precious metal which could only be obtained chemically. Industrial production of aluminium began in 1886 when the electrolytic process was discovered independently by Paul Louis Touissant Heroult in France and Charles Martin Hall in USA. In a hundred years of prodigious development, aluminium has become the most diversely used metal ever to serve mankind. In Europe, the consumption of aluminium increased gradually from 4.602 million tonnes in 1982 to 5.213 million tonnes in 1985. The consumption rate also increased in other countries such as USA and Japan.

The major advantages of aluminium are:

1. lightness (one third the weight of steel)

2. high corrosion resistance

3. high conductivity

4. high strength

5. good appearance

6. high flexibility in extrusion of profiles

Table 1.1 shows the general use of aluminium in the world and Figure 1.1 shows the major European markets for aluminium consumption in 1985. From them, we can see that aluminium is an important metal which is closely
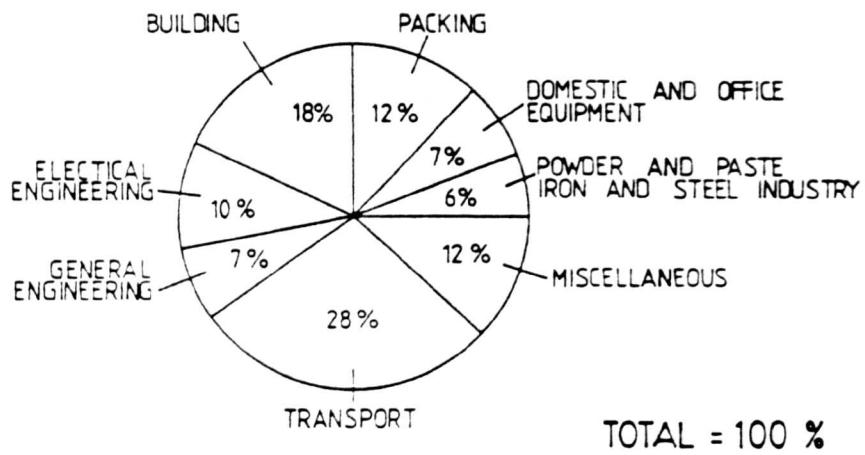
Figure 1.1 Aluminium Consumption in Europe (Year 1985)
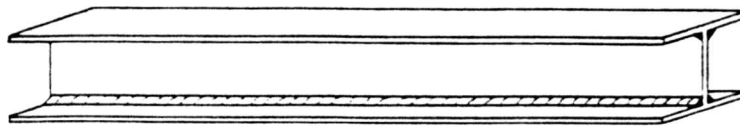
LONGITUDINAL WELDS
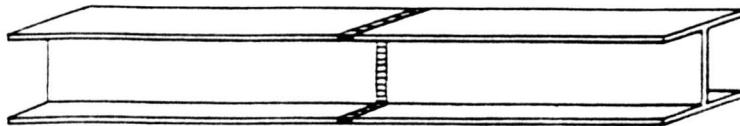
LOCAL TRANSVERSE WELDS

Figure 1.2 Longitudinal Welds and Local Transverse Welds

related to our daily life, one aspect of this being its use ^(in military) and even in civil engineering structures.

1.2   Nature of Problem and Background

One of the biggest advantages of aluminium alloys is that the structural members can be extruded to any desired profile or shape, but there exists a boundary limit of approximately 600 mm diameter circle. In practice, the above boundary limit is not adequate. Therefore, bolting or welding is necessary when a larger cross-section is desired.

Figure 1.2 shows two categories of welds which most design engineers will face during welding of aluminium alloy: (a) longitudinal welds that affect an appreciable proportion of the length; and (b) local transverse welds that affect only a small proportion of the length. However, most of the aluminium alloys commonly used for construction are heat-treated or work hardened in order to improve their mechanical properties such as 6000 series and 7000 series alloys (see Section 2.2.1). When these alloys are welded, heat-affected zones (HAZ) are found in the parent metal adjacent to the welds. These heat-affected zones possess inferior material properties and can result in a drastic loss in strength for the member as a whole. This effect is not only confined to members built-up by welding; welding an attachment to an extended section or using welding at the ends of a member to attach it to other parts of the structure will also produce localised HAZ effects.

When the current standard for the structural use of aluminium CP 118 (1969)

[1] was prepared, knowledge of the effects of longitudinal welds and local transverse welds in welded aluminium structures was rather limited. Therefore, for many years designers used rivetting or bolting instead of welding, even though the fabrication cost is higher and less rigidity is achieved by rivetting or bolting. During the 1970's extensive research programs, mainly sponsored by government agencies, were carried out to improve design recommendations. Towards the end of the decade these and other factors resulted in pressures to bring the design of aluminium structures into a limit states format. The new draft code for the design of aluminium structures BS 8118 [2], which will replace the current aluminium code CP 118, is now in circulation for the purpose of inviting public comment.

1.3   Aim of Research

The aims of the present research are

1. to investigate the general behaviour of aluminium members with or without longitudinal welds and local transverse welds using a numerical approach;

2. to conduct non-welded and transversely welded beam tests to provide comparisons with the theoretical results;

3. to give design recommendations suitable for inclusion in the new code BS 8118.

1.4 Organisation of the Thesis

Chapter 2 reviews the general information on aluminium ~~alloy~~ *alloys*; the effects of welding and the recent research works on aluminium alloys as structural members. Chapter 3 describes the computer program INSTAF which can simulate the in-plane behaviour of aluminium frames or members with or without welds. The aluminium members containing local transverse welds are studied in detail. The experimental method and the results of in-plane beam tests are given in Chapter 4. The experimental results are compared with the theoretical predictions. The 3-dimensional behaviour of aluminium members is described in Chapters 5 and 6 respectively, leading to another computer program BIAXIAL. Chapter 5 studies the general behaviour of aluminium members subject to in-plane loading but leading to out-of-plane failure. Chapter 6 studies members subject to compression plus biaxial bending. All the theoretical predictions obtained in Chapters 3, 5, and 6 are compared with ~~CP 118 and~~ the *draft* ~~new code~~ BS 8118. Design recommendations and new proposals are suggested in Chapter 7. Finally, a summary of the present research work and some suggestions for further research are given in Chapter 8.

References

[1] British Standards Institution, CP 118: 1969, "The Structural Use of Aluminium".

[2] British Standards Institution Draft British Standard BS 8118, "Code of Practice for the Design of Aluminium Structures", 1985.

[3] Buxton, P., "Recent Aluminium Structures", The Structural Use of Aluminium, The Institution of Structural Engineers, October, 1985.

LITERATURE REVIEW

2.1 Introduction

In 1979 work began in the U.K. on the revision of the code of practice for the structural use of aluminium CP 118 [1]. Recent theoretical and experimental research in U.K., and also in Germany and Italy, have provided lots of up-to-date information in many areas. To completely review all this up-to-date information would be an enormous task, and is clearly beyond the scope of this thesis. Therefore, only those publications, papers or experimental works, with direct relevance to the current research work, are considered. This chapter is divided into three parts. Part A will review the general information of aluminium alloy as a structural material. Part B will discuss those important effects of welding which give engineers or researchers some concern during analysis. Part C will focus on the development of the theoretical and experimental works on the structural use of aluminium.

Series	Major Alloying Element	
1000	Pure aluminium (> 99%)	
2000	Copper	H
3000	Manganese	N
4000	Silicon	
5000	Magnesium	N (W)
6000	Magnesium and silicon	H (W)
7000	Zinc	H (W)

NOTE

1. The letters N, H in the above list show whether the alloys concerned are non-heat-treatable (N) or heat-treatable (H). W denotes weldability.

2. 8000 and 9000 series can also be found but they are not commonly used.

Table 2.1: Numerical Designation for Aluminium Alloys

Part A :   Aluminium Alloys

2.2   General Information

2.2.1   Designation [2,3,4,5]

The new aluminium alloy classification uses the American 4-digit number-
ing system, in which the first digit indicates the alloy group based on the
major alloying element (see Table 2.1). Seven series of aluminium ~~alloy~~ *alloys* are
recognised in this system. 1000 and 4000 series are entirely non-structural,
and the application of the 3000 series is largely confined to profiled sheeting
(cladding). The 2000 series is very important structurally, but only in the
aircraft industry. 5000, 6000 and 7000 series are the most commonly used
alloys in civil structures. Typical examples are 5083, 6082, 7019, 7020 alloys,
which are commonly used in ship structures, bridges and roof structures, etc.

2.2.2   Welding Procedures [4,6]

Aluminium is one of the most weldable of all metals, particularly the 5000,
6000, and 7000 series alloys. Since the electrical conductivity and thermal
conductivity of aluminium is greater than steel, so higher capacity power
sources and more heat input are required during the welding process. For
general engineering fabrication, the two most important and widely used
methods for fusion welding of aluminium, are the Tungsten Inert Gas (TIG)

and Metal Inert Gas (MIG) processes, in which the electric arc and molten metal are shielded from the atmosphere by an envelope of inert gas. They are suitable for both manual and mechanical operation, give high quality welds in stressed structures, and are applicable to the full range of alloys and thickness likely to be required in modern designs. Depending on the application and process used, it is possible to weld thicknesses ranging from 0.5 mm to over 75 mm. With mechanised procedures, the range of thickness can be even greater.

2.2.3 Different Theoretical Models of Stress-strain Curve of Aluminium Alloy

In the theoretical analysis of stability problems of aluminium structures the idealisation of the stress-strain curve is one of the difficulties complicating computer simulations. The stress-strain curve obtained from a tension test of the alloy cannot be simplified to one of elastic/perfectly plastic behaviour as in the case of mild steel. The actual stress-strain curve is continuously increasing as if it possessed constant strain hardening; it does not exhibit a definite yield stress. In Britain, and indeed in most other countries, the common practice is to take the 0.2% proof stress, $\sigma_{0.2}$, as the 'yield point' of aluminium.

For these reasons, when conducting an accurate structural analysis, a more complex stress-strain model of aluminium alloy has to be established. Several authors have formulated various proposals in this area and these are listed below:

1. model proposed by Baehre [4]

2. model proposed by Mazzolani [4]

3. model proposed by Hong [7]

4. model proposed by Frey [8]

5. model proposed by Ramberg and Osgood [4,7,9,10]

The details of the above proposals can be found in Appendix A. The proposal (1) is only a crude approximation and cannot predict the actual behaviour of the aluminium alloy. The proposal (2) can predict quite accurately within the strain limit of $\varepsilon_{\sigma_{0.2}}$, but is quite conservative as the strain increases beyond $\varepsilon_{\sigma_{0.2}}$. Moreover, this proposal is very complicated and difficult to apply during design. The proposal (3) can give very good agreement with Ramberg-Osgood formula (proposal (5)) in all cases. The maximum difference between the two curves is less than 5%. The main disadvantage of this proposal is that the parameters used in the formula require trial and error evaluation, but it is worthwhile to consider this proposal during the computer formulation of buckling problems. The proposal (4) is not well-developed and more studies have to be carried out.

Therefore, from the detailed study, the model proposed by Ramberg and Osgood is the most suitable because its predicted behaviour is very close to the actual behaviour of aluminium alloy [4]. By using the minimum value of Young's modulus, the Ramberg-Osgood curve gives a lower bound to the experimental curves. Moreover, the parameters required by the formula are commonly given in handbooks and specifications.
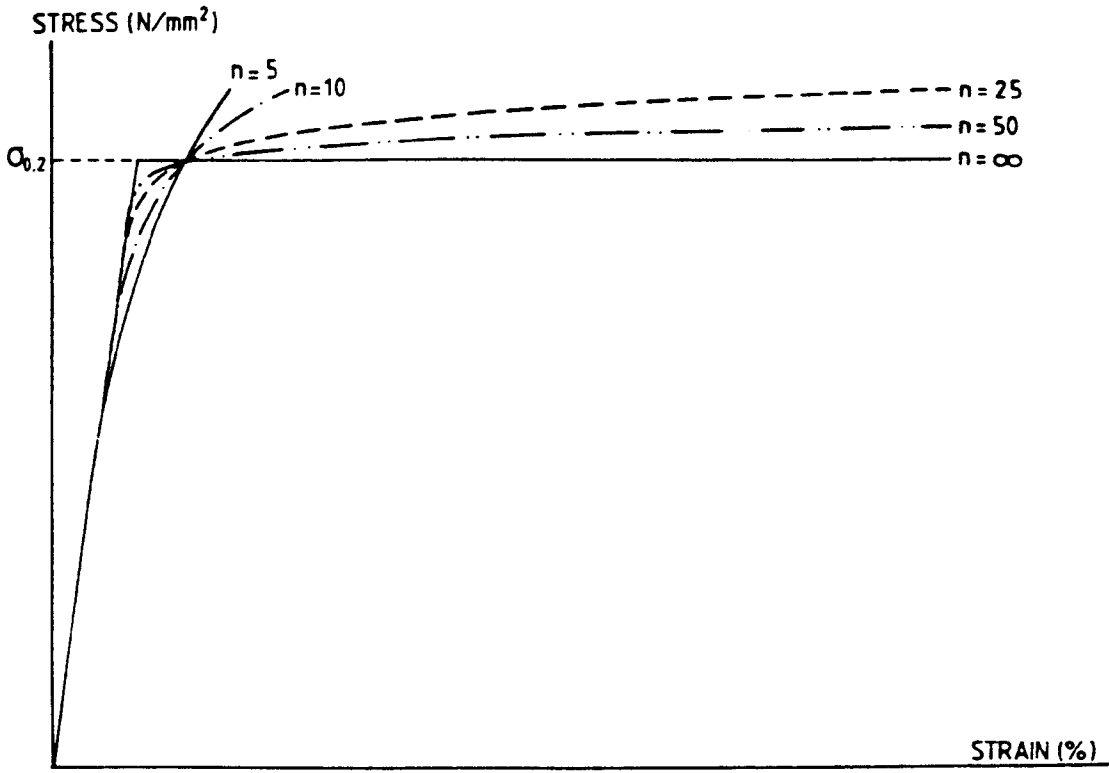
Figure 2.1 Ramberg-Osgood Curves

2.2.4 Ramberg-Osgood Formula

The Ramberg-Osgood formula is the most popular method of defining the stress-strain relationships for aluminium, and the formula is usually expressed in the following form:

$$\varepsilon = \frac{\sigma}{E} + 0.002 \left(\frac{\sigma}{\sigma_{0.2}}\right)^n \tag{2.1}$$

and the tangent modulus, E_t , is given by

$$E_t = \frac{d\sigma}{d\varepsilon} = \frac{1}{\frac{1}{E} + \frac{0.002n}{\sigma_{0.2}} \left(\frac{\sigma}{\sigma_{0.2}}\right)^{n-1}} \tag{2.2}$$

The first term of the right hand side of equation (2.1) represents the elastic component of strain, and the second term represents the plastic component of strain. When the value of n in the Ramberg-Osgood formula increases, the knee of the curve becomes sharper as shown in Figure 2.1. As n tends to infinity, the plastic component of strain will approach to zero. The curve will tend to the elastic/perfectly plastic relationship often used for mild steel with an elastic limit stress equal to $\sigma_{0.2}$.

If we examine both the equations (2.1) and (2.2), two undesirable features are apparent:

1. the Ramberg-Osgood curve starts to deviate from the linear elastic line $\sigma = E\varepsilon$ as soon as it leaves the origin.

2. ε and E_t are functions of σ, i.e. $\varepsilon = f(\sigma)$ and $E_t = f(\sigma)$.

From the detailed study, it was found that the second term on the right hand side of the formula (plastic component of strain) is insignificant at low stress
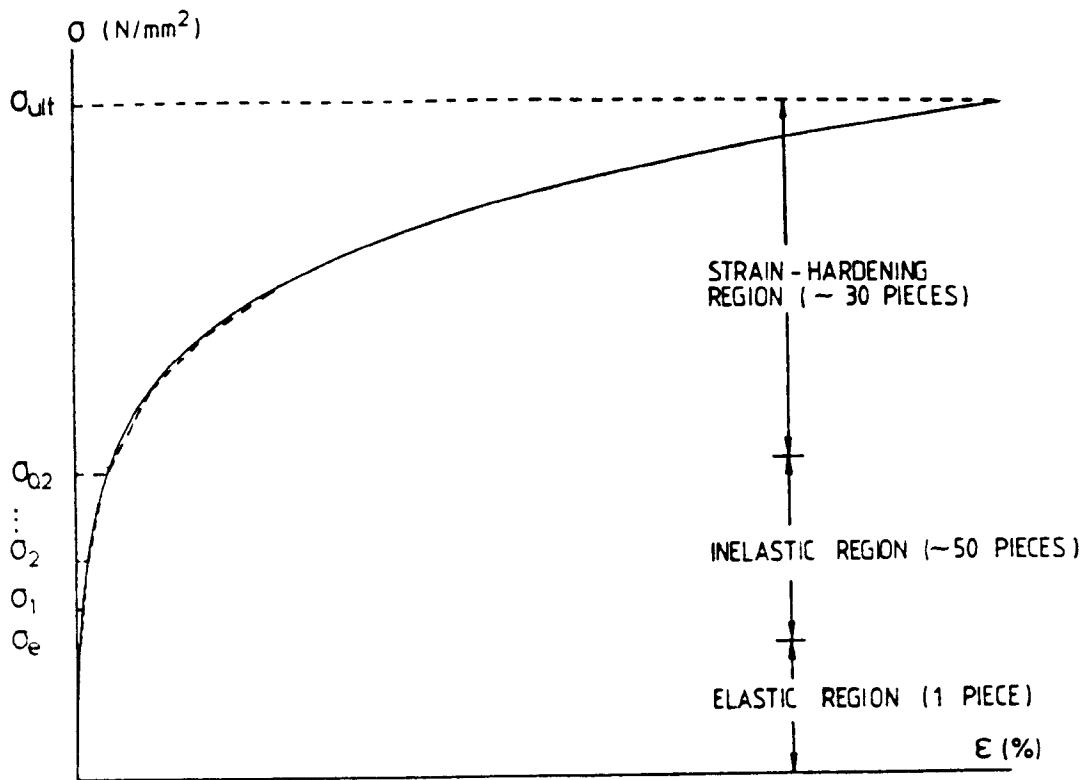
Figure 2.2 Piecewise Form of Ramberg-Osgood Curve

levels. The curve effectively follows the linear elastic line ($\sigma = E\epsilon$) at a low stress level. Therefore, the first undesirable feature can be neglected. In most modern computer programs, an ultimate strength approach is used to simulate the buckling behaviour of steel structures. These programs usually require σ as a function of ϵ (i.e. $\sigma = f(\epsilon)$); therefore, the second undesirable feature becomes significant.

If computers are used, the standard computing technique is one of 'trial and error' to solve the problem. However, in non-linear problems, iteration techniques, e.g. Direct iteration, Newton-Raphson method etc.; are necessary until the required convergence is obtained [11]. Thus the trial and error method will cause dramatic increases in computer time. For this reason a better approach is to modify the Ramberg-Osgood formula into a piecewise form (see Figure 2.2). From the author's experience, it is unnecessary to divide the elastic region into more than a single piece. For the inelastic and strain-hardening regions, dividing the curve into approximately 50 pieces and 30 pieces respectively is sufficient. The difference in stress between the original and piecewise form of the Ramberg-Osgood formula is less than 0.1%. The tangent modulus , E_t , is also determined by equation (2.2). The main advantages of the piecewise form of Ramberg-Osgood curve are the saving of computer time and retention of the simplicity of the formula. It was found that computer time is usually speeded up by 10 to 30 times. Therefore in the computer simulation (see Chapter 3 and 5), this piecewise form of Ramberg-Osgood curve was used in solving the non-linear stability problems of aluminium structures.
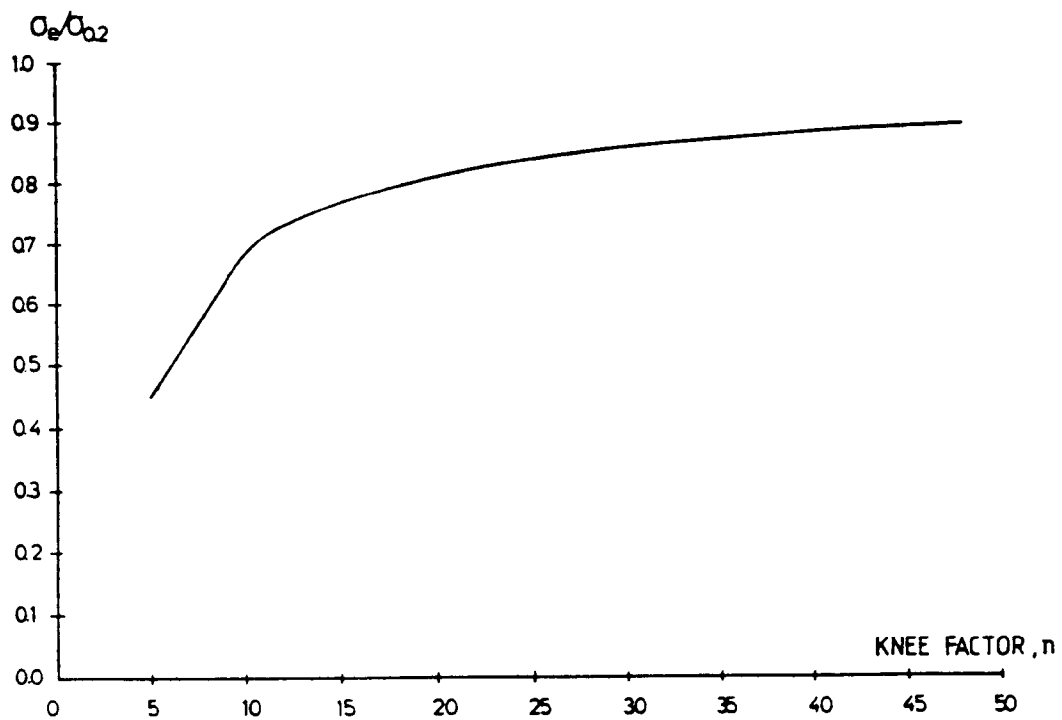
Figure 2.3 Relationship between $\frac{\sigma_e}{\sigma_{0.2}}$ and n

2.2.5   Elastic Limit Stress of Aluminium Alloy

As mentioned in Section 2.2.3, the stress-strain curve of aluminium alloy does not exhibit a definite yield stress, as well as a definite elastic limit stress. From the detailed studies, the author combined the formulae suggested by Mazzolani [4] and Ramberg-Osgood [4,10] to obtain the expression for the elastic limit stress, σ_e , as

$$\frac{\sigma_e}{\sigma_{0.2}} = 1 - \left(1 - 2^{-\frac{1}{n}}\right)^m \tag{2.3}$$

where m = $2.30 - 1.75\left(2^{\frac{1}{n}}\right)$

n = the knee factor in the Ramberg-Osgood formula

The relationship between $\frac{\sigma_e}{\sigma_{0.2}}$ and n is shown in Figure 2.3. If the knee factor, n, of the Ramberg-Osgood formula is used to classify the aluminium alloys, equation (2.3) may be simplified to:

for 5 $\leq n <$ 10   ; $\sigma_e = 0.45$

   10   $\leq n <$ 20 (non-heat-treated alloys)   ; $\sigma_e = 0.68$

   20   $\leq n <$ 40 (heat-treated alloys)   ; $\sigma_e = 0.81$
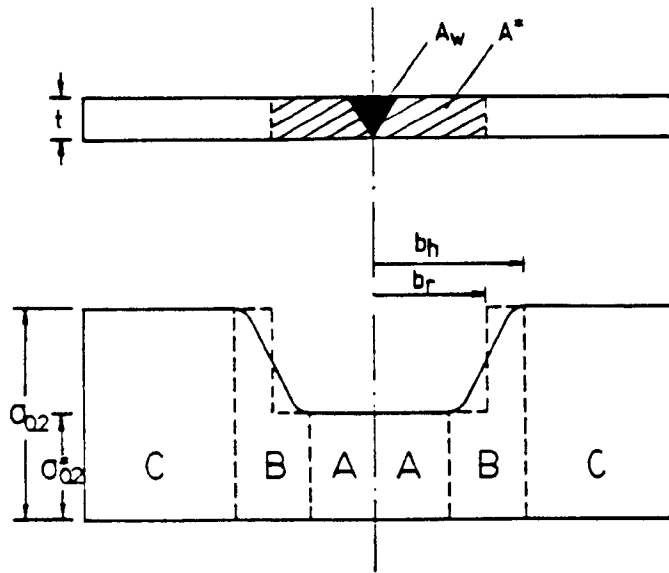
Figure 2.4 Typical Distribution of 0.2% Proof Stress in Vicinity of Weld

Part B :   Effects of Welding

2.3   Background to the Effects of Welding

The aluminium alloy could be heated up to 600F ($315°C$) during welding. The heat of welding could change the properties of parent metal adjacent to a weld in heat-treatable alloys and produce an extent of heat-affected zone. The heat-affected zone material shows a great reduction in strength. Therefore, in order to determine the buckling strength of welded members, the following information is important:

(a) the extent of softening around a weld (see Section 2.3.1)

(b) the mechanical properties of heat-affected material (see Section 2.3.2)

(c) the residual stress distribution (see Section 2.3.3)

Other general information related to the above effects of welding will also be discussed.

2.3.1   Extent of Softening around a Weld

The variation in mechanical properties in the vicinity of a weld is illustrated by the typical distribution of 0.2% proof stress shown in Figure 2.4 and three zones of material can be identified. They are :

i. zone A (fully heat-affected zone)

ii. zone B (partially heat-affected zone)

iii. zone C (unaffected parent metal)

The real extent of heat-affected zone (HAZ) is the summation of zone A and B, i.e. b_h. Since the actual strength distribution is quite complicated for design or analytical works, a step-change pattern is used for taking advantage of the strength of the material in the regions not affected by the heat of welding. The extent of the step-change pattern is called the reduced-strength zone (RSZ), which is the summation of zone A and half of zone B, i.e., b_r.

To estimate the amount of softening at a weld in heat-treated aluminium alloy, Hill, Clark and Brungraber [12] suggested the famous '1-inch rule' in 1962. This rule formed the basis for designing aluminium welded structures in U.S.A. [13] and Britain [1]. The '1-inch rule' is based on numerous hardness surveys of several alloys (3003, 5052, 5154, 5356 and 6061) with different thicknesses of welded part (maximum 2 $in.$ (50.8 mm)); and different types of welded joints (butt and fillet welds). Both the extent of heat-affected zone, b_h , and reduced-strength zone, b_r , were plotted against the thickness of welded part, and it was observed that b_h was less than 2 $in.$ (except two measurements) and b_r was less than 1.2 $in.$ (except one measurement). Therefore, the '1-inch rule' seemed reasonable and a upper bound solution for design. However, this rule can only be treated as a rough guide because there were no measurements on 7000 alloys and only one type of 6000 alloy (6061-T6) was studied. Moreover, the welding details and welding parameters were not reported, so we cannot prove that the welding process is representative of the general cases.

In 1971, Kelsey [14] obtained the hardness measurements on nine $1\frac{1}{4}in.$ (32 mm) thick specimen of 7039 alloy using butt welds in 4, 8 or 16 passes. It was observed that for continuous welding and decreasing the number of passes, the extent of heat-affected zone, b_h , and reduced-strength zone, b_r , could be more than 2 $in.$ (50.8 mm) and 1 $in.$ (25.4 mm) respectively. The width of heat-affected zone could be decreased if interpass cooling was allowed and also increase the number of passes during welding. Similar conclusions were obtained by Webber [15] when he studied the strength of welded 7019 alloy (Al Zn Mg Alloy). He compared the tensile strength of longitudinal butt and fillet weld specimens with the predicted strength obtained by the '1-inch rule' using measured strengths for parent metal, heat-affected zone and weld metal. He found that the '1-inch rule' could lead to unsafe results for most specimen widths and configurations tested. From the hardness measurements, it was observed that the reduced-strength zone could extend 25-33 mm from the weld root. The results obtained by Kelsey and Webber were important because, in some cases, the '1-inch rule' could under-estimate the extent of the softening zone.

Recent research has been carried out at University of Cambridge to improve the famous '1-inch rule'. Wong [16] studied the welding effects of 13 specimens of 6082 alloy and 8 specimens of 7019 alloy using butt welds. These specimens were 6, 7 and 10 mm in thickness. From the hardness measurements, he found that the area of reduced-strength zone, A^* , (see Figure 2.4) for both alloys could be expressed by:

$$A^* = 10 \, A_w \qquad\qquad (2.4)$$

Edward [17] proved that this relationship was correct for 6082 alloy and able to provide a reasonable upper-bound value for the extent of reduced-strength zone. However, this relationship received limited support for 7000 alloys because Wong only measured 8 specimens of 7019 alloy. In 1985, Robertson [18] carried out extensive research on 6082-T6 and 7019-T6 alloys to extend and refine Wong's predictions. He studied the effects of welding on thin, thick and intermediate thickness plates using bead; butt and fillet welds. The effects of small section, edge effects, number of heat flow paths and interpass temperature were also considered. He found that for thin plates using bead/butt welds,

$$A^* = 9.6 \ A_w \quad \text{for 6082 alloy} \tag{2.5}$$

$$A^* = 13.8 \ A_w \quad \text{for 7019 alloy} \tag{2.6}$$

Moreover, in a multi-pass weld, the extent of HAZ will be smaller if full cooling is allowed between weld passes, which also agree with Kelsey's observations.

The rules for estimating the amount of softening at a weld, listed in the new code BS 8118 [2], are mainly based on Robertson's research because his results are more comprehensive and advanced than anything previously available.

2.3.2   Mechanical Properties of Heat-affected Material

2.3.2.1   Severity of Softening within the Heat-affected Zone

In order to simplify the variation of mechanical properties within the heat-affected zone, an approximation of a step-change pattern is used in BS 8118 (see Figure 2.4). It is assumed that the mechanical properties are uniform within the reduced-strength zone [†] ($2b_r$) and the severity of softening is independent of the weld size. The properties of the heat-affected material are obtained by the application of a reduction factor to the parent material strength; i.e.

$$\text{heat-affected material strength} = \omega \times \text{ parent material strength} \qquad (2.7)$$

or

$$\omega = \frac{\text{heat-affected material strength}}{\text{parent material strength}}$$

In BS 8118, the following reduction factors are suggested according to the designation of parent material:

5000 series (non-heat-treatable alloys)   , $\omega = 1.0$

6000 series (heat-treatable alloys)   , $\omega = 0.5$

7000 series (heat-treatable alloys)   , $\omega = 0.75$

The reduction factor, ω , is assumed to be similar for both $\sigma_{0.2}$ and σ_{ult} . In order to verify the above suggestions, recent studies on material properties of aluminium alloys have been collected by the author and summarized in

---

[†]The term 'reduced-strength zone', which is used in this thesis, is same as the heat-affected zone (HAZ) used in draft BS 8118.

Author	Alloy Used in Experiment	Welding Method	Welded Joint	Parent Metal σ_0.2 (N/mm²)	Parent Metal σ_ult (N/mm²)	HAZ Material σ'_0.2 (N/mm²)	HAZ Material σ'_ult (N/mm²)	Reduction Factor σ'_0.2/σ_0.2	Reduction Factor σ'_ult/σ_ult	Comment
Mazzolani [4,19,27]	5086	MIG	Butt	145-157	-	131-145	-	0.89-0.91	-	Values likely to be the strength of weld metal but small reduction in strength
	6082	MIG	Butt and fillet	309-332	330-360	135-168	220-315	0.41-0.54	0.66-0.87	Three welded profiles (2 I-sections and 1 box-section) the strength of heat-affected material around the weld metal is considered
	7020	MIG	Butt	290-348	-	185-200	-	0.56-0.63	-	Values likely to be strength of weld metal, more reliable results for σ'_0.2/σ_0.2 are 0.85-0.87
Durrant [28]	7019	MIG	Bead	-	-	-	-	0.8	-	
Pirner [29]	6082	MIG	-	286	317	140	190	0.49	0.60	Value likely to be the strength of weld metal
		TIG	-	-	-	-	-	-	-	
	7020	MIG	-	404	443	190	275	0.47	0.62	
		TIG	-	-	-	-	-	-	-	
Wong [16]	5083 (M)	MIG	Bead	194	-	-	-	-	-	Significant drop in σ_u, but shows a small reduction in σ_0.2
	6082	MIG	Butt and fillet	-	-	-	-	-	-	
	7019	MIG		-	-	-	-	-	-	
Edward [17]	6082	MIG	Butt and fillet	275-285	-	142-233	-	0.51-0.83	-	
Soetens [30]	6082	MIG	Butt	-	317	-	200	-	0.63	
		TIG	Butt	-	316	-	158	-	0.5	
	7020	MIG	Butt	-	440	-	370	-	0.84	
Hong [7]	6082	MIG	Bead	246-297	-	123-206	-	0.5	-	Extensive research, the results are very reliable.
Baxter [20]	6082	MIG	Fillet	293	-	247	-	0.84	-	
Thomas [21]	6082	MIG	Bead	223	249	212	233	0.95	0.94	The parent metal strength is unreliable.
Webber [15]	7019	MIG	Fillet	381-391	428-438	237-287	319-386	0.61-0.74	0.73-0.89	The strength of heat-affected material due to four welds is lower than that due to one weld.
Moffin [22]	5083	TIG	Fillet	-	-	-	-	-	-	
	6082	MIG	Butt	-	-	-	-	0.5	-	
Techanti-sawad [23]	7019	MIG	Bead	371-428	415-465	261-397	403-442	0.64-0.93	0.84-1.00	Bead welds were put on extruded section
Robertson [18]	6082	MIG	Bead	304-322	336-337	147-154	239-263	0.47-0.49	0.71-0.78	Extensive research, the results are reliable
			Butt	309	315	127-161	208-237	0.41-0.52	0.66-0.75	
	7019	MIG	Butt	352	391-395	227-264	264-392	0.64-0.75	0.67-1.00	

[1]The results can also be found in reference [18]

Table 2.2 Experimental Results for the Strength of Heat-affected Material

Table 2.2. From the table, the following conclusions are arrived:

1. Limited types of aluminium alloy were studied and the experimental results were confined to those commonly used alloys (5083-M, 6082-TF, 7019-TF, 7020-TF).

2. The reduction factors for 0.2% proof stress, and ultimate tensile stress of the heat-affected material (i.e. $\frac{\sigma_{0.2}^{\bullet}}{\sigma_{0.2}}$ and $\frac{\sigma_{ult}^{\bullet}}{\sigma_{ult}}$) are not the same; and large variation is observed in some of the studies.

3. The reduction factor recommended by BS 8118 for each series of alloy (except for 7000 series alloy) is mainly based on 0.2% proof stress. For 7000 series alloy, the value ω is about the average of $\frac{\sigma_{0.2}^{\bullet}}{\sigma_{0.2}}$ and $\frac{\sigma_{ult}^{\bullet}}{\sigma_{ult}}$.

Although the experimental results available are limited, they tend to support the reduction factors suggested in BS 8118. However, attention should be paid to 7000 series alloy because the reduction factors obtained from experiment, in some cases, are lower than the value suggested by BS 8118.

2.3.2.2   Loss of Ductility of Heat-affected Material

Apart from the softening effect within the reduced-strength zone, another significant effect after welding is the drastic loss in ductility of the heat-affected material. This effect is important because it may influence the plastic design of aluminium structures. The structural members may be unable to develop full plasticity (plastic hinges) and maintain their capacity to carry load. For 5000 series alloy, it does not significantly change its mechanical

Designation	Ultimate Elongation	
	Parent Metal	Heat-affected material
6000	8%-12%	1%-4%
7000	10%-15%	2%-6%

Table 2.3: Effect of Welding on Ductility of Aluminium Alloy

properties after welding, so the loss in ductility can be neglected. But for 6000 series and 7000 series alloy, the reductions in ultimate elongation are shown in Table 2.3; and we can observe that the ductility of both alloys is drastically reduced. Since most of the authors neglect this effect and insufficient experimental data are available, therefore it is difficult to choose a suitable limit for the ultimate elongation of heat-affected material for plastic design. But the author recommends that the maximum tensile elongation for 6000 series and 7000 series alloy be 2.5% and 3.5% respectively (see Section 3.3).

2.3.2.3 Recovery of Heat-affected Material

It was found that the aluminium alloys could recover some of their original strength after welding either naturally or artificially. This effect is known as the post weld aging process. As mentioned in Section 2.3.1, three zones of material are identified after welding (see Figure 2.4). The recovery in strength can only occur in zone A (fully heat-affected zone), therefore, this effect will not affect the extent of heat-affected zone.

Figure 2.5 shows the recovery of 5050, 5056, 6082 and 7020 alloy within six months after welding obtained by Brenner [24]. We can observe that the reductions in σ_{02} and σ_{ult} for 5000 series alloy are insignificant. Moreover, it is reasonable to neglect the loss in the ductility for 5000 series alloy because the ultimate elongation is still high after welding even though some reduction in ductility has occurred. For 6082 and 7020 alloy the recovery in strength becomes steady after three months' time and higher strengths

can be obtained if artificial aging is carried out. Ultimate elongation values remain very low, and can even decrease in the case of artificial aging.

Similar results were obtained by Webber [25,26] for 7019 alloy. If all specimens were allowed to age naturally at an ambient temperature of above 18°C for about 30 days before being tested, he found that the 0.2% proof stress and ultimate tensile stress could recover up to 77% and 87% of parent metal strength respectively. If artificial aging was carried out (8 hours at 90°C followed by 16 hours at at 150°C) the 0.2% proof stress and ultimate tensile stress could be improved up to 82% and 92% of parent metal strength respectively.

Finally, it is worthwhile to point out that the reduction factor suggested by BS 8118 (see Section 2.3.2.1) is only suitable to apply for the alloys which are naturally aged (say 1-3 months after welding). The artificial aging process could improve the strength of a welded alloy better than naturally aged but this might not be possible in practice.
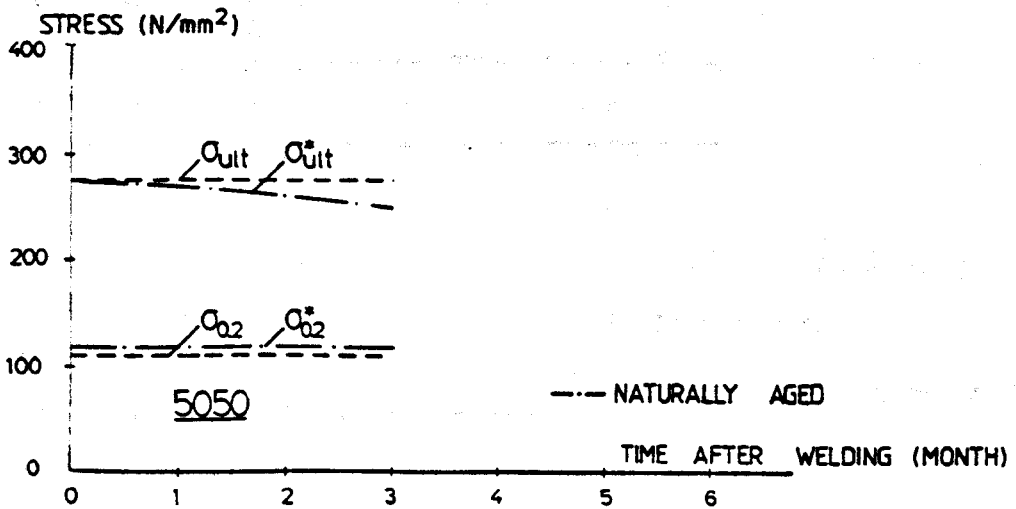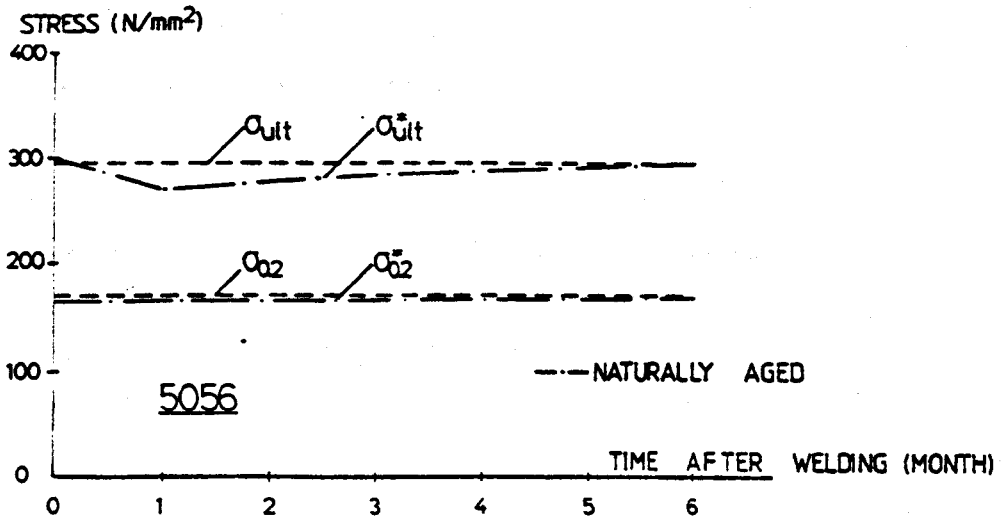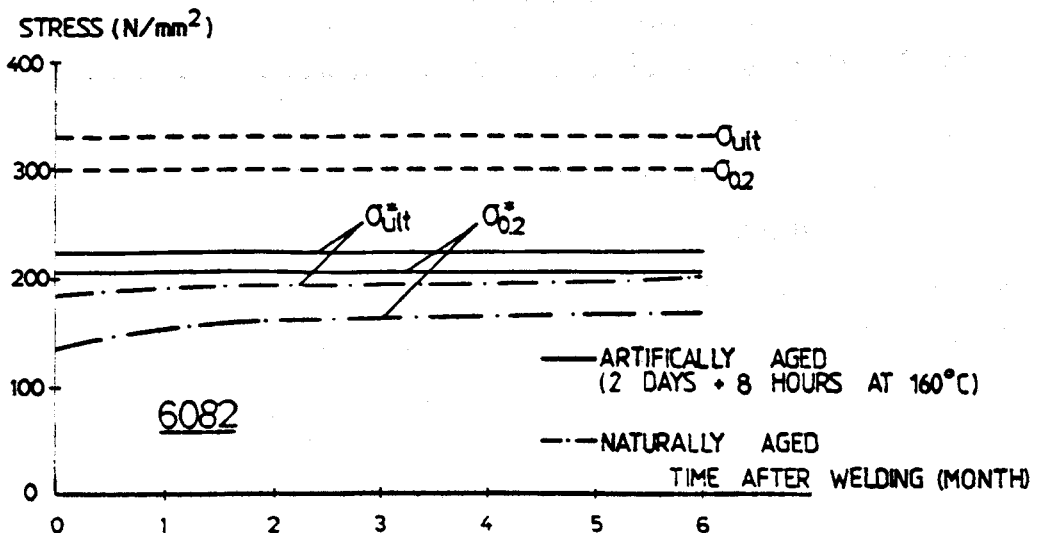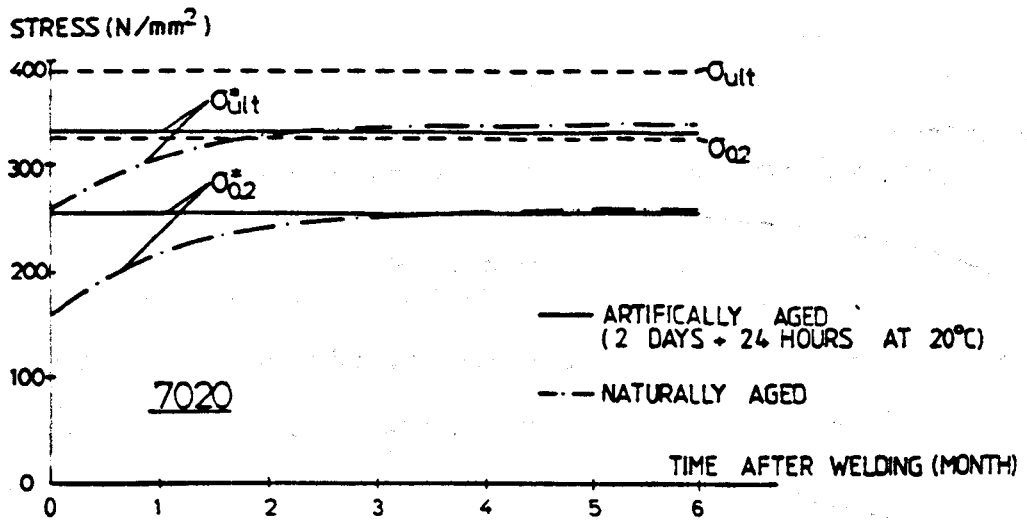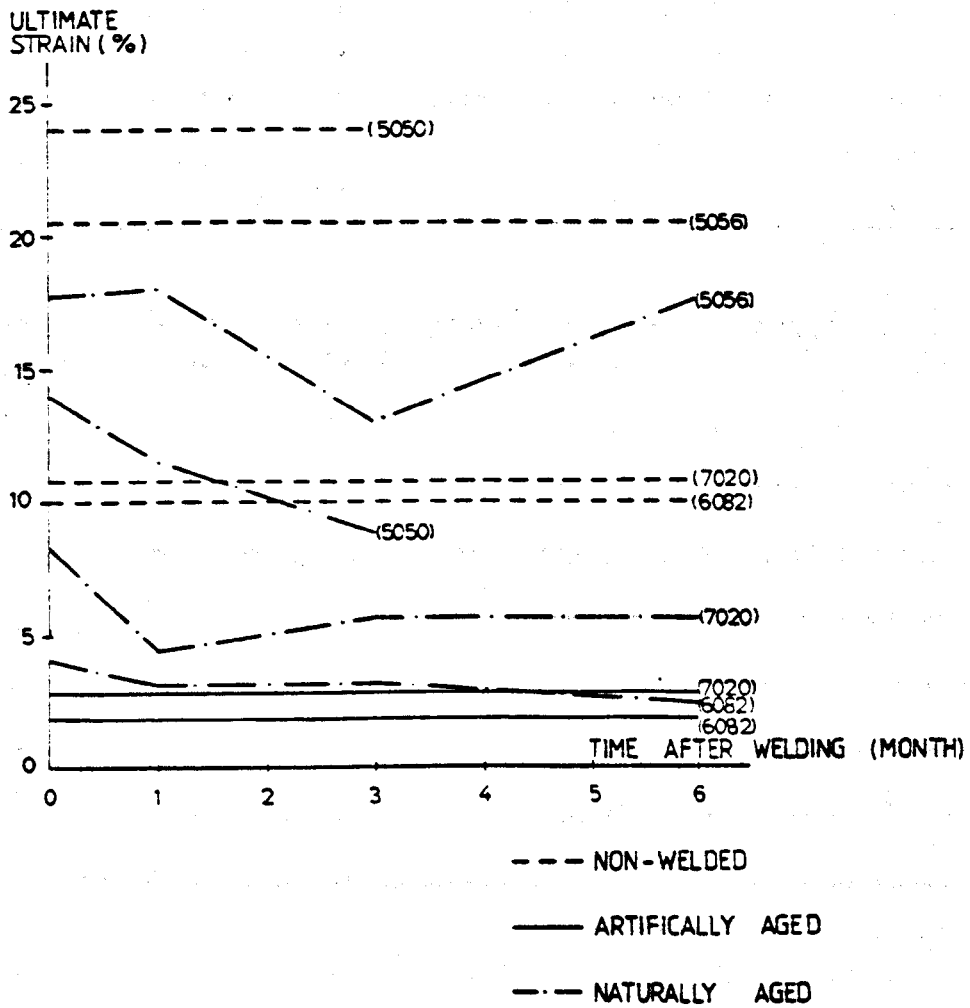
Figure 2.5 (a)

Figure 2.5 (b)

Figure 2.5 (c)

STRESS (N/mm²)

400⊤ ——————————————————— σ_{ult}

σ^*_{ult}

300⊤

σ^*_{02} ————————————————— σ_{02}

200⊢

—— ARTIFICALLY AGED
(2 DAYS + 24 HOURS AT 20°C)

100⊢   7020

—·— NATURALLY AGED

TIME AFTER WELDING (MONTH)

0 └──┬────┬────┬────┬────┬────┬────┬──
   0   1   2   3   4   5   6

Figure 2.5 (d)

ULTIMATE
STRAIN (%)

25 ⊣ — — — — — — —(5050)

20 ⊣ — — — — — — — — — — —(5056)

                                    (5056)

15 ⊣

                          (7020)
10 ⊣ — — — — — — — — — — —(6082)
              (5050)

5 ⊣   (7020)

                          (7020)
                          (6082)
                          (6082)
                    TIME AFTER WELDING (MONTH)
0 └──┬────┬────┬────┬────┬────┬────┬──
   0   1   2   3   4   5   6

— — — NON-WELDED

———— ARTIFICALLY AGED

—·— NATURALLY AGED

Figure 2.5 (e)

Figure 2.5 Effect of Natural and Artifical Aging after Welding

STRESS (N/mm^2)

PARENT MATERIAL

$E = 70000 \ (N/mm^2)$
$\sigma_{0.2} = 250 \ (N/mm^2)$
$n = 25$

RSZ MATERIAL

$E^* = 70000 \ (N/mm^2)$
$\sigma_{0.2}^* = 125 \ (N/mm^2)$
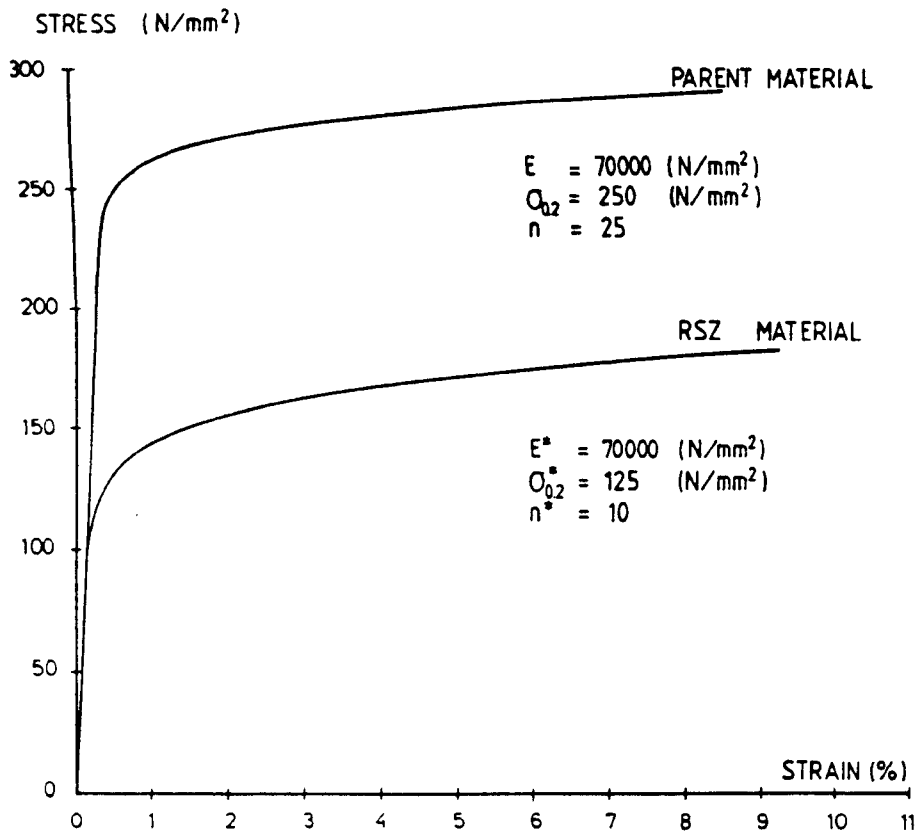$n^* = 10$

STRAIN (%)

Figure 2.6 Typical Stress-strain Curves for Parent and RSZ Material (6082-TF)

2.3.2.4 Stress-strain Relationships of Heat-affected Material

The stress-strain relationships of heat-affected material can also be expressed by the Ramberg-Osgood formula (see Section 2.2.4) as shown in Figure 2.6. From experiments [4,7], it was found that the Young's modulus of the heat-affected material is the same as the parent metal but with a reduced elastic limit stress, 0.2% proof stress and ultimate tensile stress. Moreover the heat-affected material also has a smaller knee factor, n, than the parent metal as shown below:

(a)   Heat-affected material, tension and compression $n = 5 - 10$

(b)   Parent metal, tension $n = 25 - 50$

(c)   Parent metal, compression $n = 15 - 20$

2.3.3   Residual Stress Distribution

Residual stresses are self-equilibrating internal stresses present in the members which are caused by thermal processes such as cooling after extrusion or welding. In structural problems, the presence of residual stresses can cause significant effects on structural members, particularly in buckling where the compressive residual stresses play an important role. Therefore this section will briefly review the recent studies on residual stresses existing after extrusion and welding. Moreover, the models used to represent the residual stress distribution will also be discussed.
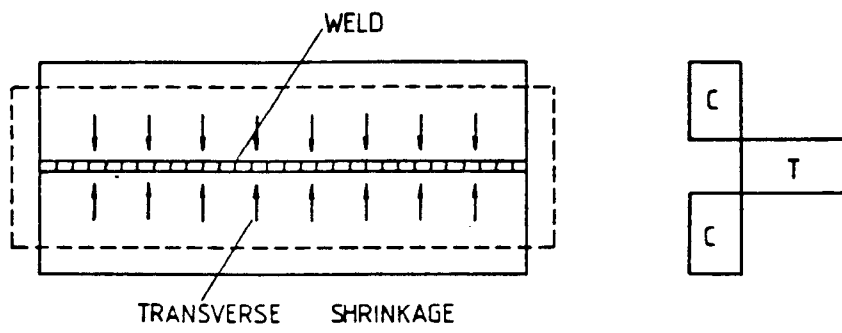
Figure 2.7 Longitudinal Residual Stresses and Transverse Shrinkage of Welded Plate

2.3.3.1   Residual Stresses Existed after Extrusion

Tests have been conducted by Mazzolani [4] to investigate the distribution and magnitude of residual stresses caused by cooling in extruded aluminium alloy profiles. French alloys A-GSM (6060-6063), A-SGM (6181), A-U4G (2017), A-Z5G (7020) and Austrian alloys AlZnMg1 (7020), AlMgSi0.5 (6060) were tested; and the sectioning method was used to determine the distribution and magnitude of residual stresses. From these test results, it was observed that the distribution of residual stresses is very irregular and does not follow any law like that for steel structures. These results are not easily explained but it was confirmed that the residual stresses produced by manufacturing are generally very low in extruded profiles (less than 20 N/mm^2) . Therefore for practical purposes, the effect of residual stresses on load-bearing capacity of extruded profiles can be neglected.

2.3.3.2   Residual Stresses Existed after Welding

Consider a rectangular plate with a longitudinal cross weld located in the middle as shown in Figure 2.7. Due to the localised heat, severe plastic strains are generated in the weld and the surrounding region during welding; after cooling, these plastic strains in turn give rise to residual stress and distortion, acting both longitudinally (parallel to the weld line) and transversely.

If we consider the transverse behaviour first, we could observe that the plane is subjected to heat treatment which is homogeneous; so a uniform transverse contraction will take place across the weld and result in a change of dimen-

sions. Therefore, the residual stresses in the transverse direction should be very small except that the plate is restrained transversely.

But for the longitudinal direction, the plate will behave differently because the heat treatment becomes inhomogeneous. The zones close to the welds are heated to very high temperatures during welding and tend to expand, but this expansion is prevented by the regions further from the weld which are at lower temperatures. Due to this restraint, residual tensile stresses are generated in the regions close to the weld; and these tensile stresses will be balanced by the compressive stresses arising further from the weld.

If we extend the above ideas to welded members, we can conclude that residual stresses can only be significant if the members containing longitudinal welds. The residual stresses in transversely welded members should have negligible effects except for members which are restrained during welding (e.g. members with both ends fixed). However, nobody has measured the intensity of residual stresses in transversely welded members with or without restraint; or the residual stresses developed due to differential cooling after welding. Therefore, more investigations in this area should be carried out.

2.3.3.3   Theoretical Models for Residual Stresses

Two models have been developed to determine the residual stresses of longitudinally welded members. The first model was developed by ECCS Committees and was based on the results obtained by Gatto, Mazzolani and Morri [4,19]. In their experiments, only three types of welded cross-sections (P, T
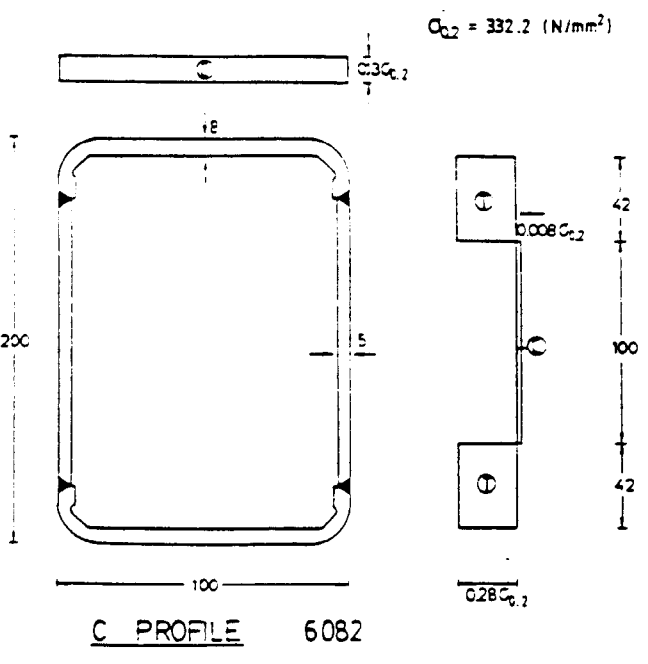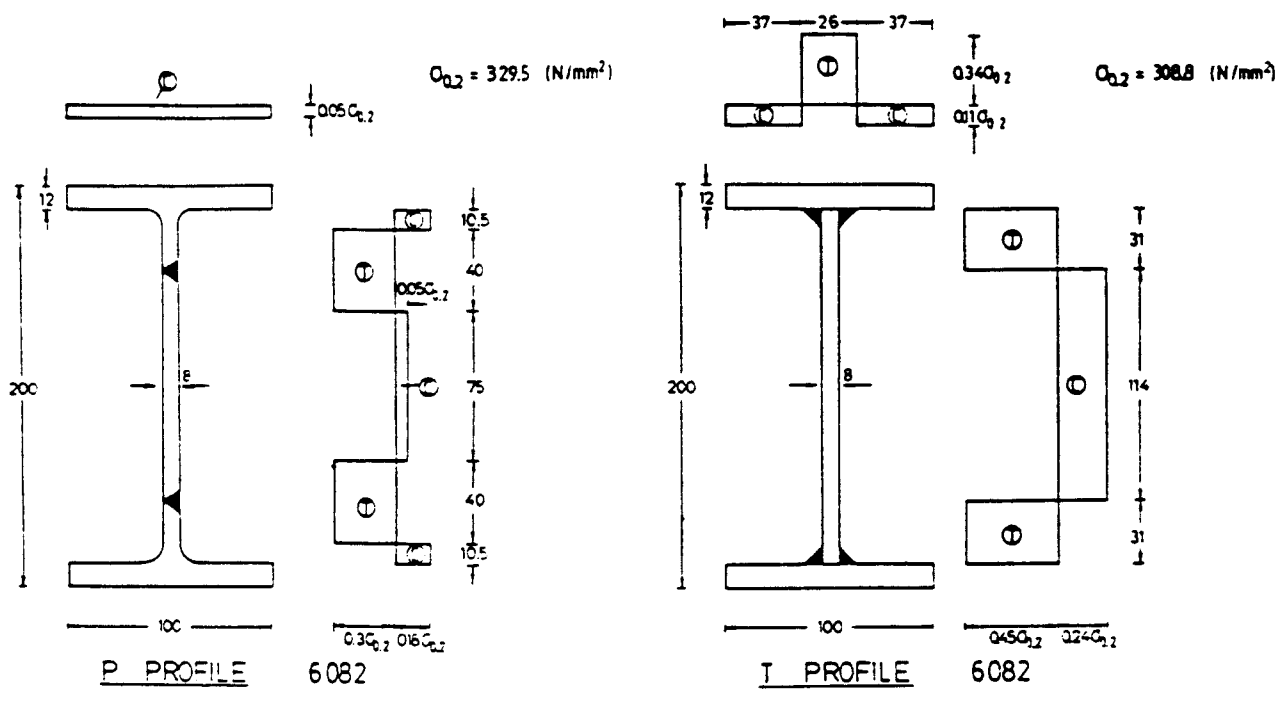
Figure 2.8 Idealised Residual Stress Distribution for T,P and C Profiles

and C profile), made of 6082 alloy were chosen using the sectioning method to determine the residual stresses and material properties. The idealised residual stress distribution for P, T and C profiles are shown in Figure 2.8. All these tests show that residual stress distributions are characterised by tension regions close to the welds, where the highest values of tensile residual stresses are observed, and compression regions located further from the welds. Moreover, the compression stresses in T profiles were different in the flange and web.

The second model to determine residual stresses was developed in the University of Cambridge and was based on the 'tendon force' approach [16]. This approach has been verified through experiment and numerical simulation. The details of the Cambridge model can be referred to Appendix B, but in here, only the important results are discussed.

It was found that the tendon force, F_t , could be expressed as (see Appendix B):

$$F_t = 20kA_w \quad \text{(KN)} \tag{2.8}$$

where k is a non-dimensional coefficient and A_w is the area of weld deposit.

Recent work by Wong has shown that $k = 0.12$ for a single pass weld on 6082 and 7019 alloys and MIG welding.

Therefore,

$$F_t = 2.4A_w \quad \text{(KN)} \qquad \text{for 6082 and 7019 alloys} \tag{2.9}$$

$$\text{(single pass)}$$

However, for T-fillet welds with two fillet welds laid sequentially, Wong has found that the tendon force could increase by 25%. Hence, for an I-section fillet welded at the web-flange junctions,

$$F_t = 3A_w \quad (KN) \qquad \text{for 6082 and 7019 alloys} \qquad (2.10)$$

$$(2 \text{ pass T-fillet weld})$$

The tendon force, F_t , is assumed to be resisted by the whole cross section, so the compressive residual stress is simply equal to

$$\sigma_c = \frac{F_t \times 10^3}{A} \quad (N/mm^2) \qquad (2.11)$$

Therefore, from equations (2.5), (2.6), (2.9), (2.10) and (2.11), the compressive residual stress can be related to the area of reduced-strength zone, A^* , by :

for 6082 alloy ,

$$\sigma_c = 250.0 \frac{A^*}{A} \quad (N/mm^2) \text{ (single pass)} \qquad (2.12)$$

$$\sigma_c = 312.5 \frac{A^*}{A} \quad (N/mm^2) \text{ (2 pass T-fillet weld)} \qquad (2.13)$$

for 7019 alloy ,

$$\sigma_c = 173.9 \frac{A^*}{A} \quad (N/mm^2) \text{ (single pass)} \qquad (2.14)$$

$$\sigma_c = 217.4 \frac{A^*}{A} \quad (N/mm^2) \text{ (2 pass T-fillet weld)} \qquad (2.15)$$

Mazzolani and De Luca [27] have compared the two models and found that the magnitude of the residual stress values given by the two models are comparable even though the Cambridge model does not permit characterization

of the actual distributions of residual stress. However, the main advantage of the Cambridge model is the flexibility $\overset{to}{\wedge}$ extend the problem to all types of joints even though rough approximations are necessary.

In addition, both the models are based on the assumption that the longitudinal welds on the cross section are symmetric, so they fail to represent the distribution of residual stress when unsymmetric longitudinal welds are found.

Part C :   Structural Use of Aluminium

2.4   Development of Structural Use of Aluminium

The research on the structural use of aluminium alloys was mainly started in America in the early 1920's with the support by the Aluminium Company of America (ALCOA). As a result of the early work ALCOA published its first Structural Aluminium Handbook in 1930 [31].

In the pre-war period, only one material has mattered very much to the design engineers, ordinary structural steel. It was mainly because the cost of aluminium on a volume basis was about six times the price of steel. During World War 2, the large demand of aluminium for the aircraft industry resulted in a vast increase in the world production of aluminium. The demand for structural efficiency and safety during this time also led to highly sophisticated manufacturing techniques and new high strength aluminium alloys. Therefore, before and during the war time, the studies and knowledge of the structural behaviour of aluminium members were rather limited. Most of the experiments that were carried out [32,33[‡],34] were mainly simple column tests; and the aluminium alloys used in tests were mainly used in the aircraft industry. After World War 2 considerable effects were made to introduce aluminium alloys into civil engineering structures, accompanied by the substantial lowering in price of aluminium and the increasing price of steel. More experimental works were started in order to increase the knowledge of

---

[‡]The results can be found in reference [43]

aluminium [35[‡],36[‡],37[‡], 38,39[‡],40]. Most of the tests, in general, were also in-plane column tests but covering a wider range of aluminium alloys and extruded sections. Limited studies on lateral buckling of aluminium members were also conducted [41,42]. Thereafter, design rules were proposed [43,44] with the support of experimental data; and resulted in the publication of the specifications for aluminium structures by A.S.C.E. Committee on Lightweight Alloys [45,46]. The specifications were written in a permissible stress format and the information on the design of welded members was very limited.

In Britain, aluminium became more widely used in civil structures soon after World War 2, therefore, a document to help guarantee safety and efficiency was required. The Institution of Structural Engineers thus drafted a report on the structural use of aluminium in 1962 [47]; and more background information could be found in the Symposium on Aluminium in Structural Engineering published in 1963 [48]. From this report came the code of Practice for Structural Aluminium CP 118 [1], published in 1969. CP 118 was also written in a permissible stress format but contained more information on welded members. At that time, knowledge of the effects of welding on aluminium structures was rather limited and there were other areas where further work was needed to improve design recommendations. Research was therefore continued during the 1970's in Britain. Recent research programs were mainly undertaken within University of Cambridge; and the studies were mainly on the general effects of welding [16,18] and the buckling strength of welded members [7,17,20,22,23]. Most of these results will be included in

---

[‡]The results can be found in reference [43]

the new British Standard for the use of structural aluminium BS 8118 [2].

As a parallel project, the ECCS Committee has carried out extensive studies and research on the instability problems of aluminium alloy structures since 1970. Several theoretical and experimental research programs have been undertaken with the cooperation and support by several European countries. Some of the tests were on extruded members carried out at Liege University [4] and Germany [71]. The purposes were to investigate the mechanical properties of the materials, their imperfections and their influence on the instability of members. There were also tests on longitudinally welded built-up members carried out at Liege University in cooperation with the University of Naples and the Experimental Institute for Light Metals of Novara [4,19]. In 1977, Mazzolani and Frey [49] concluded the experimental and theoretical studies of the extruded aluminium members; and Frey [50] also reported the results of the longitudinally welded column tests in the same year. The theoretical study and a proposed design method for welded columns were presented by Faella and Mazzolani in 1978 [51]. As a result of the research works, ECCS published the first edition of the recommendations for aluminium structures in 1978. In 1980, a series of papers [52,53,54] were written by Faella and Mazzolani to explain the bases of the ECCS buckling curves. Research programs were still continued by the ECCS Committee to refine the column buckling design curves in the recommendations [27,55,56,57,58]; and improve the plastic design of aluminium members in bending [59,60,61,62,63].

2.5   Research on Welded Aluminium Members

Most of the experimental works on aluminium members, which started from the 1930's, are shown in Table 2.4. It can be seen that the studies on welded aluminium members were rather limited. The first report on welded aluminium columns was published in 1962 by Brungraber and Clark [64]. Unfortunately, their studies were mainly on straight columns which were made from narrow rectangular plate; and some of their conclusions were questionable. After their studies, there was no research on welded aluminium members till ECCS carried out extensive research on longitudinally welded 6082-T6 aluminium columns with three different cross sections [4,19,50]. The theoretical and experimental results were reported by Faella and Mazzolani in 1978 [51].

Recent research programs on welded aluminium members were undertaken within University of Cambridge for the revision of the current standard CP 118. These included the extensive research on longitudinally welded 6082 aluminium columns conducted by Hong in 1983 [7] and some tests on longitudinally welded aluminium beams of 6082 and 7019 alloys carried out by Baxter [20] and Techanitisawad [23] respectively. Moreover, significant research was also conducted by Mofflin [22] on the study of local buckling of aluminium plates with or without longitudinal welds.

From the review of the past research, almost no work appears to have been conducted to study the effect of local transverse welds on member strength. Sample theoretical results were given by Valtinat and Muller [65]; Mazzolani

and Valtinat [62]; and limited tests were carried out in the University of Cambridge [17,18], but no general conclusions could be derived.

Finally, it is worthwhile to mention that the general behaviour of aluminium members with or without welds under compression and biaxial bending are still hardly explored, therefore, extensive theoretical and experimental works should be carried out for further examination of this subject.

Author	Alloy	Type of Cross-section	Type of Tests	Remark
Templin [32]	17S-T(2017)	Solid round rod	Column	In-plane test, without welds
	17S-T(2017) ALCOA 3S, (3003)	Round tube, angle	Column	In-plane test, without welds
Osgood [33]	2024-T4	H-section	Column	In-plane test, without welds
Hill [34]	17S-T(2017)	Unsymmetrical I-section	Beam	Elastic lateral buckling, without welds
Holt [35]	75S-T (7075-T6)	Angle, solid rolled rod, rectangular bar	Column	In-plane test, without welds
Leary [36]	14S-T (2014-T6)	Solid rolled rod, Z-section, rectangular bar	Column	In-plane test, without welds
Unpublished data [37,43]	2014-T6	Angle, channel	Column	In-plane test, without welds
	5154-F	Angle		
	5154-H34	Round tube		
	6061-T6	Round tube, angle		
	7178-T6	Angle		
Barker [72]	Duralumin S	Angle, U-section, T-section, I-section	Column	Flexural-torsional buckling, without welds
	Duralumin D	Angle		
	Mg 7	Angle		
Smith [73]	HE10 WP	Equal bulb angle, unequal bulk angle	Column	Flexural-torsional buckling, without
	HE15 WP	Equal bulk angle, unequal bulk angle, lipped channel, lipped H-channel		
Hill [38]	27S-T6 (2027), 14S-T6	I- and H-section	Column	Lateral buckling, eccentrically loaded, without welds
Clark [39]	6061-T6	Rectangular tube, rectangular bar	Column	In-plane tests, without welds
Hill [41]	17S-T6 (2017)	Channel, Z-section Z-section	Beam	Lateral buckling, without welds
Clark [42]	2014-T6	I-section	Beam	Lateral buckling of beam subjected to unequal end moments, without welds
Brungraber [64]	6061-T6, 5154-H34, 5456-H321	Solid rectangular section	Column	In-plane tests, longitudinally welded
	6061-T6	Solid rectangular section, round tube		In-plane tests, transversely welded

Table 2.4 Experimental Works on Aluminium Members

Author	Alloy	Type of Cross-section	Type of Tests	Remark
Clark [66]	2024-0, 2024-T4	Rectangular bar	Beam	Laterally supported, without welds
Augusti [67]	HE9-WP (6060)	I-section	Beam-column	Small-scale tests, without welds
Marshall [68]	HE30-WP (6082) NE6-M HE15-WP	Equal and unequal angle bulb angle	Column	Flexural-torsional buckling, without welds
Chilver [69]	–	I-section	Column	In-plane test, without welds
Cullimore [70]	HE30-WP (6082)	Double angle	Column	Flexural-torsional buckling
Kloppel [71]	AlZnMg1F36 (7020) AlMgSi1F32 (6181) AlMgMnF20 (5083-5086)	I-section, T-section, round tube	Column	Eccentrically loaded, without welds
	AlZnMg1F36 (7020)	U-section		Torsional buckling, without welds
	AlMgMnF20 (5083-5086)	U-section, I-section, T-section,		Local buckling, without welds
		Round tube		Centrally loaded, without welds
		I-section	Beam	Cantilever, without welds
Mazzolani [4,49,52]	AlMg2.5Mn (5052-5251) AlZnMg1 (7020) Al4Mg (5083-5086)	I-section, round tube	Column	In-plane test, without welds
Frey [4,50,51]	6082	P-section, T-section C-section (see Figure 2.7)	Column	In-plane test, longitudinally welded
Gilson [55,56]	Al Mg Si (6060-6063)	T-section	Column	In-plane test, without welds
Mazzolani [61]	6060-TaA, 6060-T5, 5154-HP	Square box, rectangular box,	Beam	In-plane test, without welds
Hong [7]	6082	I-section	Column	In-plane test, longitudinally welded
Edward [17]	6082	I-section	Beam	In-plane test, transversely welded
Baxter [20]	6082	I-section	Beam	In-plane test, longitudinally welded
Techaniti -sawad [23]	7019	I-section	Beam	In-plane test, longitudinally welded

Table 2.4 cont.

References

[1] British Standards Institution, CP 118: 1969, "The Structural Use of Aluminium".

[2] British Standards Institution, Draft British Standard BS 8118, "Code of Practice for the Design of Aluminium Structures", 1985.

[3] Dwight, J. B., "Principal Structural Alloys and the Effects of Welding", The Structural Use of Aluminium, The Institution of Structural Engineers, October 1985.

[4] Mazzolani, F. M., "Aluminium Alloy Structures", Pitman.

[5] Bayley, M. J., "Materials for Aluminium Structures", International Conference on Steel and Aluminium Structures, Cardiff, 1987

[6] Aluminium Federation Ltd., "You can Weld It! Aluminium".

[7] Hong, G. M., "Buckling of Non-welded and Welded Aluminium Columns", Ph.D Thesis, University of Cambridge, 1983.

[8] Frey, F., Lemaire, E., de Ville de Goyet, V., Jetteur, P., and Studer, M., "Finel - G, Nonlinear Finite Element Analysis Program User Manual", University of Liege, IREM Internal Report 85/3, July 1985.

[9] Little, G. H., "Collapse Behaviour of Aluminium Plates", BSI Committee for the Revision of CP 118, A/Paper 27, March 1981.

[10] Ramberg, W. and Osgood, W. R., "Description of Stress-strain Curves by Three Parameters", NACA Tech Note 902, 1943.

[11] Zienkiewicz, O. C., "The Finite Element Method", Third Edition, 1977.

[12] Hill, H. N., Clark, J. W., and Brungraber, R. J., "Design of Welded Aluminium Structures", Transactions, A.S.C.E., Vol. 127, Part II, 1962.

[13] Aluminium Company of America, "ALCOA Handbook of Design Stresses for Aluminium", Pittsburgh, Pennsylvania.

[14] Kelsey, R. A., "Effect of Heat Input on Welds in Aluminium Alloy 7039", Welding Journal, Welding Research Supplement, 1971.

[15] Webber, D., "Strength of Welded 232 AL Zn Mg Alloy", Project No. 7559, Royal Armament Research and Development Establishment (Christchurch), 1983.

[16] Wong, M. P., "Weld Shrinkage in Non-linear Materials", Ph.D Thesis, University of Cambridge, 1982.

[17] Edward, S. P. W., "HAZ Effects in Transversely Welded Aluminium Beams", Part II Project, University of Cambridge, April 1982.

[18] Robertson, I., "Strength Loss in Welded Aluminium Structures", Ph.D Thesis, University of Cambridge, 1985.

[19] Mazzolani, F. M., Gatto, F., and Morri, D., "Experimental Analysis of Residual Stresses and of Mechanical Characteristics in Welded Profiles of Al-Si-Mg Alloy (Type 6082)", Italian Machinery and Equipment, Vol. 11, March 1979, No. 50.

[20] Baxter, G. H. L., "HAZ Effects in Welded Aluminium Beams", Part II Project, University of Cambridge, April 1983.

[21] Thomas, T. C. P. N., "HAZ Effects in Welded Aluminium Tension Members", Part II Project, University of Cambridge, April 1983.

[22] Mofflin, D. S., "Plate Buckling in Steel and Aluminium", Ph.D Thesis, University of Cambridge, 1983.

[23] Techanitisawad, A., "Effect of HAZ Softening in Longitudinally Welded 7019 Beams", Part II Project, University of Cambridge, April 1984.

[24] Brenner, P., "Alliages d'Aluminium Durcissables comme Materiaux pour les Constructions Soudees", VDI, Vol. 103, No. 18, 1961.

[25] Webber, D., "Validation of Design Properties of Welded DGFVE 232A Al Zn Mg Alloy Naturally Aged After Welding", Project No. 7557, Royal Armament Research and Development Establishment (Christchurch), December 1983.

[26] Webber, D., "The Strength of DGFVE 232A Al Zn Mg Alloy Artificially Aged After Welding", Project No.7557, Royal Armament Research and Development Establishment (Christchurch), November 1983.

[27] Mazzolani, F. M., De Luca, A., "Models Distribution of Mechanical Imperfections in Aluminium Alloy Welded Members", Report of I tituto Di Tecnica Delle Costruzioni, Facolta' Di Ingegneria, Universita' Degli Studi Di Napoli, 1983.

[28] Durrant, P. W., "Weld Shrinkage Measurements in a Heat-treatable 4% Zn 2% Mg Aluminium Alloy", Part II Project, University of Cambridge, 1980.

[29] Pirner, M., "Properties of Gas Shielded Arc Welded Joints in Heat-treatable Al-Si-Mg and Al-Zn-Mg Alloys", Colloquium on Aluminium and its Alloys in Welded Construction, Porto, 1981.

[30] Soetens, F., "Welded Connections in Aluminium Alloy Structures", Progress Report, T. N. O. Report, 1983.

[31] Aluminium Company of America, "Structural Handbook - A Design Manual for Aluminium", Pittsburgh, Pennsylvania.

[32] Templin, R. L., Sturm, R. G., Hartmann, E. C., and Holt, M., "Column Strength of Various Aluminium Alloys", Aluminium Research Laboratories, Technical Paper No. 1, ALCOA, 1938.

[33] Osgood, W. R., and Holt, M., "The Column Strength of Two Extruded Aluminium Alloy H-Sections", Report No. 656, NACA, 1939.

[34] Hill, H. N., "The Lateral Instability of Unsymmetrical I Beams", Journal of the Aeronautical Sciences, Vol. 9, 1942.

[35] Holt, M., and Leary, J. R., "The Column Strength of Aluminium Alloy 75S-T Extruded Shapes", Technical Note No. 1004, NACA, 1946.

[36] Leary, J. R., and Holt, M., "Column Strength of Aluminium Alloy 14S-T Extruded Shapes and Rod", Technical Note No. 1027, NACA, 1946.

[37] Unpublished Data, Aluminium Research Laboratories, Aluminium Company of America.

[38] Hill, H. N., and Clark, J. W., "Lateral Buckling of Eccentrically Loaded I- and H-section Columns", Proceedings of First National Congress of Applied Mechanics, A.S.M.E., 1951.

[39] Clark, J. W., "Plastic Buckling of Eccentrically Loaded Aluminium Alloy Columns", Separate No. 299, Proceedings, A.S.C.E., October 1953.

[40] Clark, J. W., "Eccentrically Loaded Aluminium Columns", Transactions, A.S.C.E., Vol. 120, 1955.

[41] Hill, H. N., "Lateral Buckling of Channels and Z-beams", Transactions, A.S.C.E., Vol. 119, 1954.

[42] Clark, J. W., and Jombock, J. R., "Lateral Buckling of I-beams Subjected to Unequal End Moments", Journal of the Engineering Mechanics Division, A.S.C.E., Vol. 83, No. EM3, July 1957.

[43] Hill, H. N. and Clark, J. W., "Straight-line Column Formulas for Aluminium Alloys", Aluminium Research Laboratories, Technical Paper No. 12, ALCOA, 1955.

[44] Hill, H. N., Hartmann, E. C., and Clark, J. W., "Design of Aluminium Alloy Beam-columns", Transactions, A.S.C.E., Vol. 121, 1956.

[45] Committee on Lightweight Alloys, "Suggested Specifications for Structures of Aluminium Alloys 6061-T6 and 6062-T6", Journal of the Structural Division, Proceedings, A.S.C.E., December 1962.

[46] Committee on Lightweight Alloys, "Suggested Specifications for Structures of Aluminium Alloy 6063-T5 and -T6", Journal of the Structural Division, Proceedings, A.S.C.E., December 1962.

[47] Institution of Structural Engineers, "Report on the Structural Use of Aluminium", January 1962.

[48] Institution of Structural Engineers, "Symposium on Aluminium in Structural Engineering", 1963.

[49] Mazzolani, F. M., and Frey, F., "Buckling Behaviour of Aluminium - Alloy Extruded Members", Proceedings of the Second International Colloquium on Stability of Steel Structures, Liege, April 1977.

[50] Frey, Fr., "Alu - Alloy Welded Column Buckling Research Program Test Results", ECCS Committee 16, Doc. 16-77-3, 1977.

[51] Faella, C., and Mazzolani, F. M., "Buckling Behaviour of Aluminium Alloy Welded Columns", ECCS Committee, Doc. 16-78-2, 1978.

[52] Faella, C., and Mazzolani, F. M., "European Buckling Curves for Aluminium Alloy Extruded Members", Alluminio, Ottobre 1980.

[53] Faella, C., and Mazzolani, F. M., "European Buckling Curves for Aluminium Alloy Welded Members", Alluminio, Novembre 1980.

[54] Mazzolani, F. M., "The Bases of the European Recommendations for the Design of Aluminium Alloy Structures", Alluminio, Febbraio 1980.

[55] Gilson, S., and Cescotto, S., "Experimental Research on the Buckling of Aluminium Alloys Columns with Unsymmetrical Cross-section", University of Liege.

[56] Gilson, S., and Cescotto, S., "Experimental Research on the Buckling of Aluminium Alloys Columns with Unsymmetrical Cross-section - Complementary Test", University of Liege.

[57] Cescotto, S., "The In-plane Buckling of Alu-alloys Columns with Un-symmetrical Cross-sections Submitted to Eccentric Loading", University of Liege, June 1983.

[58] Mazzolani, F. M., "ECCS Stability Code for Aluminium Alloy Members: Present State and Work in Progress", Stability of Metal Structures, Preliminary Report, Paris 16-17 November 1983.

[59] Mazzolani, F. M., "Plastic Design of Aluminium Alloy Structures", University of Naples.

[60] De Martino, A., Faella, C., and Mazzolani, F. M., "Inelastic Behaviour of Aluminium Double - T Welded Beams: A Parametric Analysis", ECCS Committee T2, October 1984.

[61] Mazzolani, F. M., Cappelli, M., Spasiano, G., "Plastic Analysis of Aluminium Alloy Members in Bending : Comparison between Theoretical and Experimental Results", ECCS Committee T2, October 1984.

[62] Mazzolani, F. M., and Valtinat G., "ECCS Activity in the Field of Buckling of Aluminium Alloy Members", International Conference on Steel and Aluminium Structures, Cardiff, 1987.

[63] Cappelli, M., De Martino, A., and Mazzolani, F. M., "Ultimate Bending Moment Evaluation for Aluminium Alloy Members : A Comparison among Different Definitions", International Conference on Steel and Aluminium Structures, Cardiff, 1987.

[64] Brungraber, R. J., and Clark, J. W., "Strength of Welded Aluminium Columns", Transactions, A.S.C.E., Vol. 127, Part II, 1962.

[65] Valtinat, G., and Muller, R., "Ultimate Load of *of* Beam-columns in Aluminium Alloys with Longitudinal and Transversal Welds", Second International Colloquium on Stability, Preliminary Report, Liege, 1977.

[66] Clark, J. W., Richard, L., Rolf, A. M., "Buckling of Aluminium Columns, Plates, and Beams", Journal of Structural Division, Proceedings, A.S.C.E., Vol. 92, No. ST3, June 1966.

[67] Augusti, G., and Barbarito, B., "Small Scale Aluminium Stanchions in Combined Bending and Compression", The Structural Engineer , Vol. 44, No. 4, April 1966.

[68] Marshall, W. T., Nelson, H. M., Smith, I. A., "Experiments on Alloy Struts", Symposium on Aluminium in Structural Engineering, Institution of Structural Engineers, 1963.

[69] Chilver, A. H., and Britvec, S. J., "The Plastic Buckling of Aluminium Columns", Symposium of Aluminium in Structural Engineering, Institution of Structural Engineers, 1963.

[70] Cullimore, M. S. G., "Aluminium Double Angle Struts", Symposium of Aluminium in Structural Engineering, Institution of Structural Engineers, 1963.

[71] Kloppel, K., and Barsch, W., "Versucke Zum Kapitel Stabilitatsfalle Der Neufassung Von DIN 4113", Aluminium, Helft 10, 1973. (Translation provided by M.O.D.)

[72] Baker, J. F. and Roderick, J. W., "The Strength of Light Alloy Struts", Aluminium Development Association Report No. 3, 1948.

[73] Smith, R. E., "Column Tests on Some Proposed Aluminium Standard Structural Sections", Report B-IR-241-54-30/2, Aluminium Laboratories, Banbury, 1954.

IN-PLANE BEHAVIOUR OF ALUMINIUM MEMBERS

The general studies of longitudinally welded columns have been carried out by Hong [1] in 1983, so there is no need to repeat the works in this area. Therefore, this chapter will mainly stress the general in-plane behaviour of aluminium members with or without local transverse welds. A computer program, called Inelastic Stability Analysis of Frames (INSTAF) is used to simulate the in-plane response of the welded members. The basic assumptions and formulations of INSTAF can be referred to Section 3.1 and the parametric studies are shown in Sections 3.3 and 3.4.

3.1   Description of the Program INSTAF

In order to simulate the in-plane behaviour of various aluminium sections, the program INSTAF (originally obtained from the University of Alberta) [2,3], which is based on an ultimate strength approach, was modified to handle the special problems of aluminium structures. The original program INSTAF is a very sophisticated program for the two-dimensional, in-plane analysis of braced and unbraced multi-storey steel frames composed of I-section members. The analysis is based on a stiffness formulation which accounts for geometric as well as material nonlinearity. The effect of axial load on the stiffness and strength of the individual members is considered and partial plastification of sections is taken into account. The influence of residual stresses as well as strain hardening of the material is included in the analysis. The formulation also permits consideration of extended regions of plastic material rather than discrete hinges in beams and beam-columns. The formulation results in finite element equations and the Newton-Raphson

method is then used to solve for overall load-deformation characteristics of the structure.

Since the stress-strain relationship of the original program was a tri-linear curve, the stress-strain curve had to be modified into a continuous form. The stress-strain relationship chosen is the piecewise form of Ramberg-Osgood formula. Moreover, the original program could deal only with I-sections under major-axis bending. After the modifications INSTAF can analyse aluminium frames or isolated members with various types of cross-section (I-section, unsymmetrical I-section, box-section, tee-section, channel and lipped-channel) under major and minor axis bending. The modified INSTAF can also simulate the effect of longitudinal and transverse welds along the member.

The member containing local transverse welds is analysed by dividing the member into several elements, using elements having reduced stiffness to represent the reduced-strength zones of the transverse welds. For both the transverse and longitudinal welds, and idealized step-change model is used to represent the effect of welding within the member (see Section 2.3.1).

3.1.1   Numerical Formulation of the Problem

All the basic equations of program INSTAF have been well-explained in reference [2], so there is no intention to copy all the equations again. Therefore, the author only discusses the general considerations and procedures for simulating the effect of longitudinal and transverse welds within the member.
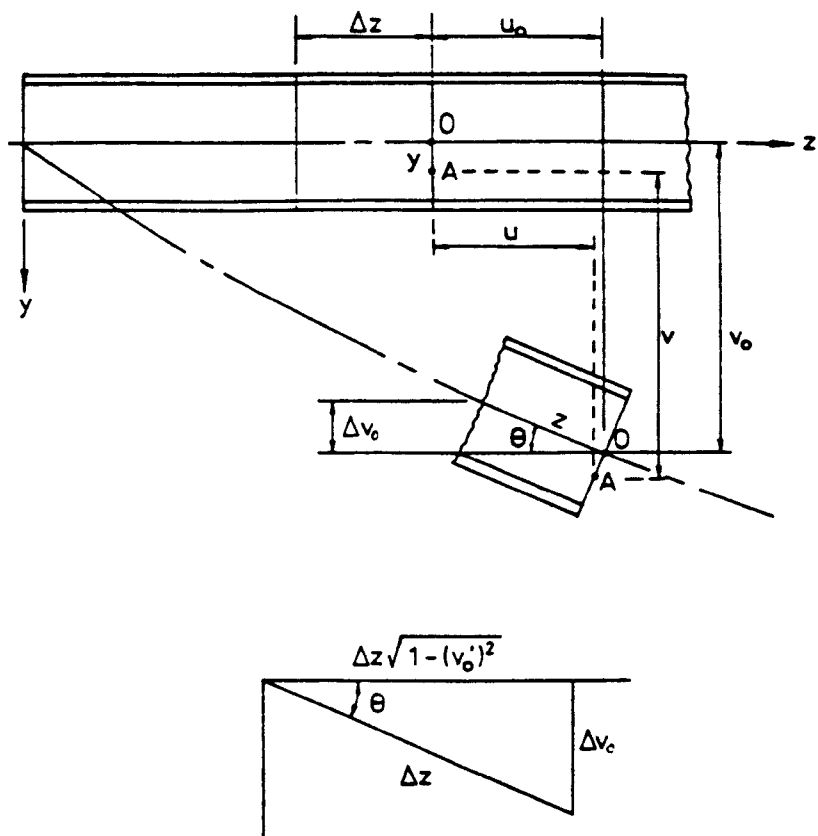
Figure 3.1 Element Deformation

The following assumptions are used to formulate the basic equations of program INSTAF.

1. The member is straight, prismatic and the member z-axis (the reference axis) coincides with the centroidal axis of the cross-section.

2. Only in-plane deformations occur and sections that were originally normal to the z-axis will remain undistorted and normal to the beam axis after deformation.

3. Shearing deformations are negligible.

4. The slope at any point along the reference axis is given by

$$v_o' = \frac{\Delta v_o}{\Delta z} = \sin\theta \tag{3.1}$$

in which the notation is shown in Figure 3.1.

Assumption 4 is basic to the nonlinear formulation developed herein. Since a Lagrangian coordinate system is used, this expression is 'exact' when the elemental length of beam Δz does not change in length. Since the axial strain in a member may be expected to be small up to the point of collapse (of the order of 1% or 2%), equation (3.1) remains valid and permits accurate solutions for large displacement problems of frames.

The above assumptions permit the displacement u and v of an an arbitrary point A on a beam cross-section to be expressed in terms of the displacements of the reference axis of the beam. Thus, referring to Figure 3.1, the displacements can be written as

$$u = u_o - y\sin\theta \tag{3.2}$$
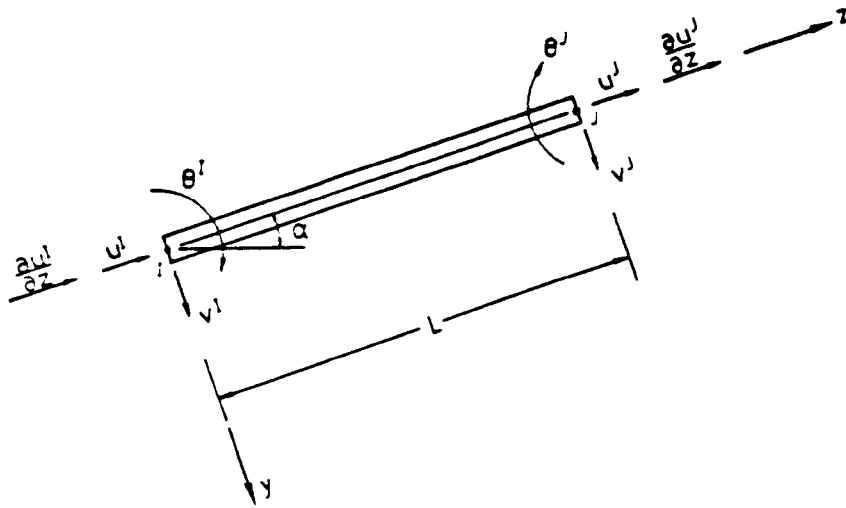
Figure 3.2 Local Nodal Displacements

and

$$v = v_o - y(1 - \cos\theta) \tag{3.3}$$

Assumption 4 permits equations (3.2) and (3.3) to be written as

$$u = u_o - yv_o' \tag{3.4}$$

and

$$v = v_o - y(1 - \cos\theta) \tag{3.5}$$

The axial strain at the arbitrary point A can be obtained from the large displacement strain-displacement equation [2] as

$$\varepsilon_z = u_o' + \frac{1}{2}\left[(u_o')^2 + (v_o')^2\right] - yv_o''\left[1 + u_o' + \frac{(v_o')^2}{\sqrt{1 - (v_o')^2}}\right]$$

$$+ \frac{1}{2}y^2(v_o'')^2\left[1 + \frac{(v_o')^2}{1 - (v_o')^2}\right] \tag{3.6}$$

The principle of virtual work may be written as

$$\delta W = \int_V \sigma_z \, \delta\varepsilon_z \, dV - [Q]\{\delta q\} = 0 \tag{3.7}$$

From equations (3.1), (3.4), (3.5), (3.6) and (3.7), an equilibrium equation for an element which relates the incremental tangent stiffness matrix $[k_T]$ and unbalance load vector $\{\Delta Q\}$ is formed; and may then be written symbolically as

$$[k_T]\{\Delta q\} = \{\Delta Q\} \tag{3.8}$$

In this equation the element stiffness matrix has been evaluated with respect to nodal displacements $\{q\}$ referenced to a local coordinate system shown in Figure 3.2. The local nodal displacements can be written as

$$\{q\} = \left\{ \ \{q'\}, \{q'\} \ \right\} \tag{3.9}$$
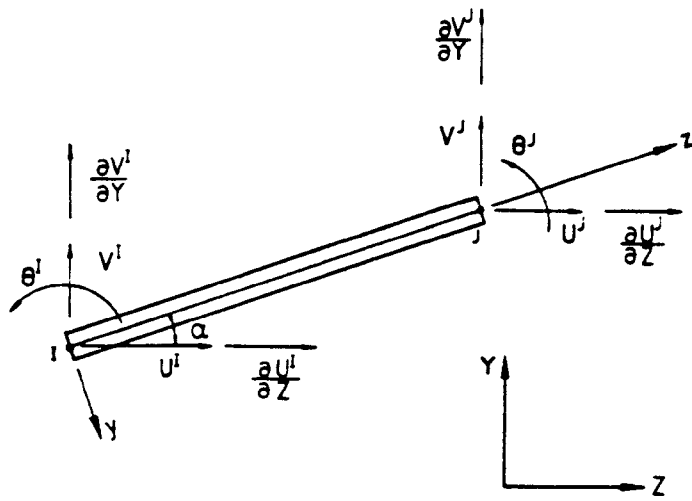
Figure 3.3 Global Nodal Displacements

in which $\left\{q^I\right\} = \left\{u^I, v^I, \theta^I, (\frac{\partial u}{\partial z})^I\right\}$

However, it is convenient to select a different set of reference axes for the global system of nodal displacements $\{r_E\}$ as shown in Figure 3.3. The global nodal displacements can be written as

$$\{r_E\}_G = \left\{ \ \{r_E^I\}, \{r_E^J\} \ \right\}_G \tag{3.10}$$

in which $\left\{r_E^I\right\} = \left\{U^I, V^I, \theta^I, (\frac{\partial U}{\partial Z})^I, (\frac{\partial V}{\partial Y})^I\right\}$

The element displacements with respect to the local coordinate system can be related to those in the global coordinate system by using the transformation matrix $[T]$ as

$$\{q\} = [T]\{r_E\}_G \tag{3.11}$$

As the corresponding force components must perform the same amount of work in either the local or global coordinate system, so

$$\{q\}^T \{Q\} = \{r_E\}_G^T \{R_E\}_G \tag{3.12}$$

By using equations (3.11) and (3.12), equation (3.8) become

$$[k_T]\{\Delta r_E\}_G = \{\Delta R_E\}_G \tag{3.13}$$

The element stiffness matrices can now be assembled to form

$$[K_T]\{\Delta r\} = \{\Delta R\} \tag{3.14}$$

in which $[K_T]$ is the structural tangent stiffness matrix assembled for the entire structure, $\{\Delta r\}$ is the assembled vector of incremental nodal displacements, and $\{\Delta R\}$ is the assembled vector of the incremental nodal forces,

Figure 3.4: Discretisation and Different Location of Welds within the Cross-section
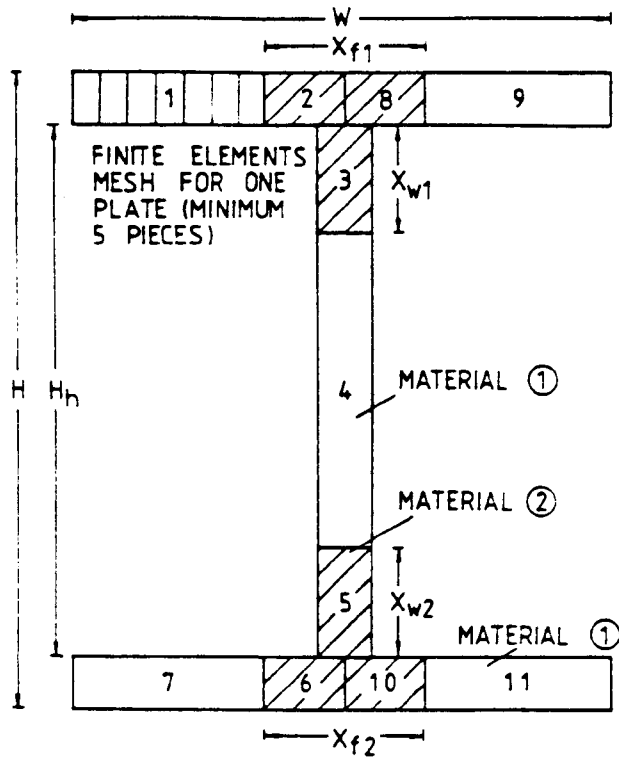
Case A (without welds)

   (a) $X_{f1} = X_{f2} = X_{w1} = X_{w2} = 0$

   (b) material ① = mechanical properties of parent metal

Case B (fully heat-affected, represent local transverse welds)

   (a) $X_{f1} = X_{f2} = X_{w1} = X_{w2} = 0$

   (b) material ① = mechanical properties of RSZ material

Case C (longitudinal welds at the flange and web)

   (a) X_{f1} and $X_{x2} < W$, X_{w1} and $X_{w2} < \frac{H_h}{2}$

   (b) material ① = mechanical properties of parent metal

      material ② = mechanical properties of RSZ material

Case D (longitudinal welds at web)

   (a) X_{f1} and $X_{f2} = W$, X_{w1} and $X_{w2} < \frac{H_h}{2}$

   (b) material ① = mechanical properties of RSZ material

      material ② = mechanical properties of parent metal

called the unbalanced forces. Once equation (3.14) is assembled the Newton-Raphson method [4] can be used to solve for the load-deformation characteristics of the structure.

In order to determine the unbalanced forces, the evaluation of internal nodal forces is necessary. Since there are different ways to build up the longitudinally welded members or the members may contain transverse welds within the structure, to include these effects, the cross-section is divided into several elements as shown in Figure 3.4. The elements having the mechanical properties of heat-affected material are used to represent the effect of welding within the cross-section. Hence, by summing the infinitesimal force of each element, the internal nodal forces can be determined. The piecewise form of Ramberg-Osgood formula is chosen to represent the stress-strain relationship for both the parent and heat-affected material.
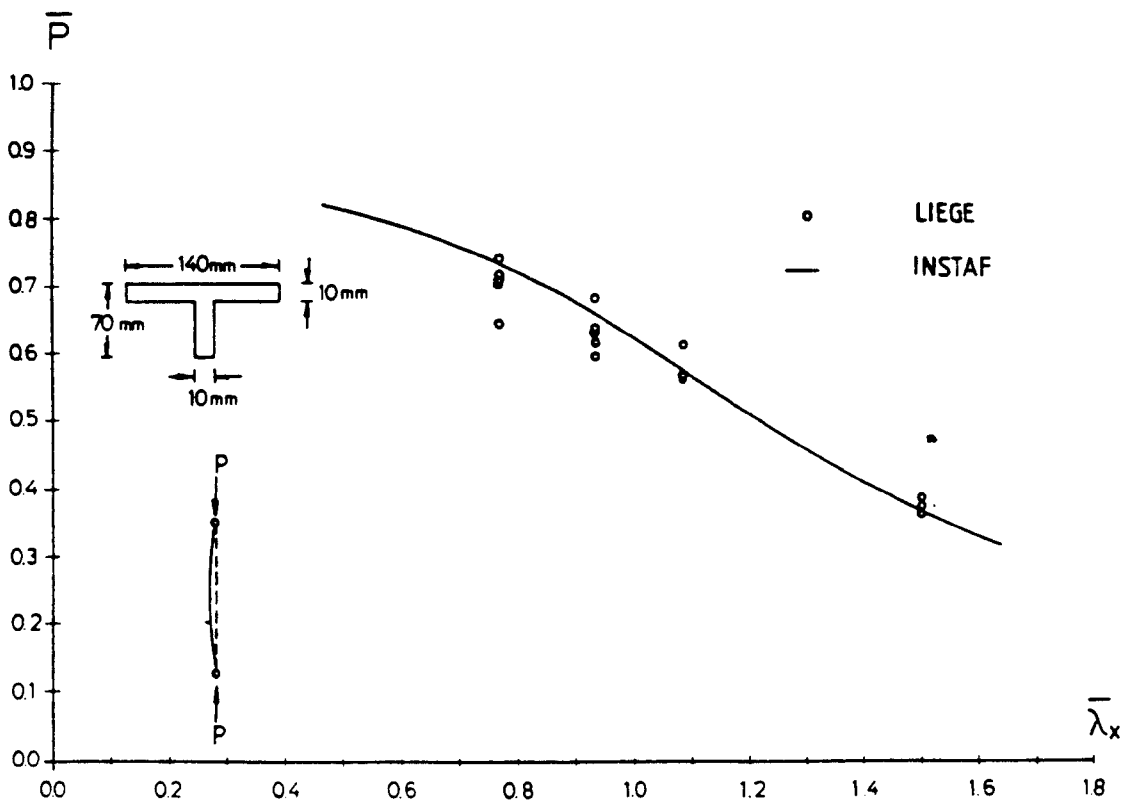
Figure 3.5 Comparison with Experimental Results Obtained by University of Liege [5,6]

Length (mm)	λ_x	$\overline{\lambda}_x$	Experimental Load (Liege) (KN)	Theoretical Load (INSTAF) (KN)	Difference (%)
660	34.9	0.719	485.0	506.4	-4.4
800	42.3	0.932	436.0	454.2	-4.2
930	49.2	1.084	399.0	396.0	0.7
1285	68.1	1.5	258.5	251.6	2.7

Table 3.1: Comparison between Experimental Results and Theoretical Results Obtained by Program INSTAF

3.2   Comparison between INSTAF with Experimental and Theoretical Results

3.2.1   Comparison with Experimental Results

An experimental research program was carried out in the University of Liege (Belgium) to study the in-plane buckling behaviour of aluminium alloy columns with unsymmetrical cross-section [5,6]. The chosen unsymmetrical cross-section is a tee-section and the columns are pin-ended without any welds. From the experimental data, the parameters to fit the Ramberg-Osgood stress-strain curve are:

$$E \quad = \quad 70180 \quad N/mm^2$$

$$\sigma_{0.2} \quad = \quad 336 \quad N/mm^2$$

$$n \quad = \quad 50$$

Figure 3.5 shows the comparison between the results obtained from the modified version of INSTAF with the experimental results. Table 3.1 shows the comparison between the mean of the experimental results with the theoretical results. It is seen that a very good correlation is obtained between the experimental buckling loads and the present computer simulation.
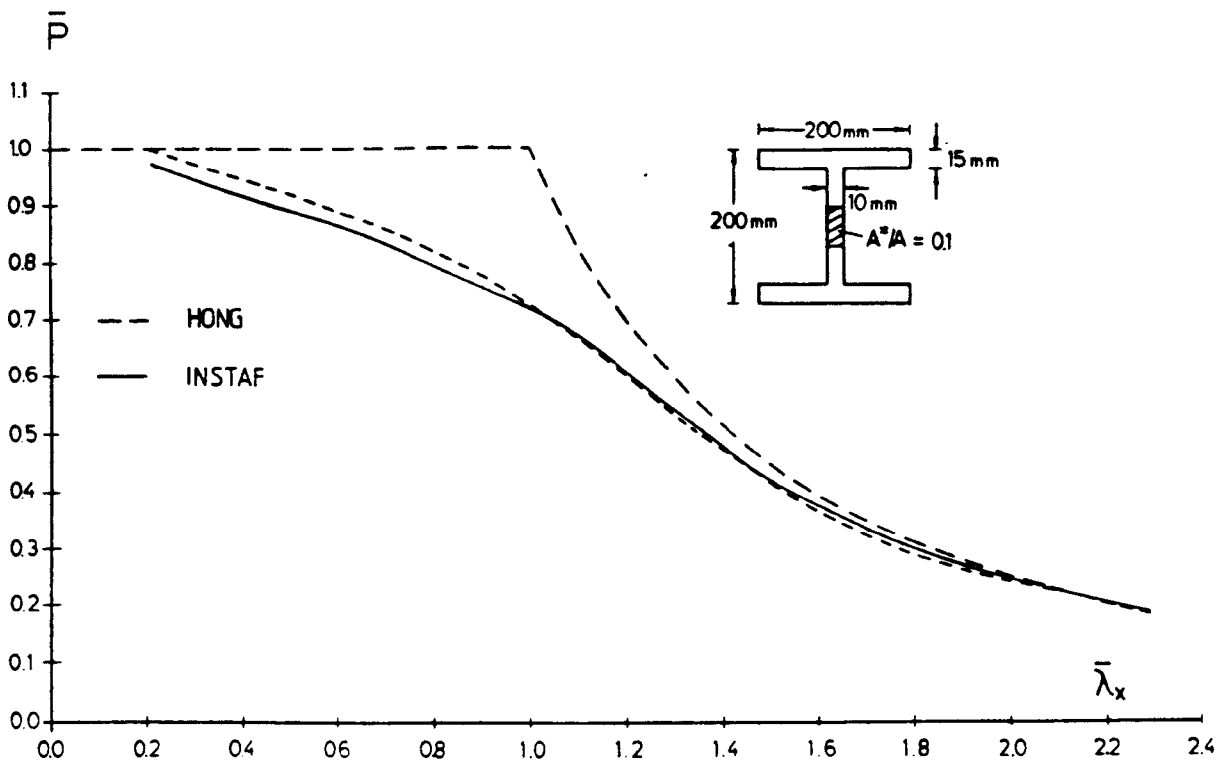
Figure 3.6 Comparison with Hong's Results [1] (Longitudinally Welded Columns)
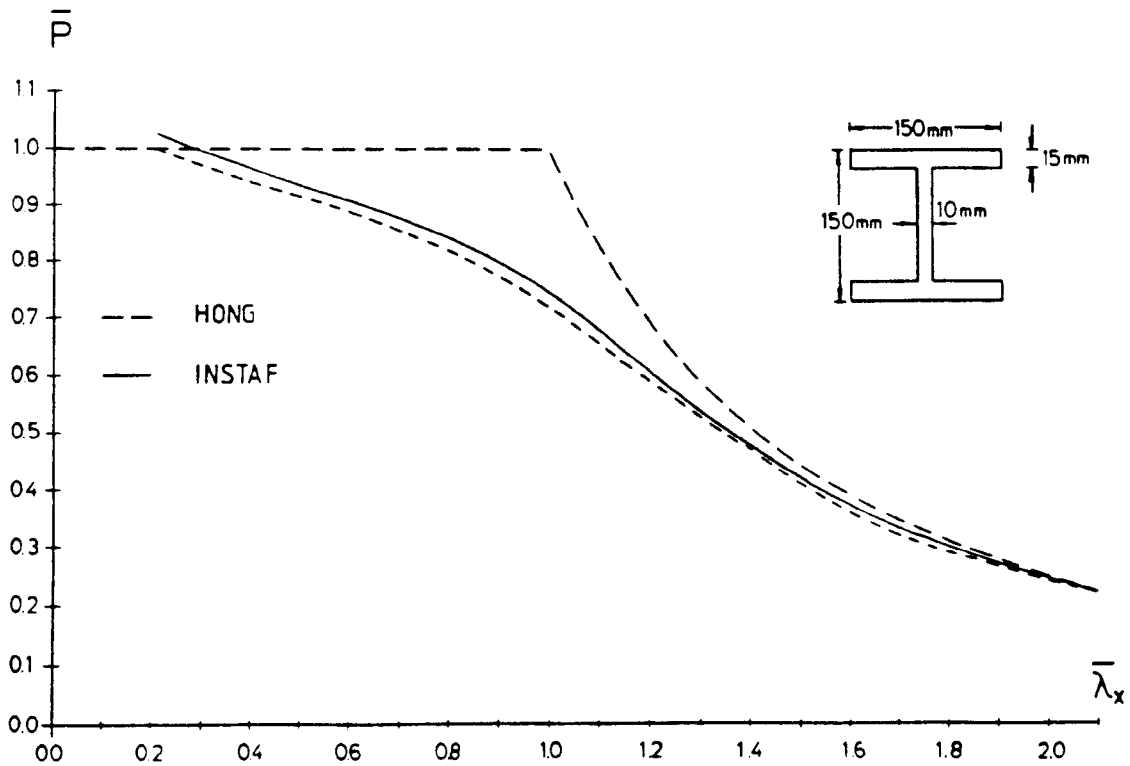
Figure 3.7 Comparison with Hong's Results [1] (Non-welded Columns)

3.2.2   Comparison with Theoretical Results

Figure 3.6 and Figure 3.7 show the comparison between the column curves obtained from the modified INSTAF and the theoretical results obtained by Hong [1] for columns with and without longitudinal welds respectively. The location of the longitudinal welds is at the centre of web with $\frac{A^*}{A} = 0.1$. The parent material properties are:

$$E \quad = \quad 70000 \quad N/mm^2$$
$$\sigma_{0.2} \quad = \quad 300 \quad N/mm^2$$
$$n \quad = \quad 25$$

and the reduced-strength zone (RSZ) material properties are:

$$E^* \quad = \quad 70000 \quad N/mm^2$$
$$\sigma_{0.2}^* \quad = \quad 150 \quad N/mm^2$$
$$n^* \quad = \quad 10$$

From the comparison, it can be seen that quite good agreement is obtained between the two different approaches with a maximum difference between the curves of less than 5%. The difference in results for the longitudinally welded columns is mainly due to the approximate nature of the program used by Hong.

3.3   Choice of ε_{limit}

As mentioned in Section 2.3.2.2, the ductility of the heat-affected material will greatly reduce after welding, therefore, a suitable choice of strain limit, ε_{limit} , becomes important in order to take into account this effect. Figure 3.8 show the results for the bending strength of a beam under moment gradient, $\beta_x = 0$, with different strain limit. We can observe that the most suitable strain limit is $\varepsilon_{limit} = 5\varepsilon_{\sigma_{0.2}}$. The main reasons are the solution obtained by INSTAF will tend to the exact value and the ε_{limit} also directly depends on the type of aluminium alloys used in the analysis. For 6000 series and 7000 series alloy, the ε_{limit} will be around 2.5% and 3.5% respectively. Therefore in the future parametric studies, the above strain limit will be used in the program INSTAF.
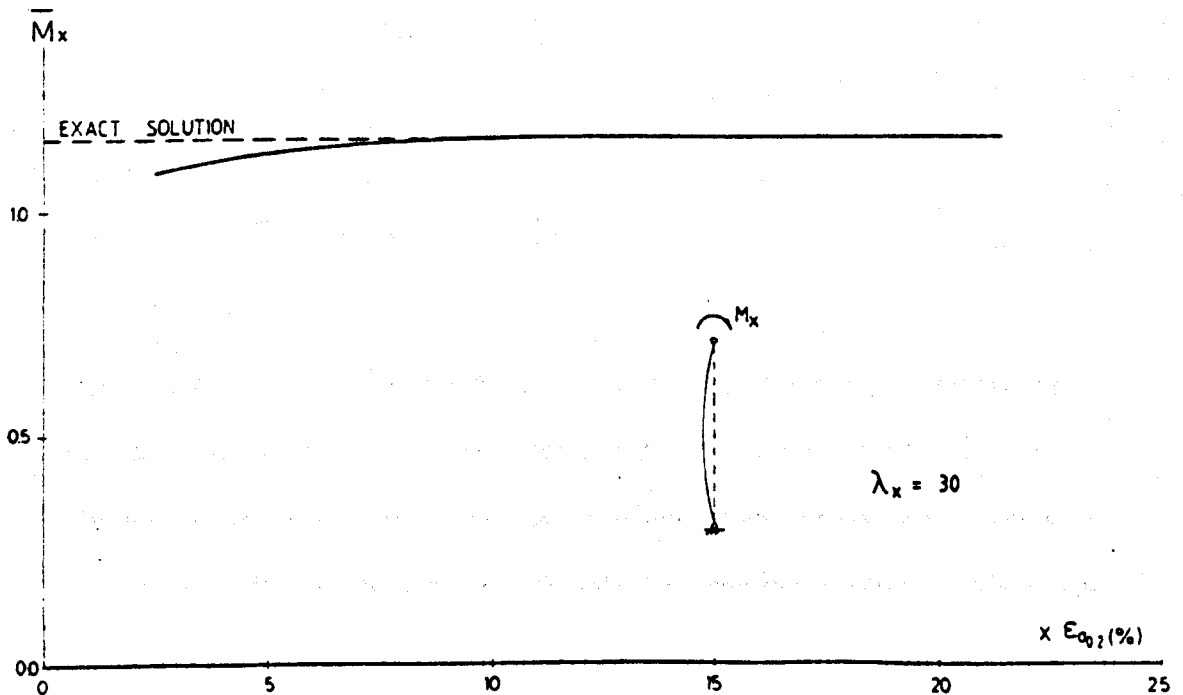
Figure 3.8 Effect of ε_{limit}
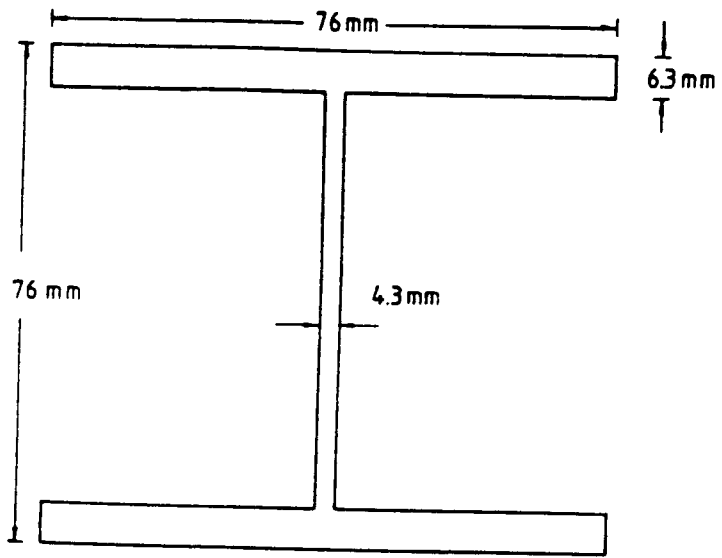
Figure 3.9 Cross-section Used for Parametric Studies

3.4   Parametric Studies of Transversely Welded Members

The aim of the parametric studies is to investigate the general behaviour of aluminium members with local transverse welds. The parametric studies are divided into three main areas: (1) columns (2) beams (3) beam-columns; and the principal results can be found in Table 3.2. Figure 3.9 shows the cross-section chosen for the parametric studies. Amongst all the commonly used aluminium alloys, 6082-TF gives the most severe reduction in strength; therefore, the mechanical properties of 6082-TF alloy were chosen for the parametric studies. The mechanical properties of the parent and reduced-strength zone (RSZ) material are:

Parent: E $=$ 70000 N/mm^2

$\sigma_{0.2}$ $=$ 250 N/mm^2

n $=$ 25

RSZ: E^* $=$ 70000 N/mm^2

$\sigma_{0.2}^*$ $=$ 125 N/mm^2

n^* $=$ 10

An initial sinusoidal deflection with maximum amplitude $\frac{L}{1000}$ was introduced into each member in all the cases. For this particular section the relationship between slenderness ratio λ_x and the non-dimensional slenderness parameter $\overline{\lambda}_x$ is $\lambda_x = 52.6\overline{\lambda}_x$. Furthermore the effect of residual stresses is neglected throughout the parametric studies (see Section 2.3.3.2).

Cases	Reference	Buckling Axis	Extent of RSZ (Located in the Middle)	Principal Results	Remark
Column	C1	Major axis	$\frac{L^*}{L}$ = 0.0, 0.1, 0.2, 0.3, 1.0; 0.05 and 0.1 located at both ends	Figure 3.10	Investigate the effect of location and extent of RSZ on column strength
	C2	Major axis	$\frac{L^*}{L}$ = 0.0, 0.05, 0.1, 0.2, 0.3, 1.0 and 0.1 located at both ends	Figure 3.11	Column curves
	C3	Minor axis	$\frac{L^*}{L}$ = 0.0, 0.1, 0.2, 0.3 and 1.0	Figure 3.12	Column curves
	C4	Major axis	L^* = 10 mm, 30mm, 50mm, 60 mm and 30 mm located at both ends	Figure 3.13	Column curves
	C5	Major axis	L^* = 30 mm, 45 mm and 60 mm	Figure 3.14	Study the effect of HAZ models on column strength
	C6	Major axis	L^* = 50 mm	Figure 3.15	Study the effect of $\sigma_{0.2}^*$ on column strength
	C7	Major axis	L^* = 50 mm	Figure 3.16	Study the effect of n^* on column strength
	C8	Major axis	L^* = 50 mm	Figure 3.17	Study the effect of $\delta_{y(max)}$ on column strength
Beam	B1	Major axis	$\frac{L^*}{L}$ = 0.0, 0.1, 0.2, 0.3, 1.0 and 1.0 located at both ends	Figure 3.18	Investigate the effect of location and extent of RSZ on ultimate strength of beams
	B2	Major axis	L^* = 50 mm	Figure 3.19	In-plane buckling curves of beam
Beam-column	BC1	Major axis	$\frac{L^*}{L}$ = 0.0, 0.1, 0.2, 0.3 and 1.0	Figure 3.20	$\lambda_x = 30, \beta_x = 0$, interaction curves
	BC2	Major axis	$\frac{L^*}{L}$ = 0.0, 0.1, 0.2, 0.3 and 1.0	Figure 3.21	$\lambda_x = 50, \beta_x = 0$, interaction curves
	BC3	Major axis	$\frac{L^*}{L}$ = 0.0, 0.1, 0.2, 0.3 and 1.0	Figure 3.22	$\lambda_x = 70, \beta_x = 0$, interaction curves
	BC4	Major axis	$\frac{L^*}{L}$ = 0	Figure 3.23	$\lambda_x = 90, \beta_x = 0$, interaction curves
	BC5	Major axis	$\frac{L^*}{L}$ = 0.0, 0.1, 0.2, 0.3 and 1.0	Figure 3.24	$\lambda_x = 30, \beta_x = 1$, interaction curves
	BC6	Major axis	$\frac{L^*}{L}$ = 0.0, 0.1, 0.2, 0.3 and 1.0	Figure 3.25	$\lambda_x = 30, \beta_x = -1$, interaction curves
	BC7	Major axis	$\frac{L^*}{L}$ = 0.0, 0.1, 0.2, 0.3 and 1.0	Figure 3.26	$\lambda_x = 30$, interaction curve for member under axial load and lateral point load acting in the middle

NOTE

An initial sinuosidal deflection with maximum amplitude $\frac{L}{1000}$ is introduced in all cases.

Table 3.2: List of Cases in Parametric Studies of Transversely Welded Aluminium Members
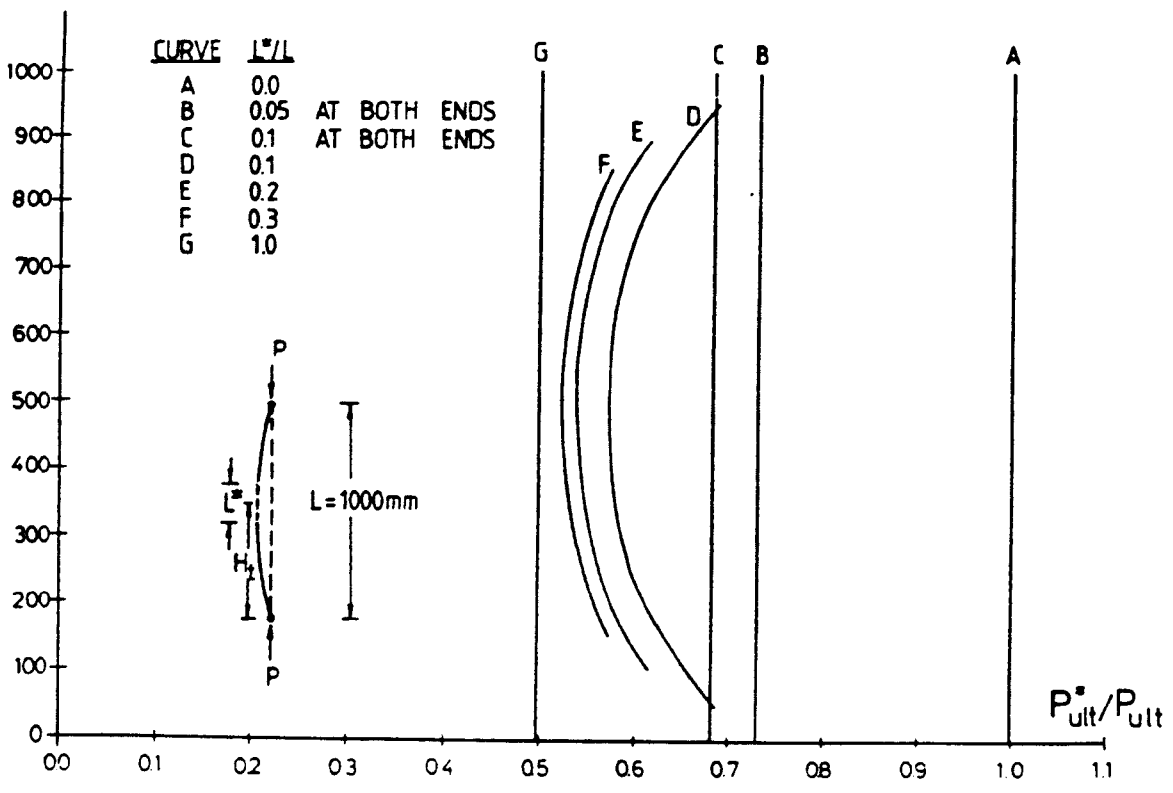
Figure 3.10 Effect of Location and Dimension of RSZ on Ultimate Strength of Columns
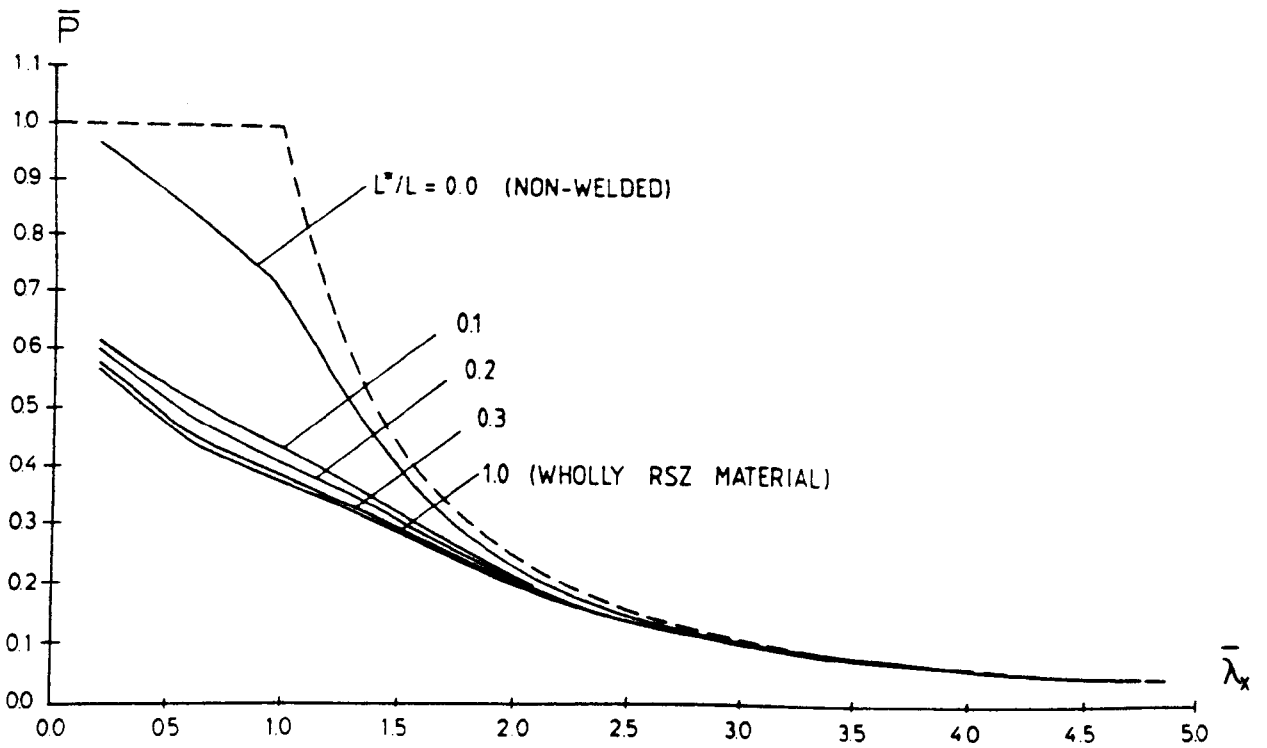
Figure 3.11 Column Curves for I-section Columns with RSZ Located at Mid-height (Major Axis Buckling)

3.4.1   Parametric Studies of Transversely Welded Columns

3.4.1.1   Effect of Local Transverse Welds on Columns

The aim of these parametric studies is to investigate the effect of local transverse welds on the buckling strength of columns. The columns are pin-ended with axial load only and the results are shown in Figure 3.10 to Figure 3.13.

Figure 3.10 covers the effect of the location and dimensions of the reduced-strength zone (RSZ) on the buckling strength of i-section columns. The column with length $L = 1000\ mm$ ($\lambda_x = 31$) is chosen and the ratio of length of reduced-strength zone to the column length (i.e. $\frac{L^*}{L}$) varies from 0.0, 0.05, 0.1, 0.2, 0.3 to 1.0. The location of the RSZ is shifted from one end of the column to the other end. Moreover, RSZ located at both ends of the column with length $0.05L$ and $0.1L$ are also considered. From Figure 3.10, we can observe that the maximum reduction in column strength will occur when the RSZ is located at the mid-height of the column. The reduction in strength will increase as the length of RSZ increases.

Brungraber and Clark [3] pointed out that transverse welds where reduced-strength zones do not extend more than $0.05L$ from the ends of the column have a negligible effect on the buckling strength of pin-ended columns. However, the studies presented herein suggest that it is unsafe to neglect this effect even if the extent of RSZ is small. The buckling strength of the column could be reduced by approximately 30% of the original value when both ends of the column are welded.
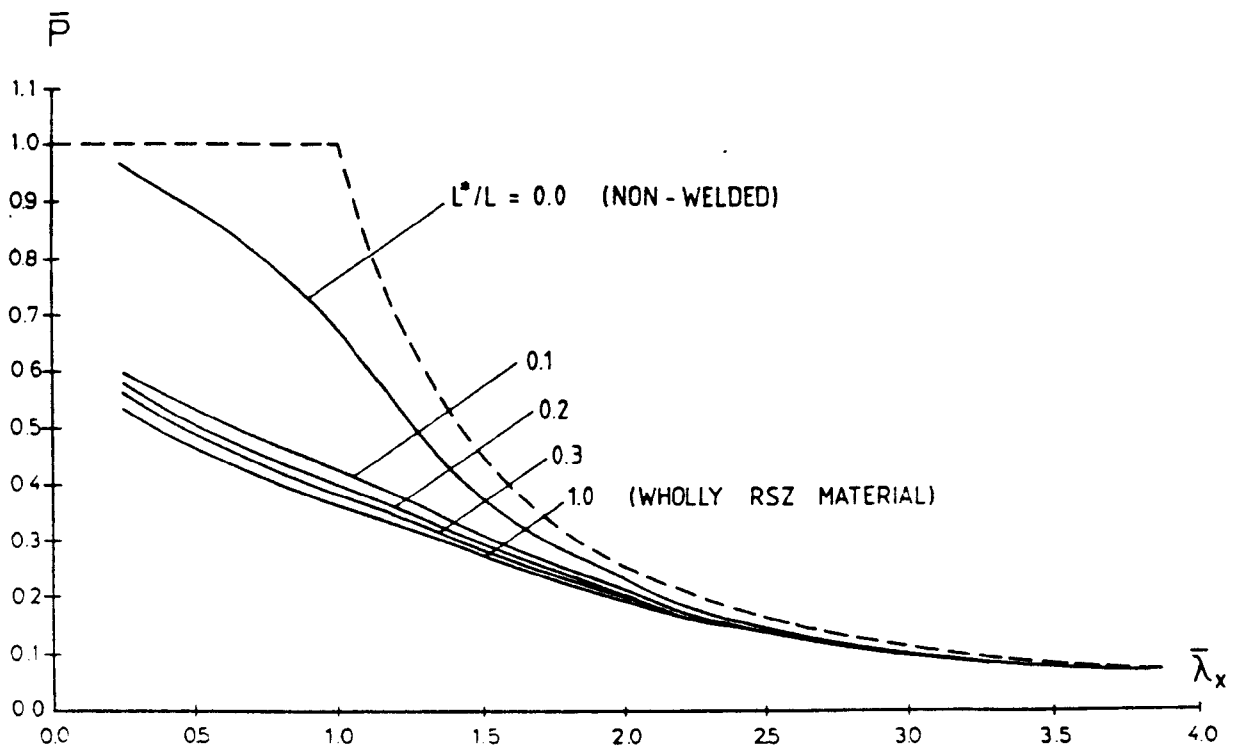
Figure 3.12 Column Curves for I-section Columns with RSZ Located at Mid-height (Minor Axis Buckling)
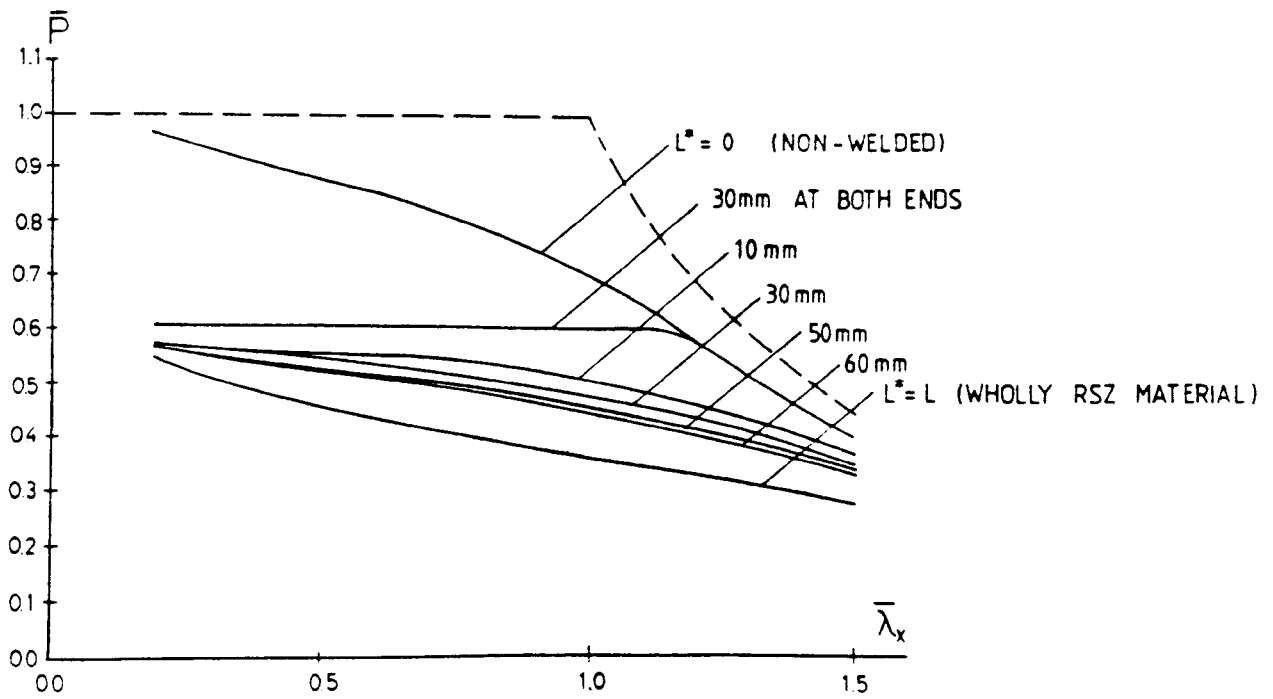
Figure 3.13 Effect of Constant RSZ on Ultimate Strength of Columns

Figure 3.11 to Figure 3.13 cover the reduction in column strength over a wide range of slenderness under major and minor axis in-plane buckling. The RSZ is located at mid-height of the column because it will give the maximum reduction in strength (see Figure 3.10). However , columns with RSZ located at both ends are also considered. Since , the practical range of RSZ are between 30 mm - 60 mm , so in Figure 3.13, constant length of RSZ is used rather than varying the length of RSZ as shown in Figure 3.11. From these figures , it can be seen that the transversely welded column does not have much difference in buckling strength from the column containing wholly RSZ material (i.e. $\frac{L^{\bullet}}{L} = 1$) even though the RSZ is small.

Figure 3.14 Effect of Different HAZ Models on Ultimate Strength of Columns
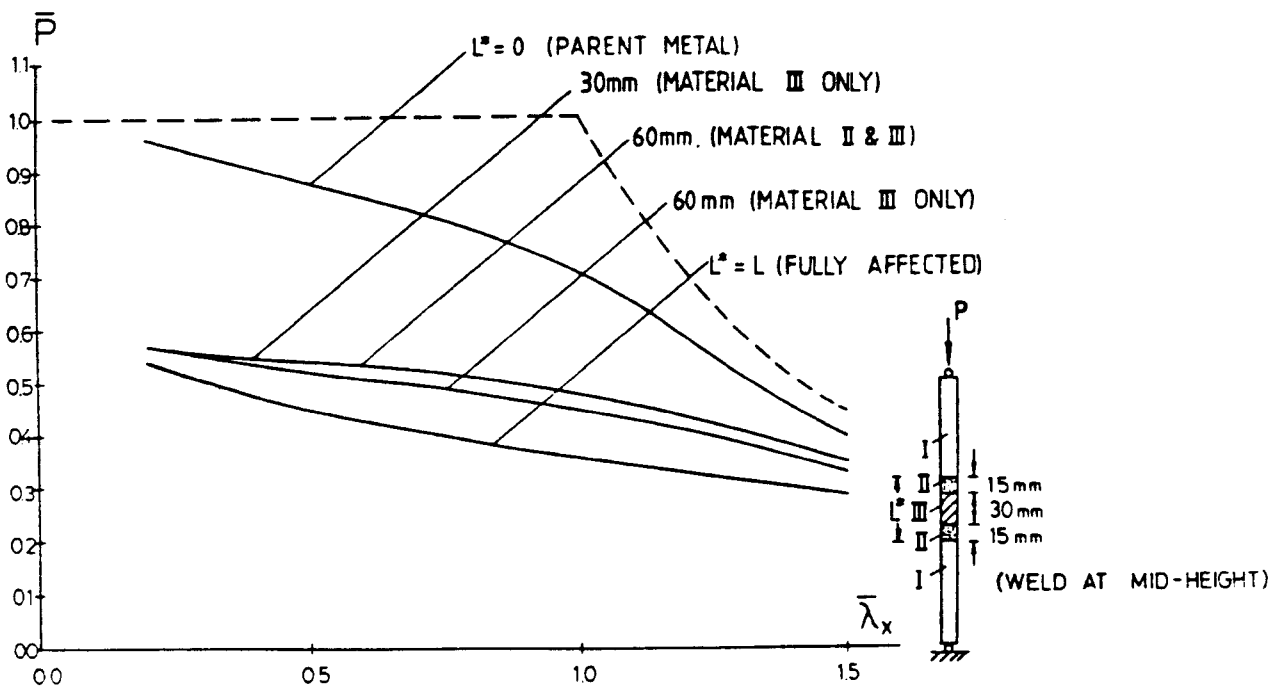
MATERIAL I (PARENT)

$E = 70000$ (N/mm^2)
$\sigma_{0.2} = 250$ (N/mm^2)
$n = 25$

MATERIAL II (PARTIALLY AFFECTED)

$E^* = 70000$ (N/mm^2)
$\sigma_{0.2}^* = 200$ (N/mm^2)
$n^* = 20$

MATERIAL III (FULLY AFFECTED)

$E^* = 70000$ (N/mm^2)
$\sigma_{0.2}^* = 125$ (N/mm^2)
$n^* = 10$

3.4.1.2 Effect of Heat-affected Zone Models on Buckling Strength of Columns

Figure 3.14 shows the effect of different models of heat-affected zone material properties on the buckling strength of columns. ~~Four~~ *Three* different models are chosen to represent the distribution of material properties within the heat-affected zone. Since three zones of material can be found after welding (see Figure 2.4), so the mechanical properties of the parent, partially-affected and fully-affected material are:

<u>Parent:</u>

$$E \quad = \quad 70000 \quad N/mm^2$$
$$\sigma_{0.2} \quad = \quad 250 \quad N/mm^2$$
$$n \quad = \quad 25$$

<u>Partially-affected:</u>

$$E^* \quad = \quad 70000 \quad N/mm^2$$
$$\sigma_{0.2}^* \quad = \quad 200 \quad N/mm^2$$
$$n^* \quad = \quad 20$$

<u>Fully-affected:</u>

$$E^* \quad = \quad 70000 \quad N/mm^2$$
$$\sigma_{0.2}^* \quad = \quad 125 \quad N/mm^2$$
$$n^* \quad = \quad 10$$

From Figure 3.14, we can find that the ultimate buckling strength is controlled by the length of ~~full-affected~~ *fully heat-affected* softening zone only. The length of ~~partially-affected~~ *partially heat-affected* material has negligible effect on the ultimate strength of transversely welded aluminium columns.

3.4.1.3   Effect of $\sigma_{0.2}^*$, n^* and $\delta_{y(max)}$ on Columns

From the experimental results, great variation in mechanical properties was found within the heat-affected zone. Moreover, the heat input during welding can also distort the overall geometry of the member, so it is necessary to perform some sensitivity tests of certain important parameters on the strength of aluminium column. Three important parameters, $\sigma_{0.2}^*$, n^* , and $\delta_{y(max)}$ are chosen in the sensitivity studies and the results are shown in Figure 3.15 to Figure 3.17. We can observe that the variation of $\sigma_{0.2}^*$ has a serious effect on the buckling strength of stocky and intermediate columns ($\lambda_x > 90$ or $\overline{\lambda}_x > 1.7$). The effect of n^* can be neglected as $n^* > 20$ or $\lambda_x > 60$ ($\overline{\lambda}_x > 1.1$). Therefore, if the mechanical properties of heat-affected zone material are uncertain, choosing a lower value of $\sigma_{0.2}^*$ and a higher value of n^* should give a design on the safe side.

Figure 3.17 covers the practical range of initial-out-of-straightness which may be found in welded aluminium columns. A sinusoidal deflection shape is assumed in each column with maximum deflection , $\delta_{y(max)}$, at mid-height. As expected, columns with the greater maximum deflection, $\delta_{y(max)}$, result in the greater reduction in strength.
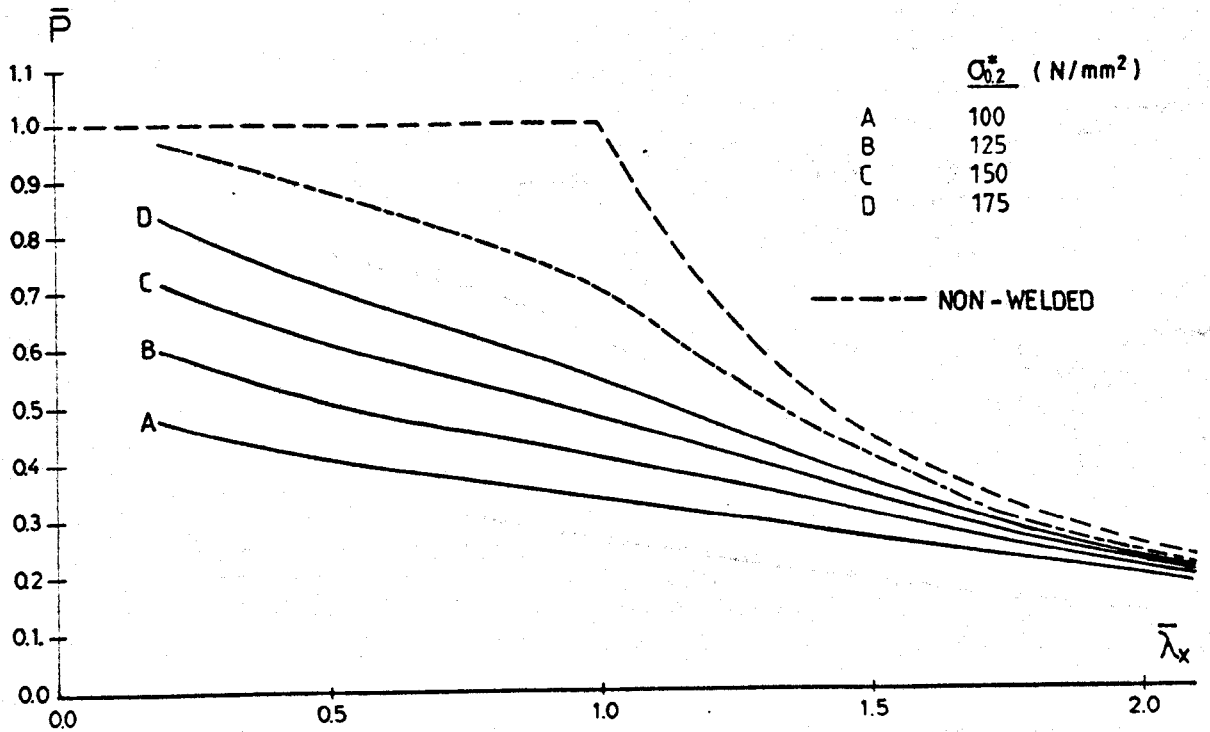
Figure 3.15 Effect of $\sigma_{0.2}^*$
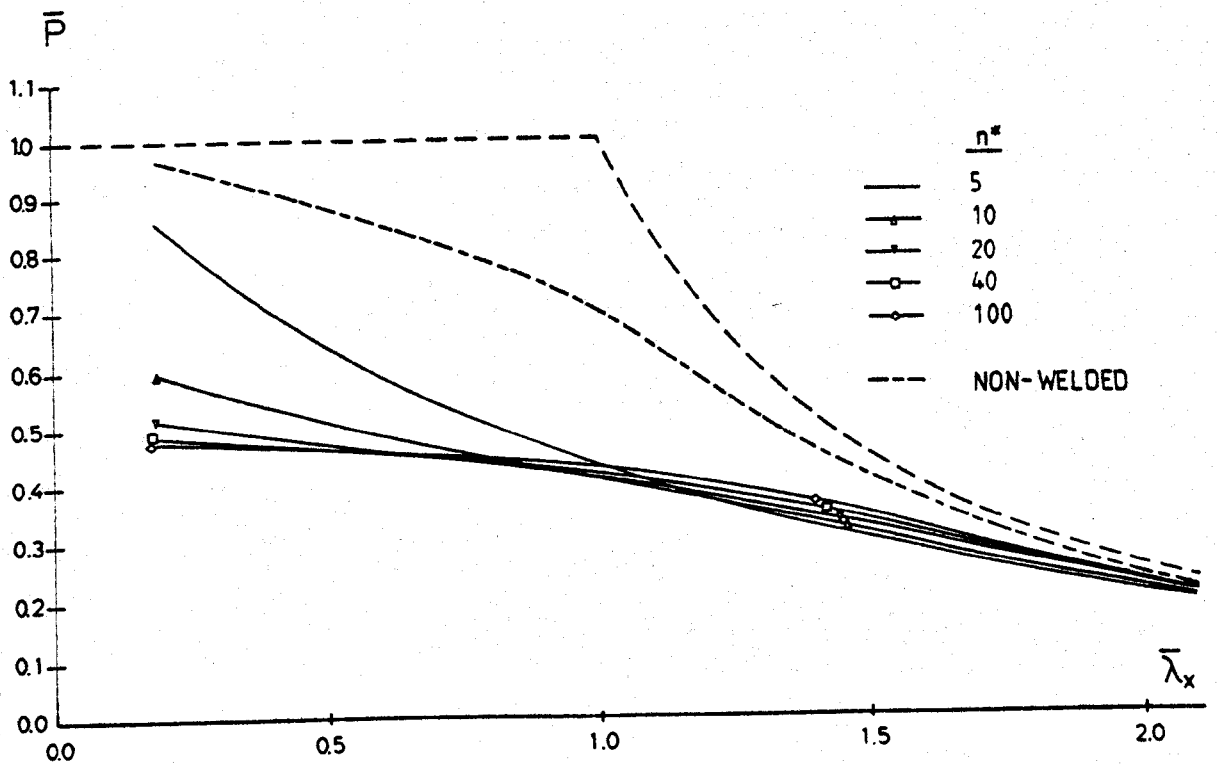
Figure 3.16 Effect of n^*
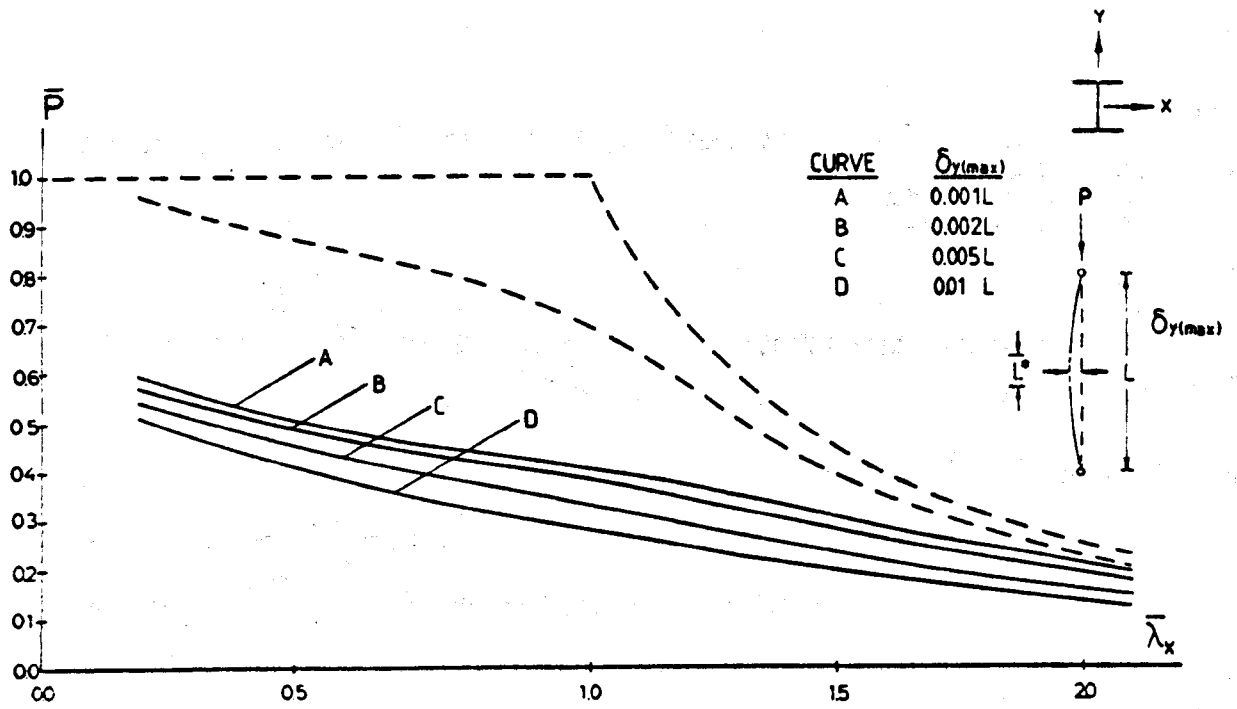
Figure 3.17 Effect of Initial Out-of-straightness
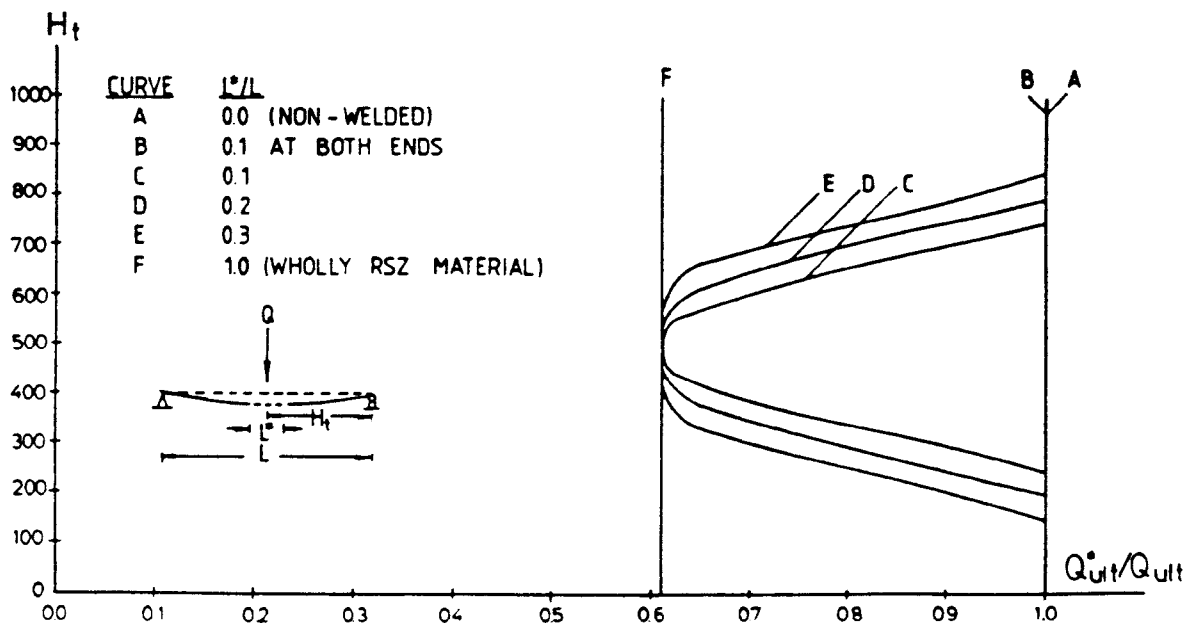
Figure 3.18 Effect of Location and Dimension of RSZ on Ultimate Strength of Beams
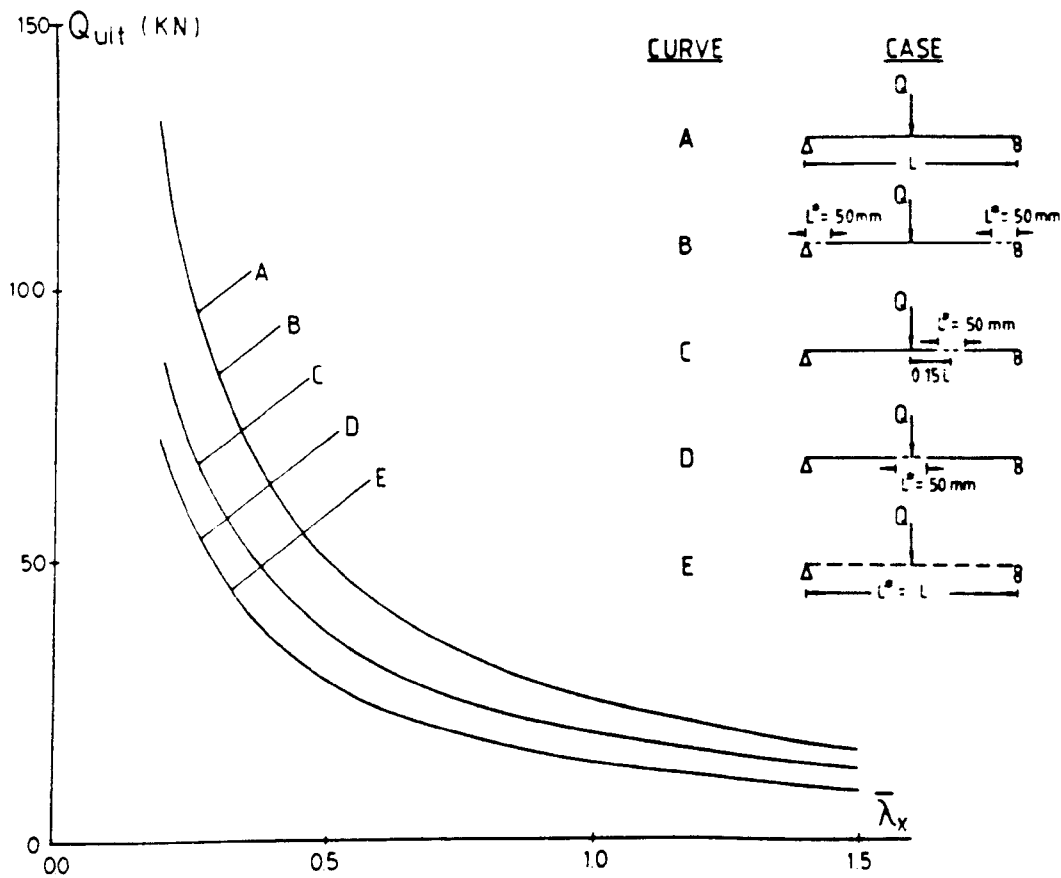
Figure 3.19 Effect of Location of RSZ on Beams

3.4.2   Parametric Studies of Transversely Welded Beams

3.4.2.1   Effect of Local Transverse Welds on Beams

The aim of these parametric studies is to investigate the effect of local transverse welds on the bending strength of beams. In Figure 3.18, the length of the beam selected is 1000 mm assuming simply-supported ends with a central point load. Following parametric study C1, the location of the RSZ is moved along the beam from one end to the other with different $\frac{L^*}{L}$ ratio. The results show that the effect of RSZ can be neglected if the welds are located at the two ends. The maximum reduction in bending strength will occur if the RSZ is located at the point of maximum bending moment and is independent of the dimensions of the RSZ. The reason can be referred to the stress-strain relationship of the parent and heat-affected material of the aluminium alloy (see Figure 2.6). When the RSZ is located near the two ends of the beam, the stress level in the RSZ material is low$\underset{\wedge}{}$ and the beam will behave as if $(\sigma < \sigma_e^*)$ it is a single-phase material. But if the RSZ is located in the middle of the beam, the stress level in the RSZ material is high$\underset{\wedge}{}$ and hence, causes serious $(\sigma > \sigma_e^*)$ reductions in bending strength. Therefore, it was found that the best way to investigate the strength of aluminium members containing local transverse welds is through the stress-strain relationship of the RSZ material and then to determine the stress-level on the RSZ under the applied loading.

Figure 3.19 shows the reduction in bending strength of beams over a wide range of slenderness under major axis in-plane bending. The length of RSZ is

equal to 50 *mm* and three locations of RSZ within the beam are considered. From Figure 3.18 and Figure 3.19, similar conclusions are arrived at and the beams will show significant reduction in bending strength only when the RSZ material is sufficiently stressed.

3.4.3   Parametric Studies of Transversely Welded Beam-columns

3.4.3.1   Effect of Local Transverse Welds on Beam-columns

In these studies, the general behaviour of transversely welded aluminium beam-columns are investigated. All the members were simply-supported with the RSZ located at mid-height. The results are presented in Figure 3.20 to Figure 3.26 in the form of interaction plots using the axial and bending strengths of the unwelded section. The first six of these cover the behaviour of aluminium members under axial load and unequal major axis end moments ($\beta_x = 0, 1, -1$). Figure 3.26 covers the behaviour of aluminium members under axial load and a central lateral point load.

In the case of uniform single curvature bending (see Figure 3.24) and central point load (see Figure 3.26) all cases have similar strengths and it would therefore seen reasonable for the purpose of design to treat members containing any internal transverse welding as if they consisted solely of RSZ material. However, for cases of non-uniform end moments (see Figures 3.20, 3.21, 3.22 and 3.25) the proportions of axial load and moment are more important. In particular, for the case of double curvature bending of $\beta_x = -1$, members with localised yet quite extensive central welding subjected to high moments will behave as if free from RSZ effects. This follows directly from the beam results of Figure 3.18 and Figure 3.19, the central RSZ material being insufficiently stressed for any significant loss of stiffness to occur. In the case of $\beta_x = 0$ the curves diverge as bending becomes more important,

intersecting the moment axis at progressively higher values as the extent of the RSZ decreases, the moment gradient loading meaning that there is correspondingly less scope for this material to reach 'yield'. Thus whilst Figures 3.20, 3.21, 3.22 and 3.25 support the count of a safe design based on the assumption of a wholly RSZ member, they also show such an approach to be potentially very conservative in cases where the exact nature of the problem is such that the presence of the RSZ can have little effect on the member's behaviour.
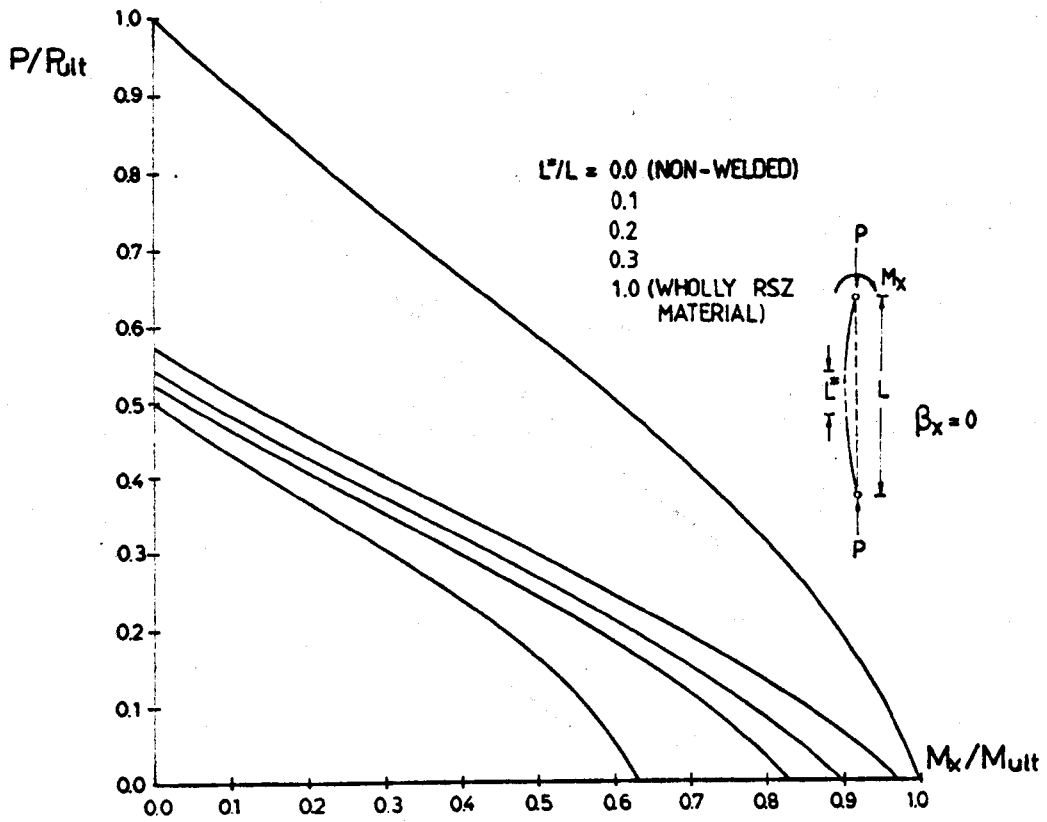
Figure 3.20 Interaction Curves for $\lambda_x = 30$ ($\beta_x = 0$)
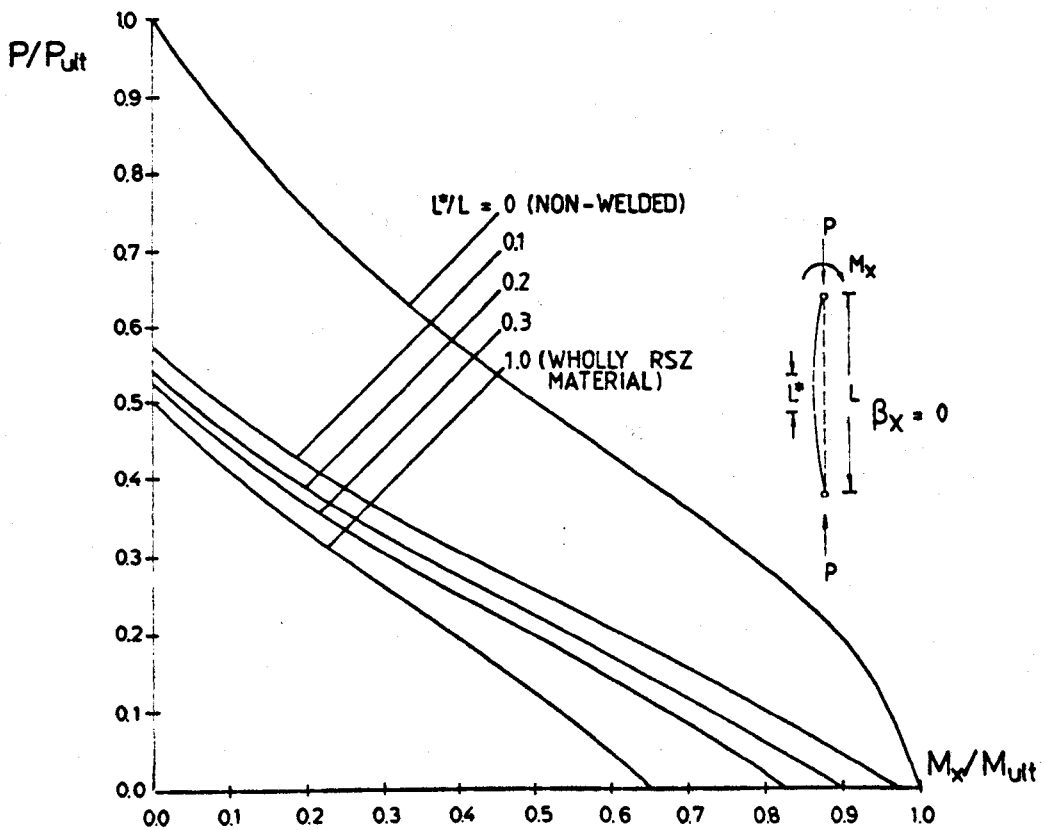
Figure 3.21 Interaction Curves for $\lambda_x = 50$ ($\beta_x = 0$)
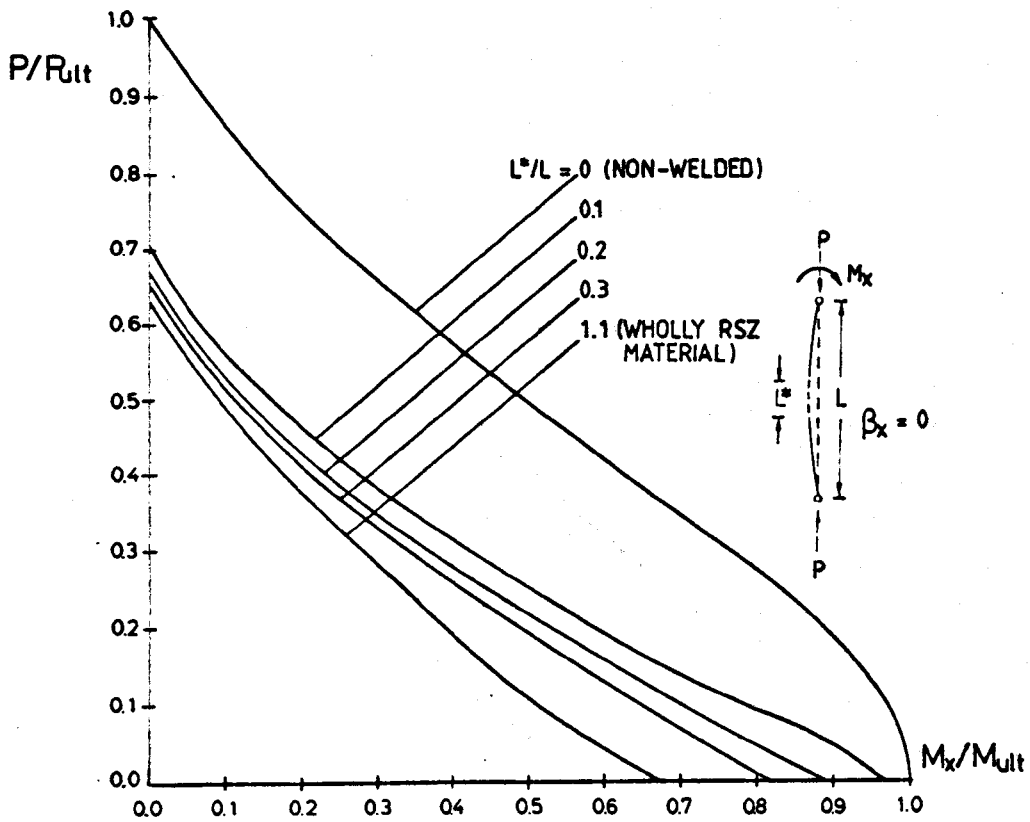
Figure 3.22 Interaction Curves for $\lambda_x = 70$ $(\beta_x = 0)$
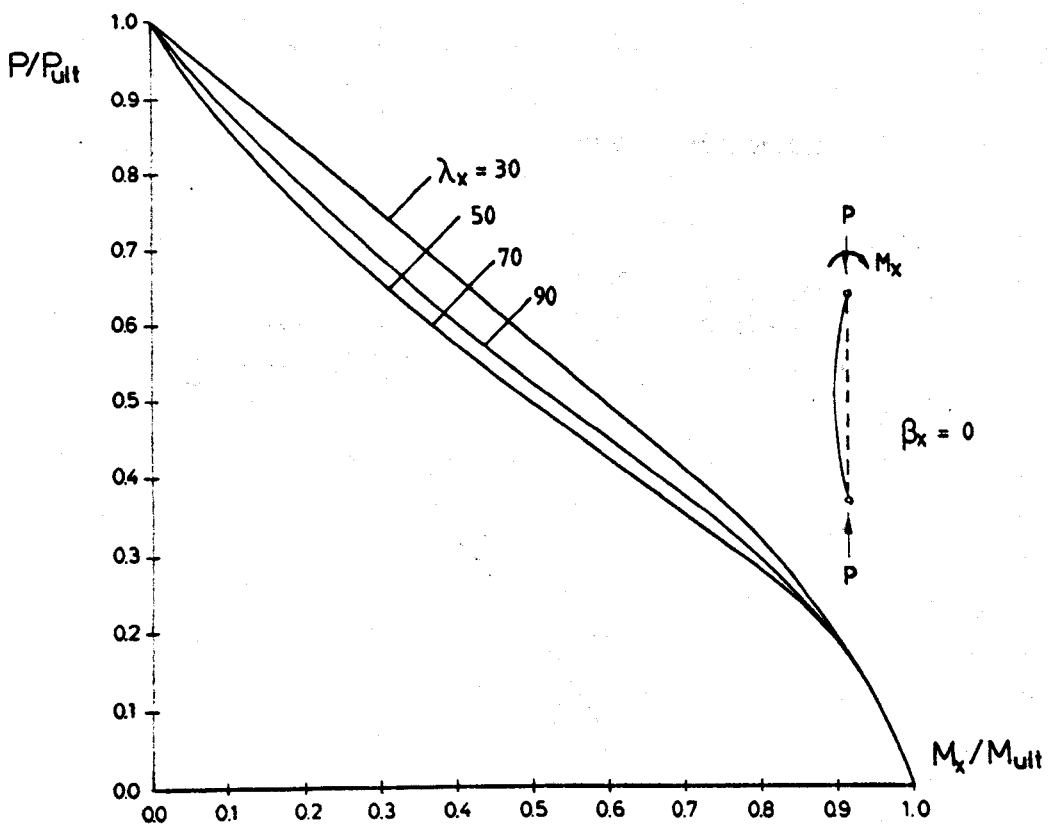
Figure 3.23 Interaction Curves for Non-welded Beam-columns with Different λ_x
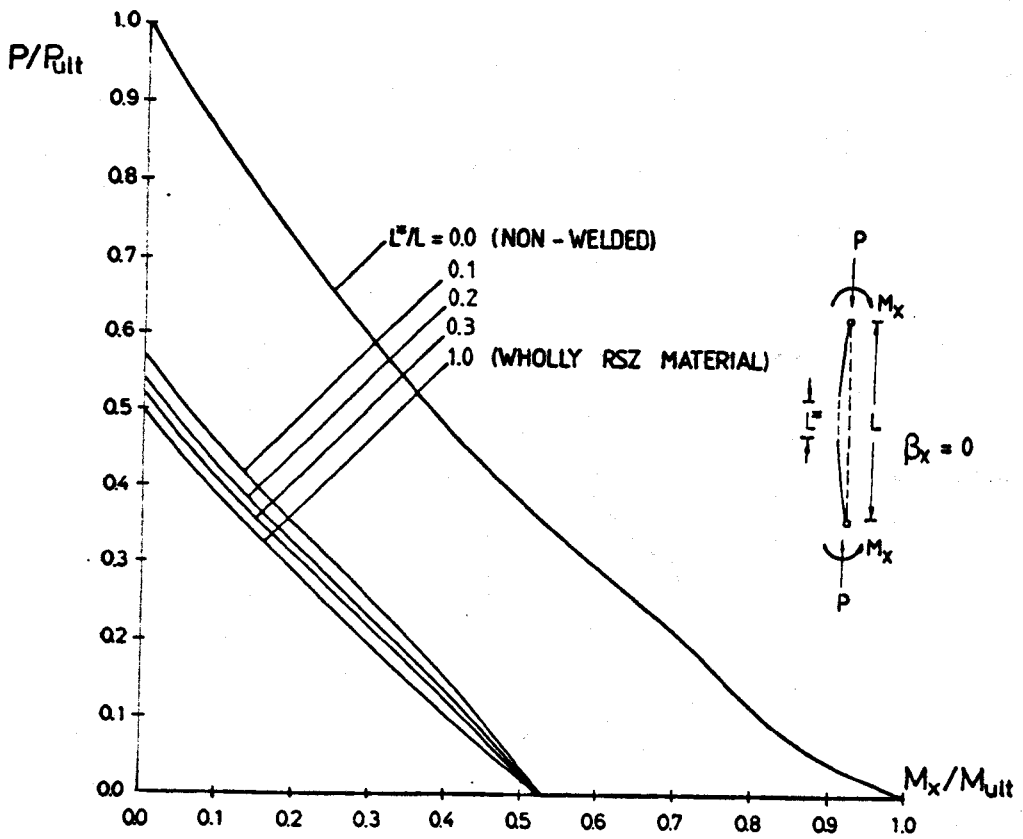
Figure 3.24 Interaction Curves for $\lambda_x = 30$ ($\beta_x = 1$)
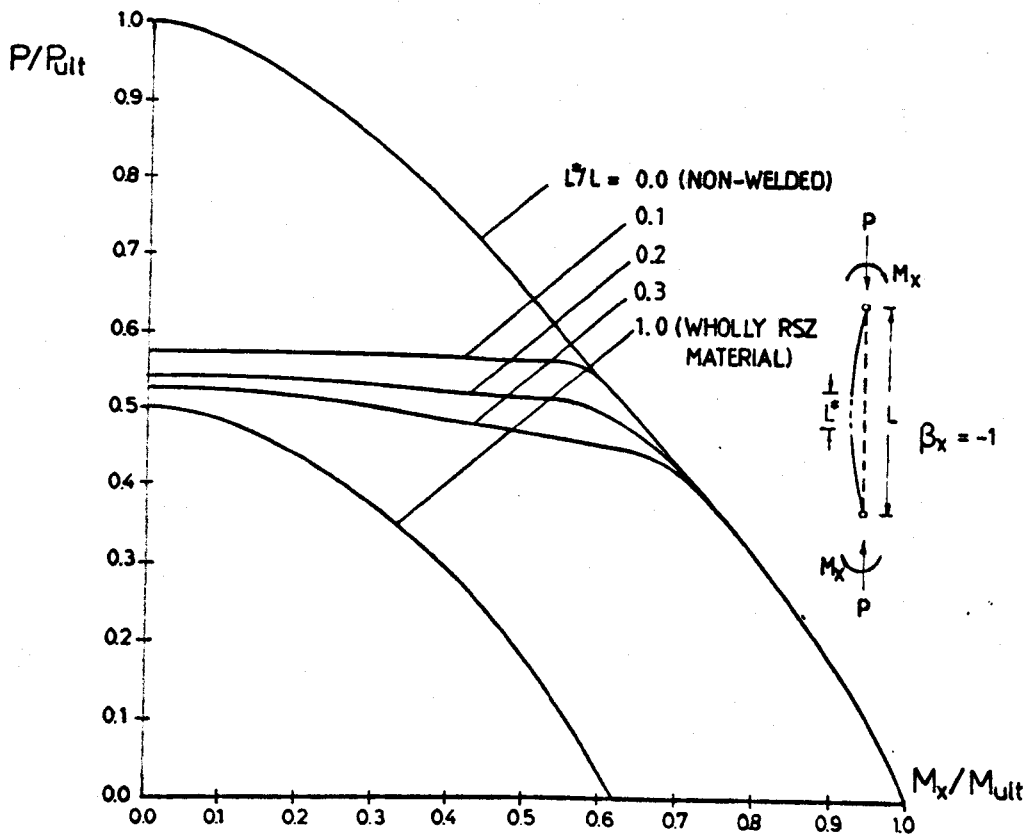
Figure 3.25 Interaction Curves for $\lambda_x = 30$ ($\beta_x = -1$)
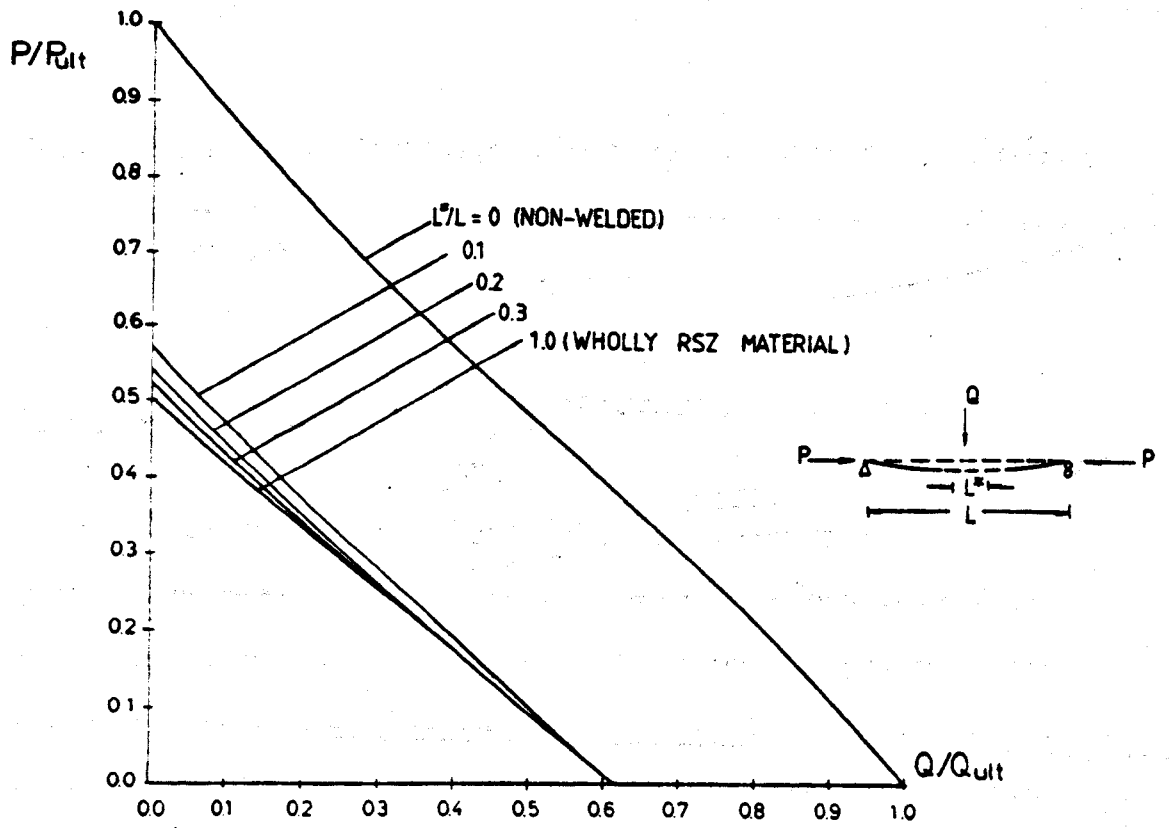
Figure 3.26 Interaction Curves for Laterally Loaded Beam-columns with $\lambda_x = 30$
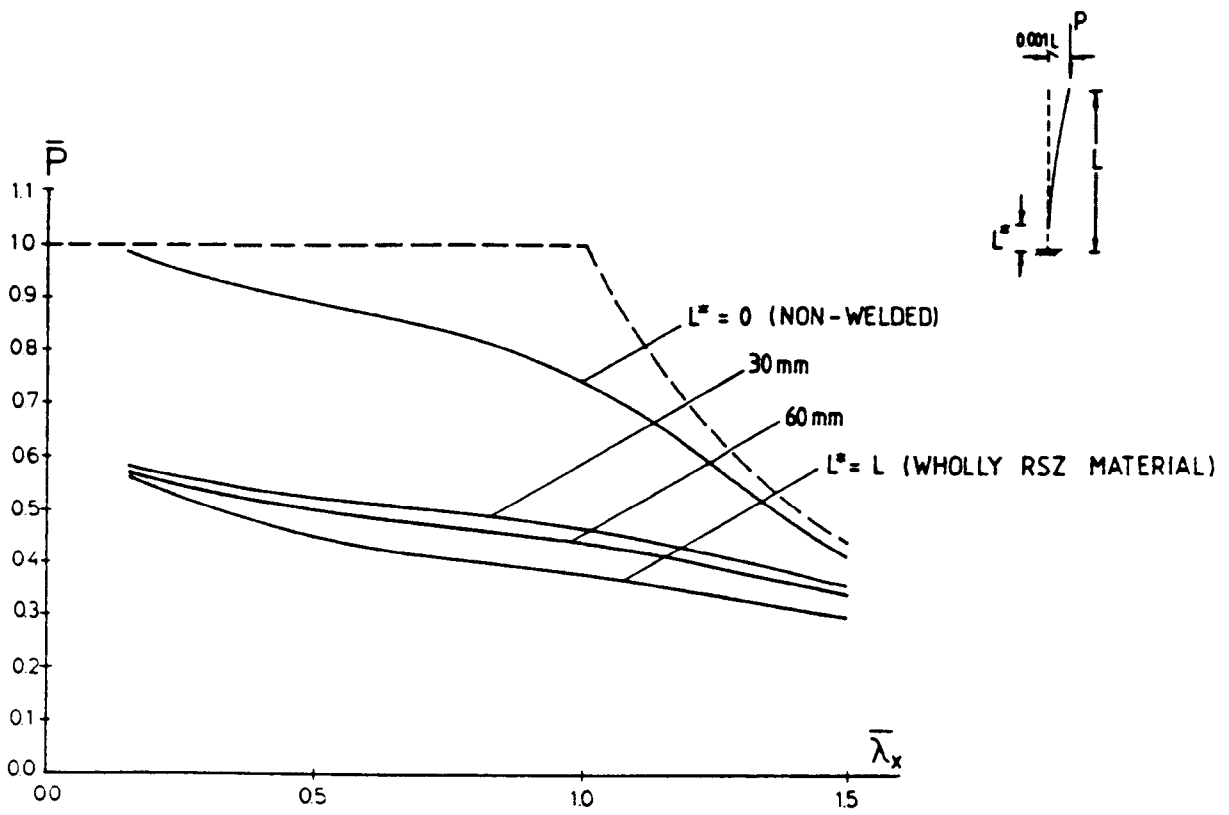
Figure 3.27 Effect of RSZ on Fixed-ended Columns

3.5 Further Parametric Studies on Aluminium Members

3.5.1 Effect of RSZ on Fixed Joints

Figure 3.27 shows the effect of RSZ on the fixed base columns. The RSZ is located at the base of the column and it can be seen that the presence of RSZ at the joint can cause a complete loss of fixity and result in great reductions in column strength. This effect is also considered on the sub-frame as shown in Figure 3.28. The RSZ is located at the joint and three slendernesses of the column ($\lambda_x = 30$, 50 and 70) are chosen. In Figures 3.28 (a) and 3.28 (b), the loading is applied exactly at the joint and at a distance of 30 mm from the joint respectively. The maximum load, which the sub-frame can resist, is greater in the case of Figure 3.28 (b) because the reaction force in the column is greater in the cases of Figure 3.28 (a). From the results tabulated in Figure 3.28, similar observations are obtained; and therefore special considerations should be paid especially to the situations where the presence of RSZ at the joints may influence or destroy the overall stability of the structures.

L_c (mm)	λ_x (column)	Without RSZ P_{ult} (KN)	$L^* = 30\ mm$ Located at Joint $P^*_{ult(1)}$ (KN)	Fully RSZ $P^*_{ult(2)}$ (KN)	$\frac{P^*_{ult(1)}}{P_{ult}}$	$\frac{P^*_{ult(2)}}{P_{ult}}$
954	30	298.5 (278.7)	183.5	155.5 (139.5)	0.61	0.52
1590	50	280.9 (236.3)	180.5	138.1 (118.7)	0.64	0.49
2226	70	253.5 (158.5)	173.9	125.7 (100.1)	0.69	0.50

NOTE

The values in brackets are the buckling load of pin-ended columns.

Figure 3.28 (a)
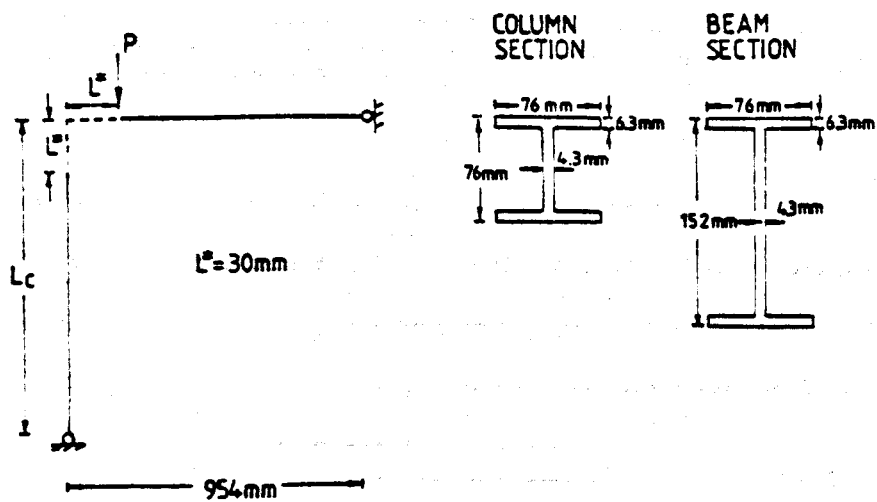
L_c	λ_x	Without RSZ	$L^* = 30\ mm$ Located at Joint	Fully RSZ		
		P_{ult}	$P^*_{ult(1)}$	$P^*_{ult(2)}$	$\frac{P^*_{ult(1)}}{P_{ult}}$	$\frac{P^*_{ult(2)}}{P_{ult}}$
(mm)	(column)	(KN)	(KN)	(KN)		
954	30	301.7	191.3	158.7	0.63	0.53
1590	50	282.1	190.7	140.3	0.68	0.50
2226	70	254.7	180.1	126.7	0.71	0.50

Figure 3.28 (b)

Figure 3.28 Effect of RSZ on Simple Frame
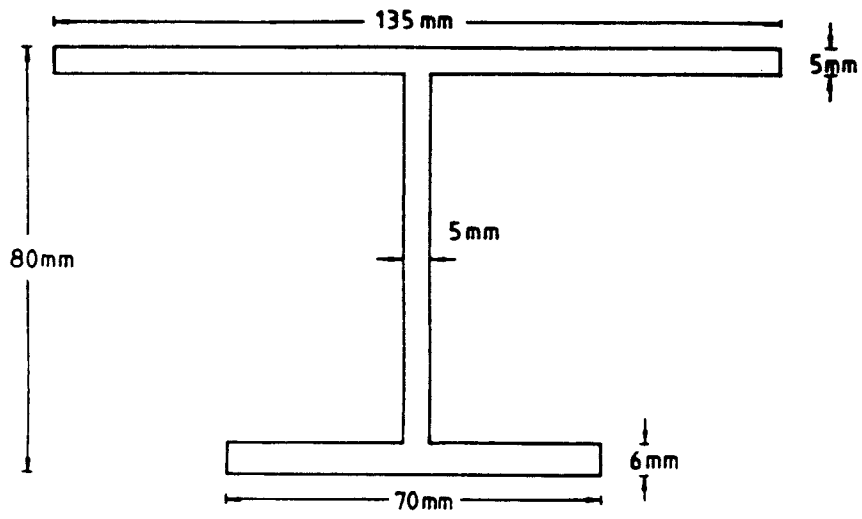
Figure 3.29 Cross-section Used for Parametric Studies on 7019 Alloy

3.5.2   Studies on 7019 Aluminium Alloy

The parametric studies which were carried out previously are mainly based on 6082-TF alloy. However, some studies on 7019 aluminium alloy have also been conducted and will be discussed below. An unsymmetrical I-section is used in these parametric studies and is shown in Figure 3.29. This unsymmetrical I-section of 7019 alloy is commonly used in the design of bridges. From experiments, the mechanical properties of the parent and RSZ material are:

Parent: $E \quad = \quad 70000 \quad N/mm^2$

                $\sigma_{0.2} \quad = \quad 386 \quad N/mm^2$

                $n \quad = \quad 33$

RSZ: $E^* \quad = \quad 70000 \quad N/mm^2$

                $\sigma_{0.2}^* \quad = \quad 239 \quad N/mm^2$

                $n^* \quad = \quad 9$
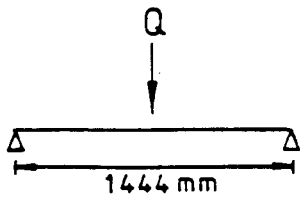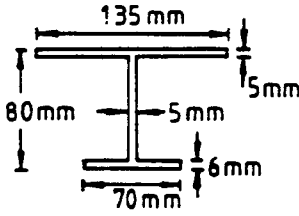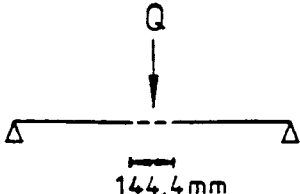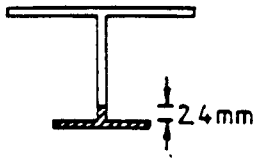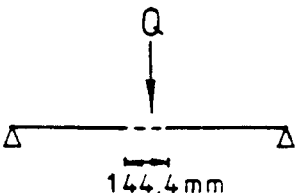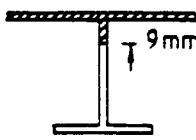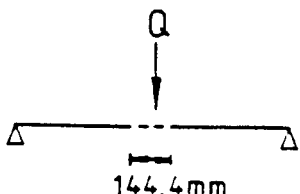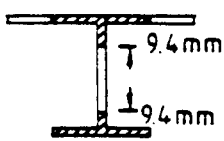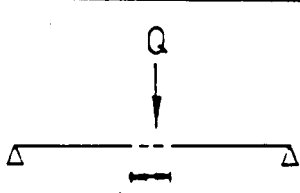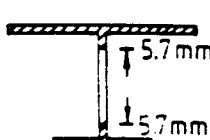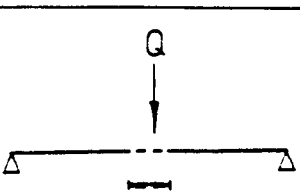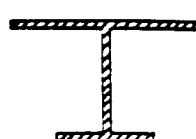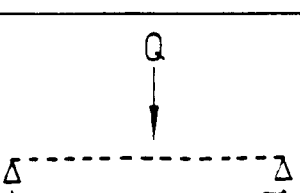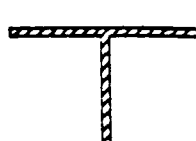
Cases	Condition	Degree of Softening on Cross-section	$\frac{A^*}{A}$	Q^*_{ult} (KN)	$\frac{Q^*_{ult}}{Q_{ult}}$
(a)	Q, 1444 mm	135 mm, 5mm, 80mm, 5mm, 6mm, 70mm	0.0	43.55	1.0
(b)	Q, 144.4 mm	2.4mm	0.3	38.97	0.895
(c)	Q, 144.4 mm	9mm	0.5	40.07	0.920
(d)	Q, 144.4mm	9.4mm, 9.4mm	0.6	34.71	0.797
(e)	Q, 144.4 mm	5.7mm, 5.7mm	0.8	32.11	0.737
(f)	Q, 144.4mm		1.0	31.55	0.720
(g)	Q, 1444 mm		1.0	31.25	0.718

Table 3.3: Effect of Partially Affected Cross-section on Member Strength

3.5.2.1 Effect of Partially-affected Cross-section on Member Strength

In some cases, the local transverse welds may only affect part of the cross-section and the other part is still undisturbed. Table 3.3 covers the response of the unsymmetrical I-sections which are partially affected by the local transverse welds. The beams are simply-supported under a central point load and the length of the RSZ is kept constant at 144.4 mm (i.e. $\frac{L^*}{L} = 0.1$) located at mid-span.

Cases (a) and (g) in Table 3.3 are for the beams which are unaffected or fully-affected by RSZ respectively. Cases (b) to (f) show the different degree of softening effects on the cross-section. The ratios between the softening area on the cross-section to the cross-sectional area of beam are (i.e. $\frac{A^*}{A}$) equal to 0.3, 0.5, 0.6, 0.8 and 1.0. From the table, we can observe that the decrease in ultimate strength varies from 8% to 28% depending on the degree of softening.
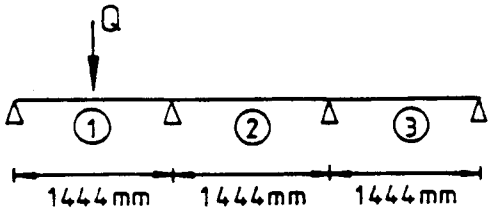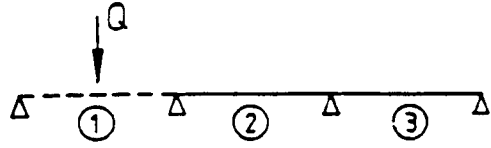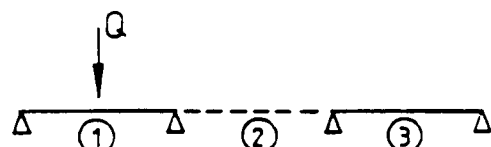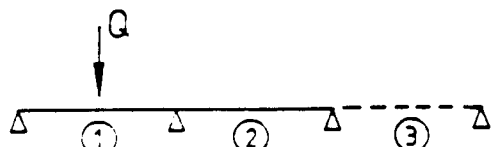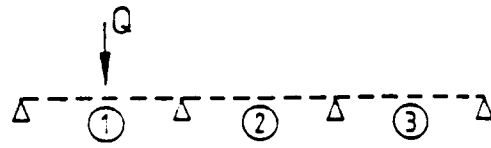
Cases	Condition	$Q^*_{ult}(KN)$	$\frac{Q^*_{ult}}{Q_{ult}}$
(a)

1444mm 1444mm 1444mm

(Without welds) | 61.94 | 1.0 |
| (b) |

(Fully RSZ on span 1) | 44.94 | 0.73 |
| (c) |

(Fully RSZ on span 2) | 60.90 | 0.98 |
| (d) |

(Fully RSZ on span 3) | 61.94 | 1.0 |
| (e) |

(Fully RSZ on span 1, 2, and 3) | 44.62 | 0.72 |

Table 3.4: Effect of RSZ on Continuous Beam

3.5.2.2 Effect of RSZ on Continuous Beams

A continuous three-equal-span beam as shown in Table 3.4 is considered in this analysis and the concentrated load is applied at the middle of span 1. Cases (a) and (e) in Table 3.4 are for the whole continuous beams which are unaffected or fully-affected by RSZ respectively. In cases (b) to (d), the RSZ is shifted from one span to the other and it is assumed that only one span is ~~full~~ fully-affected by RSZ. From the results, cases (b) and (e) ~~are~~ have a similar reduced strength because the RSZ is under maximum bending moment. For cases (c) and (d), ~~the reductions in strength are smaller and the decreases in ultimate strength are 27% and 25% respectively.~~ the bending moment within the RSZ is significatly reduced, and therefore the reductions in strength become negligible

3.6   Conclusions

From the parametric studies for transversely welded aluminium members, the main findings are summarised below:

1. For slender columns ($\lambda_x > 90$), the effect of local transverse welds is insignificant.

2. For stocky and intermediate columns, the effect of local transverse welds become significant. The reduction in ultimate strength is approximately 40% to 50%.

3. If both ends of the column are welded, it is unsafe to neglect the softening effect even if the extent of RSZ is small.

4. Maximum reductions in bending strength will occur if the RSZ is located at the point of maximum bending moment in the beam.

5. ~~If the stress level in the RSZ is low~~ Providing stresses within the RSZ remain below the σ_o^* value of the RSZ material, the effect of local transverse welds can be neglected.

6. From the column curves and the interaction curves, the behaviour of the partially welded members or aluminium members containing wholly RSZ material is quite similar. Thus, it is quite accurate and reasonable to design the partially welded members as members containing wholly RSZ material.

7. Special considerations should be paid to the presence of local transverse welds at the rigid joints because they can cause a complete loss of fixity and result in great reduction in overall structural stability and strength.

References

[1] Hong, G. M., "Buckling of Non-welded and Welded Aluminium Columns", Ph.D Thesis, University of Cambridge, 1983.

[2] Murray, D. W., El-Zanaty, M. H. and Bjorhovde, R., "Inelastic Behaviour of Multi-storey Steel Frames", University of Alberta, Structural Engineering Report Number 83, April 1980.

[3] El-Zanaty, M. H. and Murray, D. W., "Finite Element Programs for Frame Analysis", University of Alberta, Structural Engineering Report No. 84, April 1980.

[4] Zienkiewicz, O. C., "The Finite Element Method", Third Edition, 1977.

[5] Gilson, S., and Cescotto, S., "Experimental Research on the Buckling of Aluminium Alloys Columns with Unsymmetrical Cross-section", University of Liege.

[6] Gilson, S., and Cescotto, S., "Experimental Research on the Buckling of Aluminium Alloys Columns with Unsymmetrical Cross-section - Complementary Test", University of Liege.

TEST ON ALUMINIUM BEAMS WITH OR WITHOUT LOCAL TRANSVERSE WELDS

4.1   Introduction

In 1982, Edward [1] carried out experiments on three I-section beams of 6082 aluminium alloy under pine bending. One was unwelded, one had a bead weld laid round its perimeter at mid-span and the third had stiffeners fillet welded between the flanges at mid-span. The behaviour of the welded beams was compared with the unwelded beam and he found that, although the material in the RSZ is softened to about half the strength of the parent metal, the three beams all failed at similar loads. However, the welded beams did show a loss of ductility.

Due to the limited number of test specimens, his results can only be treated as a rough guide and no special conclusions can be arrived at. Apart from the experiments done by Edward, there are no test of a similar nature known to have been carried out before. The author, therefore, conducted an extensive test on aluminium beams with or without local transverse welds, and the experimental results will be presented in this chapter. The main objectives of the tests were:

1. to study the real behaviour of transversely welded aluminium beam under pure bending;

2. to compare the theoretical predictions obtained by program INSTAF with the experimental results. This can also serve as a experimental support to the theoretical studies described in Chapter 3.
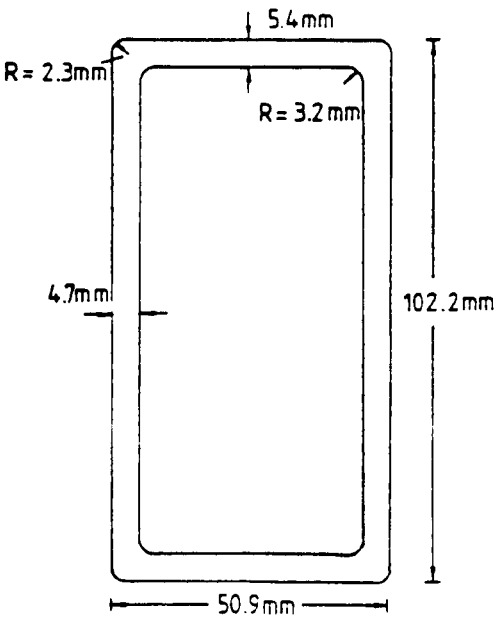
Cross-sectional Properties

A = 1413.1 mm^2

I_x = 1799628.8 mm^4

r_x = 35.7 mm

(a) Non-welded Section
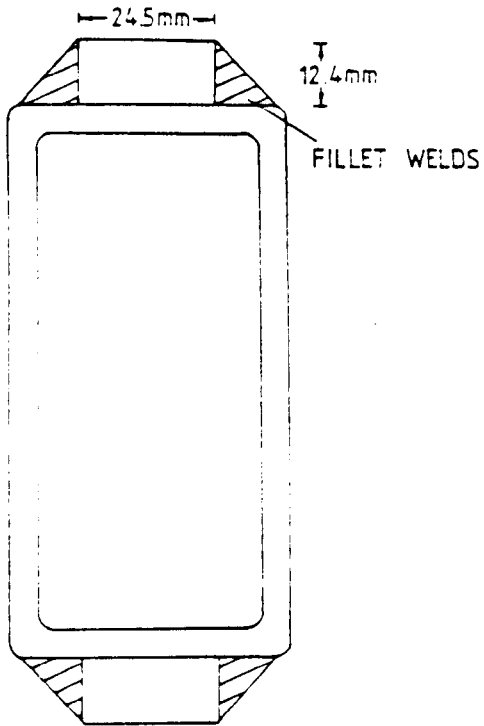
Approximate Cross-sectional Properties

A = 2348.1 mm^2

I_x = 4803809.6 mm^4
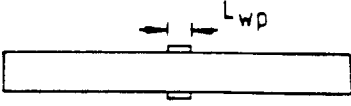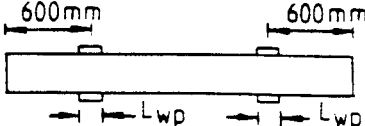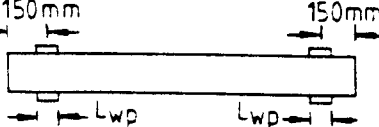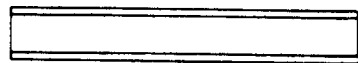
r_x = 45.2 mm

(b) Welded Section
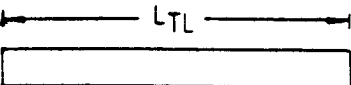
Figure 4.1 Cross-sectional Dimensions of Test Specimen

4.2   Specimen
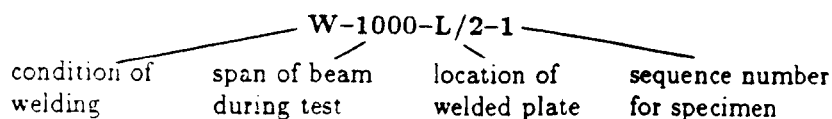
4.2.1   Basic Dimensions and Specimen Designations

All the beams used in the tests were 7019 aluminium alloy and the cross-section chosen for the tests was a 50.9mm × 102.2mm extruded rectangular box section. Due to the high torsional stiffness of the box section, the beams, therefore, were expected to fail in bending rather than lateral buckling. In order to represent the most commonly occurring welding situation and produce different extents of heat-affected zones, two 7019 aluminium plates with thickness 12.4 mm and approximate width 24.5 mm were fillet welded to the top and bottom flanges of the box-section. The heat-affected zones could also be produced by cutting the beam into halves and joined again using butt welds, but this methods was not recommended. The main reason is that the weld metal (alloy type: 5556A) possesses inferior material properties than the parent metal or the heat-affected zone material. The beams, therefore, will be likely to fail due to reduction in strength or ductility of the weld metal rather than the heat-affected zone material. The cross-sectional properties and the average dimensions for the non-welded and welded sections are shown in Figure 4.1.

Altogether 5 non-welded and 22 welded beams were tested. The beams were either 1200 mm or 2200 mm in length and were simply supported over a span of 1000 mm or 2000 mm respectively. The welded plates were either located at mid-span, symmetrically at quarter-span or near both ends of the span. Plates were also welded for the whole length on the flanges to represent the

Location of Welded Plates	Specimen Designation		Length of Welded Plate $L_{wp}(mm)$	
	$L_{TL} = 1200mm$	$L_{TL} = 2200mm$	$L_{TL} = 1200mm$	$L_{TL} = 2200mm$
L_{TL} (without welds)	N-1000-P-1 N-1000-P-2 N-1000-P-3	N-2000-P-1 N-2000-P-2	–	–
L_{wp} (at mid-span)	W-1000-L/2-1 W-1000-L/2-2 W-1000-L/2-3 W-1000-L/2-4	W-2000-L/2-1 W-2000-L/2-2 W-2000-L/2-3 W-2000-L/2-4	50	200
600mm 600mm L_{wp} L_{wp} (symmetrically at quarter-span)	–	W-2000-L/4-1 W-2000-L/4-2 W-2000-L/4-3	–	200
150mm 150mm L_{wp} L_{wp} (near the two ends)	W-1000-E-1 W-1000-E-2 W-1000-E-3	–	25	–
(along the whole specimen)	W-1000-F-1 W-1000-F-2 W-1000-F-3 W-1000-F-4 W-1000-F-5	W-2000-F-1 W-2000-F-2 W-2000-F-3	1200	2200

NOTE

1. The specimen designation convention is as shown below:

$$W-1000-L/2-1$$

| condition of welding | span of beam during test | location of welded plate | sequence number for specimen |

2. N - Non-welded beam
   W - Welded beam
   P - Parent metal
   E - welded plates locate near the two ends
   F - fully-welded

Table 4.1: Test Scheme and Specimen Designation

fully heat-affected beam (see Plates 4.1 and 4.2). The details for the beam designations, locations and length of the welded plates can be referred to Table 4.1.
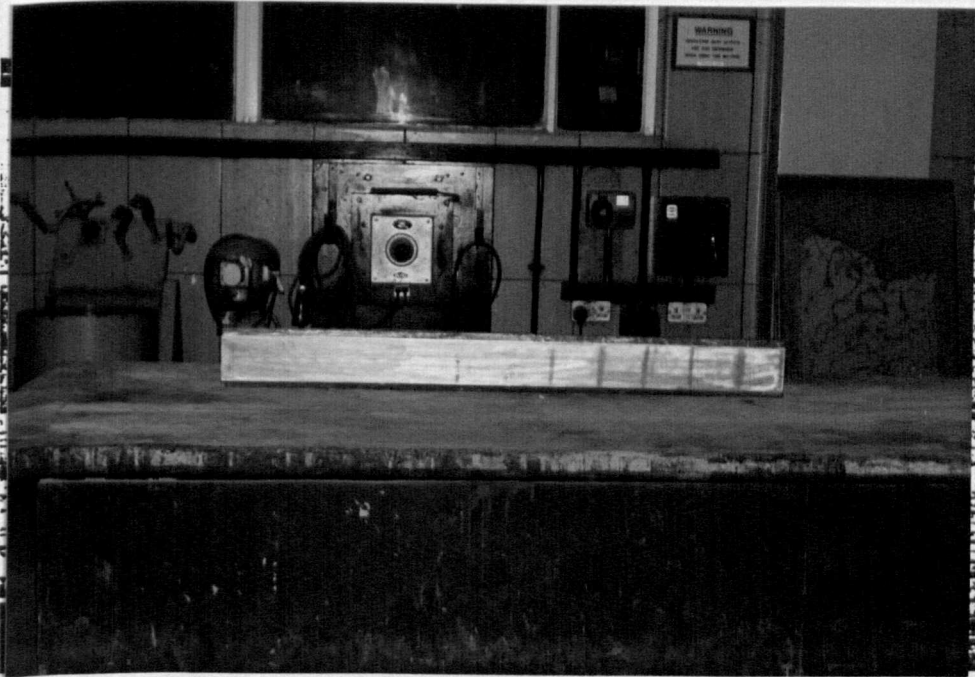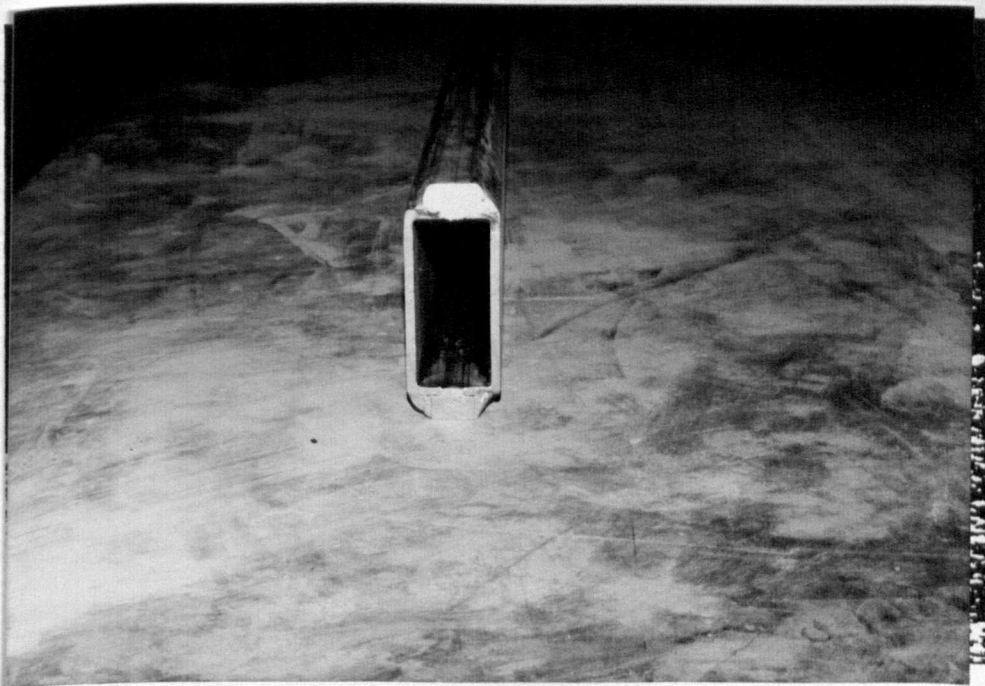

Plate 4.1 Fully Welded Beam (W-1000-F-1)

Plate 4.2 Fully Welded Beam (W-1000-F-1)

Process	:	Metal Inert Gas (MIG)
Welding Set Type	:	SPR BOC
Wire Feed Type	:	Transmatic 2S $3\frac{3}{4}$ setting
Wire	:	Bostrand 2861 1.6 mm dia. (BS NG61)
Shielding Gas	:	Argor 30 ft^3/hr
Work	:	-VC

Table 4.2: Welding Details
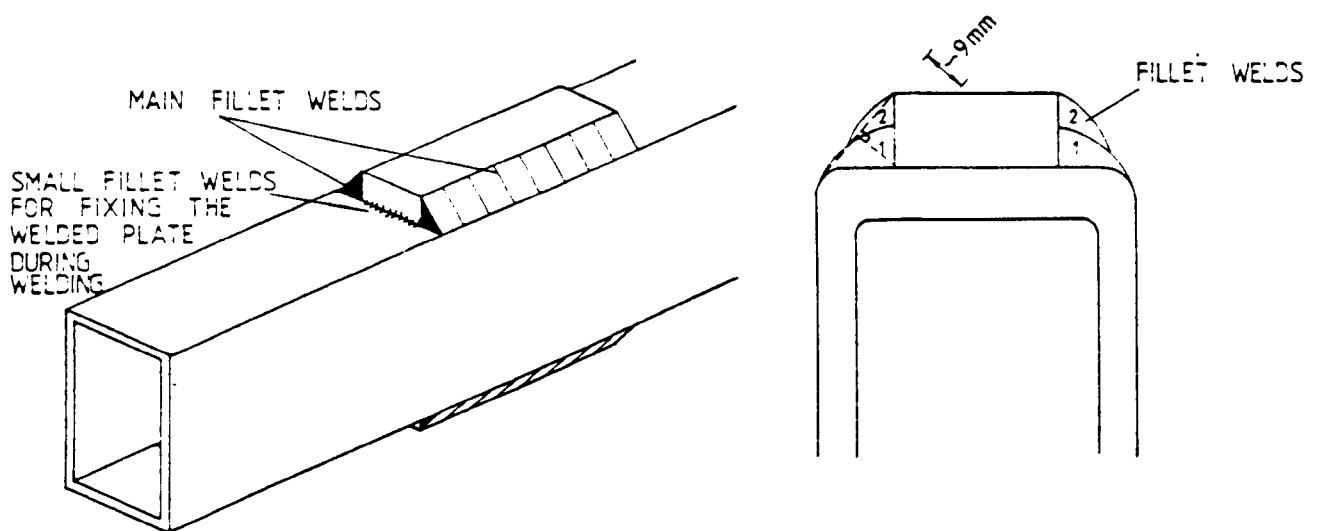
Figure 4.2 Fillet Welds in Test Specimen

4.2.2   Welding

All the welding was conducted by the qualified welder of R.A.R.D.E. and the welding details can be referred to Table 4.2, Two passes of main fillet welds were laid on each side and along the whole length of the welded aluminium plates with an approximate throat thickness of 9 mm. Small fillet welds were also laid transversely on the two ends of the welded aluminium plates for fixing during welding (see Figure 4.2). The welding wire was 1.6 mm diameter to the old British Standard Registration designation NG61 which corresponds to the Aluminium Association international designation 5556A. All the specimens were welded by the same welder and no special treatments were carried out in order to disturb the thermal effects during welding, so the welding process was typical of that commonly used in the construction industry. All the welded specimens were left to age naturally for more than 4 weeks before conducting any tests. For tensile coupons tests and beam tests, all the welded specimens were aged for at least 8 weeks after welding.

4.2.3   Initial Out-of-straightness

The non-welded specimens were very straight with maximum out-of-straightness smaller than $\frac{L}{4000}$ in both the major and minor axis directions. The initial twists of the cross-sections were also very small with maximum magnitudes smaller than 0.003 radian. But for the welded specimens, the beams were found to be quite severely distorted after welding. Since it was difficult to measure the out-of-straightness in the major axis direction due to the pres-
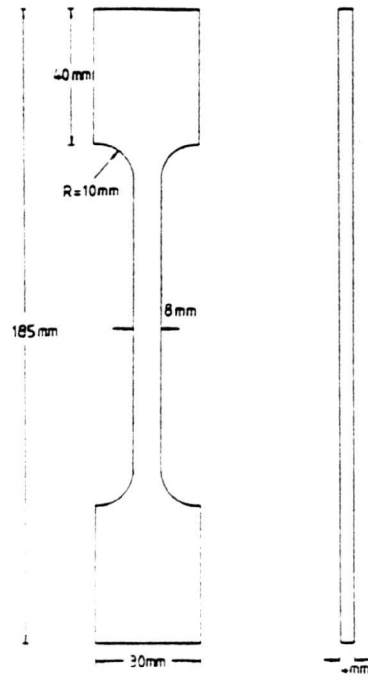
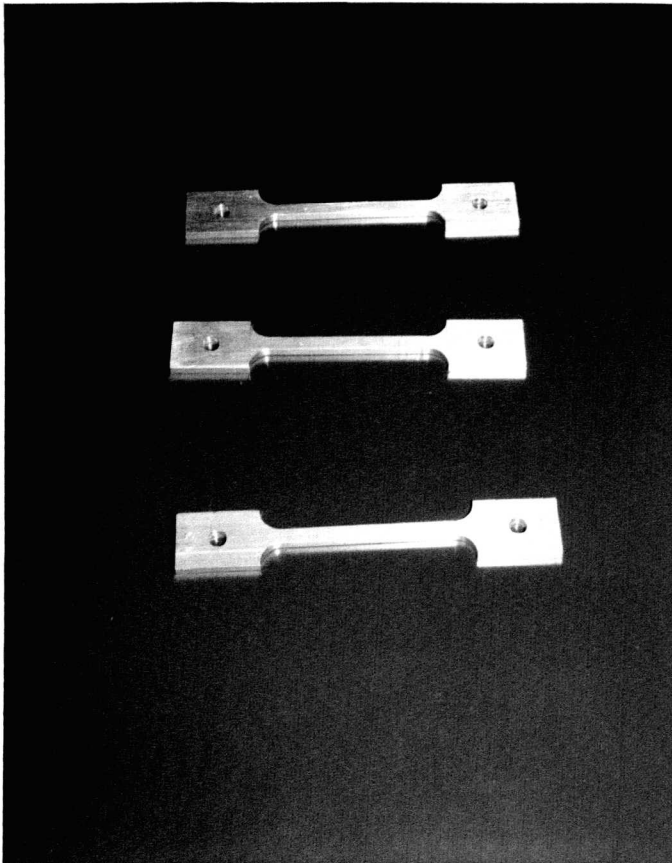Figure 4.3 Nominal Dimensions of Tensile Coupon

Plate 4.3 Tensile Coupons

ence of the welded plates, therefore only the out-of-straightness in the minor axis direction was considered. The maximum out-of-straightness in the minor axis direction was about $\frac{L}{930}$ and the maximum initial twist was about 0.04 radian.

4.3   Auxiliary Tests

4.3.1   Tensile Coupon Tests [2]

Before performing the beam tests, tensile coupon tests were conducted in order to obtain the mechanical properties of parent and heat-affected material. The nominal dimensions and shapes of the tensile specimens are shown on Figure 4.3 and Plate 4.3. Each tensile coupon was labelled with a letter followed by a number where the letter indicated parent or heat-affected material (see Tables 4.3 and 4.4). For parent metal, all the seven coupons were obtained from beam N-1000-P-1 (see Section 4.2.1). The first three coupons were cut from the top flange and the rest were cut from the web. Since the beams N-1000-P-1 and N-1000-P-2 were actually cut from the same beam of length 2500 mm, therefore, the parent material properties of the two beams should be similar. For softened material, all the five coupons were cut from the top flange of beam W-1000-F-1 with the welded plate being removed.

The tensile coupon tests were conducted in the 20 KN Hounsfield Tensometer at a displacement speed of about 1.00 mm/min. A clip-on extensometer with a 50 mm gauge length was used to give strain reading. The extensome-

| Specimen	Location	E (N/mm^2)	$\sigma_{0.1}$ (N/mm^2)	$\sigma_{0.2}$ (N/mm^2)	σ_{ult} (N/mm^2)	ε_t (%)	n	$\frac{\sigma_{ult}}{\sigma_{0.2}}$
N-1	Flange	68500	363	370	432	10.4	36.3	1.168
N-2	Flange	69800	376	385	431	11.6	29.3	1.119
N-3	Flange	68300	358	366	420	10.4	31.4	1.173
N-4	Web	72000	373	380	436	10.2	37.3	1.147
N-5	Web	72900	370	378	439	9.0	32.4	1.161
N-6	Web	70200	366	374	434	9.1	32.1	1.165
N-7	Web	74600	352	359	415	10.6	35.1	1.156
Maximum		74600	376	385	439	11.6	37.3	1.173
Minimum		68300	352	359	415	9.1	29.3	1.119
Mean		70900	365.4	373.1	429.6	10.3	33.4	1.155
Standard deviation		2175.2	7.8	8.2	8.1	0.73		
Coefficent of variation (%)		3.07	2.15	2.20	1.89	7.11		

NOTE

1. $n = \dfrac{\ln 2}{\ln\left(\frac{\sigma_{0.2}}{\sigma_{0.1}}\right)}$ (see APPENDIX A)

2. All the tensile coupons were obtained from beam N-1000-P-1.

Table 4.3: Parent Metal Properties

ter was attached to the centre of the specimen well away from the jaws. The failures of the tensile coupons showed necking across the width and through the thickness.

4.3.2   Coupon Results and Material Properties

All the coupon results were fitted with Ramberg-Osgood formulae as shown in Figures4.4(a)-(g) and Figures4.5(a)-(e). The mechanical properties for the parent and heat-affected material are summarised in Tables4.3 and 4.4.

The parent and heat-affected material properties were generally very consistent and of the form expected. For parent metal (see Table 4.3), the results showed very little variation, the coefficient of variation being less than 3.1%. Values of Young's modulus obtained varied from 68300 N/mm^2 to 74600 N/mm^2 with a mean value of 70900 N/mm^2. From draft BS 8118 [3], the recommended Young's modulus is 71700 N/mm^2 for 7000 series aluminium alloys. When compared with the mean value, a very good agreement was obtained with a difference of 1.1%. The mean values for $\sigma_{0.1}, \sigma_{0.2}$ and σ_{ult} were 365.4 N/mm^2, 373.1 N/mm^2 and 429.6 N/mm^2 respectively. These values were also in good agreement when compared with the experimental results obtained Webber [4], Techanitisawad [5] and Robertson [6]. Each Ramberg-Osgood curve for the parent metal showed a sharper knee; and the mean values of the knee factor, n, and the ratio $\frac{\sigma_{ult}}{\sigma_{0.2}}$ were 33.4 and 1.155 respectively.

For heat-affected material (see Table 4.4), the results also showed small coef-

Specimen	E^* (N/mm^2)	$\sigma_{0.1}^*$ (N/mm^2)	$\sigma_{0.2}^*$ (N/mm^2)	σ_{ult}^* (N/mm^2)	ε_t^* (%)	n^*	$\frac{\sigma_{ult}^*}{\sigma_{0.2}^*}$
W-1	72900	224	237	388	13.8	12.3	1.637
W-2	72700	232	248	355	12.8	10.4	1.431
W-3	70700	232	245	353	12.4	12.7	1.441
W-4	69000	221	235	331	10.5	11.3	1.408
W-5	73600	229	243	362	11.7	11.7	1.490
Maximum	73600	231	248	388	13.8	12.7	1.637
Minimum	69000	221	235	331	10.5	10.4	1.408
Mean	71780	227.6	241.6	357.8	12.2	11.7	1.481
Standard deviation	1691.6	4.4	4.9	18.3	1.10		
Coefficent of variation (%)	2.36	1.94	2.02	5.12	9.05		

NOTE

1. $n = \dfrac{\ln 2}{\ln\left(\frac{\sigma_{0.2}^*}{\sigma_{0.1}^*}\right)}$ (see APPENDIX A)

2. All the tensile coupons were cut from the top flange of beam W-1000-F-1.

Table 4.4: Heat-affected Material Properties

ficients of variations similar to those for the parent metal. The Young's modulus ranged from 69000 N/mm^2 to 73600 N/mm^2. Therefore, the Young's moduli of parent and heat-affected material were similar. All the heat-affected coupons showed reduction in strength and the mean ratios of $\frac{\sigma_{0.1}^*}{\sigma_{0.1}}$, $\frac{\sigma_{0.2}^*}{\sigma_{0.2}}$ and $\frac{\sigma_{ult}^*}{\sigma_{ult}}$ were 0.62, 0.65 and 0.83 respectively. The knee factors of softened material were all smaller than those of the parent metal, therefore the Ramberg-Osgood curves for the softened material showed less sharper knee. The mean values for n^* and $\frac{\sigma_{ult}^*}{\sigma_{0.2}^*}$ were 11.7 and 1.481 respectively.

STRESS (N/mm^2)
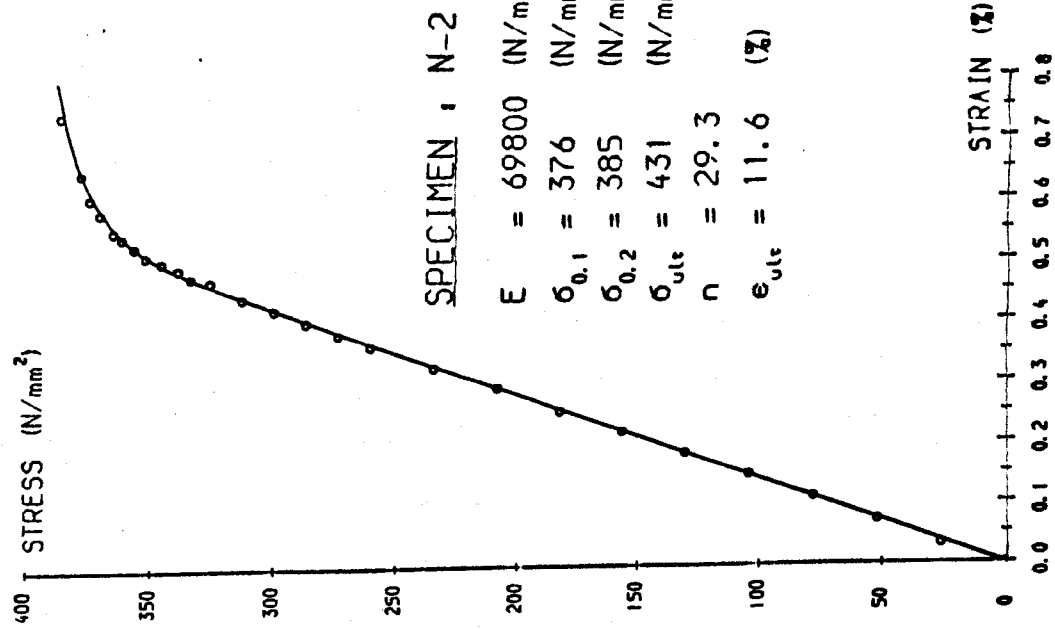
SPECIMEN : N-1

E	= 68500	(N/mm^2)
$\sigma_{0.1}$	= 363	(N/mm^2)
$\sigma_{0.2}$	= 370	(N/mm^2)
σ_{ult}	= 432	(N/mm^2)
n	= 36.3	
e_{ult}	= 10.4	(%)

STRAIN (%)

0.0 0.1 0.2 0.3 0.4 0.5 0.6 0.7 0.8

400 350 300 250 200 150 100 50 0

Figure 4.4 (a)

STRESS (N/mm^2)

SPECIMEN : N-2

E	= 69800	(N/mm^2)
$\sigma_{0.1}$	= 376	(N/mm^2)
$\sigma_{0.2}$	= 385	(N/mm^2)
σ_{ult}	= 431	(N/mm^2)
n	= 29.3	
e_{ult}	= 11.6	(%)

STRAIN (%)

0.0 0.1 0.2 0.3 0.4 0.5 0.6 0.7 0.8

400 350 300 250 200 150 100 50 0

Figure 4.4 (b)
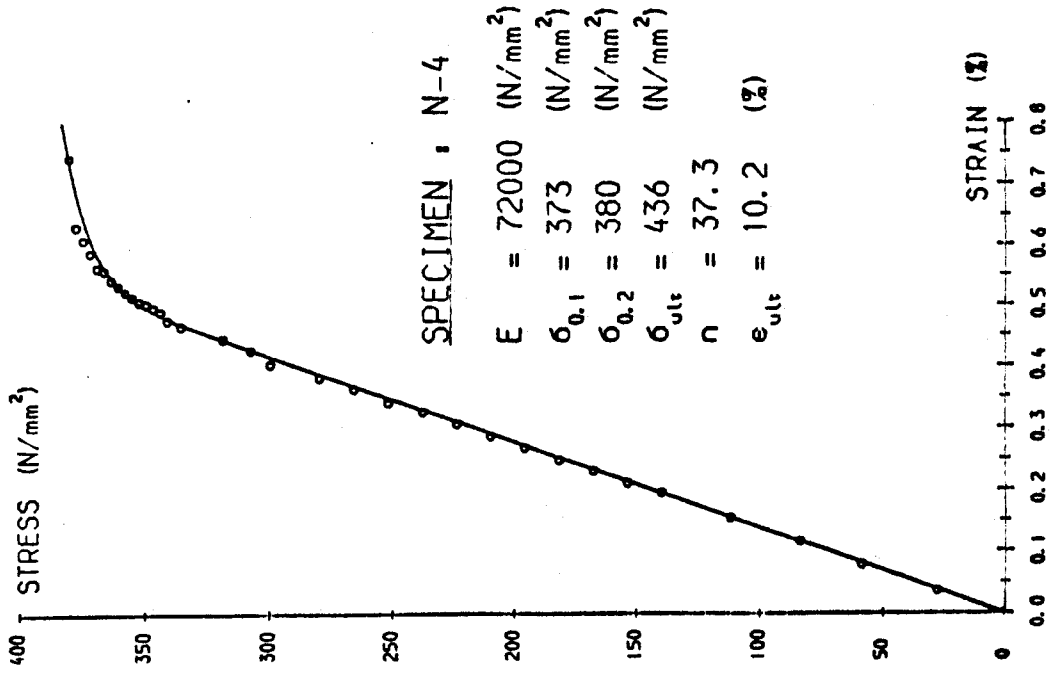
STRESS (N/mm^2)

SPECIMEN : N-4

E = 72000 (N/mm^2)
$\sigma_{0.1}$ = 373 (N/mm^2)
$\sigma_{0.2}$ = 380 (N/mm^2)
σ_{ult} = 436 (N/mm^2)
n = 37.3
e_{ult} = 10.2 (%)

STRAIN (%)

Figure 4.4 (d)
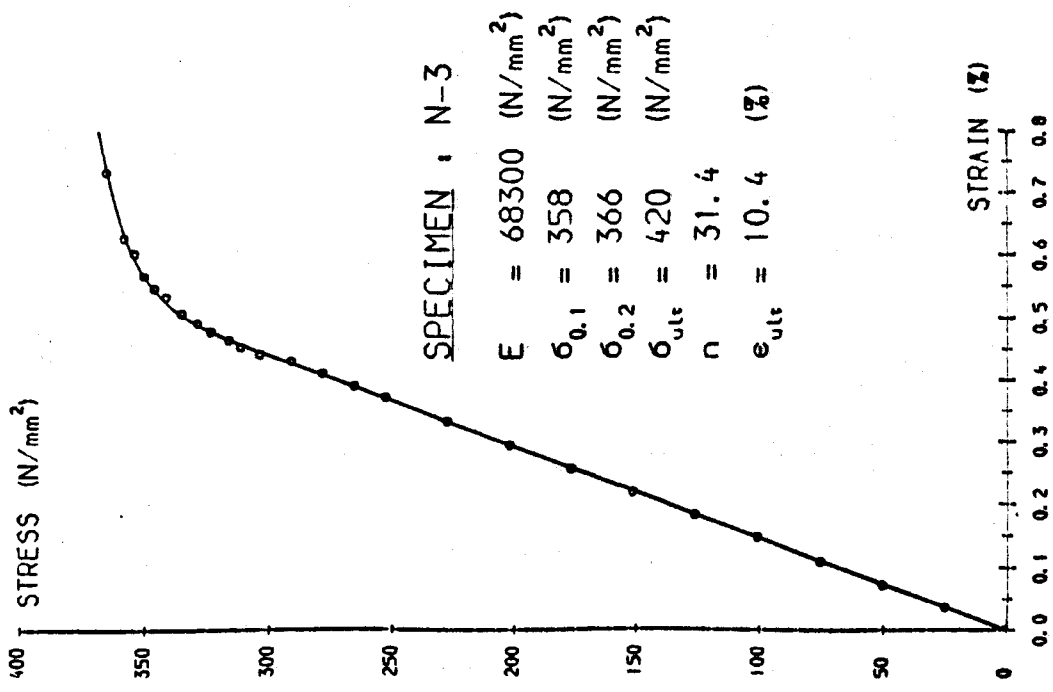
STRESS (N/mm^2)

SPECIMEN : N-3

E = 68300 (N/mm^2)
$\sigma_{0.1}$ = 358 (N/mm^2)
$\sigma_{0.2}$ = 366 (N/mm^2)
σ_{ult} = 420 (N/mm^2)
n = 31.4
e_{ult} = 10.4 (%)

STRAIN (%)

Figure 4.4 (c)

SPECIMEN : N-6

E	=	70200	(N/mm^2)
$\sigma_{0.1}$	=	366	(N/mm^2)
$\sigma_{0.2}$	=	374	(N/mm^2)
σ_{ult}	=	434	(N/mm^2)
n	=	32.1	
e_{ult}	=	9.1	$(\%)$
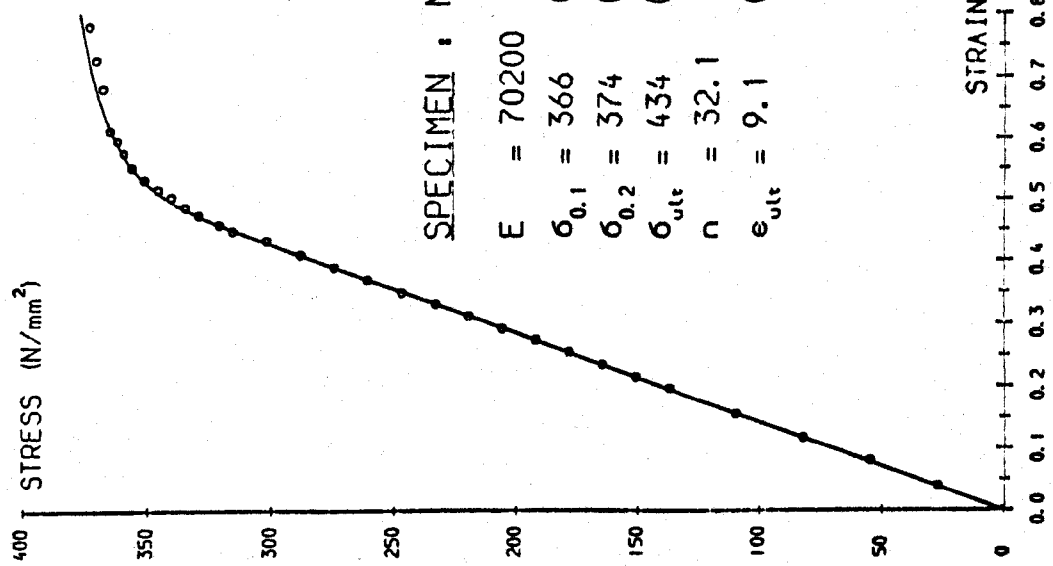
Figure 4.4 (f)

SPECIMEN : N-5

E	=	72900	(N/mm^2)
$\sigma_{0.1}$	=	370	(N/mm^2)
$\sigma_{0.2}$	=	378	(N/mm^2)
σ_{ult}	=	439	(N/mm^2)
n	=	32.4	
e_{ult}	=	9.6	$(\%)$

Figure 4.4 (e)

STRESS (N/mm²)

SPECIMEN : N-7

$E = 74600$ (N/mm²)
$\sigma_{0.1} = 352$ (N/mm²)
$\sigma_{0.2} = 359$ (N/mm²)
$\sigma_{ult} = 415$ (N/mm²)
$n = 35.1$
$e_{ult} = 10.6$ (%)

STRAIN (%)

0.0 0.1 0.2 0.3 0.4 0.5 0.6 0.7 0.8

400 350 300 250 200 150 100 50 0
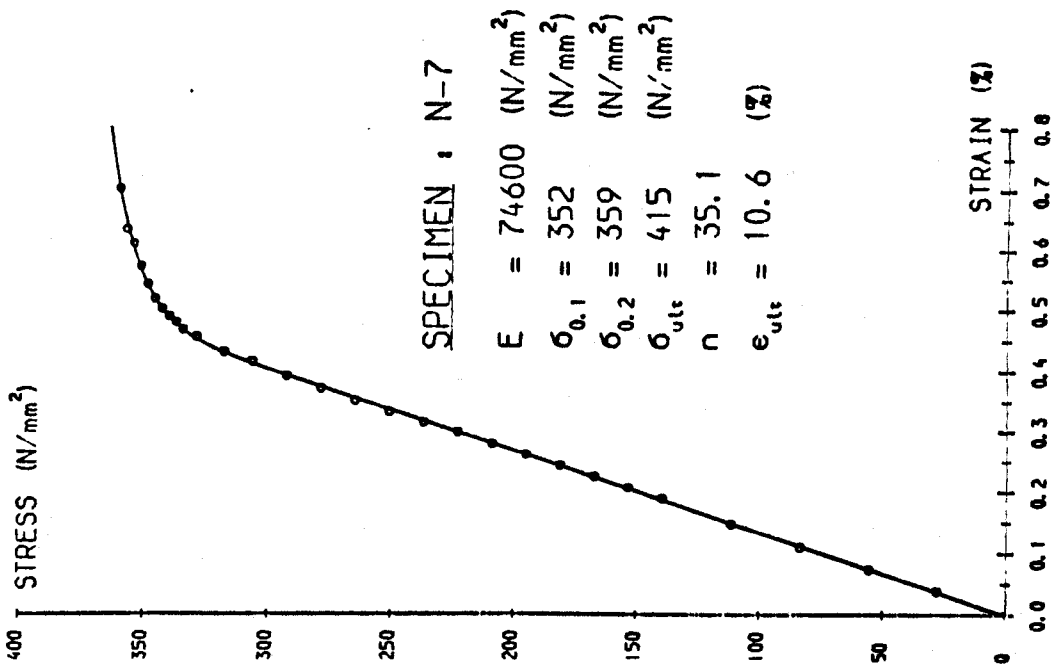
Figure 4.4 (g)

Figure 4.4 Mechanical Properties of Parent Metal Fitted with Ramberg-Osgood Formula

STRESS (N/mm²)

SPECIMEN : W-2

$E = 72700$ (N/mm²)
$\sigma_{0.1} = 232$ (N/mm²)
$\sigma_{0.2} = 248$ (N/mm²)
$\sigma_{ult} = 355$ (N/mm²)
$n = 10.4$
$e_{ult} = 12.8$ (%)

STRAIN (%)

Figure 4.5 (b)

STRESS (N/mm²)

SPECIMEN : W-1

$E = 72900$ (N/mm²)
$\sigma_{0.1} = 224$ (N/mm²)
$\sigma_{0.2} = 237$ (N/mm²)
$\sigma_{ult} = 388$ (N/mm²)
$n = 12.3$
$e_{ult} = 13.8$ (%)

STRAIN (%)

Figure 4.5 (a)

STRESS (N/mm^2)

SPECIMEN : W-4

E = 69000 (N/mm^2)
$\sigma_{0.1}$ = 221 (N/mm^2)
$\sigma_{0.2}$ = 235 (N/mm^2)
σ_{ult} = 331 (N/mm^2)
n = 11.3
e_{ult} = 10.5 (%)

STRAIN (%)

Figure 4.5 (d)

STRESS (N/mm^2)

SPECIMEN : W-3

E = 70700 (N/mm^2)
$\sigma_{0.1}$ = 232 (N/mm^2)
$\sigma_{0.2}$ = 245 (N/mm^2)
σ_{ult} = 353 (N/mm^2)
n = 12.7
e_{ult} = 12.4 (%)

STRAIN (%)

Figure 4.5 (c)

STRESS (N/mm²)

SPECIMEN : W-5

E = 73600 (N/mm²)
$\sigma_{0.1}$ = 229 (N/mm²)
$\sigma_{0.2}$ = 243 (N/mm²)
σ_{ult} = 362 (N/mm²)
n = 11.7
ϵ_{ult} = 11.7 (%)

STRAIN (%)
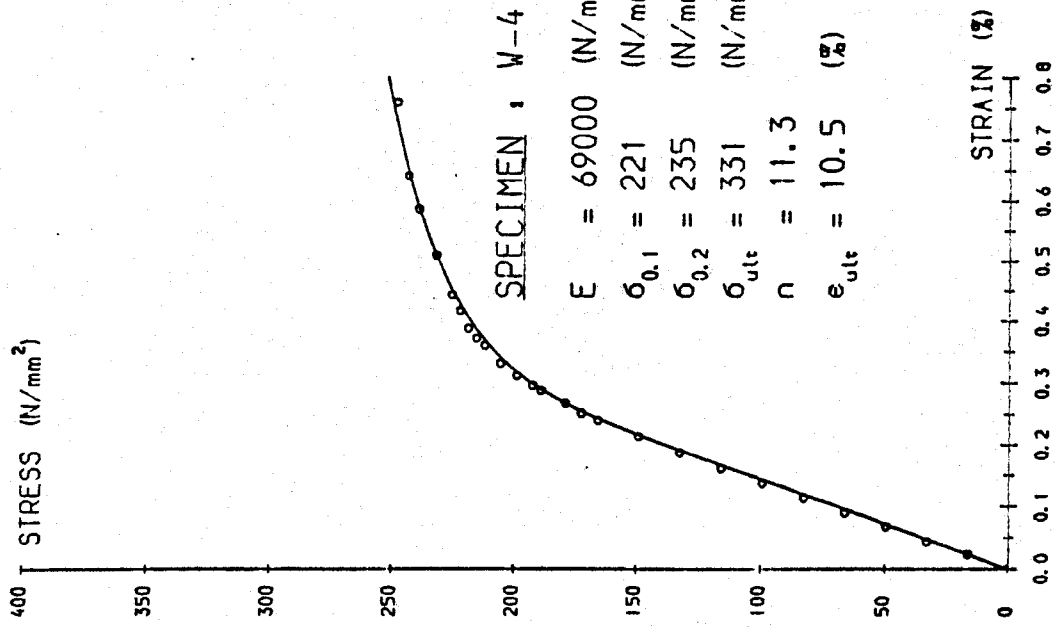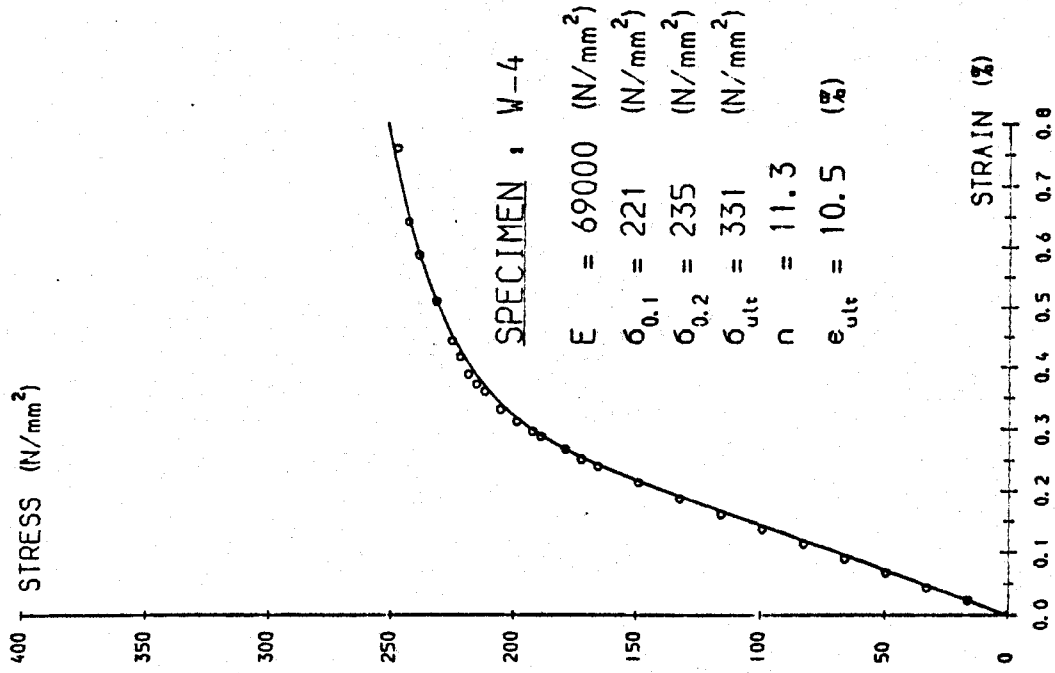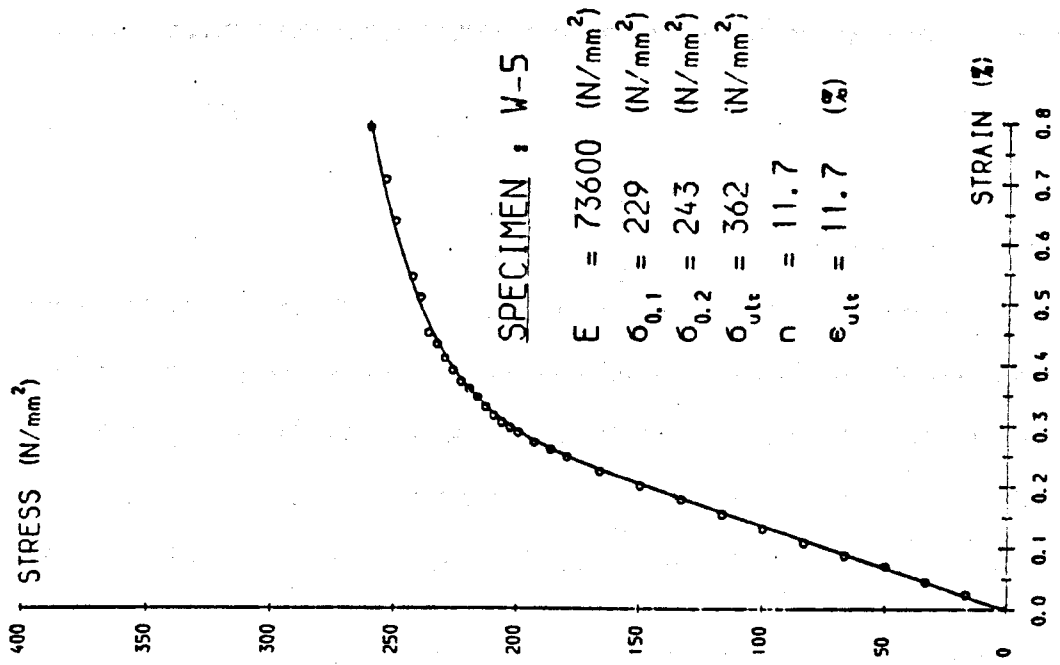
Figure 4.5 (e)

Figure 4.5 Mechanical Properties of RSZ Material Fitted with Ramberg-Osgood Formula
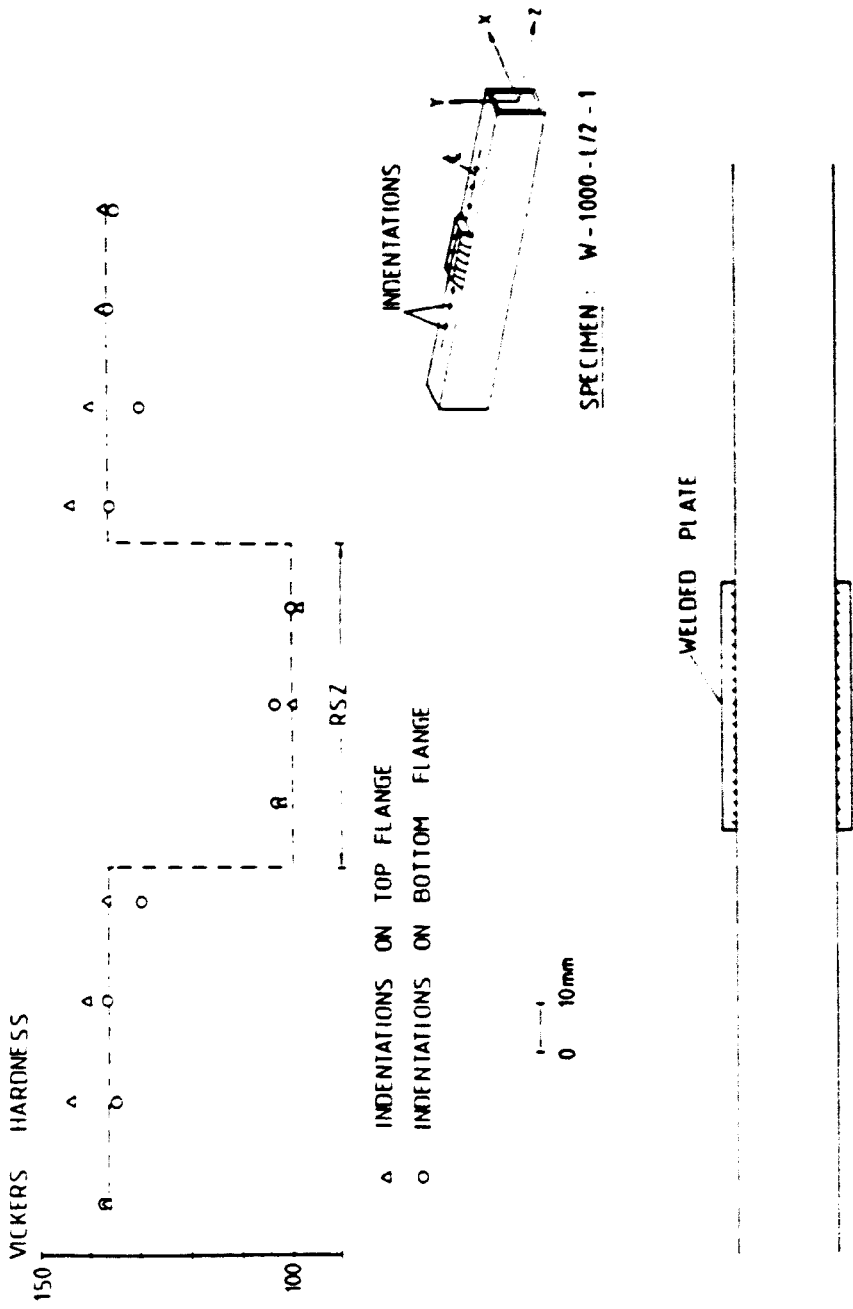
Figure 4.6 Hardness Surveys along the Member

4.3.3 Hardness Surveys and Extent of Reduced-strength Zone

In order to determine the extent of RSZ, hardness surveys were carried out on all the beam specimens, the hardness measurements were being done on a Vickers hardness machine using a 5 Kg weight. The hardness measurements were taken longitudinally along the centre-lines of the welded plates ($y - z$ plane) and the flanges, and transversely along the webs and the centre-lines of the welded plates ($x - y$ plane). Typical results are shown in Figures 4.6 and 4.7.

Figure 4.6 shows the hardness measurements taken along the centre-lines of the welded plates ($y - z$ plane) and the flanges. The measurements were done as close to the welded plates as possible, but the closest distance was about 15 mm. The main reason is in those regions, the surfaces become rippled and proper indentations cannot be made except unless the surfaces are polished. However, the polishing will over-cut the surfaces and may introduce local weaknesses within the beam. The author, therefore, did not disturb the specimens but from the texture and colour of those regions, it is quite clear that those regions were heat-affected after welding. Therefore, it is quite reasonable to assume that the length of HAZ is equal to the length of the welded plate plus 15 mm on both sides (i.e. total length of HAZ = length of welded plate + 30 mm) and the length of RSZ is equal to the length of the welded plate plus 7.5 mm on both sides (i.e. total length of RSZ = length of welded plate + 15 mm)
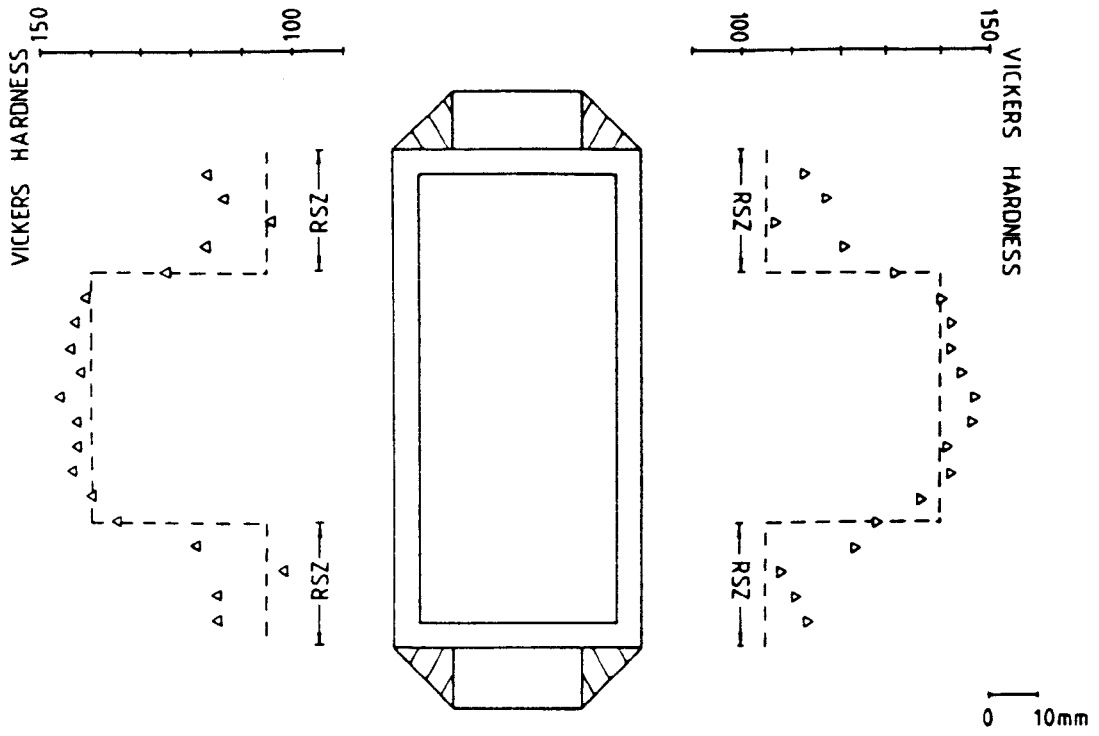
Figure 4.7 Hardness Surveys within the Cross-section

Figure 4.7 shows the hardness measurements taken transversely along the webs and the centre-lines of the welded plates ($x-y$ plane). The main purpose is to investigate the area of RSZ within the cross-section. The indentations, were about 5 mm apart and were done on both webs of the box-section. From the figure, we can observe that only both flanges and parts of the webs were affected by welding. The extents of HAZ and RSZ are about 27.3 mm and 22.3 mm respectively measured from the mid-thickness of the flange. The areas of HAZ and RSZ are about 0.72 and 0.65 of the area of the original cross-section respectively.
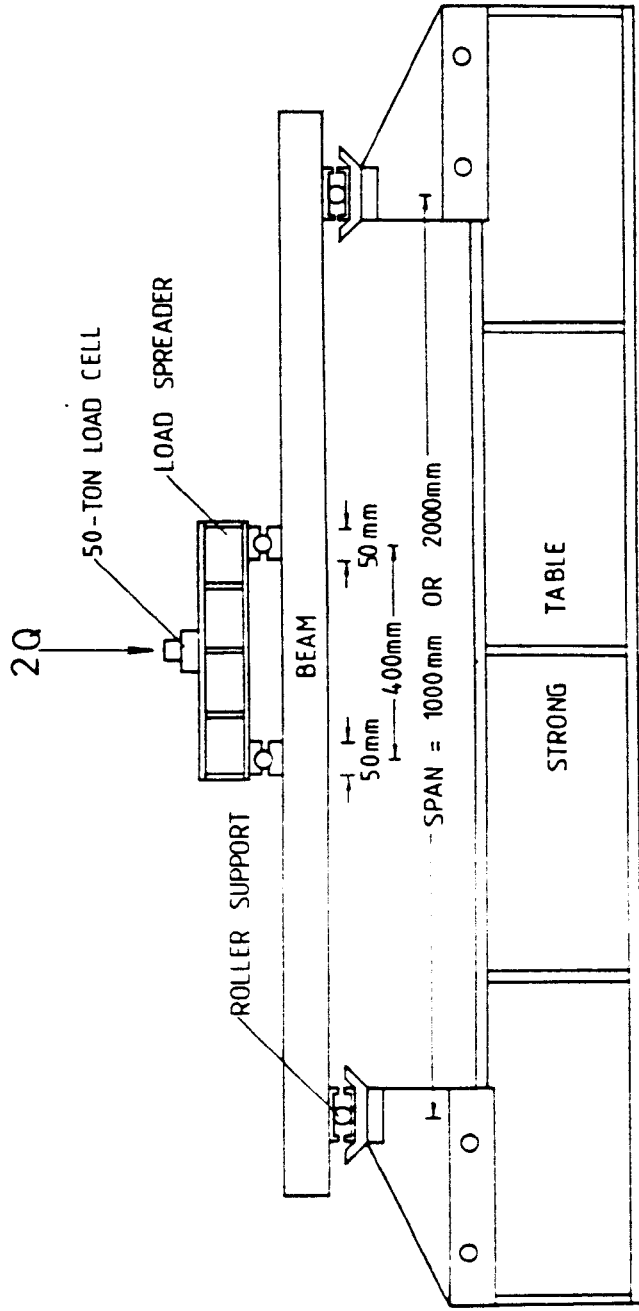
Figure 4.8 Set-up of Beam Test

4.4   Beam Tests

4.4.1   Set-up of Beam Test with 1000 mm Span

The beams with 1000 mm span were tested in a 400 KN Amsler Hydraulic Press and the complete set-up is shown in Figure 4.8 and Plates 4.4 and 4.5. The Amsler testing machine consists of a strong table attached to a hydraulic ram which rises vertically from the floor, and two vertical columns astride the ram, between which is a movable crosshead. Two adjustable end-support stands were slotted into the table and were made to be ~~exactly~~ 1000 mm apart. Above the stands were the roller supports on which the test beam would be placed (see Plate 4.6). A load spreader (see Plate 4.7) was placed symmetrically at mid-span to provide the two patch loading with 400 mm apart. The crosshead was then lowered to touch a 50-ton load cell (manufacturer: Davy-United, type: H500) which sat on top of the load spreader. Three DC rectilinear potentiometers (manufacturer: Novatech) were used to measure the deflections at mid-span and quarter-span (see Plates 4.4 and 4.5). The loading increment was controlled by a Losenhausen Close-loop Servo-hydraulic Control System as shown in Plate 4.8. The load and the deflections were recorded automatically by the Opus computer and a data logger (see Plate 4.9). The load versus deflections at mid-span and quarter-span were displayed on the screen during testing and were stored on the hard disk of the Opus computer when finished.
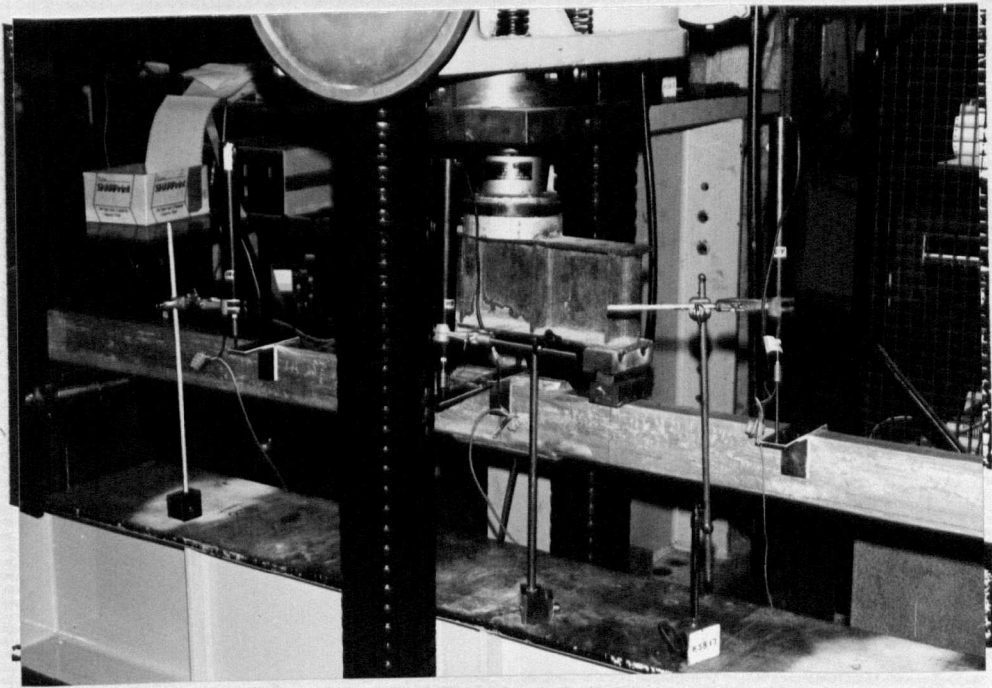
Plate 4.4 Set-up of Beam Test with 1000 mm Span
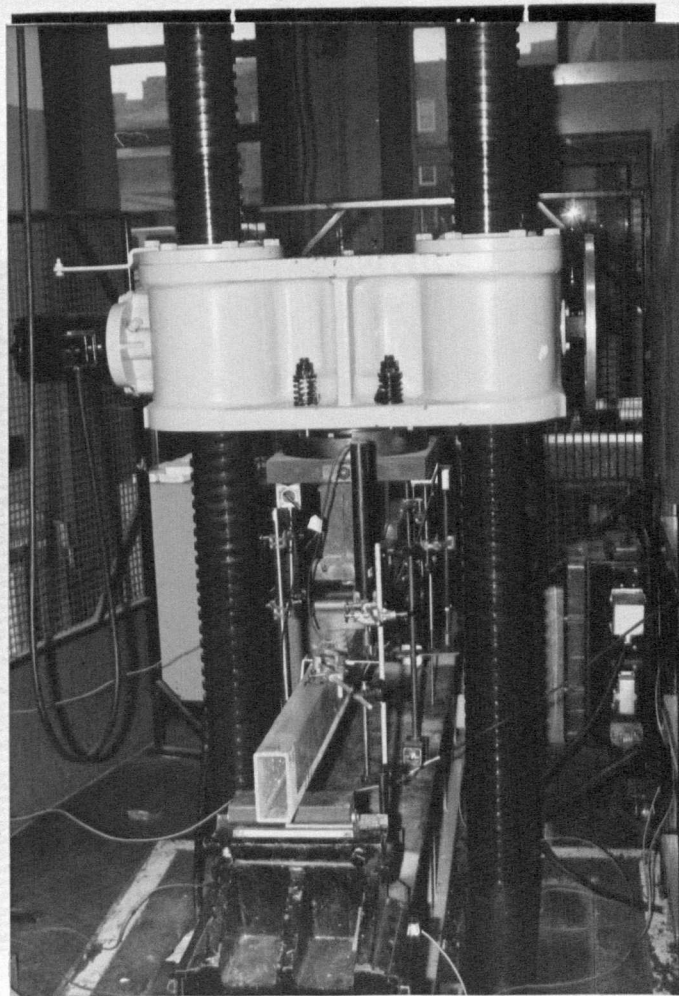
Plate 4.5 Set-up of Beam Test with 1000 mm Span
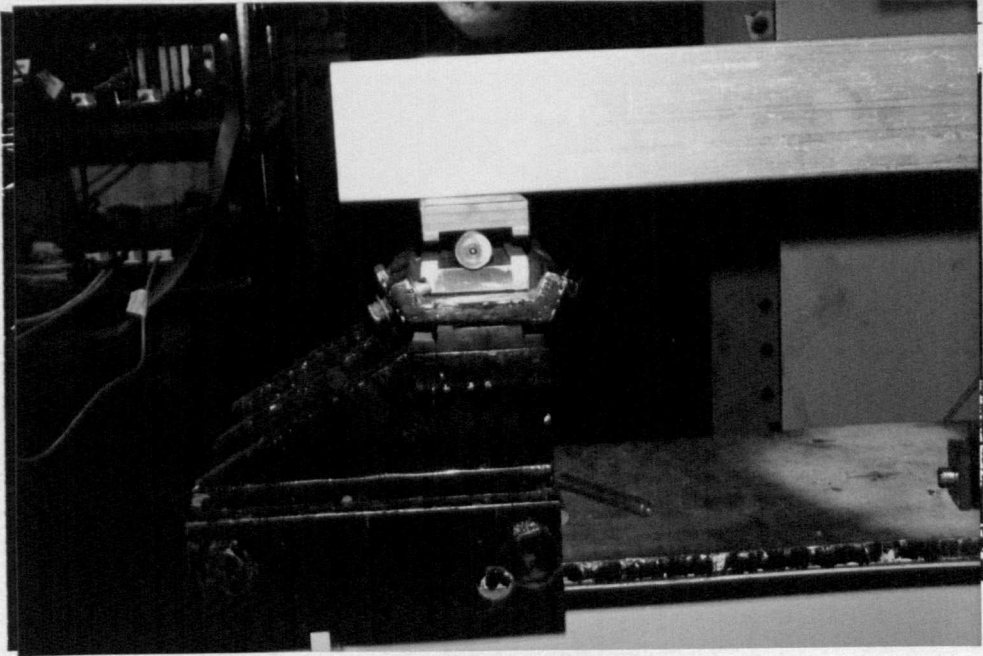
Plate 4.6 Roller Support
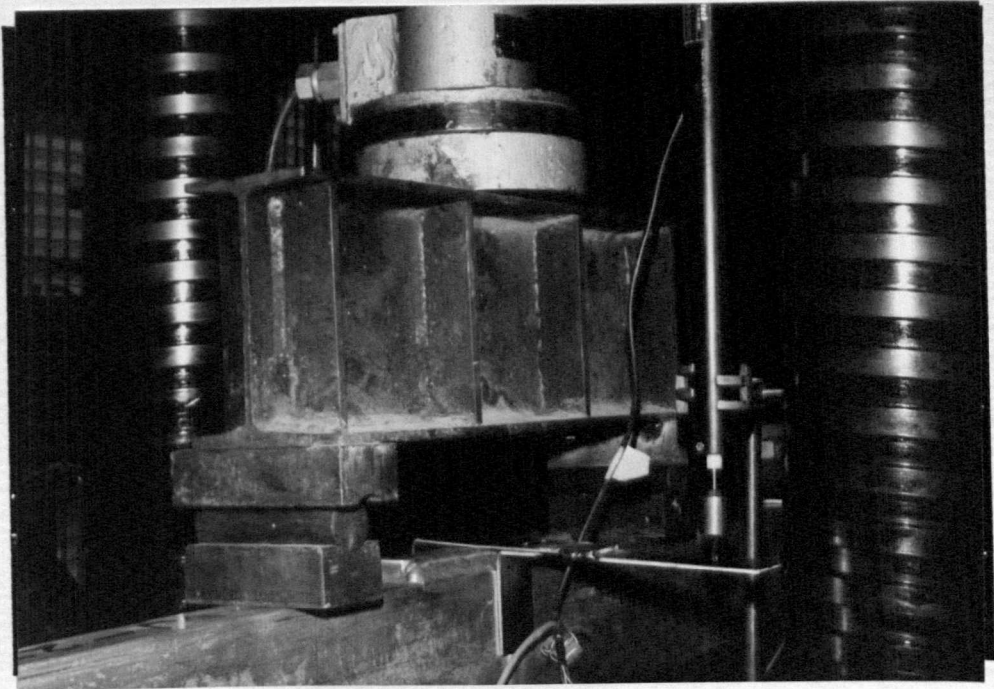
Plate 4.7 Load Spreader and Load Cell
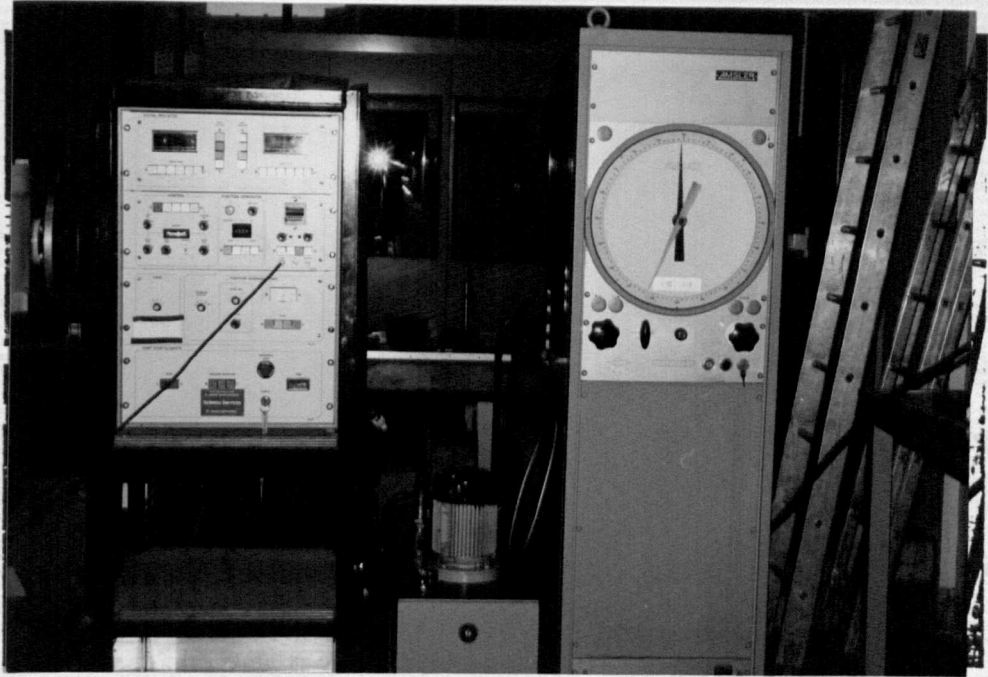
Plate 4.8 Losenhausen Close-loop Servo-hydraulic Control System

Plate 4.9 Opus Compter and Data Logger

4.4.2   Set-up of Beam Test with 2000 mm Span

During the testing of beams with 1000 mm span, one centrally-welded beam was fractured and damaged some of the testing equipment. In order to prevent any further damage and so as not to endanger the safety of other people, the beams with 2000 mm span were therefore tested on the 500 KN 4 Post Denison Universal Testing Machine with screw thread displacement control. The instrumentation and experimental set-up were basically the same as before but without the Losenhausen Close-loop Servo-hydraulic Control System.

4.4.3   Testing Procedure

For the beams with 1000 mm span, a constant loading increment about 5 KN per minute was applied and the total load on the beam was measured by the 50-ton load cell. The load cell and the three DC rectilinear potentiometers were connected to a data logger and the data logger was controlled by the Opus computer. During testing, the load and the deflections at mid-span and quarter-span were recorded automatically for every 5 seconds by the Opus computer, and all the results were stored in the hard disk after completion.

For the beams with 2000 mm span, a constant vertical displacement of about 5 mm per minute was applied initially. As the deflections became progressively larger, smaller displacement of about 2 mm per minute were applied. The total load on the beam was also measured by the same 50-ton load cell and the testing procedure was the same as before.

Due to safety reasons, the welded beams were not intended to be tested up to failure. Therefore, when the mid-span of the welded beam showed a reasonably large amount of deflection, the test was terminated and all the deflections and the corresponding maximum applied load were recorded.

4.4.4 Beam Test Results and Computer Simulation Using Program INSTAF

All the experimental results were compared with the theoretical predictions obtained by program INSTAF. The input parameters required by the program INSTAF were as follows:

1. Span of beam (either 1000 mm or 2000 mm)

2. Dimensions of the non-welded and welded beam cross-section (see Figure 4.1)

3. Stress-strain properties of parent and RSZ material (see Tables 4.3 and 4.4)

4. The positions and the length of RSZ within the beam (see Figure 4.6)

5. The area of RSZ within the cross-section (see Figure 4.7)

6. The initial out-of-straightness (see Section 4.2.3)

7. The locations of load (see Figure 4.8)

8. The boundary conditions (simply-supported beam)

From the load-deflection curves of the fully-welded beams, it was found that the area of the fillet welds cannot strengthen the members due to lack of fusion. Therefore, in the comparisons, the area of the fillet welds is neglected and only the area of the welded plates is taken into account.

All the test results are summarised in Tables 4.5(a) and 4.5(b). Moreover, all the experimental and theoretical results are also presented in Figures 4.9 to 4.16 in the form of non-dimensionalised plots of $\frac{Q}{Q_{0.2x}}$ versus $\frac{\Delta_C}{\text{span}} \times 100\%$ or $\frac{\Delta_Q}{\text{span}} \times 100\%$ for mid-span and quarter-span deflection respectively where

$$Q_{0.2x} = \frac{M_{0.2x}}{0.3} \quad (KN) \quad \text{(for beam with span } 1000mm\text{)}$$

or

$$Q_{0.2x} = \frac{M_{0.2x}}{0.8} \quad (KN) \quad \text{(for beam with span } 2000mm\text{)}$$

The mean value of $\sigma_{0.2}$ is used to evaluate the value of $M_{0.2x}$ for a heat-unaffected cross-section. For the partially heat-affected cross-section, both the mean values of $\sigma_{0.2}$ and $\sigma_{0.2}^*$ are required to evaluate the value of $M_{0.2x}$. Therefore, for the cross-section as shown in Figure 4.1, the values of $Q_{0.2x}$ are:

$$Q_{0.2x} \;=\; 68.1 \;\; KN \quad \text{(specimen designation: W-1000-F-1, W-1000-F-2,}$$
$$\text{W-1000-F-3, W-1000-F-4, W-1000-F-5)}$$
$$=\; 25.5 \;\; KN \quad \text{(specimen designation: W-2000-F-1, W-2000-F-2,}$$
$$\text{W-2000-F-3)}$$
$$=\; 57.5 \;\; KN \quad \text{(other beam specimens with span } 1000\ mm)$$
$$=\; 21.6 \;\; KN \quad \text{(other beam specimens with span } 2000\ mm)$$

From Tables 4.3 and 4.4, we can observe that the mechanical properties for the parent and heat-affected material show a certain variability, to take into

account this effect, therefore three theoretical curves were drawn in Figures 4.9 to 4.16 and these three curves were obtained by inputting the maximum, mean and minimum values of $\sigma_{0.2}$ and $\sigma_{0.2}^*$ respectively into the program INSTAF. Moreover, the effect of residual stresses is neglected in the computer simulation.

Specimen Designation	Q_{30} (KN)	Q_{max} (KN)	$\Delta_{C(max)}$ (mm)	$\Delta_{Q(max)}$ (mm)	Remark
N-1000-P-2	62.7	68.2	51.7	36.6	LB
N-1000-P-3	61.9	69.7	63.1	45.3	LB
W-1000-L/2-1	57.2	58.8	31.7	22.2	BF
W-1000-L/2-2	54.8	62.7	62.3	43.2	LB
W-1000-L/2-3	60.3	64.2	48.1	34.4	LB
W-1000-L/2-4	51.7	57.2	60.1	45.1	LB
W-1000-E-1	57.2	64.4	61.1	44.3	LB
W-1000-E-2	55.2	64.4	65.9	46.6	LB
W-1000-E-3	55.6	64.4	64.4	45.2	LB
W-1000-F-2	88.5	> 102.6	> 51.9	> 38.1	NB
W-1000-F-3	87.7	> 104.2	> 59.0	> 41.0	NB
W-1000-F-4	89.3	> 98.7	> 56.7	> 38.5	NB
W-1000-F-5	89.3	> 97.9	> 54.0	> 38.5	NB

Table 4.5: (a) Test Results for Beam with 1000 mm Span

Plate 4.10 Beam Failed in Local Buckling (W-1000-L/2-2)
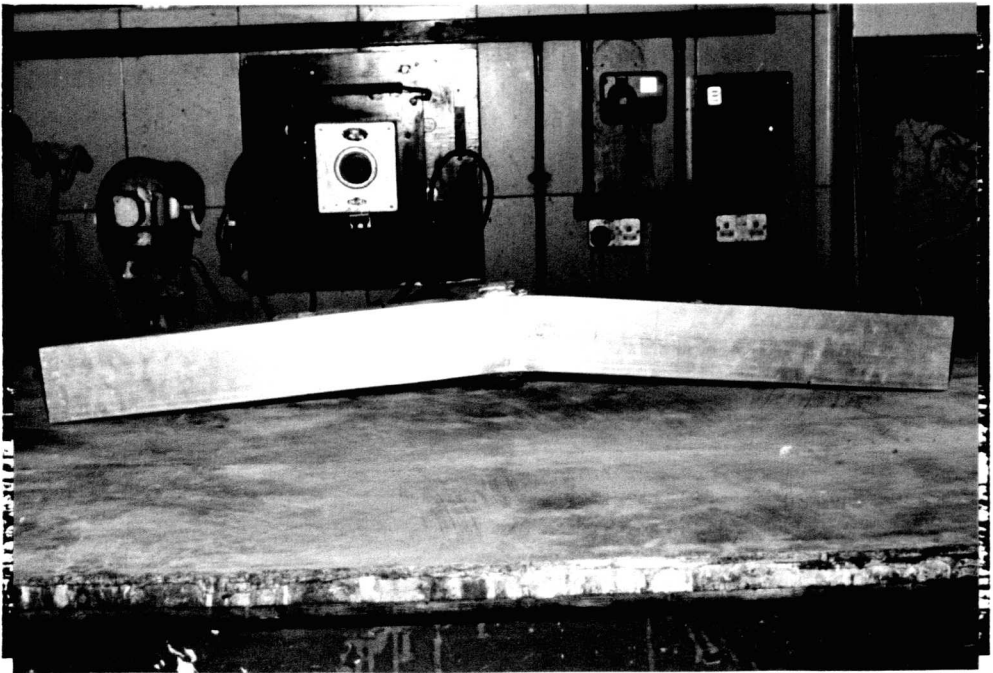
Plate 4.11 Beam Fractured during Test (W-1000-L/2-1)

Specimen Designation	Q_{60} (KN)	Q_{max} (KN)	$\Delta_{C(max)}$ (mm)	$\Delta_{Q(max)}$ (mm)	Remark
N-2000-P-1	20.0	23.0	126.7	79.9	LB
N-2000-P-2	20.5	23.6	128.7	82.2	LB
W-2000-L/2-1	17.0	20.7	208.5	135.7	BF
W-2000-L/2-2	19.6	23.6	155.2	103.8	BF
W-2000-L/2-3	21.2	23.7	105.3	69.8	BF
W-2000-L/2-4	18.2	> 20.9	> 105.1	> 67.8	NB
W-2000-L/4-1	19.9	> 22.9	> 128.7	> 83.0	NB
W-2000-L/4-2	21.7	> 24.7	> 127.4	> 81.9	NB
W-2000-L/4-3	20.7	> 23.3	> 122.7	> 78.2	NB
W-2000-F-1	31.6	> 39.3	> 153.4	> 98.5	NB
W-2000-F-2	31.5	> 38.6	> 144.6	> 95.6	NB
W-2000-F-3	31.8	> 39.6	> 146.8	> 95.9	NB

Table 4.5: (b) Test Results for Beam with 2000 mm Span

NOTE
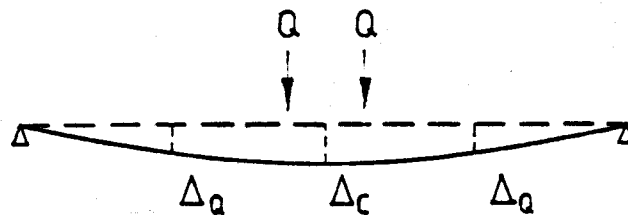
Q_{30} = corresponding applied lateral patch load when the mid-span of beam deflect 30 mm

Q_{60} = corresponding applied lateral patch load when the mid-span of beam deflects 60 mm

Q_{max} = maximum applied lateral patch load measured in test

$\Delta_{C(max)}$ = maximum mid-span deflection of beam measured in test

$\Delta_{Q(max)}$ = maximum quarter-span defection of beam measured in test

LB = beam failed in local buckling (see Plate 4.10)

BF = beam fractured during test (see Plate 4.11)

NB = no local buckling or fracture up to Q_{max}
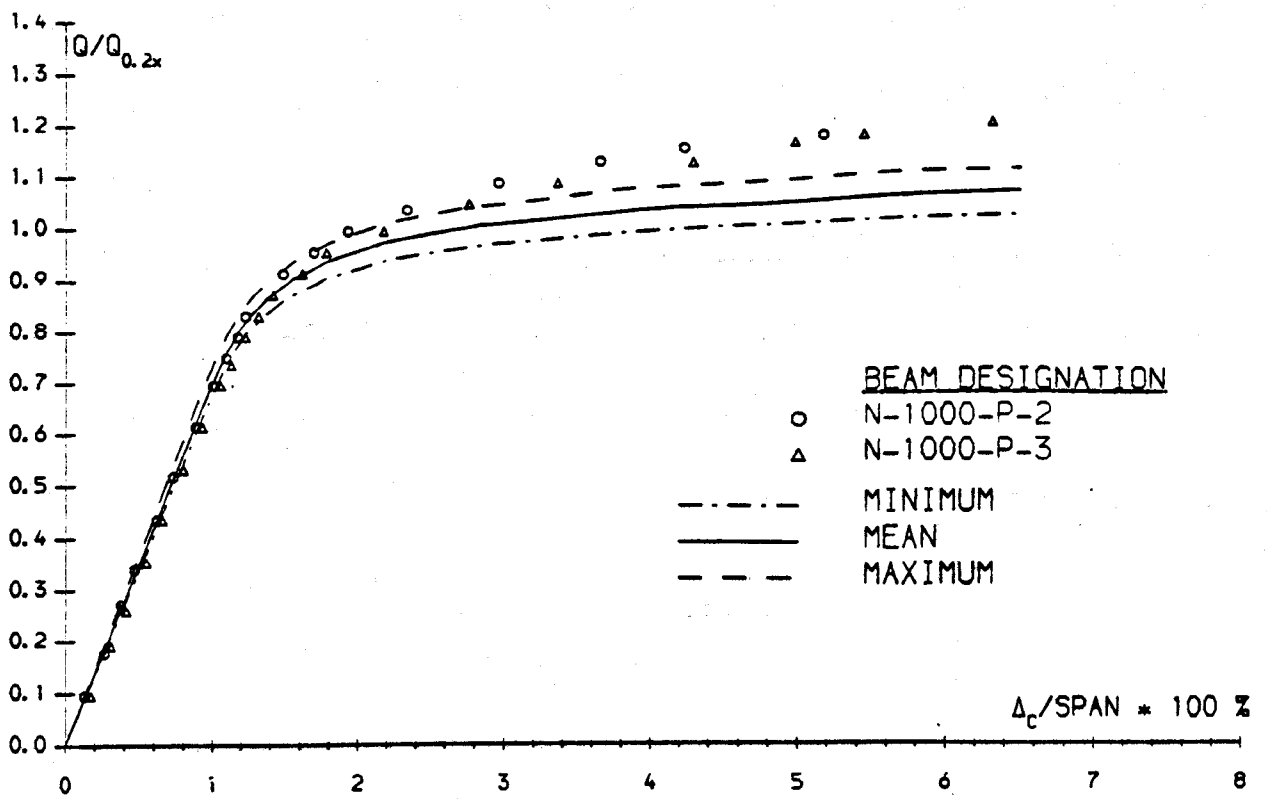
Figure 4.9 (a)
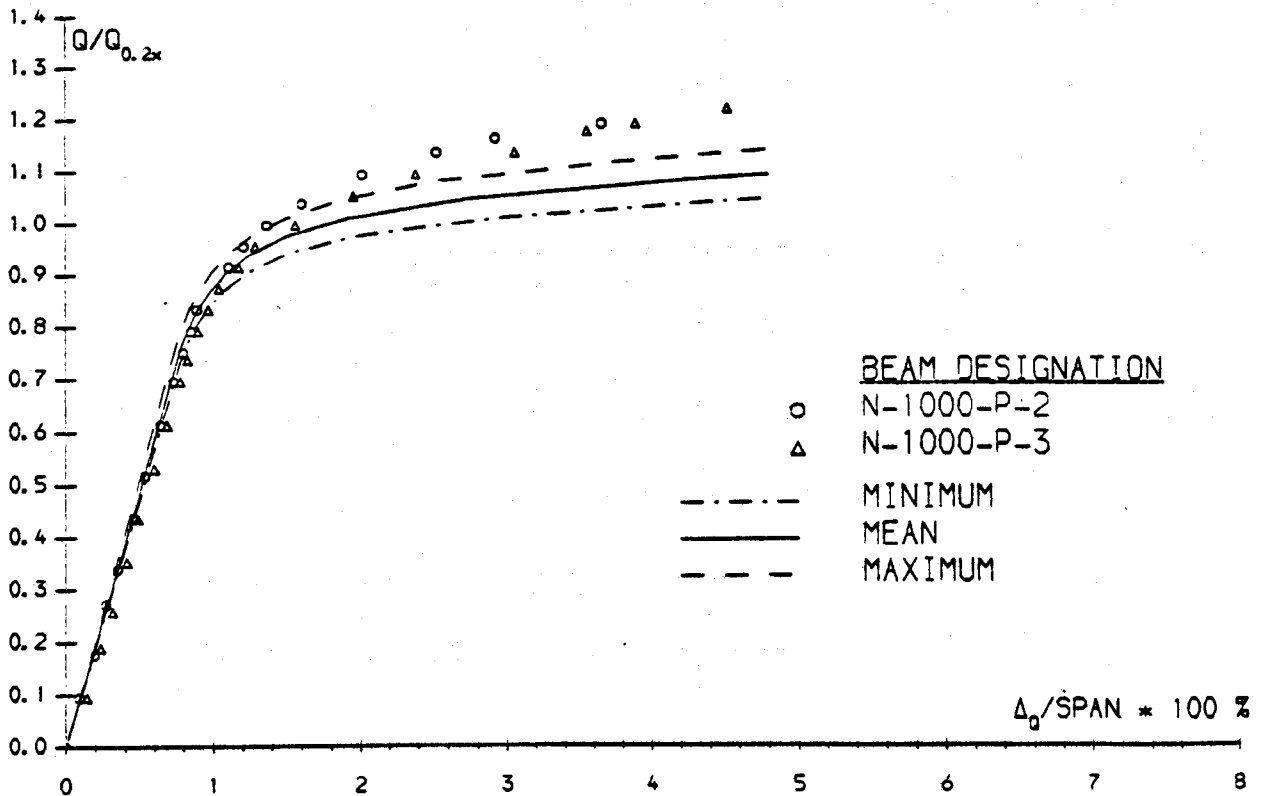
Figure 4.9 (b)

Figure 4.9 Comparison with Theoretical Load-deflection Curves at Mid-span
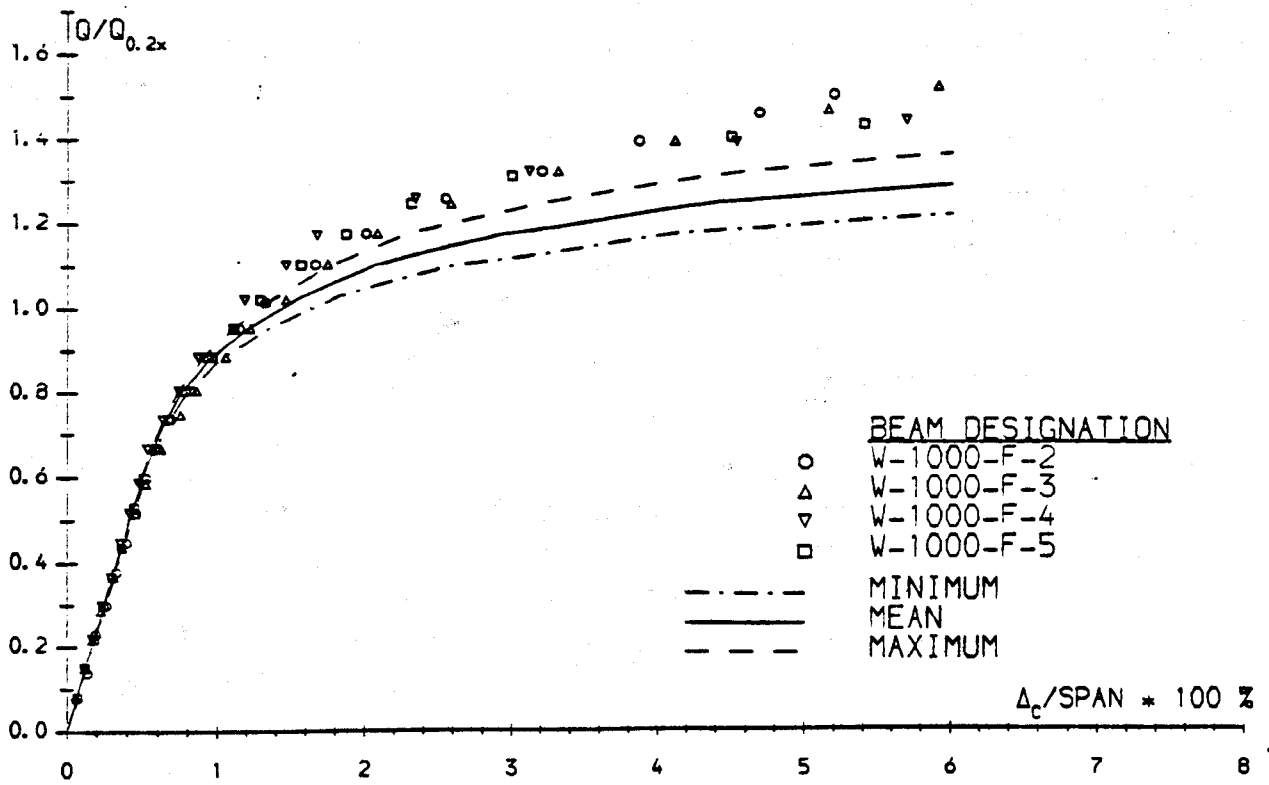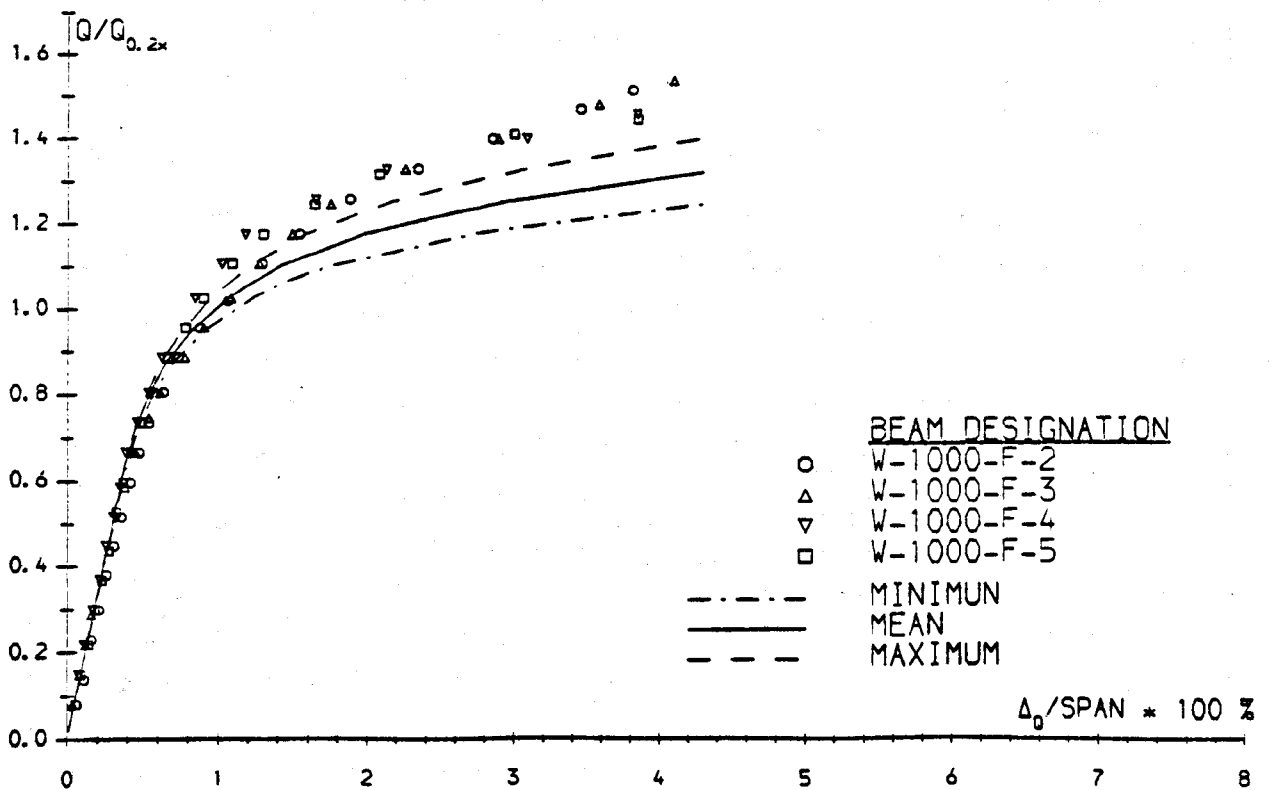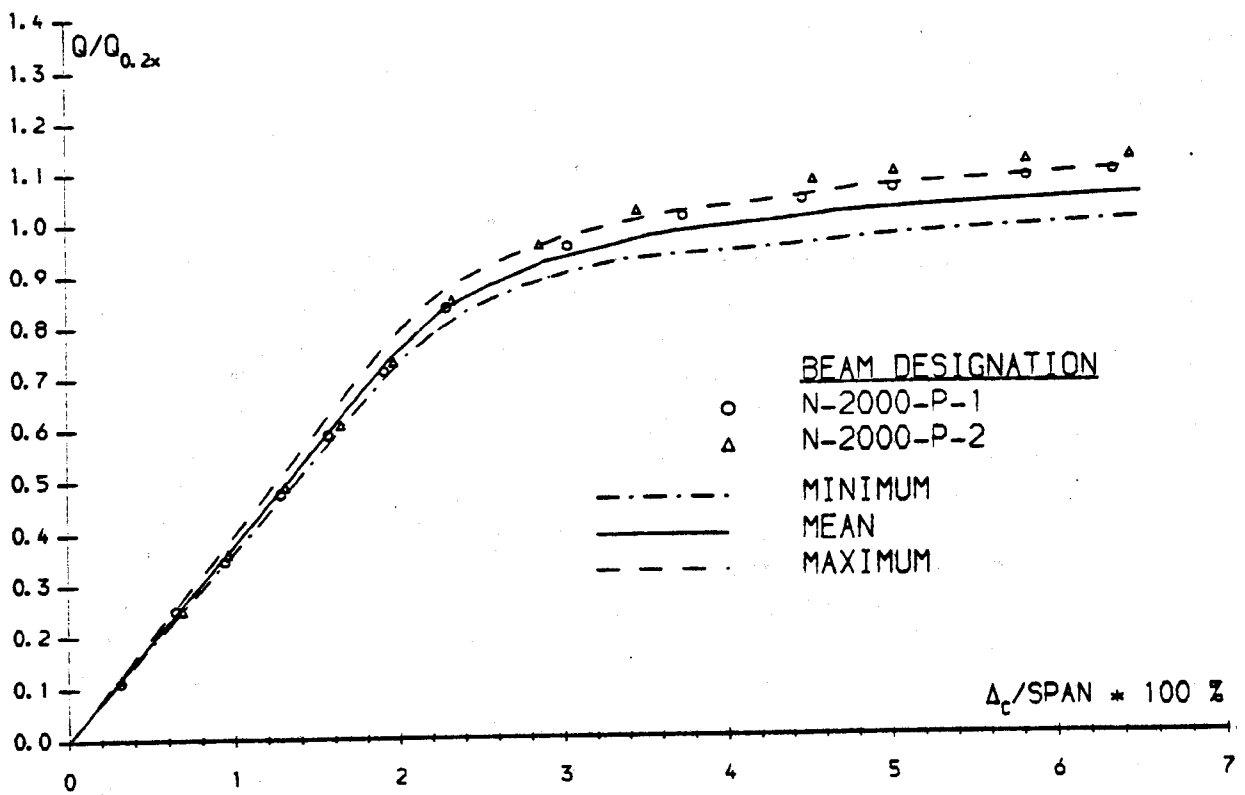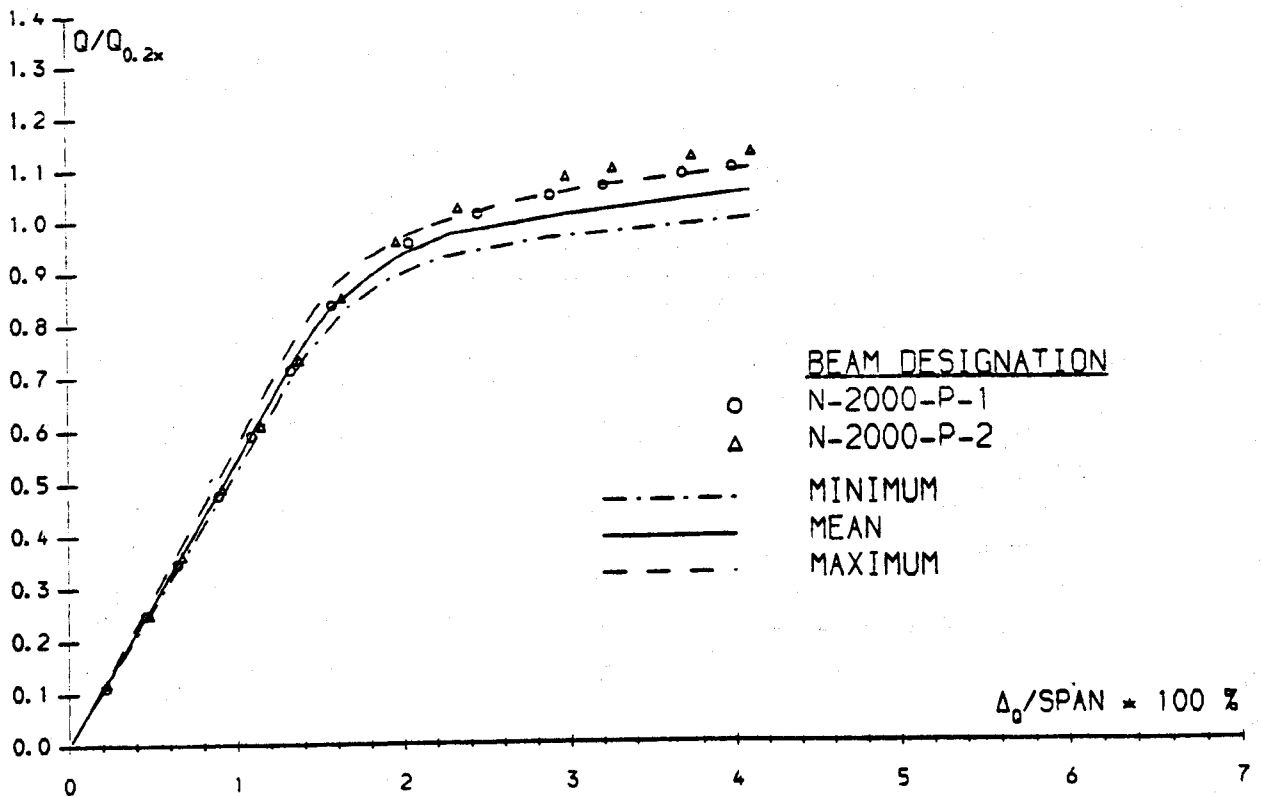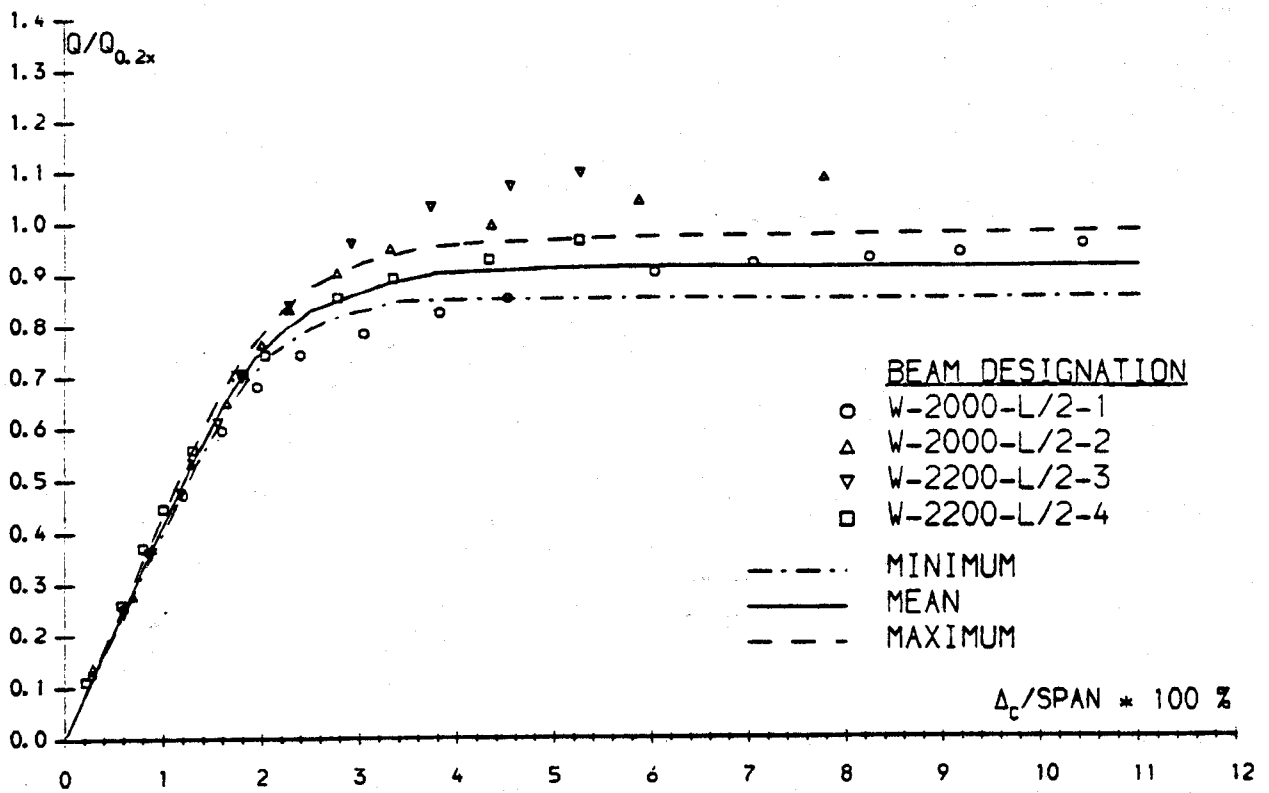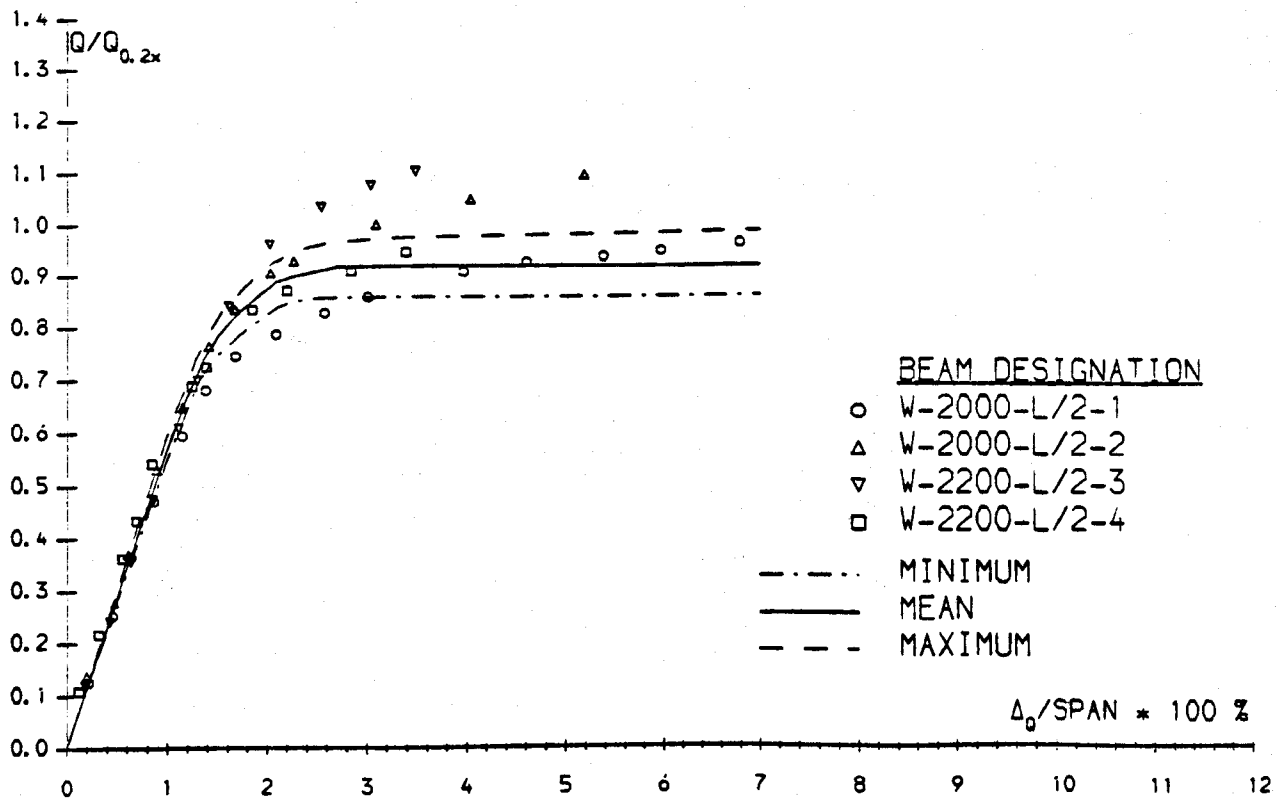(a) and Quarter-span (b) (Specimen : N-1000-P-2,3)
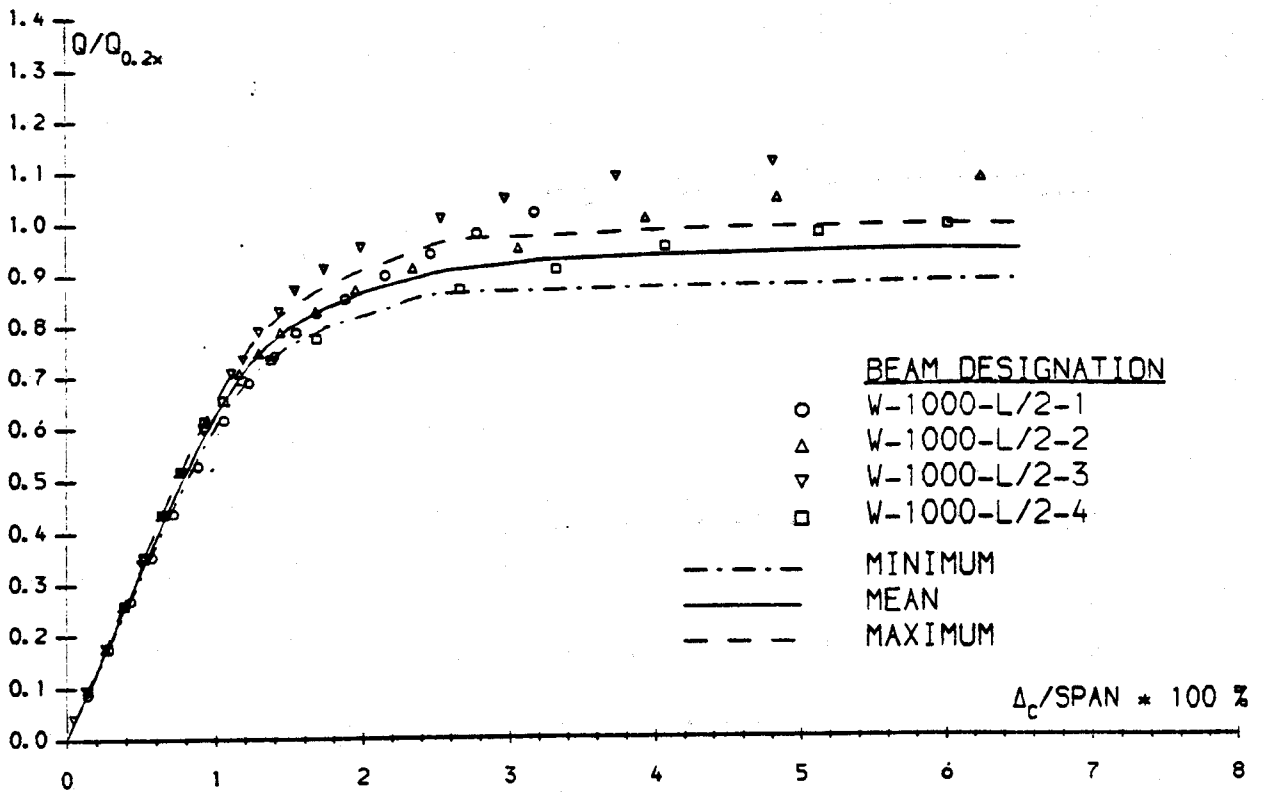
Figure 4.10 (a)
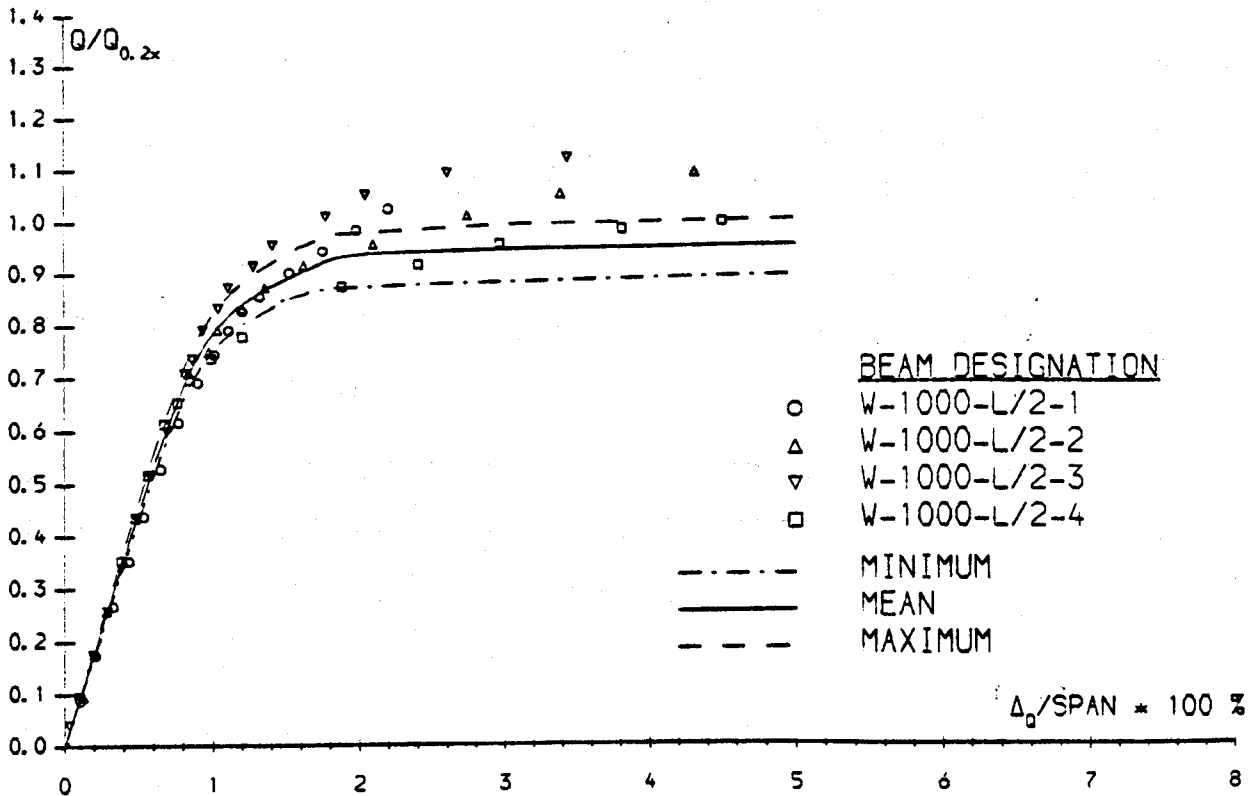
Figure 4.10 (b)

Figure 4.10 Comparison with Theoretical Load-deflection Curves at Mid-span
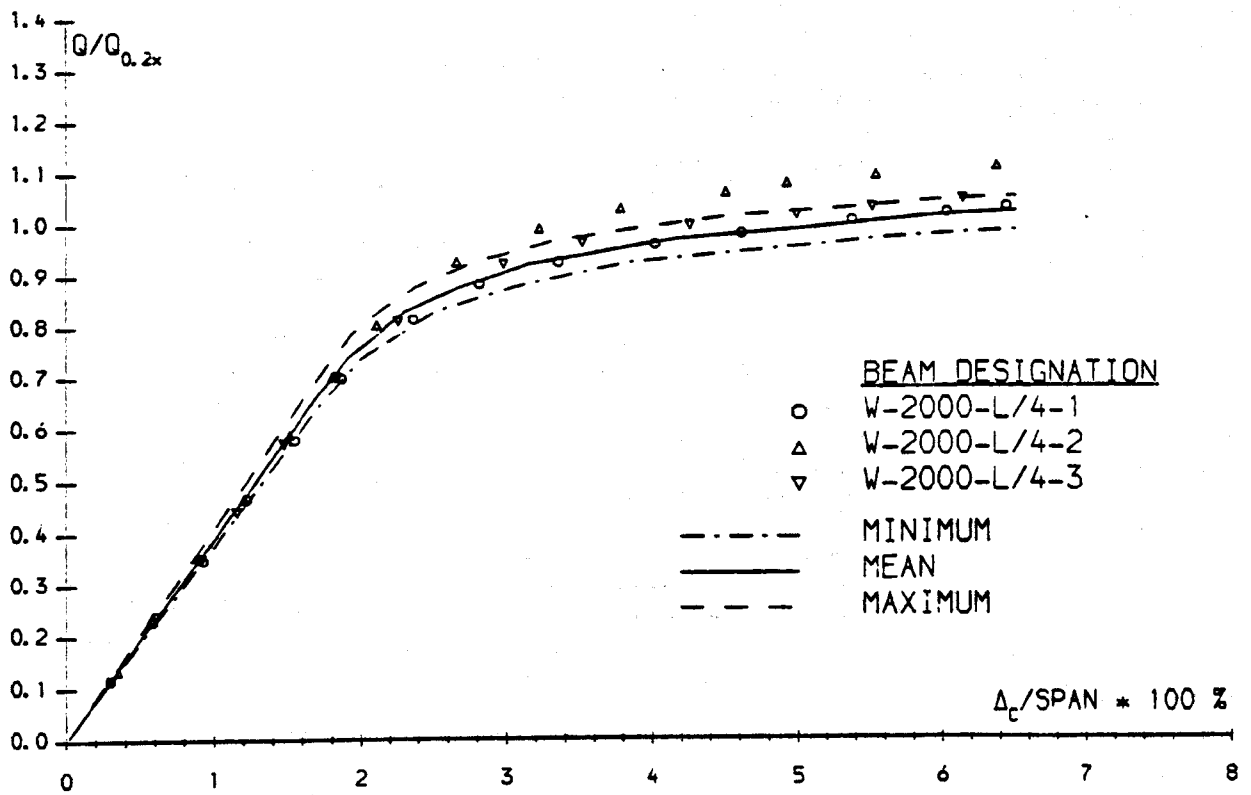(a) and Quarter-span (b) (Specimen : W-1000-L/2-1,2,3,4)
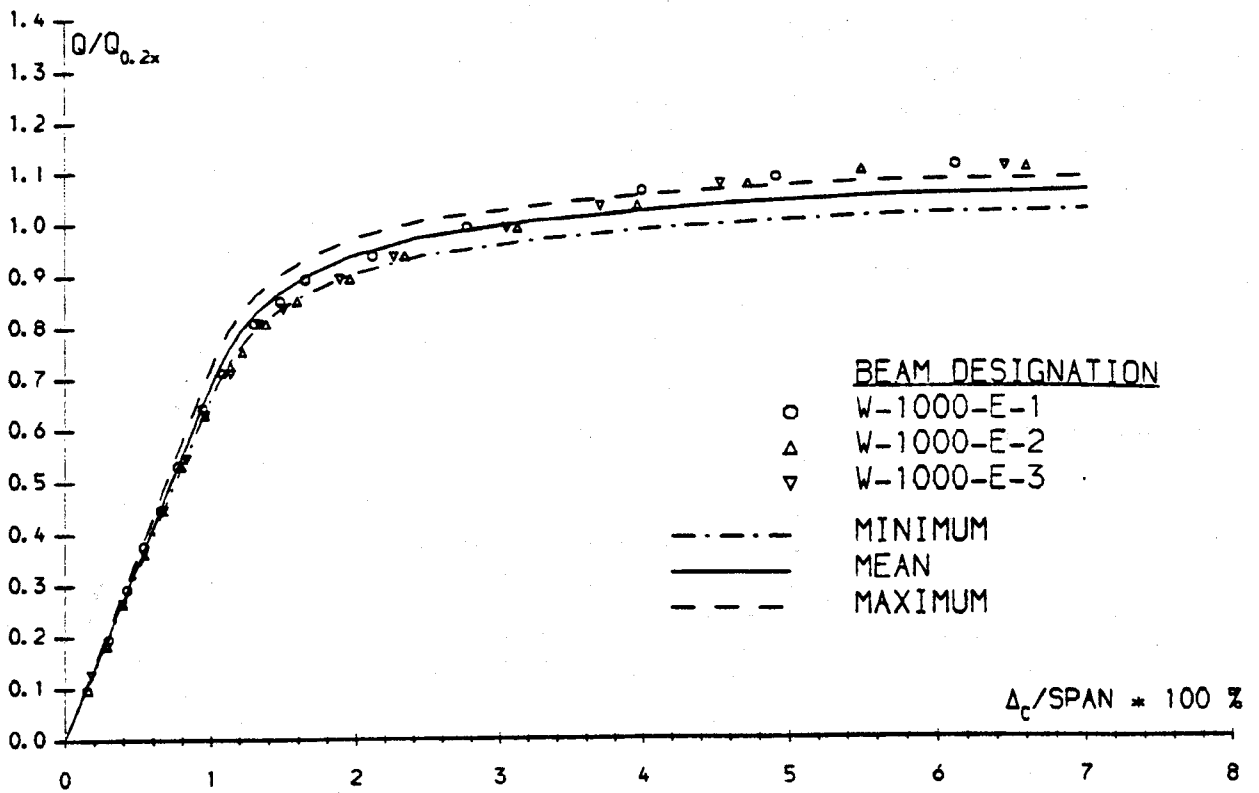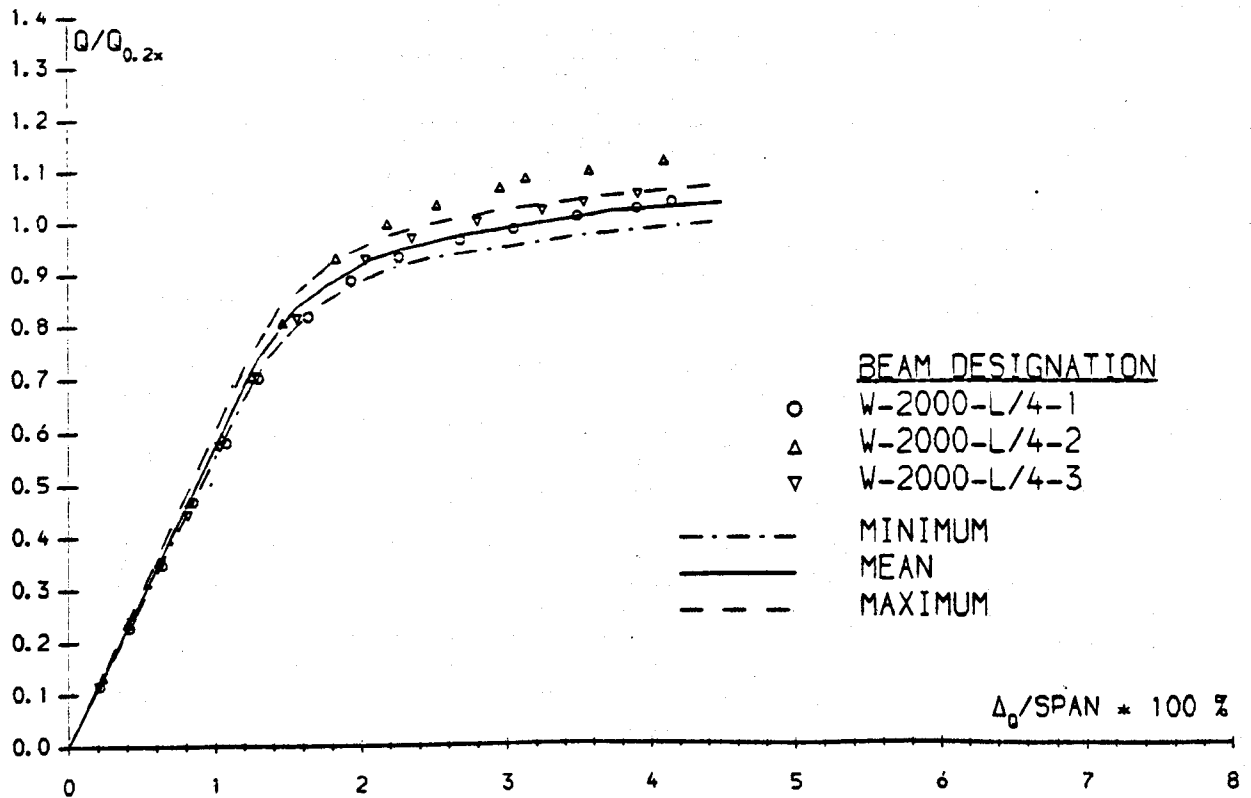
Figure 4.11 (a)
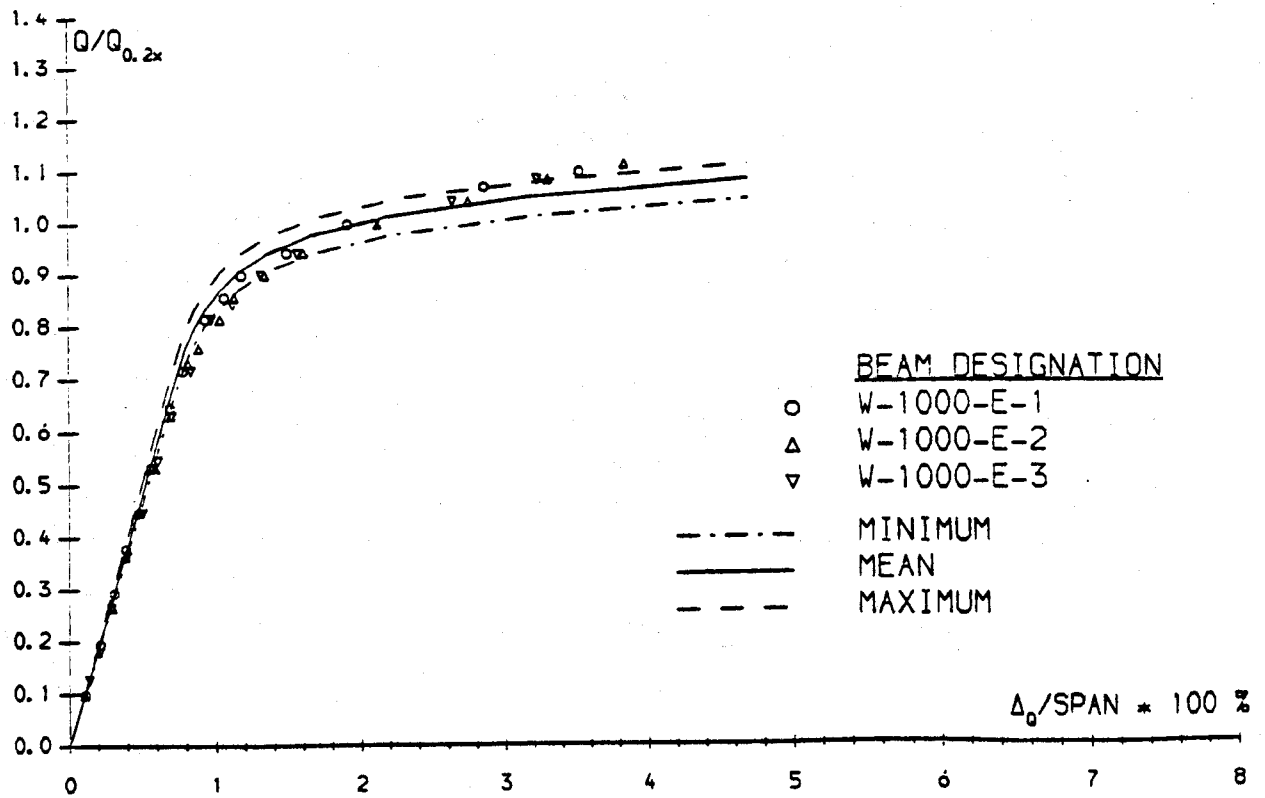
Figure 4.11 (b)

Figure 4.11 Comparison with Theoretical Load-deflection Curves at Mid-span
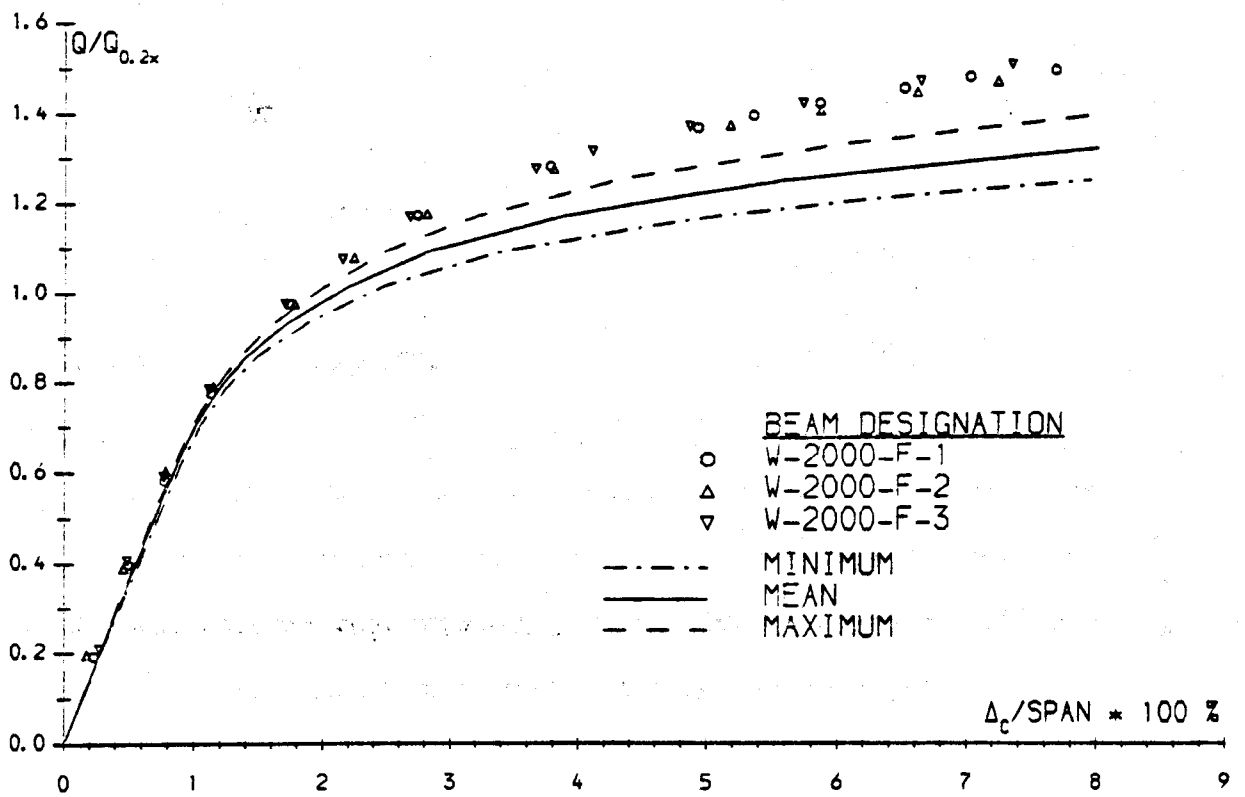(a) and Quarter-span (b) (Specimen : W-1000-E-1,2,3)

Figure 4.12 (a)

Figure 4.12 (b)

Figure 4.12 Comparison with Theoretical Load-deflection Curves at Mid-span
(a) and Quarter-span (b) (Specimen : W-1000-F-2,3,4,5)

Figure 4.13 (a)

Figure 4.13 (b)

Figure 4.13 Comparison with Theoretical Load-deflection Curves at Mid-span
(a) and Quarter-span (b) (Specimen : N-2000-P-1,2)

Figure 4.14 (a)

Figure 4.14 (b)

Figure 4.14 Comparison with Theoretical Load-deflection Curves at Mid-span
(a) and Quarter-span (b) (Specimen : W-2000-L/2-1,2,3,4)

Figure 4.15 (a)

Figure 4.15 (b)

Figure 4.15 Comparison with Theoretical Load-deflection Curves at Mid-span
(a) and Quarter-span (b) (Spceimen : W-2000-L/4-1,2,3)
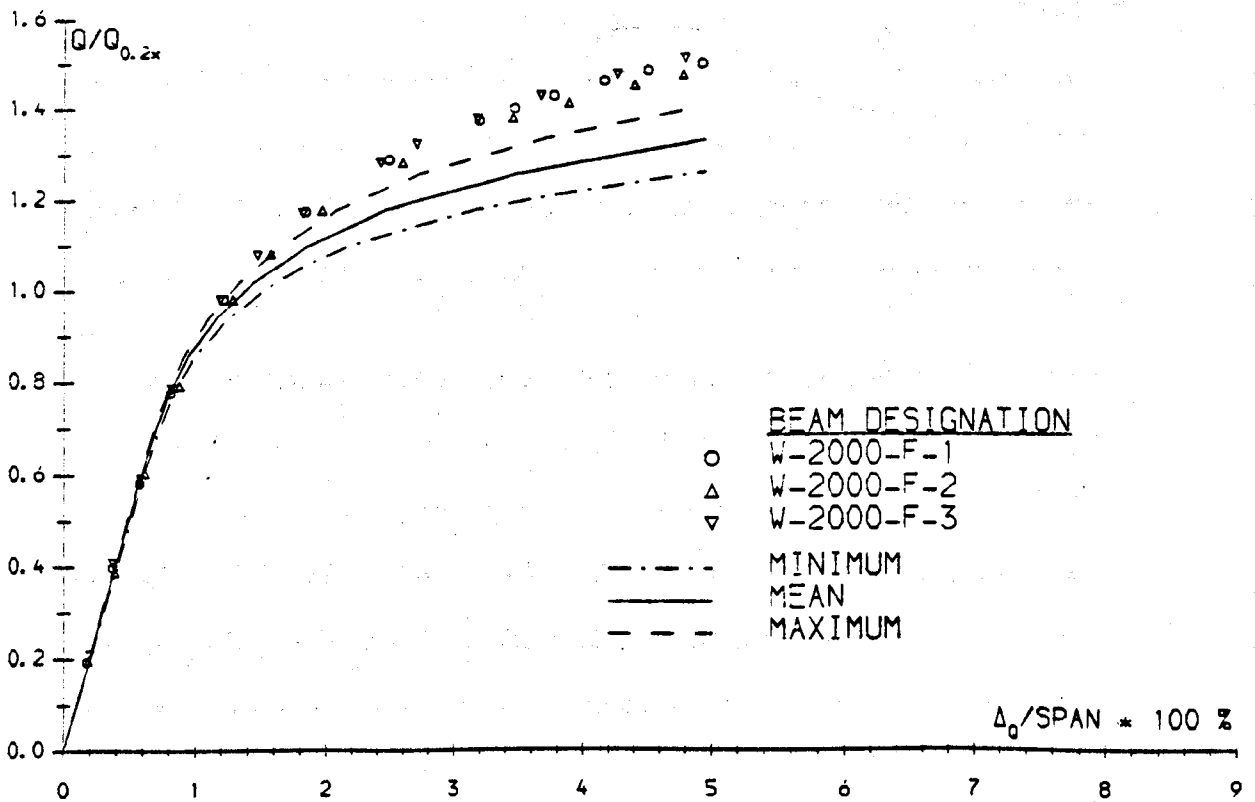
Figure 4.16 (a)

Figure 4.16 (b)

Figure 4.16 Comparison with Theoretical Load-deflection Curves at Mid-span
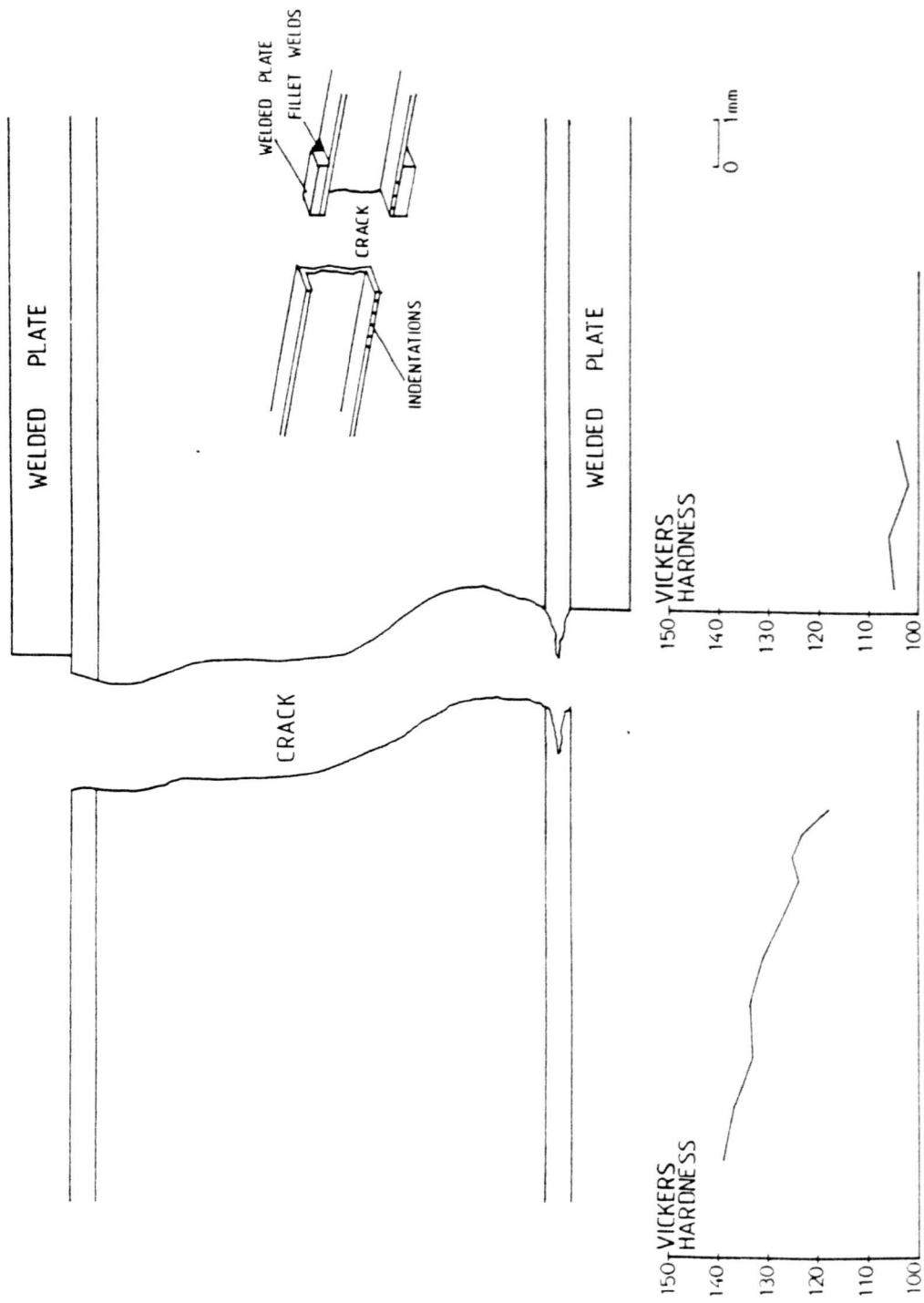(a) and Quarter-span (b) (Specimen : W-2000-F-1,2,3)

Figure 4.17 Hardness Surveys around the Crack

4.5 Discussion

4.5.1 Test Results

From the test results, as expected, we can observe that the load-deflection curves of the non-welded extruded beams; and the beams with transverse welds near the two ends show very small variation. The fully-welded beams also show similar behaviour because the change in temperature during welding and cooling was quite uniform within the whole beam. The material properties, therefore, were affected uniformly along the length and these were reflected in the tensile coupon tests for the heat-affected material as mentioned in Section 4.3.2.

For other transversely welded beams, especially the centrally-welded beams, the load-deflection curves vary considerably. It is because the heat input is so localised and the cooling temperature become rather non-uniform. The material properties, thus, show great variability within the heat-affected zone.

In the beam tests, several centrally-welded beams fractured at relatively small deflections. Therefore, the heat-affected material did show a loss of ductility, but, this effect was not apparent in the tensile coupon tests for the heat-affected material. After the beam tests, one of the fractured beam was selected and the region around the crack was cut into halves along the centre line of the welded plates and flanges. Hardness surveys around the crack were then carried out and the results are shown in Figure 4.17. The measurements were taken as close to the crack as possible and it seemed that the crack was

initiated around the boundary of fully heat-affected zone and partially heat-affected zone (see Section 2.3.1). The author, therefore, suspected that the loss of ductility may occur only on the partially heat-affected zone and not on the fully heat-affected zone.

Kelsey [7] reported that for 7039 aluminium alloy, the temperature within the fully heat-affected zone was above 600F (316°C); and the temperature within the partially heat-affected zone ranged from 400F to 600F (204°C to 316°C); and the parent material properties appeared to be unaffected in locations where the heat of welding did not exceed 400F (204°C). For 7019 alloy, similar results were obtained by Robertson [6] and these transition points were about 275°C and 205°C. Therefore, the author suspects that for the region close to the welds, the energy input during welding is large enough to break the original crystal structure of the parent metal. After welding, temperature within this region is still high, and the material, therefore, recrystalize to form another stable lattice structure. This new stable lattice structure will give inferior material properties but does not show any loss of ductility. This region is the same as the fully heat-affected zone as mentioned before. For the region further away from the welds, the energy input during welding may or may not be large enough to break the original crystal structure depending on the distance from the welds. After welding, the temperature within this region is relatively lower and the material cannot recrystalize to form another stable lattice structure. The material in this region, therefore, resembles the parent metal and shows less reduction in strength, but the material gives poor ductility. This region is the same as the partially heat-affected zone. For the tests conducted by Webber [4],
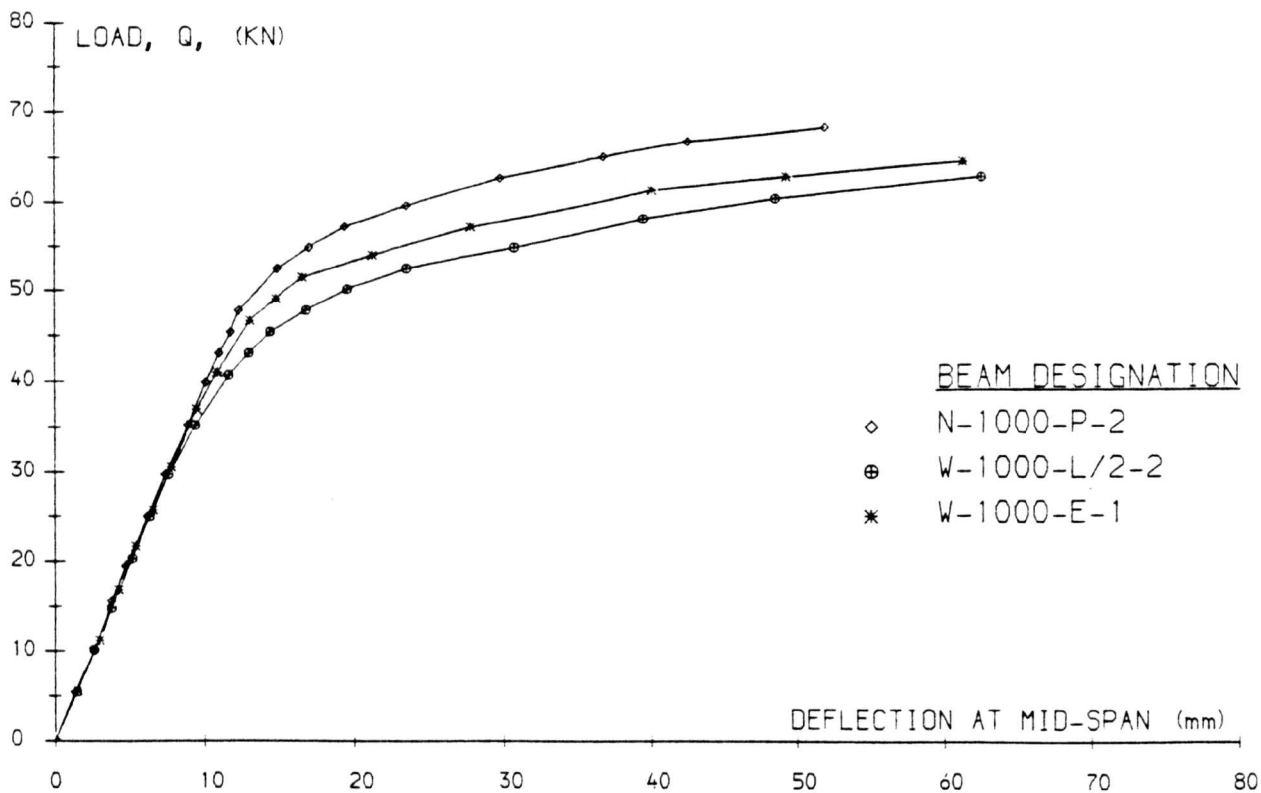
Figure 4.18 Comparison between the Load-deflection Curves of Non-welded; Centrally-welded and End-welded Beams of 1000 mm Span

combined zones of material were found within the tensile specimens and all those ~~those~~ specimens resulted in a loss of ductility. The above suggestion, therefore, is reasonable but experiments should be carried out for verification.

For the beams with 1000 mm span, the non-welded beams; centrally-welded beams and beams with welds near the two ends are still comparable because the strengthening effect due to the welded plates is not too much. Figure 4.18 shows the comparisons of their typical load versus central deflection curves and we can observe that the centrally-welded beam did show reduction in strength as predicted by the author. The HAZ material within the centrally-welded beam is under pure moment, so the load-deflection characteristics of the beam should depend on the progressive 'yielding' of the HAZ material. From Figure 4.18, we can find that the centrally-welded beam is mainly elastic until the load reaches about 30 KN. However, for the non-welded beam, the deflection starts to deviate from linearity at about 45 KN. By comparing the relative curvature of the knees on Figure 4.18, the load-deflection curve of the non-welded beam has ~~more~~ a sharper knee and this can all be explained in terms of the mechanical properties of the parent metal and heat-affected zone material (see Section 4.3.2).

For the beam with welds near the two ends, the beams also show reductions in strength and this behaviour ~~is~~ cannot, at present, be explained by the author. From Figure 4.18, it can be seen that the end-welded beam is mainly elastic until the load reaches about 39 KN. Therefore, the author suspected that the reduction in strength is mainly due to the presence of residual stresses after welding because, from the hardness surveys, the cross-section is only partially-affected. The ratio of $\frac{A^*}{A}$ for RSZ material is only 0.65 and the

Specimen Designation	Experimental Load (mean)		Theoretical Load (INSTAF)		Different
	Q_{30} (KN)	Q_{60} (KN)	Q_{30} (KN)	Q_{60} (KN)	(%)
N-1000-P-2 N-1000-P-3	62.3	–	58.2	–	6.6
W-1000-L/2-1 W-1000-L/2-2 W-1000-L/2-3 W-1000-L/2-4	56.0	–	52.5	–	6.2
W-1000-E-1 W-1000-E-2 W-1000-E-3	56.0	–	57.6	–	-2.9
W-1000-F-2 W-1000-F-3 W-1000-F-4 W-1000-F-5	88.7	–	80.3	–	9.5
N-2000-P-1 N-2000-P-2	–	20.3	–	20.0	1.5
W-2000-L/2-1 W-2000-L/2-2 W-2000-L/2-3 W-2000-L/2-4	–	19.1	–	18.6	2.6
W-2000-L/4-1 W-2000-L/4-2 W-2000-L/4-3	–	20.8	–	19.6	5.8
W-2000-F-1 W-2000-F-2 W-2000-F-3	–	31.6	–	28.5	9.8

Table 4.6: Comparison between Test Results and Theoretical Results Obtained by Program INSTAF

central parts of the webs are still unaffected by welding. The residual stresses, therefore, should be developed within the cross-section, and could result in 'yielding' of material as the loading is applied progressively. Since the welding was not conducted by the author and it is impossible to determine the actual distributions and magnitudes of the residual stresses within the cross-section. However, the results suggest that we should not under-estimate the effect of residual stresses due to local transverse welds, especially when the cross-section is only partially affected by welding. Further investigation in this area should be carried out.

4.5.2   Comparisons of Test Results

From Figures 4.9 to 4.16, it can be seen that the program INSTAF can give conservative predictions of the behaviour of aluminium members with or without welds. Since the welded beams were not intended to be tested up to failure, using the maximum applied load for comparisons become less suitable. The load, which corresponds to a central deflection of 30 mm and 60 mm for beams with 1000 mm span and 2000 mm span respectively, are chosen ~~arbitrary~~ arbitrary for comparisons. The comparisons are shown in Table 4.6 on which the experimental loads of Q_{30} and Q_{60} are the mean values of the test results. The theoretical values of Q_{30} and Q_{60} are obtained by inputting the mean values of $\sigma_{0.2}$ and/or $\sigma_{0.2}^{*}$ (see Tables 4.3 and 4.4) into the program INSTAF. From Table 4.6, we can observe that the maximum difference between the experimental and theoretical values of Q_{30} or Q_{60} is less than 10%. The difference is larger for fully-welded beams because the area of

fillet welds is neglected in the computer simulation (see Section 4.4.4). However, for centrally-welded beams, the average reduction in bending strength is about 10.1% in test. The theoretical reduction predicted by INSTAF is about 9.8%. Therefore, we can conclude that the reliability of the program INSTAF is strongly supported by the generally good agreement between the experimental and theoretical results of aluminium beams with or without welds.

4.6   Conclusions

1. For heat-affected material, the reductions in 0.2% proof stress and ultimate stress are about 35% and 17% respectively.

2. The fully heat-affected zone material shows a reduction in strength but not in ultimate elongation. Therefore, loss of ductility may occur only on the partially heat-affected zone.

3. The effect of residual stresses due to local transverse welds should not be under-estimated. Particular attention has to be paid to those cross-section which is only partially affected by local transverse welds.

4. The program INSTAF can predict the behaviour of aluminium members with or without welds, erring on the conservative side. The reliability of the theoretical studies described in Chapter 3 is strongly supported by the generally good agreement between the experimental and theoretical results of the aluminium beams.

References

[1] Edward, S. P. W., "HAZ Effects in Transversely Welded Aluminium Beams", Part II Project, University of Cambridge, April 1982.

[2] British Standards Institution, BS 18, "Methods for Tensile Testing of Metals Part I Non-ferrous Metals", 1970.

[3] British Standards Institution, Draft British Standard BS 8118, "Code of Practice for the Design of Aluminium Structures", 1985.

[4] Webber, D., "Strength of Welded 232 Al Zn Mg Alloy", Project No. 7559, Royal Armament Research and Development Establishment (Christchurch), 1983.

[5] Techanitisawad, A., "Effect of HAZ Softening in Longitudinally Welded 7019 Beams", Part II Project, University of Cambridge, April 1984.

[6] Robertson, I., "Strength Loss in Welded Aluminium Structures", Ph.D Thesis, University of Cambridge, 1985.

[7] Kelsey, R. A., "Effect of Heat Input on Welds in Aluminium Alloy 7039", Welding Journal, Welding Research Supplement, 1971.

FLEXURAL-TORSIONAL BUCKLING OF ALUMINIUM MEMBERS

When an unrestrained member is bent about its major axis, it may buckle by deflecting laterally and twisting at a load which is significantly less than the maximum load predicted by an in-plane analysis. This flexural-torsional buckling may occur while the member is still elastic, or after some yielding due to in-plane bending and compression has occurred. However, most of the studies on flexural-torsional behaviour of members were mainly confined to steel structures and the research on aluminium structures was very limited. A computer program called BIAXIAL is, therefore, used to analyse the flexural-torsional buckling and biaxial bending of aluminium members. The members subjected to biaxial bending will be discussed in Chapter 6. The basic assumptions and formulations of BIAXIAL will be discussed in Section 5.1. The parametric studies for flexural-torsional buckling of aluminium members will be presented in Sections 5.3 and 5.4. In this chapter, aluminium members both with or without longitudinal and local transverse welds will be studied.

5.1   Description of the Program BIAXIAL

The program BIAXIAL was originally developed by one of the research students in Civil and Structural Engineering Department at University of Sheffield [1]. The program was then modified to simulate the three dimensional behaviour of aluminium members having almost any open cross-section composed of a series of flat plates. Program BIAXIAL is a finite element program and the displacement model is used to arrive at the force displacement relationship for a beam-column element by considering the principle of vir-

tual work. The program can follow the loss of stiffness due to spread of yield within the cross-section and hence trace the three dimensional load-deflection response up to collapse. The effect of twisting and warping on stiffness is taken into account. The influence of residual stresses and initial out-of-straightness is also included in the analysis. The formulation results in finite element equations and the Newton-Raphson method is used to solve the load-deformation characteristics of the beam-column for both the elastic and inelastic ranges. The stress-strain relationship chosen is also the piece-wise form of Ramberg-Osgood formula (see Section 2.2.4). The simulation of longitudinal and local transverse welds within the member is basically the same as in the program INSTAF (see Section 3.1)

5.1.1 General Formulation of the Program BIAXIAL

The following assumptions have been used in the analysis:

1. The beam-column has a general open cross-section.

2. Transverse displacements are much larger than the longitudinal ones.

3. The member length is assumed very large compared with its cross-sectional dimensions.

4. No distortion of the cross-section occurs apart from warping.

5. The shearing deformation in the mid-surface of the thin-walled plate is extremely small and can be neglected.

6. Yielding is governed by normal stresses only.
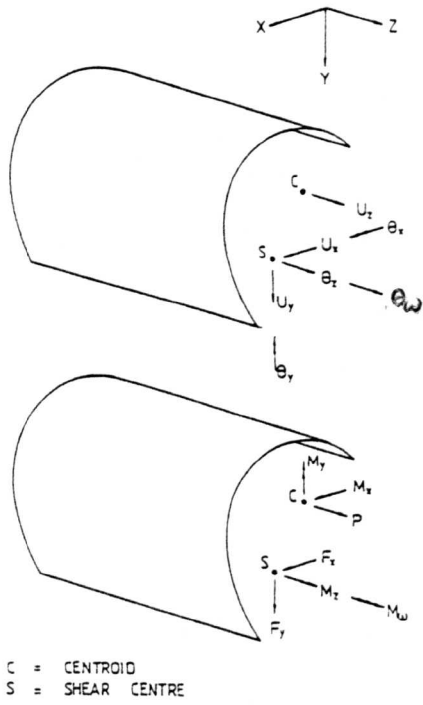
Figure 5.1 Finite Element Nodal Displacements and Stress Resultants
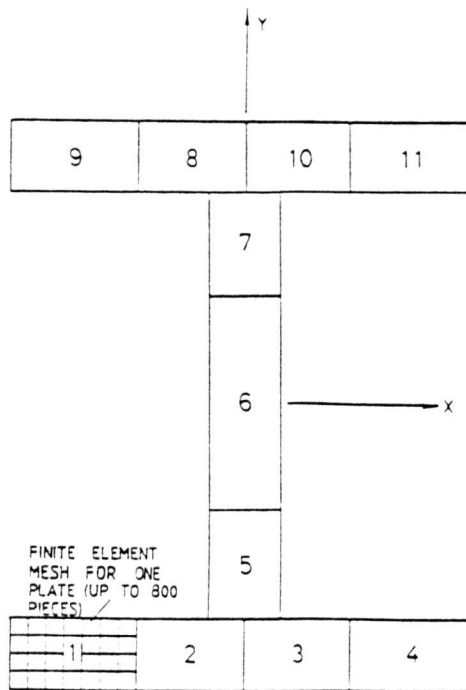
Figure 5.2 Finite Element Mesh within the Cross-section

The steps involved in the finite element program BIAXIAL are basically the same as for program INSTAF (see Section 3.1.1). The background theory and the derivation of the governing differential equations for beam-columns in three dimensions can be referred to references [1] and [2].

At each node of a beam-column element there are seven degrees of freedom $(u_z, u_x, u_y, \theta_x, \theta_y, \theta_z, \theta_\omega)$ and the element undergoes axial, flexural and torsional displacements under the action of joint forces $(P, F_x, F_y, M_x, M_y, M_z, M_\omega)$ as shown in Figure 5.1. Figure 5.2 shows the cross-section and gives details about the pattern of the finite elements. The program is capable of analysing any type of residual stress pattern whether it is symmetrical or not. The cross-section is divided into a series of plates and each plate can have different material properties to represent the heat-affected material. Each plate is then sub-divided into lots of small elements (up to 800) to trace the spread of yield within the cross-section. This method of sub-division is accurate enough to evaluate the sectorial properties of the cross-section and the determination of the sectorial properties can be referred to references [2], [3], [4] and [5].
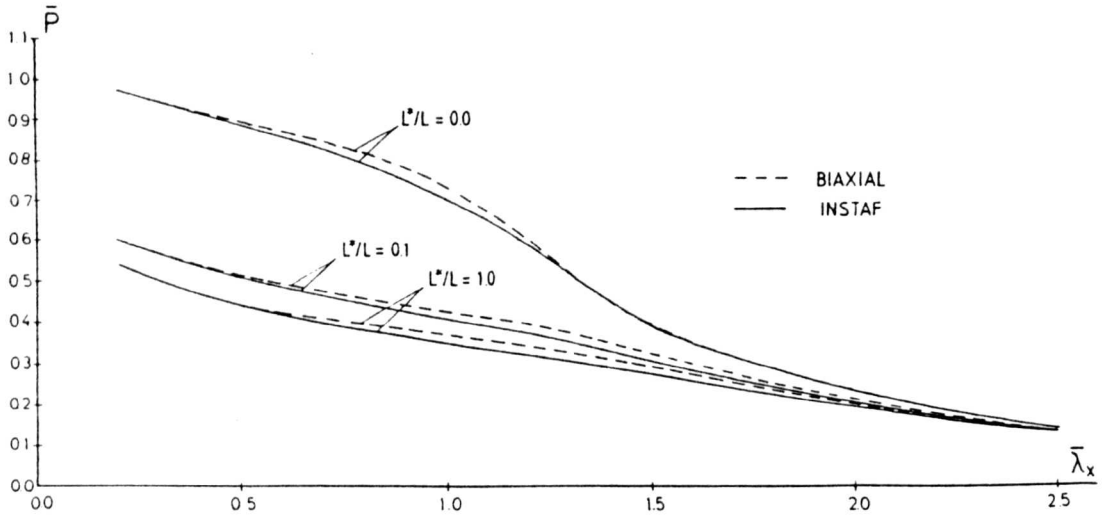
Figure 5.3 Comparison between the Column Curves Obtained by Programs BIAXIAL and INSTAF

5.2   Comparisons with Theoretical and Experimental Results

5.2.1   Comparison with the Program INSTAF

Figure 5.3 shows the comparison between the column curves obtained by programs INSTAF and BIAXIAL. The columns are pin-ended with axial load and fail by major axis buckling. The ratios $\frac{L^*}{L}$ equal to 0, 0.1, and 1.0 are considered (see Figure 3.10). Since program INSTAF can only simulate the in-plane behaviour of aluminium members, apart from the degrees of freedom corresponding to the major axis buckling all other degrees of freedom are restrained in the program BIAXIAL. From the comparison, the maximum difference between the curves is less than 6% and the difference is mainly caused by the effect of axial load on the column stiffness being considered in program INSTAF while this effect is neglected in program BIAXIAL.

Specimen No.	Length (in.)	Eccentricity (in.)	P_{ult} (BIAXIAL) (lb.)	P_{ult} (Hill and Clark) (lb.)	Difference (%)
A1	39.94	0.0	10520	10500	0.19
A2	39.97	0.25	10340	10250	0.88
A5	39.97	1.0	8270	8140	1.60
A7	60.00	0.5	4630	4540	1.98
A9	60.03	1.0	3820	3840	-0.52
A10	69.94	0.0	3415	3335	2.40
		0.5	3244	3100	4.64
		1.0	2835	2680	5.78
A13	100.06	0.0	1670	1655	0.91
		0.5	1625	1610	0.93
B1	29.91	0.0	107100	105600	1.42
B2	29.94	1.0	60630	60500	0.21
B5	50.07	0.0	74790	71900	4.02
B9	70.14	0.0	42961	42000	2.29
B10	70.08	1.0	29090	27600	5.40

Table 5.1: Comparison between Experimental Results Obtained by Hill and Clark and Theoretical Results Obtained by Program BIAXIAL

5.2.2 Comparison with the Experimental Column Results Obtained by Hill and Clark [6]

In 1951, Hill and Clark carried out experimental studies on the lateral buckling of I- and H-section columns of high strength aluminium alloy subjected to simultaneous axial load and bending in the plane of web. The combined loading was obtained by testing the members as eccentrically loaded columns. Some of their column results which failed in a lateral torsional buckling are selected for comparison and presented in Table 5.1. It can be seen that a very good correlation is obtained and the maximum difference between the experimental and theoretical buckling loads is less than 6%.

TEST 68

TEST 24

LOAD (T)

LOAD (T)

DEFL. (MM)

DEFL. (MM)

DEFLECTION IN X-DIRECTION (LIEGE)
DEFLECTION IN Y-DIRECTION (LIEGE)
DEFLECTION IN X-DIRECTION (BIAXIAL)
DEFLECTION IN Y-DIRECTION (BIAXIAL)
O
Δ
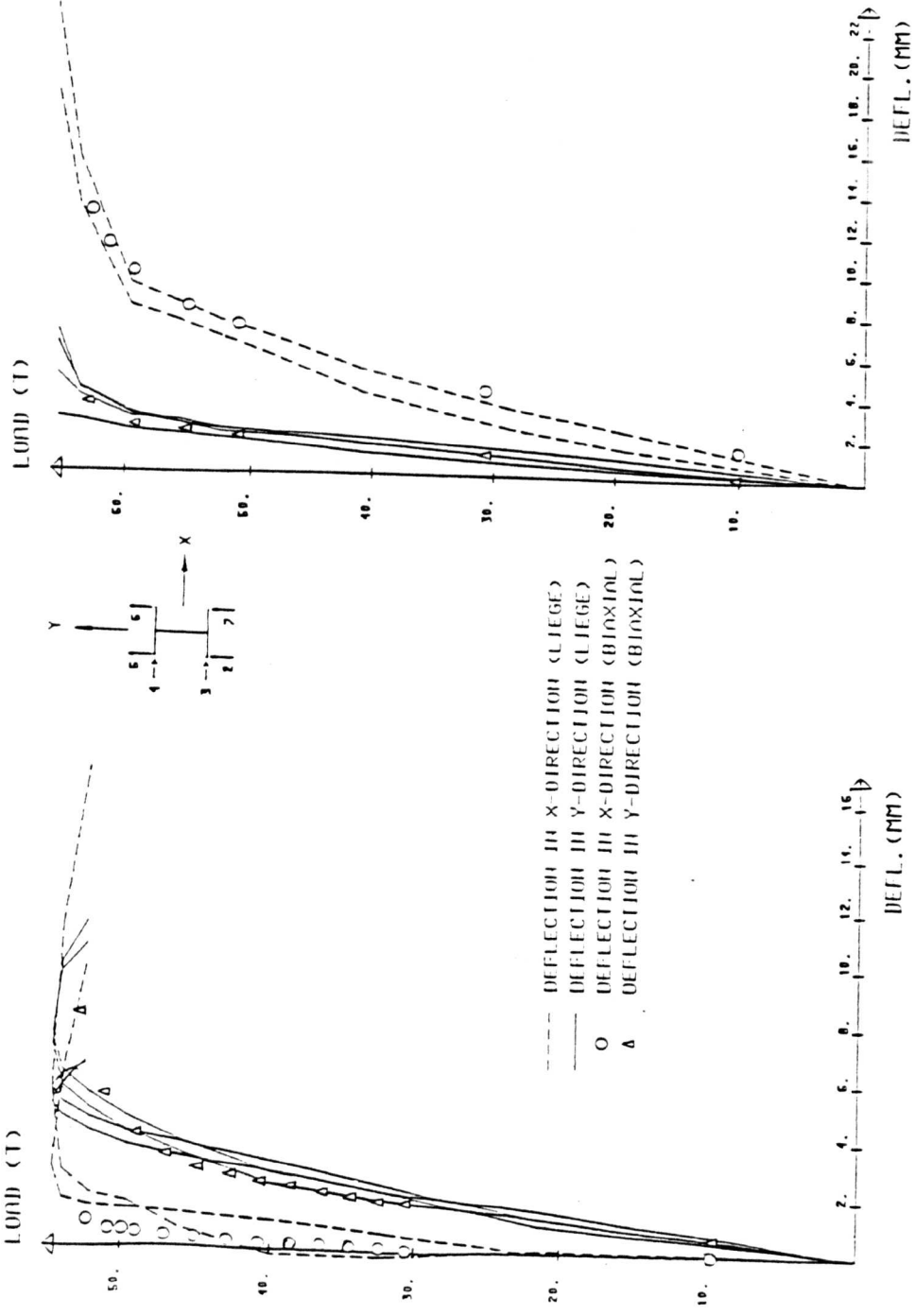
Figure 5.4 Comparison with Anslijn's Results [7]

Test No.	λ_y	β_x	β_y	σ_y (Kg/cm^2)	P_{ult} (Anslign) (Kg)	P_{ult} (BIAXIAL) (Kg)	Difference (%)
18	60.2	-1	-1	2066	53500	51700	3.4
24	60.2	1	-1	2245	55000	52400	4.7
59	60.2	-1	-1	2479	60000	58300	2.8
68	60.2	0	0	2347	65000	63500	2.3
75	96.4	-1	1	2401	26200	25700	1.9
80	96.3	0	1	2401	25200	24100	4.4

Table 5.2: Comparison between Anslign's Test Results [7] and Program BIAXIAL
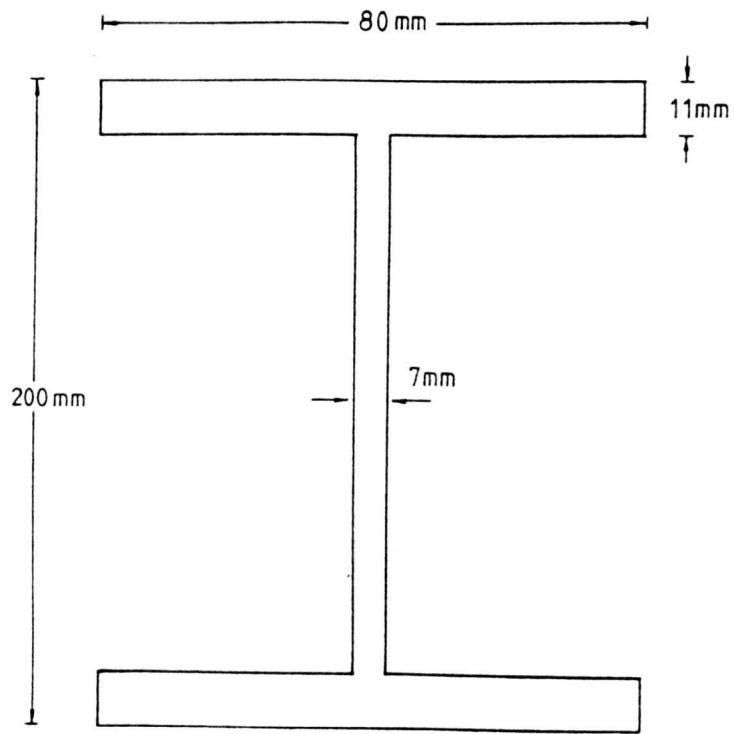
Figure 5.5 Cross-section Used for Parametric Studies

5.2.3   Comparison with the Tests on Beam-columns Subjected to Thrust and Biaxial Bending

From the literature review (see Sections 2.4 and 2.5), there are no experimental or theoretical studies which have been carried out on biaxial bending of aluminium members, therefore, the author can only select the biaxial tests on steel members to compare with program BIAXIAL. As mentioned in Section 2.2.4, when the value of knee factor, n, in the Ramberg-Osgood formula tends to infinity, the stress-strain curve will tend to the elastic/perfectly plastic relationship of mild steel. Therefore program BIAXIAL can also analyse the three dimensional behaviour of steel members when a large value of n is input (say $n > 1000$). Several comparisons have been made with the tests on steel I beam-columns subjected to biaxially eccentric compression conducted by Anslijn in 1983 [7]. Table 5.2 shows the comparisons and the maximum difference of less than 5% is obtained. A typical comparison between the theoretical and experimental in-plane and out-of-plane deflections at mid-height of the beam-column is shown in Figure 5.4 for test no. 24 and 68. It can be seen that very good agreement for both the in-plane and out-of-plane deflection is obtained.

5.3   Parametric Studies of Aluminium Members

The aim of the parametric studies is to investigate the general behaviour of aluminium members under flexural-torsional buckling. Similar to Chapter 3, the parametric studies are also divided into three main areas (1) column (2) beam (3) beam-column; and both the effects of longitudinal welds and local transverse welds will be studied. All the principal results can be found in Table 5.3. ~~Except~~ Unless otherwise stated, the cross-section chosen for parametric studies is shown in Figure 5.5. and the mechanical properties of parent and RSZ material are:

$$
\begin{aligned}
\underline{Parent:} \quad E &= 70000 \quad N/mm^2 \\
\sigma_{0.2} &= 250 \quad N/mm^2 \\
n &= 25 \\
\underline{RSZ:} \quad E^* &= 70000 \quad N/mm^2 \\
\sigma_{0.2}^* &= 125 \quad N/mm^2 \\
n^* &= 10
\end{aligned}
$$

The aluminium members considered herein are initially twisted in a sine function shape with initial twisting angle of 0.01 radian at mid-span. The initial displacements in the major and minor axis directions are also assumed to be sine functions, and the maximum values at mid-span are equal and are arbitrary assumed to be $\frac{L}{1000}$. All the aluminium members are pin-ended and warping deformation is unrestrained but the rotation is prevented at both ends.

Cases	Reference	$\frac{A^*}{A}$ or $\frac{L^*}{L}$	Principal Results	Remark
Column	C1-N	$\frac{L^*}{L} = 0.0$	Figure 5.6	Study the effect of section geometry on non-welded columns
	C2-LW	$\frac{A^*}{A} = 0.0, 0.1, 0.2,$ 0.3, 0.4, 0.5 and 1.0	Figure 5.7	Study the effect of symmetric longitudinal welds (without residual stresses)
	C3-LW	$\frac{A^*}{A} = 0.0, 0.1, 0.2,$ 0.3,0.4, 0.5 and 1.0	Figure 5.8	Study the effect of symmetric longitudinal welds (with residual stresses)
	C4-LW	$\frac{A^*}{A} = 0.1$	Figure 5.9	Study the effect of unsymmetric longitudinal welds
	C5-LW	$\frac{A^*}{A} = 0.3$	Figure 5.10	
	C6-LW	$\frac{A^*}{A} = 0.5$	Figure 5.11	
	C7-TW	$L^* = 30mm$ at both ends	Figure 5.12	Study the behaviour of end-welded columns
	C8-TW	$L^* = 50mm$ at mid-height	Figure 5.13	Study the behaviour of centrally-welded columns
Beam	B1-N	$\frac{L^*}{L} = 0.0$	Figure 5.15	Study the effect of section geometry on non-welded beam
	B2-N	$\frac{L^*}{L} = 0.0$	Figure 5.16	Study the effect of E on non-welded beams
	B3-N	$\frac{L^*}{L} = 0.0$	Figure 5.17	Study the effect of $\sigma_{0.2}$ on non-welded beams
	B4-N	$\frac{L^*}{L} = 0.0$	Figure 5.18	Study the effect of n on non-welded beams
	B5-N	$\frac{L^*}{L} = 0.0$	Figure 5.19	Study the effect of $\delta_{x(max)}$ on non-welded beams
	B6-N	$\frac{L^*}{L} = 0.0$	Figure 5.20	Study the effect of unequal end moments ($\beta_x = 1,0,-1$) on non-welded beams
	B7-LW	$\frac{A^*}{A} = 0.0, 0.1, 0.2,$ 0.3, 0.4, 0.5 and 1.0	Figure 5.21	Study the effect of symmertic longitudinal welds on beams
	B8-LW	$\frac{A^*}{A} = 0.1$	Figure 5.22	Study the effect of unsymmetric longitudinal welds on beams
	B9-LW	$\frac{A^*}{A} = 0.3$	Figure 5.23	
	B10-LW	$\frac{A^*}{A} = 0.5$	Figure 5.24	
	B11-TW	$L^* = 30mm$ at both ends	Figure 5.25	Study the behaviour of end-welded beams
	B12-TW	$L^* = 50mm$ at mid-span	Figure 5.26	Study the behaviour of centrally-welded beams

Table 5.3: List of Cases in Parametric Studies of Aluminium Members under Flexural-torsional Buckling

Cases	Reference	$\frac{A^*}{A}$ or $\frac{L^*}{L}$	Principal Results	Remark
Beam-column	BC1-N	$\frac{L^*}{L} = 0.0$	Figures 5.27 and 5.28	$\lambda_y = 30,50,70,90$ and 120, $\beta_x = 1$
	BC2-N	$\frac{L^*}{L} = 0.0$	Figure 5.29	$\lambda_y = 50,70,120$ and 170, $\beta_x = 0$
	BC3-N	$\frac{L^*}{L} = 0.0$	Figure 5.30	$\lambda_y = 90,120$ and 170, $\beta_x = -1$
	BC4-LW	$\frac{A^*}{A} = 0.0, 0.1, 0.3,$ 0.5 and 1.0	Figure 5.31	$\lambda_y = 30, \beta_x = 1$
	BC5-LW	$\frac{A^*}{A} = 0.0, 0.1, 0.3,$ 0.5 and 1.0	Figure 5.32	$\lambda_y = 70, \beta_x = 1$
	BC6-LW	$\frac{A^*}{A} = 0.0, 0.1, 0.3,$ 0.5 and 1.0	Figure 5.33	$\lambda_y = 90, \beta_x = 1$
	BC7-TW	$L^* = 30mm$ at both ends	Figure 5.34	$\lambda_y = 30, \beta_x = 1$
	BC8-TW	$L^* = 30mm$ at both ends	Figure 5.35	$\lambda_y = 70, \beta_x = 1$
	BC9-TW	$L^* = 30mm$ at both ends	Figure 5.36	$\lambda_y = 90, \beta_x = 1$
	BC10-TW	$L^* = 50mm$ at mid-height	Figure 5.37	$\lambda_y = 30, \beta_x = 1$
	BC11-TW	$L^* = 50mm$ at mid-height	Figure 5.38	$\lambda_y = 70, \beta_x = 1$
	BC12-TW	$L^* = 50mm$ at mid-height	Figure 5.39	$\lambda_y = 90, \beta_x = 1$

Table 5.3: cont.

5.3.1 Parametric Studies of Aluminium Columns

5.3.1.1 Effect of Section Geometry on Non-welded Columns

Figure 5.6 shows the effect of section geometry for I-section columns with different $\frac{H}{W}$ values of 1.0, 2.0, 2.5, 4.375 and 5.625, and the curves cross over one another at $\overline{\lambda}_y = 0.95$. For $\overline{\lambda}_y < 0.95$, before the cross over, the $\overline{P} - \overline{\lambda}_y$ curves are higher for higher values of $\frac{H}{W}$. However for $\overline{\lambda}_y > 0.95$, the $\overline{P} - \overline{\lambda}_y$ curves are higher for lower values of $\frac{H}{W}$, and all the curves will join together as the columns buckle elastically. The cause of the cross over of curves with different values of $\frac{H}{W}$ has been explained schematically by Hong [8], and is due mainly to the combined effects of strain hardening and initial out-of-straightness of columns with different $\overline{\lambda}_y$.

CURVE	W	H	T_F	T_W	y/r_y
A	80	80	11	7	1.92
B	80	160	11	7	4.30
C	80	200	11	7	5.60
D	80	350	11	7	11.45
E	80	450	11	7	15.91
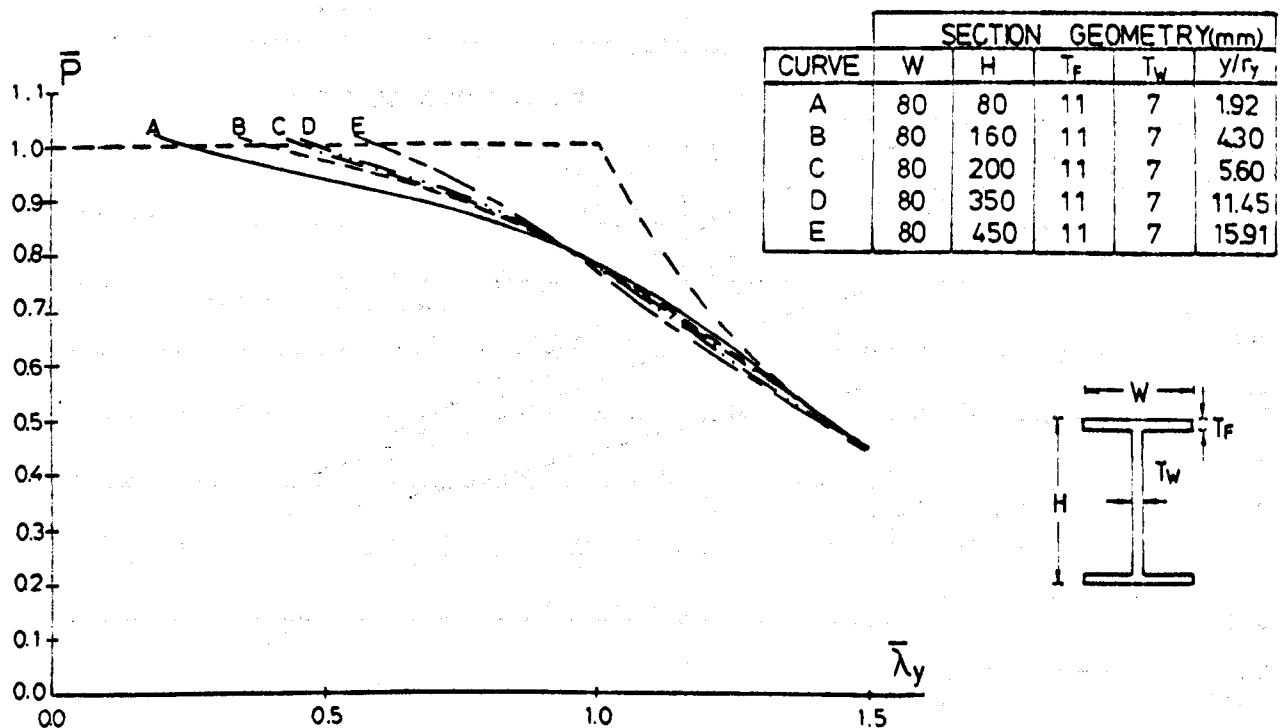
Figure 5.6 Effect of Section Geometry on Columns
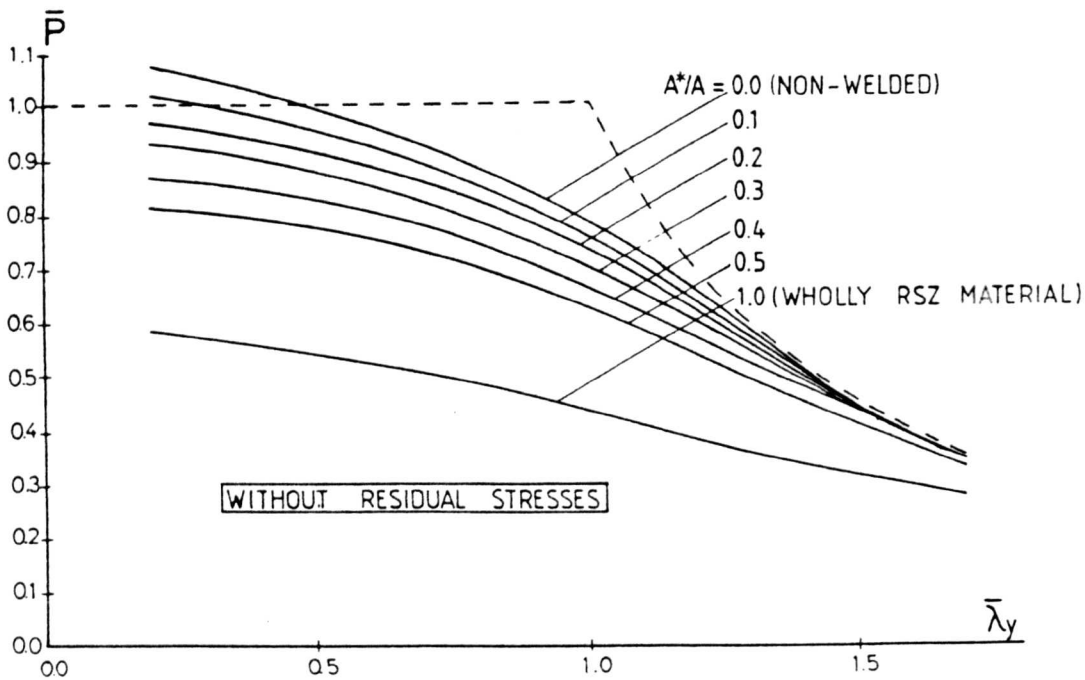
Figure 5.7 Study of Symmetric Longitudinally Welded Columns (without Residual Stresses)
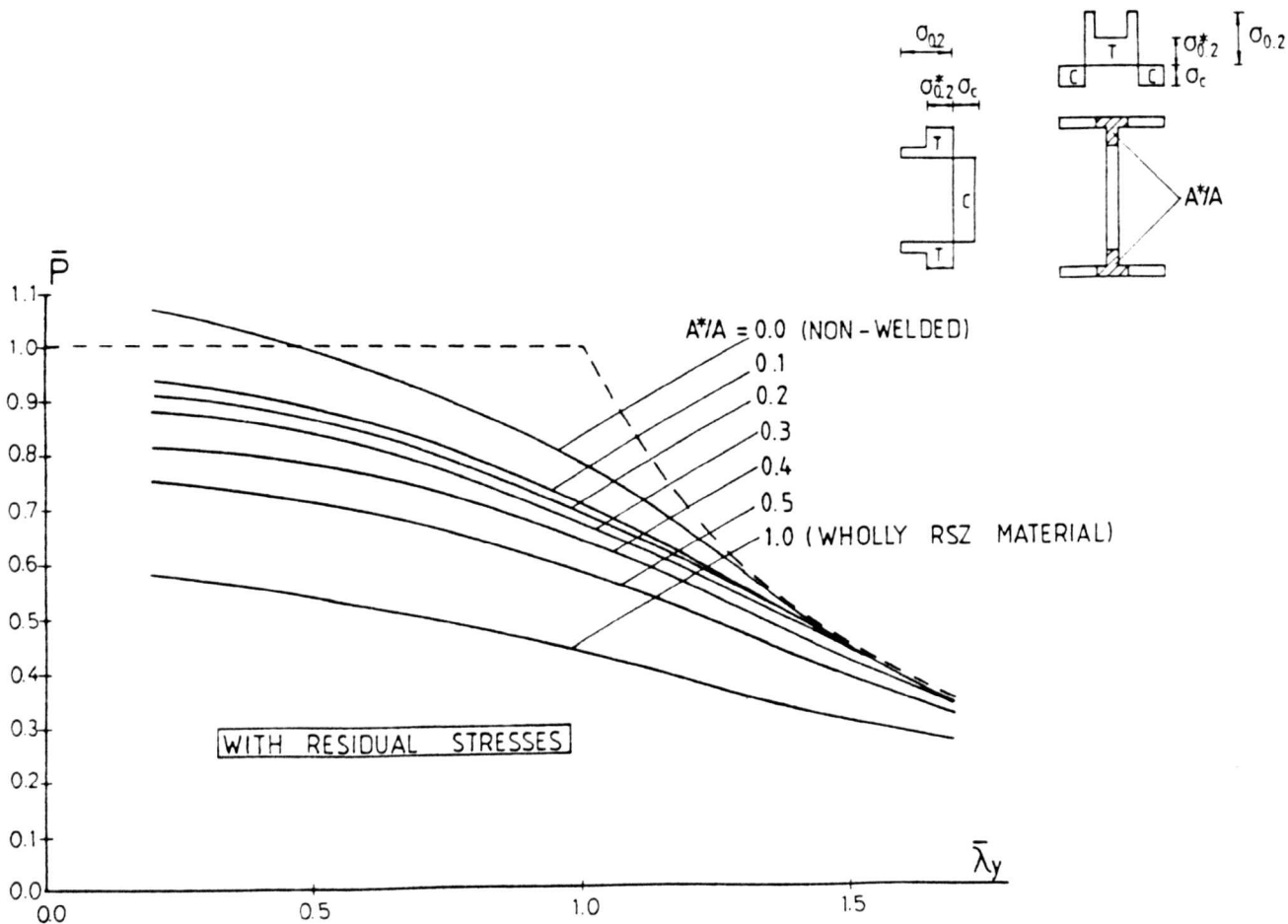
Figure 5.8 Study of Symmetric Longitudinally Welded Columns (with Residual Stresses)

5.3.1.2   Effect of Symmetric Longitudinal Welds on Columns

Figures 5.7 and 5.8 show the $\overline{P} - \overline{\lambda}_y$ curves for the longitudinally welded columns with different values of $\frac{A^\bullet}{A}$, ranging from 0.0, 0.1, 0.2, 0.3, 0.4, 0.5 to 1.0, and it is assumed that the RSZ is located symmetrically at the two flange-web junctions. The purpose of Figure 5.7 is to investigate the effect of RSZ softening only, so the residual stresses are neglected in the analysis. But the combination of the two effects are studied in Figure 5.8 and the idealized residual stress distribution is also presented in the figure. The Cambridge tendon force model is used to determine the value of compressive residual stress, σ_c, and can be referred to equation (2.13). The tensile residual stresses are assumed to be equal to $\sigma_{0.2}^*$ in the reduced-strength zones and $\sigma_{0.2}$ outside the reduced-strength zones. The widths of the tension zones are determined by considering the equilibrium between the tensile and compressive residual stresses. It is worthwhile to point out that for for $\frac{A^\bullet}{A} < 0.5$, the tension zones are always greater than the reduced-strength zones.

From Figure 5.7, we can observe that the buckling strength of longitudinally welded columns will be decreased as the ratio of $\frac{A^\bullet}{A}$ is increased. The weakening effect becomes insignificant as the $\overline{\lambda}_y$ becomes larger and the welded columns tend to buckle elastically. The reason can be explained in terms of the mechanical properties of the parent metal and RSZ material; and the stress level within the welded columns. When the effect of residual stresses is included in the longitudinally welded columns, Figure 5.8 shows that the presence of residual stresses could further reduce the strength of columns by about 8%, and the reduction is more or less independent of the values of $\frac{A^\bullet}{A}$.
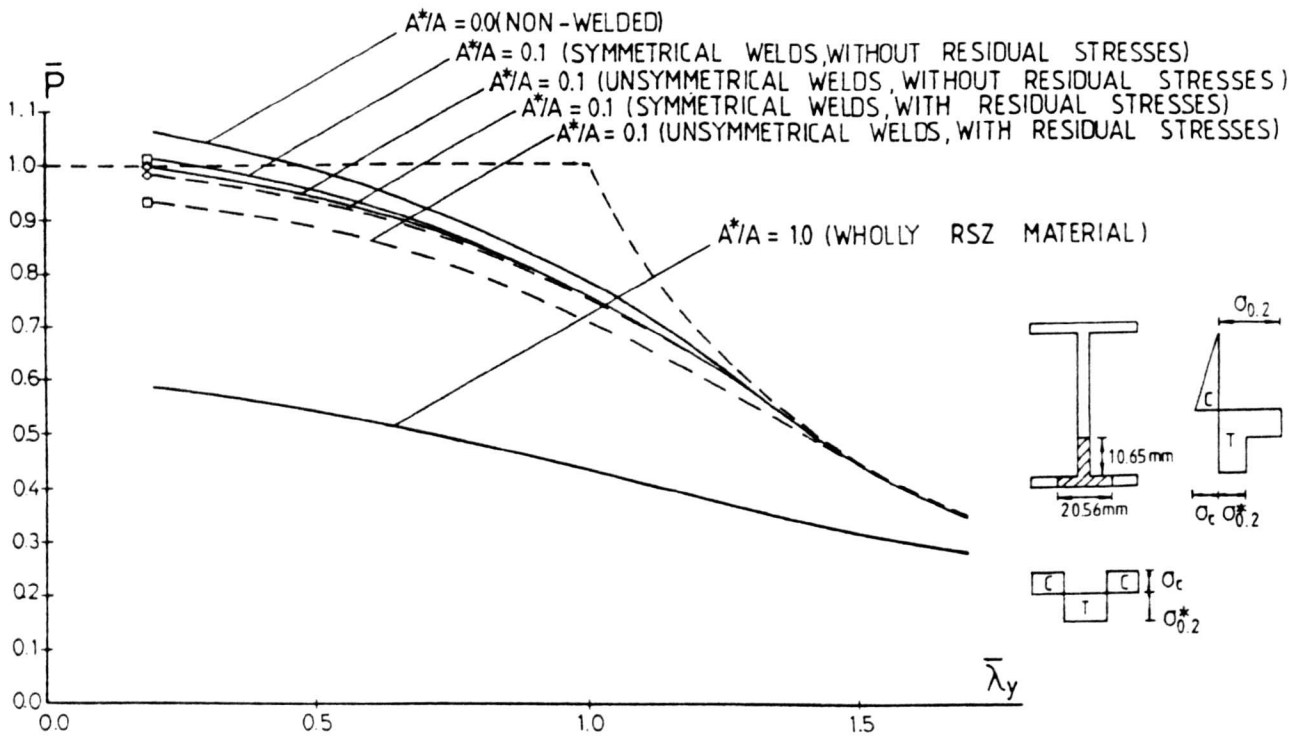
Figure 5.9 Study of Unsymmetric Longitudinally Welded Columns
($\frac{A^{\bullet}}{A} = 0.1$)
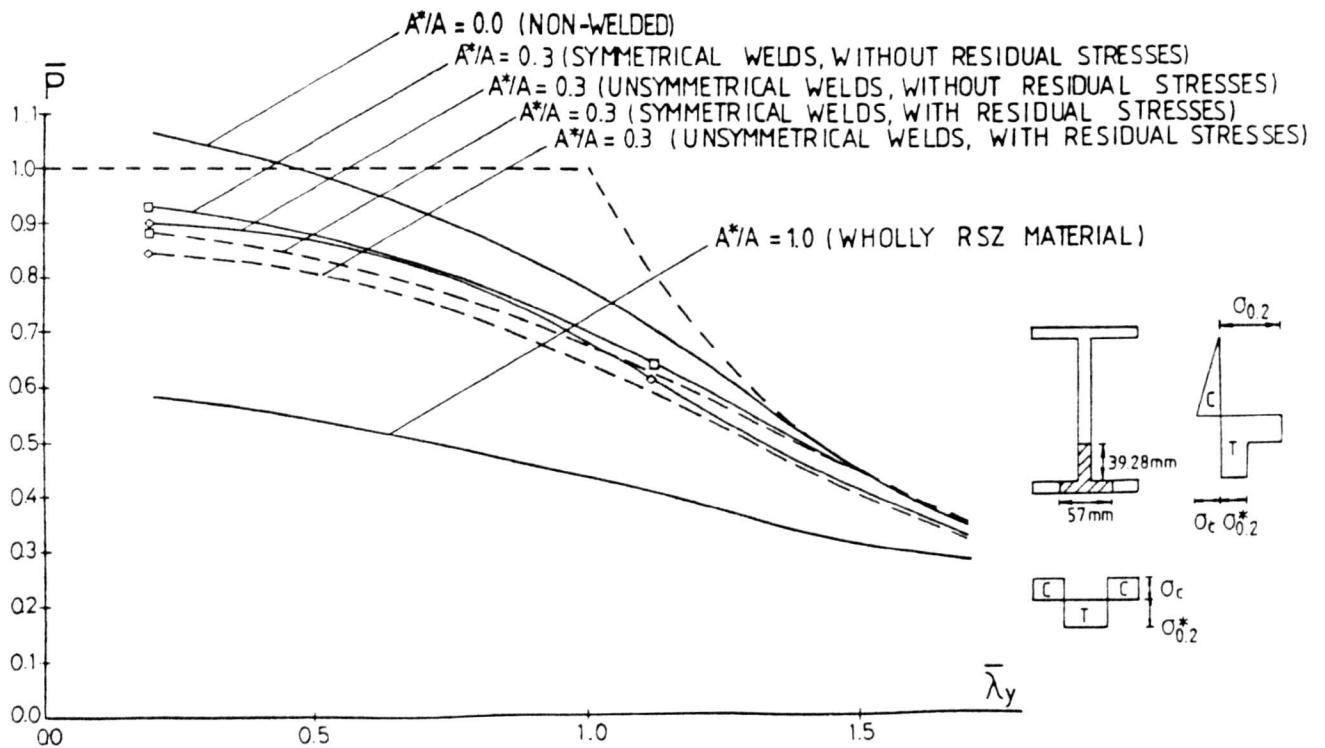
Figure 5.10 Study of Unsymmetric Longitudinally Welded Columns
($\frac{A^{\bullet}}{A} = 0.3$)

5.3.1.3   Effect of Unsymmetric Longitudinal Welds on Columns

In practice, the longitudinal welds are very often laid on one side of the member and result in unsymmetric RSZ softening within the cross-section. This situation is very common in ship and bridge structures. However, in this type of analysis, the determination of a rational pattern of residual stress distribution becomes difficult. The Cambridge tendon force model (see Section 2.3.3.3) sometimes fails to represent the distribution of residual stress because of the relatively high tensile stresses and the equilibrium condition becomes unsatisfactory.

Figures 5.9 to 5.11 show the effect of unsymmetric longitudinal welds on welds on columns with $\frac{A^\bullet}{A} = 0.1, 0.3$ and 0.5 respectively, and the comparison between columns with symmetric and unsymmetric longitudinal welds is also presented. The RSZ within the cross-section is located at the concave side of the column. The assumed residual stress distributions shown in Figures 5.9 and 5.10 are based on Cambridge tendon force model and reference [9]. In order to satisfy the equilibrium equation, it was found that the tension zones in the flange had to be smaller than the reduced-strength zones.[‡] For columns with $\frac{A^\bullet}{A} = 0.5$ where one of the flanges is fully-affected by welding (see Figure 5.11), the residual stress distribution is uncertain because the equilibrium condition cannot be satisfied and the Cambridge tendon force model fails to represent the residual stress distribution. Therefore, the effect of residual stresses is neglected in Figure 5.11.

[‡]For the member with symmetric longitudinal welds, the tension zones are greater than the reduced-strength zones for $\frac{A^\bullet}{A} < 0.5$
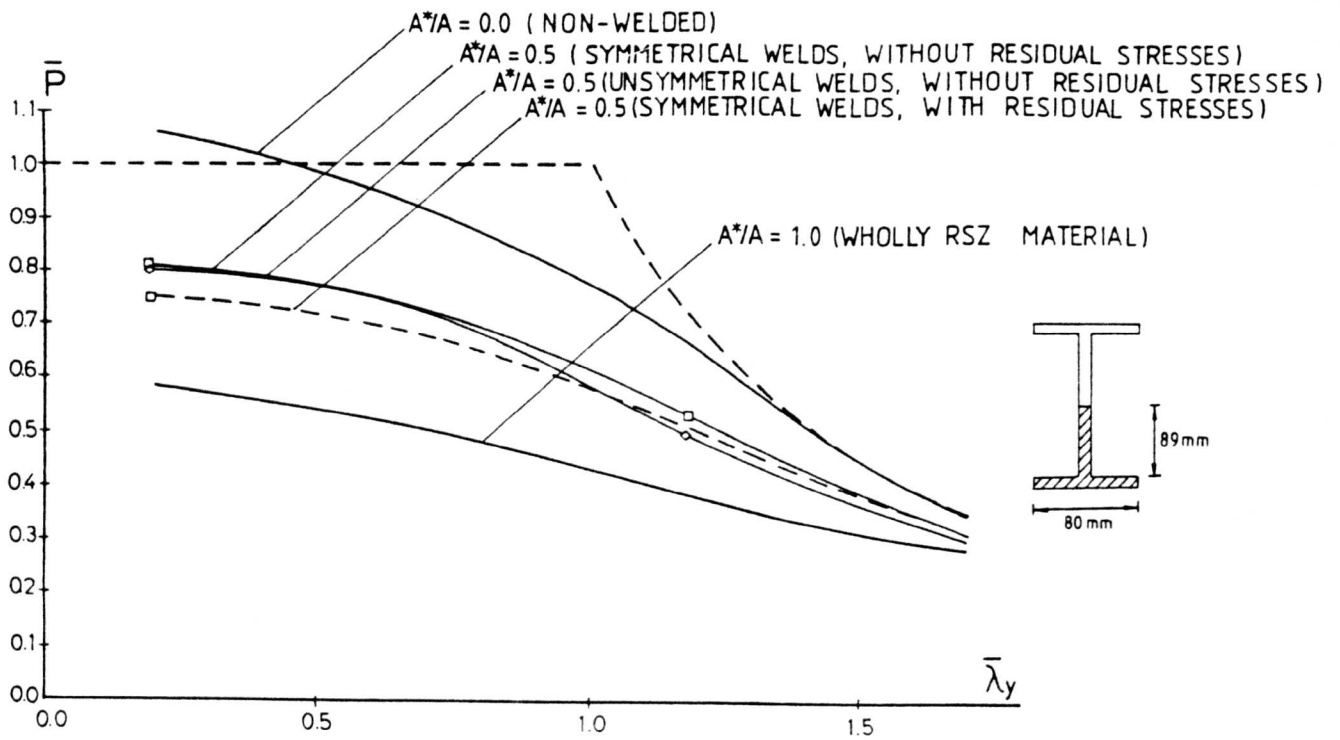
Figure 5.11 Study of Unsymmetric Longitudinally Welded Columns $(\frac{A^{\bullet}}{A} = 0.5)$

For columns with $\frac{A^*}{A} = 0.1$ and the effect of residual stresses neglected, the buckling strength of columns with symmetric or unsymmetric longitudinal welds are quite similar (see Figure 5.9). However, when the residual stresses are included in the analysis, their further reduction in buckling strength is about 8% and 2% respectively. This is expected because the area of compressive residual stress is relatively larger for columns having symmetric longitudinal welds. For columns with $\frac{A^*}{A} = 0.3$ and the effect of residual stresses neglected, both types of column show similar buckling strengths as $\overline{\lambda}_y \leq 0.85$ or the columns tend to buckle elastically (see Figure 5.10). As $\overline{\lambda}_y > 0.85$, columns having unsymmetrical longitudinal welds show lower strengths than the symmetric longitudinally welded columns by about 9%. When residual stresses are included, both types of column show about 8% maximum reduction in strength. For columns with $\frac{A^*}{A} = 0.5$ as shown in Figure 5.11, although the effect of residual stresses is neglected, similar observations are obtained. It is because for intermediate columns, instability of the members becomes important. Due to the unsymmetric nature of the RSZ, the effective cross-section will become unsymmetric as the RSZ material is sufficiently stressed and will result in extra twisting on the column. This action takes place because the axis of twist through the shear centre does not coincide with the loading axis through the centroid, and flexural-torsional buckling will occur in the columns. Since the column having an asymmetric cross-section will have a lower critical load than the column having a symmetric cross-section [10,11,12,13], thus the unsymmetric longitudinally welded columns showing lower ultimate strengths is expected.
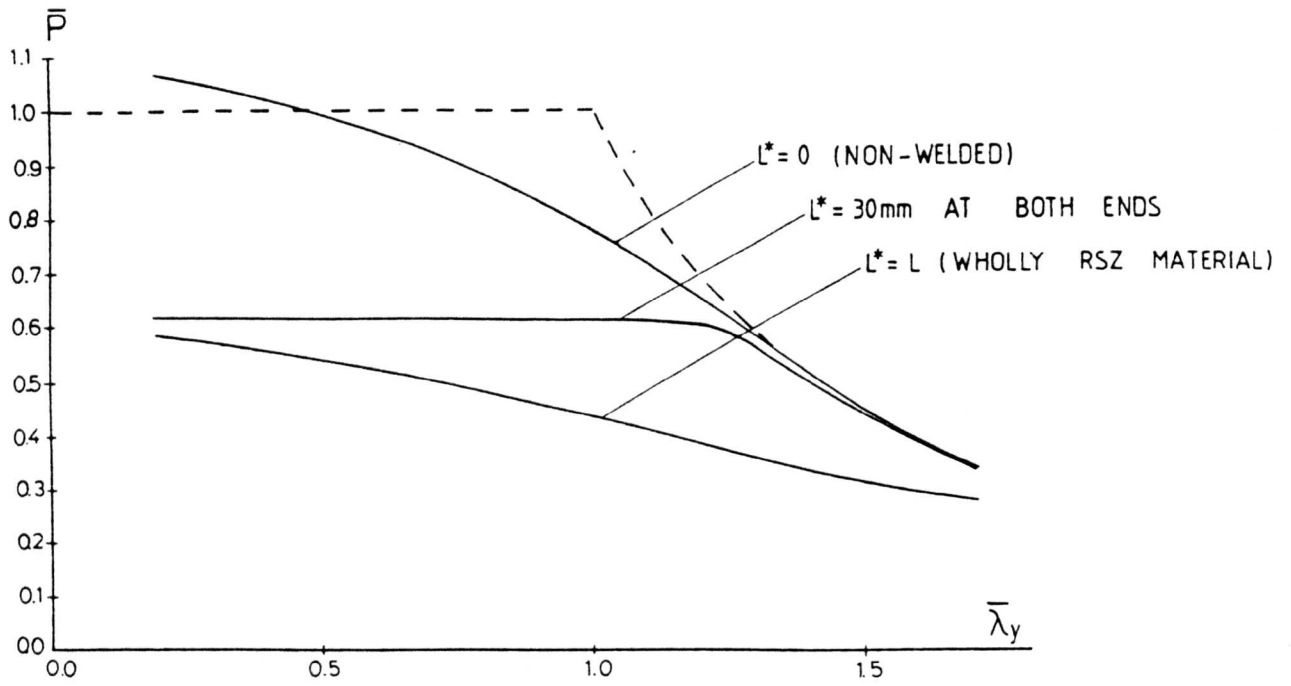
Figure 5.12 Study of End-welded Columns ($L^* = 30\ mm$ at Both Ends)
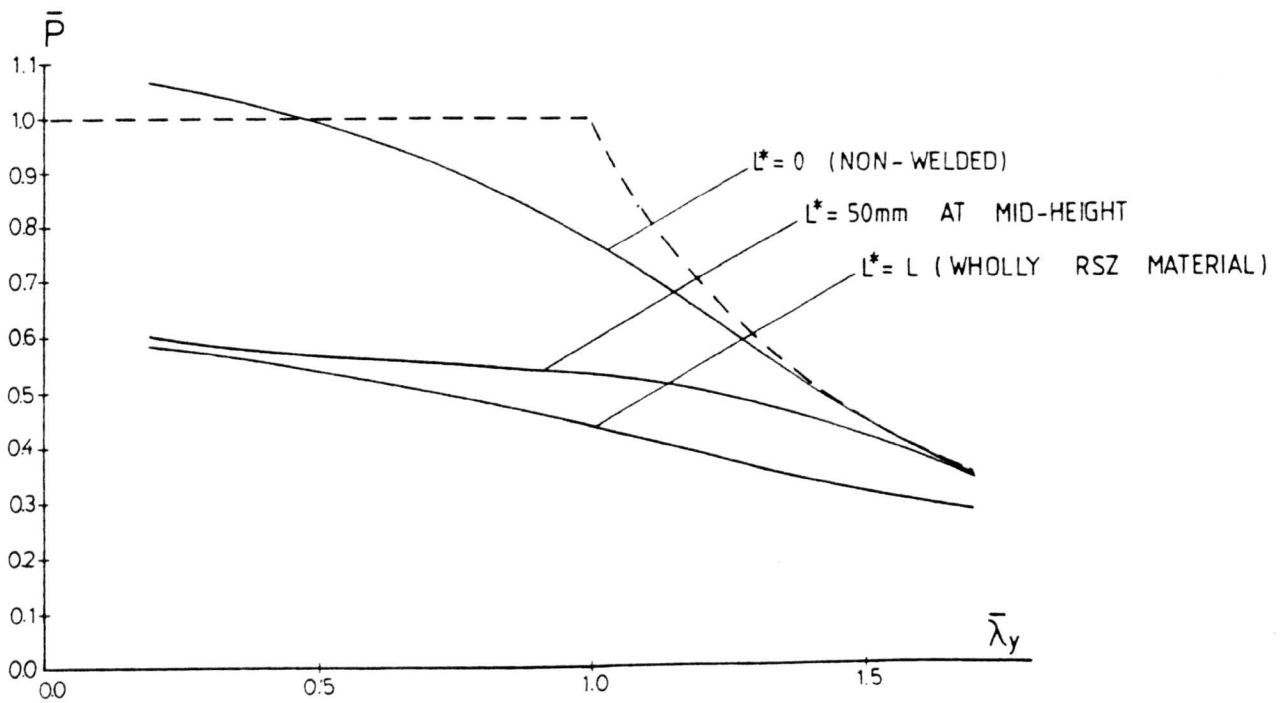
Figure 5.13 Study of Centrally-welded Columns ($L^* = 50\ mm$ at Mid-height)

5.3.1.4 Effect of Local Transverse Welds on Columns

Figures 5.12 and 5.13 show the effect of local transverse welds on columns with $L^* = 30mm$ located at both ends and $L^* = 50mm$ located at mid-height respectively. The effect of residual stresses is neglected in the analysis. Both the figures show that the presence of local transverse welds can cause severe reductions in the buckling strength of columns. Moreover, it further shows that it is unsafe to neglect this effect even if the extent of RSZ is small.

Up to now, it is worthwhile to further discuss the behaviour of columns having local transverse welds located at both ends. In BS 8118, the maximum permissible axial capacity of a non-welded aluminium column is equal to $A\sigma_{0.2}$. (or $\overline{P} = 1$). Although the strain hardening of the material is beneficial to the aluminium columns, this effect is neglected in BS 8118. For transversely welded 6000 series aluminium columns, the RSZ material shows a 50% reduction in strength (see Section 2.3.2.1). Therefore, the maximum permissible axial capacity of a transversely welded column is equal to $0.5\ A\sigma_{0.2}$ (or $\overline{P} = \omega$ and $\omega = 0.5$). in other words, we can say that two cut-off lines ($\overline{P} = 1$ and $\overline{P} = 0.5$) have to be drawn in the $\overline{P} - \overline{\lambda}_x$ or $\overline{P} - \overline{\lambda}_y$ curves to represent the maximum strength that the non-welded and transversely welded columns can carry. Therefore in BS 8118, any non-welded and transversely welded columns having $\overline{P} > 1$ or $\overline{P} > 0.5$ respectively will be controlled by material failure. In Figure 5.14, the simulation of the behaviour of end-welded columns using program INSTAF (see Figure 3.13) and BIAXIAL (see Figure 5.12) are compared. If we draw the two cut-off lines ($\overline{P} = 1$ and $\overline{P} = 0.5$) in Figure 5.14, we can observe that the non-welded and end-welded columns
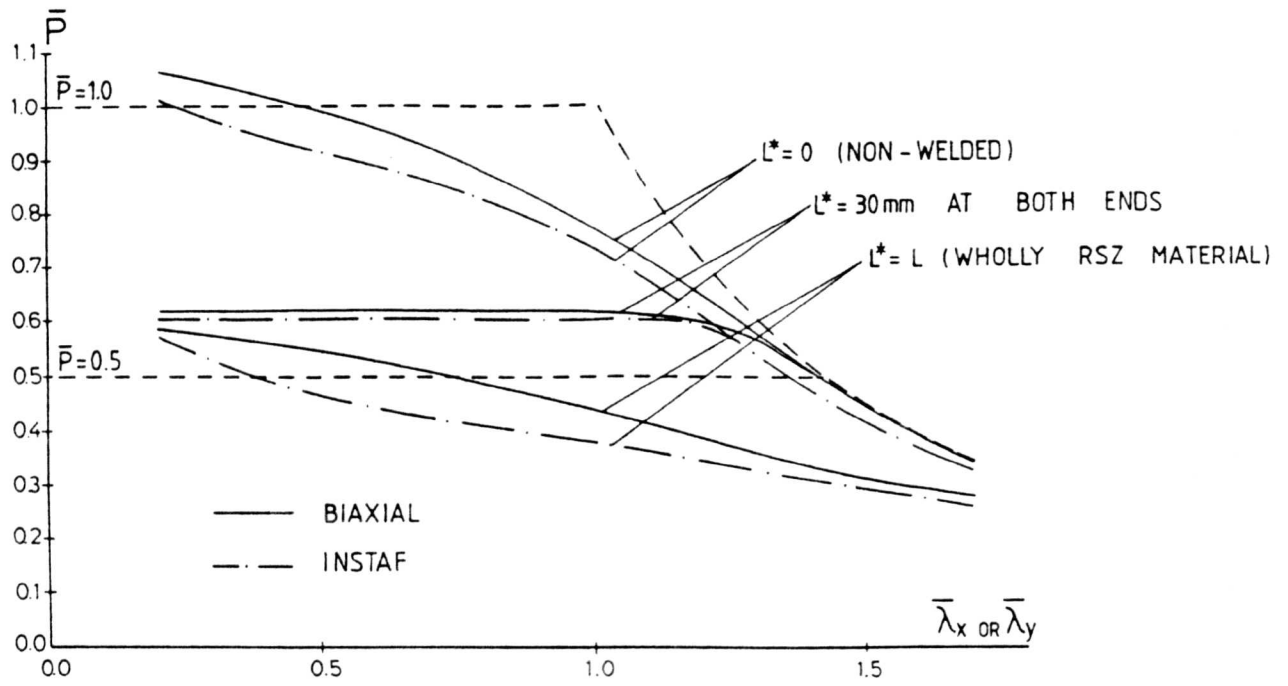
Figure 5.14 Column Curves for End-welded Columns Obtained by Programs
BIAXIAL and INSTAF

are having similar strengths as $\overline{\lambda}_x > 1.35$ or $\overline{\lambda}_y > 1.4$. When compared with the fully-welded columns, the maximum improvement in strength is about 30% in design. Therefore, two possible methods for designing end-welded columns are:

1. design the end-welded columns as if non-welded columns but the maximum strength of columns cannot be greater than $\overline{P} = \omega$ (a cut-off line)

2. design the end-welded columns as if containing wholly RSZ material

The author would recommend using method (1) in design because it tends to give higher design strengths of columns and method (2) is potentially too conservative for designing end-welded columns. But from the beam tests discussed in Chapter 4, special attentions should be paid to the effect of residual stresses because their presence may lower the buckling strength of columns. Moreover, it is worthwhile to point out that method (1) is also potentially very conservative for designing end-welded columns if the transverse welds only affect part of the cross-section. The author, therefore, suggested that a modified cut-off line $\overline{P} = 1 - (1 - \omega)\frac{A^*}{A}$ should be used in the $\overline{P} - \overline{\lambda}_x$ or $\overline{P} - \overline{\lambda}_y$ curves rather than using $\overline{P} = \omega$. When the cross-section is fully-affected by local transverse welds, i.e. $A^* = A$, the above equation will become $\overline{P} = \omega$. Finally, if the local transverse welds are not located at the ends, design method (2) should be used.

Figure 5.15 Effect of Section Geometry

CURVE	SECTION GEOMETRY (mm)				
	W	H	T_F	T_W	y/r_y
—◇—	80	80	11	7	1.92
—△—	80	160	11	7	4.30
—○—	80	200	11	7	5.60
—□—	80	350	11	7	11.45
—▽—	80	450	11	7	15.91

5.3.2   Parametric Studies of Aluminium Beams

5.3.2.1   Effect of Section Geometry on Non-welded Beams

Similar to case C1-N, Figure 5.15 shows the effect of section geometry for
I-section beams under single curvature major axis bending. The values of $\frac{H}{W}$
also range from 1.0 to 5.625. However, the $\overline{M}_x - \overline{\lambda}_M$ curves for beams behave
differently from the $\overline{P} - \overline{\lambda}_y$ curves for columns. The curves do not show any
cross over and the $\overline{M}_x - \overline{\lambda}_M$ curves are higher for lower values of $\frac{H}{W}$. The
reason is due to the compactness of the cross-section and is the same as for
steel members. For the beams with high values of $\frac{H}{W}$, the beams will fail due
to lateral-torsional instability and cannot reach the 'plastic moment' unless
the beams are very stocky.

5.3.2.2 Effect of $E, \sigma_{0.2}$, n and and $\delta_{x(max)}$ on Non-welded Beams

The effects of $E, \sigma_{0.2}$, n and $\delta_{x(max)}$ on non-welded beams under single curvature bending are shown on Figures 5.16 to 5.19. In Figure 5.16, the Young's modulus E, is varied from 65,000 N/mm^2 to 75,000 N/mm^2 and we can observe that the variation of E will have no effect on $\overline{M}_x - \overline{\lambda}_M$ curves. In Figure 5.17, the 0.2% proof stresses, $\sigma_{0.2}$, is varied from 125 N/mm^2 to 500 N/mm^2 and we can find that the $\overline{M}_x - \overline{\lambda}_M$ curves are higher for higher values of $\sigma_{0.2}$. All the curves will converge together as the beam buckles elastically. In Figure 5.18, the knee factor, n, is varied from 10 to 200 and the curves cross over one another at $\overline{\lambda}_M = 0.55$. The reason can be explained in terms of the mechanical properties of the parent metal (see Figure 2.1). The parent metal having higher values of n will have lower increase in hardening strain but higher values of σ_e and σ_e will approach to $\sigma_{0.2}$ as n tends to infinity.

For stocky beams $(\overline{\lambda}_M < 0.55)$, the hardening strength is more pronounced, and therefore, a lower ultimate strength is obtained for beams with higher values of n. However, for intermediate and slender beams $(\overline{\lambda}_M \geq 0.55)$, the variation of σ_e will be controlling, and so the beams having higher values of n will result in higher ultimate strengths. The combination of these two effects, therefore, results in the curves crossing over one another as is evident in Figure 5.17. Figure 5.19 shows the familiar weakening effect similar to the case of transversely welded aluminium columns (see Figure 3.17); the greater the initial out-of-straightness $\delta_{x(max)}$, the greater is the strength reduction.
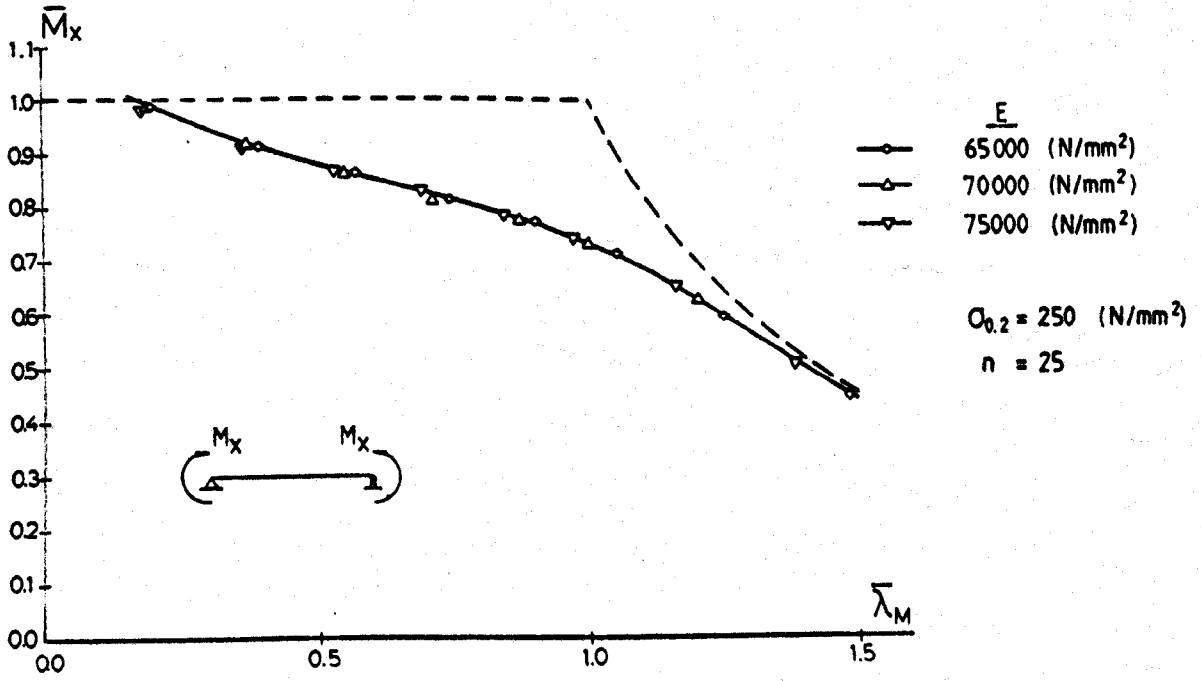
Figure 5.16 Effect of Young's Modulus
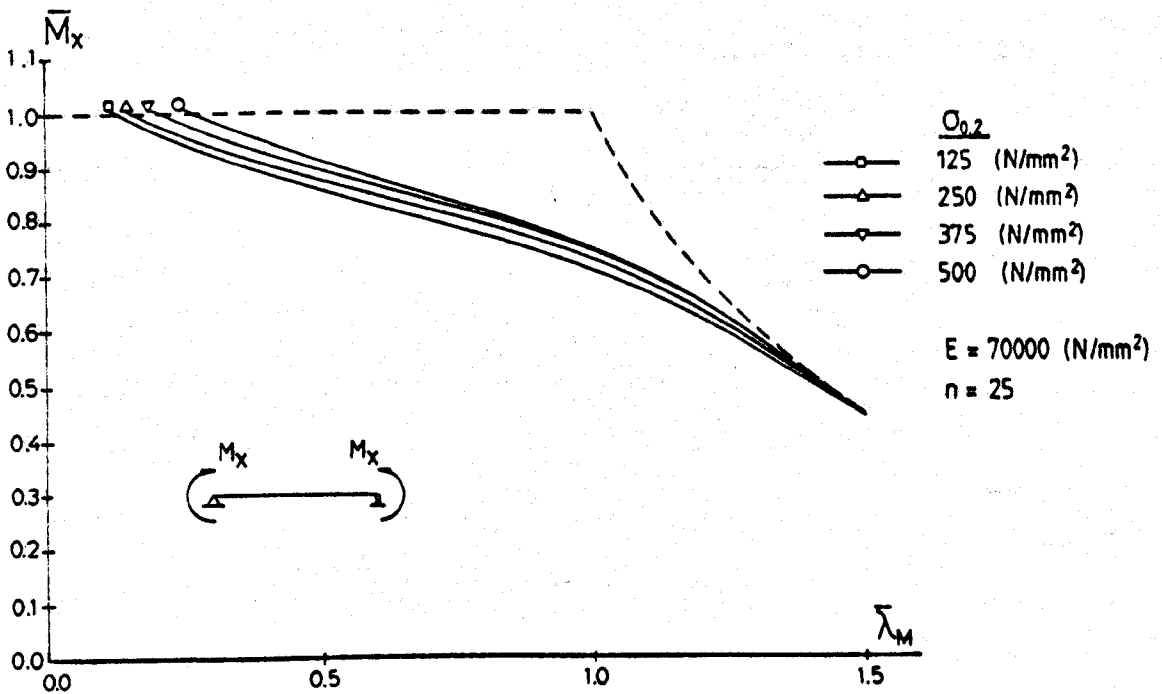
Figure 5.17 Effect of $\sigma_{0.2}$

Figure 5.18 Effect of n

n

―⊙―	10
―◯―	25
―△―	40
―▽―	55
―◯―	200

$E = 70000$ (N/mm^2)

$\sigma_{0.2} = 250$ (N/mm^2)

CURVE	$\delta_{x(max)}$ (mm)	θ_z (radian)
―△―	0	0
―▽―	0.001 L	0
―◯―	0.001 L	0.01
―◯―	0.005 L	0
―◇―	0.005 L	0.01
―■―	0.01 L	0
―●―	0.01 L	0.01

$\delta_{y(max)} = 0.001 L$
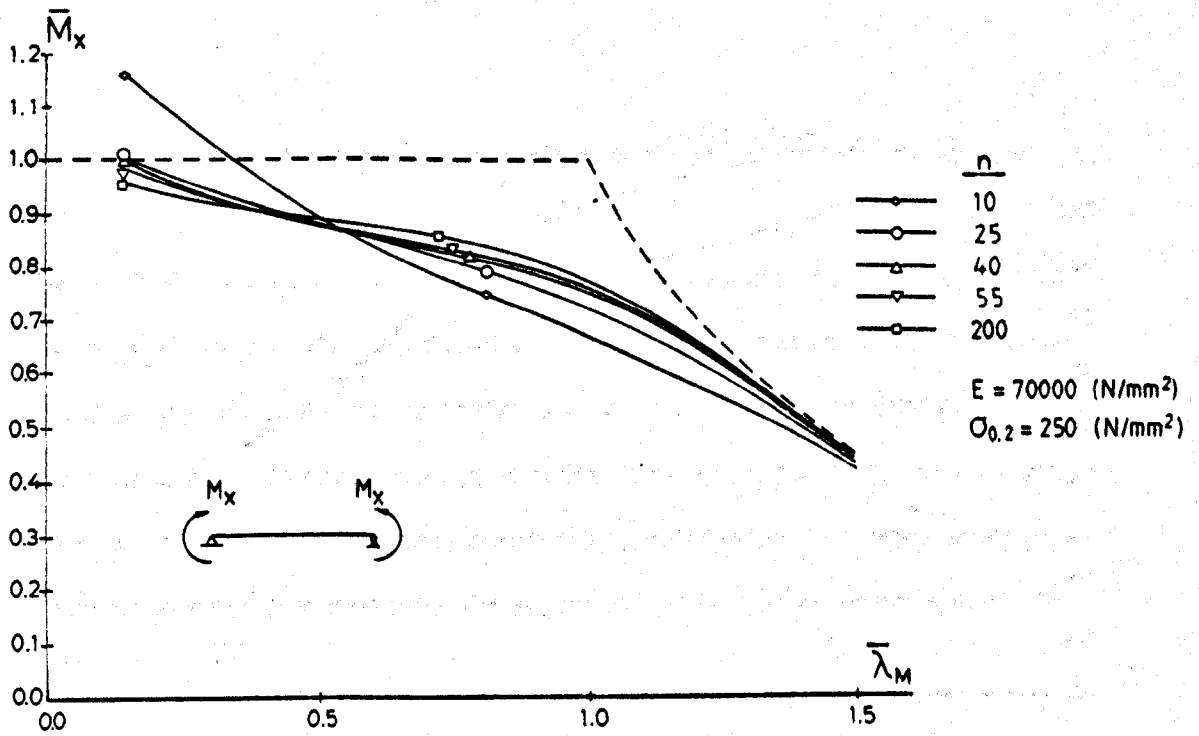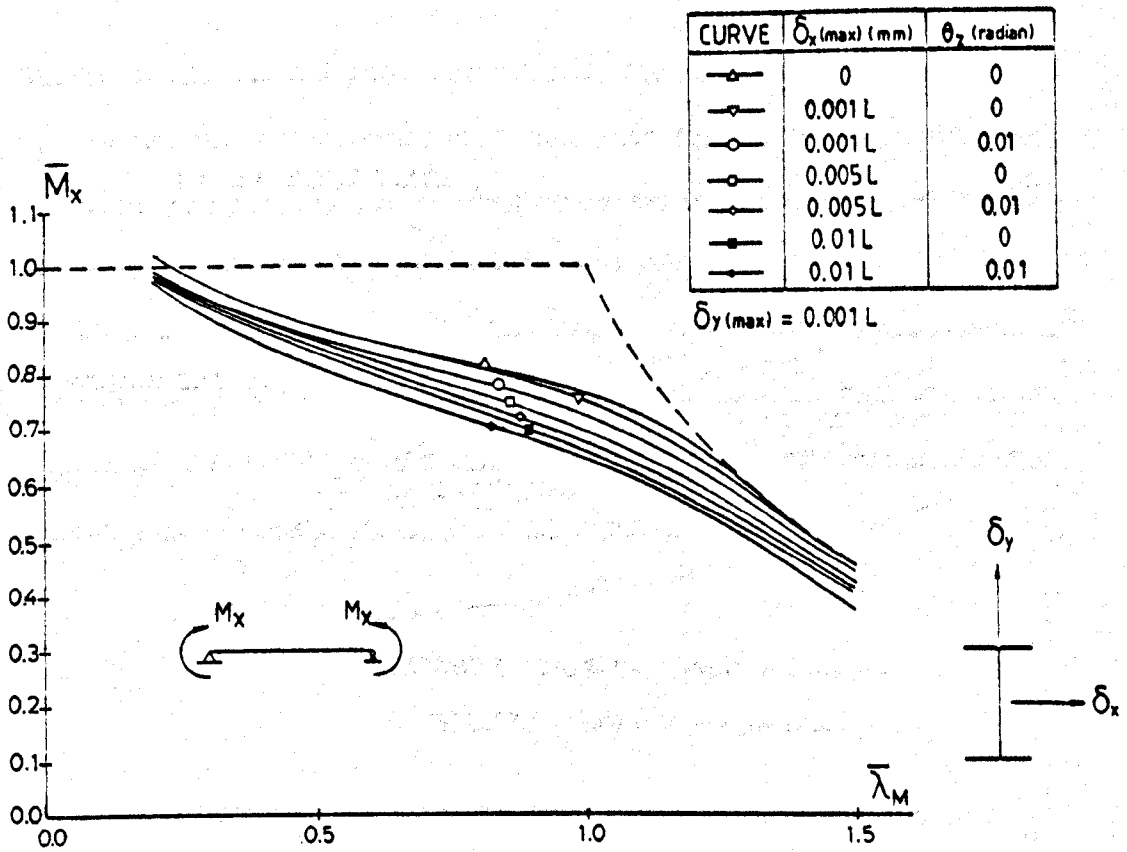
Figure 5.19 Effect of Intial Out-of-straightness
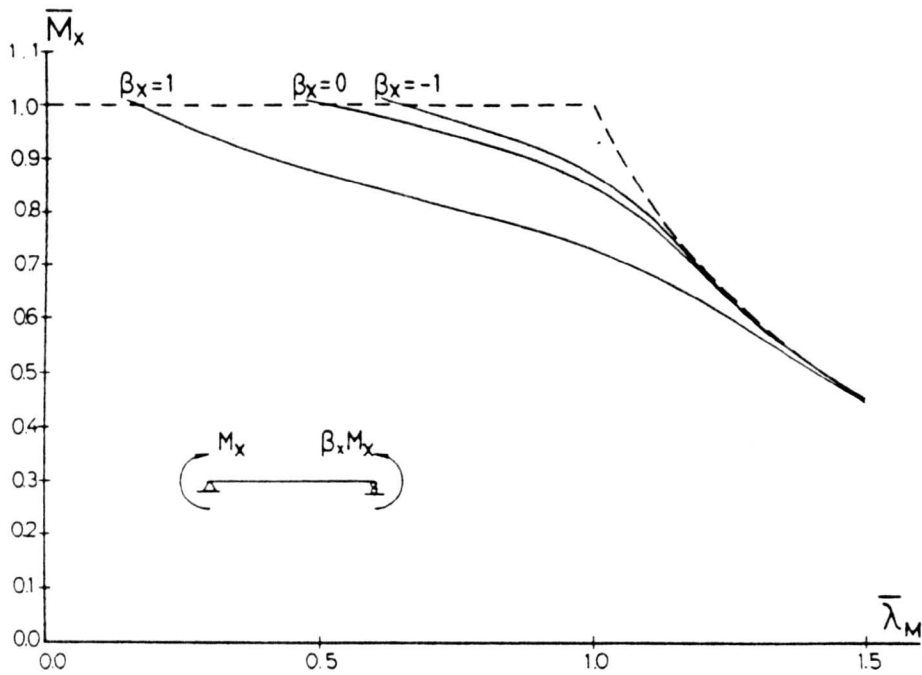
Figure 5.20 Buckling of Non-welded Beams under Unequal End Moments $(\beta_x = 1, 0, -1)$
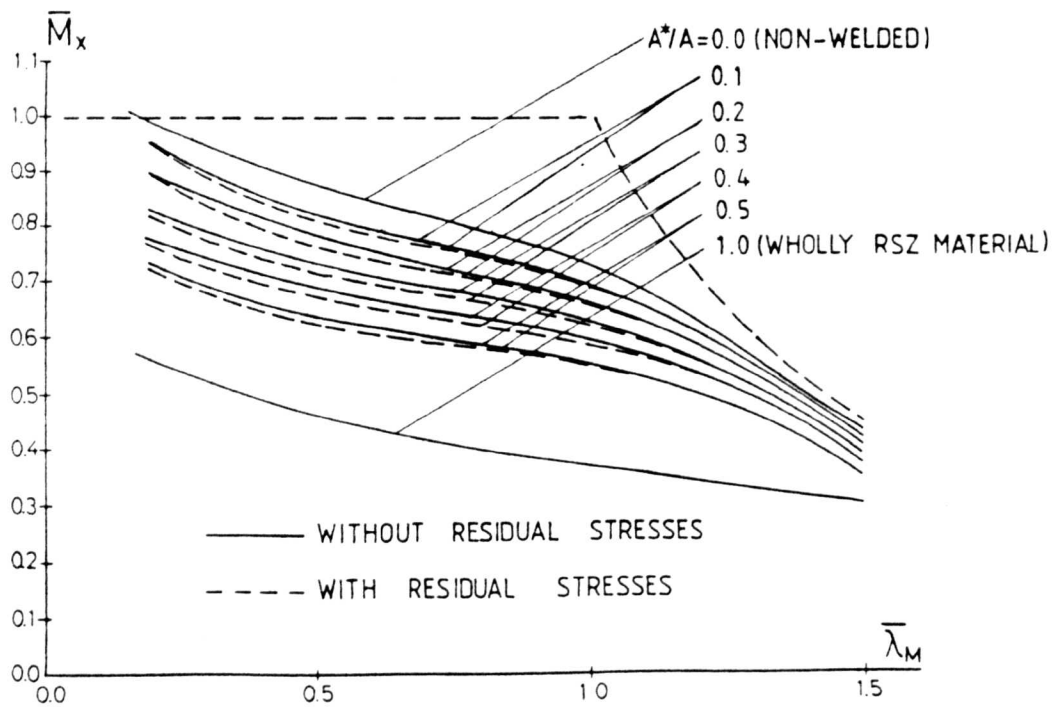
Figure 5.21 Study of Symmetric Longitudinally Welded Beams $(\beta_x = 1)$

5.3.2.3 Effect of Unequal End Moments on Non-welded Beams

Figure 5.20 shows the effect of unequal end moments ($\beta_x = 1$, 0, -1) for non-welded beams. The most severe loading case is that of single curvature bending ($\beta_x = 1$), for which yielding is constant along the beam so that the resistance to lateral buckling is reduced everywhere. Less severe cases are those beams under moment gradient ($\beta_x = 0$ and -1) because yielding is confined to small portions near the supports, for which the reductions in the sectional properties are comparatively unimportant.

5.3.2.4 Effect of Symmetric Longitudinal Welds on Beams

Similar to the cases C2-LW and C3-LW, Figure 5.21 shows the effect of symmetric longitudinal welds on beams. All the beams are under single curvature bending and the residual stress distribution is the same as for symmetric longitudinally welded columns (see Figure 5.8). From Figure 5.21, we can observe that the beams show progressive reductions in strength as the value of $\frac{A^*}{A}$ is increased. Moreover, the presence of residual stresses can only cause about a 2% reduction in strength, therefore, this weakening effect is negligible on symmetric longitudinally welded beams.

5.3.2.5   Effect of Unsymmetric Longitudinal Welds on Beams

Figures 5.22 to 5.24 shows the effect of unsymmetric longitudinal welds on beams. The residual stress distributions can be referred to Figure 5.9 and Figure 5.10. In Figure 5.24, the effect of residual stresses is not included because the residual stress distribution is uncertain. All the beams are under single curvature bending and the RSZ is under compression. From Figures 5.22 to 5.24, if the effect of residual stresses is neglected, we can observe that the shapes of the $\overline{M}_x - \overline{\lambda}_M$ curves for beams having symmetric or unsymmetric longitudinal welds are quite similar to the $\overline{P} - \overline{\lambda}_y$ curves of columns as shown in Figures 5.9 to 5.11. For the beams with $\frac{A^{\bullet}}{A} = 0.3$ and 0.5, the unsymmetric longitudinally welded beams show lower strengths than the symmetric longitudinally welded beams as $\overline{\lambda}_y > 0.85$. The reasons have been explained in Section 5.3.1.3. If the effect of residual stresses is taken into account, the strength of unsymmetric longitudinally welded beams with $\frac{A^{\bullet}}{A}$ = 0.1 and 0.3 show about 5% and 8% further reductions in strength respectively. These reductions in strength are higher than for beams having symmetric longitudinal welds.
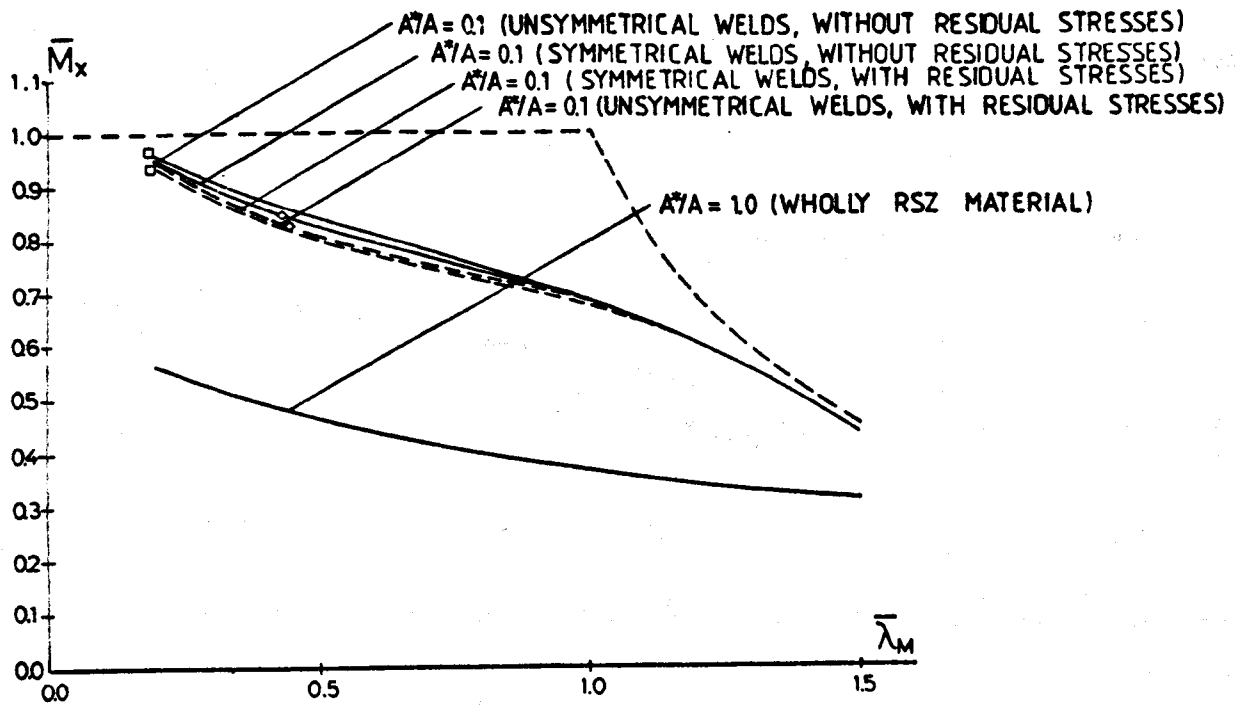
Figure 5.22 Study of Unsymmetric Longitudinally Welded Beams
$(\frac{A^*}{A} = 0.1, \beta_x = 1)$
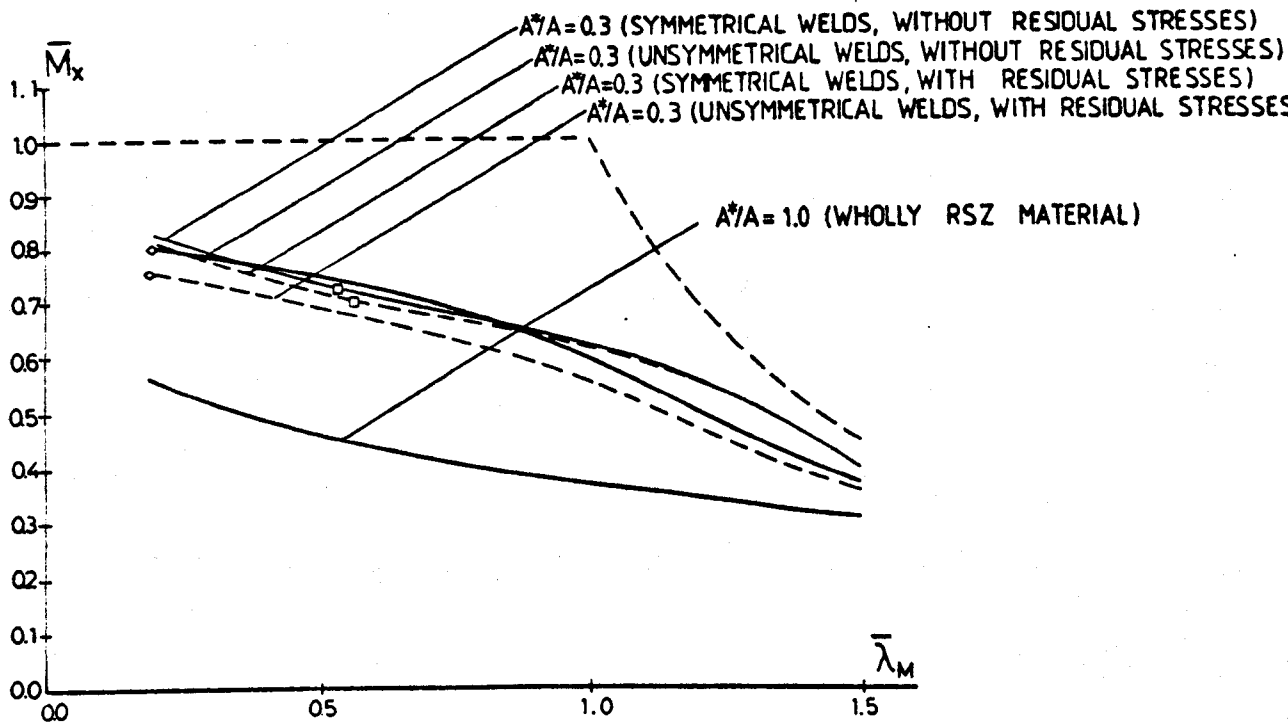
Figure 5.23 Study of Unsymmetric Longitudinally Welded Beams
$(\frac{A^*}{A} = 0.3, \beta_x = 1)$
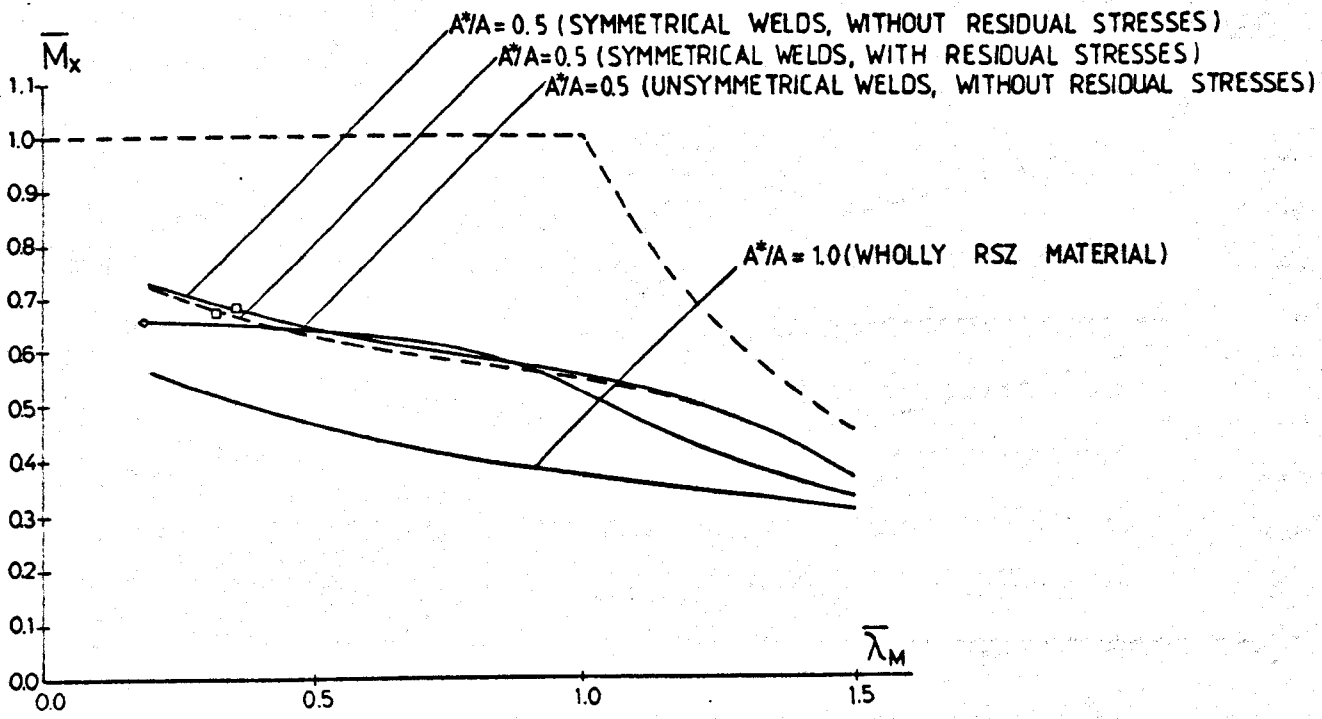
Figure 5.24 Study of Unsymmetric Longitudinally Welded Beams
$(\frac{A^*}{A} = 0.5, \beta_x = 1)$
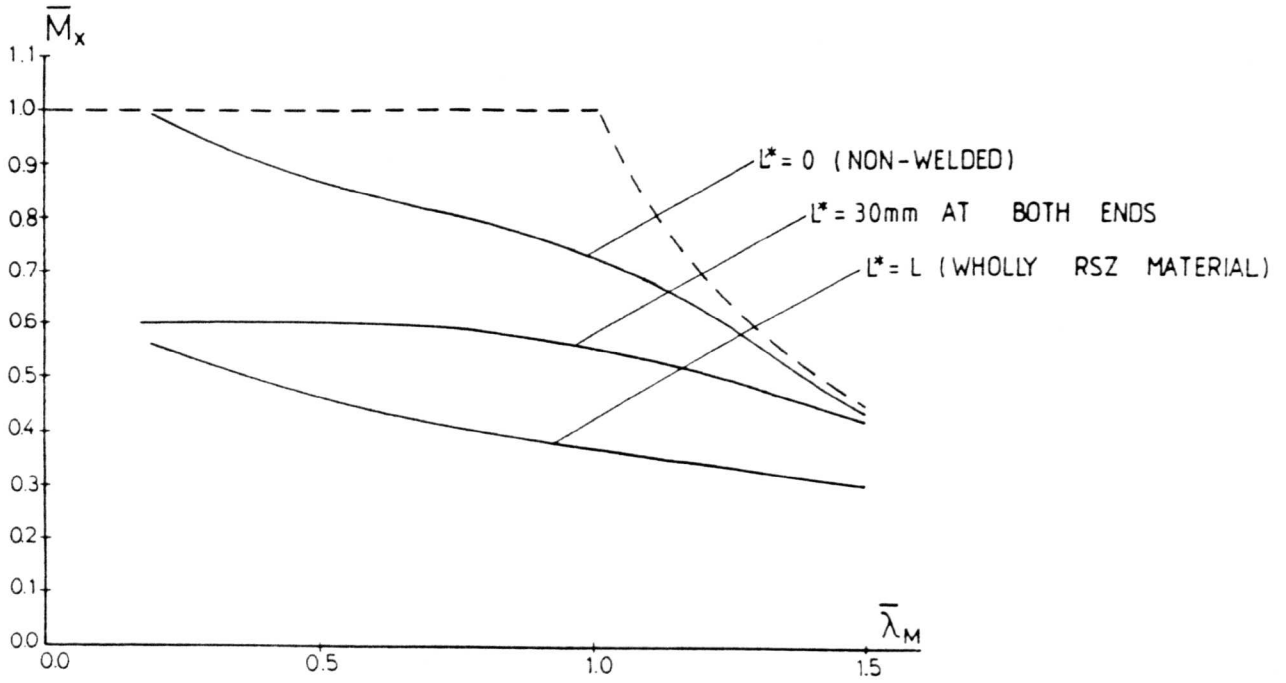
Figure 5.25 Study of End-welded Beams ($L^* = 30\ mm$ at Both Ends, $\beta_x = 1$)
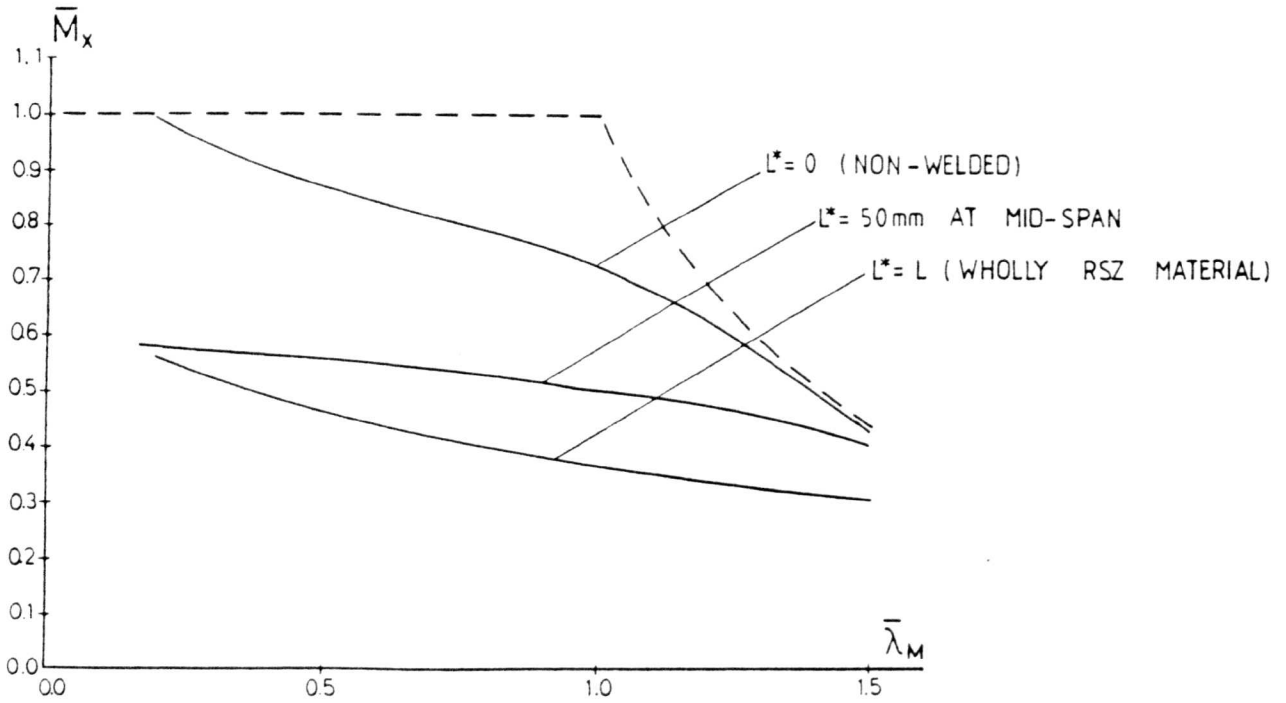
Figure 5.26 Study of Centrally-welded Beams ($L^* = 50\ mm$ at Mid-span, $\beta_x = 1$)

5.3.2.6 Effect of Local Transverse Welds on Beams

Figures 5.25 and 5.26 show the effect of local transverse welds on beams with $L^* = 30mm$ located at both ends and $L^* = 50mm$ located at mid-span respectively. The effect of residual stresses is also neglected in the analysis and the beams are under single curvature bending. From the figures, we can find that the transversely welded beams show severe reductions in strength because the RSZ material is sufficiently stressed. Therefore, it further supports the idea that the most suitable method for designing transversely welded beams is using the stress-strain relationship of the RSZ material as a basis and determining the stress level within the RSZ. If the RSZ material is sufficiently stressed, the transversely welded beams should be designed as if containing wholly RSZ material.

5.3.3   Parametric Studies of Aluminium Beam-columns

5.3.3.1   Effect of Moment Gradient on Non-welded Beam-columns

Figures 5.27 to 5.30 show the interaction of axial load and moment gradient
($\beta_x = 1, 0, -1$) on non-welded aluminium beam-columns, and the details can
be referred to Table 5.3. In Figure 5.27, the effect of axial load plus single
curvature bending ($\beta_x = 1$) is investigated and a wide range of slenderness
($\lambda_y = 30, 50, 70, 90, 120$) is considered. The axial load P and moment M_x
were normalised with respect to the values $P_{0.2}$ and $M_{0.2x}$, and as expected,
the $\overline{P} - \overline{M}_x$ curves show that the beam-columns will gradually reduce in
strength as the slenderness, λ_y. increased. However, if the axial load P and
moment M_x were normalised with respect to the values P_{ult} and M_{ult}, ob-
tained from the program BIAXIAL, Figure 5.28 shows that small disparities
between the curves with different slenderness, λ_y, are apparent. Therefore,
when the axial load and moment are plotted in this way, we can observe
that the straight line formula will give lower bound solutions for designing
aluminium beam-columns.

In Figure 5.29 for which the moment gradient $\beta_x = 0$, the effect of end
moments is insignificant when $\lambda_y \leq 50$ and the value of end moment is small
(say $\overline{M}_x \leq 0.2$). For the moment gradient $\beta_x = -1$ (see Figure 5.30), the
effect of end moments is also less critical, even though the slenderness of the
beam-column is increased ($\lambda_y \geq 90$). The strength of the beam-column is
more or less controlled by the axial load and the end moments will only have
effects when the values become higher (say $\overline{M}_x = 0.5$).
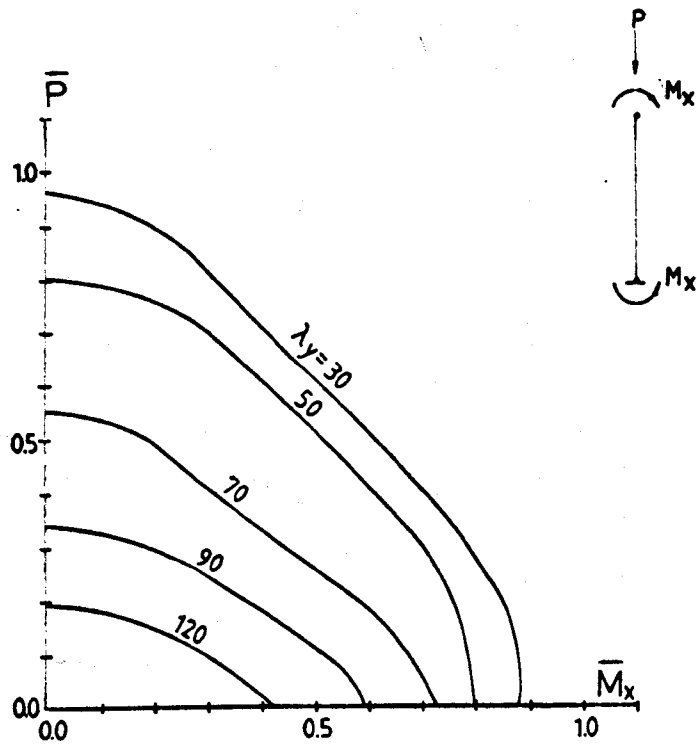
Figure 5.27 Study of Non-welded Beam-columns ($\beta_x = 1$)
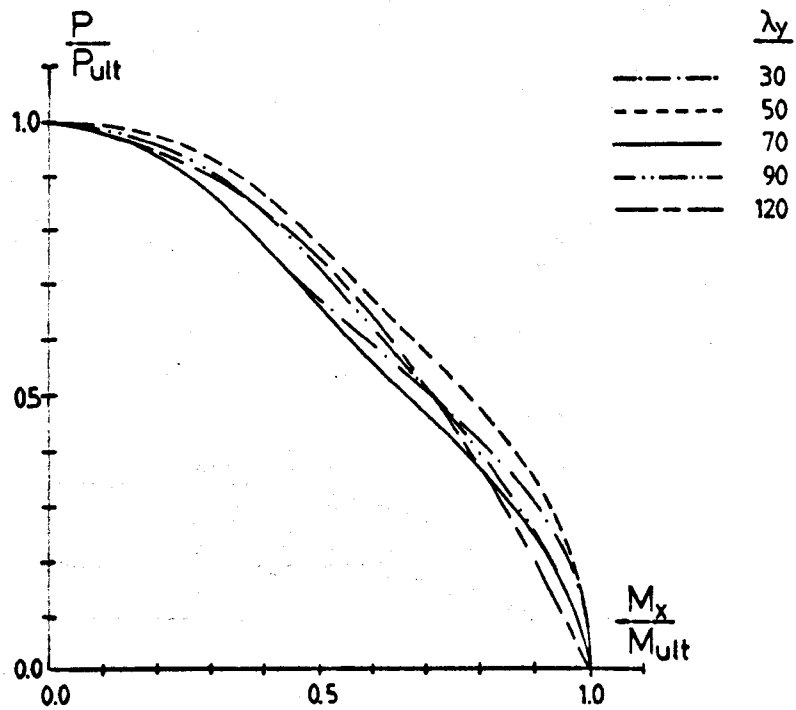
Figure 5.28 Study of Non-welded beam-columns ($\frac{P}{P_{ult}}$ against $\frac{M_x}{M_{ult}}$)
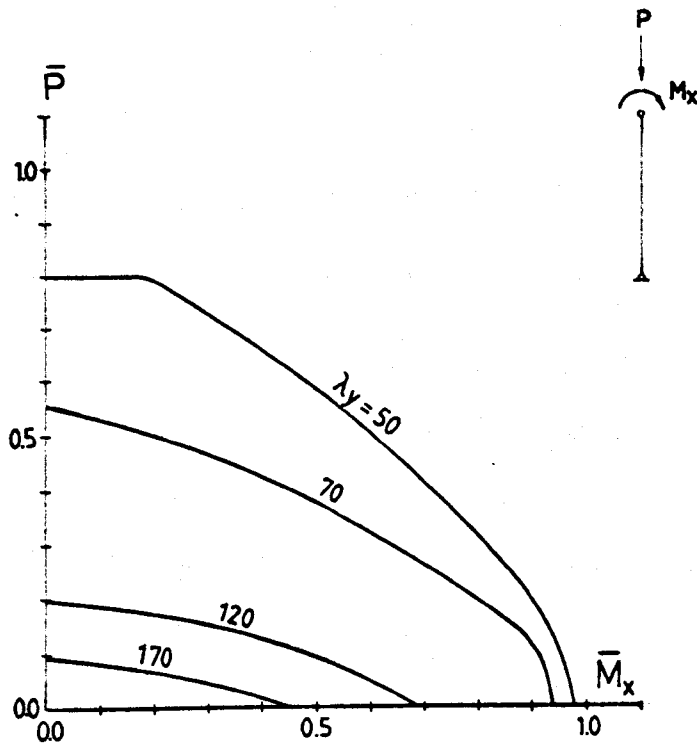
Figure 5.29 Study of Non-welded Beam-columns ($\beta_x = 0$)
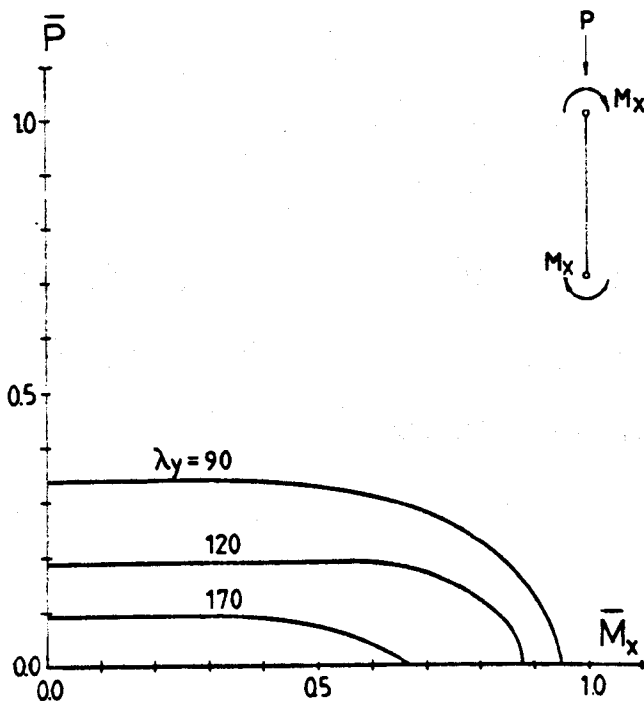
Figure 5.30 Study of Non-welded Beam-columns ($\beta_x = -1$)

5.3.3.2 Effect of Symmetric Longitudinal Welds on Beam-columns

Figures 5.31 to 5.33 show the effect of symmetric longitudinal welds on beam-columns with $\lambda_y =$ 30, 70 and 90 respectively. The value of $\frac{A^*}{A}$ is varied from 0.1, 0.3, 0.5 to 1.0 and the residual stress distributions can be referred to Figure 5.8. All the symmetric longitudinally welded beam-columns are under axial load and single curvature bending ($\beta_x = 1$). From the figures, when the beam-columns are having material failure, the reduction in ultimate strength is gradually increased as the value of $\frac{A^*}{A}$ is also increased. However, as the slenderness of the beam-column is increased and they tend to buckle elastically, the presence of RSZ within the cross-section become less significant because the RSZ material is not sufficiently stressed.
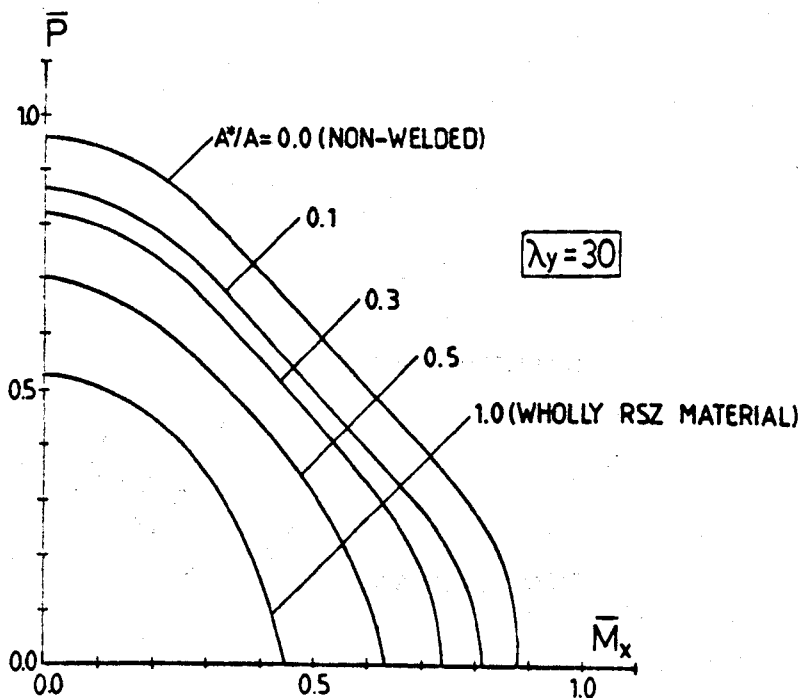
Figure 5.31 Study of Longitudinally Welded Beam-columns ($\lambda_y = 30$, $\beta_x = 1$)
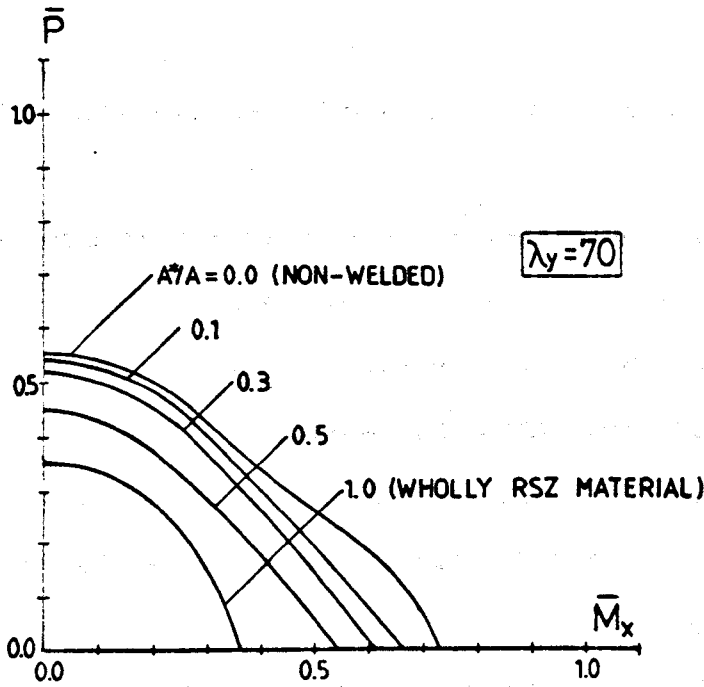
Figure 5.32 Study of Longitudinally Welded Beam-columns
($\lambda_y = 70$, $\beta_x = 1$)
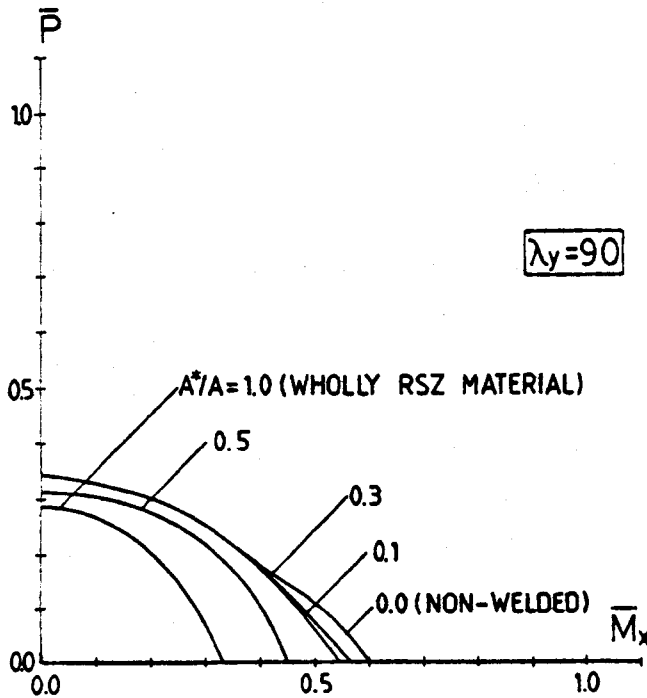
Figure 5.33 Study of Longitudinally Welded Beam-columns
($\lambda_y = 90$, $\beta_x = 1$)

5.3.3.3   Effect of Local Transverse Welds on Beam-columns

The effect of local transverse welds on beam-columns are presented in Figures 5.34 to 5.39. The local transverse welds are either $L^* = 30mm$ located at both ends or $L^* = 50mm$ located at mid-height, and $\lambda_y = 30, 70$ and 90 are considered. All the transversely welded beam-columns are also under axial load and single curvature bending ($\beta_x = 1$). Same as the behaviour of longitudinally welded beam-columns, the figures show that the transversely welded beam-columns will have severe reductions in strength as the RSZ material is sufficiently stressed no matter that the RSZ is located at both ends or at mid-height or the extent of RSZ is small. The strength of the transversely welded beam-columns is quite similar to the beam-columns containing wholly RSZ. However, the effect of local transverse welds become less critical as the beam-columns tend to buckle elastically.
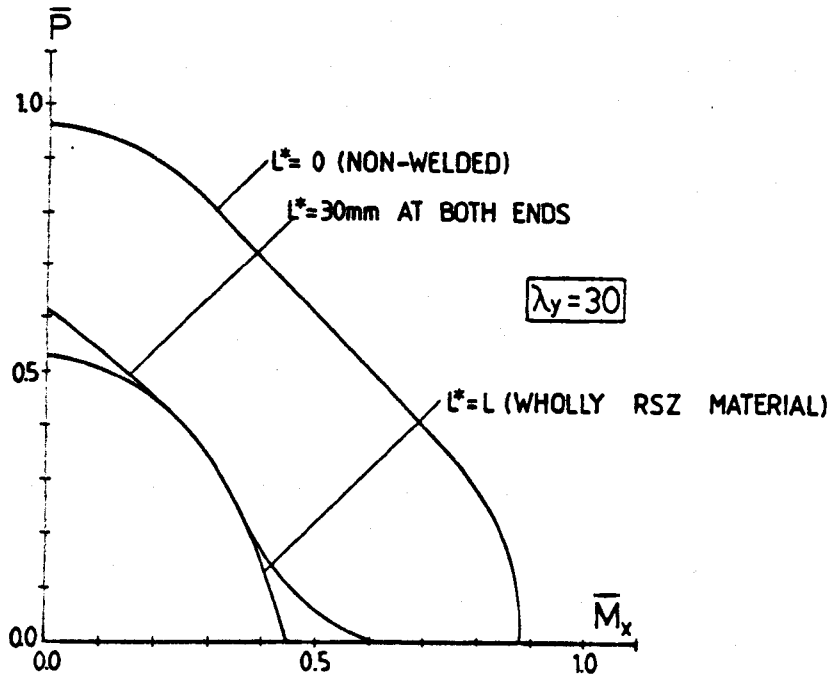
Figure 5.34 Study of End-welded Beam-columns ($\lambda_y = 30$, $\beta_x = 1$)
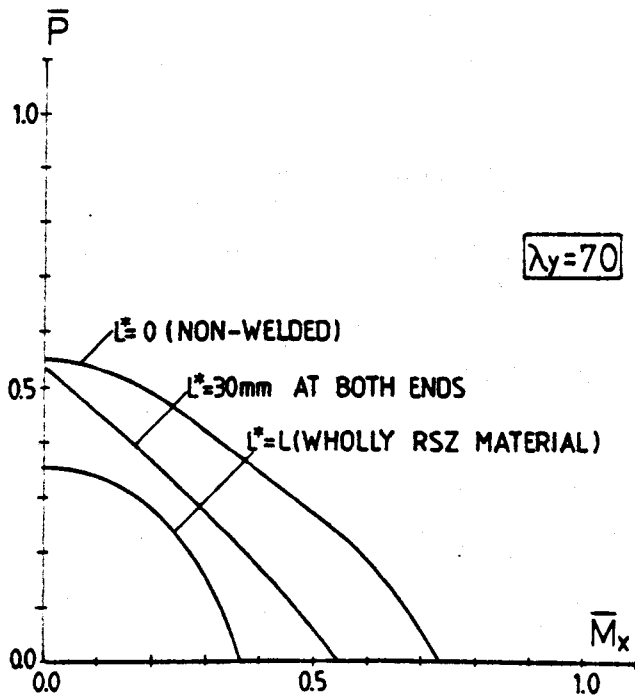
Figure 5.35 Study of End-welded Beam-columns ($\lambda_y = 70$, $\beta_x = 1$)
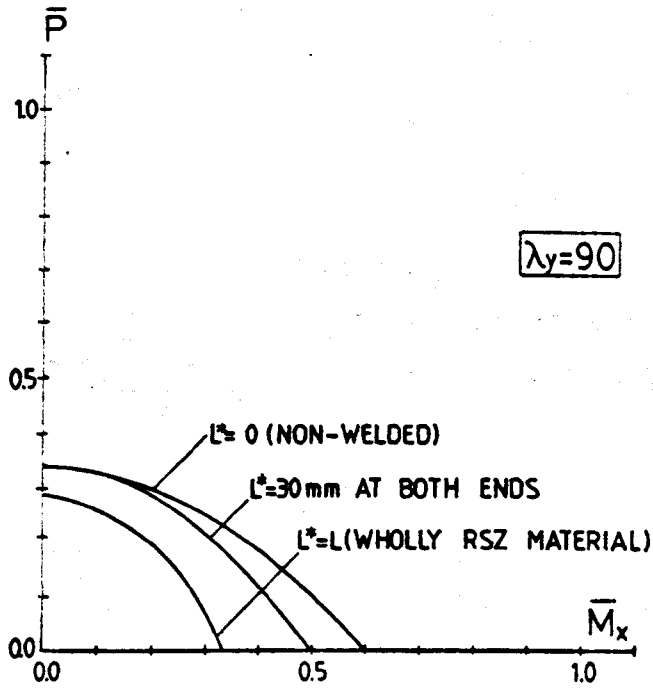
Figure 5.36 Study of End-welded Beam-columns ($\lambda_y = 90$, $\beta_x = 1$)
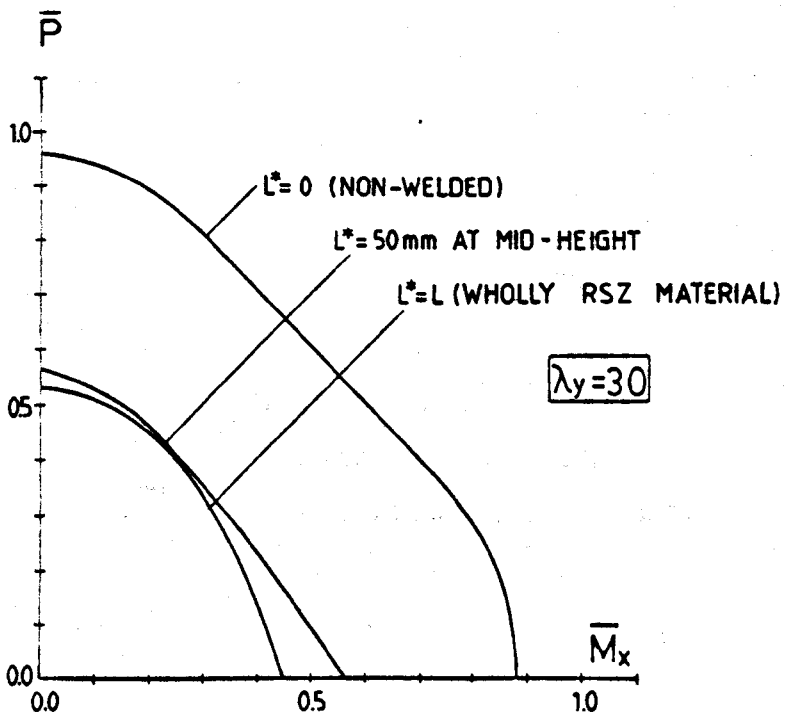
Figure 5.37 Study of Centrally-welded Beam-columns ($\lambda_y = 30$, $\beta_x = 1$)
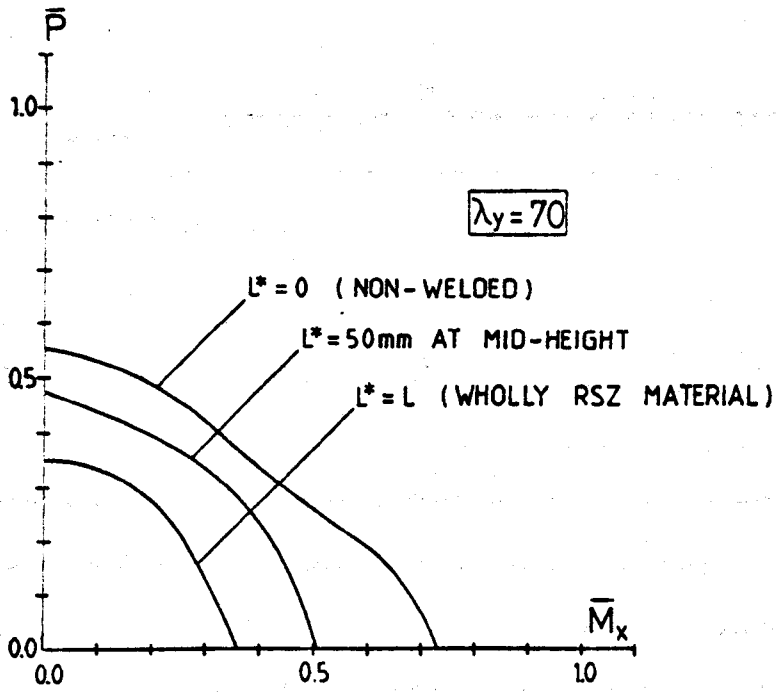
Figure 5.38 Study of Centrally-welded Beam-columns ($\lambda_y = 70, \beta_x = 1$)
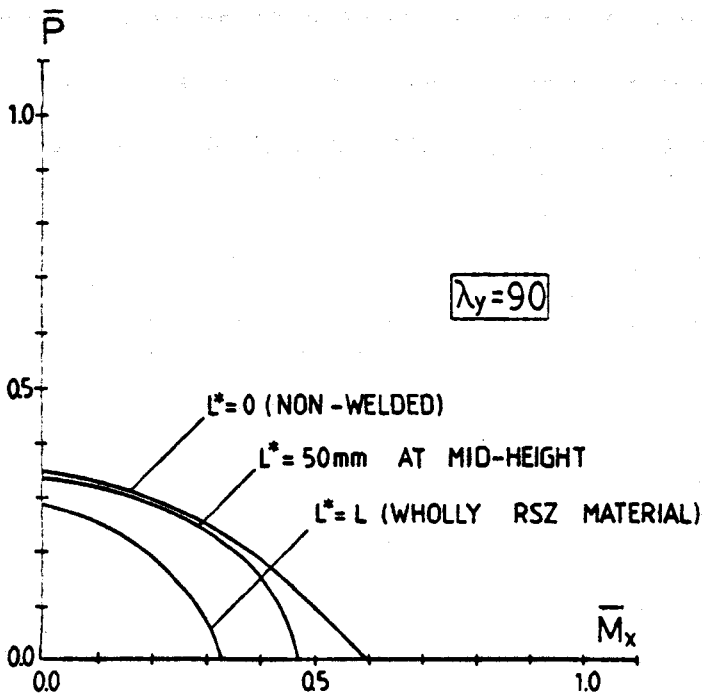
Figure 5.39 Study of Centrally-welded Beam-columns ($\lambda_y = 90, \beta_x = 1$)
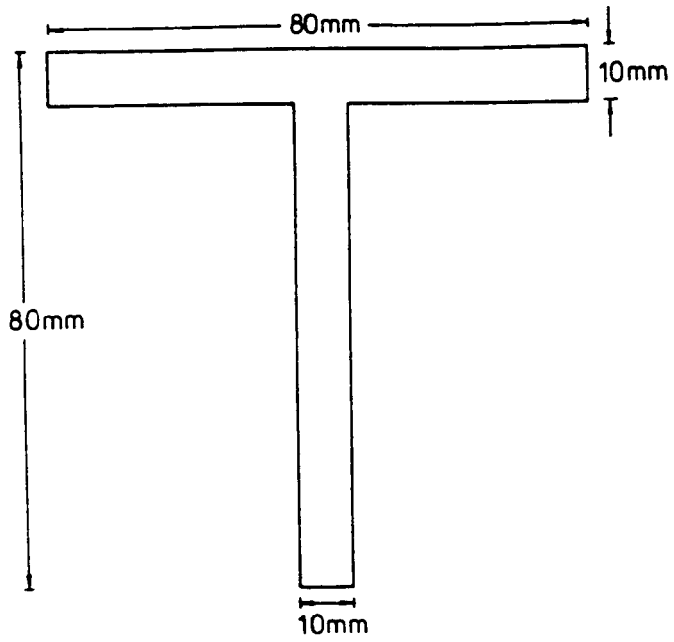
Figure 5.40 Cross-section Used for Parametric Studies

5.4   Further Parametric Studies of Aluminium Members

5.4.1   Study of Tee-section Aluminium Members

The parametric studies which were carried out in Section 5.3 are confined to doubly symmetric I-sections. However, in this section, limited studies are carried out to investigate the behaviour of tee aluminium members. It is because structural members of asymmetric thin-walled open-sections, such as tee-sections have relatively low bending and torsional stiffnesses and tend to bend and twist as load is applied.

The cross-section chosen for the parametric studies is shown in Figure 5.40 and the mechanical properties of parent metal and RSZ material are the same as Section 5.3. All the tee members are also pin-ended and warping deformation is unrestrained but the rotation is prevented at both ends.

5.4.1.1   Study of Non-welded and Longitudinally Welded Columns

Figure 5.41 shows the $\overline{P} - \overline{\lambda}_y$ curves for the non-welded and longitudinally welded aluminium columns. Moreover, the theoretical elastic buckling curve for tee-section columns [10,11,12,13] is also presented. For the longitudinally welded columns, the values of $\frac{A^*}{A} = 0.3$ and 0.5 are considered and the residual stress distributions can also be referred to Figure 5.41. The figures clearly shows that the weakening effect of $\frac{A^*}{A}$ is quite substantial for low $\overline{\lambda}_y$ and much less for high $\overline{\lambda}_y$. The presence of residual stresses can only cause further maximum reductions of about 7% on the buckling strength of columns.
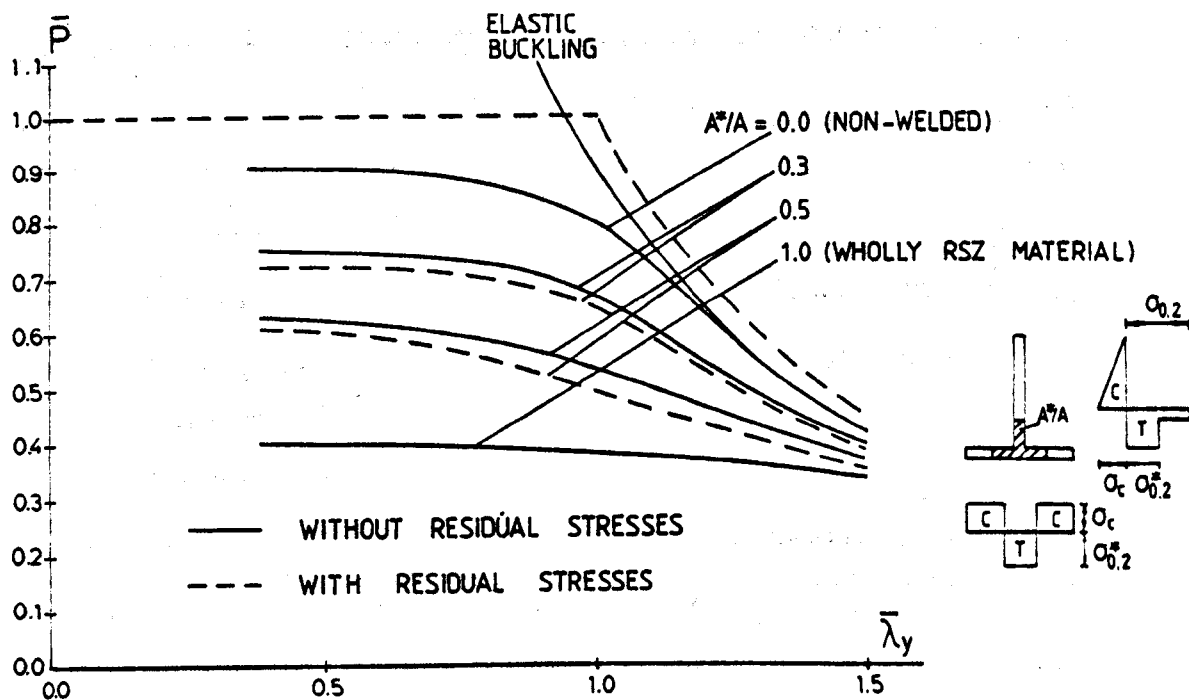
Figure 5.41 Study of Longitudinally Welded Tee-columns
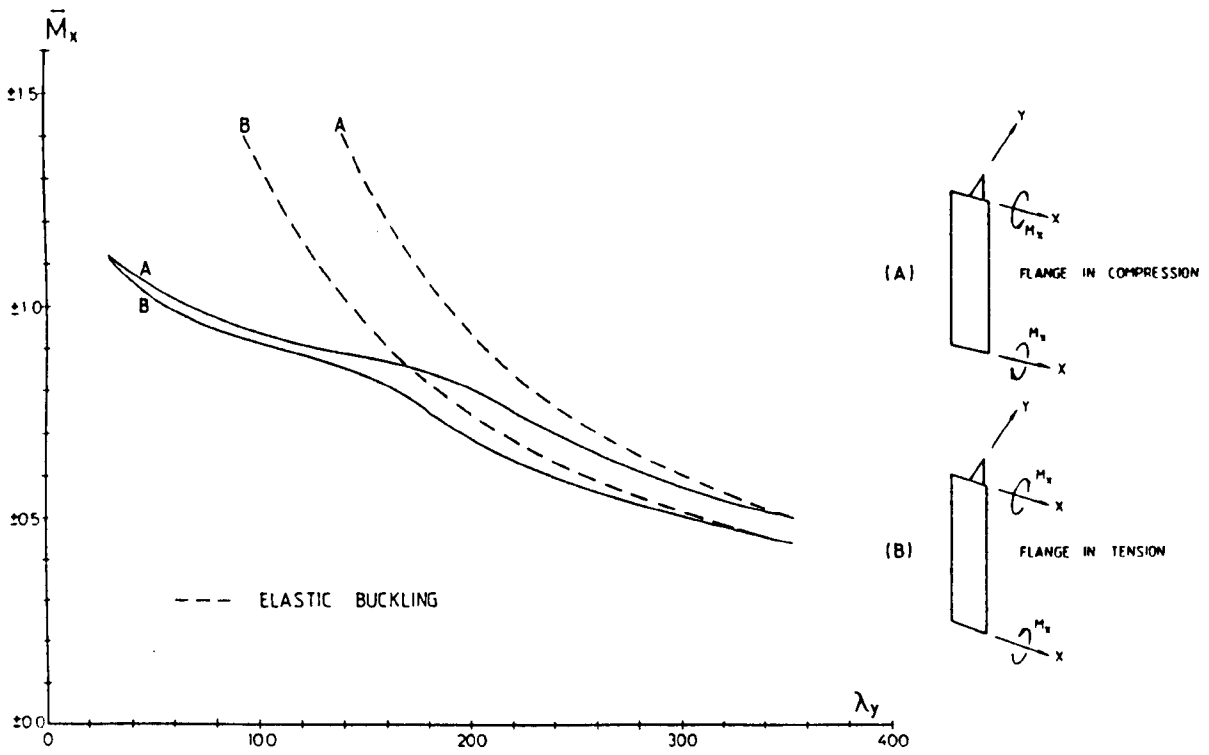
Figure 5.42 Study of Non-welded Tee-beams
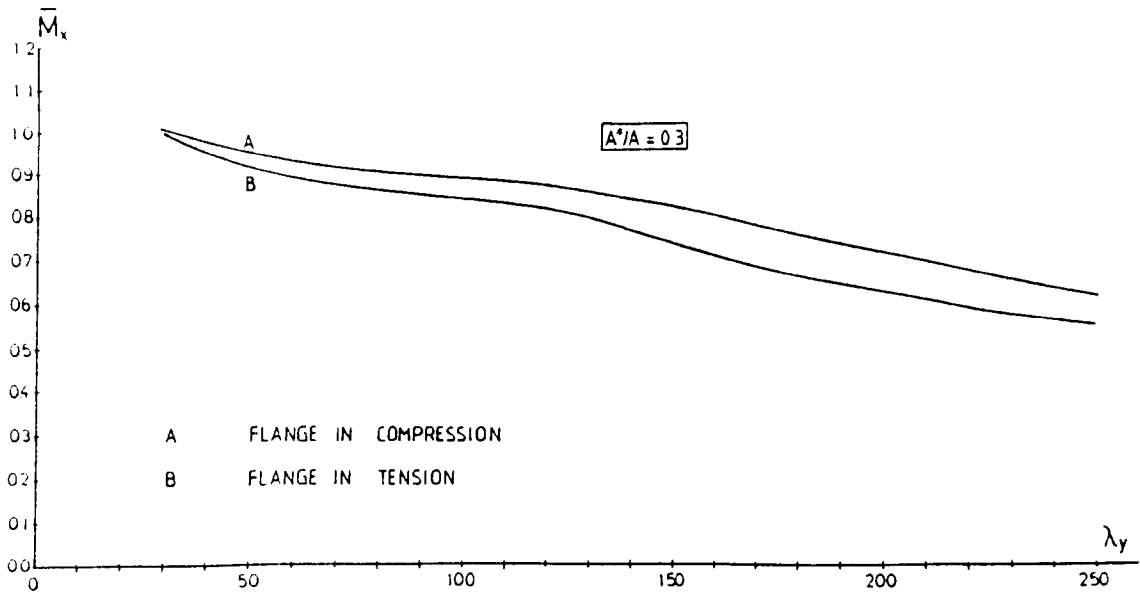
Figure 5.43 Study of Longitudinally Welded Tee-beams (without Residual Stresses)

5.4.1.2 Study of Non-welded and Longitudinally Welded Beams under Single Curvature Major Axis Bending

As mentioned by other authors [10,11], when a monosymmetric beam is bent in its plane of symmetry and twisted, the longitudinal bending stresses exert a torque which is similar to that which causes some short concentrically loaded compression members to buckle torsionally. In doubly symmetric beams the disturbing torque exerted by the compressive bending stresses is exactly balanced by the restoring torque due to the tensile stresses. In monosymmetric beams, however, there is an imbalance that results in a disturbing torque so that there is a reduction in the effective torsional rigidity. The effective torsional rigidity, therefore, is ~~depended~~ *dependent* on the directions of the applied end moments, and this can be demonstrated in Figure 5.42. The solid curves shown in Figure 5.42 correspond to the tee-section which the applied and moments cause compression in the flange, and the dashed curves B are for tension in the flange. The figure clearly shows that the ultimate bending strength of tee-beams depend on the direction of the applied end moments, and the tee-beams for which the flanges are in tension will give lower ultimate strengths. However, the difference in ultimate strength become less significant as the tee-beams suffer failure due to yielding of material.

The above phenomenon also holds for longitudinally welded tee-beams as shown in Figure 5.43. The curves of the longitudinally welded tee-beams are for the value of $\frac{A^*}{A} = 0.3$ only and the effect of residual stresses is neglected. The weakening effects due to RSZ softening and residual stresses are shown in Figures 5.44 to 5.45, and the residual stress distribution is the same as
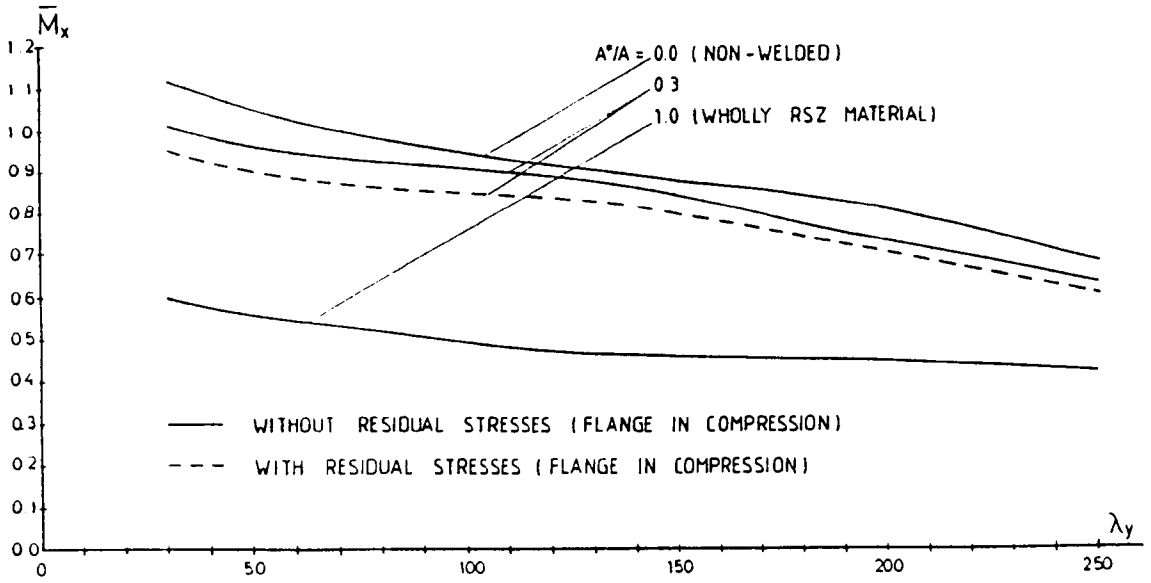
Figure 5.44 Study of Longitudinally Welded Tee-beams (with Residual Stresses and Flange in Compression)
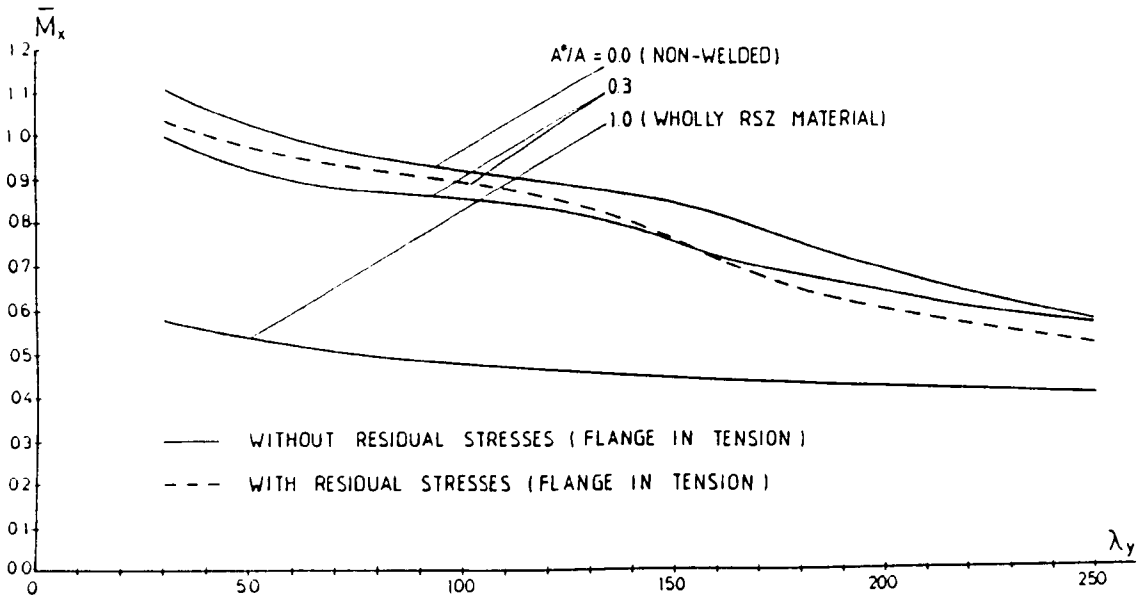

Figure 5.45 Study of Longitudianlly Welded Tee-beams (with Residual Stresses and Flange in Tension)

Figure 5.41. In Figure 5.44, the tee-beams are under single curvature bending with the flanges in compression. The presence of residual stresses will cause a further reduction in strength of a maximum 7%. In Figure 5.45, the tee-beams are also under single curvature bending but with the flanges in tension. We can observe that as the tee-beams tend to fail due to yielding of material ($\lambda_y \leq 155$), the presence of residual stresses will strengthen the tee-beams by a maximum of 6%. The reason is due mainly to the fact that the area of residual compressive zone is larger than the area of residual tensile zone. As the tension is applied, the residual compressive stresses in the flange will cancel some of the applied tensile bending stresses, and hence, the tee-beam is strengthened. However, as the instability of the tee-beam is pronounced ($\lambda_y > 155$), the presence of residual stresses can cause initial yielding of the cross-section and the tee-beams, therefore, will tend to buckle laterally and twist. But when compared with the non-welded tee-beams, the longitudinally welded tee-beams generally will give lower ultimate strengths.

5.4.1.3   Study of Non-welded Tee Beam :-columns

Figure 5.46 shows the interaction curves for the non-welded tee beam-columns under axial loading and major axis single curvature bending. Both the cases with the flange in compression or tension are considered. From the figure, it can be seen that the beam-columns for which the flanges are in tension will give lower ultimate strengths. The difference become less significant as the applied end moments become small.
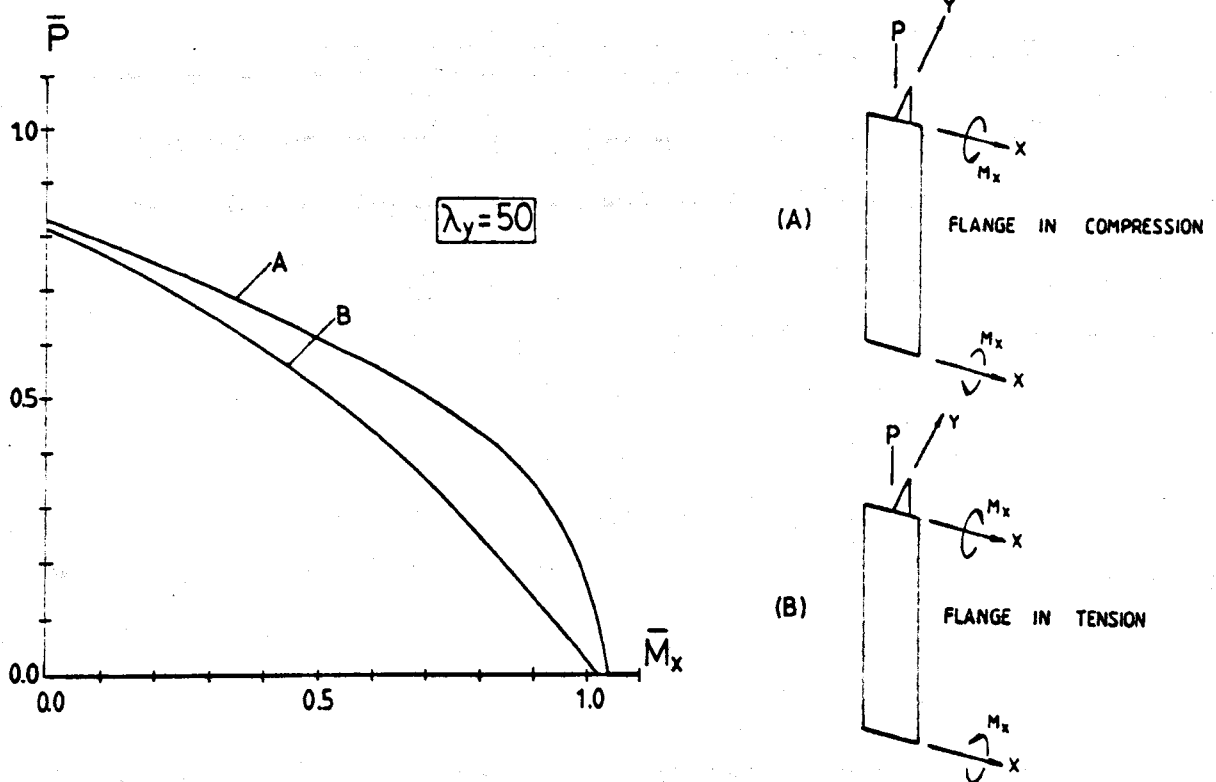
Figure 5.46 Study of Non-welded Tee Beam-columns
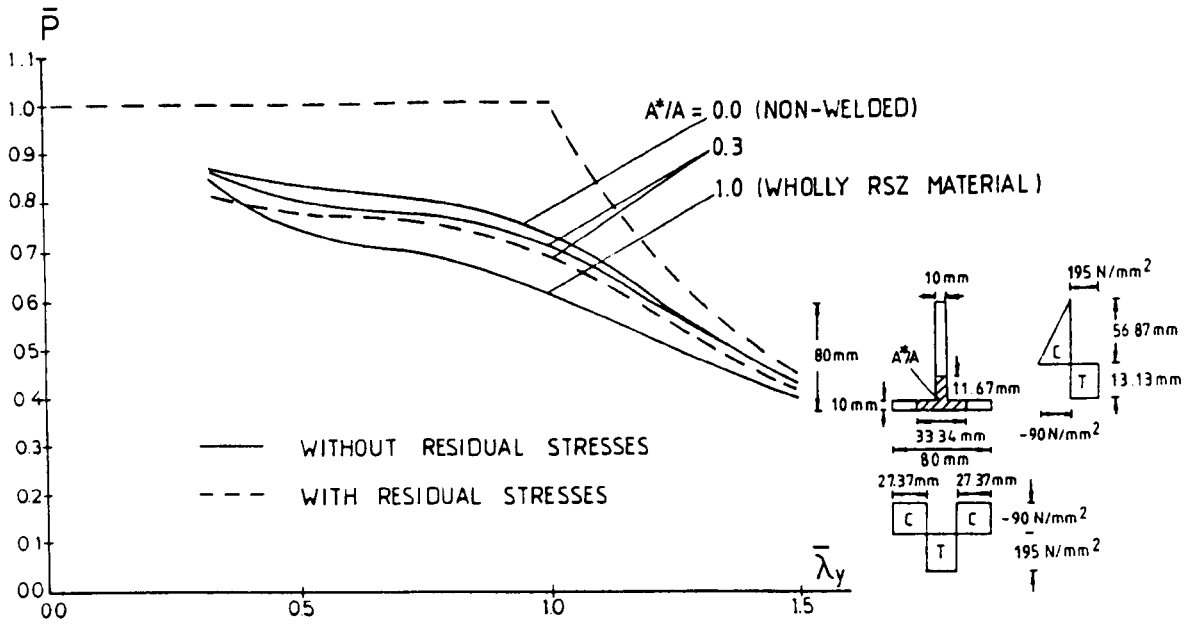
Figure 5.47 Study of Longitudinally Welded 5083-M Columns

5.4.2 Study of 5083-M Aluminium Columns

5083-M aluminium alloy (formerly known as NP8-M) is a non-heat-treatable alloy as used in marine construction, with a somewhat round stress-strain curve. From the experimental results obtained by Wong [14], it was found that the effect of welding can only produce a small change on the value of $\sigma_{0.2}$, but a significant drop in the elastic limit stress, σ_e, for the regions near to the weld. This means that the RSZ material of 5083-M alloy does not show any change in $\sigma_{0.2}$ but has an increase in knee factor, n. This behaviour is completely different from the 6000 or 7000 series alloy, and therefore, it is worthwhile to carry out limited studies on this type of alloy.

The cross-section chosen in the parametric study is the same tee-section as shown in Figure 5.40. From the experimental results obtained by Wong [14] and Mofflin [15], the mechanical properties of the parent metal and RSZ material are:

Parent :
$$E \;=\; 70000 \quad N/mm^2$$
$$\sigma_{0.2} \;=\; 195 \quad N/mm^2$$
$$n \;=\; 13$$

RSZ :
$$E^* \;=\; 70000 \quad N/mm^2$$
$$\sigma_{0.2}^* \;=\; 195 \quad N/mm^2$$
$$n^* \;=\; 6$$

The behaviour of the non-welded and longitudinally welded 5083-M aluminium columns are shown in Figure 5.47. For the longitudinally welded columns, only the value of $\frac{A^*}{A} = 0.3$ are considered and the residual stress distributions shown in Figure 5.47 are based on the experimental results ob-

tained by Wong [14]. For the longitudinally welded columns without residual stresses, Figure 5.47 shows that the maximum reduction in ultimate strength is less than 4%. When the effect of residual stresses is included, the longitudinally welded columns show total reduction of about 7% in ultimate strength. If we compare the ultimate strength of non-welded ($\frac{A^\bullet}{A} = 0.0$) and fully-welded ($\frac{A^\bullet}{A} = 1.0$) columns, the maximum reduction in strength is only about 15% and the reduction become less significant as $\overline{\lambda}_y < 0.3$. Therefore as $\overline{\lambda}_y < 0.3$, the effect of residual stresses may be more critical than the effect of RSZ softening.
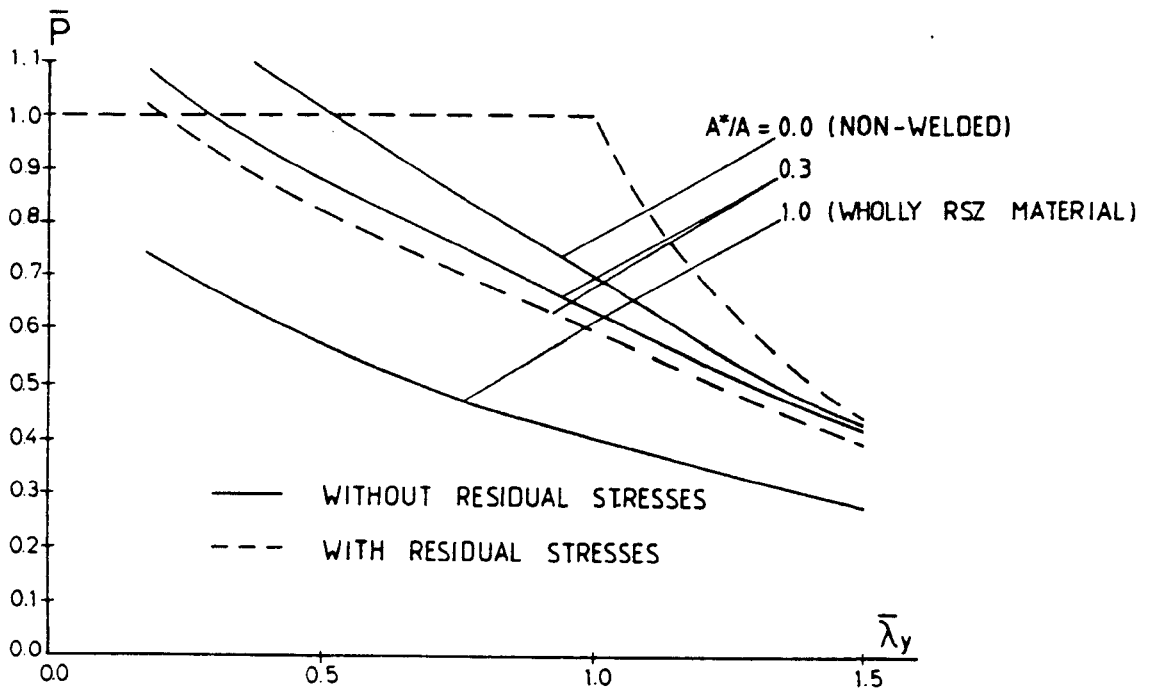
Figure 5.48 Study of Longitudinally Welded 6061-TB Columns

5.4.3   Study of 6061-TB Aluminium Columns

From the stress-strain relationship of 6000 and 7000 series aluminium alloys (see Section A.2.2 in Appendix A), it was found that those alloys usually possesses high knee factor, ($n > 15$). However, from draft BS 8118, 6061-TB aluminium alloy shows a more round stress-strain curve (i.e. low n) than the other alloys in the same series. Since there are no experimental results on 6061-TB alloy, therefore it is difficult to determine the mechanical properties of the RSZ material after welding. But, ~~different from 5083-M~~ referring to 6082 alloy, it is quite reasonable to assume that the RSZ material of 6061-TB alloy also shows 50% reduction is 0.2% proof stress (see Section 2.3.2.1). Therefore, in the parametric studies, the assumed mechanical properties of the parent metal and RSZ material are:

<u>Parent</u> : E =   70000 N/mm^2

$\sigma_{0.2}$ =   230 N/mm^2

n =   8.4

<u>RSZ</u> : E^* =   70000 N/mm^2

$\sigma_{0.2}^*$ =   115 N/mm^2

n^* =   5

The cross-section chosen is also the same I-section as shown in Figure 5.5. The effect of symmetric longitudinal welds ($\frac{A^*}{A} = 0.3$) on columns with or without residual stresses is studied and the results are shown in Figure 5.48. Similar to previous studies on columns (see Figures 5.7 and 5.8), the reduction in ultimate strength of longitudinally welded columns is due mainly to the effect of RSZ softening within the cross-section. The presence of residual stresses

can only cause a further reduction in ultimate strength of about 7%.

5.5   Conclusions

The general inelastic behaviour of aluminium members with or without welds under flexural-torsional buckling has been studied. Limited but significant results on aluminium members with asymmetric cross-section are also presented. From the parametric studies, several important observations emerge.

1. For the longitudinally welded aluminium members, the weakening effect is mainly due to the presence of RSZ within the cross-section. The presence of residual stresses can only cause a further reduction in ultimate strength of up to 8%, and the reduction is more or less independent of the value $\frac{A^*}{A}$.

2. For the aluminium members having unsymmetric longitudinal welds, the Cambridge tendon force model ~~sometime~~ _Sometimes_ fails to represent the distribution of residual stresses. When compared with the aluminium members having symmetric longitudinal welds, they will give a maximum decrease in strength of about 9% for members within the intermediate and slender ranges ($\overline{\lambda}_y$ and $\overline{\lambda}_M \geq 0.85$).

3. For the end-welded aluminium columns, we can design the columns as if non-welded but the maximum strength cannot be greater than $\overline{P} = 1 - (1 - \omega)\frac{A^*}{A}$ (a cut-off line). For other transversely welded aluminium columns, we should design the columns as if containing wholly RSZ material.

4. For the transversely welded beams or beam-columns, the best design approach is to consider the stress level within the RSZ. If the stress level in the RSZ is high, we should also design the members as if containing wholly RSZ material. If the stress level in the RSZ is low, we can neglect the presence of local transverse welds but special attention should be paid to the effect of residual stresses because these may be present after welding.

5. Tee-section aluminium members for which the applied end moments cause tension in the flanges will generally give lower strengths than tees with moments causing compression in the flanges.

References

[1] El-Khenfas, M. A., "Three Dimensional Ultimate Strength Analysis of Beam-columns", Ph.D Thesis, University of Sheffield, 1987.

[2] Chen, W. F., and Atsuta, T., "Theory of Beam-columns, Vol. 2, Space Behaviour and Design", Chapter 12, McGraw-Hill.

[3] Zbirohowski - Koscia, K., "Thin Walled Beams, from Theory to Practice", Crosby Lockwood and Son Ltd, 1967.

[4] Murray, N. W., "Introduction to the Theory of Thin-walled Structures", Clarendon Press, Oxford, 1984.

[5] Vlasov, V. Z., "Thin-walled Elastic Beam", Israel Program for Scientific Translations, 2nd Edition, Translated from Russian, Jerusalem, 1961.

[6] Hill, H. N., and Clark, J. W., "Lateral Buckling of Eccentrically Loaded I- and H-section Columns", Proceedings of First National Congress of Applied Mechanics, A.S.M.E., 1951.

[7] Anslijn, R., "Tests on Steel I Beam-columns Subjected to Thrust and Biaxial Bending", Report MT 157, Centre de Recherches Scientifiques et Techniques de L'industrie des Fabrications Metalliques, University of Liege, August 1983.

[8] Hong, G. M., "Buckling of Non-welded and Welded Aluminium Columns", Ph.D Thesis, University of Cambridge, 1983.

[9] Smith, C. S., and Kirkwood, W., "Influence of Initial Deformations and Residual Stresses on Inelastic Flexural Buckling of Stiffened Plates and Shells", International Conference on Steel Plated Structures, Imperial College, London, July 1976.

[10] Trahair, N. S., "The Behaviour and Design of Steel Structures", Chapman and Hall, London, England, 1977.

[11] Galambos, T. V., "Structural Members and Frames", Prentice-hall, Englewood Cliffs, 1968.

[12] Bleich, F., "Buckling Strength of Metal Structures", McGraw-Hill.

[13] Allen, H. G. and Bulson, P. S., "Background to Buckling", McGraw-Hill.

[14] Wong, M. P., "Weld Shrinkage in Non-linear Materials", Ph.D Thesis, University of Cambridge, 1982.

[15] Mofflin, D. S., "Plate Buckling in Steel and Aluminium", Ph.D Thesis, University of Cambridge, 1983.

BIAXIAL BENDING OF ALUMINIUM BEAM-COLUMNS

6.1   Introduction

A three-dimensional space structure is often treated as a collection of two-dimensional planar structures. This idealization does not represent the true loading condition existing in a space structure and may not give the optimum design. In an actual building framework, the beam-columns are frequently subjected to bending moments acting in two perpendicular directions in addition to an axial compression. The obvious example is a corner column in a building frame. The beam-column which is loaded with biaxial eccentricity will usually deflect and twist at all load levels. The importance of this twisting lies in the fact that the ultimate load carrying capacity of such beam-columns, especially beam-columns with open thin-walled sections that have small torsional rigidity, may be less than the maximum load carrying capacity for in-plane loading.

The behaviour of biaxially loaded beam-columns has been studied extensively in recent years by many researchers and lots of tests have been conducted, but their work was mainly confined to steel structures. Therefore in this chapter, the author attempts to study the general behaviour of biaxially loaded aluminium beam-columns theoretically and hence give some recommendations for the design of aluminium structures.

6.2   Factors Affecting the Solution of Biaxially Loaded Beam-column

Beam-columns under biaxial bending are far more complicated than beam-columns under flexural-torsional buckling. The flexural-torsional response of a beam-column subjected to loading in its plane is of the bifuraction type of instability and the out-of-plane deformations remain zero until the critical loading condition is reached. Thus the in-plane behaviour of a beam-column up to the critical or buckling load can be analysed independently of the out-of-plane buckling behaviour. However, biaxially loaded beam-columns exhibit the non-bifuraction type of instability in which both the in-plane and out-of-plane deflection increase until a maximum load is reached. In this situation, the in-plane and the out-of-plane buckling behaviour are interactive and the analysis is extremely load path dependent and requires step-by-step solutions that follow the history of loading.

In program BIAXIAL, similar to other numerical methods which have been used by various researchers, the accurate solution of the biaxially loaded beam-column requires consideration of compatibility and equilibrium which directly depends on the instantaneous positions of the centroid and the shear centre. Their exact positions are principally affected by:

1. the stress-strain relationship of aluminium

2. the loading increment

3. the loading paths

4. the initial out-of-straightness
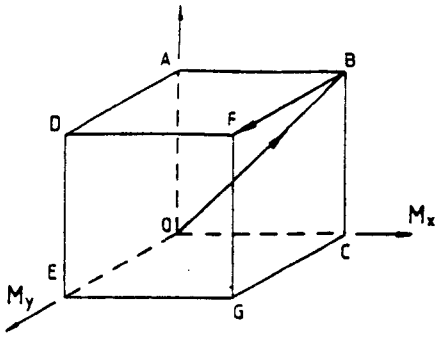
Figure 6.1 (a) Loading Path I
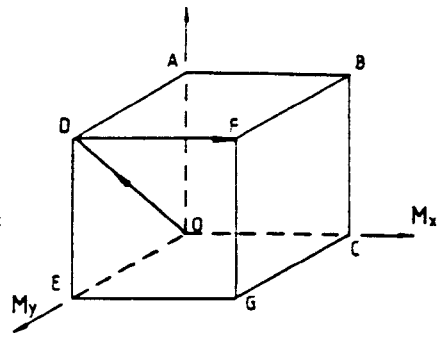
Figure 6.1 (b) Loading Path II
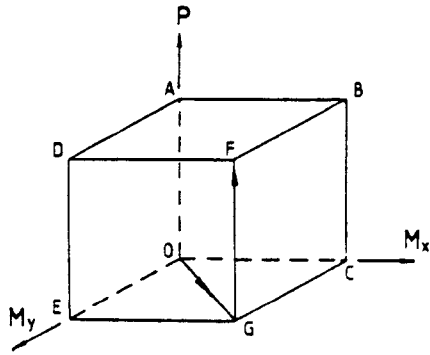
Figure 6.1 (c) Loading Path III
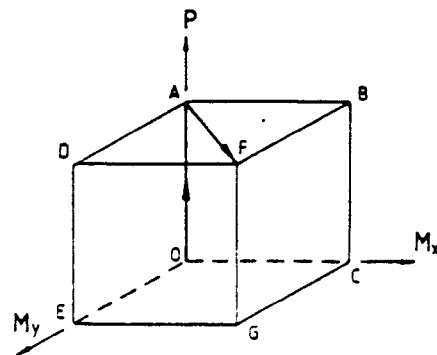
Figure 6.1 (d) Loading Path IV
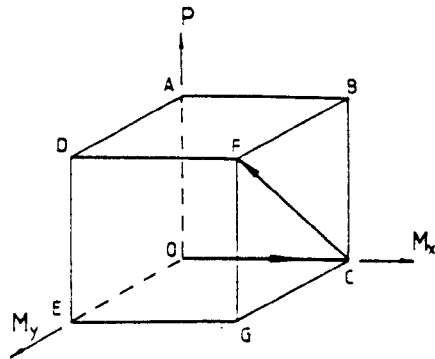
Figure 6.1 (e) Loading Path V
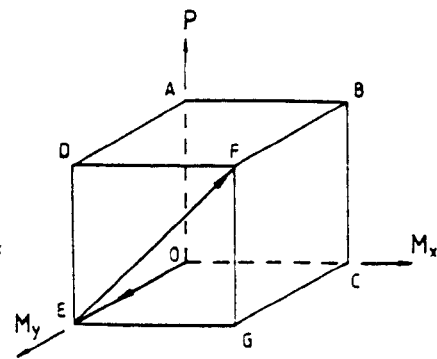
Figure 6.1 (f) Loading Path VI
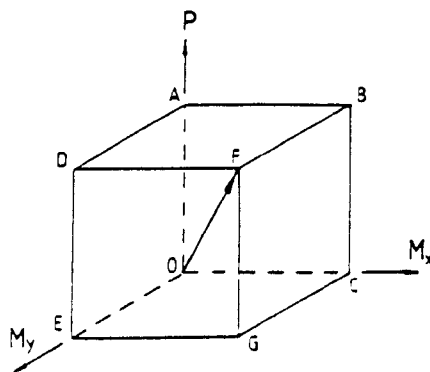
Figure 6.1 (g) Loading Path VII

Figure 6.1 Various Loading Paths

5. the type of cross-section

6. the boundary conditions

7. the residual stress distribution

The extreme difficulty in obtaining an exact inelastic analysis of aluminium beam-columns under biaxial loading, even with the aid of digital computers, is due mainly to the fact that the stress-strain relationship of aluminium shows constant strain hardening. In the inelastic range and using a tangent stiffness approach, the sectorial properties of the member depend on the stress-strain relationship which in turn affects the rotation of the principal axes and the instantaneous positions of the centroid and shear centre. During the Newton-Raphson iteration, each iteration can vary the rotation of the principal axes and the positions of the centroid and the shear centre. This situation, therefore, often introduces convergence problems when considering the equilibrium at joints and updating the geometry. This situation can be improved by using a smaller loading increment but it will cause a dramatic increase in computer time.

As mentioned by other authors, the behaviour of biaxially loaded beam-columns is load path dependent. Seven different loading paths, therefore, were chosen by the author to study which loading path will give the minimum ultimate strength. These loading paths are shown in Figure 6.1; they are:

1. Path I (OB → BF)

   The beam-column is first loaded axially and bent by M_x simultaneously to point B, finally, it is bent by M_y to failure while keeping P and M_x constant.

Loading Path	Ultimate Loading Point		
	$\overline{P}$	$\overline{M}_x$	$\overline{M}_y$
I	0.50	0.35	0.48	(minimum)
II	0.50	0.35	0.50
III	0.57	0.35	0.50
IV	0.50	0.39	0.56
V	0.54	0.35	0.54
VI	0.54	0.38	0.50
VII	0.52	0.36	0.52

NOTE

1. $\lambda_y = 30$
2. The beam-column is pin-ended and warping deformation is free but the twisting is prevented at both ends.

Table 6.1: Effect of Loading Path on Biaxially Loaded Beam-column

2. Path II (OD → DF)

   The beam-column is first loaded axially and bent by M_y simultaneously to point D, finally, it is bent by M_x to failure while keeping P and M_y constant.

3. Path III (OG → GF)

   The beam-column is first bent by M_x and M_y simultaneously to point G, finally, it is loaded axially to failure while keeping M_x and M_y constant.

4. Path IV (OA → AF)

   The beam-column is first loaded axially to point A, finally, it is bent by M_x and M_y simultaneously to failure while keeping P constant.

5. Path V (OC → CF)

   The beam-column is first bent by M_x to point C, finally, it is loaded axially and bent by M_y simultaneously to failure while keeping M_x constant.

6. Path VI (OE → EF)

   The beam-column is first bent by M_y to point E, finally, it is loaded axially and bent by M_x simultaneously to failure while keeping M_y constant.

7. Path VII (O → F)

   P, M_x and M_y are increased proportionally to point F (radial loading).

Table 6.1 shows the results of the ultimate strength analysis of biaxially
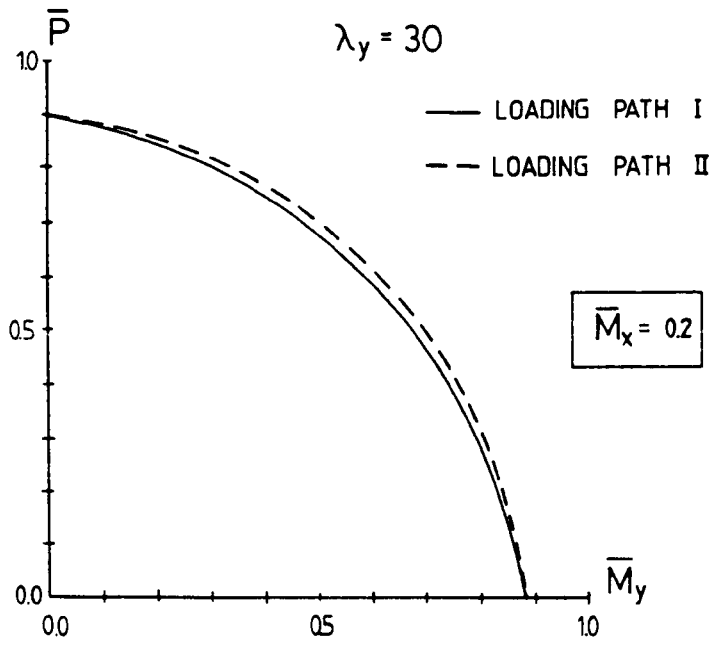
Figure 6.2 Effect of Loading Path ($\beta_x = 1, \beta_y = 1$)

loaded beam-columns for the above different loading paths. The slenderness ratio of the aluminium beam-columns is equal to 30 and the cross-section chosen is the same as Figure 5.5. The beam-columns are under single curvature bending about both major and minor axes and warping is free at the ends. From Table 6.1, we can observe that loading path I will give the minimum strength but loading path II also gives a similar strength. Therefore, loading paths I and II are compared again and the interaction curves obtained by the above two loading paths are shown in Figure 6.2. The ratio $\overline{M}_x = 0.2$ is chosen in the comparison and it further shows that loading path I will give the minimum ultimate strength of the beam-columns.

Although the loading paths I to VII are statically equivalent to each other and they are identical in term of stress resultants, the behaviour of those beam-columns are quite different. For short aluminium beam-columns, the strength is limited only by full plastic yielding of the material of the cross-section. However, the loading path, the types of cross-section and the initial out-of-straightness can influence the initial yielding and the elastic core pattern of the cross-section which directly affects the instantaneous positions of the centroid and the shear centre. If the beam-column is first loaded axially and bent by M_x and bent by M_x simultaneously (i.e. loading path I), the shear centre, which is determined from the elastic core pattern of the cross-section, will be further away from the centroid and will result in more twisting of the beam-column. For intermediate length beam-columns, the initial yielding of the cross-section will affect the instability of the member. The above phenomenon will act as a secondary effect to the beam-columns causing reductions in their ultimate strength. For slender beam-columns, the

material is still elastic up to buckling and the shear centre should coincide with the centroid for doubly symmetric sections. However, different loading paths will have different magnification effects on the laterally instability of beam-columns. The axial load and major axis bending will have the greatest tendency to buckle laterally. This effect is then magnified by the minor axis bending and causes buckling of the whole member.

Finally, the author wants to point out that the effect of loading path on bi-axially loaded beam-column is a very complicated problem. The studies presented herein only concern beam-columns of doubly symmetric cross-section under axial load plus biaxial bending. The problem will be further complicated if the loading paths include the effect of warping and torsion. Problems of this type, which involve the interaction of flexural-torsional buckling; bi-moment and applied torsion in the inelastic range, are certainly beyond the scope of this thesis and the author's knowledge. For asymmetric cross-section in which the shear centre and centroid do not coincide, the member will buckle by a combination of twisting and bending. The twisting of the asymmetric cross-section will play an important role in the effect of loading paths because it can affect the initial position of yielding on the section. Moreover, the effect of residual stresses can be ignored in extruded aluminium profiles, but this cannot be neglected in welded profiles especially in unsymmetric welded cross-sections. Therefore, further studies on the effect of loading paths should be carried out and more parameters, which could affect the ultimate strength of the beam-columns should be included.

6.3   Parametric Studies of Biaxially Loaded Aluminium Beam-columns

The general behaviour of aluminium members under biaxial bending is also simulated by the program BIAXIAL and the principal results can be found in Tables 6.2(a), 6.2(b) and 6.2(c). The doubly symmetric I-section is chosen for the parametric studies and is the same as Figure 5.5. The mechanical properties of parent and reduced-strength zone (RSZ) material are:

$$
\begin{array}{llll}
\underline{\text{Parent}}: & E & = & 70000 \quad N/mm^2 \\
& \sigma_{0.2} & = & 250 \quad N/mm^2 \\
& n & = & 25 \\
\underline{\text{RSZ}}: & E^* & = & 70000 \quad N/mm^2 \\
& \sigma_{0.2}^* & = & 250 \quad N/mm^2 \\
& n^* & = & 10
\end{array}
$$

The beam-columns considered herein are initially twisted in a sine function shape with an initial twisting angle of 0.01 radian at mid-span. The initial displacements in the major and minor axis directions are also assumed to be sine functions, and the maximum values at mid-span are equal and are arbitrarily assumed as $\frac{L}{1000}$. The arrangement of the initial twist and deflections is that they will produce inferior initial conditions and hence the ultimate load capacity is reduced. Moreover, all the beam-columns are pin-ended and warping deformation is unrestrained but the rotation is prevented at both ends. In all the analyses, loading path I is used to obtain the ultimate solutions of the beam-columns (see Section 6.2).

Reference	λ_y	β_x	β_y	Principal Results
NW1	30	1	1	Figure 6.3
NW2	50	1	1	Figure 6.4
NW3	70	1	1	Figure 6.5
NW4	90	1	1	Figure 6.6
NW5	120	1	1	Figure 6.7
NW6	30	1	-1	Figure 6.8
NW7	50	0	1	Figure 6.9
NW8	50	0	0	Figure 6.10
NW9	50	0	-1	Figure 6.11
NW10	70	1	0	Figure 6.12
NW11	70	1	-1	Figure 6.13
NW12	90	-1	1	Figure 6.14
NW13	90	-1	0	Figure 6.15
NW14	90	-1	-1	Figure 6.16
NW15	120	-1	1	Figure 6.17

Table 6.2: (a) List of Cases in Parametric Studies of Non-welded Aluminium Beam-columns under Biaxial Bending

Reference	λ_y	β_x	β_y	$\frac{A^*}{A}$	Principal Results
LW1	30	1	1	0.0, 0.1, 0.5 and 1.0	Figure 6.18
LW2	70	1	1	0.0, 0.1, 0.3 and 1.0	Figure 6.19
LW3	90	1	1	0.0, 0.3, 0.5 and 1.0	Figure 6.20

Table 6.2: (b) List of Cases in Parametric Studies of Longitudinally Welded Aluminium Beam-columns under Biaxial Bending

Reference	λ_y	β_x	β_y	L^* (mm)	$\frac{L^*}{L}$	Principal Results
TW1	30	1	1	30mm at both ends	0.056 at both ends	Figure 6.21
TW2	70	1	1	30mm at both ends	0.024 at both ends	Figure 6.22
TW3	70	1	1	50mm at mid-height	0.040 at mid-height	Figure 6.23
TW4	90	1	1	50mm at mid-height	0.031 at mid-height	Figure 6.24

Table 6.2: (c) List of Cases in Parametric Studies of Transversely Welded Aluminum Beam-columns under Biaxial Bending

6.3.1 Parametric Studies of Non-welded Aluminium Beam-columns

6.3.1.1 Non-welded Aluminium Beam-columns under Compression Plus Uniform Biaxial Bending

The results for the non-welded aluminium beam-columns under compression plus uniform biaxial bending ($\beta_x = 1$, $\beta_y = 1$) are shown in Figures 6.3 to 6.7. This loading condition is the worst and gives minimum ultimate load capacities of the beam-column in the analysis. All the beam-columns are pin-ended and the slenderness ratios, λ_y, range from 30 to 120 ($0.57 \leq \overline{\lambda}_y \leq 2.3$ or $0.49 \leq \overline{\lambda}_M \leq 1.54$). All the figures are presented in the form of interaction plots using the axial and bending strengths of the non-welded section. The largest loop of the curves represents the interaction curve without major axis bending ($\overline{M}_x = 0$). When $\overline{M}_x$ increases, the loop becomes closer to a triangle.

For short beam-columns (say, $\lambda_y = 30$), the effect of lateral deflections on the magnitudes of bending moments is negligible. As a result, the maximum strength occurs when the entire cross-section is fully 'plastic' or 'yielded'. Therefore the failure criteria primarily ~~primary~~ depend on the strain (or stress) limit of the material. Strain limit is chosen in the analysis and the prescribed value is also $\varepsilon_{limit} = 5\varepsilon_{\sigma_{0.2}}$ (see Section 3.3). Beam-columns having material failure will give convex interaction curves and the degree of convexity is dependent ~~depended~~ on the value of ε_{limit}. This convexity condition is not violated even if $\overline{M}_x$ increased.

For intermediate length and slender beam-columns, the instability of the members becomes important and the interaction curves tend to be a straight line. For beam-columns under minor axis bending, M_y, only (i.e. $\overline{P} = 0, \overline{M}_x = 0$), the instability of the members can be neglected and the failure criteria also depend on the material strength. Under this special loading condition, therefore, the interaction curves show the same value of $\overline{M}_y$ for all slenderness ratios as expected. Moreover, for beam-columns under major and minor axis bending only ($\overline{P} = 0$), the interaction curves change from convex shape to concave as the slenderness ratio increases. The reason for obtaining the concave curves is because the beam-columns are controlled by yielding of material rather than lateral buckling as the value of $\overline{M}_x$ is decreased.
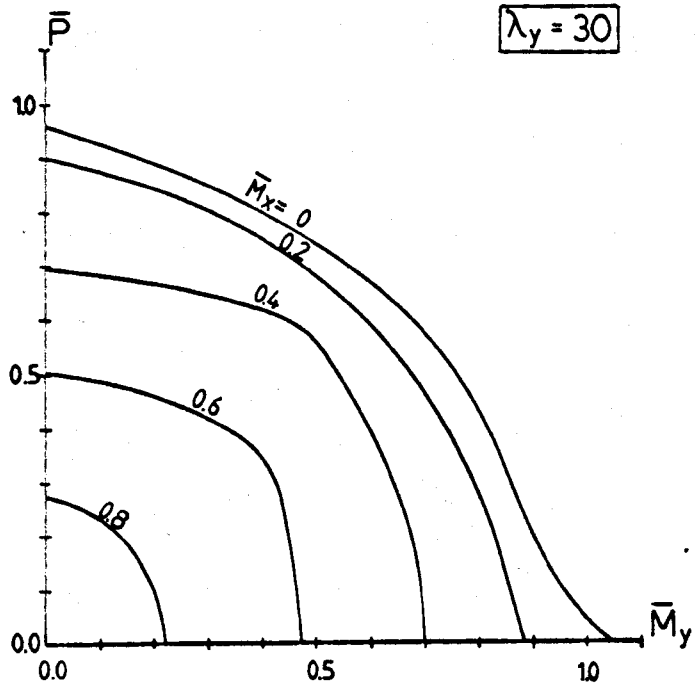
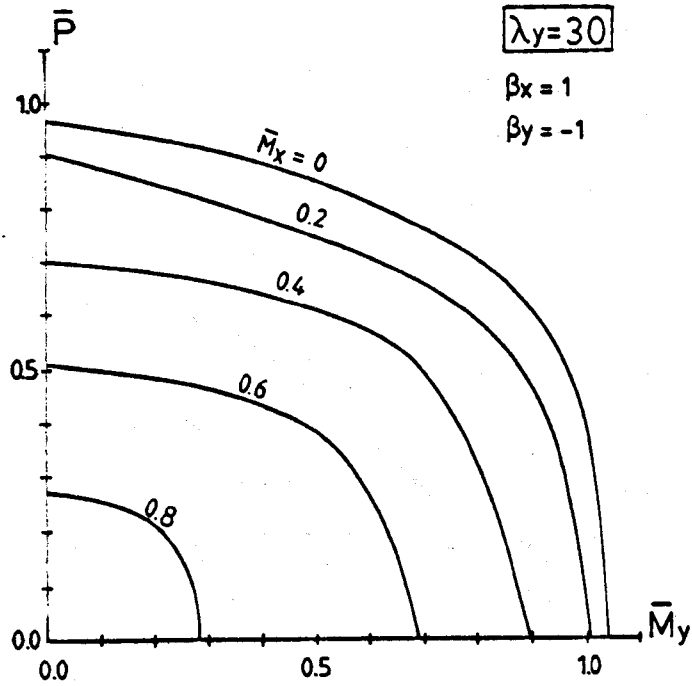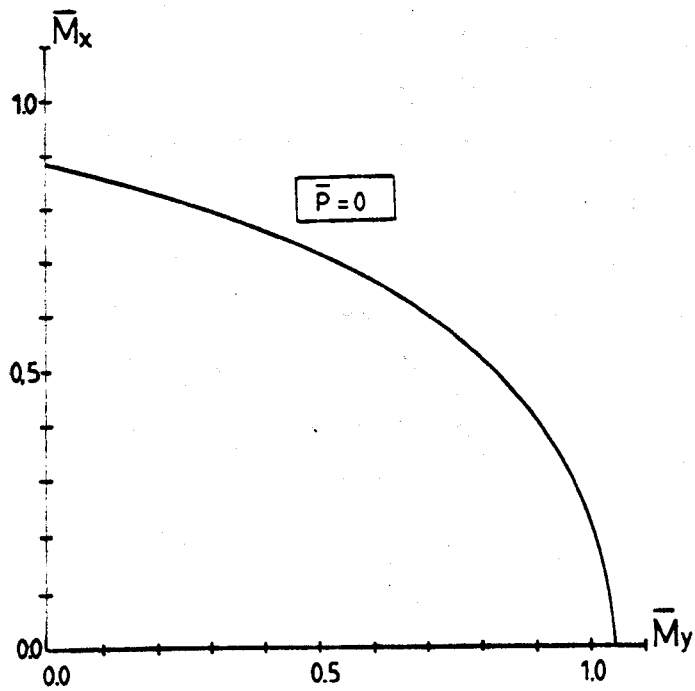Figure 6.3 (a)
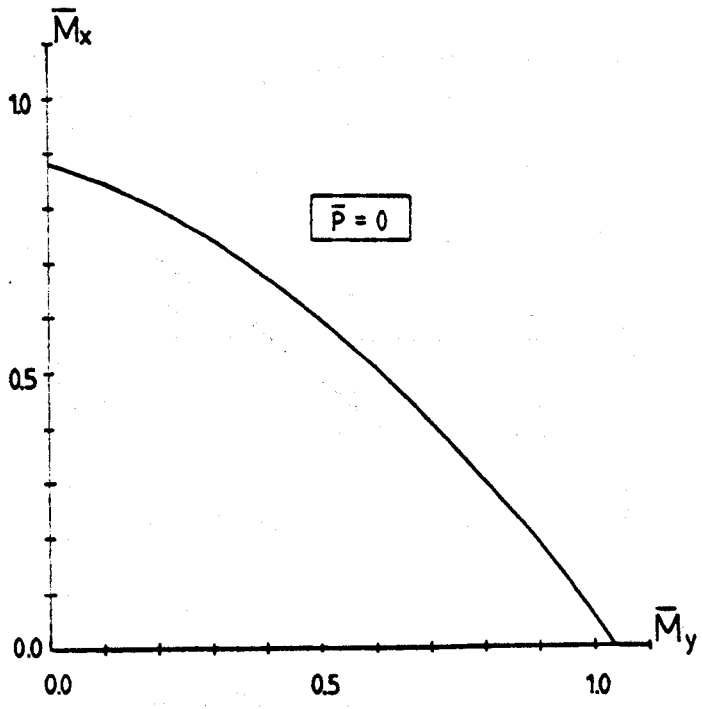
Figure 6.3 (b)

Figure 6.3 Interaction Curves for Non-welded Aluminium Beam-columns
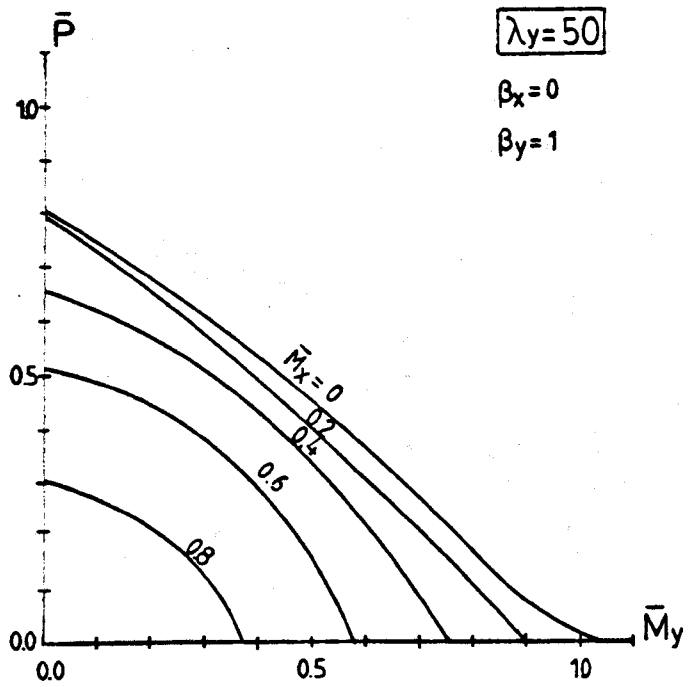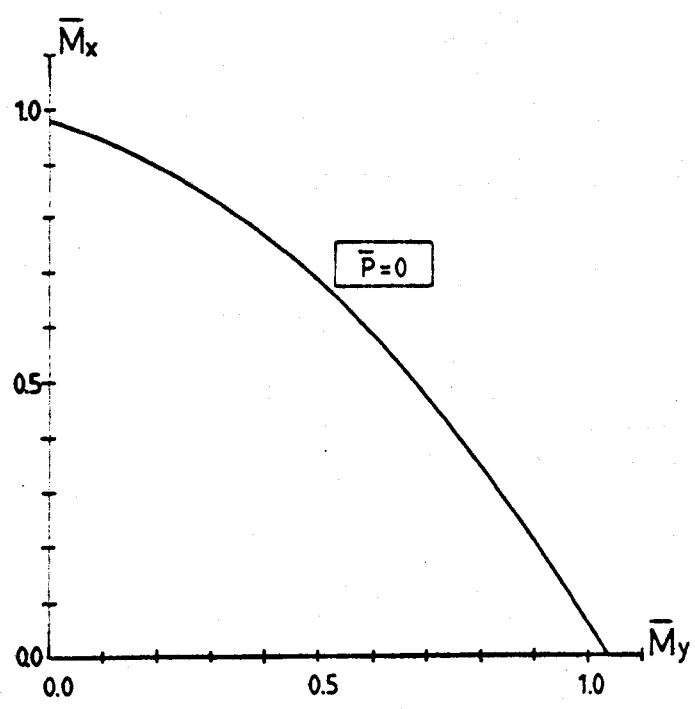with $\lambda_y = 30$ ($\beta_x = 1, \beta_y = 1$)
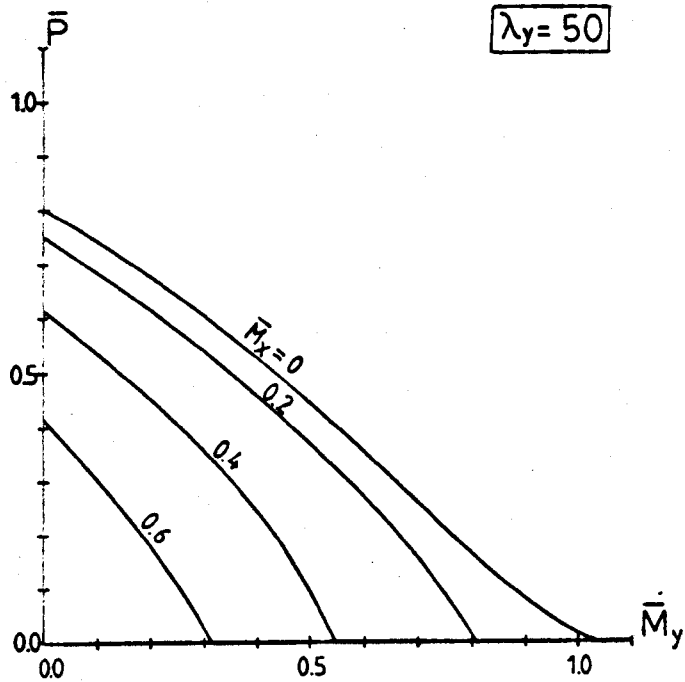
Figure 6.4 (a)
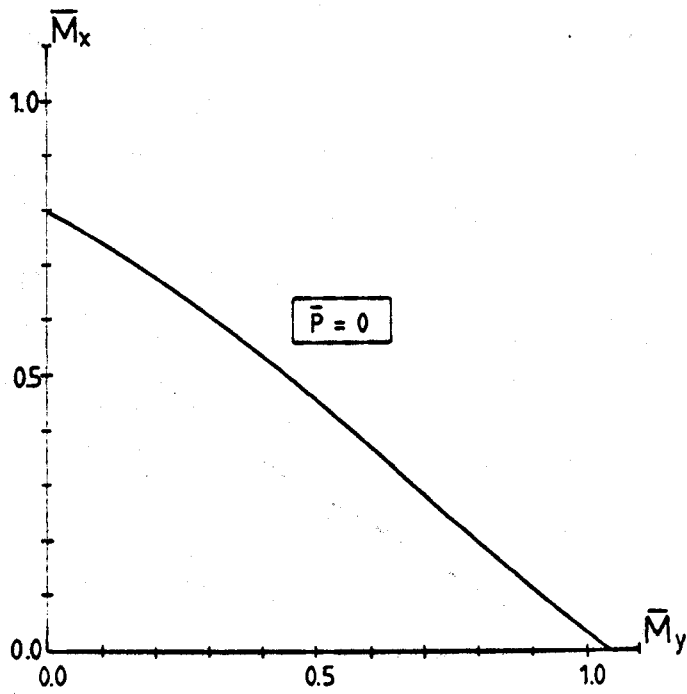
Figure 6.4 (b)

Figure 6.4 Interaction Curves for Non-welded Alumiunum Beam-columns with $\lambda_y = 50$ ($\beta_x = 1, \beta_y = 1$)
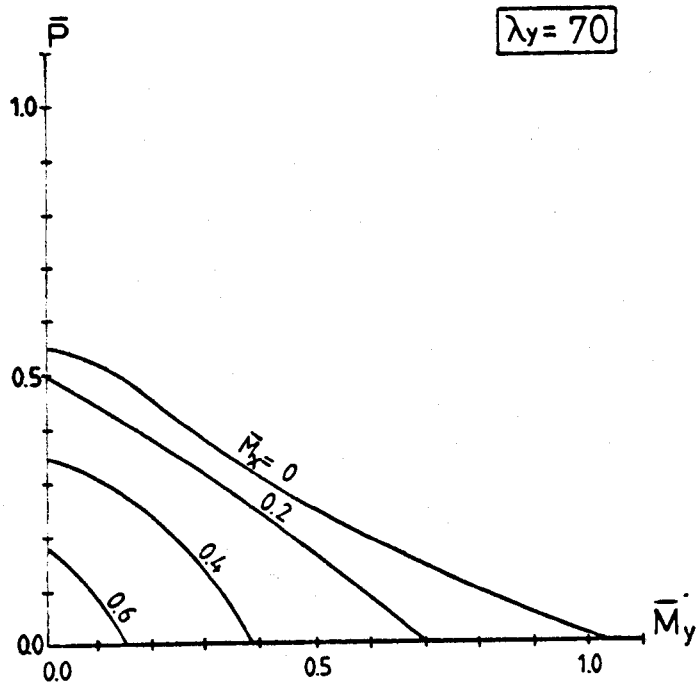
Figure 6.5 (a)
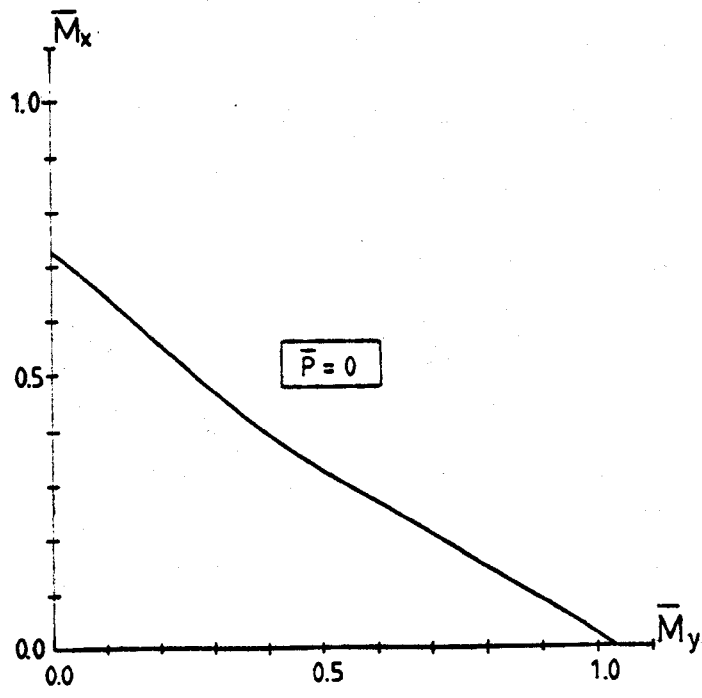
Figure 6.5 (b)

Figure 6.5 Interaction Curves for Non-welded Aluminium Beam-columns with $\lambda_y = 70$ ($\beta_x = 1, \beta_y = 1$)
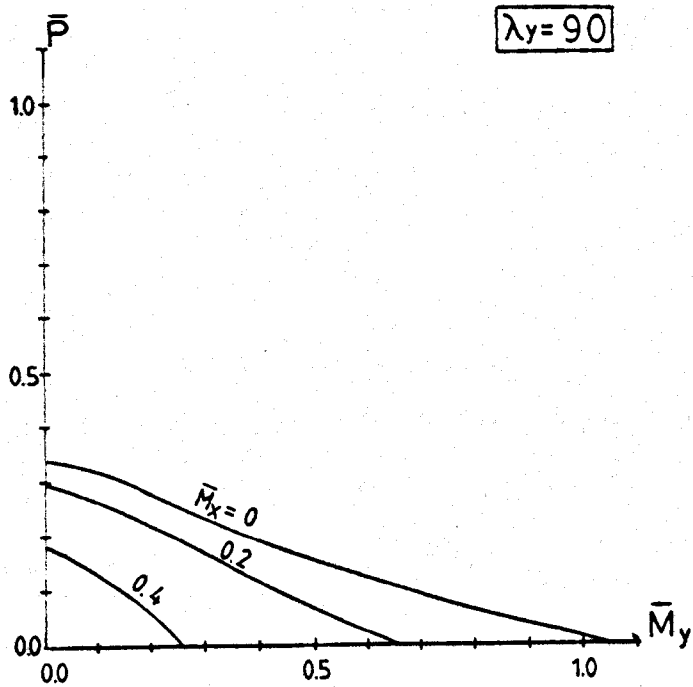
Figure 6.6 (a)
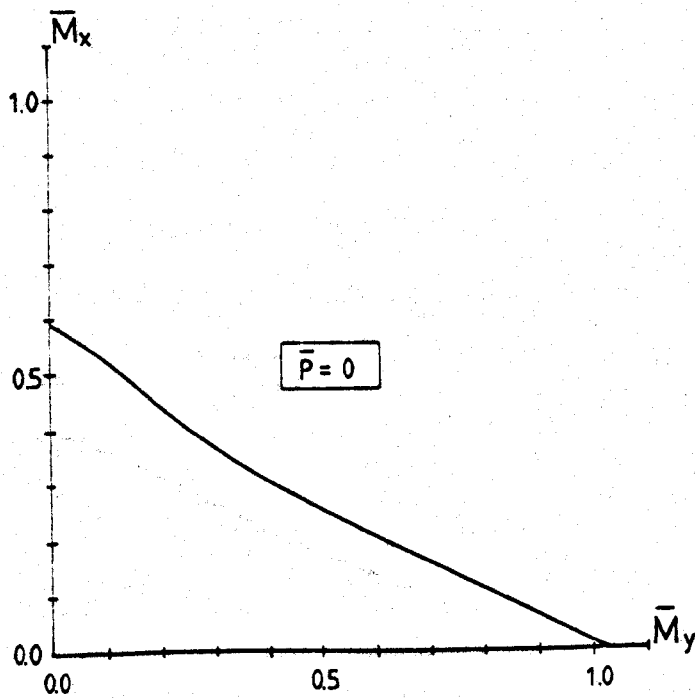
Figure 6.6 (b)

Figure 6.6 Interaction Curves for Non-welded Aluminium Beam-columns with $\lambda_y = 90$ ($\beta_x = 1, \beta_y = 1$)
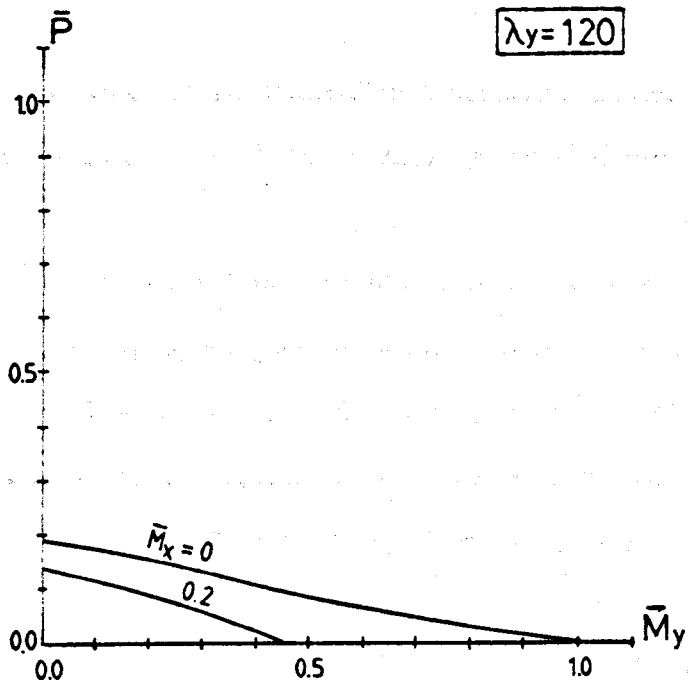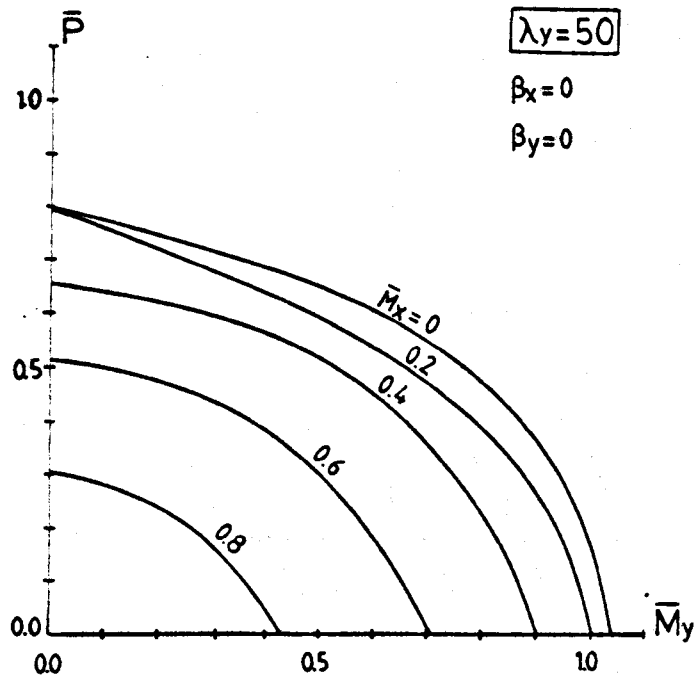
Figure 6.7 (a)
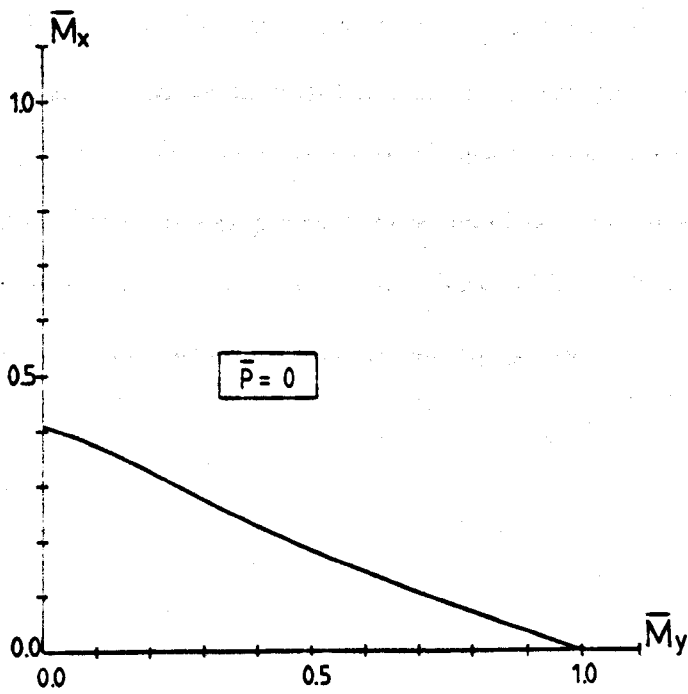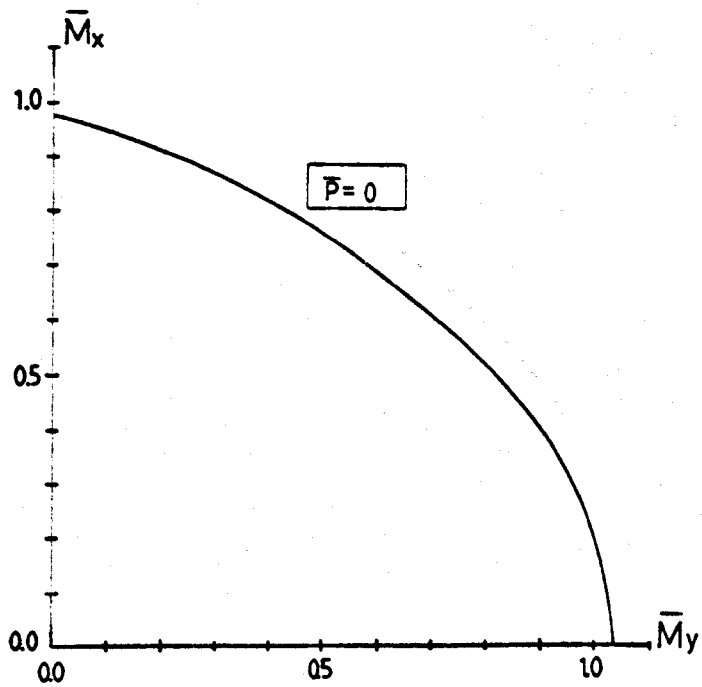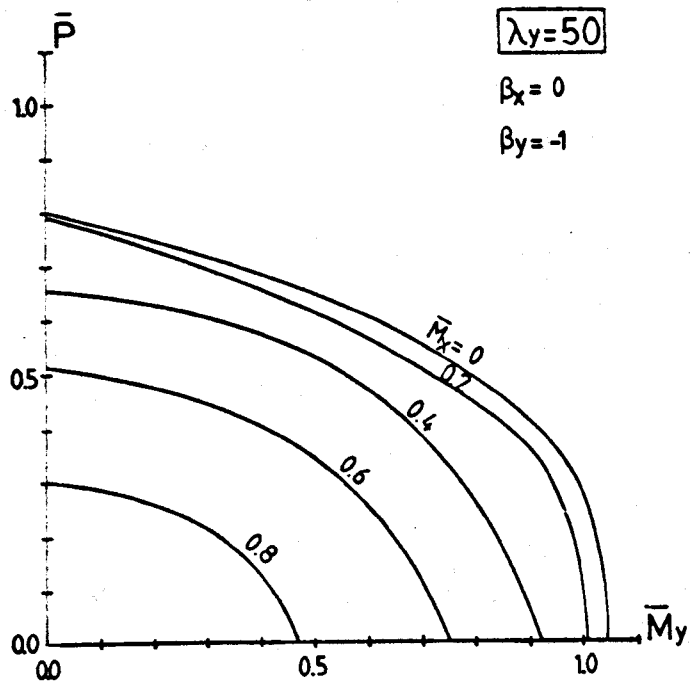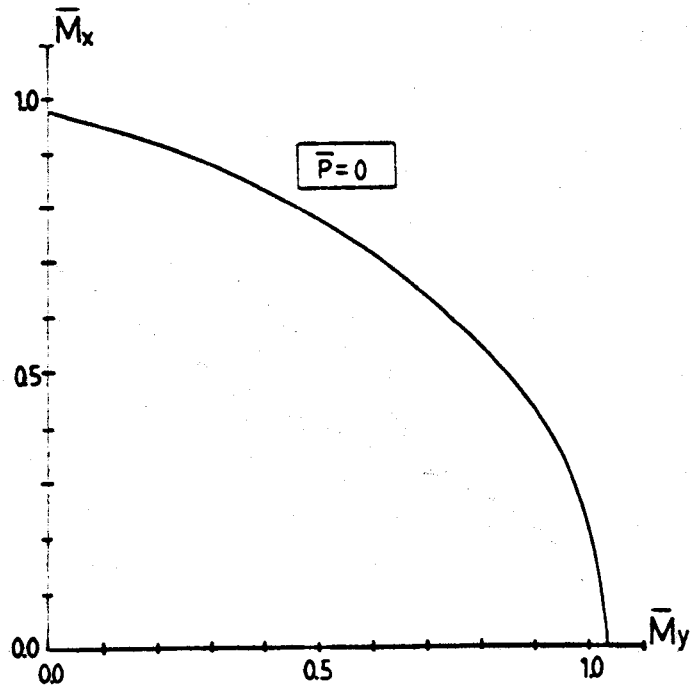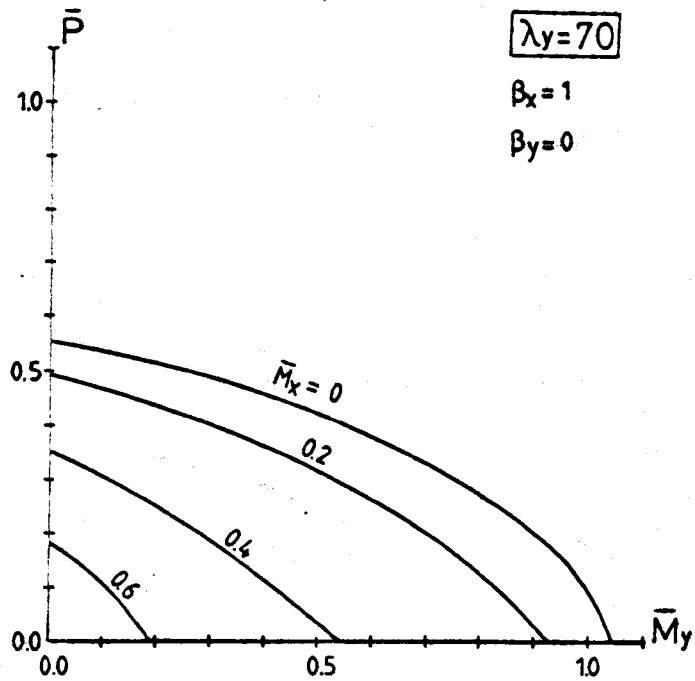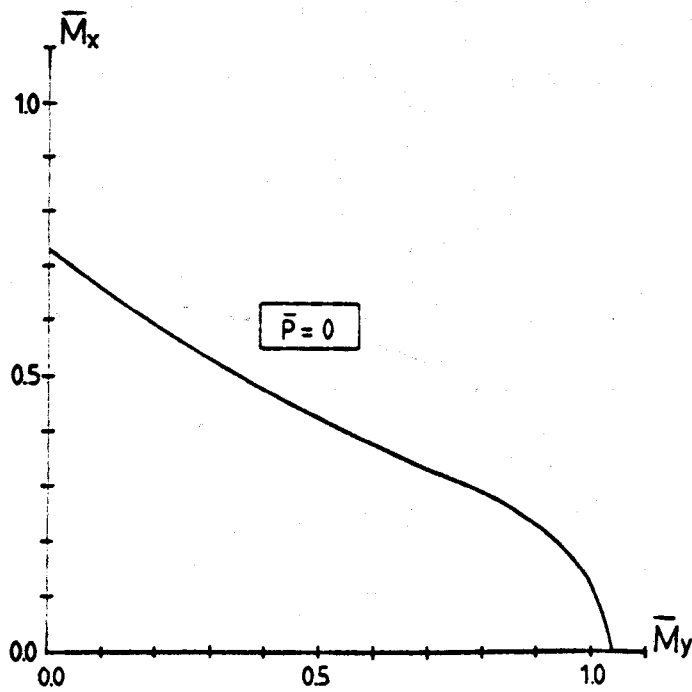

Figure 6.7 (b)

Figure 6.7 Interaction Curves for Non-welded Aluminium Beam-columns with $\lambda_y = 120$ ($\beta_x = 1, \beta_y = 1$)

6.3.1.2   Non-welded Aluminium Beam-columns under
Compression Plus Non-uniform Biaxial Bending

The results for the non-welded aluminium beam-columns under compression plus non-uniform biaxial bending are shown in Figures 6.8 to 6.17. The combination of β_x and β_y and with the slenderness ratio can be referred to Table 6.2(a). The values of β_x and β_y are either 1, 0 or -1. The slenderness ratios, λ_y, also range from 30 to 120 ($0.57 \leq \overline{\lambda}_y \overset{\leq}{_\wedge} 2.3$ or $0.49 \leq \overline{\lambda}_M \leq 1.54$). From the figures, we can observe that beam-columns under non-uniform bending about either axis show an increase in ultimate strength and the interaction curves tend to be convex in shape. The reason is that for the instability problem of beam-columns, minor axis deflection and twists are often significant due to minor axis bending and torsional stiffnesses being small. These deformations will be magnified by the axial load and major axis moment and cause deterioration of the member stiffness. The minor axis deflection and twists will be smaller if the beam-column is under moment gradient about either axis rather than under single curvature bending about both axes. Furthermore, it is quite obvious that the most favourable loading condition is the beam-column under double curvature bending ($\beta_x = -1, \beta_y = -1$) about both axis.
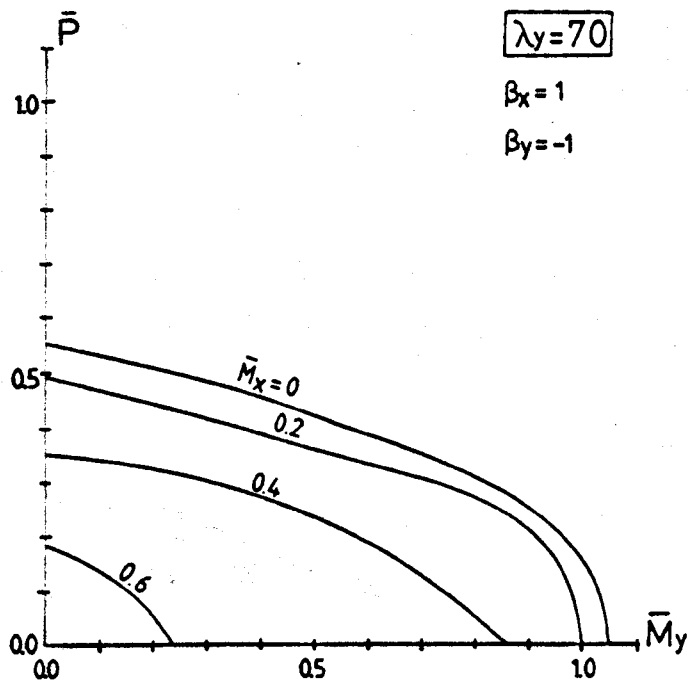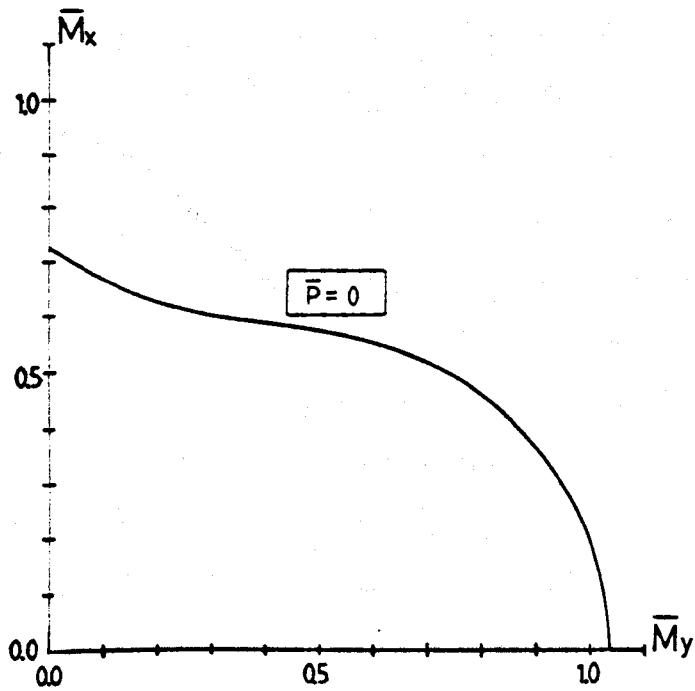
Figure 6.8 (a)

Figure 6.8 (b)

Figure 6.8 Interaction Curves for Non-welded Aluminumn Beam-columns with $\lambda_y = 30$ ($\beta_x = 1, \beta_y = -1$)
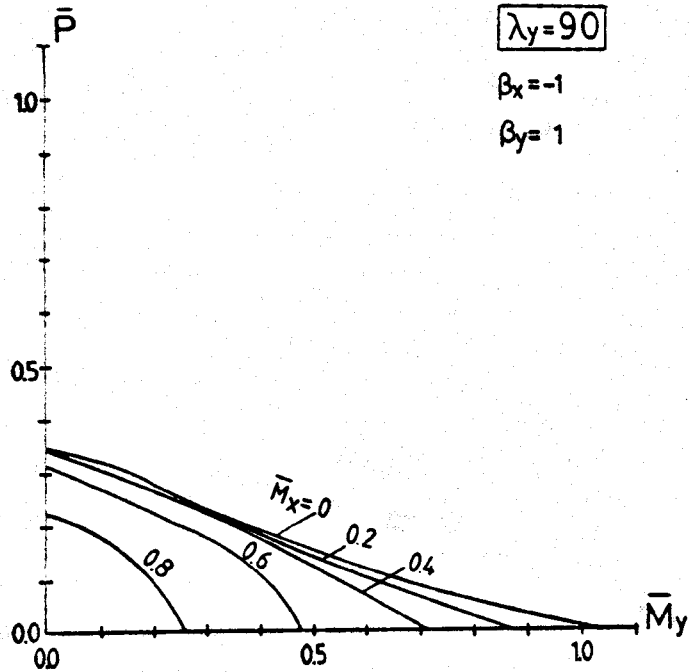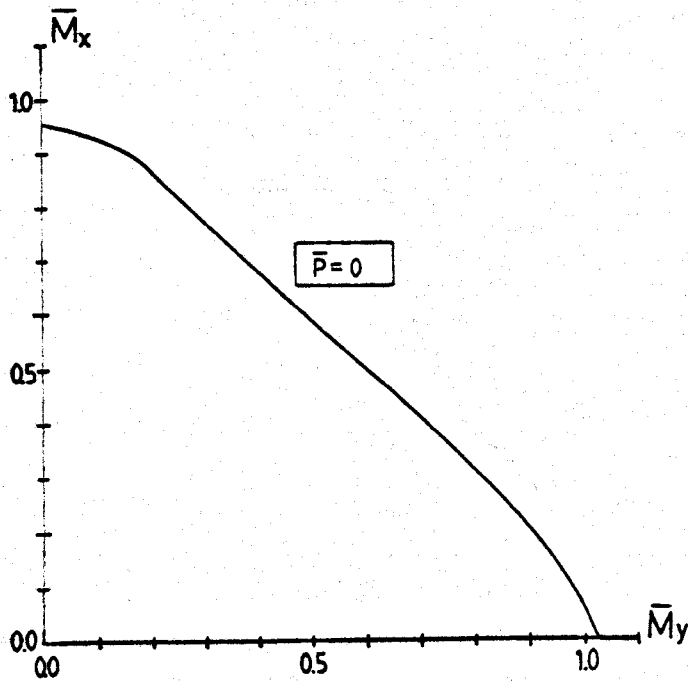
Figure 6.9 (a)

Figure 6.9 (b)

Figure 6.9 Interaction Curves for Non-welded Aluminium Beam-columns with $\lambda_y = 50$ ($\beta_x = 0, \beta_y = 1$)
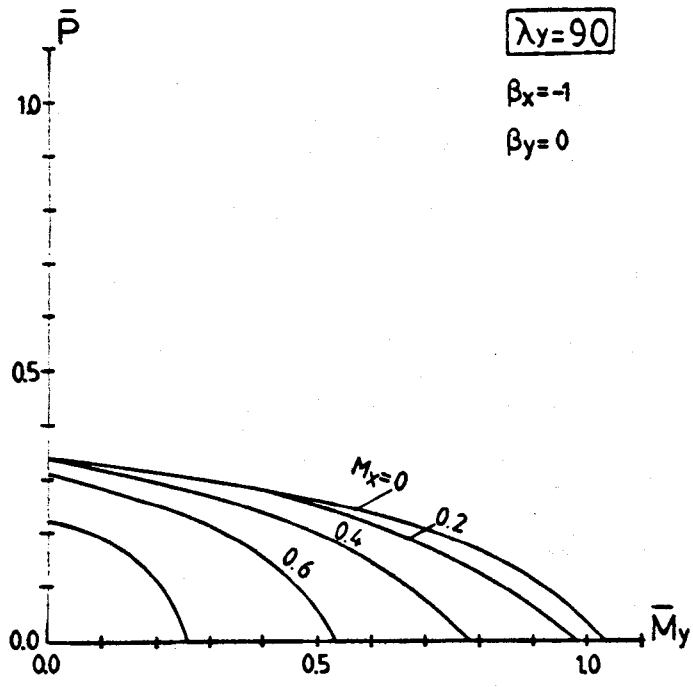
Figure 6.10 (a)

Figure 6.10 (b)

Figure 6.10 Interaction Curves for Non-welded Aluminium Beam-columns with $\lambda_y = 50$ ($\beta_x = 0, \beta_y = 0$)

Figure 6.11 (a)

Figure 6.11 (b)

Figure 6.11 Interaction Curves for Non-welded Aluminium Beam-columns
with $\lambda_y = 50$ ($\beta_x = 0, \beta_y = -1$)
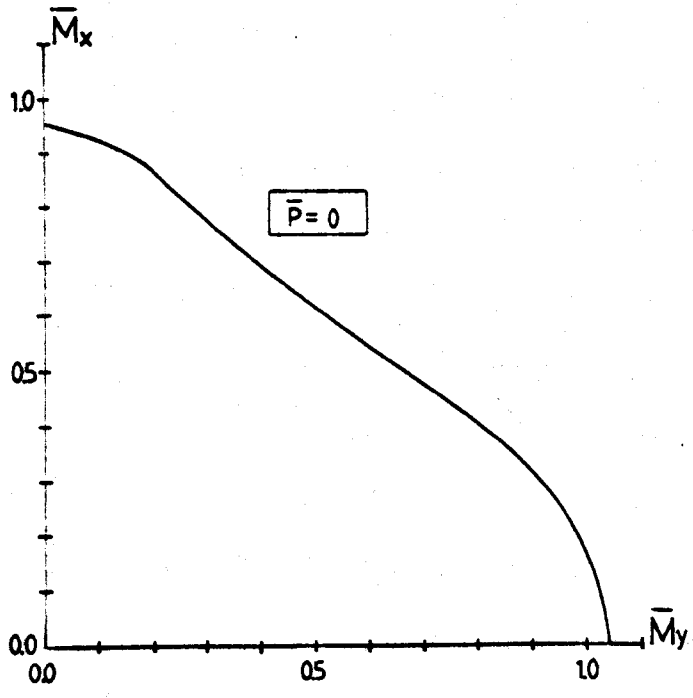
Figure 6.12 (a)

Figure 6.12 (b)

Figure 6.12 Interaction Curves for Non-welded Aluminium Bean-columns with $\lambda_y = 70$ ($\beta_x = 1, \beta_y = 0$)

Figure 6.13 (a)

Figure 6.13 (b)

Figure 6.13 Interaction Curves for Non-welded Aluminium Beam-columns
with $\lambda_y = 70$ ($\beta_x = 1, \beta_y = -1$)
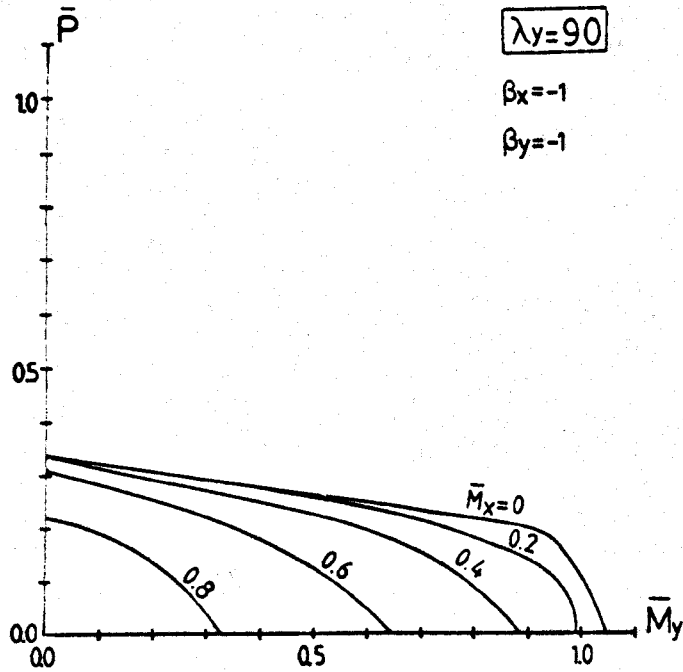
Figure 6.14 (a)

Figure 6.14 (b)

Figure 6.14 Interaction Curves for Non-welded Aluminium Beam-columns
with $\lambda_y = 90$ ($\beta_x = -1, \beta_y = 1$)

Figure 6.15 (a)

Figure 6.15 (b)

Figure 6.15 Interaction Curves for Non-welded Aluminium Beam-columns with $\lambda_y = 90$ ($\beta_x = -1, \beta_y = 0$)
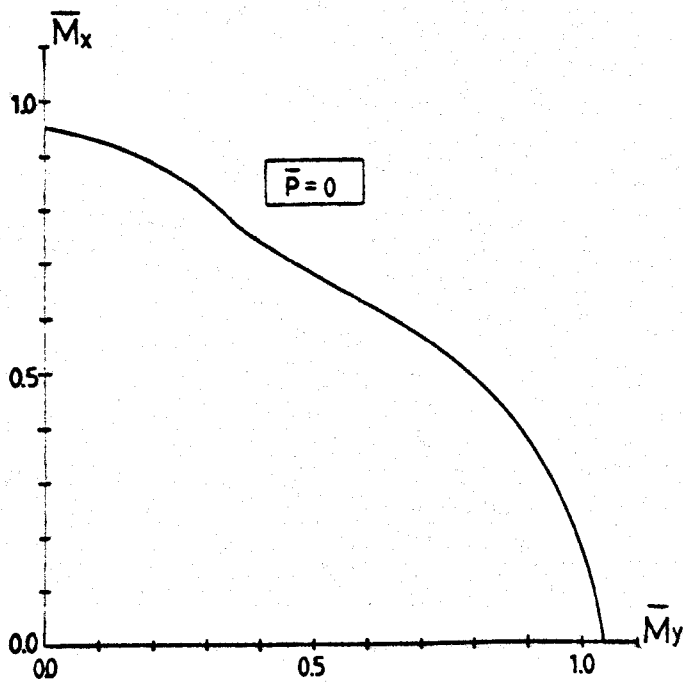
Figure 6.16 (a)

Figure 6.16 (b)

Figure 6.16 Interaction Curves for Non-welded Aluminium Beam-columns with $\lambda_y = 90$ ($\beta_x = -1, \beta_y = -1$)
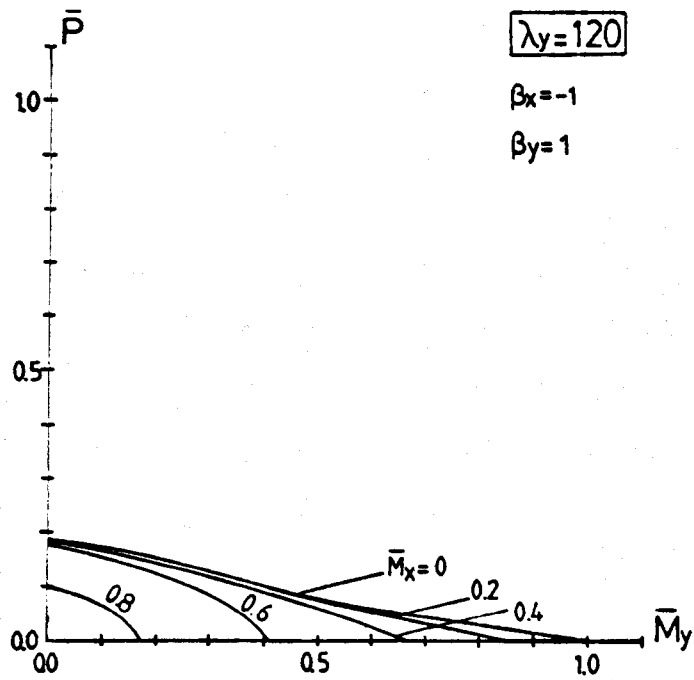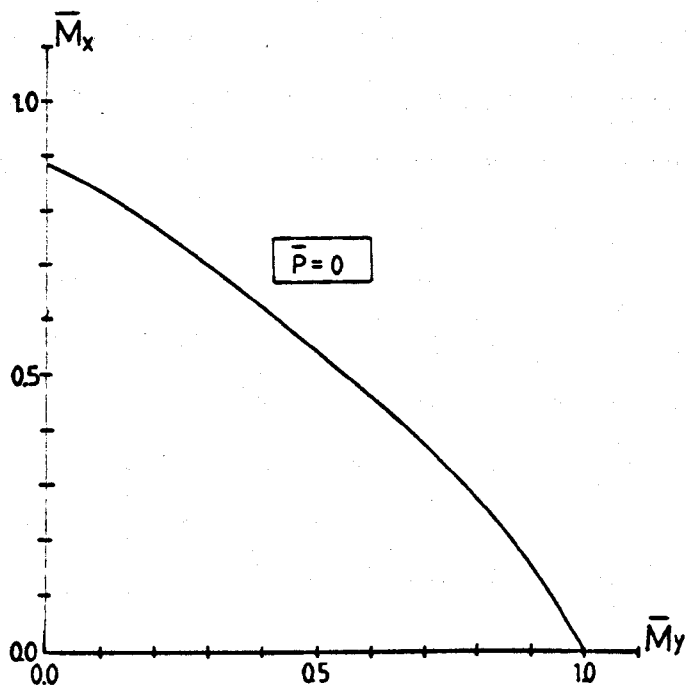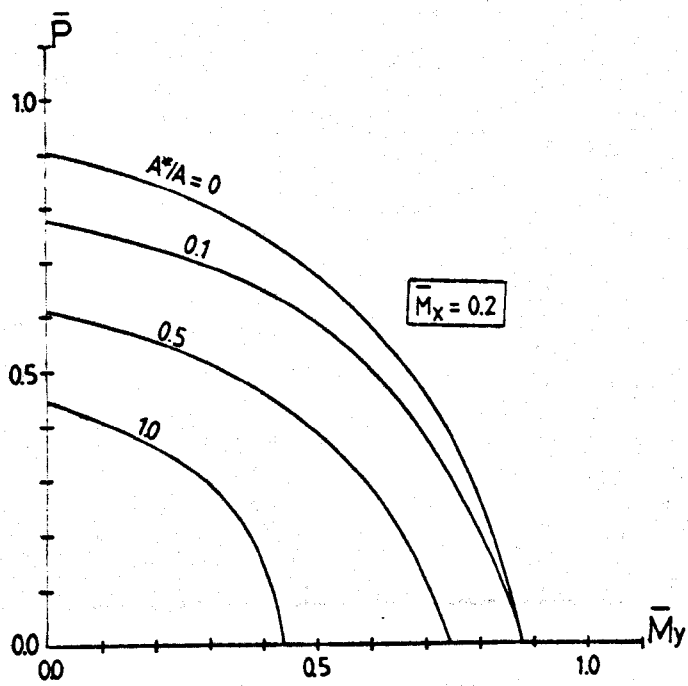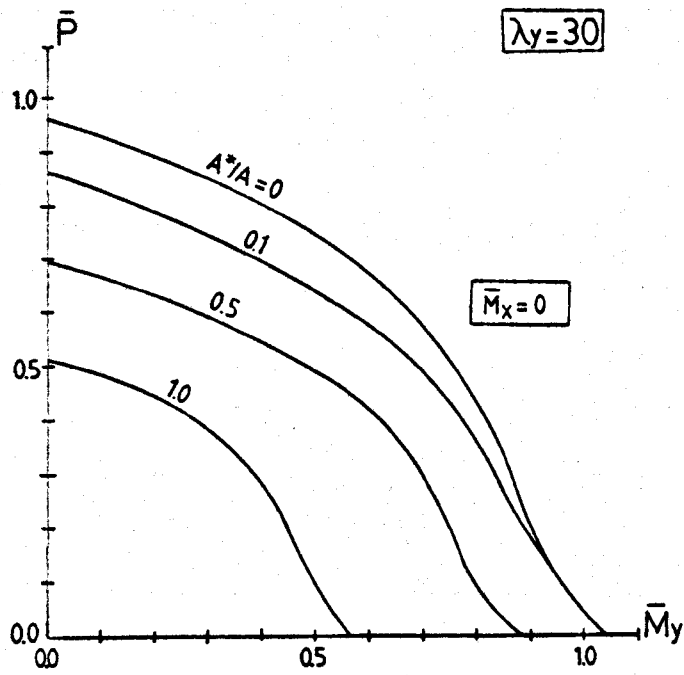
Figure 6.17 (a)

Figure 6.17 (b)

Figure 6.17 Interaction Curves for Non-welded Aluminium Beam-columns with $\lambda_y = 120$ ($\beta_x = -1, \beta_y = 1$)

6.3.2   Parametric Studies of Longitudinally Welded Aluminium Beam-columns

The results for the longitudinally welded aluminium beam-columns under compression plus uniform biaxial bending ($\beta_x = 1, \beta_y = 1$) are shown in Figures 6.18 to 6.20. The slenderness ratio chosen in the parametric studies is either $\lambda_y = 30$, 70 or 90 ($\overline{\lambda}_y = 0.57$, 1.33 and 1.71 or $\overline{\lambda}_M = 0.49$, 1.04 and 1.26). The values of $\frac{A^*}{A}$ vary from 0.1, 0.3, 0.5 to 1.0 as shown in Table 6.2(b) where $\frac{A^*}{A} = 1.0$ represents the member fully-affected by welding. The area of the RSZ zone, A^*, on the cross-section is symmetrically located at the joints of flange-web and the residual stress distribution is also determined by the Cambridge model (see Section 2.3.3.3 and Figure 5.8)

In Figure 6.18, the longitudinally welded beam-columns are quite stocky ($\lambda_y = 30$) and the ultimate load is controlled by the strength of parent metal and RSZ material. The reduction in ultimate load, therefore, is increased as the area of the RSZ zone, A^*, is also increased. The convexity condition is also observed in the interaction curves for the longitudinally welded beam-columns. As the slenderness of the beam-columns is increased ($\lambda_y = 70$ in Figure 6.19 and $\lambda_y = 90$ in Figure 6.20), the interaction curves also tend to be a straight line. Moreover, the interaction curves of $\frac{A^*}{A} = 0.1$, 0.3 and 0.5 are quite close together because the RSZ material is stressed about to the elastic limit up to failure. Therefore, it shows that the ultimate strength of longitudinally welded beam-columns under biaxial bending also depend on the stress level of RSZ material. Severe reduction in ultimate strength will occur only when the RSZ material is sufficiently stressed.
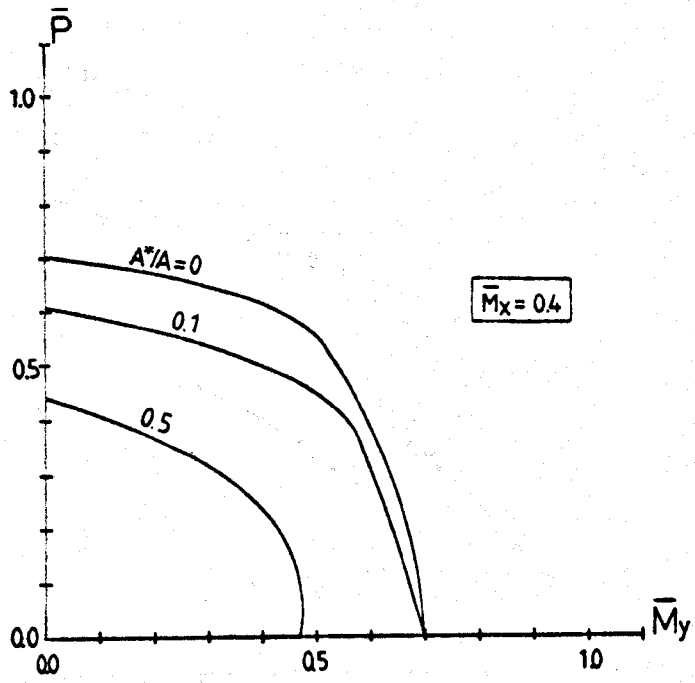
Figure 6.18 (a)
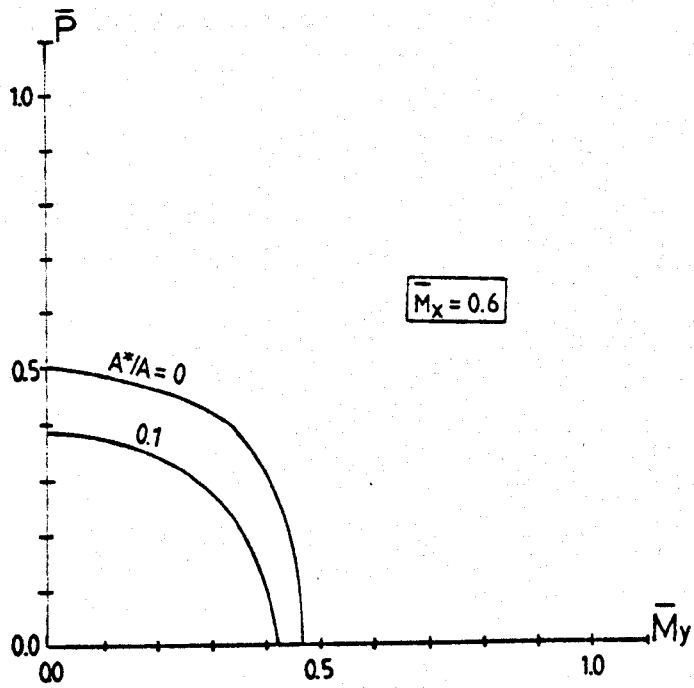

Figure 6.18 (b)

Figure 6.18 (c)

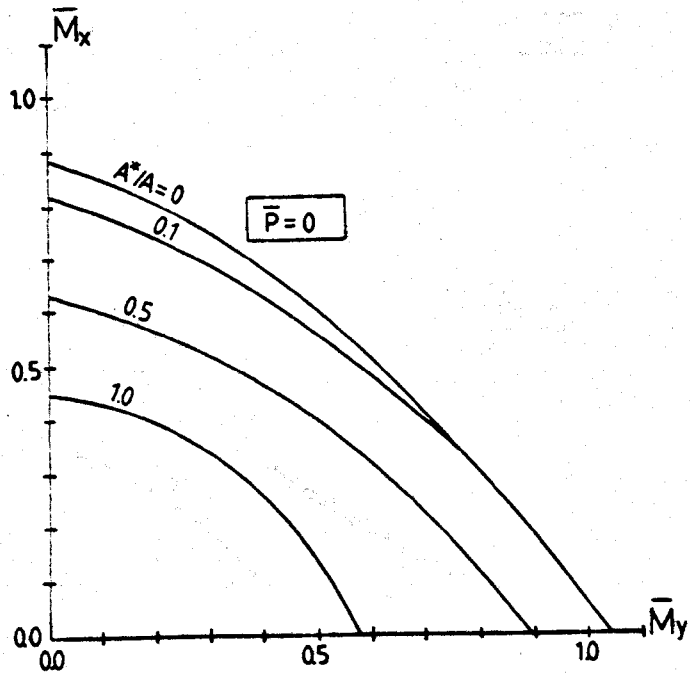Figure 6.18 (d)

Figure 6.18 (e)

Figure 6.18 Interaction Curves for Longitudinally Welded Aluminium Beam-columns with $\lambda_y = 30$ ($\beta_x = 1, \beta_y = 1$)

Figure 6.19 (a)

Figure 6.19 (b)

Figure 6.19 (c)
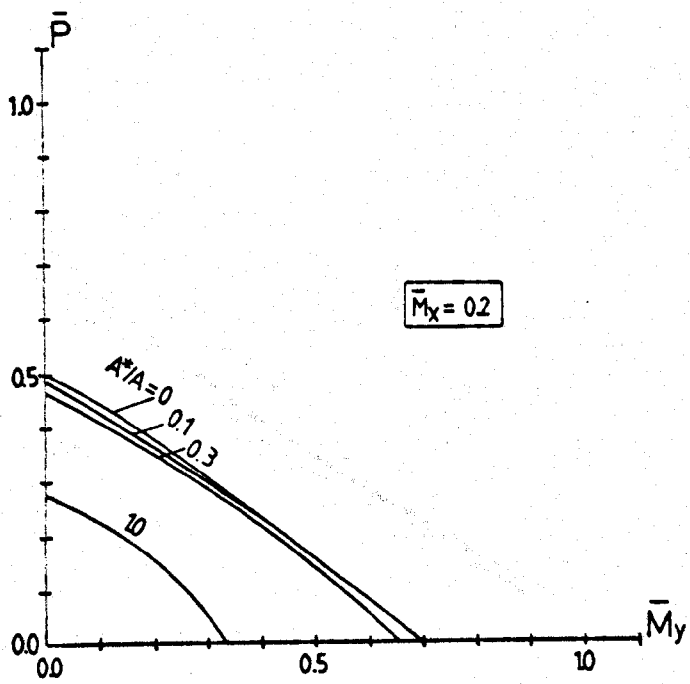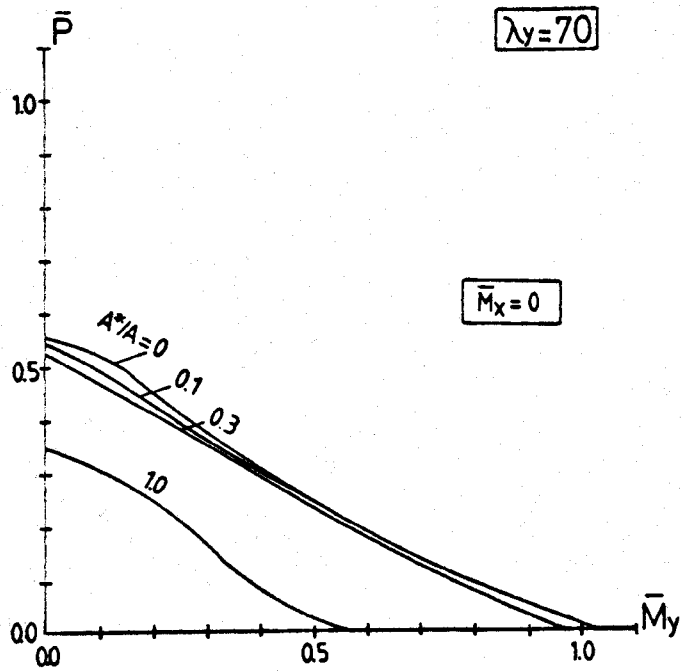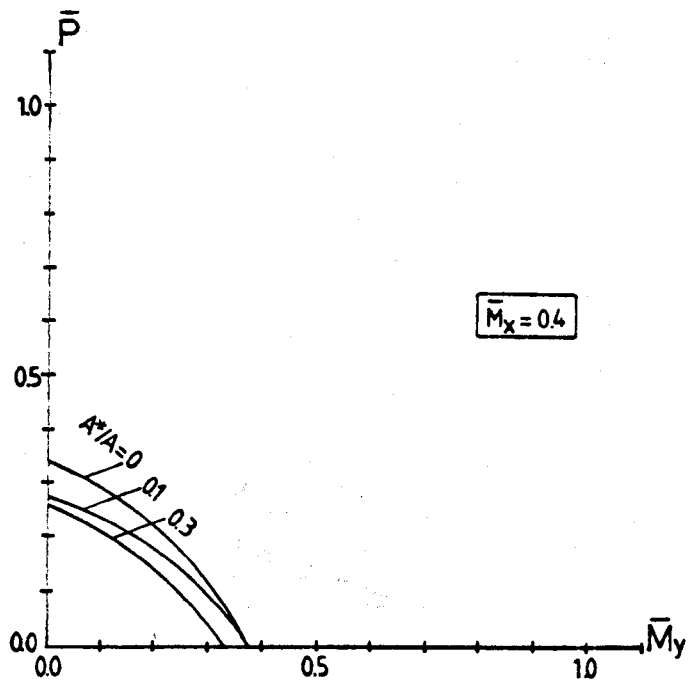

Figure 6.19 (d)

Figure 6.19 Interaction Curves for Longitudinally Welded Aluminium Members with $\lambda_y = 70$ ($\beta_x = 1, \beta_y = 1$)

Figure 6.20 (a)
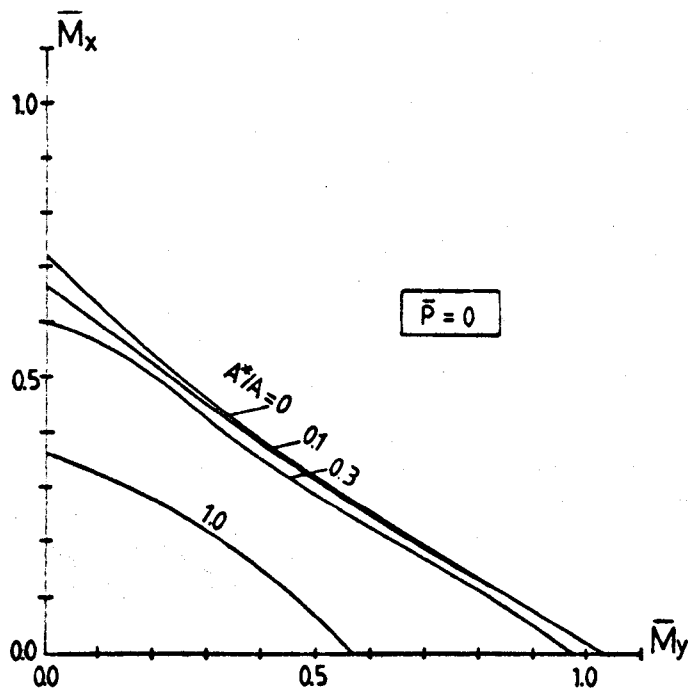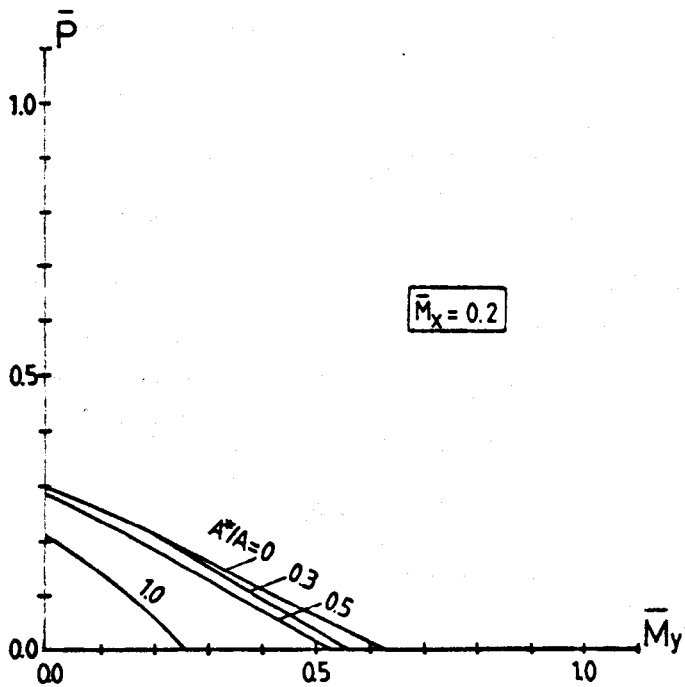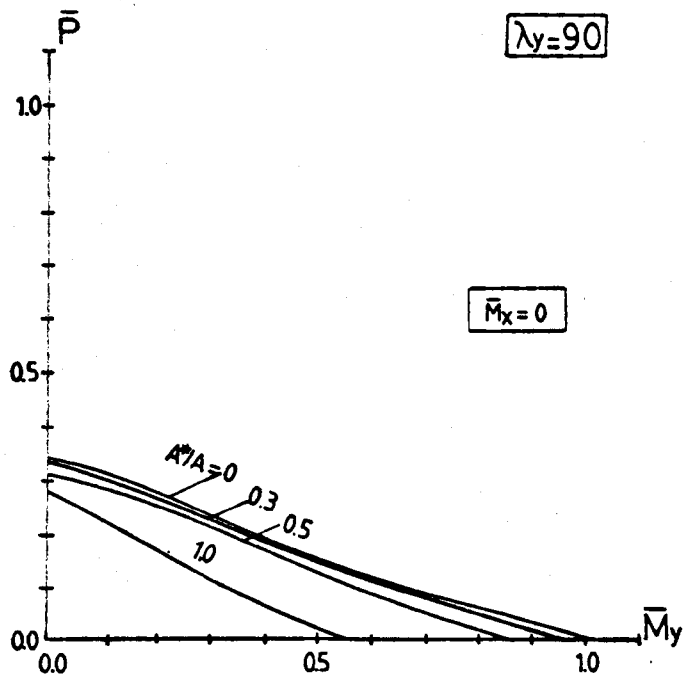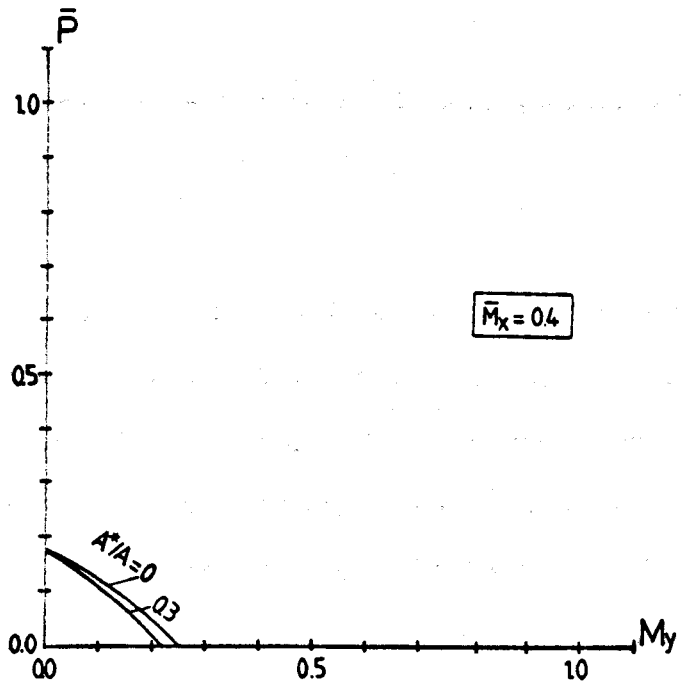

Figure 6.20 (b)
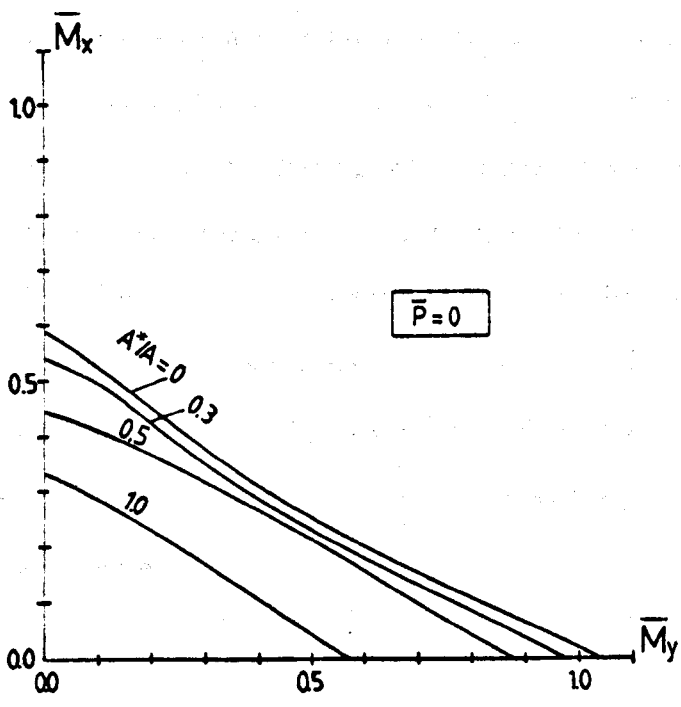
Figure 6.20 (c)

Figure 6.20 (d)

Figure 6.20 Interaction Curves for Longitudinally Welded Aluminium Members with $\lambda_y = 90$ ($\beta_x = 1, \beta_y = 1$)

6.3.3   Parametric Studies of Transversely Welded Beam-columns

The results for the transversely welded aluminium beam-columns under compression plus biaxial bending ($\beta_x = 1, \beta_y = 1$) are shown in Figure 6.21 to 6.24. The slenderness ratio chosen in the parametric studies is also either λ_y= 30, 70 or 90 ($\overline{\lambda}_y$= 0.57, 1.33 and 1.71 or $\overline{\lambda}_M$= 0.49, 1.04 and 1.26). The positions and the extent of the reduced-strength-zone (RSZ) are either 30 *mm* located at both ends or 50 *mm* located at mid-height as shown in Table 6.2(c).

Since the beam-columns are under single curvature bending about both axis ~~axis~~ from the bending moment diagram, the RSZ material should be sufficiently stressed to cause reductions in ultimate strength of the beam-columns except for members buckling elastically. Therefore, from the interaction curves shown in Figures 6.21 to 6.24, in keeping with the previous investigation, we can observe that the presence of RSZ can cause severe reductions in ultimate strength even if the extent of RSZ is small. Moreover, the strength of the transversely welded beam-column is also quite similar to the beam-column which is fully heat-affected, so it further supports the concert that to design the transversely welded members as members containing wholly RSZ material is quite reasonable.

Figure 6.21 (a)

Figure 6.21 (b)

Figure 6.21 (c)

Figure 6.21 (d)

Figure 6.21 Interaction Curves for Transversely Welded Aluminium Beam-columns with $\lambda_y = 30$ ($L^* = 30\ mm$ at Both Ends, $\beta_x = 1, \beta_y = 1$)
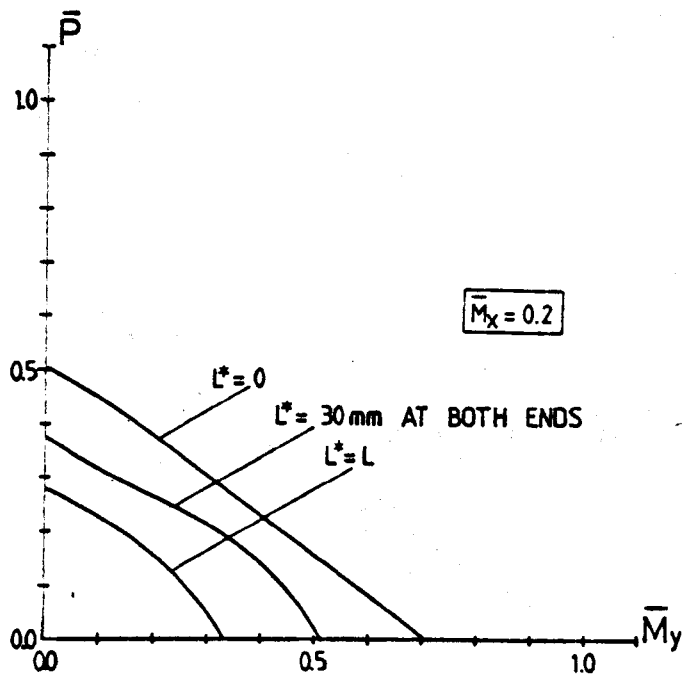
Figure 6.22 (a)
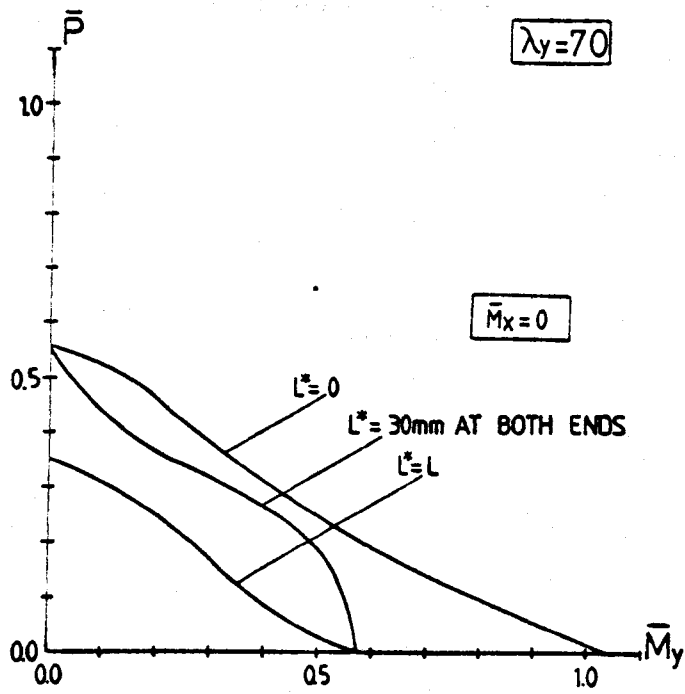
Figure 6.22 (b)
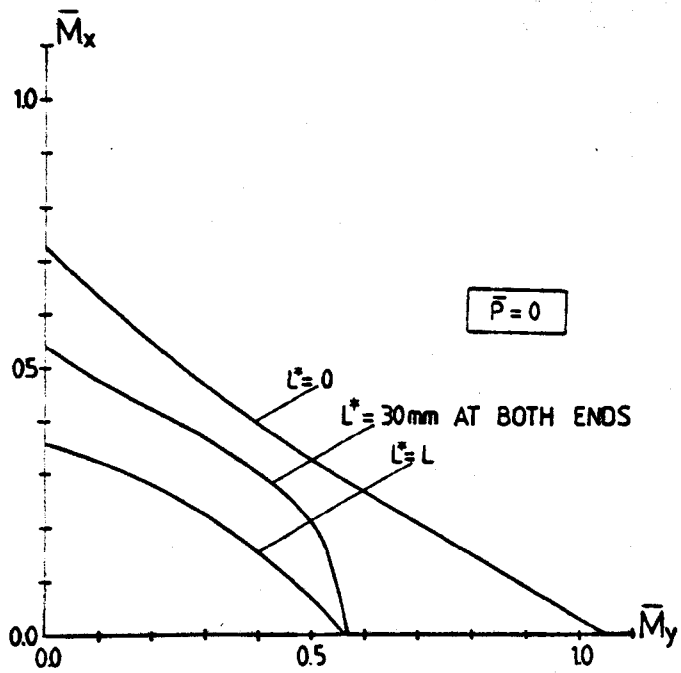
Figure 6.22 (c)

Figure 6.22 Interaction Curves for Transversely Welded Aluminium Beam-columns with $\lambda_y = 70$ ($L^* = 30\ mm$ at Both Ends, $\beta_x = 1, \beta_y = 1$)
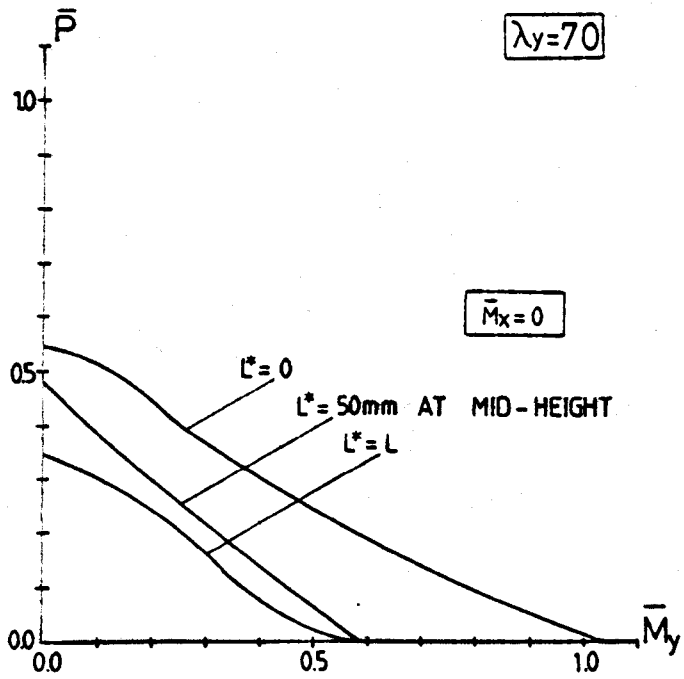
Figure 6.23 (a)
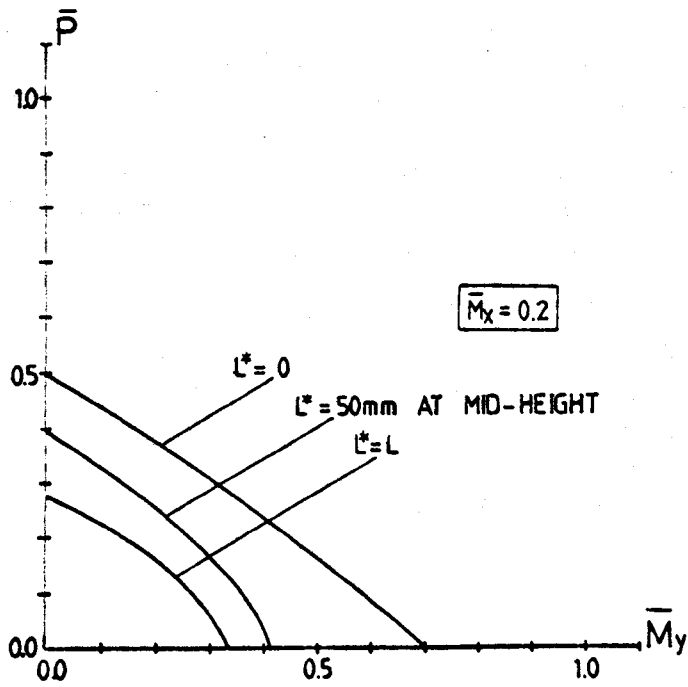
Figure 6.23 (b)
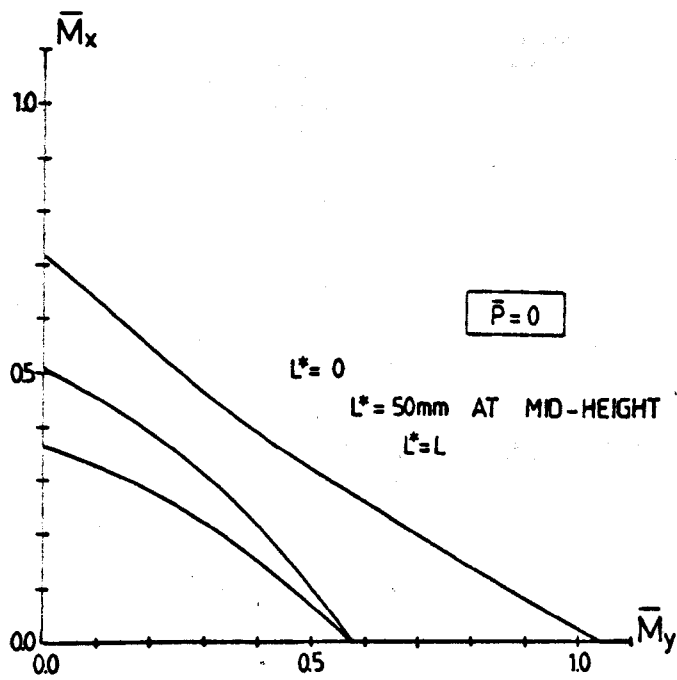
Figure 6.23 (c)

Figure 6.23 Interaction Curves for Transversely Welded Aluminium Beam-columns with $\lambda_y = 70$ ($L^* = 50\ mm$ at Mid-height, $\beta_x = 1, \beta_y = 1$)
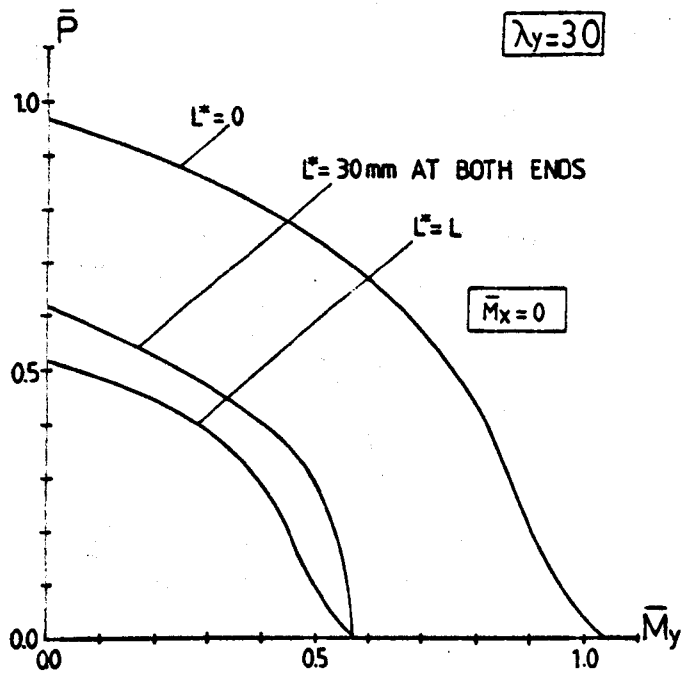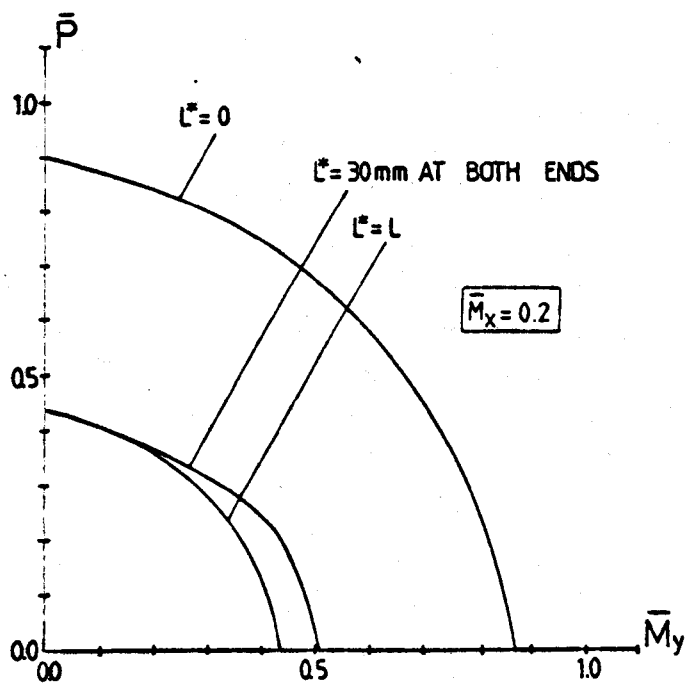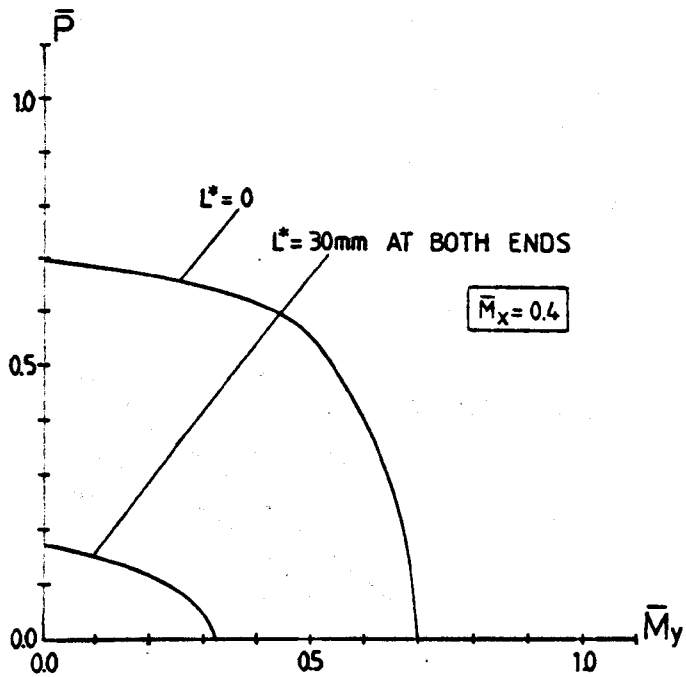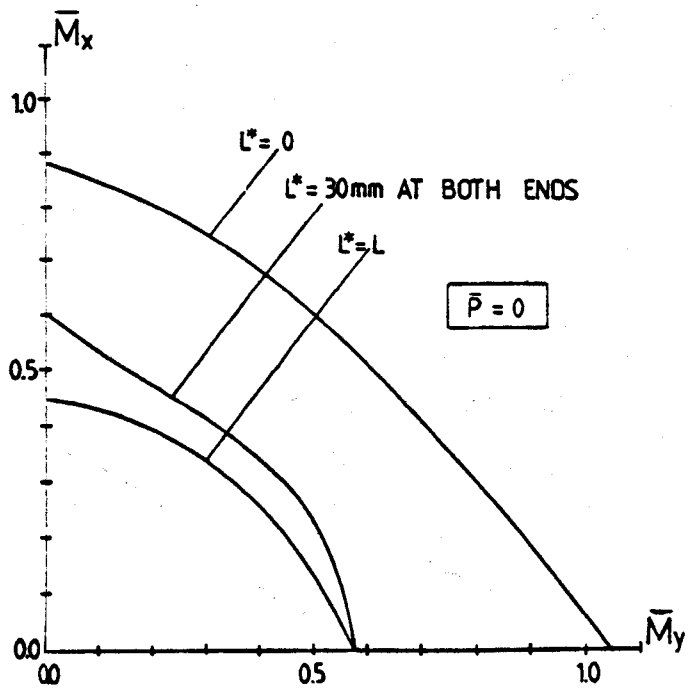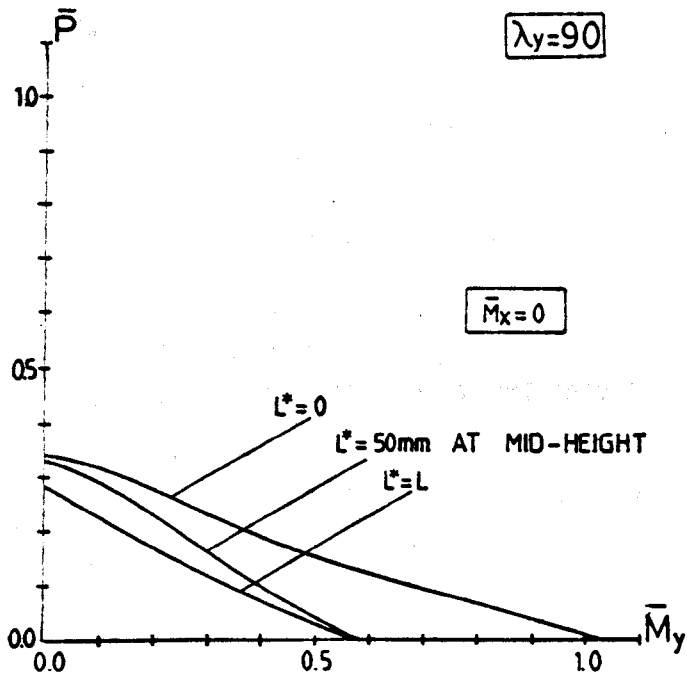
Figure 6.24 (a)
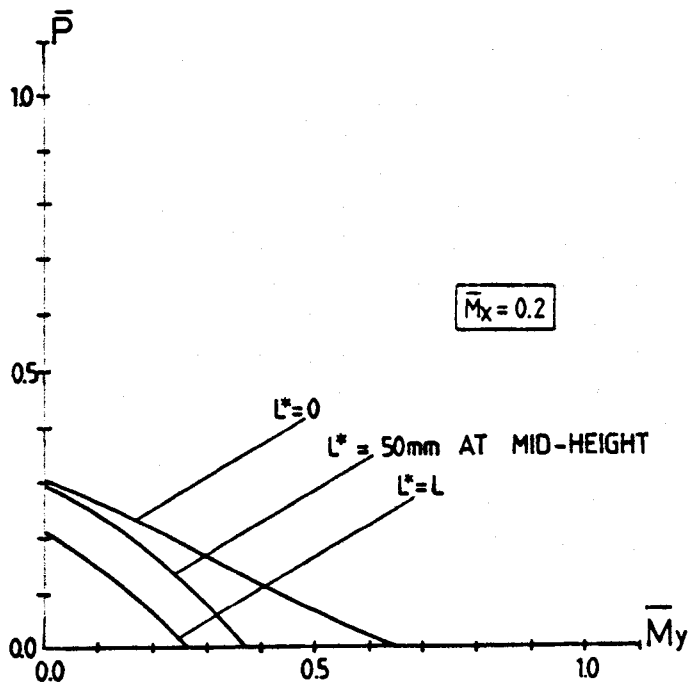
Figure 6.24 (b)
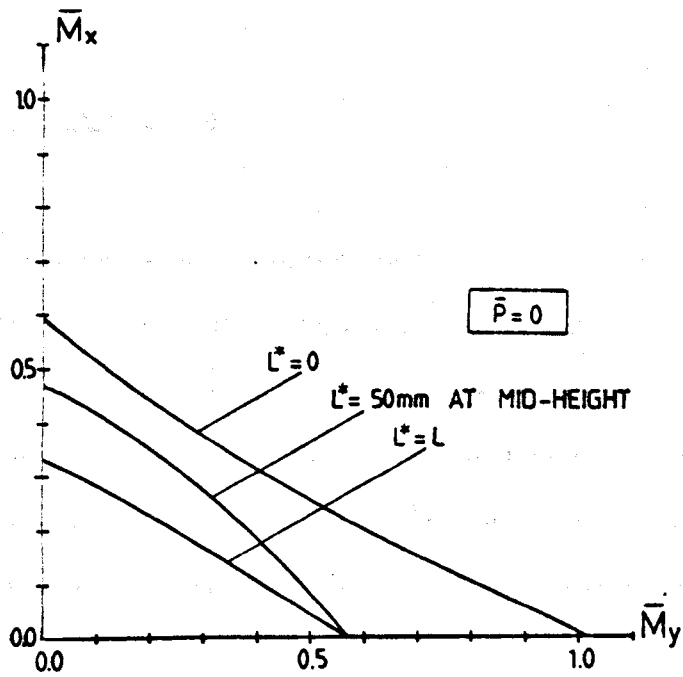
Figure 6.24 (c)

Figure 6.24 Interaction Curves for Transversely Welded Aluminium Beam-columns with $\lambda_y = 90$ ($L^* = 50\ mm$ at Mid-height, $\beta_x = 1, \beta_y = 1$)

6.4   Conclusions

The 3-dimensional behaviour of aluminium beam-columns under compression plus biaxial bending has been studied and presented herein. The ultimate strength of the beam-column depend on the loading paths and has been discussed. The aluminium beam-columns containing longitudinal welds or local transverse welds are also investigated but the studies are confined to doubly symmetric I-section and symmetric RSZ within the cross-section. From the studies, several important observations are obtained:

1. For all the seven loading paths studied by the author, loading path I tends to give the minimum ultimate strengths of the beam-columns.

2. For the aluminium beam-columns which fail due to 'yielding' of the material, the interaction curves are convex in shape.

3. For the aluminium beam-columns which fail by buckling due to instability of the members, the interaction curves tend to be straight lines. Therefore, in this situation, using the straight line interaction equations to represent the ultimate strength of aluminium beam-column is quite reasonable.

4. The ultimate strength of the aluminium beam-columns will be increased if the members are under non-uniform bending about either axis. The most favourable loading condition is the beam-columns under double curvature bending ($\beta_x = -1, \beta_y = -1$) about both axis.

5. For the aluminium beam-columns containing longitudinal welds or local transverse welds, the ultimate strength also depend on the stress level of the RSZ material. If the RSZ material is sufficiently stressed, severe reduction in ultimate strength will occur.

6. For the biaxially loaded beam-columns containing local transverse welds, in keeping with the previous investigation, to design the members as if they contain wholly RSZ material is reasonable.

References

[1] Chen, W. F., and Atsuta, T., "Theory of Beam-columns, Vol. 2, Space Behaviour and Design", McGraw-Hill.

[2] Johnston, B. G., "Guide to Stability Design Criteria for Metal Structures", 3rd Edition, John Wiley and Sons, New York, 1976.

COMPARISON BETWEEN DRAFT BS 8118 WITH THEORETICAL RESULTS

7.1   Introduction

7.1.1   Basic Design Philosophy of Draft BS 8118

The existing standard for the Structural Use of Aluminium CP 118 [1] is one of a generation of working stress type codes in which the maximum permissible stresses are obtained by applying all the safety factors (on materials and loading) to the yield stress of the material. The new standard BS 8118 [2], which will replace CP 118, uses the more modern philosophy of limit state design in which the ultimate unfactored design strength of the member, based upon the yield stress of material or its equivalent, is obtained. An adequate margin of safety can then be ensured by applying a material safety factor (γ_m) to give an ultimate factored capacity which is compared with the effects on the structure produced by the factored (γ_f) nominal loads, i.e.

$$\frac{\text{ultimate resistance}}{\gamma_m} \geq \text{effect due to nominal load} \times \gamma_f$$

(both γ_m and $\gamma_f \geq 1$)

The load factor γ_f , which depends on the type of load, can be referred to Section 3 of draft BS 8118. Under static loading conditions, the values of γ_m used are 1.2 for extruded sections and 1.25 for welded sections.

7.1.2   Scope and Layout of this Chapter

A comparison between the draft BS 8118 and CP 118 has been conducted by Nethercot, Weston and Davison [3], so there is no intention to repeat the work in this area. However, many areas of the draft BS 8118 are still uncertain and without support from experimental or theoretical results. In this chapter, therefore, most of the theoretical results presented in Chapters 3, 5 and 6 will be compared with the design procedures of the new draft code BS 8118 so as to check its accuracy when used for the design of aluminium members. The comparisons are also divided into three main categories: (1) column (2) beam (3) beam- column, and the design principle and procedures of draft BS 8118 are also discussed in each category. The safety factor on material strength, γ_m , is taken as 1.0 in all the comparisons. Since the programs INSTAF and BIAXIAL cannot simulate the effect of local buckling, in order to make a fair comparison between draft BS 8118 and theoretical results; therefore, the effect of local buckling is neglected in the comparison.

7.2   Design of Aluminium Columns

7.2.1   Basic Principle and Design Procedures

The factored axial capacity of column, P_c, which is influenced by the compressive proof stress of the material, the area, HAZ effects, slenderness and the degree of end fixity, thicknesses of the plate elements and torsional properties of the cross-section, is given by

$$P_c = \frac{P_{ac}\, C_c}{\gamma_m} \qquad (7.1)$$

where P_{ac} =   basic axial capacity

C_c =   reduction factor for overall flexual buckling

In determining P_{ac} due account must be taken of both HAZ and local buckling effects, so

$$P_{ac} = C_L\, \sigma_{0.2}\left[A - \sum(1-\omega)A^*\right] \qquad (7.2)$$

in which C_L = reduction factor for local buckling

and the second term in the square brackets allows for the reduction in strength due to the presence of RSZ material. Compression members for which $C_L = 1$ are sometimes called 'compact' members, and in this instance there is no loss of factored resistance by local buckling effects.

The value of C_c depends on the non-dimensional slenderness parameter $\frac{L}{r}\sqrt{(\frac{\sigma_{0.2}}{250})C_L}$. The set of five column curves for the determination of C_c is provided in Figure 5.9 of BS 8118 and the selection of the the appropriate curve will be discussed later in Section 7.2.3. For the column which may fail

due to torsional instability, it is necessary to check whether the reduction factor for torsional buckling C_T is less than C_c . If the value of C_T is less than the value of C_c for flexural buckling, then C_T is substituted for C_c in the determination of the factored axial capacity of column. The torsional buckling parameter, C_T , is determined from Figure 5.10 of draft BS 8118 in which the four curves are exactly the same as the first four curves of Figure 5.9 of draft BS 8118.

7.2.2   Design of Columns Having Local Transverse Welds

The design of columns having localised welds along their length is discussed only in Appendix 5A of the draft BS 8118. To measure the effect of local transverse welds on the buckling strength of a column, a parameter $\frac{L_{m}}{L_{cr}}$ is used and the design is then divided into the following cases:

1. If $\frac{L_{m}}{L_{cr}} > 0.2$, design the column as if fully affected by the welded zone.

2. If $\frac{L_{m}}{L_{cr}} = 0$, design the column as if affected by longitudinal welds only.

3. If $0 < \frac{L_{m}}{L_{cr}} < 0.2$, interpolate the basic axial capacity , P_{ac} , of the column between (a) and (b), based on the value of $\frac{L_{m}}{L_{cr}}$.

Moreover, for end-welded columns, the effect of transverse welds may be neglected, account being taken of longitudinal welds only.

The above design philosophy is actually based on the results obtained by Brungraber and Clark [4] and the validity will be discussed in Section 7.2.4.6.

7.2.3   Selection of Column Curves

The representation of the column curves is based on the Perry-Robertson type equation and the selection of column curves for the determination of C_c depends on:

(a)   aluminium alloy with high n value (H) or low n value (L)

In BS 8118, for columns having

$$\frac{\sigma_{ult}}{\sigma_{0.2}} \leq 1.2 \; : \; \text{high } n \text{ value}$$

$$\frac{\sigma_{ult}}{\sigma_{0.2}} > 1.2 \; : \; \text{low } n \text{ value}$$

(b)   the cross-section is symmetric (S) or asymmetric (A)

In BS 8118, it is suggested that

$$\frac{y_1}{y_2} \leq 1.2 \; : \; \text{symmetric}$$

$$\frac{y_1}{y_2} > 1.2 \; : \; \text{asymmetric}$$

where y_1 and y_2 are the perpendicular distance from the axis of buckling to the further and nearer extreme fibres respectively.

(c)   the column is non-welded (NW) or welded (W)

Class	Conditions	Rating	Column Curve in Figure 5.9 of Draft BS 8118
A	H-S-NW	0	Curve 1
B	H-S-W	1	Curve 2
C	H-A-NW	1	Curve 2
D	H-A-W	2	Curve 3
E	L-S-NW	1	Curve 3
F	L-S-W	2	Curve 4
G	L-A-NW	2	Curve 4
H	L-A-W	3	Curve 5

Table 7.1: Grading and Selection of Column Curves

Aluminium alloy having low a value will give higher strength but this is only valid as $\sigma > \sigma_{0.2}$. Since in the draft BS 8118, the maximum permissible stress is equal to $\sigma_{0.2}$ and most of the columns will buckle at $\sigma < \sigma_{0.2}$, so condition (L) together with conditions (A) and (W) are actually weakening in effects. Therefore, the columns can be graded into eight classes according to the combinations of these conditions and be rated according to the number of weakening conditions they have. The grading of columns together with the selection of column curves is shown in Table 7.1. The higher the rating number the weaker is that class of column. Although the positioning of the design column curves was based largely on test data and accurate numerical studies [5], the accuracy is still uncertain especially for the welded-columns. Moreover, some of the test results (carried out in USA) are somewhat old (see Section 2.4) and some of the aluminium alloys chosen in tests (2000 series alloy) were only commonly used in aircraft industries, so the reliability of the column curves in many areas is still questionable. The author, therefore, carried out extensive comparisons between the design column curves with theoretical results presented in Chapter 3 and 5, and the details of the comparison will be discussed in Section 7.2.4.

7.2.4 Comparison between Design Column Curves of Draft BS 8118 with Theoretical Results of Columns

In order to check the accuracy of the draft BS 8118, the author, therefore, carried out extensive comparison between all the design column curves with the theoretical column results. The details of the comparisons can be referred to Table 7.2 (a) and (b), and the theoretical column curves have already been presented in Chapter 3 and 5. It is worthwhile to point out that the theoretical column curves presented in Chapter 3 are obtained by using program INSTAF which is for the simulation of 2-D or in-plane behaviour of aluminium members. The theoretical column curves presented in Chapter 5 are obtained by using program BIAXIAL which is for the simulation of 3-D behaviour of aluminium members.

The comparisons with welded columns listed in Table 7.2 (a) are only limited to the columns having longitudinal welds. The comparisons with transversely welded columns listed in Table 7.2 (b) will be discussed separately in Section 7.2.4.6. Since the effect of local buckling is neglected in the comparison, therefore, the value of $C_L = 1$ is assumed. However, the inclusion of local buckling in the comparison will also be discussed in Section 7.2.4.7.

Class	Condition	Design Column Curves in Figure 5.9 of BS 8118	$\frac{\sigma_{ult}}{\sigma_{0.2}}$	n	$\frac{\Delta}{A}$ or $\frac{\Delta}{L}$	Theoretical Curve Reference	Source of Theoretical Curves	Principal Results
A	H-S-NW	1	1.17	25	$\frac{\Delta}{L} = 0.0$	C-A-1	Figure 3.11	Figure 7.1
					$\frac{\Delta}{A} = 0.0$	C-A-2	Figure 5.7	
B	H-S-W	2	1.17	25	$\frac{\Delta}{A} = 0.1$	C-B-1	Figure 5.8	Figure 7.2
					$\frac{\Delta}{A} = 0.3$	C-B-2		
					$\frac{\Delta}{A} = 0.5$	C-B-3		
					$\frac{\Delta}{A} = 0.1$	C-B-4	Figure 5.9	Figure 7.3
					$\frac{\Delta}{A} = 0.3$	C-B-5	Figure 5.10	
					$\frac{\Delta}{A} = 0.5$	C-B-6	Figure 5.11	
C	H-A-NW	2	1.08	50	$\frac{\Delta}{A} = 0.0$	C-C-1	Figure 3.5	Figure 7.4
			1.17	25	$\frac{\Delta}{A} = 0.0$	C-C-2	Figure 5.41	
D	H-A-W	3	1.17	25	$\frac{\Delta}{A} = 0.3$	C-D-1	Figure 5.41	Figure 7.5
					$\frac{\Delta}{A} = 0.5$	C-D-2		
E	L-S-NW	3	1.49	10	$\frac{\Delta}{A} = 1.0$	C-E-1	Figure 3.11	Figure 7.6
			1.61	8.4	$\frac{\Delta}{A} = 0.0$	C-E-2	Figure 5.48	
F	L-S-W	4	1.61	8.4	$\frac{\Delta}{A} = 0.3$	C-F-1	Figure 5.48	Figure 7.7
G	L-A-NW	4	1.36	13	$\frac{\Delta}{A} = 0.0$	C-G-1	Figure 5.47	Figure 7.8
			1.95	6	$\frac{\Delta}{A} = 1.0$	C-G-2		
H	L-A-W	5	1.95	6	$\frac{\Delta}{A} = 0.3$	C-H-1	Figure 5.47	Figure 7.9

NOTE

The value of σ_{ult} is obtained by $n = \frac{1}{\ln\left(\frac{\sigma_{ult}}{\sigma_{0.2}}\right)}$ (see Section A.2.1.4 of APPENDIX A)

Table 7.2: (a) List of Theoretical Column Curves (Non-welded and Longitudinally Welded Columns)

Theoretical Curve Reference	$\frac{\sigma_{ult}}{\sigma_{0.2}}$	n	$\frac{L^*}{L}$	Source of Theoretical Curves	Principal Results
C-TW-1	1.17	25	0.1	Figure 3.11	Figure 7.10
C-TW-2			0.2		
C-TW-3			0.3		
C-TW-4			1.0		
C-TW-5	1.17	25	0.0	Figure 3.11	Figure 7.11
C-TW-6	1.17	25	0.05	Figure 3.11	Figure 7.12
C-TW-7	1.17	25	0.1 at both ends	Figure 3.11	Figure 7.13
C-TW-8	1.17	25	$L^* = 50mm$ at mid-height	Figure 5.13	Figure 7.14
C-TW-9			$L^* = L$		
C-TW-10	1.17	25	$L^* = 0$	Figure 5.12	Figure 7.15
C-TW-11			$L^* = 30mm$ at both ends		

NOTE

The value of σ_{ult} is obtained by $n = \dfrac{4}{\ln\left(\frac{\sigma_{ult}}{\sigma_{0.2}}\right)}$ (see Section A.2.1.4 of APPENDIX A)

Table 7.2: (b) List of Theoretical Column Curves (Transversely Welded Columns)

7.2.4.1   Comparison between Design Column Curve 1 with Class A Column

Class A columns is the strongest class of column and design column curve 1 is used in draft BS 8118. Figure 7.1 shows that design column curve 1 is slightly unsafe for columns under in-plane buckling as $0.25 < \lambda_x < 0.75$ ($13.1 < \overline{\lambda}_x < 39.4$). For the columns having flexural-torsional buckling, design column curve 1 safely covers all the theoretical results and the maximum difference is about 20% below the theoretical curve.
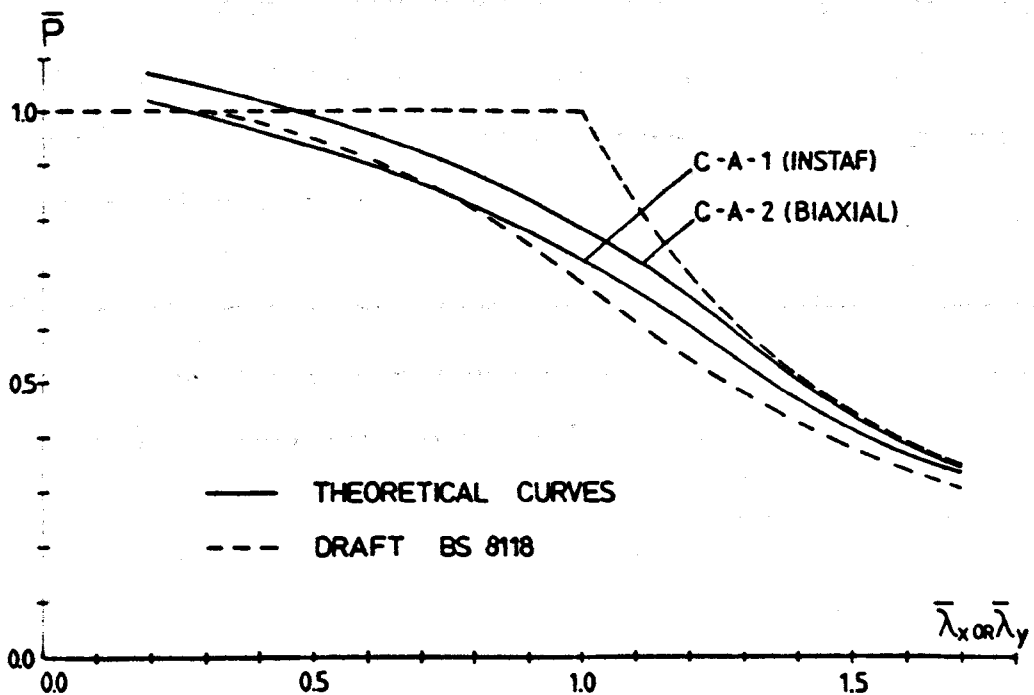

Figure 7.1 Comparison between Design Column Curve 1 with Theoretical Column Curves (Class A Columns)

7.2.4.2 Comparison between Design Column Curve 2 with Class B and C Columns

The comparison between design column curve 2 with class B and C columns is shown in Figures 7.2 to 7.4. Figures 7.2 and 7.3 are for the columns with symmetric or unsymmetric longitudinal welds respectively, and the effect of residual stresses is included in the comparison (except unsymmetric longitudinally welded columns with $\frac{A^{\bullet}}{A} = 0.5$). Generally, except for stocky columns ($\bar{\lambda}_y \leq 0.4$ or $\lambda_y \leq 21$) in some cases, design column curve 2 safely covers all the theoretical results of class B and C columns. But, in the range of intermediate slenderness, design curve 2 tends to be slightly too conservative and gives a maximum difference of about 30% below the theoretical curves. However, from Figures 7.2 and 7.3, we can conclude that draft BS 8118 can give safe design for longitudinally welded columns no matter the RSZ within the cross-section is symmetric or not.

For the asymmetric non-welded columns (Tee-section) which are under in-plane buckling, same as design column curve 1, design column curve 2 tends to give slightly unsafe design as $\bar{\lambda}_x < 0.5$.
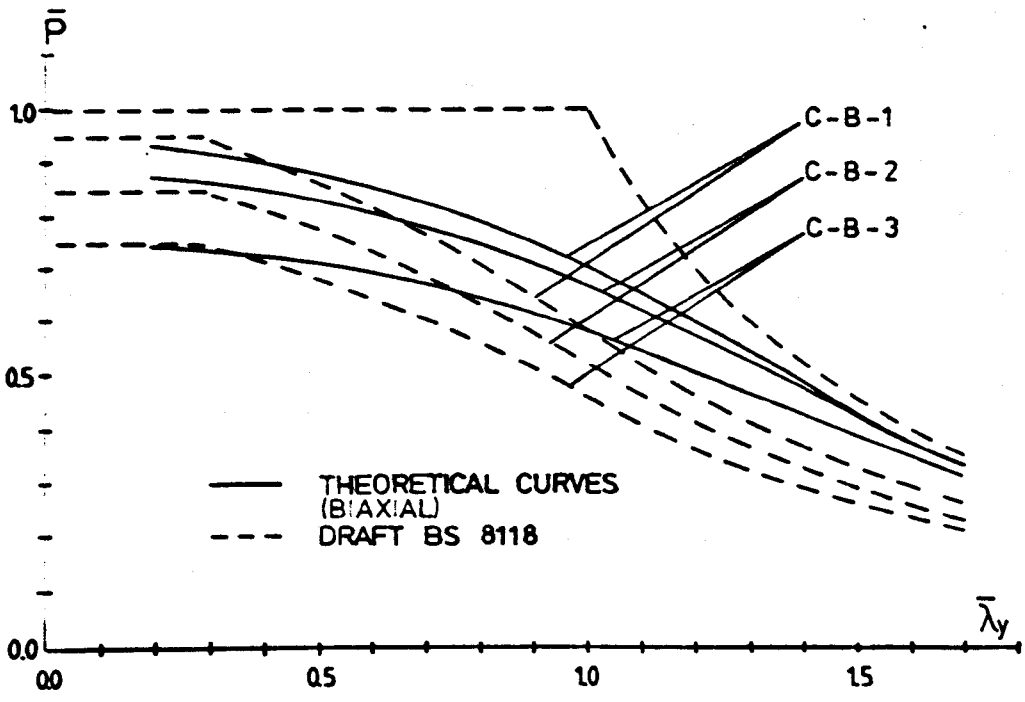
Figure 7.2 Comparison between Design Column Curve 2 with Theoretical Column Curves (Class B Columns, with Symmetric Longitudinal Welds)
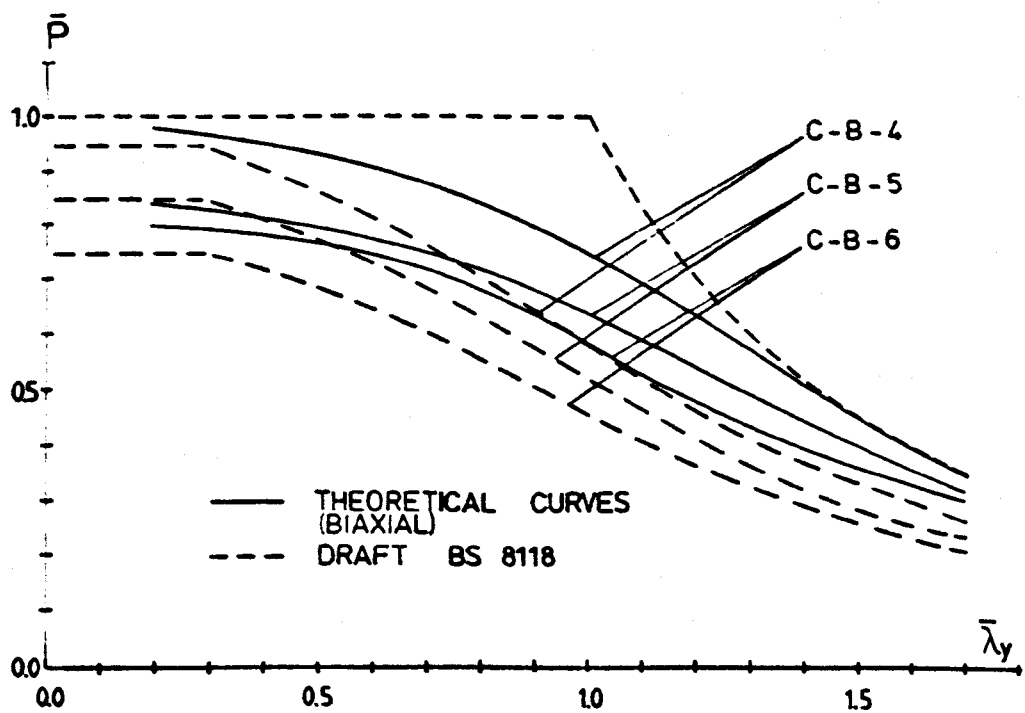
Figure 7.3 Comparison between Design Column Curve 2 with Theoretical Column Curves (Class B Columns, with Unsymmetric Longitudinal Welds)

Figure 7.4 Comparison between Design Column Curve 2 with Theoretical Column Curves (Class C Columns)

Figure 7.5 Comparison between Design Column Curve 3 with Theoretical Column Curves (Class D Columns)

Figure 7.6 Comparison between Design Column Curve 3 with Theoretical Column Curves (Class E Columns)

7.2.4.3 Comparison between Design Column Curve 3 with Class D and E Columns

Figures 7.5 and 7.6 show the comparison between design column curve 3 with class D and E columns respectively. In Figure 7.5, the effect of residual stresses is included, and we can observe that design column curve 3 also tends to give very conservative design for intermediate and slender columns. For the comparison with class E columns as shown in Figure 7.6, design column curve 3 will give slightly unsafe design for columns under in-plane buckling as $0.28 < \bar{\lambda}_x < 0.63$ $(14.7 < \lambda_x < 33.1)$. Generally, for the columns under flexural-torsional buckling, design column curve 3 tends to give the results with a maximum of about 30% below the theoretical curves.
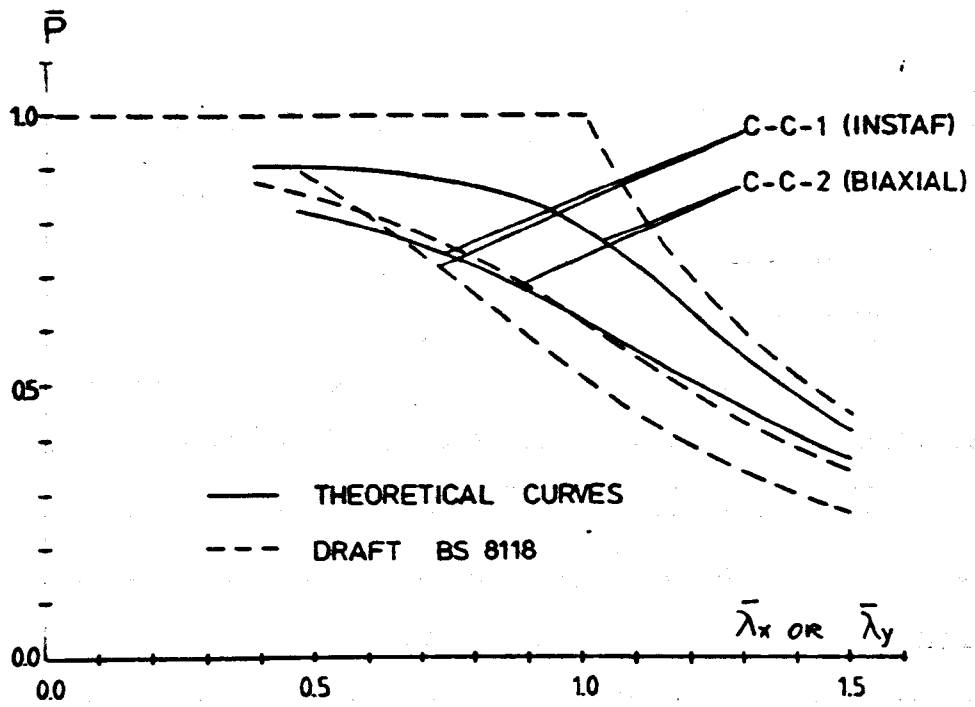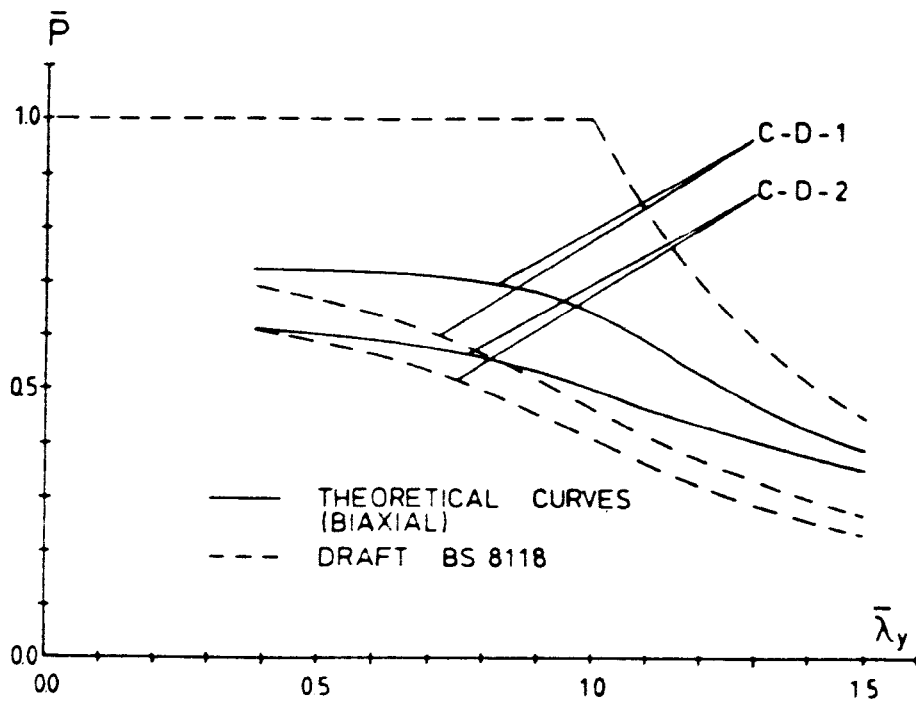
Figure 7.7 Comparison between Design Column Curve 4 with Theoretical Column Curves (Class F Columns)

Figure 7.8 Comparison between Design Column Curve 4 with Theoretical Column Curves (Class G Columns)
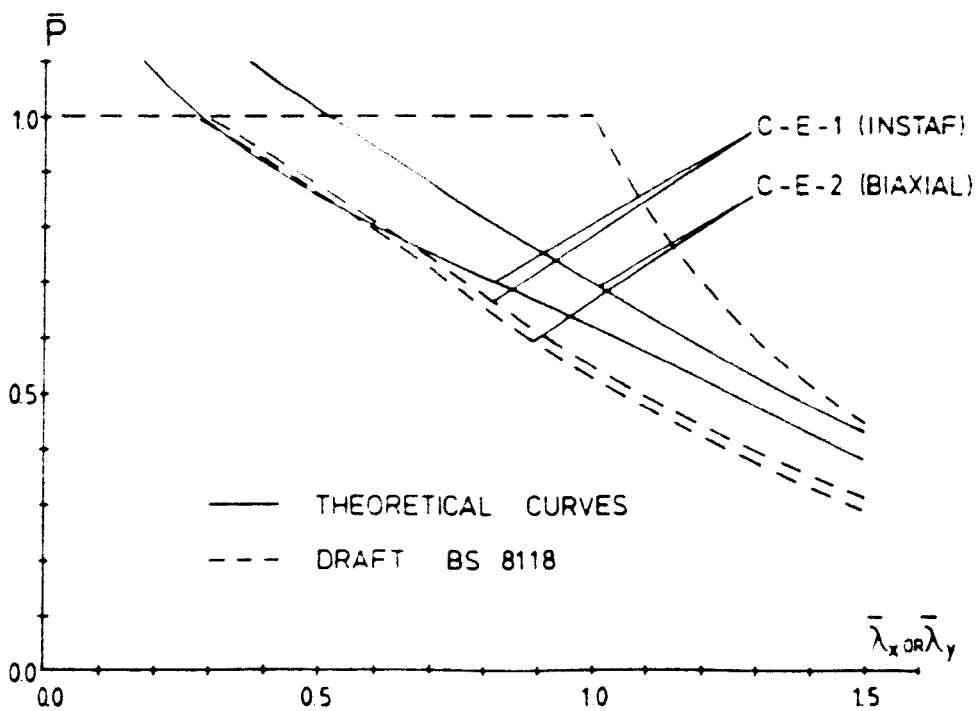
7.2.4.4 Comparison between Design Column Curve 4 with Class F and G Columns

Figures 7.7 and 7.8 show the comparison between design column curve 4 with class F and G columns. For both class of columns , draft BS 8118 also gives very conservative results. For class F columns, the design column curve 4 gives a maximum difference of about 35% below the theoretical curve. For class G columns, the design column curve 4 is even more conservative and give a maximum difference of about 42% below the theoretical curve.

7.2.4.5   Comparison between Design Column Curve 5 with Class H Columns

This class of columns is the weakest and design column curve 5 is used in draft BS 8118. Due to lack of theoretical and experimental results, the behaviour of this class of columns is quite uncertain. Draft BS 8118, therefore, is extremely conservative in designing class H columns. From Figure 7.9, we can find that the design column curve 5 gives a maximum difference of about 60% below the theoretical curve.
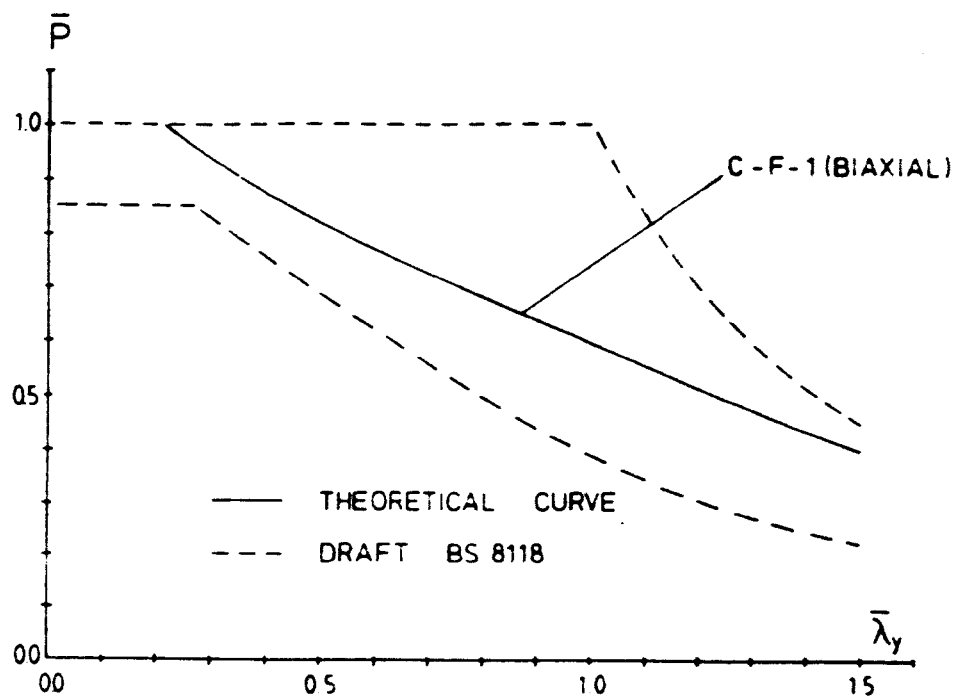

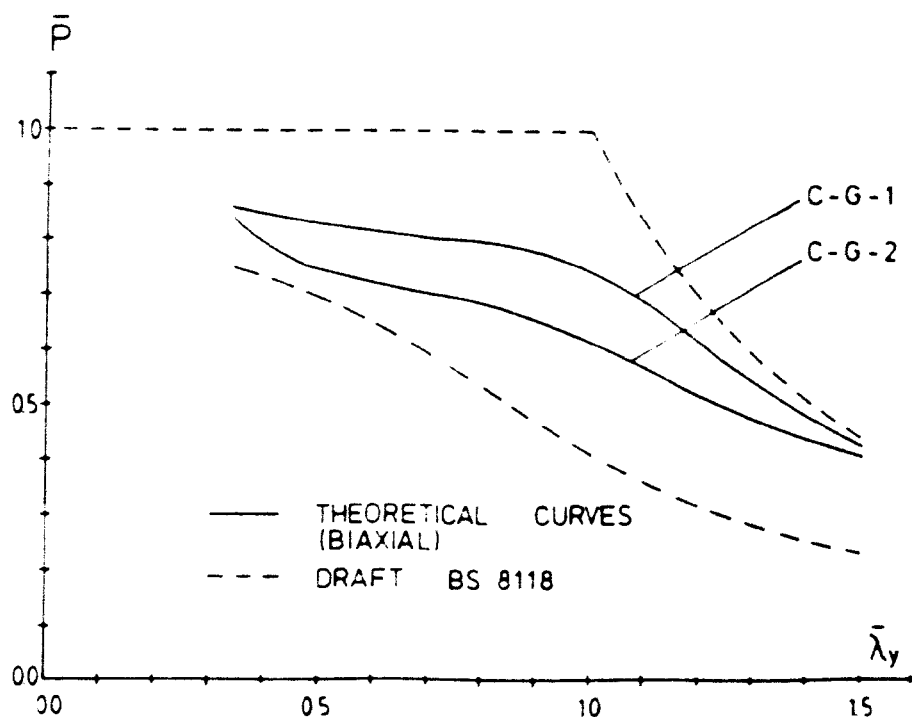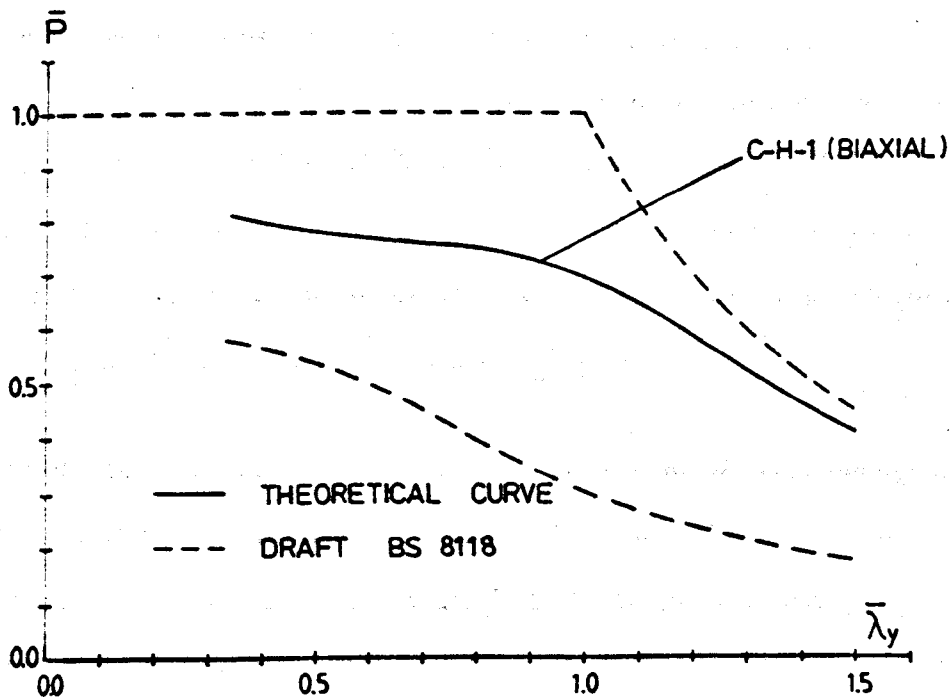Figure 7.9 Comparison between Design Column Curve 5 with Theoretical Column Curves (Class H Columns)

7.2.4.6 Comparison with Columns Having Local Transverse Welds

As mentioned in Section 7.2.2, the design of columns having local transverse welds is divided into four cases: (i) $\frac{L_w}{L_{cr}} > 0.2$; (ii) $\frac{L_w}{L_{cr}} = 0$; (iii) $0 < \frac{L_w}{L_{cr}} < 0.2$; and (iv) end-welded columns.

For the columns under in-plane buckling, the design of transversely welded columns according to draft BS 8118 for the above cases are shown in Figures 7.10 to 7.13. For cases (i) and (ii), the columns are treated as if fully-affected by welding and non-welded columns respectively. In case (i), the transversely welded columns are designed as if non-welded members but the material properties are based on RSZ material (see Section 7.7). As mentioned in Sections 7.2.4.1 and 7.2.4.3, draft BS 8118 will give slightly unsafe design on intermediate columns. For case (iii), in which the columns are considered as partially affected by RSZ ($\frac{L_w}{L_{cr}} = 0.1$ is chosen by the author), Figure 7.12 shows that the draft BS 8118 can lead to unsafe design as for $\overline{\lambda}_x < 1.05$ ($\lambda_x < 55$). For end-welded columns (case (iv)), neglecting the welded zone can also lead to very unsafe predictions throughout the practical range of slenderness of column as shown in Figure 7.13.

Figures 7.14 to 7.15 show the design of transversely welded columns suggested by the author as mentioned in Section 5.3.1.4, and the columns are under flexural-torsional buckling. In Figure 7.14, the centrally welded columns are designed as if containing wholly RSZ material no matter the extent of RSZ is large or small. In Figure 7.15, the end-welded columns are designed as if non-welded columns but with a cut-off line $\overline{P} = 1 - (1 - \omega)\frac{A^*}{A}$. Since the cross-section is fully-affected by local transverse welds, i.e. $A^* = A$, the

above equation, therefore, becomes $\overline{P} = \omega$. From Figures 7.14 and 7.15, it can be seen that the suggested design procedures can give the design on the safe side and with high degree of accuracy.
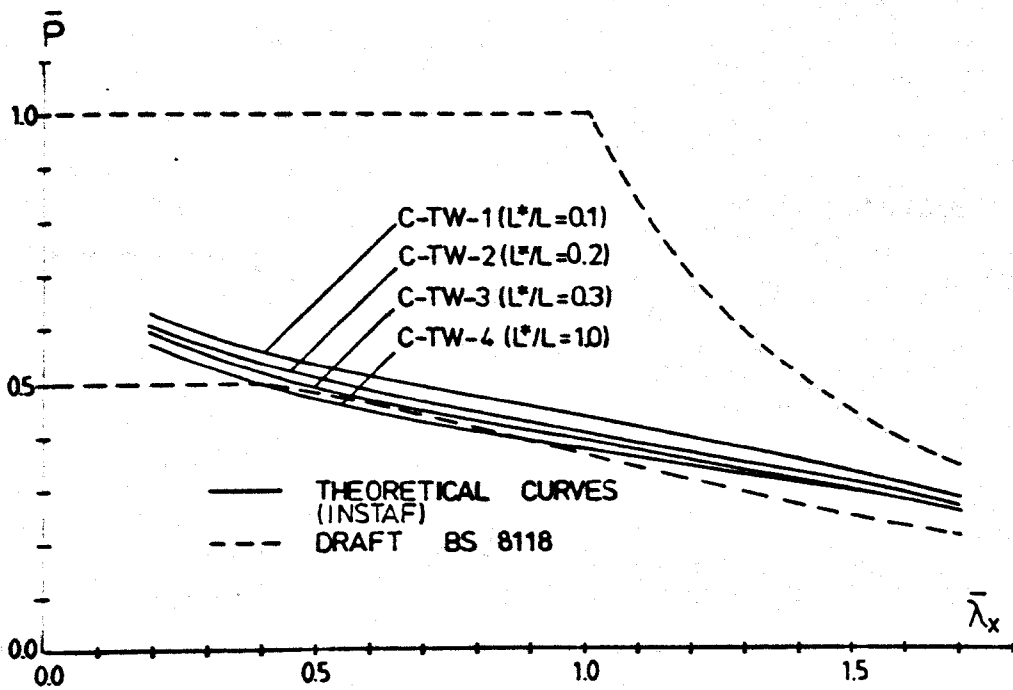
Figure 7.10 Comparison with Transversely Welded Column Curves Obtained by Program INSTAF ($\frac{L_{uz}}{L_{cr}} > 0.2$)
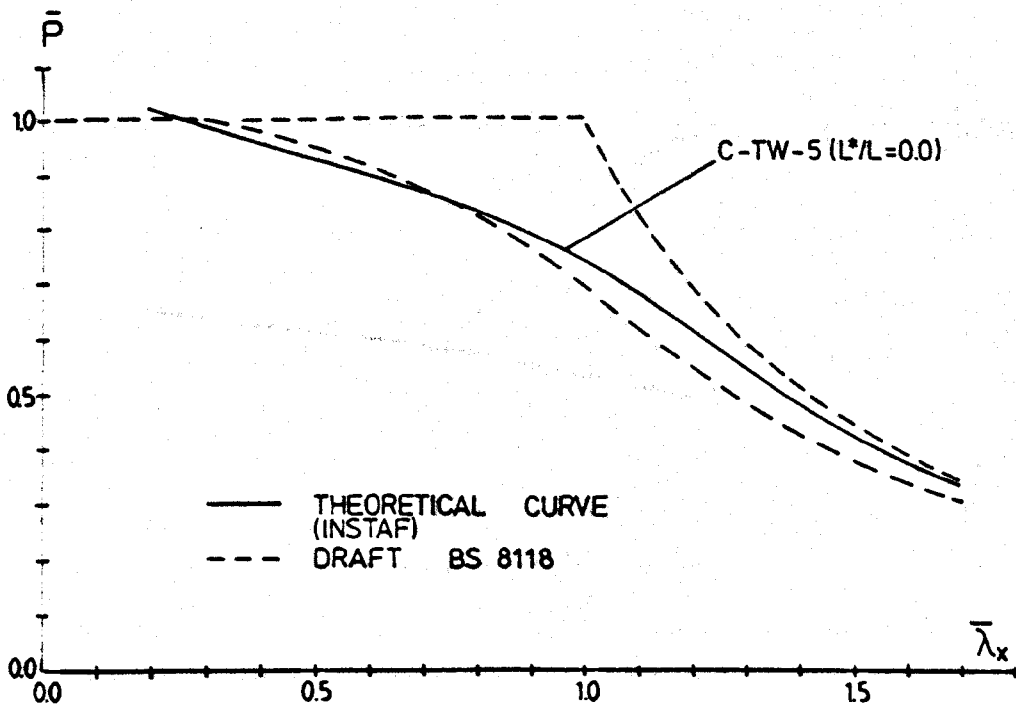
Figure 7.11 Comparison with Transversely Welded Column Curves Obtained by Program INSTAF ($\frac{L_{uz}}{L_{cr}} = 0$)
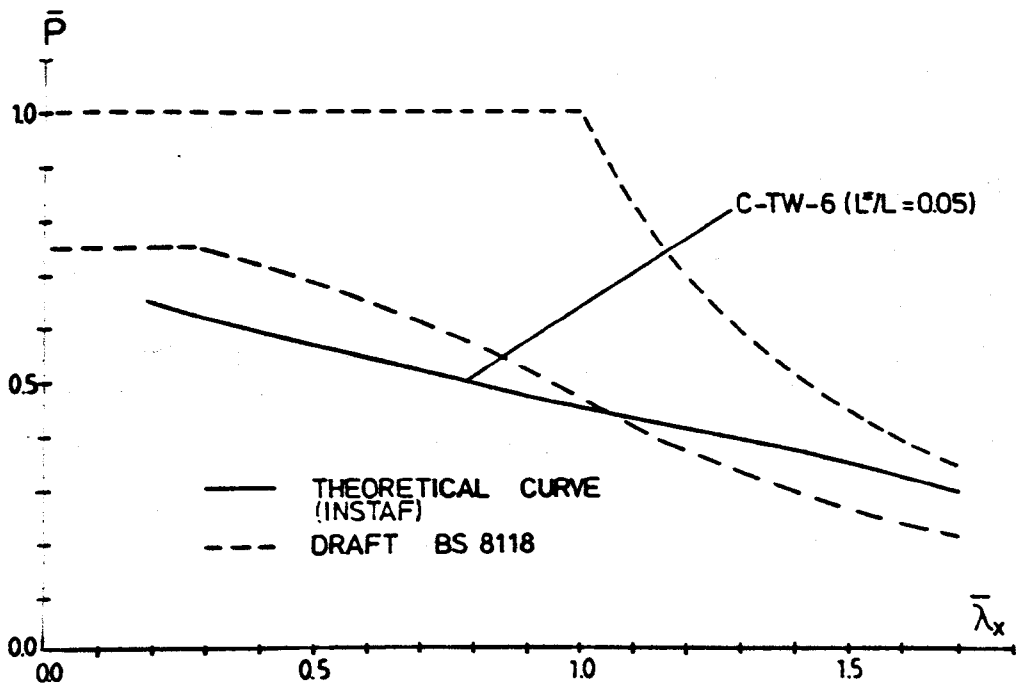
Figure 7.12 Comparison with Transversely Welded Column Curves Obtained by Program INSTAF ($\frac{L_{aa}}{L_{cr}} = 0.1$)
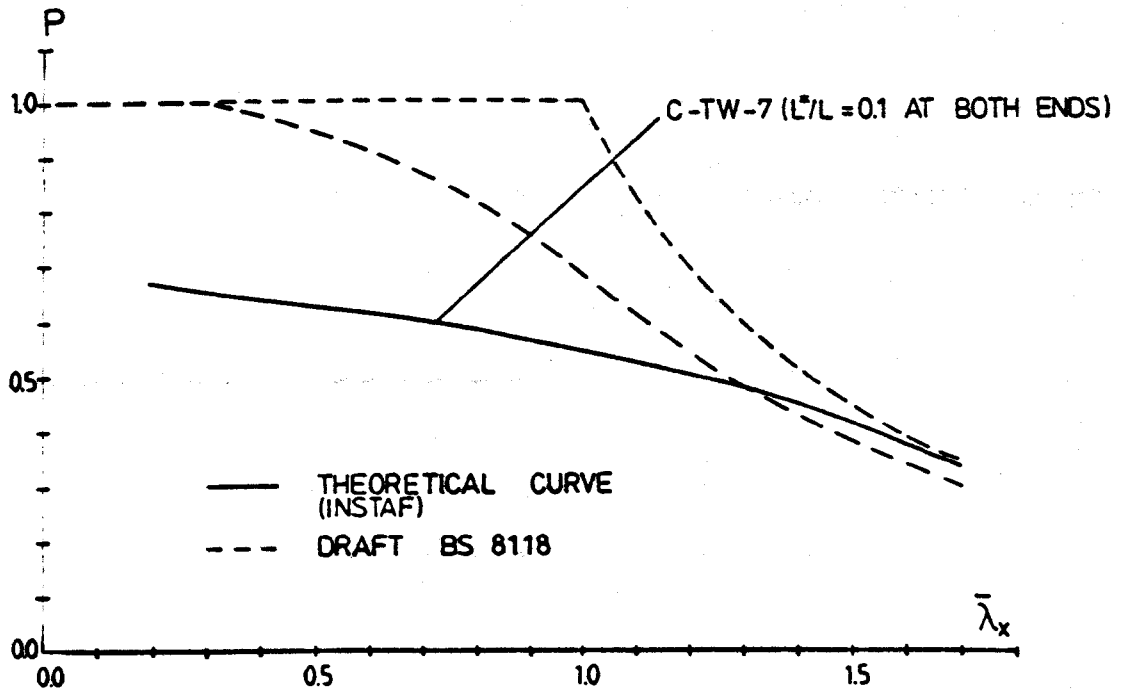
Figure 7.13 Comparison with Transversely Welded Column Curves Obtained by Program INSTAF (End-welded Columns)
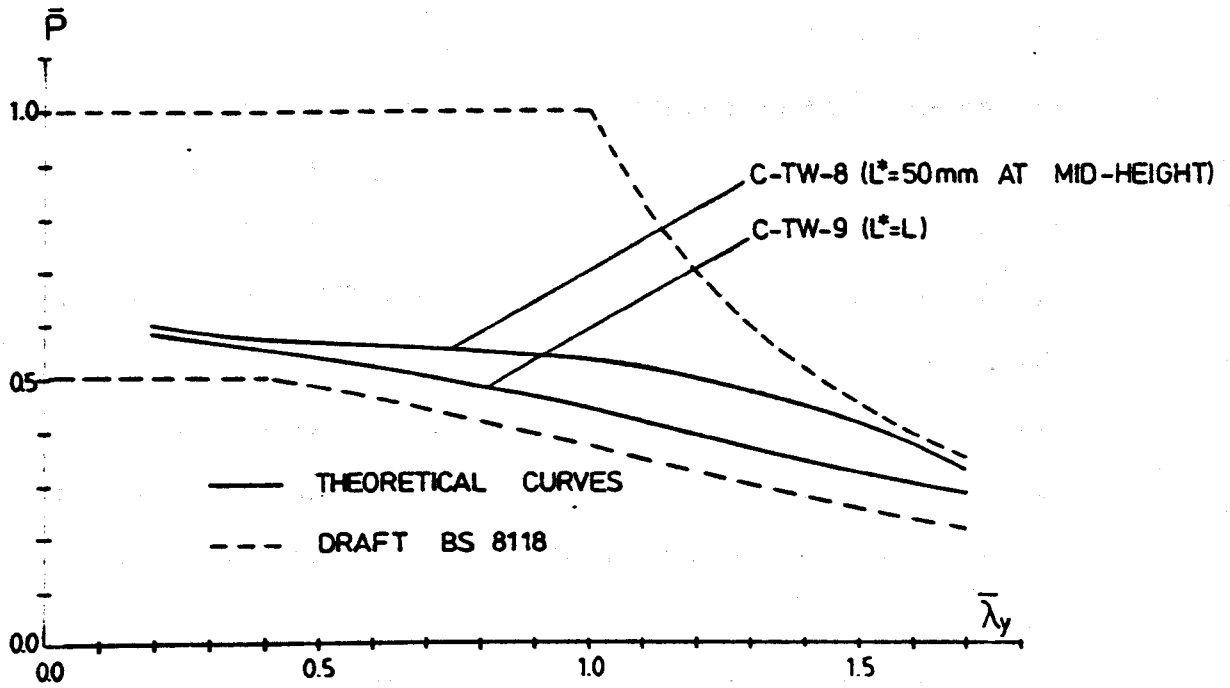
Figure 7.14 Comparison with Transversely Welded Column Curves Obtained by Program BIAXIAL (Centrally-welded Columns)
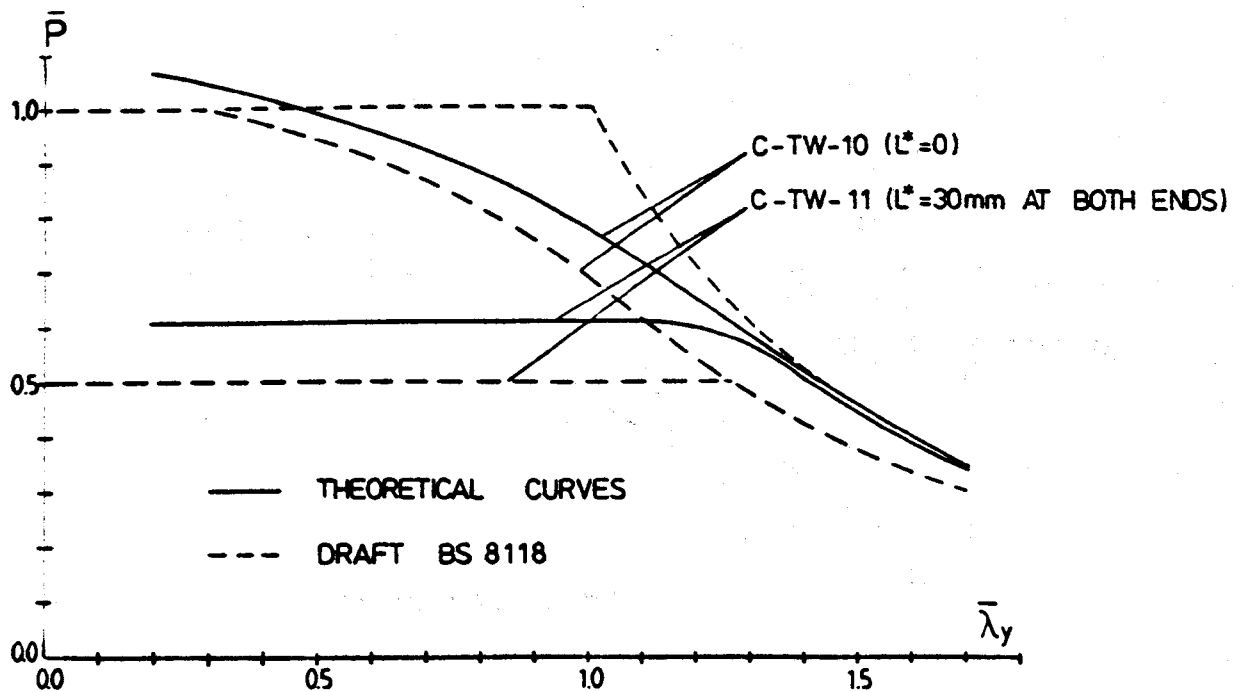
Figure 7.15 Comparison with Transversely Welded Column Curves Obtained by Program BIAXIAL (End-welded Columns)

7.2.4.7   Effect of Local Buckling on Comparison with Theoretical Column Results

Since the programs INSTAF and BIAXIAL cannot simulate the effect of local buckling, therefore in the comparison presented in Sections 7.2.4.1 to 7.2.4.6, this effect is neglected by assuming $C_L = 1$ in all the cases. For the cross-sections of column shown in Figure 3.5 and 3.9 which are under in-plane buckling, the section are compact and the value of C_L is equal to 1 even the effect of local buckling is taken into account. However, for the cross-section of column shown in Figure 5.5 which contains slender web, the inclusion of local buckling in the comparison will only give the design column curve about 5% lower than before (see Figure 7.16). But for the more reasonable comparison between draft BS 8118 and theoretical results, the effect of local buckling should be neglected.
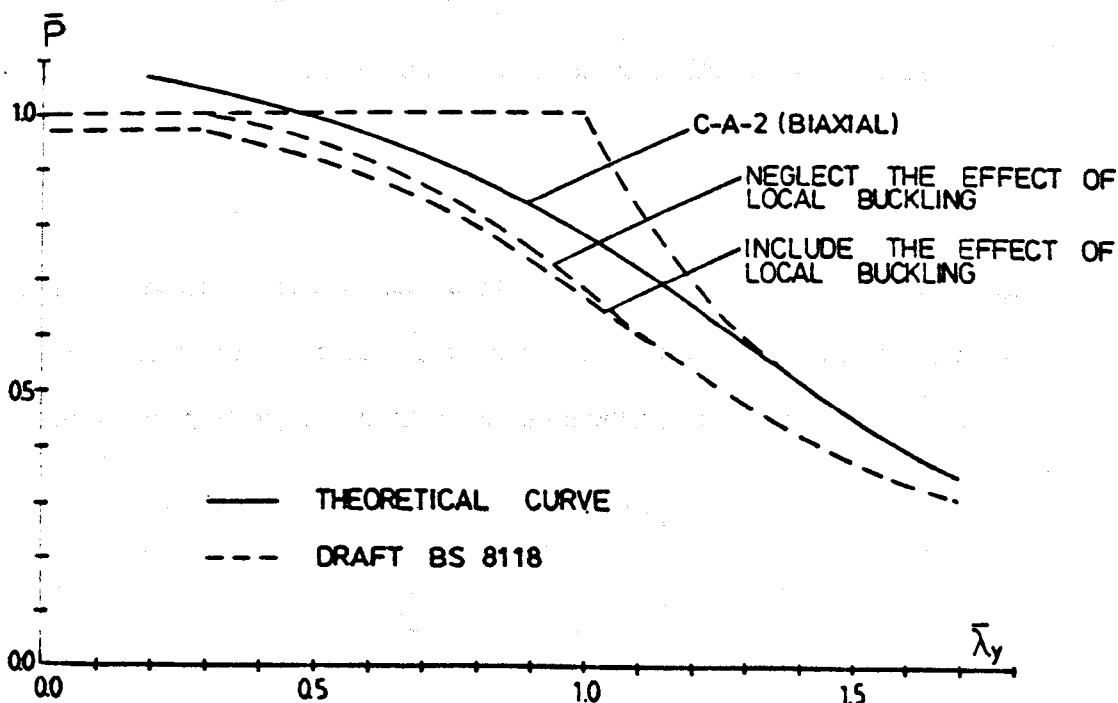
Figure 7.16 Effect of the Inclusion of Local Buckling on Comparison

7.3   Design of Aluminium Beams

7.3.1   Basic Principle and Design Procedures [7]

The factored moment resistance, M_{max} , of a beam is given by

$$M_{max} = \frac{M_s \, C_{LT}}{\gamma_m} \qquad (7.3)$$

where M_s =   basic moment capacity

C_{LT} =   reduction factor for lateral buckling

The basic moment capacity of a beam is based on the 0.2% proof stress, and is influenced by the local buckling parameters of elements of the cross-section that are wholly or partly in compression when bending takes place. Similar to aluminium column, the value of M_s is determined by the following conditions;

    i. welded or non-welded

    ii. aluminium alloy with high n value or low n value

    iii. types of section

The parameter $\frac{\sigma_{ult}}{\sigma_{0.2}}$ is also used to determine whether the aluminium beam is having high n or low n value but the limit is different from that for aluminium column. BS 8118 suggested that for the aluminium beam having

$$\frac{\sigma_{ult}}{\sigma_{0.2}} \leq 1.4 \quad : \quad \text{high } n$$

$$\frac{\sigma_{ult}}{\sigma_{0.2}} > 1.4 \quad : \quad \text{low } n$$

Moreover, similar to the steel code BS 5950 [6], three types of section are identified. They are

(a) Compact sections for which the fully plastic moment capacity may be attained, i.e. $M_s = M_p = \sigma_{0.2} Z_p$

(b) Semi-compact sections which are unable to achieve M_p but for which M_s is greater than or equal to the elastic yield moment based upon the full cross-sectional properties, i.e. $\sigma_{0.2} Z_e \leq M_s < M_p$

(c) Slender sections for which M_s is based upon an effective elastic section modulus, Z_{eff} which is obtained by taking a reduced thickness for the critical elements in compression, i.e. $M_s = \sigma_{0.2} Z_{eff}$.

Sections made from material having $\frac{\sigma_{ult}}{\sigma_{0.2}} > 1.4$ are not permitted to be designed for M_p due to concern about the high strain (and hence deformations) involved.

The value of C_{LT} depends on the beam slenderness λ_{LT} , and there are three possible ways to determine C_{LT} and their differences have been discussed in reference [3]. The three possible ways are:

(a) $\lambda_{LT} = u \; v \; \lambda_y \sqrt{\frac{\sigma_{0.2}}{250}}$

where u = 0.85 for I beams, 0.75 for channels, 1.0 for Tee-sections

v is obtained from Figure 5.15 of draft BS 8118

(b) $\lambda_{LT} = 53 \sqrt{\frac{M_s}{M_{cr}}}$ and $M_{max} = M_s C_{LT}$

where M_{cr} = elastic critical buckling moment

(c) $\lambda_{LT} = 53 \sqrt{\frac{M_p}{M_{cr}}}$ and $M_{max} = M_p C_{LT} < M_s$

The determination of C_{LT} is based on one single design curve which is given in Figure 5.16 of draft BS 8118. The reason of using one single design curve is due mainly to the absence of either a comprehensive theoretical treatment or a sufficiently large and well structured body of test data. Therefore, differentiation between classes of section, as was done for aluminium column curves, become impossible.

Equivalent uniform moment concept is also used in the draft code, i.e.

$$\tilde{M} = m\, M_1 \tag{7.4}$$

in which $\quad m = (0.6 + 0.4 \dfrac{M_2}{M_1} \geq 0.4)$ $\hfill$ (7.5)

$M_1, M_2 \quad = \quad$ larger and smaller end moments respectively

Guidance is also provided, through the use of effective length factors, on the approximate effects of end fixity and destabilising loads i.e. those applied above the level of the shear centre in such a way that they are free to move sideways with the beam as it buckles.

The design procedures of beams with local transverse welds are identical to the situation of columns. The effect of local transverse welds is also neglected when the welds are located at the ends.

Theoretical Curve Reference	Source of Theoretical Curves	$\frac{A^*}{A}$ or $\frac{L^*}{L}$	Principal Results	Remark
B-NW-1	Figure 5.18	$\frac{A^*}{A} = 0.0$	Figure 7.17	$n = 25$
B-NW-2				$n = 40$
B-NW-3				$n = 55$
B-NW-4				$n = 200$
B-NW-5	Figure 5.42	$\frac{A^*}{A} = 0.0$	Figure 7.18	$n = 25$, T-section
B-NW-6				
B-NW-7	Figure 5.18	$\frac{A^*}{A} = 0.0$	Figure 7.19	$\sigma_{0.2} = 250$, $n = 10$
B-NW-8	Figure 5.21	$\frac{A^*}{A} = 1.0$		$\sigma_{0.2} = 125$, $n = 10$
B-NW-9	Figure 5.44	$\frac{A^*}{A} = 1.0$	Figure 7.20	$\sigma_{0.2} = 125$, $n = 10$,
B-NW-10	Figure 5.45	$\frac{A^*}{A} = 1.0$		T-section
B-LW-1	Figure 5.8	$\frac{A^*}{A} = 0.1$	Figure 7.21	Symmetric
B-LW-2		$\frac{A^*}{A} = 0.3$		longitudinal
B-LW-3		$\frac{A^*}{A} = 0.5$		welds
B-LW-4	Figure 5.9	$\frac{A^*}{A} = 0.1$	Figure 7.22	Unsymmetric
B-LW-5	Figure 5.10	$\frac{A^*}{A} = 0.3$		longitudinal
B-LW-6	Figure 5.11	$\frac{A^*}{A} = 0.5$		welds
B-LW-7	Figure 5.44	$\frac{A^*}{A} = 0.3$	Figure 7.23	Longitudinally
B-LW-8	Figure 5.45			welded T-beams
B-TW-1	Figure 3.18	$L^* = 0.0$	Figure 7.24	Transversely
B-TW-2		$L^* = 0.1$ at both ends		welded beams
B-TW-3		$L^* = 0.1$		
B-TW-4	Figure 5.25	$L^* = 30mm$ at both ends	Figure 7.25	Transversely welded beams
B-TW-5	Figure 5.26	$L^* = 50mm$ at mid-span		
B-TW-6		$L^* = L$		
B-E-1	Figure 5.20	$\frac{A^*}{A} = 0.0$	Figure 7.28	$\beta_x = 1$
B-E-2				$\beta_x = 0$
B-E-3				$\beta_x = -1$

Table 7.3: List of Theoretical Beam Results

7.3.2   Comparison between Draft BS 8118 with Theoretical Results of Beams

Most of the theoretical beam results presented in Chapter 5 will be compared with draft BS 8118. The details of comparison and the principal results can be referred to Table 7.3. The validity of the basic design principle will also be discussed. Similar to the comparison with theoretical column curves, the effect of local buckling is also neglected in all the cases. Therefore, the basic moment capacity, M_s , is always equal to $M_p(= \sigma_{0.2} \, Z_p)$ even though the cross-section shown in Figure 5.5 is a slender section according to draft BS 8118.

7.3.2.1   Comparison with Non-welded Beams

The comparison between draft BS 8118 with non-welded I- and Tee-beams are shown in Figures 7.17 to 7.20. Figures 7.17 and 7.18 show the non-welded beams with $\frac{\sigma_{ult}}{\sigma_{0.2}} \leq 1.4$ (i.e. high n value). From Figure 7.17, we can observe that draft BS 8118 cannot give safe design for doubly symmetrical I-beams throughout the practical range of beam slenderness. For asymmetrical cross-section *sections*, draft BS 8118 tends to give very conservative results [3], and therefore safe design can be obtained for non-welded Tee-beams as shown in Figure 7.18. However, from the figure, it can be seen that the ultimate moment capacities of Tee-beams are drastically underestimated by the draft code, especially when the Tee-beams tends to buckle elastically.

The comparison with non-welded I- and Tee-beams with $\frac{\sigma_{ult}}{\sigma_{0.2}} > 1.4$ (i.e. low n value) are shown in Figures 7.19 to 7.20, and similar observations are obtained. Moreover, it is worthwhile to point out that the theoretical curves: B-NW-8, B-NW-9 and B-NW-10 are obtained by inputting the RSZ material properties into the program BIAXIAL and represent the members which are fully-affected by welding. However, the mechanical properties of the RSZ material (6082-TF alloy) is quite similar to the parent 5083-M alloy as quoted in CP 118. Therefore, those theoretical curves can also be treated as if non-welded 5083-M members (see Section 7.7) during the comparison with draft BS 8118.

Figure 7.17 Comparison with Non-welded I-beams ($\frac{\sigma_{ult}}{\sigma_{0.2}} \leq 1.4$)

Figure 7.18 Comparison with Non-welded Tee-beams ($\frac{\sigma_{ult}}{\sigma_{0.2}} \leq 1.4$)
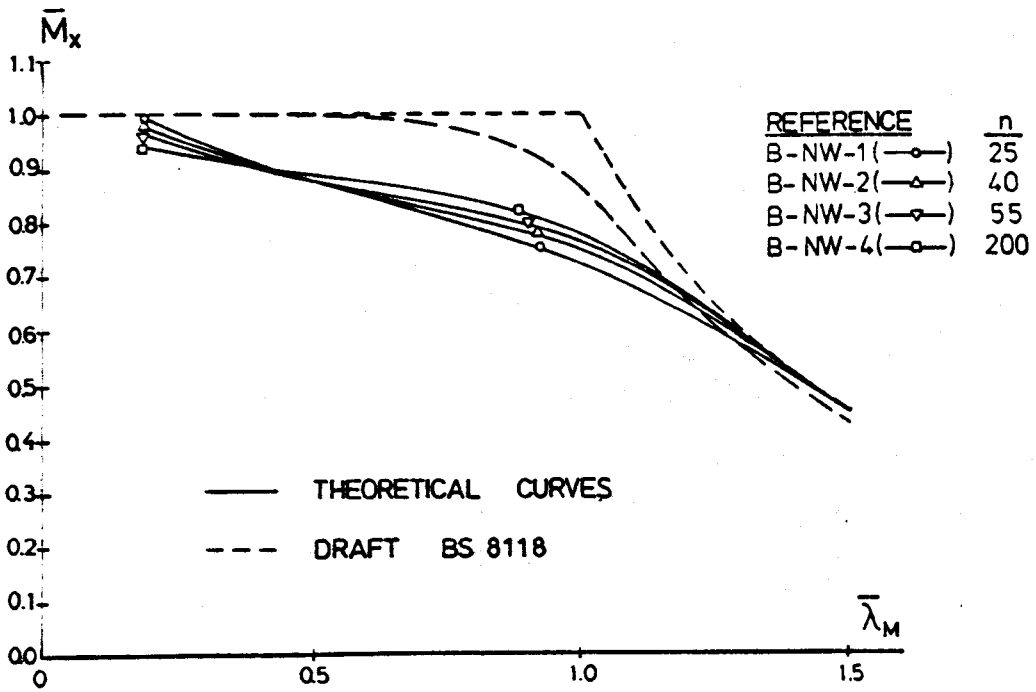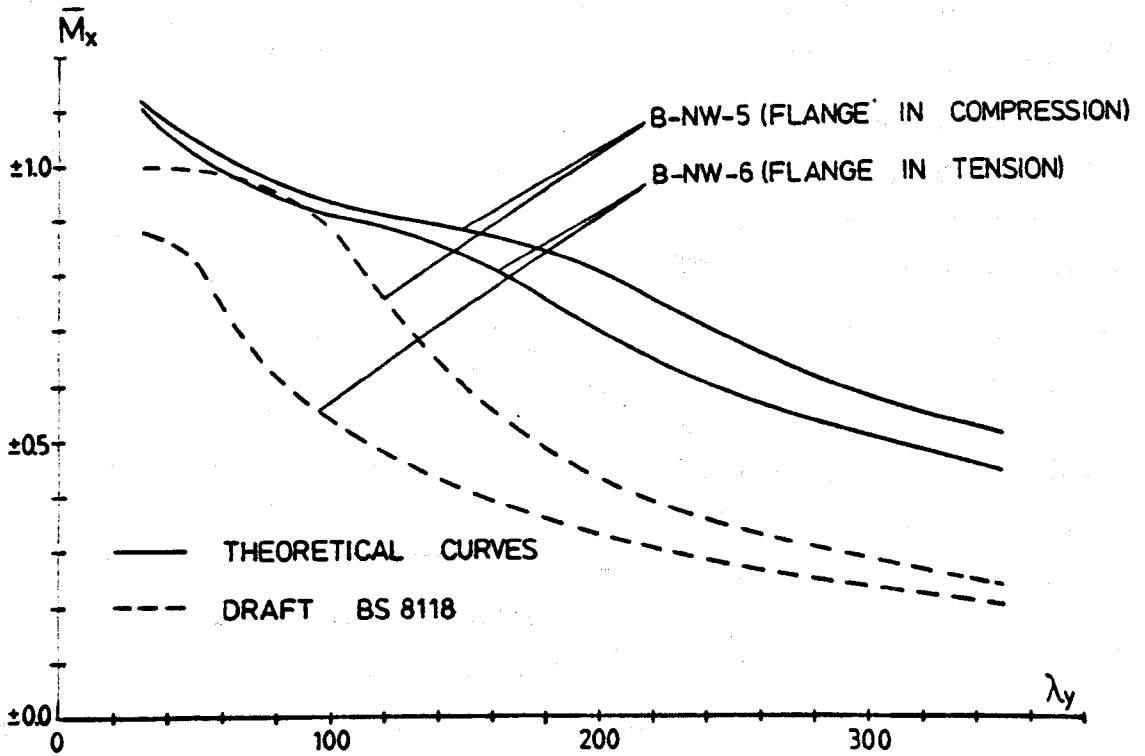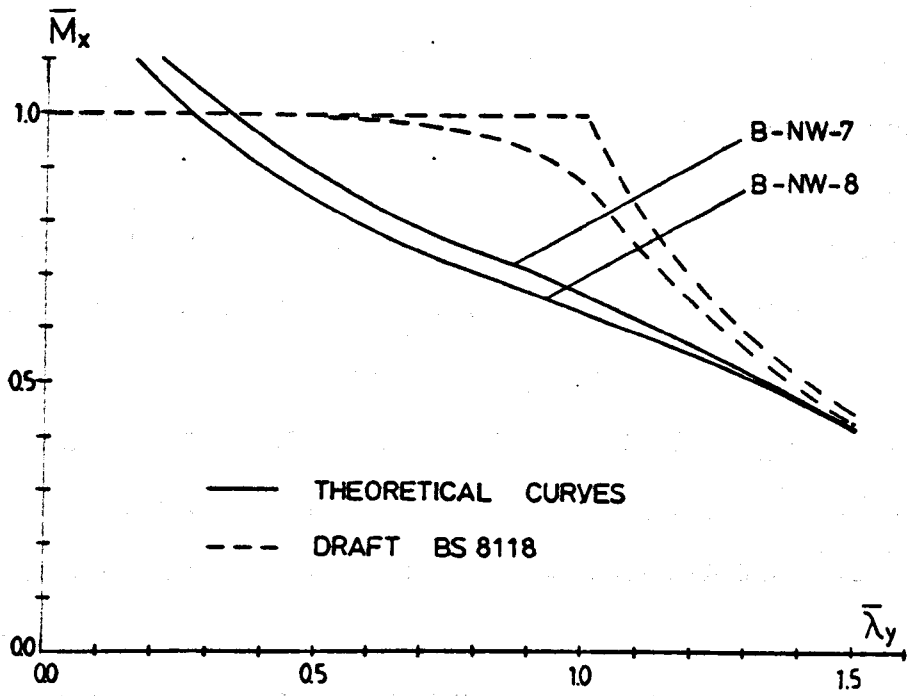
Figure 7.19 Comparison with Non-welded I-beams ($\frac{\sigma_{ult}}{\sigma_{0.2}} > 1.4$)
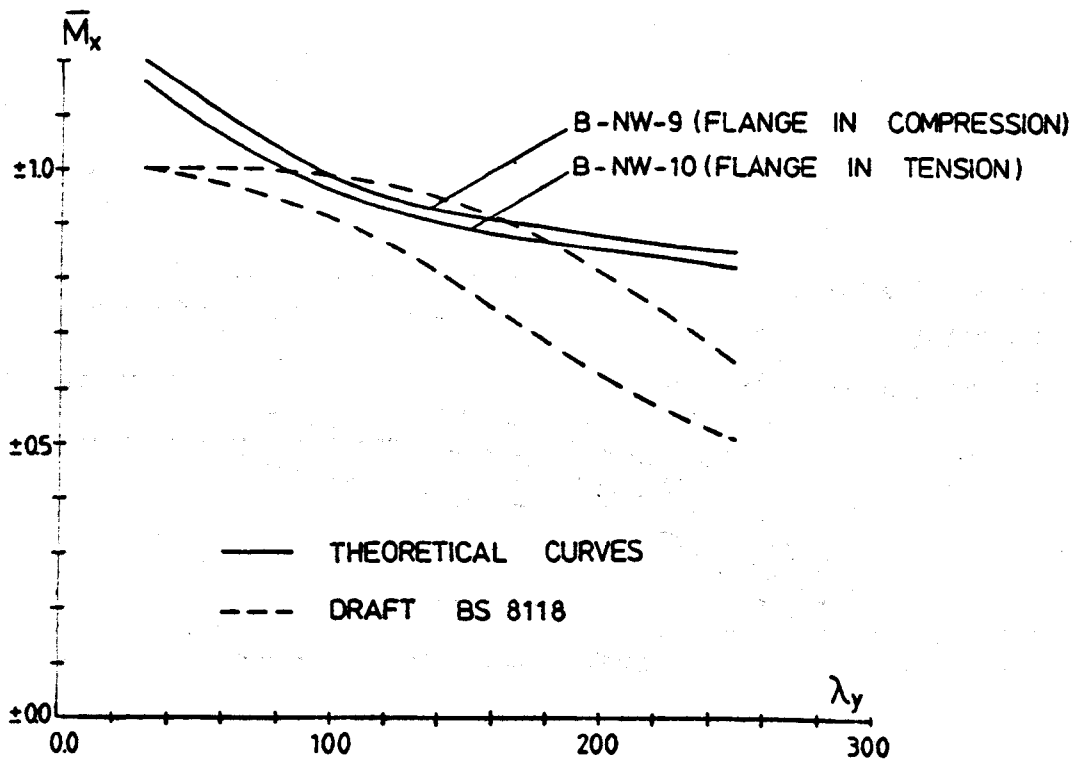
Figure 7.20 Comparison with Non-welded Tee-beams ($\frac{\sigma_{ult}}{\sigma_{0.2}} > 1.4$)

7.3.2.2   Comparison with Longitudinally Welded Beams

Figures 7.21 to 7.23 shows the comparison between draft BS 8118 with longitudinally welded I- and Tee-beams. The effect of residual stresses is also included in the comparison (except unsymmetric longitudinally welded I-beams with $\frac{A^{*}}{A} = 0.5$). Figures 7.21 and 7.22 clearly clearly show that the draft code will give unsafe design for longitudinally welded I-beams. For the longitudinally welded Tee-beams, the draft code also tends to give very conservative results especially when the flanges of the Tee-beams are under tension during bending or the Tee-beams tend to buckle elastically (see Figure 7.23). However, the draft code also gives unsafe design when the flanges of the longitudinally welded Tee-beams are under compression during bending as $\lambda_y \le 100$.

Figure 7.21 Comparison with Symmetric Longitudinally Welded I-beams
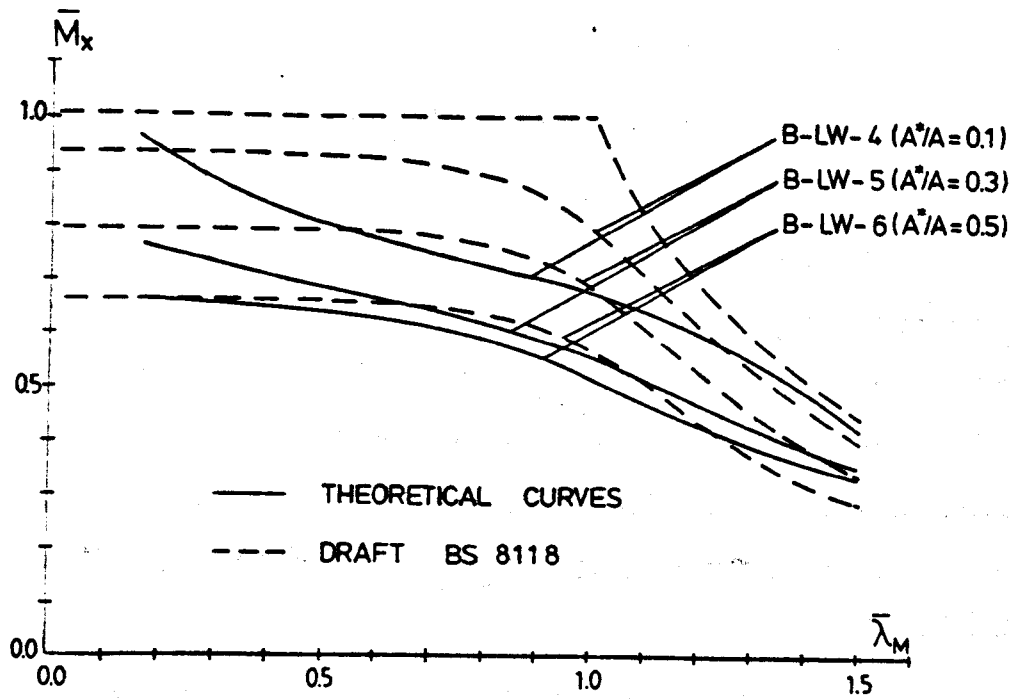
Figure 7.22 Comparison with Unsymmetric Longitudinally Welded I-beams
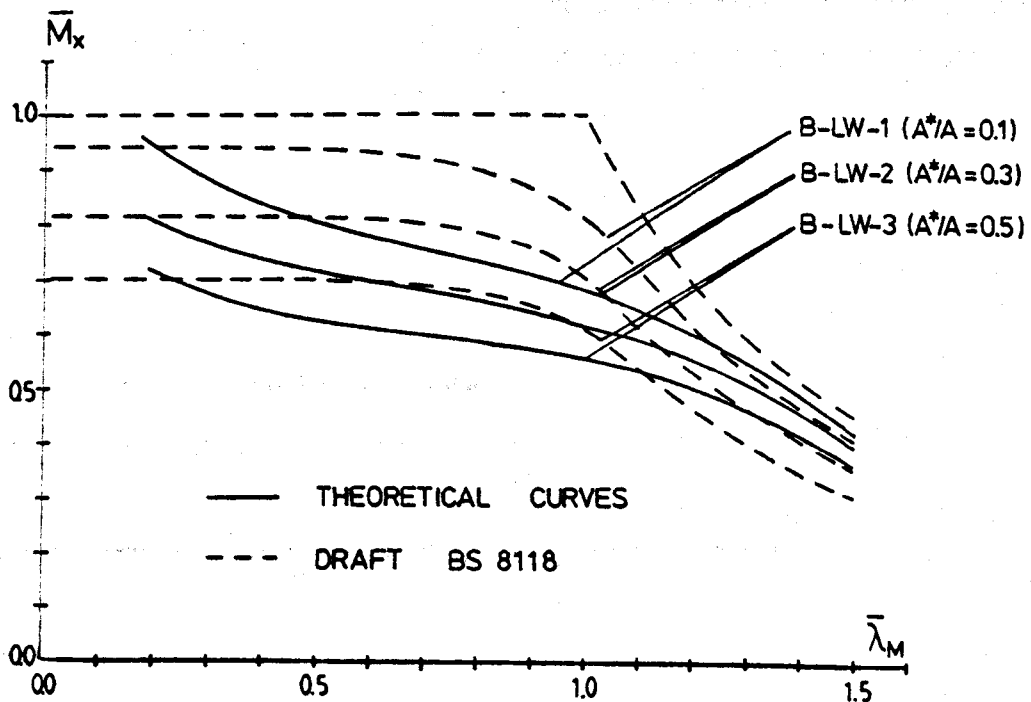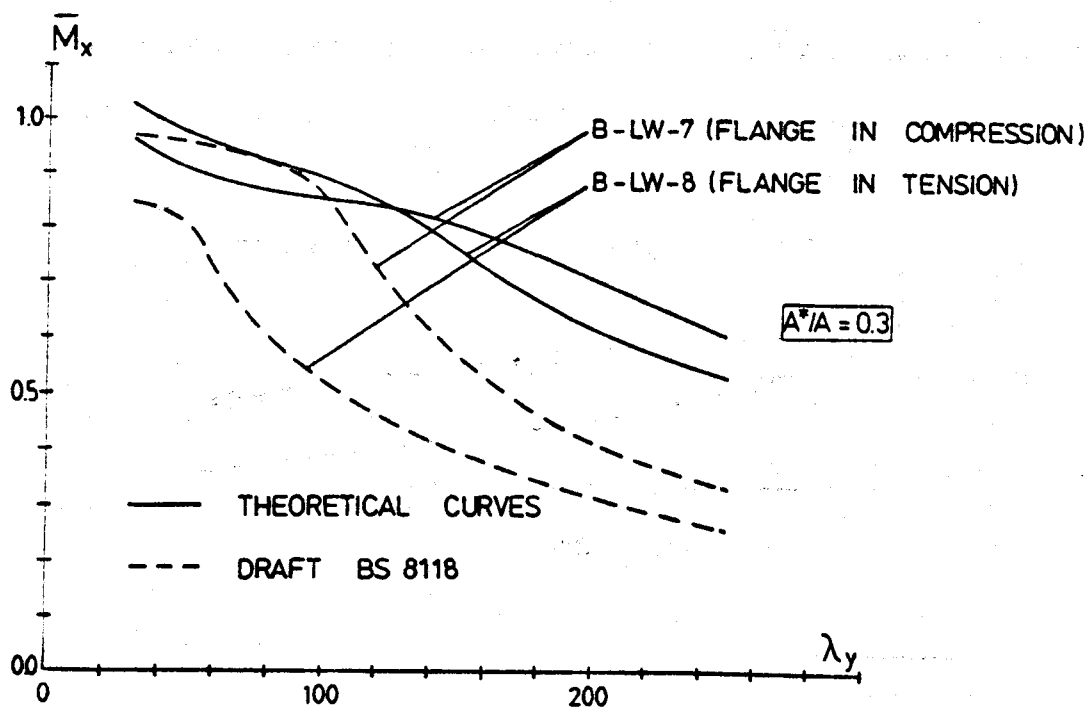

Figure 7.23 Comparison with Longitudinally Welded Tee-beams
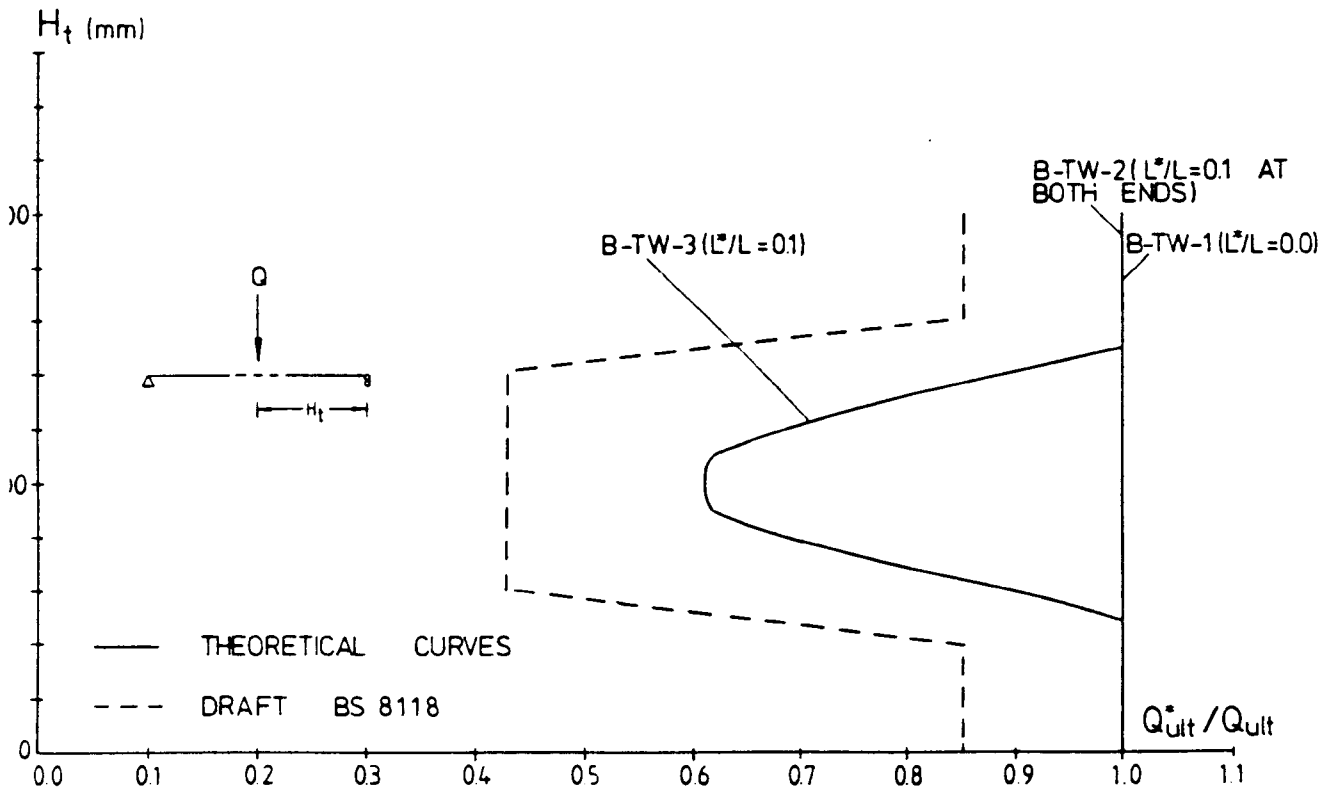
Figure 7.24 Comparison with Transversely Welded Beams Obtained by Program INSTAF
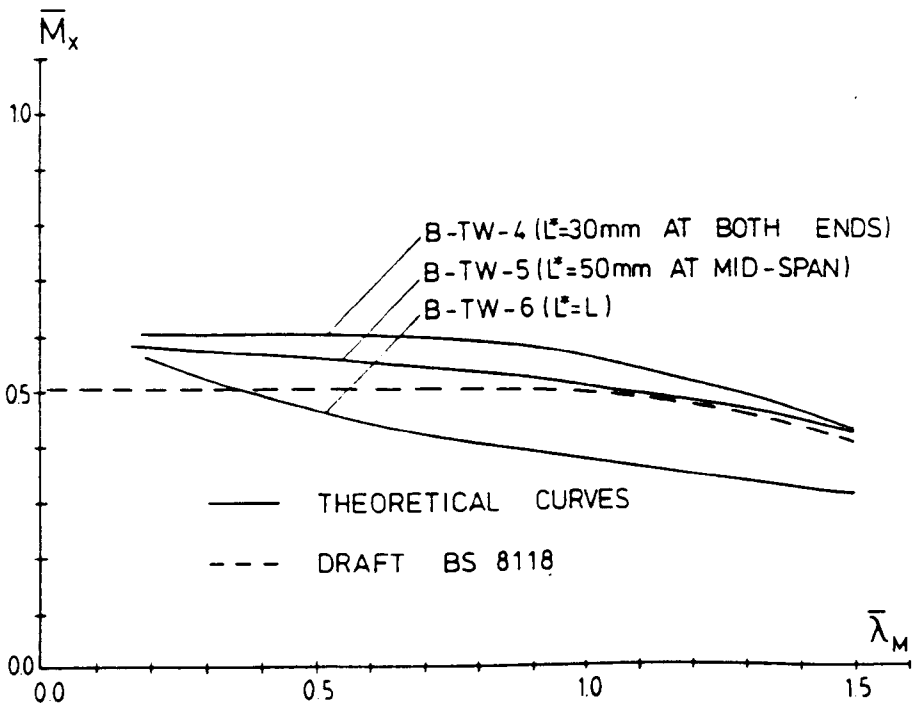
Figure 7.25 Comparison with Transversely Welded Beams Obtained by Program BIAXIAL

7.3.2.3   Comparison with Transversely Welded Beams

A similar approach, to that given for transversely welded columns is used in
the draft BS 8118 for the design of transversely welded beams. For the trans-
versely welded beams with central point load and under in-plane bending as
shown in Figure 7.24 , the draft can give a very safe design because the RSZ
located at the ends are not sufficiently stressed. However, if the RSZ material
is sufficiently stressed (e.g. the welded beam is loaded by uniform end mo-
ments), the design approach according to draft BS 8118 will become unsafe
even though the transverse welds are located at the ends. For the laterally
unrestrained beams with local transverse welds and under uniform end mo-
ments as shown in Figure 7.25, the draft code cannot give the safe design
even though the welded beams are designed as if fully-affected by welding.
The reason is due mainly to the reduction in ultimate strength due to lateral
buckling not being well-estimated by draft BS 8118. Safe design should be
obtained if the design curve for the determination of C_{LT} is revised.
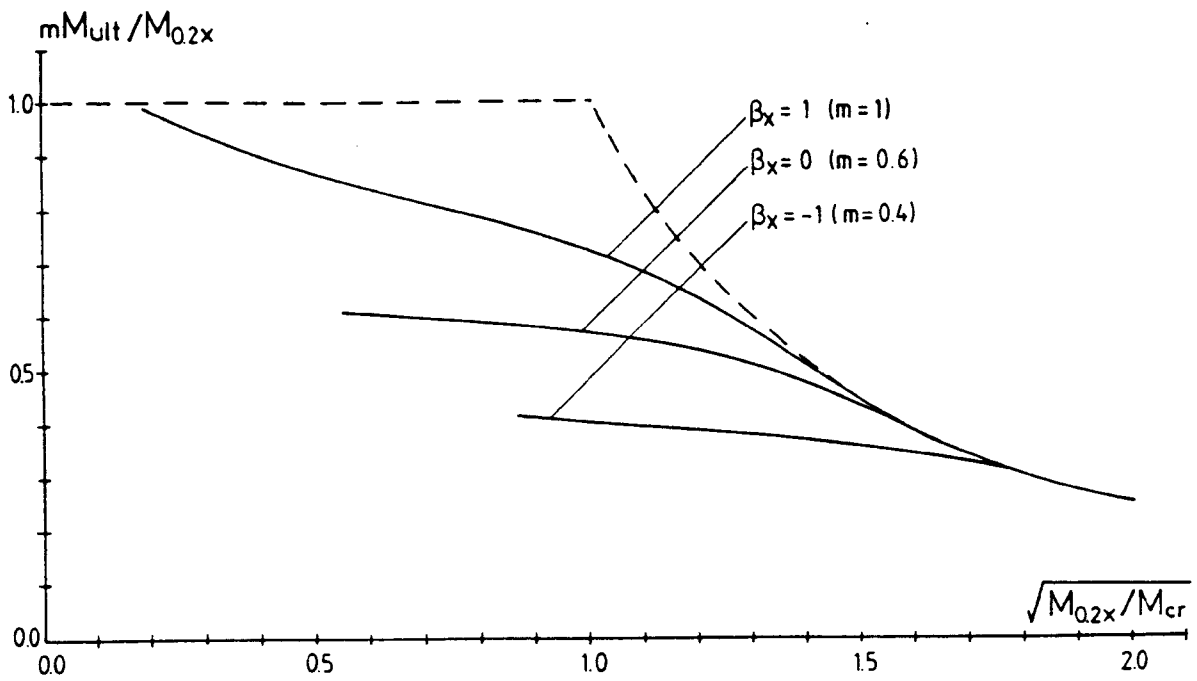
Figure 7.26 Effect of Unequal End Moments on Non-welded Beams

λ_y	Equivalent Uniform Moment Factor, m	
	$\beta_x = 0$	$\beta_x = -1$
40	0.83	–
50	0.81	–
60	0.79	0.74
70	0.76	0.71
80	0.73	0.67
90	0.69	0.62
100	0.65	0.56
110	0.63	0.52
120	0.60	0.47
130	0.60	0.44
140	0.60	0.42
150	0.60	0.41
160	0.60	0.40
170	0.60	0.40

Table 7.4: Variation of Equivalent Uniform Moment Factor

7.3.2.4 Validity of Equivalent Uniform Moment Factor

When the aluminium beam is under unequal end moments, draft BS 8118 suggested that the equivalent moment concept can be applied to design [8] and the equivalent uniform moment factor, m, can be referred to equation (7.5). The background of the equivalent moment concept is based on limited experimental results obtained by Clark and Jombock [9] in 1957. In theory [10], the m-factor should be valid for elastic aluminium beams but the suitability is still questionable for inelastic aluminium beams.

Figure 7.26 shows the plot of m($\frac{M_{ult}}{M_{0.2x}}$) Vs $\sqrt{\frac{M_{0.2x}}{M_{cr}}}$ for beams under unequal ends moments ($\beta_x = 1, 0$ and -1). The value of M_{ult} is the larger ultimate major axis end moment obtained by program BIAXIAL, and the value of M_{cr} is referred to the beam under single curvature bending ($\beta_x = 1$) for all the cases. From equation (7.5), the values of m for $\beta_x = 1, 0, -1$ are 1, 0.6 and 0.4 respectively. Figure 7.26 clearly shows that the m-factor suggested by draft BS 8118 is not correct for the inelastic beams. It is because the three curves for $\beta_x = 1, 0$ and -1 should be approximately coincide if the values of m are correct. The value of m given in equation (7.5), therefore, should be modified. Table 7.4 shows the value of m for $\beta_x = 0$ and -1 with a wide range of slenderness of beam. The value of m is then plotted in Figure 7.27. From the figure, we can observe that the value of m actually is varied with λ_y in the inelastic range and the relationship between m and λ_y is approximately approaching linear. Therefore, using a unique value of m given in equation (7.5) becomes incorrect. Using curve fitting, the linear relationship between
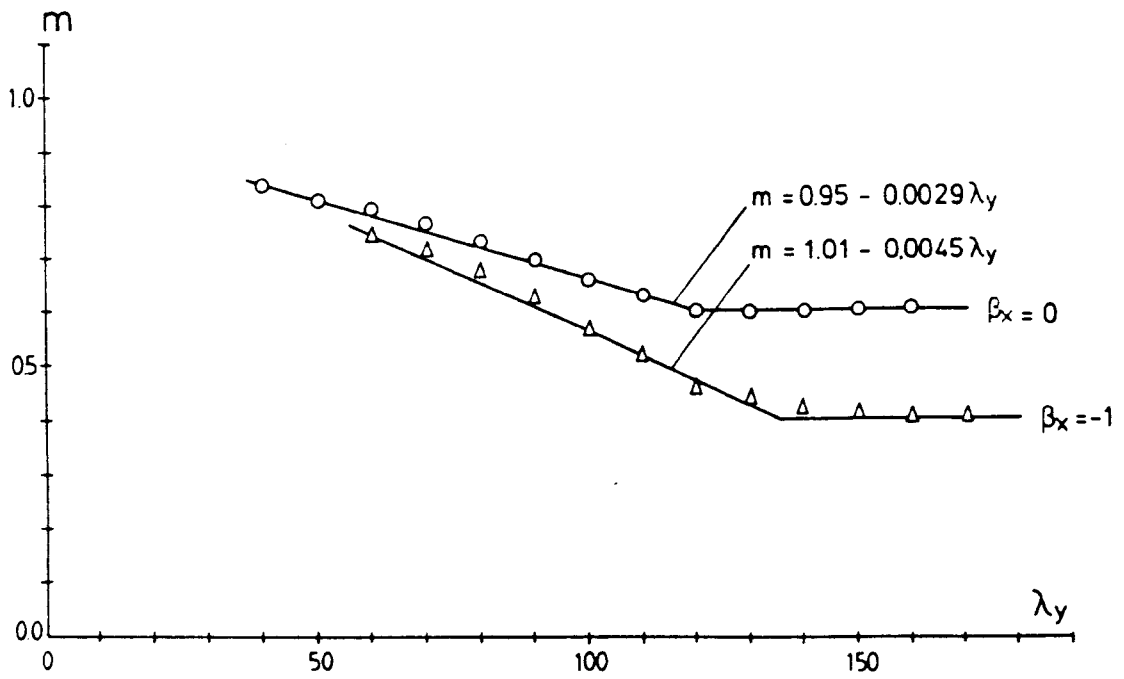
Figure 7.27 Determination of Equivalent Uniform Moment Factor , m
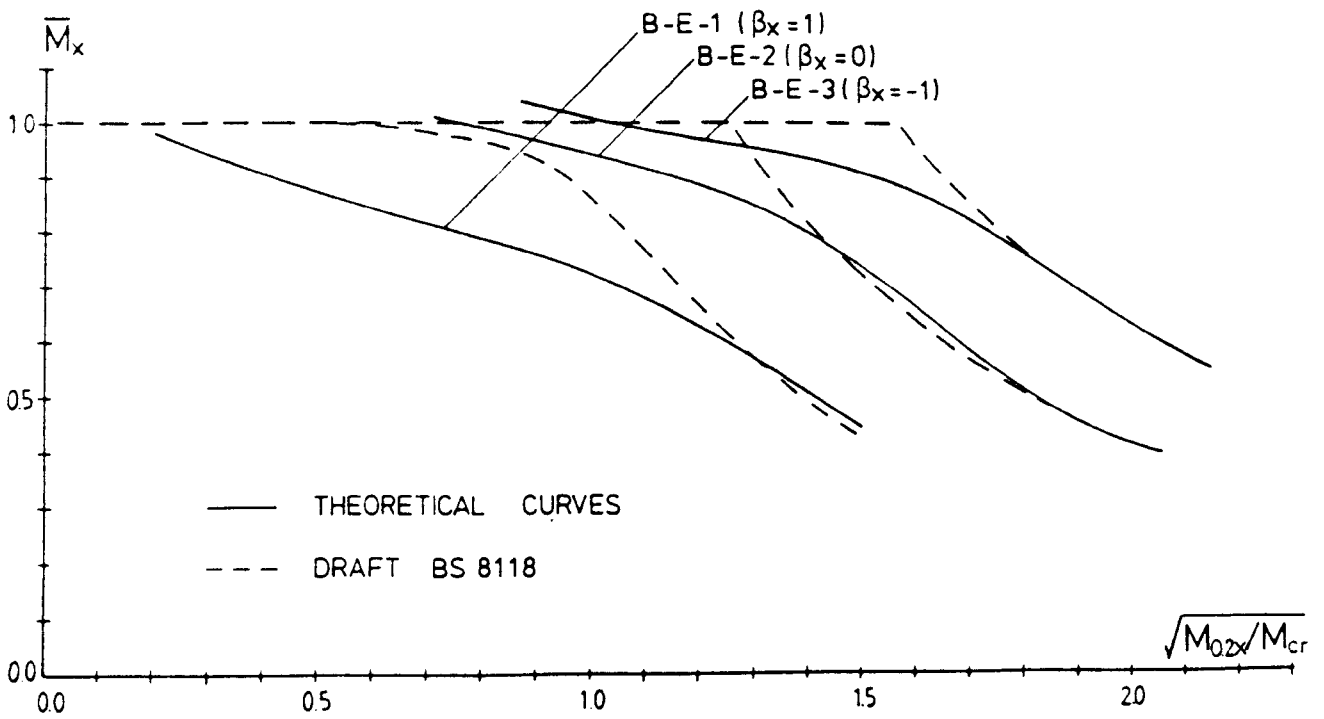
Figure 7.28 Comparison with Non-welded Beams under Unequal End Moments

m and λ_y for $\beta_x = 0$ and -1 are:

$$m = 0.95 - 0.029\lambda_y \geq 0.6 \qquad (\beta_x = 0) \tag{7.6}$$

$$m = 1.01 - 0.0045\lambda_y \geq 0.4 \qquad (\beta_x = -1) \tag{7.7}$$

If the m-value given in equation (7.5) is still used for comparison, Figure 7.28 clearly shows that the draft BS 8118 will over-estimate the ultimate strength of inelastic beams under unequal end moments.

However, from the above investigations, we can reflect that the application of m-factor is not so straight forward. The determination of the value of m actually is very complex because the value of m is not only affected by the loading conditions. The mechanical properties of the parent metal and RSZ material (i.e. with high or low knee factor, n) also can influence the value of m. Further research in this area, therefore, is necessary.

7.4 Design of Aluminium Beam-columns

7.4.1 Basic Principle and Design Procedures

In the draft BS 8118 a series of interaction equations in clause 5.39 must be checked where appropriate. Basically, the purposes of those interaction equations are to check the adequacy of

1. the strength of the most highly stressed cross-section(s),

2. the stability of members under loads and the values of $\tilde{M}_x$ and $\tilde{M}_y$ should be used when appropriate.

The first expression in clause 5.39 of draft BS 8118 is

$$\frac{P}{\frac{P_{ac}}{\gamma_m}} + \frac{M_x}{\frac{M_{ax}}{\gamma_m}} + \frac{M_y}{\frac{M_{sy}}{\gamma_m}} \leq 1 \tag{7.8}$$

This expression is a 'basic strength' equation that must be satisfied for all members and in addition one or more of the buckling equations must be checked.

For moments are applied about the major axis,

$$\frac{P}{P_{cx}} + \frac{\tilde{M}_x}{\frac{M_{ax}}{\gamma_m}} + \frac{1}{2}\frac{P}{P_{cx}}\frac{\tilde{M}_x}{\frac{M_{ax}}{\gamma_m}} \leq 1 \tag{7.9}$$

$$\frac{P}{P_{cy}} + \frac{\tilde{M}_x}{M_{max}} \leq 1 \tag{7.10}$$

where $\tilde{M}_x = m\, M_x$

Equation (7.9) is to avoid the in-plane buckling about the major axis and the third term in equation (7.9) is an amplification factor to allow for secondary bending effects. Equation (7.10) is to avoid the flexural-torsional buckling about the minor axis which involves the interaction of column buckling and beam buckling.

For moments applied about the minor axis, it is only possible for buckling to occur in the plane of bending; and therefore only one equation needs to be checked as a buckling condition. The equation is

$$\frac{P}{P_{cy}} + \frac{\tilde{M}_y}{\frac{M_{sy}}{\gamma_m}} + \frac{1}{2}\frac{P}{P_{cy}}\frac{\tilde{M}_y}{\frac{M_{sy}}{\gamma_m}} \leq 1 \tag{7.11}$$

where $\tilde{M}_y = m\,M_y$ and this expression is similar to equation (7.9) for major axis bending.

When moments are applied about both axes, it is necessary to first determine, at any given level of axial load, the maximum applied moment about each axis that just satisfies equations (7.9), (7.10) and (7.11); and these values $(\tilde{M}_{ax}, \tilde{M}_{ay})$ are then used as the denominators in an interaction equation for the moments about both axes as a buckling check. The interaction equation is

$$\frac{\tilde{M}_x}{\tilde{M}_{ax}} + \frac{\tilde{M}_y}{\tilde{M}_{ay}} \leq 1 \tag{7.12}$$

The above interaction equations for beam-columns are based on the design principle of the steel code BS 5950 [6]. The suitability of the above interaction equations on aluminium beam-columns, up to now, is uncertain because there is no test data or theoretical results available for checking especially for aluminium members under compression plus biaxial bending. Therefore,

Theoretical Curve Reference	$\frac{A^{\bullet}}{A}$ or $\frac{L^{\bullet}}{L}$	Source of Theoretical Curves	Principal Results	Remark
BC-N-1	$\frac{L^{\bullet}}{L} = 0.0$	Figures 3.20, 3.24 and 3.25	Figure 7.29	$\lambda_x = 30$, $\beta_x = 0, 1, -1$
BC-N-2	$\frac{L^{\bullet}}{L} = 0.0$	Figure 5.27	Figure 7.30	$\lambda_y = 30, 50, 70, 90$ and 120, $\beta_x = 1$
BC-N-3	$\frac{L^{\bullet}}{L} = 0.0$	Figure 5.29	Figure 7.31	$\lambda_y = 50, 70$, and 120, $\beta_x = 0$
BC-N-4	$\frac{L^{\bullet}}{L} = 0.0$	Figure 5.30	Figure 7.32	$\lambda_y = 90$ and 120, $\beta_x = -1$
BC-N-5	$\frac{L^{\bullet}}{L} = 0.0$	Figure 5.46	Figure 7.33	$\lambda_y = 50$, $\beta_x = 1$
BC-LW-1	$\frac{A^{\bullet}}{A} = 0.1, 0.3$ and 0.5	Figure 5.31	Figure 7.34	$\lambda_y = 30$, $\beta_x = 1$
BC-LW-2	$\frac{A^{\bullet}}{A} = 0.1, 0.3$ and 0.5	Figure 5.32	Figure 7.35	$\lambda_y = 70$, $\beta_x = 1$
BC-LW-3	$\frac{A^{\bullet}}{A} = 0.1, 0.3$ and 0.5	Figure 5.33	Figure 7.36	$\lambda_y = 90$, $\beta_x = 1$
BC-TW-1	$\frac{L^{\bullet}}{L} = 0.1, 0.2, 0.3$ and 1.0	Figure 3.24	Figure 7.37	$\lambda_x = 30$, $\beta_x = 1$
BC-TW-2	$\frac{L^{\bullet}}{L} = 0.1, 0.2, 0.3$ and 1.0	Figure 3.20	Figure 7.38	$\lambda_x = 30$, $\beta_x = 0$
BC-TW-3	$\frac{L^{\bullet}}{L} = 0.1, 0.2, 0.3$ and 1.0	Figure 3.25	Figure 7.39	$\lambda_x = 30$, $\beta_x = -1$
BC-TW-4	$L^{\bullet} = 0, 30\ mm$ at both ends, 50 mm at mid-height and L	Figures 5.34, and 5.37	Figure 7.40	$\lambda_y = 30$, $\beta_x = 1$
BC-TW-5	$L^{\bullet} = 0, 30\ mm$ at both ends, 50 mm at mid-height and L	Figures 5.35, and 5.38	Figure 7.41	$\lambda_y = 70$, $\beta_x = 1$
BC-TW-6	$L^{\bullet} = 0, 30\ mm$ at both ends, 50 mm at mid-height and L	Figures 5.36, and 5.39	Figure 7.42	$\lambda_y = 90$, $\beta_x = 1$

Table 7.5: (a) List of Theoretical Beam-column Results (In-plane and Out-of-plane Failure)

the comparison with theoretical results which will be presented in Section 7.4.2 can be used as a background studies for the design of aluminium beam-columns in general.

7.4.2   Comparison between Draft BS 8118 with Theoretical Results of Beam-columns

In this section, the comparison will be confined to the beam-columns which are under compression plus uniaxial bending but leading to in-plane or out-of-plane failure. The effect of local buckling is also neglected in the comparison and the principal results can be referred to Table 7.5 (a).

For the beam-columns which are under in-plane buckling, only the interaction equations (7.8) and (7.9) are needed to be checked and the reduction factor for lateral torsional buckling, C_{LT}, is equal to 1 in all the cases.

For the beam-columns which are under out-of-plane failure, interaction equations (7.8) to (7.10) are needed to be checked. For stocky beam-columns, interaction equations (7.8) and (7.9) usually control the design. For intermediate and slender beam-columns, interaction equation (7.10) usually controls the design and the interaction curve will result in a straight line.

7.4.2.1   Comparison with Non-welded Beam-columns

Figure 7.29 shows the comparison with non-welded beam-columns which are under in-plane buckling for $\lambda_x = 30$, and three moment patterns under major axis bending ($\beta_x = 1, 0, -1$) are considered. The m-factor given in equation (7.5) is also used in the comparison. In Figure 7.29, some discrepancy results at the end point on the $\overline{M}_x$ axis. It is due mainly to the limiting strain, ε_{limit}, chosen by the authors in the computer simulation (see Section 3.3) being higher than the ultimate strain used in the draft BS 8118. From the comparison, Figure 7.29 clearly shows that the draft code can give safe design for non-welded beam-columns which are under in-plane failure.

For the non-welded beam-columns which are subject to out-of-plane failure, the comparison can be referred to Figures 7.30 to 7.33. Figures 7.30 to 7.32 are for the non-welded beam-columns with doubly symmetric I-sections under compression plus unequal end moments ($\beta_x = 1, 0$ and -1). Due to the ultimate strength of beams given by the draft BS 8118 being overestimated, therefore Figures 3.30 to 7.32 clearly show that unsafe results can be obtained as the values of $\overline{M}_x$ are high. But as the values of $\overline{M}_x$ are relatively lower or the beam-columns tend to buckle elastically, safe design can also be obtained.

For the non-welded beam-columns with Tee-section under compression plus single curvature bending ($\beta_x = 1$), Figure 7.33 shows that the draft BS 8118 can give very safe design because the ultimate compressive and bending strength of Tee-section are under-estimated, especially when the flange of the Tee-section are under tension during bending.

Figure 7.29 Comparison with Non-welded Beam-columns (In-plane Buckling, $\beta_x = 1, 0, -1$)

Figure 7.30 Comparison with Non-welded Beam-columns (Lateral Torsional Buckling, $\beta_x = 1$)

Figure 7.31 Comparison with Non-welded Beam-columns (Lateral Torsional Buckling, $\beta_x = 0$)
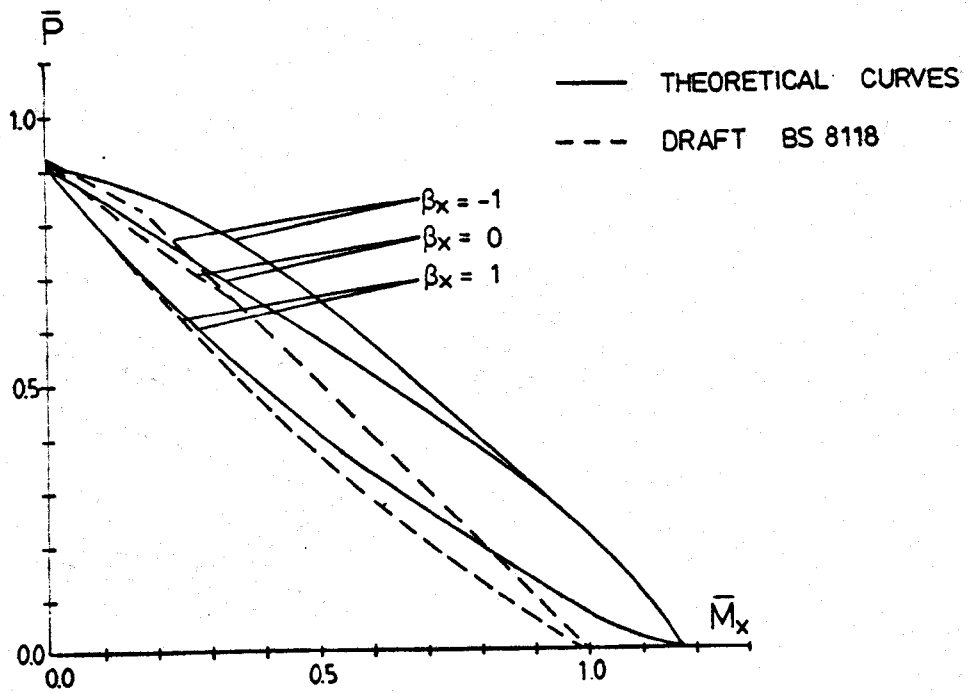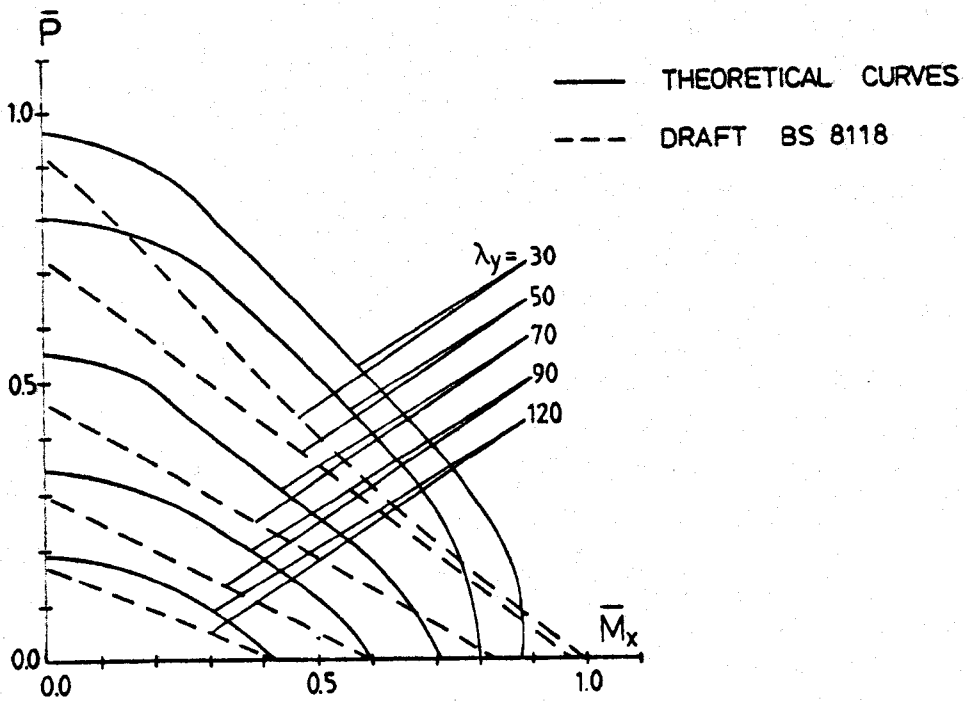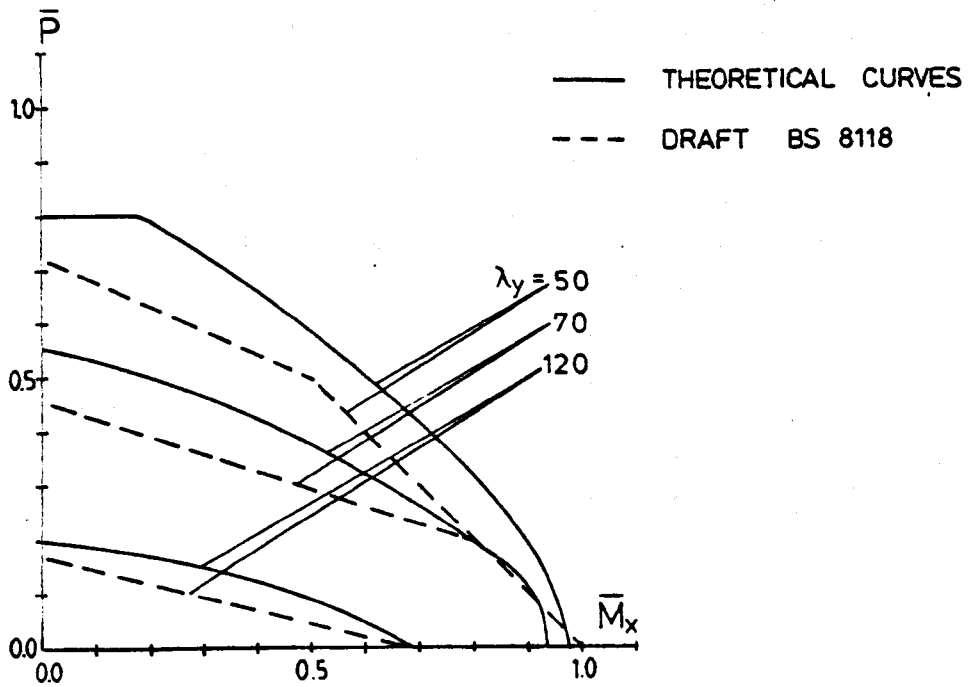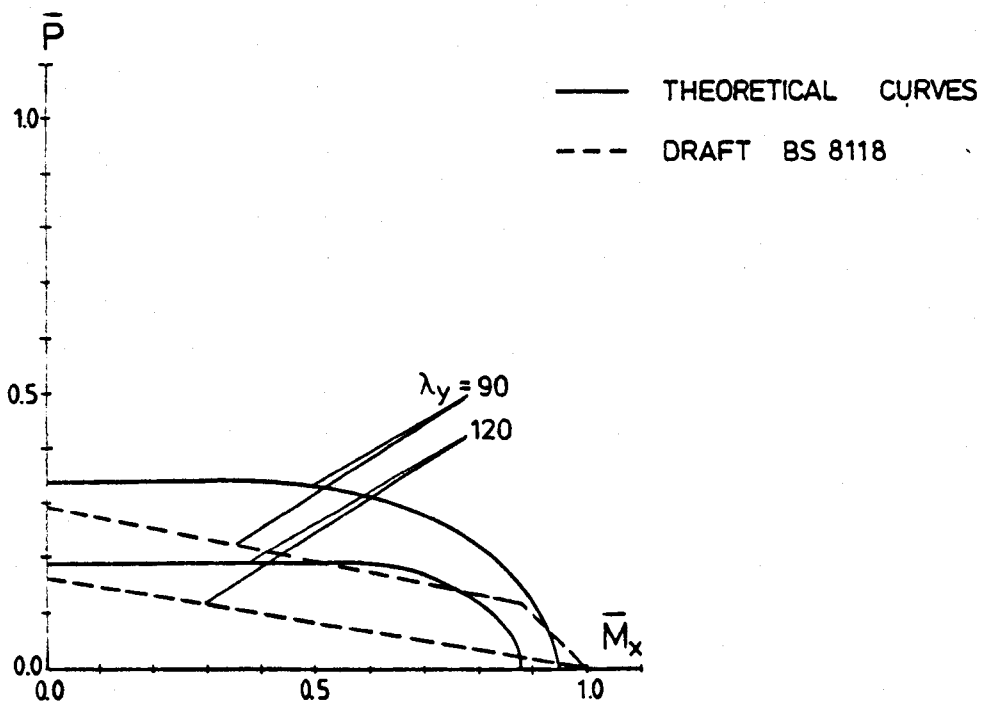

Figure 7.32 Comparison with Non-welded Beam-columns (Lateral Torsional Buckling, $\beta_x = -1$)
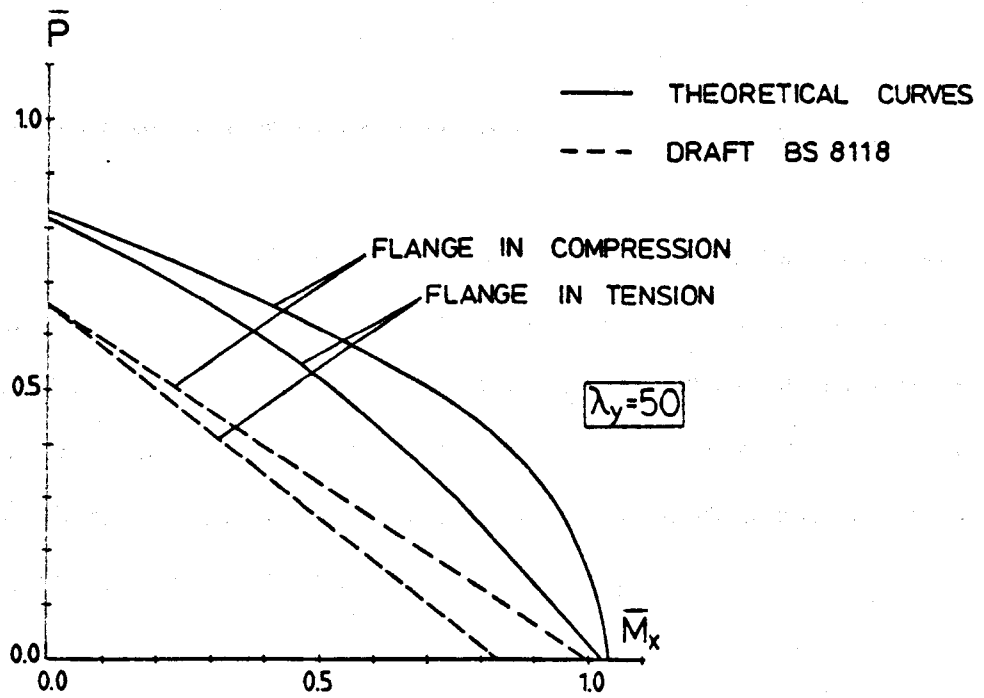
Figure 7.33 Comparison with Non-welded Tee Beam-columns ($\beta_x = 1$)

7.4.2.2   Comparison with Longitudinally Welded Beam-columns

Figures 7.34 to 7.36 show the comparison between draft BS 8118 with longitudinally welded beam-columns under compression plus single curvature bending ($\beta_x = 1$). The effect of residual stresses is also included in the comparison. From the figures, we can observe that the draft code can generally give safe design except when the values of $\overline{M}_x$ are high. It is due mainly to the ultimate strength of longitudinally welded beams being over-estimated by the draft code.

Figure 7.34 Comparison with Longitudinally Welded Beam-columns ($\lambda_y = 30, \beta_x = 1$)

Figure 7.35 Comparison with Longitudinally Welded Beam-columns ($\lambda_y = 70, \beta_x = 1$)

Figure 7.36 Comparison with Longitudinally Welded Beam-columns ($\lambda_y = 90, \beta_y = 1$)

7.4.2.3 Comparison with Transversely Welded Beam-columns

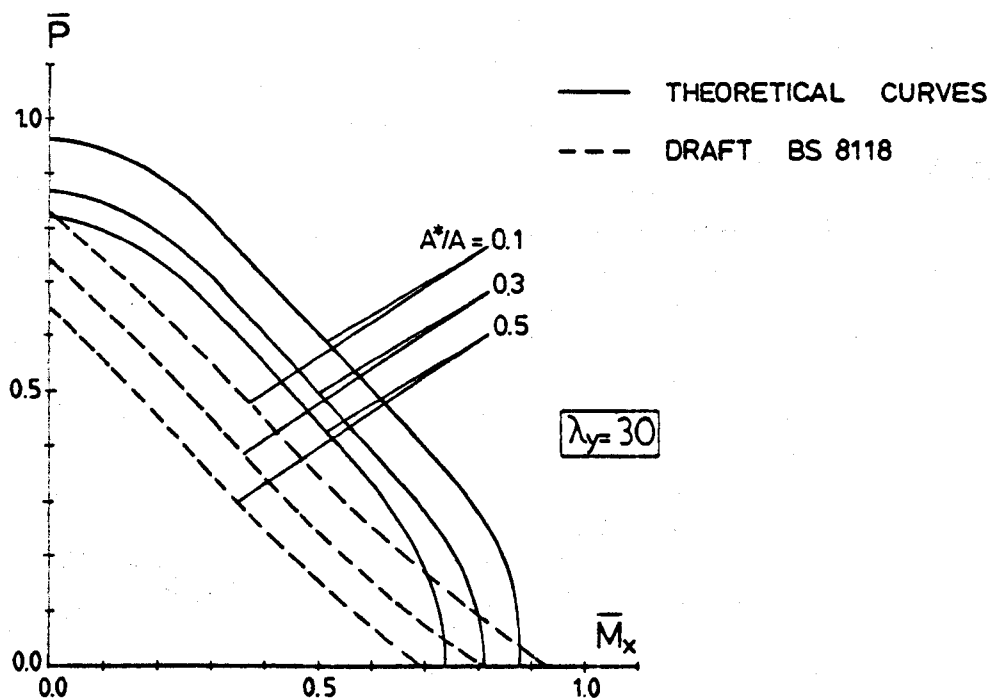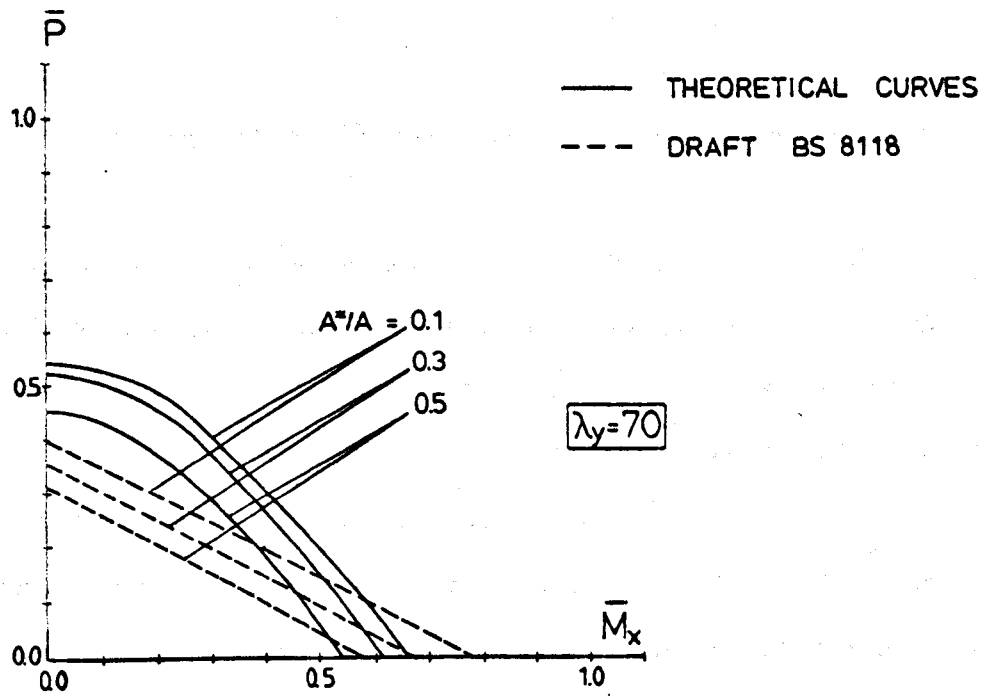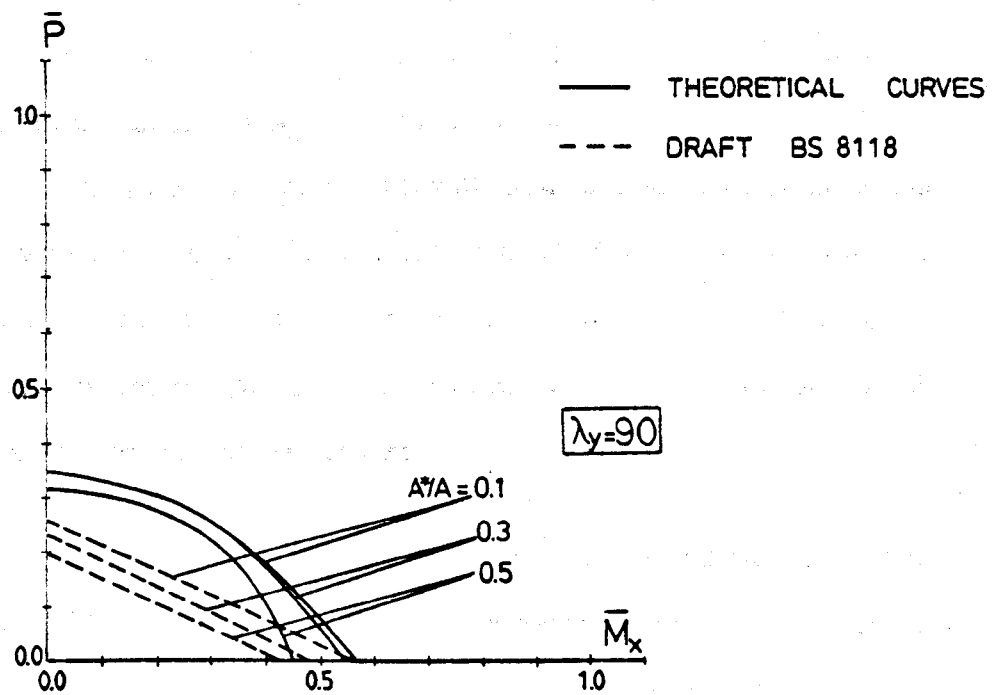For the design of transversely welded beam-columns, the draft BS 8118 did not give any guidance and some of the design procedures are questionable. From the detailed studies, the author would recommend that the effect of local transverse welds on compressive and bending strength of beam-columns should be considered separately, which means the design depends upon the positions of the local transverse welds and the moment patterns. For example, if the local transverse welds are located at mid-height and the beam-column is under compression plus single curvature bending ($\beta_x = 1$), this position of the local transverse welds and the moment pattern are the worst and will cause severe reduction in both the ultimate compressive strength and ultimate bending strength. Therefore, the basic axial capacity, P_{sc}, and the basic moment capacity, M_s, of the beam-columns should be based on RSZ material. However, if the local transverse welds are located at mid-height but the beam-column is so under double curvature bending ($\beta_x = -1$), this position of the local transverse welds will cause severe reduction in ultimate compressive strength but the moment pattern ($\beta_x = -1$) will not cause any reduction in ultimate bending strength. Therefore, the basic axial capacity, P_{sc}, should be referred to the RSZ material but the basic moment capacity, M_s, can be based on the parent metal.

The accuracy of the above suggested design principle can be demonstrated in Figures 7.37 to 7.42 for the transversely welded beam-columns which are under in-plane or out-of-plane failure. Since the presence of local transverse welds will cause severe reductions in ultimate compressive strength, therefore

in Figures 7.37 to 7.42, the end point of the dotted line on the vertical axis shows great reduction in the $\overline{P}$ value because the basic axial capacity, P_{sc}, is based on the RSZ material.

For the determination of basic moment capacity, M_s, the value is either based on the parent metal or RSZ material depending on the moment; the position and the extent of RSZ. For uniform end moments ($\beta_x = 1$), the basic moment capacity will be referred to the RSZ material (see Figures 7.37, 7.40, 7.41 and 7.42). For the moment pattern $\beta_x = 0$, if the extent of RSZ is small ($\frac{L^\bullet}{L} = $ 0.1 and 0.2), the value of M_s will be based on the parent metal. If the extent of RSZ becomes larger ($\frac{L^\bullet}{L} = 0.3$), the RSZ material will be able to reach 'yield', and therefore, the value of M_s should be based on the RSZ material (see Figure 7.38). For the double curvature bending ($\beta_x = -1$), there is less scope for the RSZ to reach 'yield' because the RSZ is located at mid-height (see Figure 7.39), so the value of M_s can be based on the parent metal.

From Figures 7.37 to 7.42, it can be seen that the suggested design method by the author can give safe and accurate design. The more generalized concepts for the design of transversely welded beam-columns will be further discussed in Section 7.6.3.

Figure 7.37 Comparison with Transversely Welded Beam-columns (Centrally-welded, $\lambda_x = 30, \beta_x = 1$)

Figure 7.38 Comparison with Transversely Welded Beam-columns (Centrally-welded, $\lambda_x = 30, \beta_x = 0$)

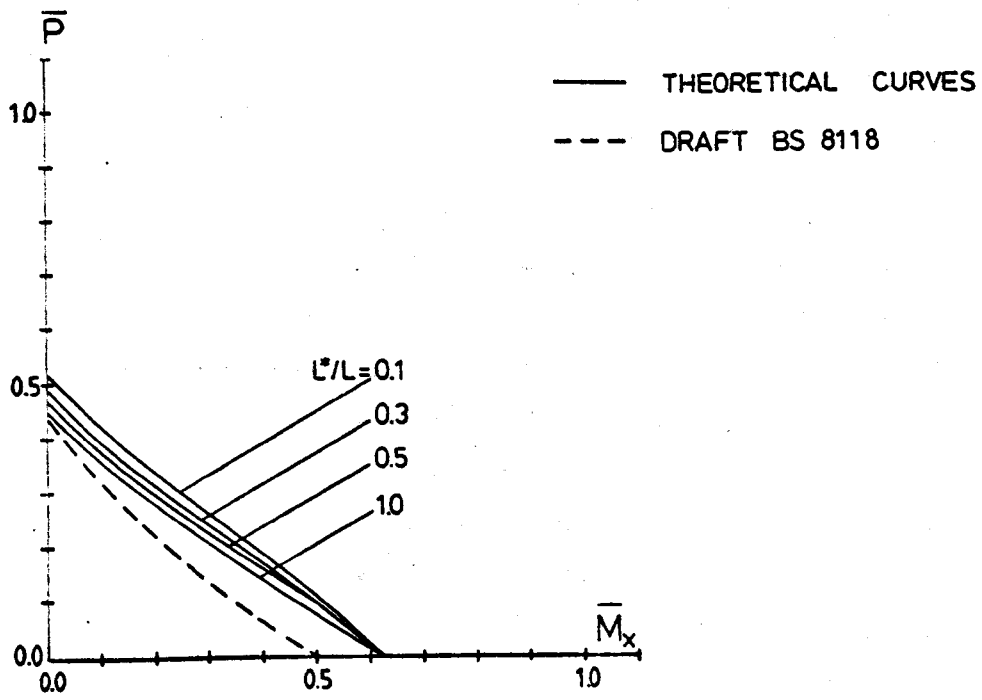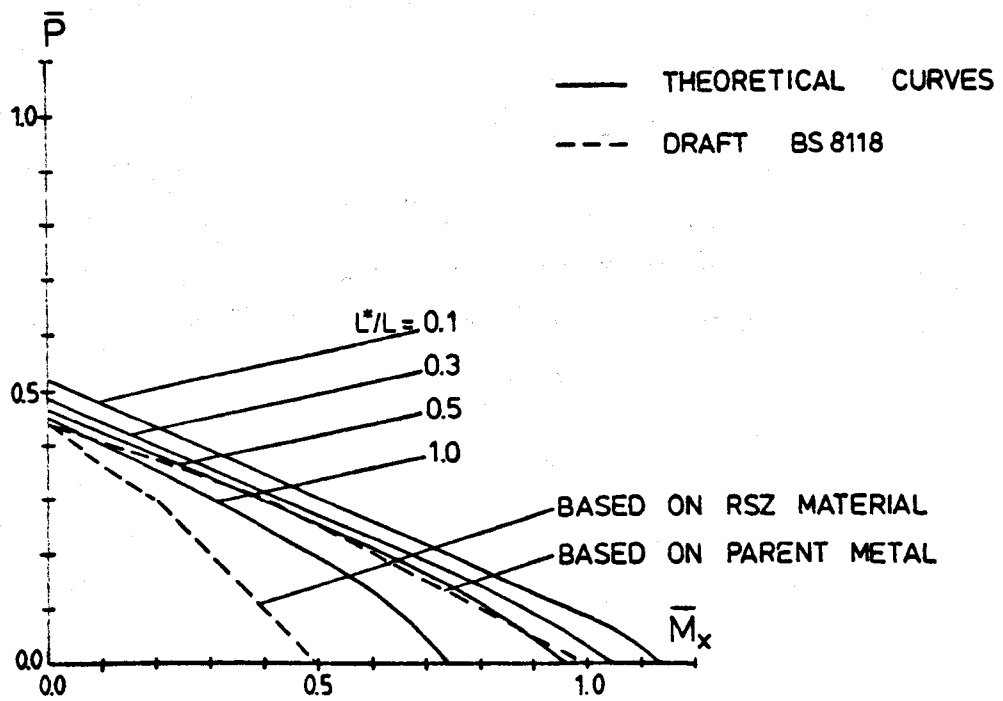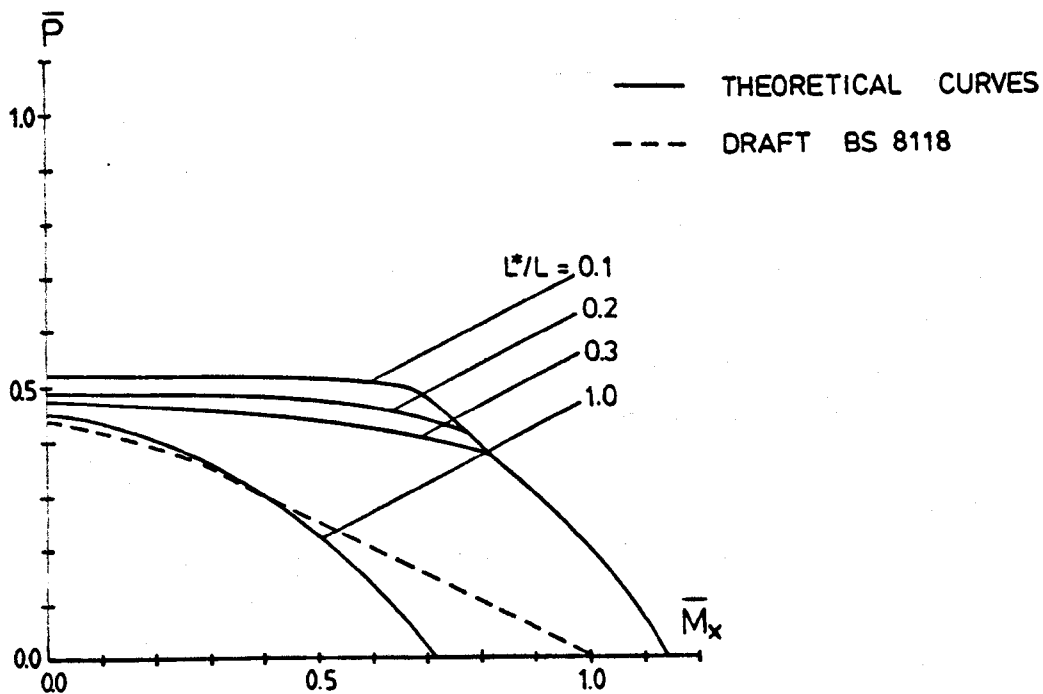Figure 7.39 Comparison with Transversely Welded Beam-columns (Centrally-welded, $\lambda_x = 30, \beta_x = -1$)
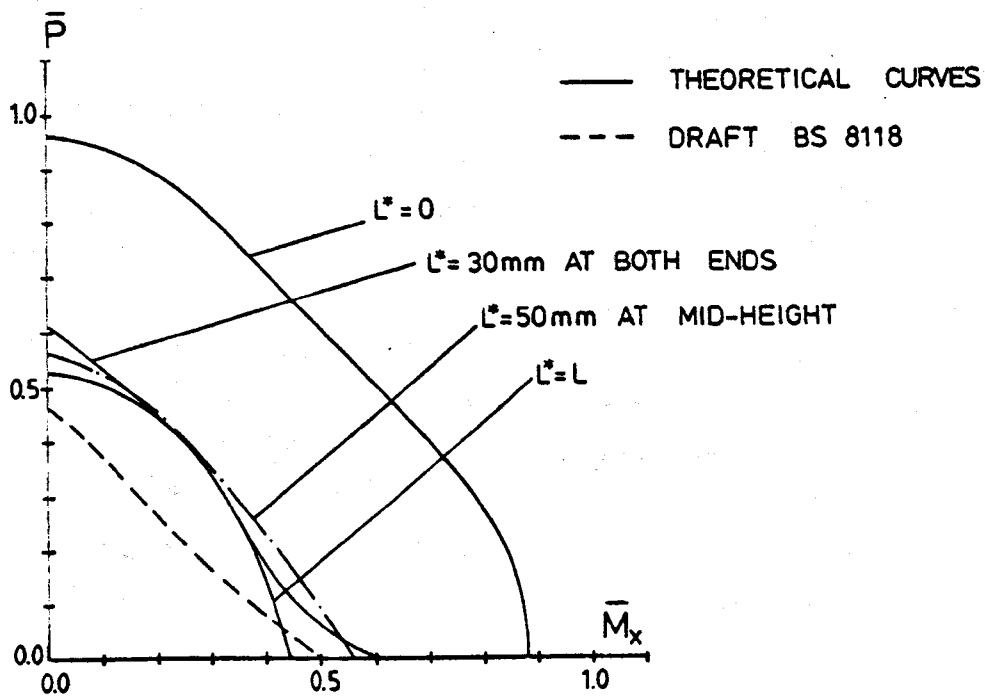

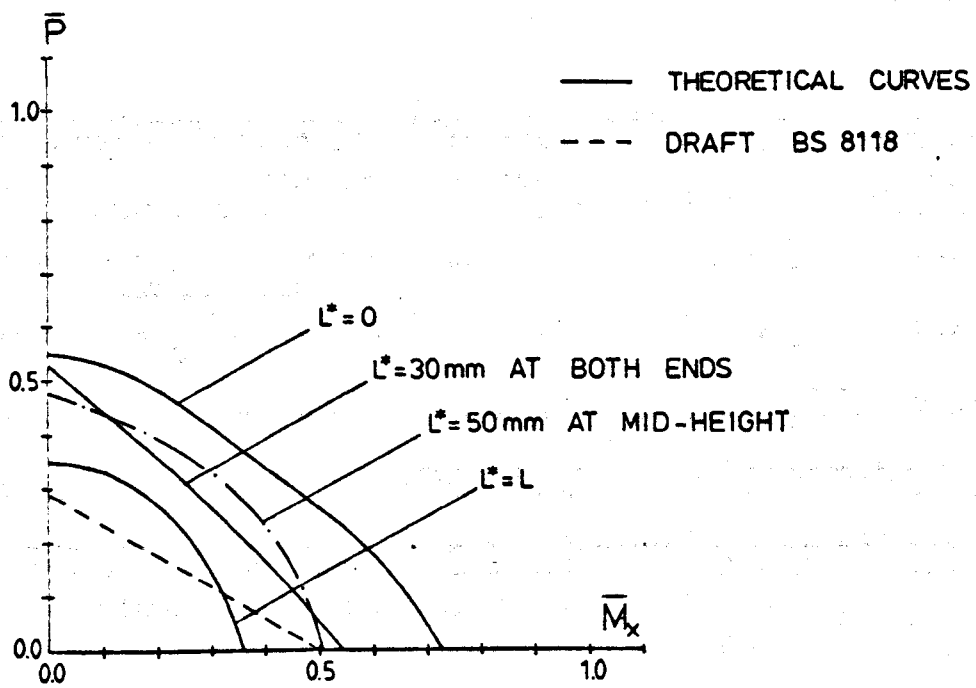Figure 7.40 Comparison with Transversely Welded Beam-columns ($\lambda_y = 30, \beta_x = 1$)

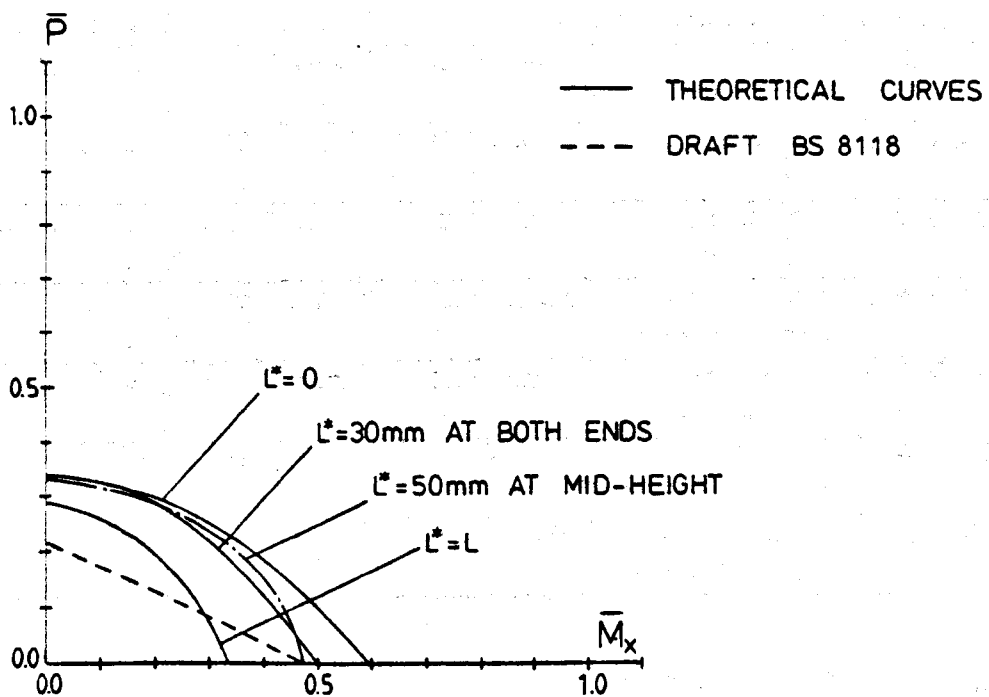Figure 7.41 Comparison with Transversely Welded Beam-columns ($\lambda_y = 70, \beta_x = 1$)

Figure 7.42 Comparison with Transversely Welded Beam-columns ($\lambda_y = 90, \beta_x = 1$)

Theoretical Curve Reference	$\frac{A^\bullet}{A}$ or $\frac{L^\bullet}{L}$	Source of Theoretical Curves	Principal Results	Remark
BA-N-1	$\frac{A^\bullet}{A} = 0.0$	Figure 6.3	Figure 7.43	$\lambda_y = 30,\ \beta_x = 1,\ \beta_y = 1$
BA-N-2	$\frac{A^\bullet}{A} = 0.0$	Figure 6.4	Figure 7.44	$\lambda_y = 50,\ \beta_x = 1,\ \beta_y = 1$
BA-N-3	$\frac{A^\bullet}{A} = 0.0$	Figure 6.5	Figure 7.45	$\lambda_y = 70,\ \beta_x = 1,\ \beta_y = 1$
BA-N-4	$\frac{A^\bullet}{A} = 0.0$	Figure 6.6	Figure 7.46	$\lambda_y = 90,\ \beta_x = 1,\ \beta_y = 1$
BA-N-5	$\frac{A^\bullet}{A} = 0.0$	Figure 6.7	Figure 7.47	$\lambda_x = 120,\ \beta_x = 1,\ \beta_y = 1$
BA-N-6	$\frac{A^\bullet}{A} = 0.0$	Figure 6.8	Figure 7.48	$\lambda_y = 30,\ \beta_x = 1,\ \beta_y = -1$
BA-N-7	$\frac{A^\bullet}{A} = 0.0$	Figure 6.10	Figure 7.49	$\lambda_y = 50,\ \beta_x = 0,\ \beta_y = 0$
BA-N-8	$\frac{A^\bullet}{A} = 0.0$	Figure 6.11	Figure 7.50	$\lambda_y = 50,\ \beta_x = 0,\ \beta_y = -1$
BA-N-9	$\frac{A^\bullet}{A} = 0.0$	Figure 6.12	Figure 7.51	$\lambda_y = 70,\ \beta_x = 1,\ \beta_y = 0$
BA-N-10	$\frac{A^\bullet}{A} = 0.0$	Figure 6.16	Figure 7.52	$\lambda_y = 90,\ \beta_x = -1,\ \beta_y = -1$
BA-LW-1	$\frac{A^\bullet}{A} = 0.1$ and 0.5	Figure 6.18	Figure 7.53	$\lambda_y = 30,\ \beta_x = 1,\ \beta_y = 1$
BA-LW-2	$\frac{A^\bullet}{A} = 0.1$ and 0.3	Figure 6.19	Figure 7.54	$\lambda_y = 70,\ \beta_x = 1,\ \beta_y = 1$
BA-LW-3	$\frac{A^\bullet}{A} = 0.3$ and 0.5	Figure 6.20	Figure 7.55	$\lambda_y = 90,\ \beta_x = 1,\ \beta_y = 1$
BA-TW-1	$L = 30mm$ at both ends	Figure 6.21	Figure 7.56	$\lambda_y = 30,\ \beta_x = 1,\ \beta_y = 1$
BA-TW-2	$L = 30mm$ at both ends	Figure 6.22	Figure 7.57	$\lambda_y = 70,\ \beta_x = 1,\ \beta_y = 1$
BA-TW-3	$L = 50mm$ at mid-height	Figure 6.23	Figure 7.58	$\lambda_y = 70,\ \beta_x = 1,\ \beta_y = 1$
BA-TW-4	$L = 50mm$ at mid-height	Figure 6.24	Figure 7.59	$\lambda_y = 90,\ \beta_x = 1,\ \beta_y = 1$

Table 7.5: (b) List of Theoretical Beam-column Results (Compression Plus Biaxial Bending)

7.4.3   Comparison between Draft BS 8118 with Theoretical Results of Beam-columns under Biaxial Bending

The draft BS 8118 and the theoretical results of biaxially loaded beam-columns as presented in Chapter 6 will be compared in this section and the principal results can be referred to Table 7.5 (b). Since the beam-columns are under compression plus biaxial bending, so the interaction equations (7.8) to (7.12) have to be checked; and $\tilde{M}_{ax}$ is determined from interaction equation (7.9) or (7.10) and $\tilde{M}_{ay}$ is obtained from interaction equation (7.11). For stocky beam-columns, the value of $\tilde{M}_{ax}$ is usually governed by interaction equation (7.9) for buckling about the major axis. For the intermediate and slender beam-columns buckling about the minor axis is the critical condition, therefore, the value of $\tilde{M}_{ax}$ will be governed by interaction equation (7.10).

7.4.3.1 Comparison with Non-welded Beam-columns under Compression Plus Biaxial Bending

The comparisons with non-welded beam-columns under compression plus uniform biaxial bending in both axes ($\beta_x = 1$ and $\beta_y = 1$) are presented in Figures 7.43 to 7.47. For the beam-columns which are under compression plus non-uniform biaxial bending in either axis, the comparisons are shown in Figures 7.48 to 7.52. Since the moment capacities of beams are over-estimated by the draft code, some discrepancy near the end points of the $\overline{M}_x$ and $\overline{M}_y$ axis are expected. For stocky beam-columns, the draft code tends to give very conservative results. But for intermediate and slender beam-columns, the draft BS 8118 can give very good predictions of the ultimate strength of the biaxially loaded beam-columns.

Figure 7.43 (a)

Figure 7.43 (b)

Figure 7.43 Comparison with Non-welded Beam-columns under Compression Plus Uniform Biaxial Bending ($\lambda_y = 30, \beta_x = 1, \beta_y = 1$)

Figure 7.44 (a)

Figure 7.44 (b)

Figure 7.44 Comparison with Non-welded Beam-columns under Compression Plus Uniform Biaxial Bending ($\lambda_y = 50, \beta_x = 1, \beta_y = 1$)

Figure 7.45 (a)

Figure 7.45 (b)

Figure 7.45 Comparison with Non-welded Beam-columns under Compression
Plus Uniform Biaxial Bending ($\lambda_y = 70, \beta_x = 1, \beta_y = 1$)

Figure 7.46 (a)

Figure 7.46 (b)

Figure 7.46 Comparison with Non-welded Beam-columns under Compression
Plus Uniform Biaxial Bending ($\lambda_y = 90, \beta_x = 1, \beta_y = 1$)
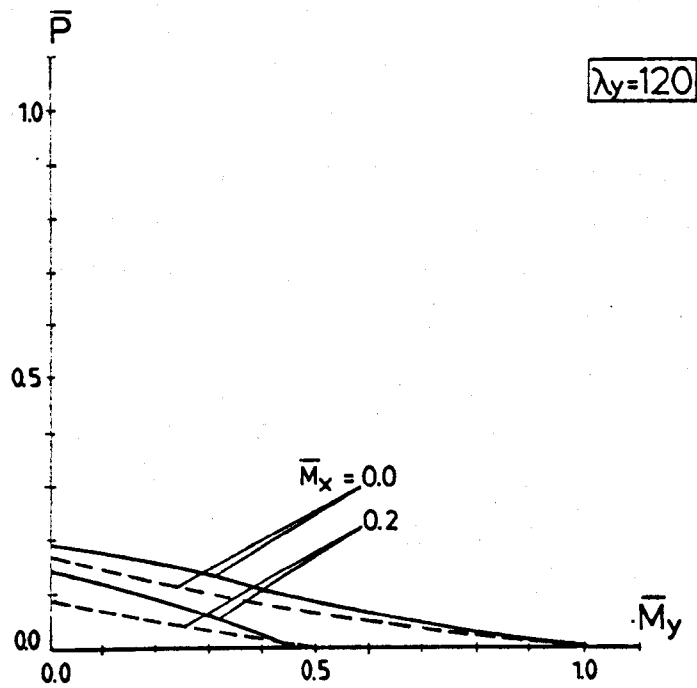
Figure 7.47 (a)
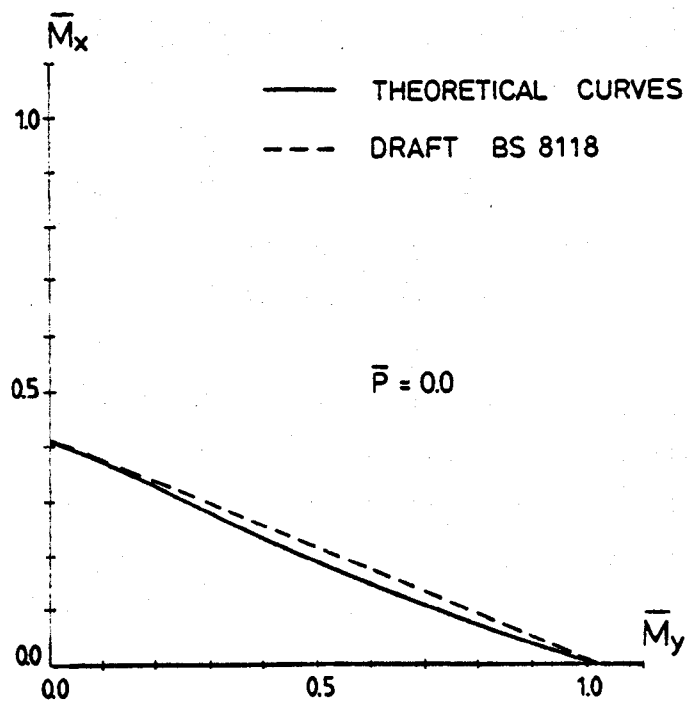
Figure 7.47 (b)

Figure 7.47 Comparison with Non-welded Beam-columns under Compression Plus Uniform Biaxial Bending ($\lambda_y = 120, \beta_x = 1, \beta_y = 1$)
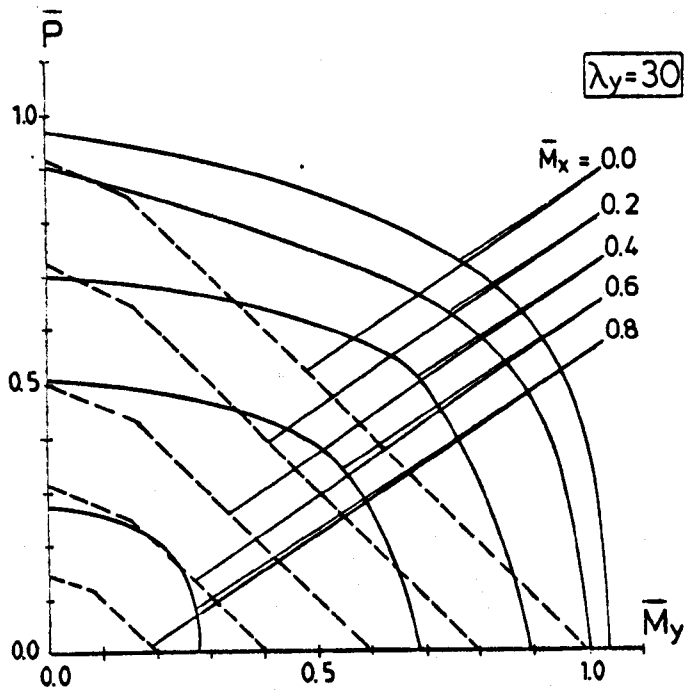
Figure 7.48 (a)
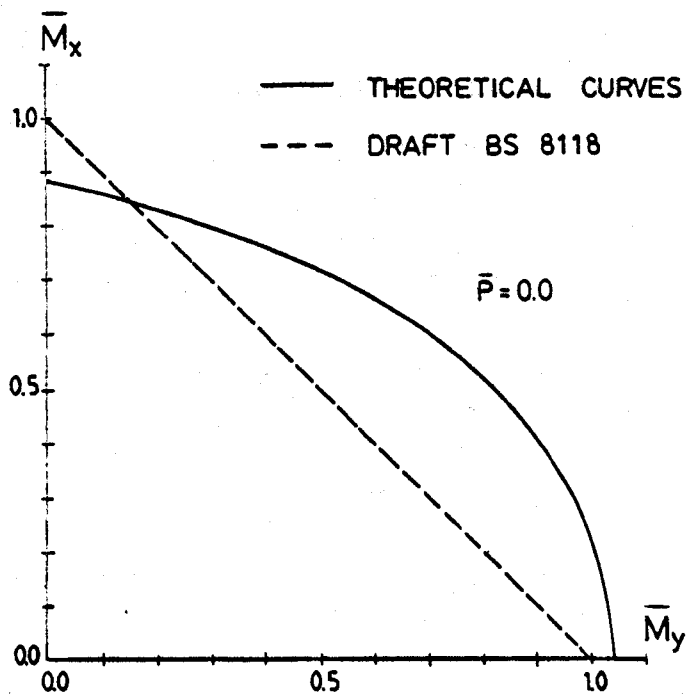
Figure 7.48 (b)

Figure 7.48 Comparison with Non-welded Beam-columns under Compression Plus Non-uniform Biaxial Bending ($\lambda_y = 30, \beta_x = 1, \beta_y = -1$)

Figure 7.49 (a)

Figure 7.49 (b)

Figure 7.49 Comparison with Non-welded Beam-columns under Compression Plus Non-uniform Biaxial Bending ($\lambda_y = 50$, $\beta_x = 0$, $\beta_y = 0$)
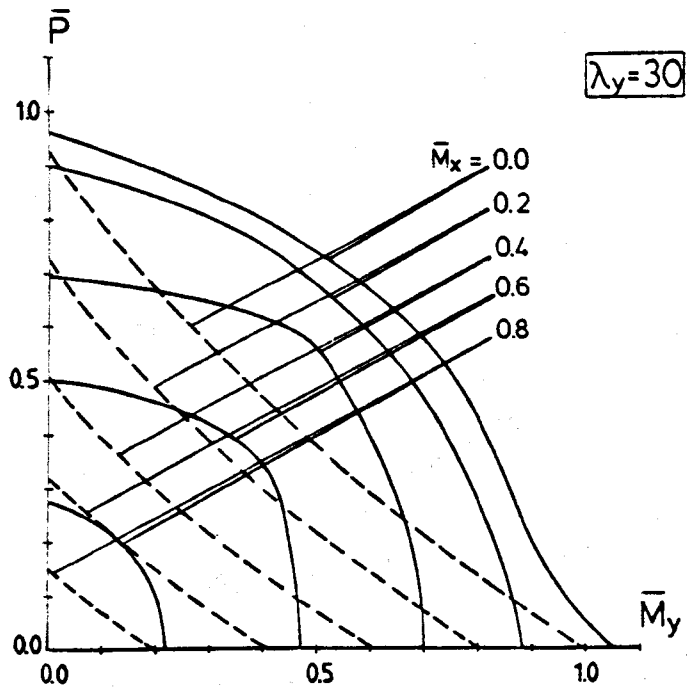
Figure 7.50 (a)

Figure 7.50 (b)

Figure 7.50 Comparison with Non-welded Beam-columns under Compression Plus Non-uniform Biaxial Bending ($\lambda_y = 50, \beta_x = 0, \beta_y = -1$)
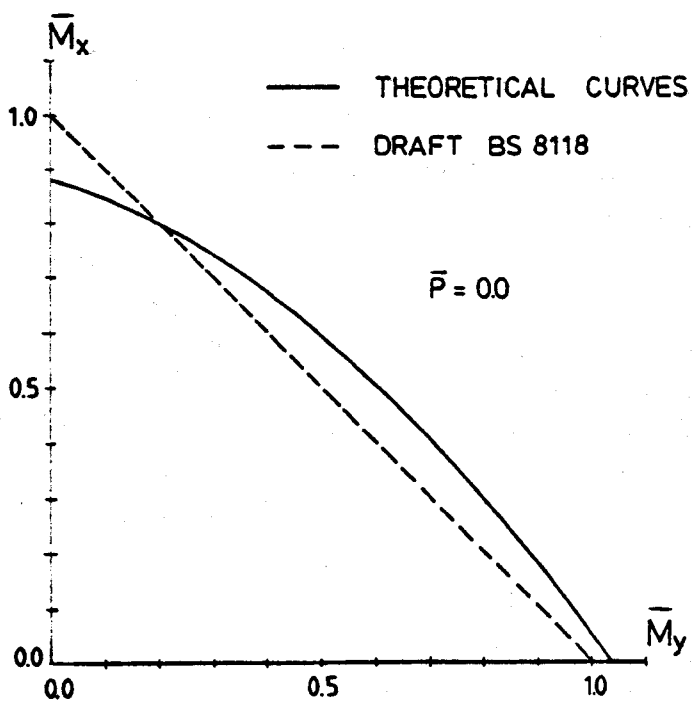
Figure 7.51 (a)

Figure 7.51 (b)

Figure 7.51 Comparison with Non-welded Beam-columns under Compression Plus Non-uniform Biaxial Bending ($\lambda_y = 70, \beta_x = 1, \beta_y = 0$)

Figure 7.52 (b)

Figure 7.52 (a)

Figure 7.52 Comparison with Non-welded Beam-columns under Compression Plus Non-uniform Biaxial Bending ($\lambda_y = 90, \beta_x = -1, \beta_y = -1$)
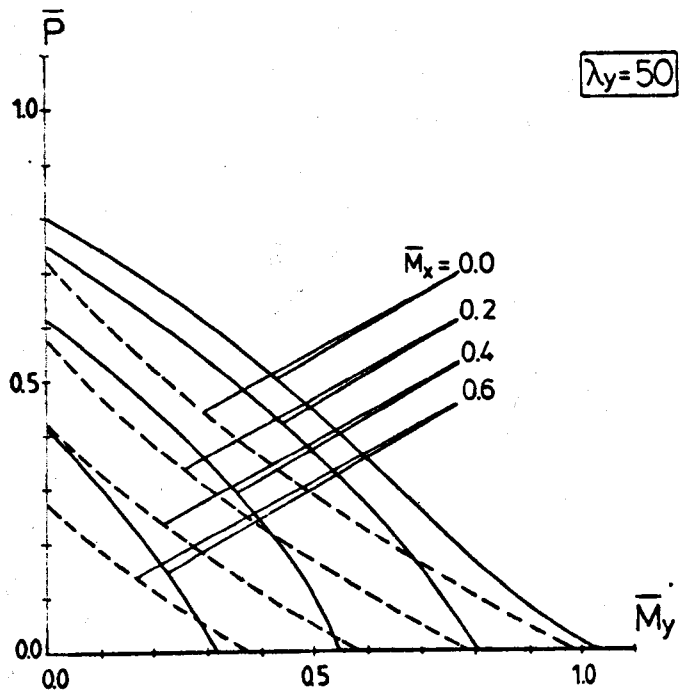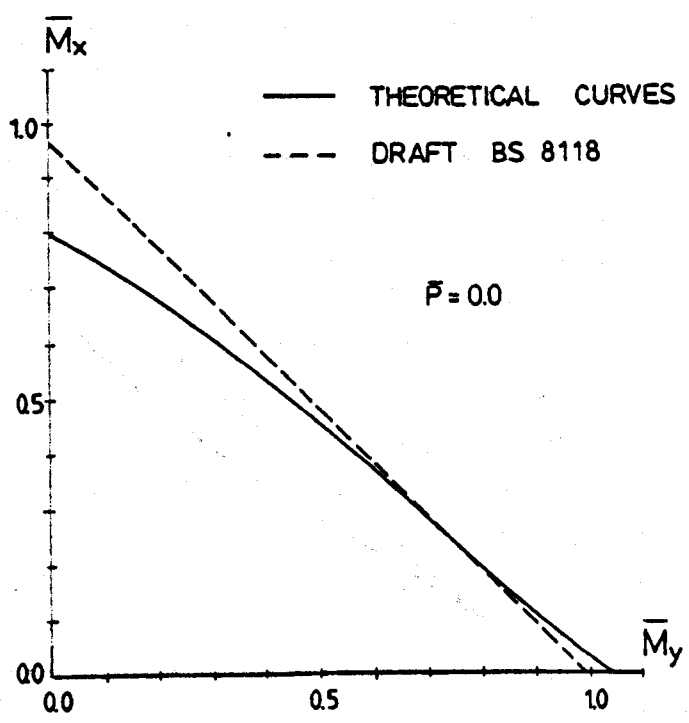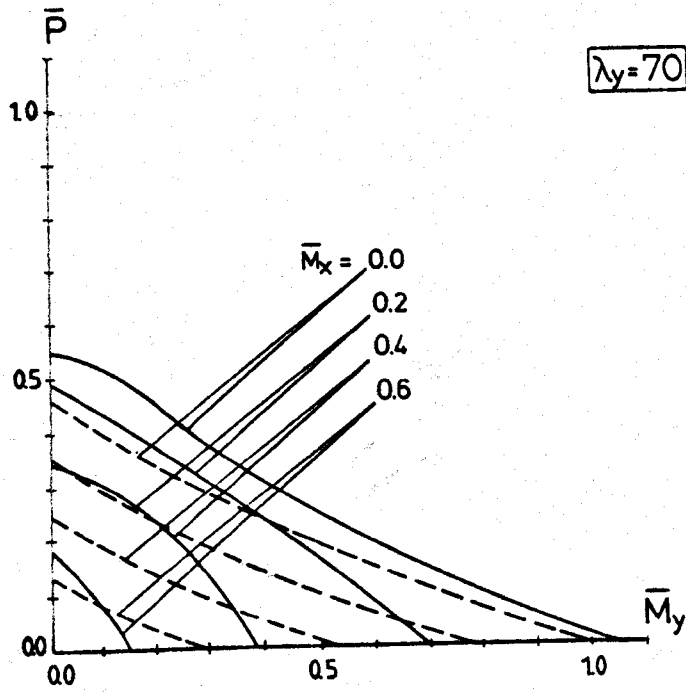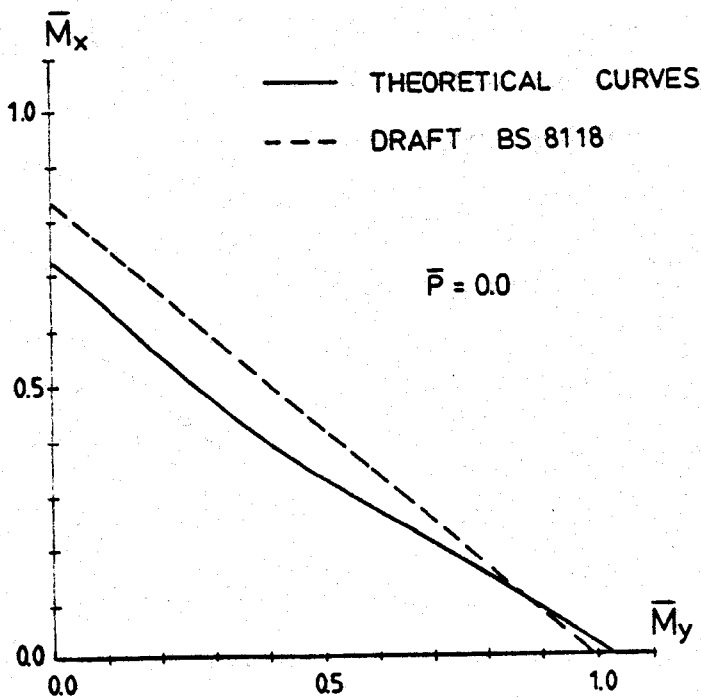
7.4.3.2 Comparison with Longitudinally Welded Beam-columns under Compression Plus Uniform Biaxial Bending

The comparison between draft BS 8118 with longitudinally welded beam-columns under compression plus uniform biaxial bending are presented in Figures 7.53 to 7.55. From the figures, we can observe that the draft code can generally give safe design for the longitudinally welded beam-columns with different $\frac{A^{\bullet}}{A}$ ratios.

Figure 7.53 (a)

Figure 7.53 (b)
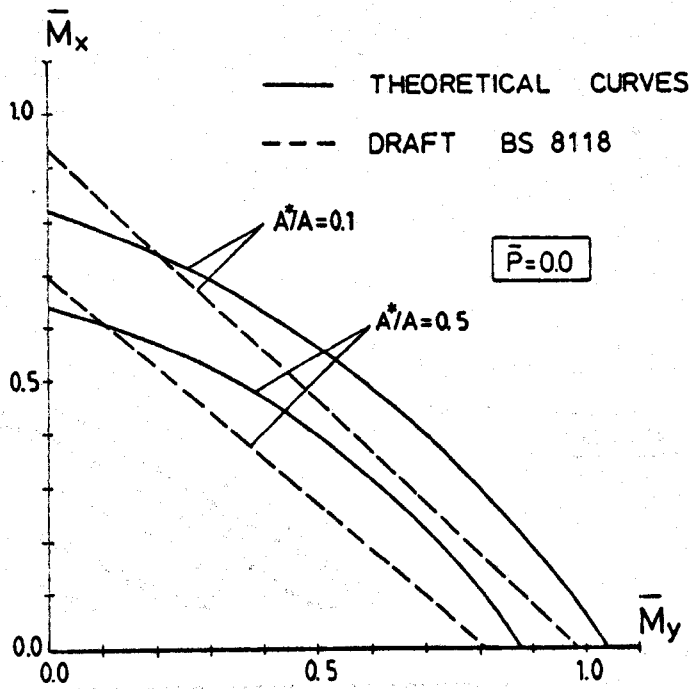
Figure 7.53 (c)

Figure 7.53 Comparison with Longitudinally Welded Beam-columns under Compression Plus Uniform Biaxial Bending ($\lambda_y = 30, \beta_x = 1, \beta_y = 1$)
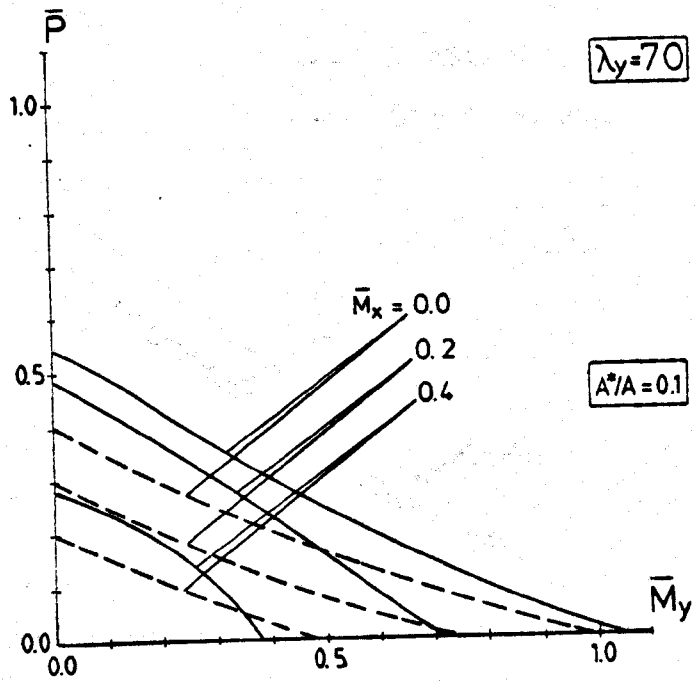
Figure 7.54 (a)
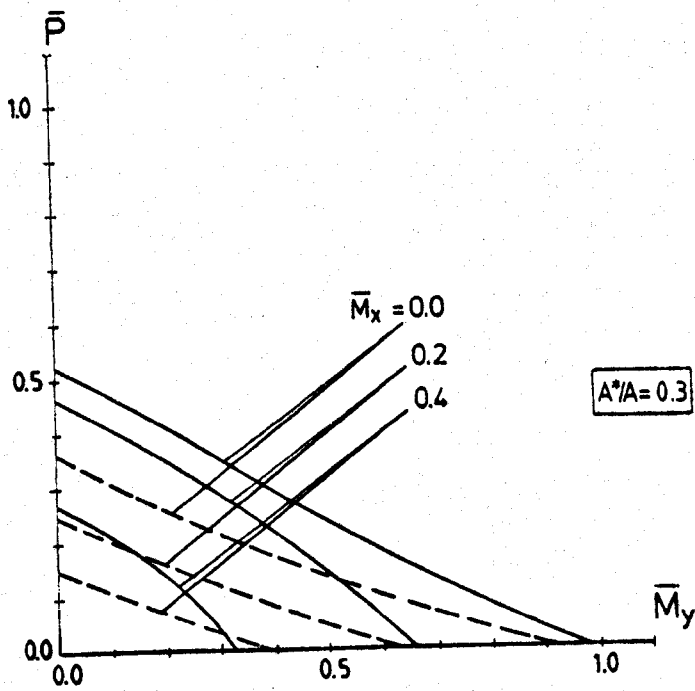
Figure 7.54 (b)
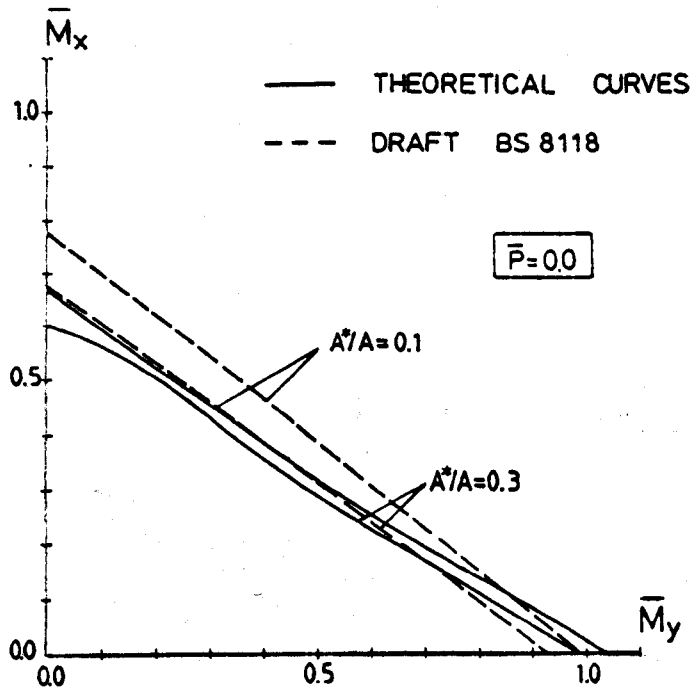
Figure 7.54 (c)

Figure 7.54 Comparison with Longitudinally Welded Beam-columns under Compression Plus Uniform Biaxial Bending ($\lambda_y = 70, \beta_x = 1, \beta_y = 1$)
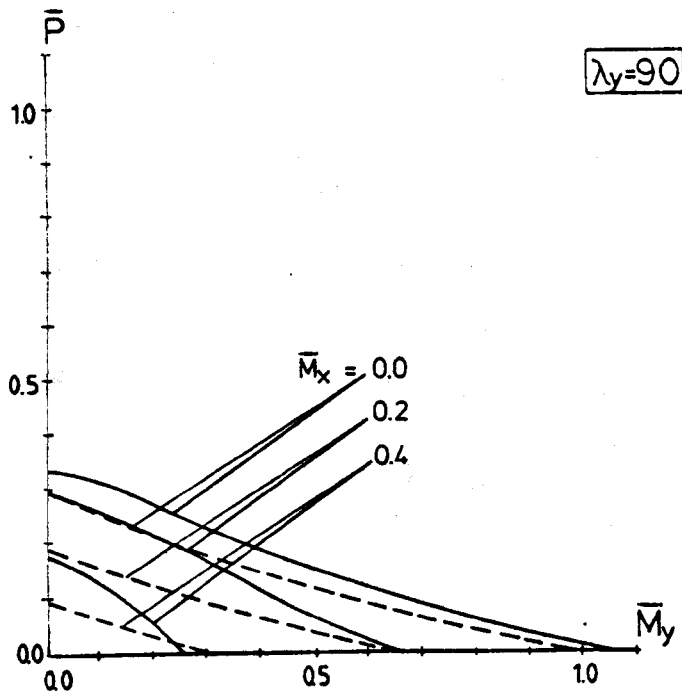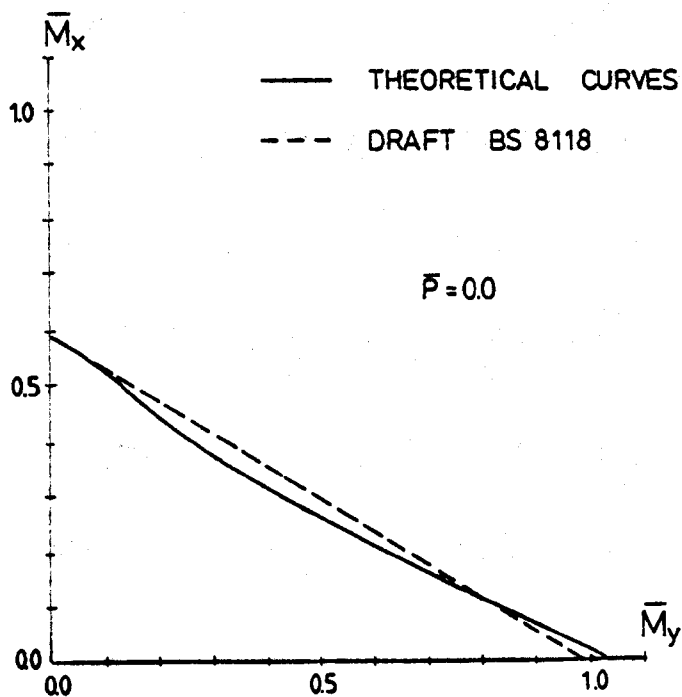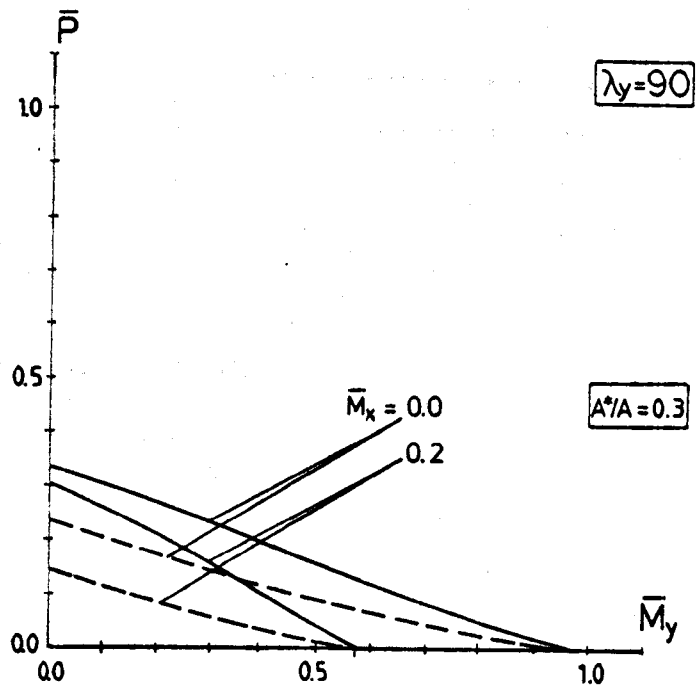
Figure 7.55 (a)
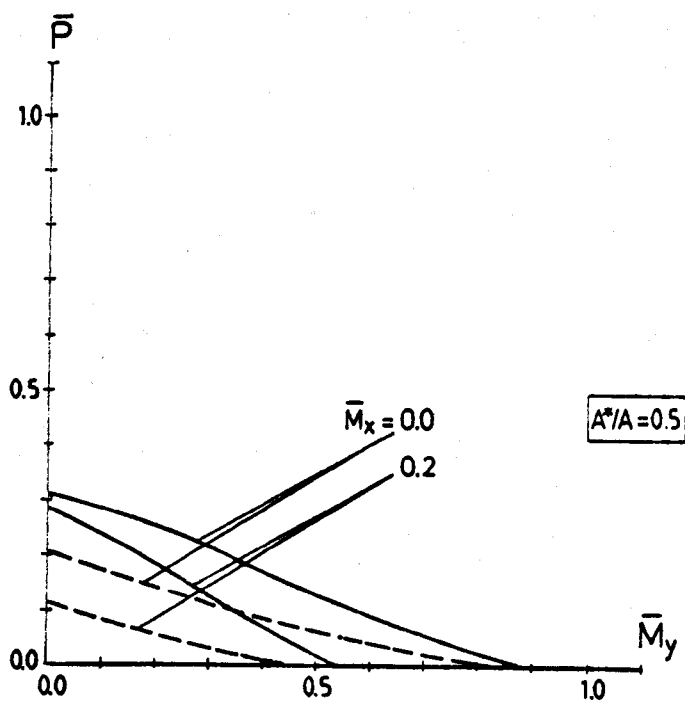
Figure 7.55 (b)
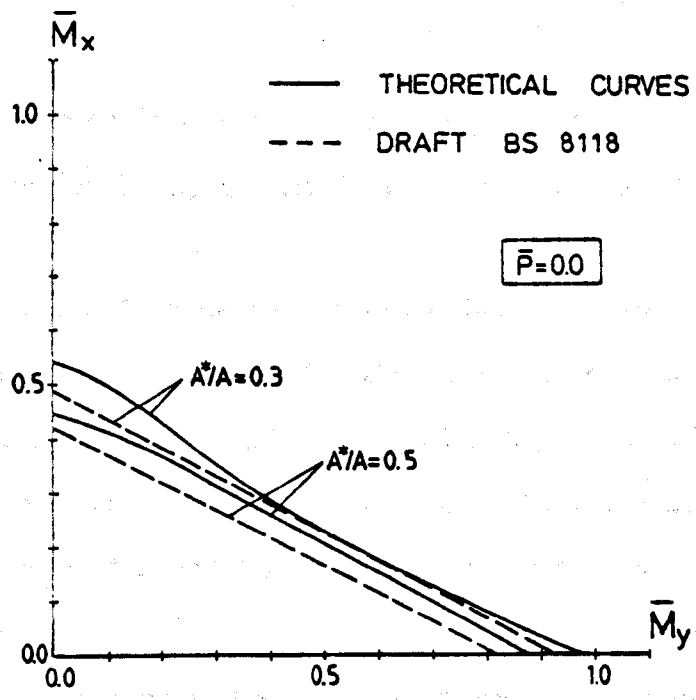
Figure 7.55 (c)

Figure 7.55 Comparison with Longitudinally Welded Beam-columns under Compression Plus Uniform Biaxial Bending ($\lambda_y = 90, \beta_x = 1, \beta_y = 1$)

7.4.3.3   Comparison with Transversely Welded Beam-columns under Compression Plus Uniform Biaxial Bending

Figures 7.56 to 7.59 show the comparison between draft BS 8118 with the theoretical curves of transversely welded beam-columns under compression plus uniform biaxial bending ($\beta_x = 1$, $\beta_y = 1$). The transversely welded beam-columns are designed as if containing wholly RSZ material. The basic moment capacities, M_{sx} and M_{sy}, are based on the RSZ material because the RSZ material within the members is sufficiently stressed due to the applied moment pattern in both axes. From the figures, it can be seen that the suggested design method by the author (see Section 7.6.3) for the transversely welded members can give the design on the safe side.
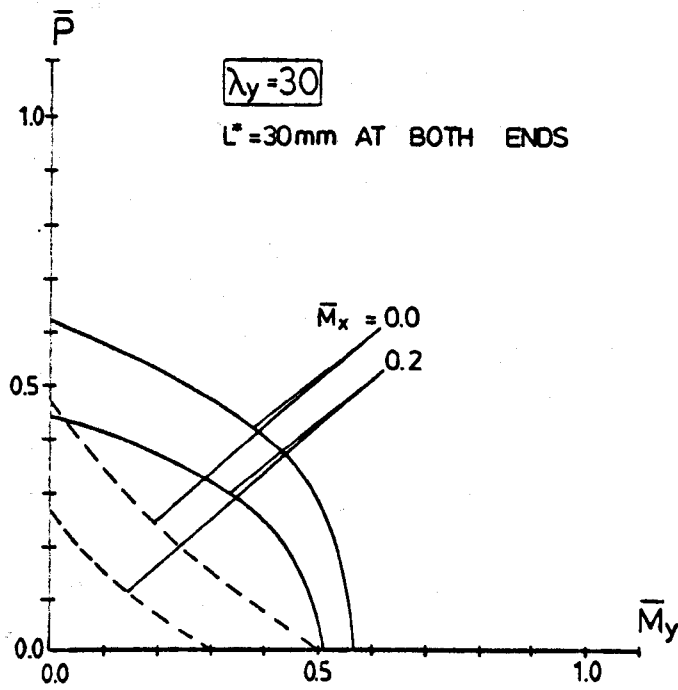
Figure 7.56 (a)
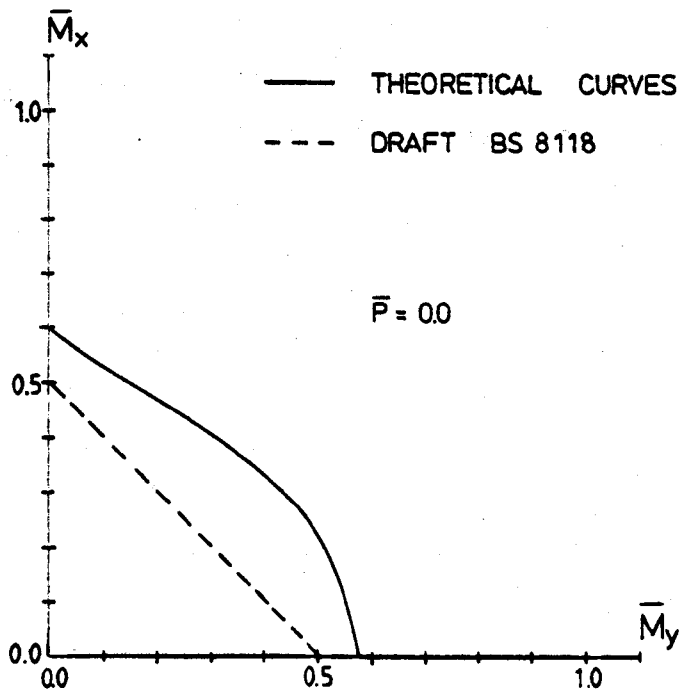
Figure 7.56 (b)

Figure 7.56 Comparison with Transversely Welded Beam-columns under Compression Plus Uniform Biaxial Bending ($\lambda_y = 30$, $L^* = 30\ mm$ at Both Ends, $\beta_x = 1, \beta_y = 1$)
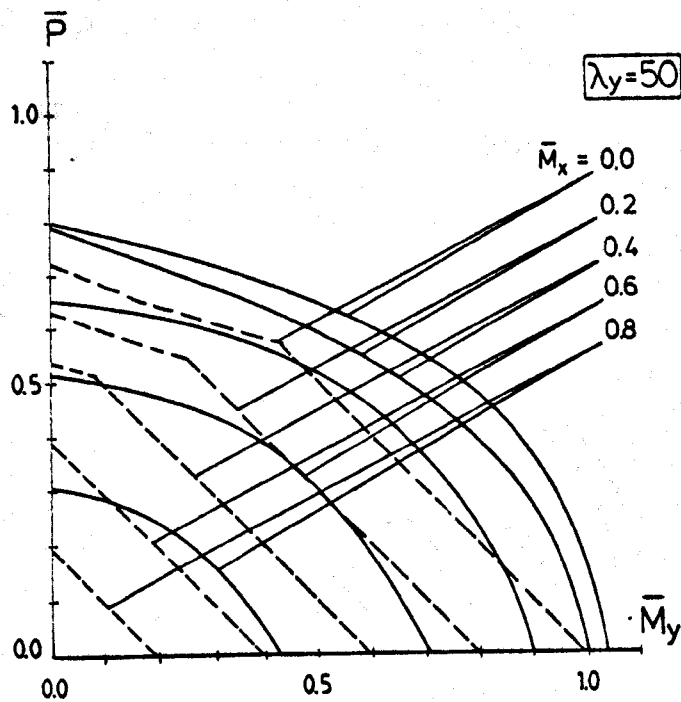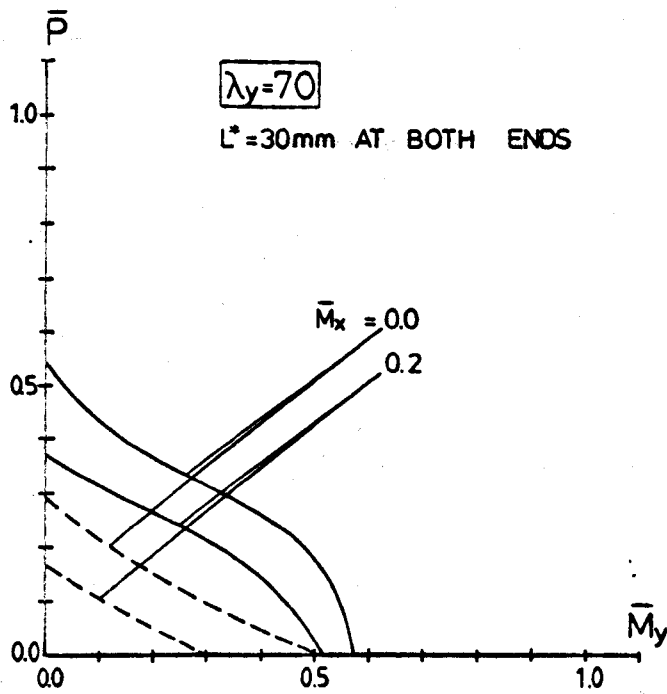
Figure 7.57 (a)
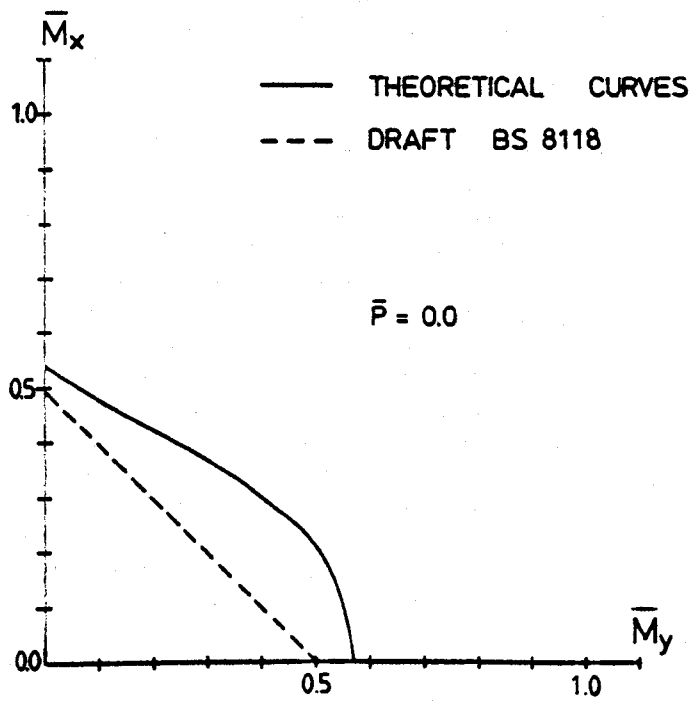
Figure 7.57 (b)

Figure 7.57 Comparison with Transversely Welded Beam-columns under Compression Plus Uniform Biaxial Bending ($\lambda_y = 70, L^* = 30 \ mm$ at Both Ends, $\beta_x = 1, \beta_y = 1$)
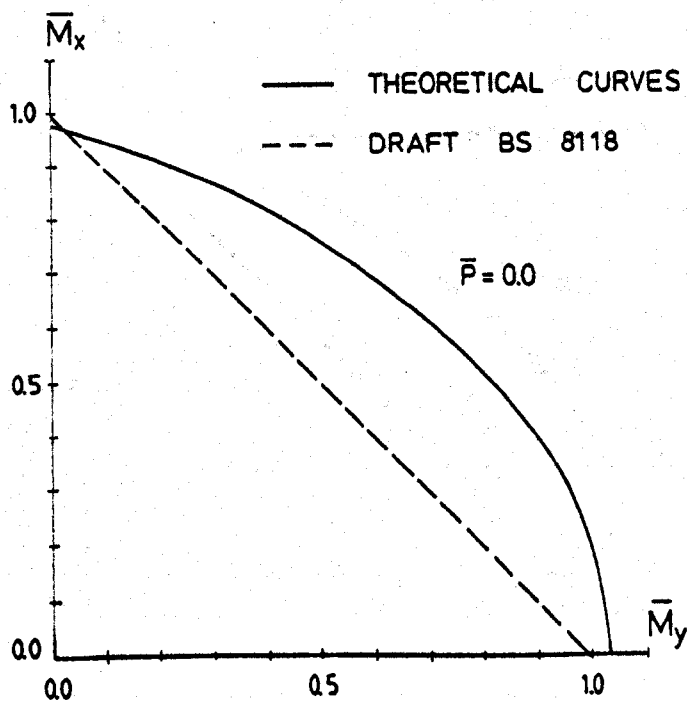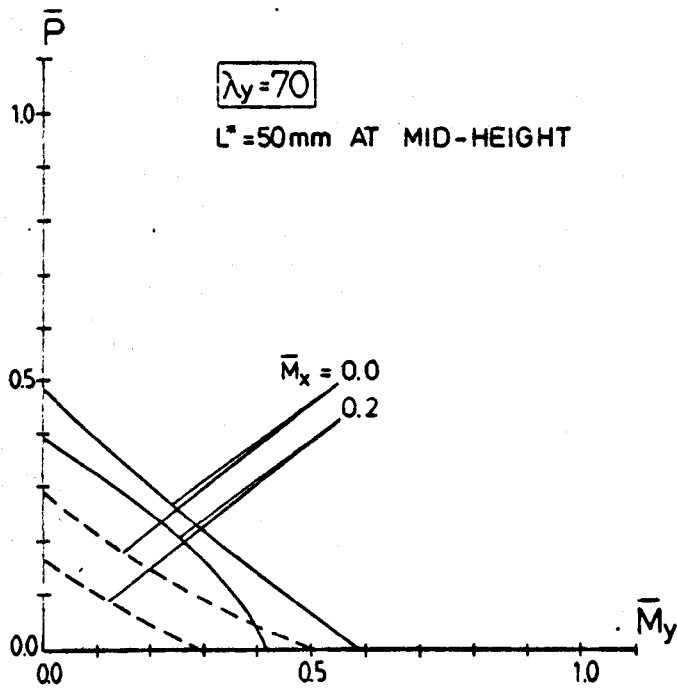
Figure 7.58 (a)
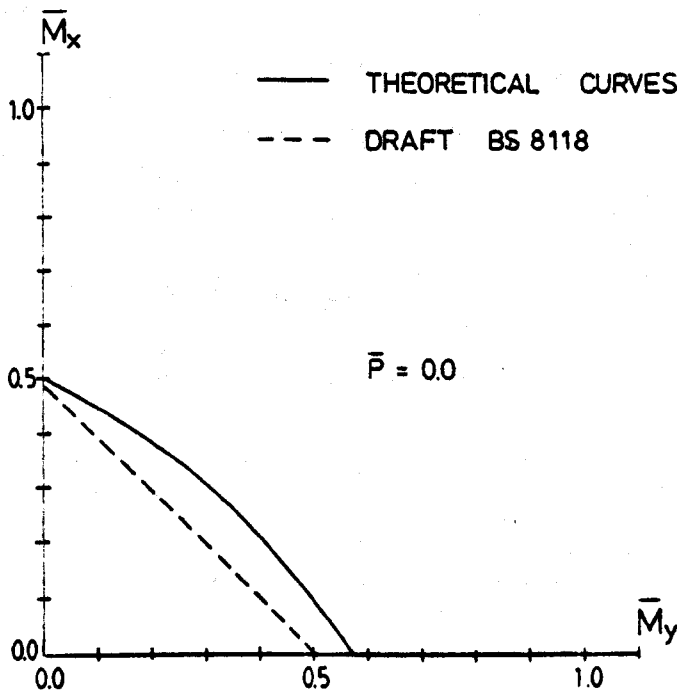
Figure 7.58 (b)

Figure 7.58 Comparison with Transversely Welded Beam-columns under Compression Plus Uniform Biaxial Bending ($\lambda_y = 70$, $L^* = 50\ mm$ at Mid-height, $\beta_x = 1, \beta_y = 1$)
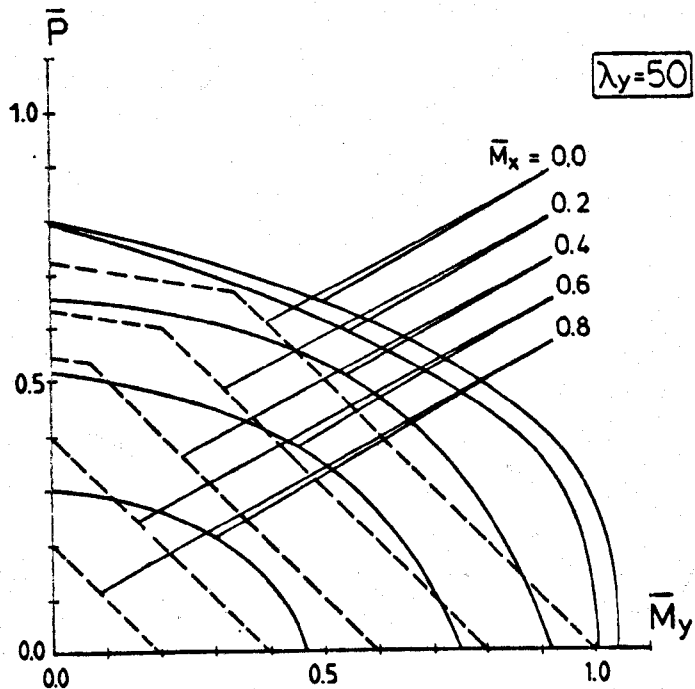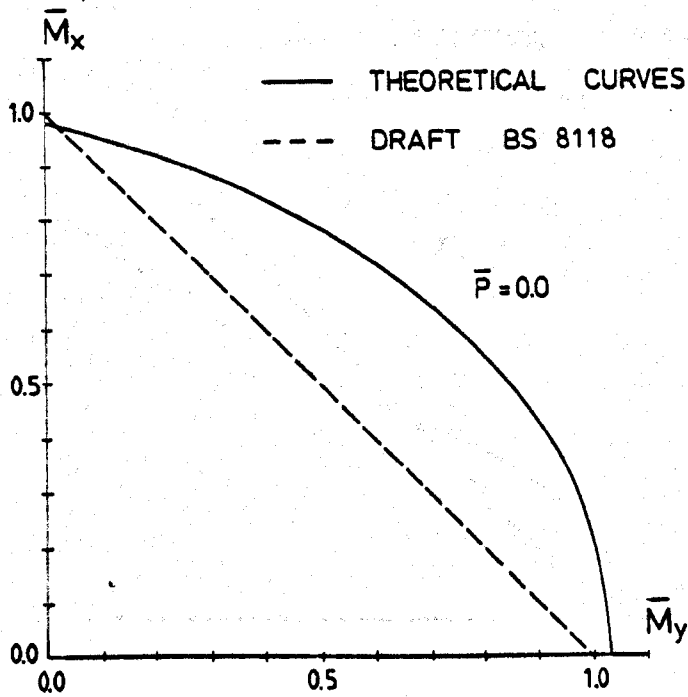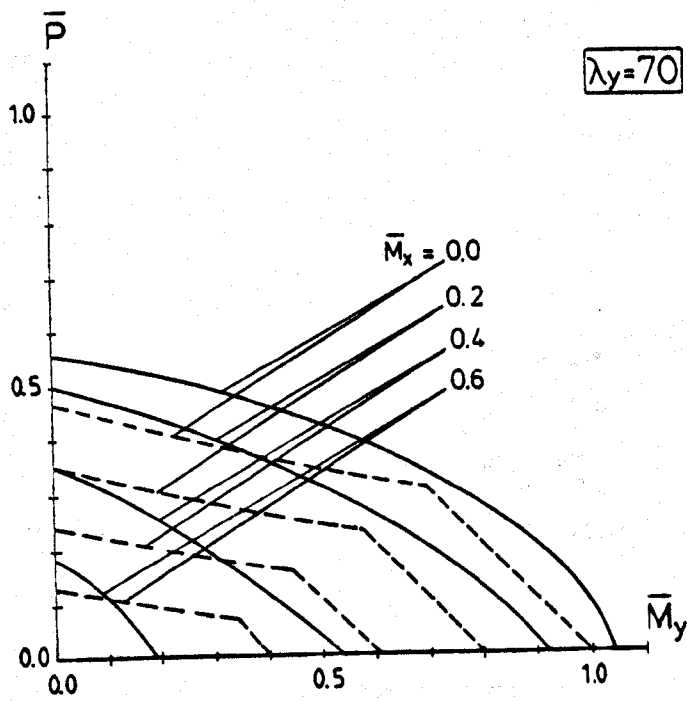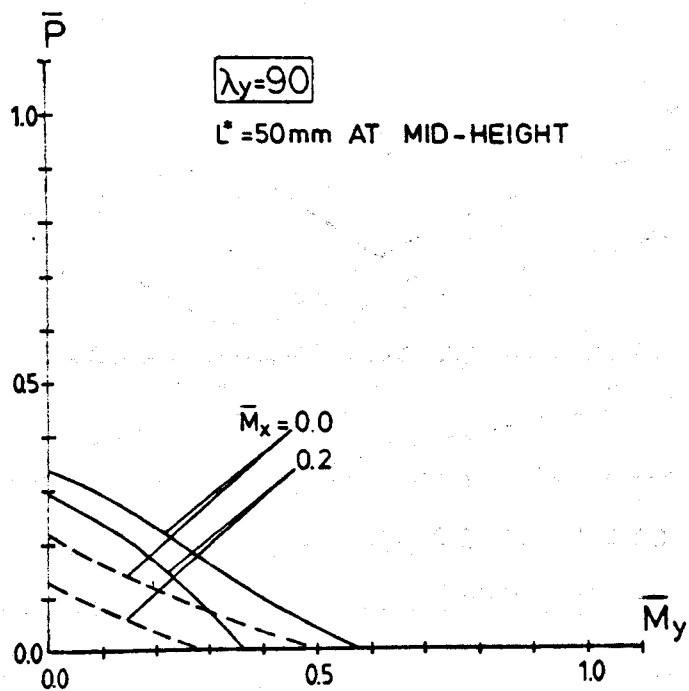
Figure 7.59 (a)
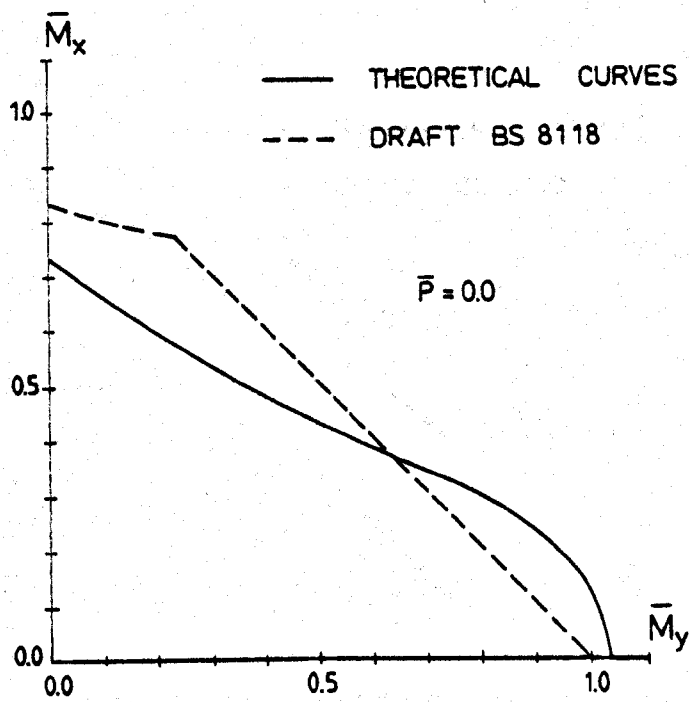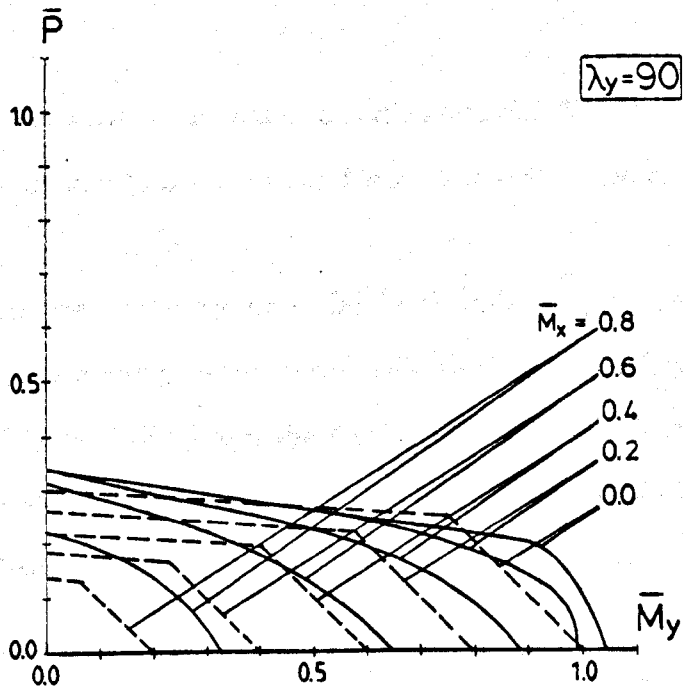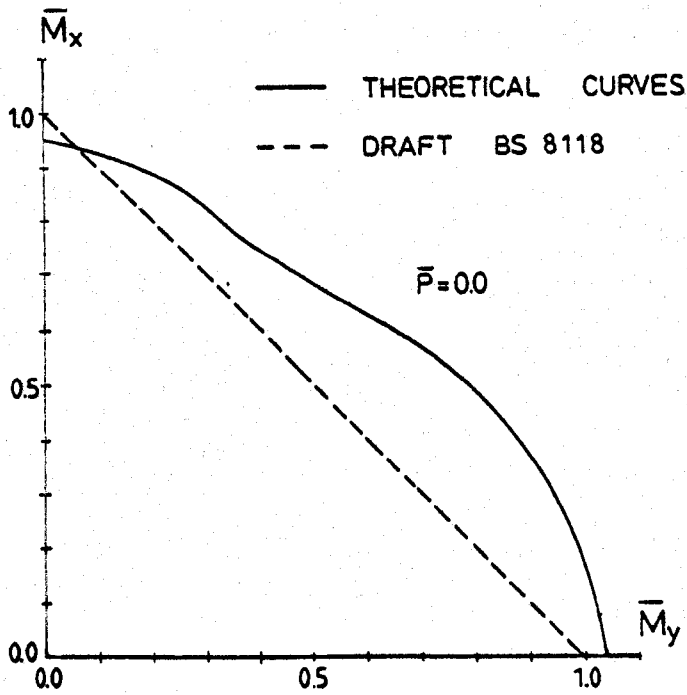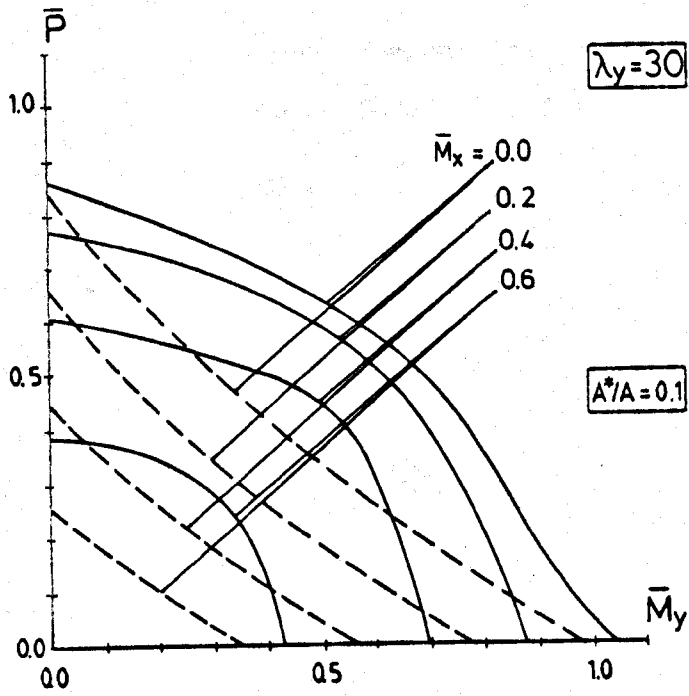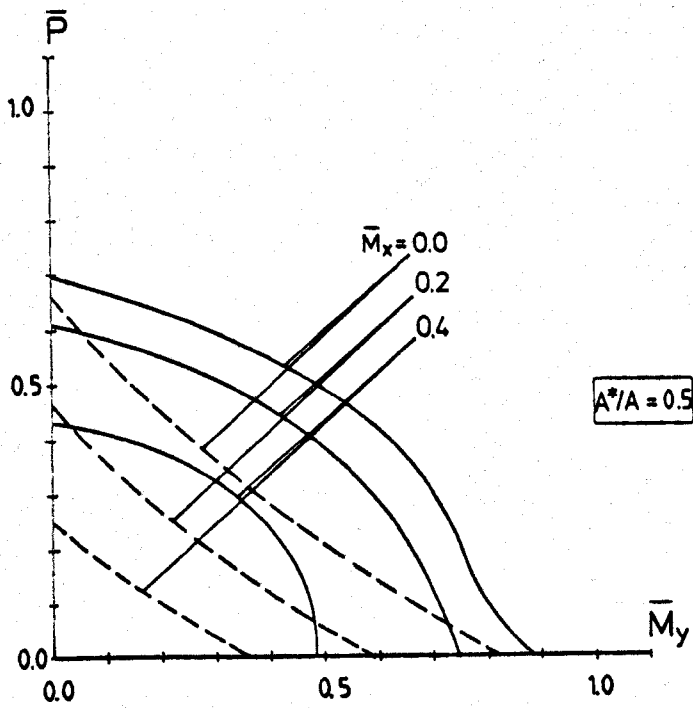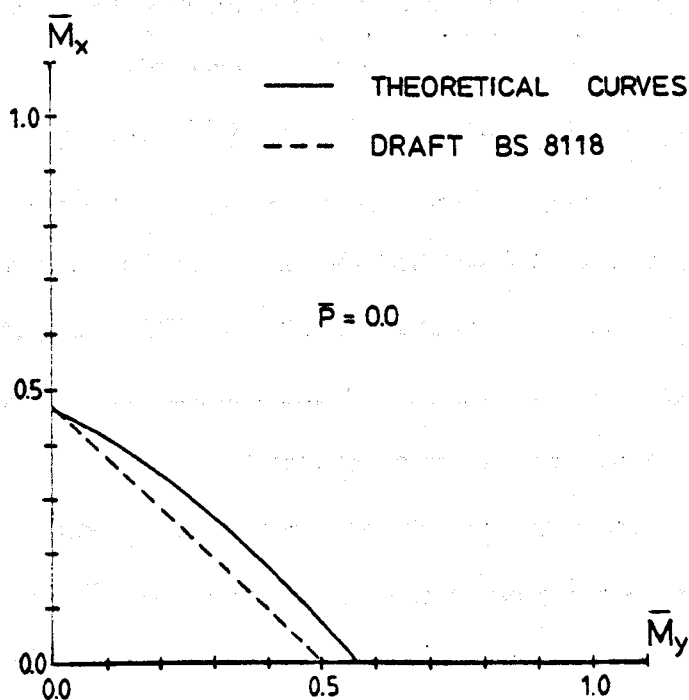

Figure 7.59 (b)

Figure 7.59 Comparison with Transversely Welded Beam-columns under Compression Plus Uniform Biaxial Bending ($\lambda y = 90$, $L^* = 50\ mm$ at Mid-height, $\beta_x = 1, \beta_y = 1$)
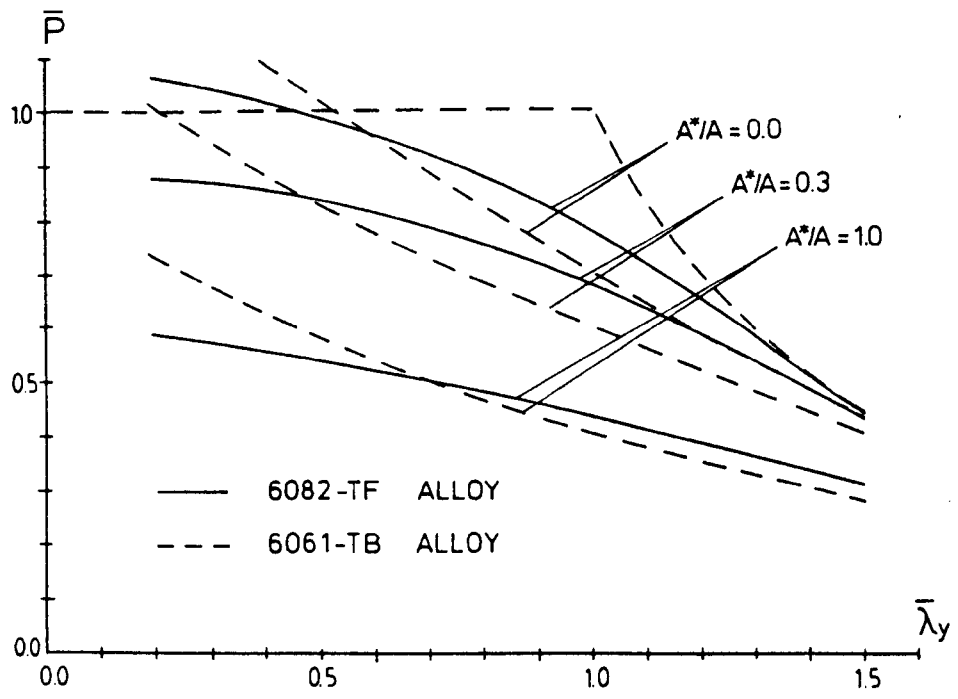
Figure 7.60 Comparison between 6061-TB and 6082-TF Aluminium Column Curves

7.5   Discussion

7.5.1   Discussion on the Design of Aluminium Columns

From the comparison presented in Section 7.2.4, it can be seen that the draft BS 8118 can generally give the design of non-welded and longitudinally welded aluminium columns on the safe side. However, for the aluminium columns having asymmetric cross-sections or having material properties $\frac{\sigma_{ult}}{\sigma_{0.2}} > 1.2$, the draft code tends to under-estimate the ultimate strength especially for intermediate and slender columns.

For 5083-M alloy (low n value), it was found that the effect of welding can only cause a significant drop in the elastic limit stress, σ_e but has nearly no effect on $\sigma_{0.2}$, so the reduction in column strength after welding is actually less than expected. Moreover, if we compare the column curves of 6000 series alloy which has $\frac{\sigma_{ult}}{\sigma_{0.2}} \leq 1.2$ (e.g. 6082-TF) and $\frac{\sigma_{ult}}{\sigma_{0.2}} > 1.2$ (e.g. 6061-TB) as shown in Figure 7.60, we find the 6061-TB columns only show a maximum about 12% lower for ultimate strength and the reduction is only limited to the intermediate and slender columns. As the columns become more stocky, the 6061-TB columns even possess higher strength than the 6082-TF columns irrespective of whether the columns contain longitudinal welds or not. Therefore similar to 5083-M alloy, the reductions in ultimate strength of the 6000 series columns having $\frac{\sigma_{ult}}{\sigma_{0.2}} > 1.2$ are also overestimated by the draft code. One of the possible methods to improve the ultimate strength of columns, perhaps, is to use four design column curves instead of five. For classes A, B, C and D columns, the selection of design column

curves is the same as before, but using design column curves 2 for class E columns; design column curve 3 for classes F and G columns; and design column curve 4 for classes H columns. The design column curve 5 can be left out from the draft code.

For the transversely welded columns, the draft BS 8118 can lead to unsafe design, and the improvement will be discussed in Section 7.6.1.

7.5.2   Discussion on the Design of Aluminium Beams

From all the comparisons for aluminium beams, we can find that the draft BS 8118 can lead to very unsafe predictions for most of the cases. It is due mainly to the fact that the lateral buckling reduction factor, C_{LT}, is not estimated correctly by the draft code. The positioning of the $C_{LT} - \lambda_{LT}$ design curve for beams [8] was mainly based on the test data conducted by Clark and Jombock [9] in 1957, and there was no complete theoretical studies available to support the $C_{LT} - \lambda_{LT}$ curve. Therefore, the combined effects of inelastic material behaviour, initial geometrical imperfections etc. are not well-considered by the draft code; and poor estimation of the lateral buckling reduction factor, C_{LT}, is expected. Moreover, if we consider the experimental investigation carried out by Clark and Jombock, we can find that the condition of end fixity, such as the warping restraint, was not reported in detail. Clark also mentioned that the stiffness of the test apparatus relative to the stiffness of the beams is very great. The ultimate buckling strength of beams, therefore, may be higher but the stiffening effect is very difficult to quantify in the analysis. The effect of end restraint on beams can
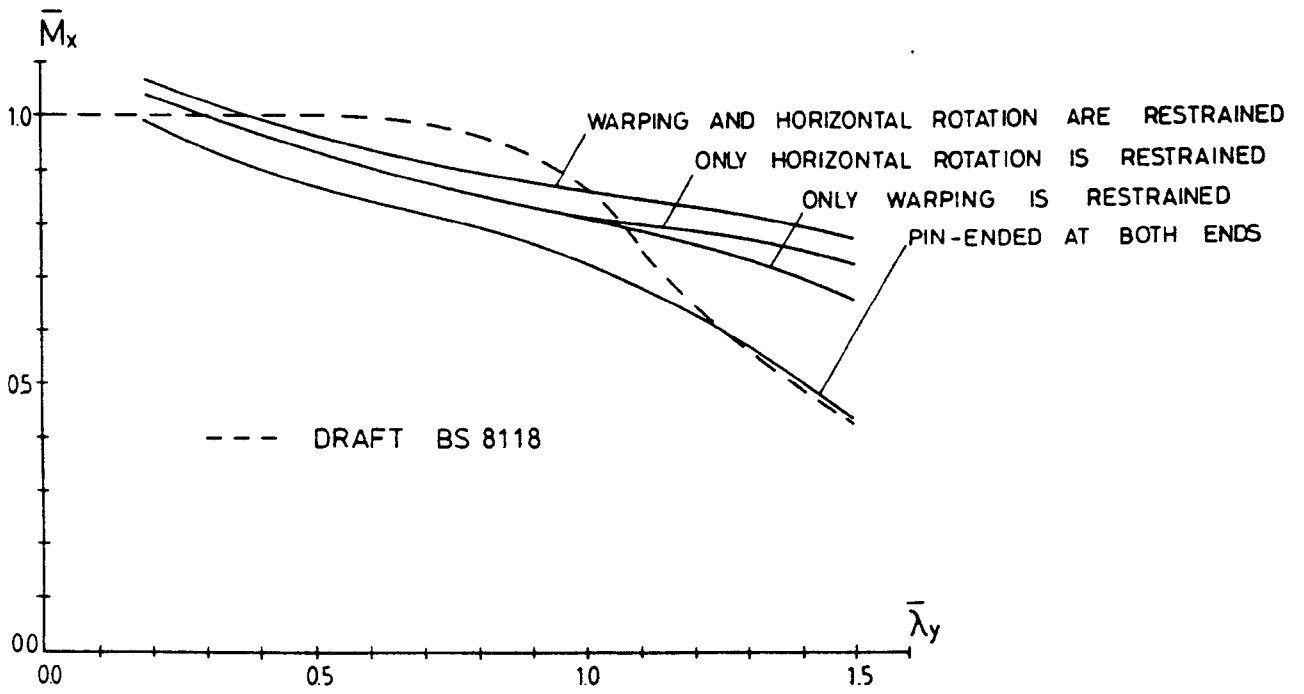
Figure 7.61 Effect of End Restraint on Beams ($\beta_x = 1$)

be illustrated in Figure 7.61 where the increase in strength due to the restraint of horizontal rotation and warping is considered. From the figure, we can find that the bending strength of inelastic beams is increased by at least 10% if both the warping and horizontal rotation are restrained. Moreover, if we compare with the design beam curve as suggested by the draft BS 8118, we can observe that the discrepancy becomes much smaller in the inelastic range, and therefore Figure 7.61 explains why the value of C_{LT} is higher than expected.

If we consider the basic equation for the $C_{LT} - \lambda_{LT}$ curve, we could find that the representation is also based on Perry-Robertson type equation which is similar to the design column curves; and the $C_{LT} - \lambda_{LT}$ curve is expressed by:

$$\left(\frac{M_{cr}}{M_p} - C_{LT} \right) (1 - C_{LT}) = \eta \, \frac{M_{cr}}{M_p} \qquad (7.13)$$

where η = imperfection constant

        = $0.0007 \, (\, \lambda_{LT} - 21.2 \,)$

Since the original $C_{LT} - \lambda_{LT}$ curve is over-estimated by the draft BS 8118, therefore, the imperfection constant, η, should be modified. From the parametric studies and the comparison with the draft code, the author found that it is not reasonable and appropriate to use only one design beam curve to represent the lateral buckling behaviour of beams due to the variation of material properties. In order to give safe predictions and simple design procedures to the design engineers, the author would recommend that two design beam curves should be used instead of one. The suggested design beam curves are also based on equation (7.13) but with different imperfec-
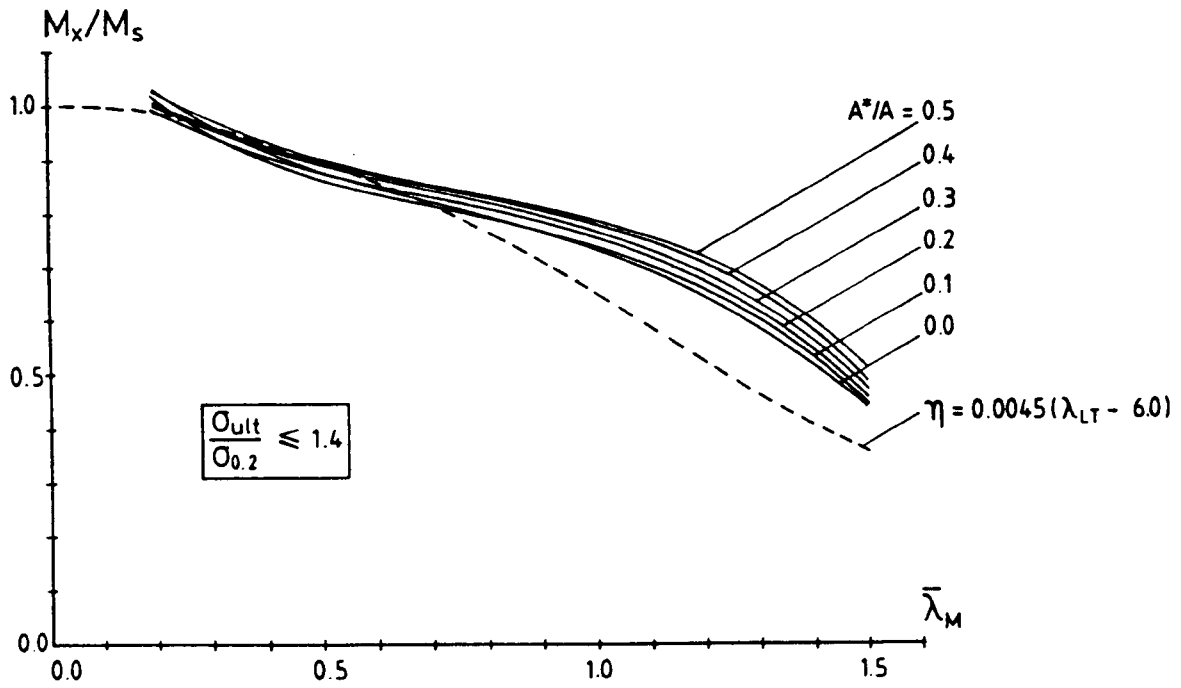
Figure 7.62 Comparison between the Suggested Design Curve with Theoretical Results of Non-welded and Symmetric Longitudinally Welded Beams ($\frac{\sigma_{ult}}{\sigma_{0.2}} \leq 1.4$)
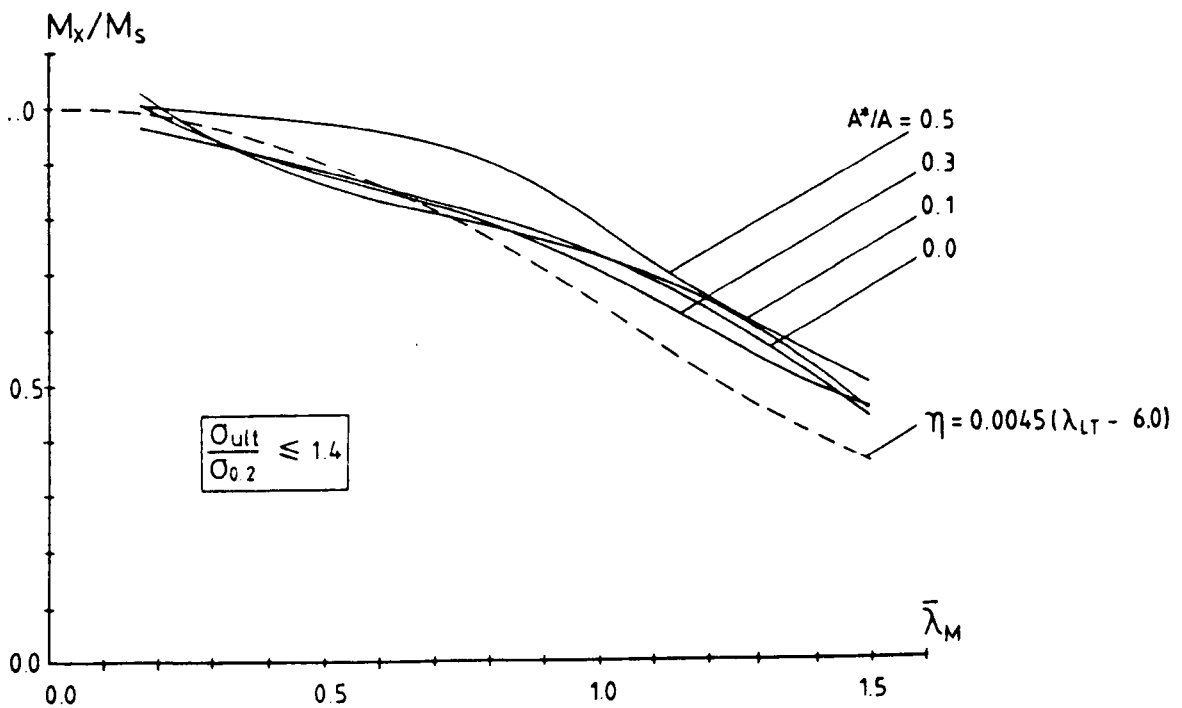
Figure 7.63 Comparison between the Suggested Design Curve with Theoretical Results of Non-welded and Unsymmetric Longitudinally Welded Beams ($\frac{\sigma_{ult}}{\sigma_{0.2}} \leq 1.4$)

tion constants. They are:

Curve 1: For $\frac{\sigma_{ult}}{\sigma_{0.2}} \leq 1.4$ (high n)

$$\eta = 0.0045 \ (\lambda_{LT} - 6.0) \tag{7.14}$$

Curve 2: For $\frac{\sigma_{ult}}{\sigma_{0.2}} > 1.4$ (low n)

$$\eta = 0.01 \ (\lambda_{LT} - 12.0) \tag{7.15}$$

The above suggested design curves can be applied to the aluminium beams with or without any welds. The accuracy of the suggested design curves can be demonstrated in Figures 7.62 to 7.64. Figures 7.62 and 7.63 show the non-dimensionalised plots of $\frac{M_x}{M_s}$ against $\overline{\lambda}_M$ for the aluminium beams having $\frac{\sigma_{ult}}{\sigma_{0.2}} \leq 1.4$ and with symmetric or unsymmetric longitudinal welds. The basic moment capacity, M_s, is calculated according to the draft BS 8118 which takes into account the reduction due to RSZ softening only because the effect of local buckling cannot be simulated by the program BIAXIAL. For the beams with symmetric longitudinal welds, Figure 7.62 shows that the discrepancies between the curves with different $\frac{A^*}{A}$ ratios are small. For the beams with unsymmetric longitudinal welds, similar observations are found (see Figure 7.63) except for the curve with $\frac{A^*}{A} = 0.5$ because the effect of residual stresses is neglected in the analysis. Therefore, for the beams with $\frac{\sigma_{ult}}{\sigma_{0.2}} \leq 1.4$, Figures 7.62 and 7.63 suggest that only one design curve is sufficiently accurate to represent the lateral buckling behaviour no matter for beams with or without longitudinal welds; and for RSZ softening within the cross-section being symmetric or not. Moreover, they further suggest that we can also use one design curve for the beams having $\frac{\sigma_{ult}}{\sigma_{0.2}} > 1.4$ as shown in
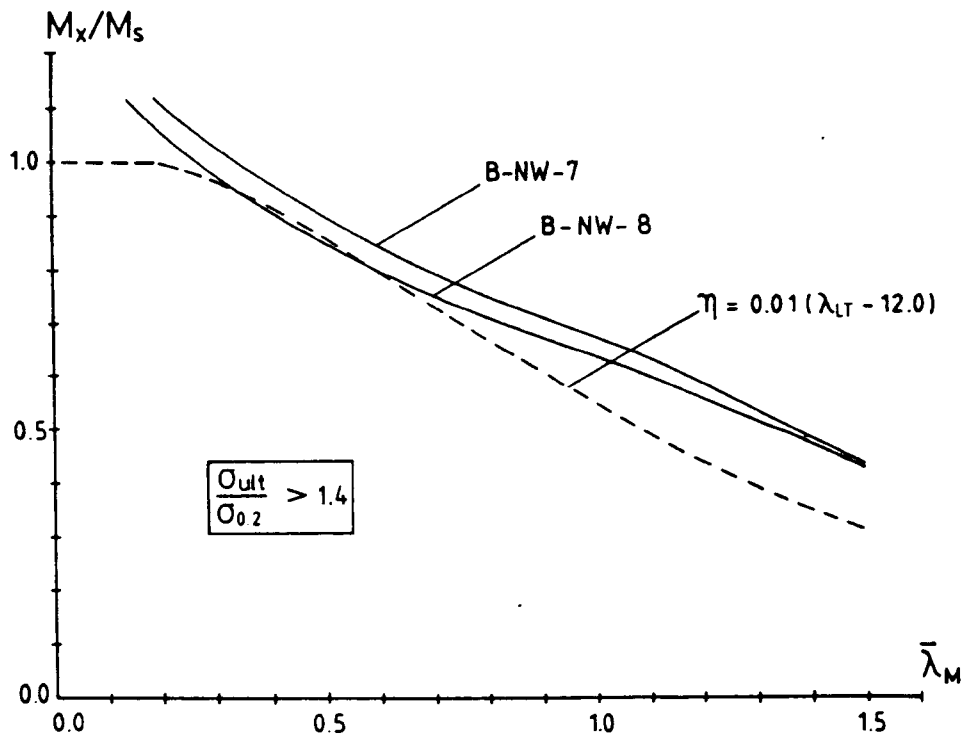
Figure 7.64 Comparison between the Suggested Design Curve with Theoretical Results of Non-welded Beams ($\frac{\sigma_{ult}}{\sigma_{0.2}} > 1.4$)
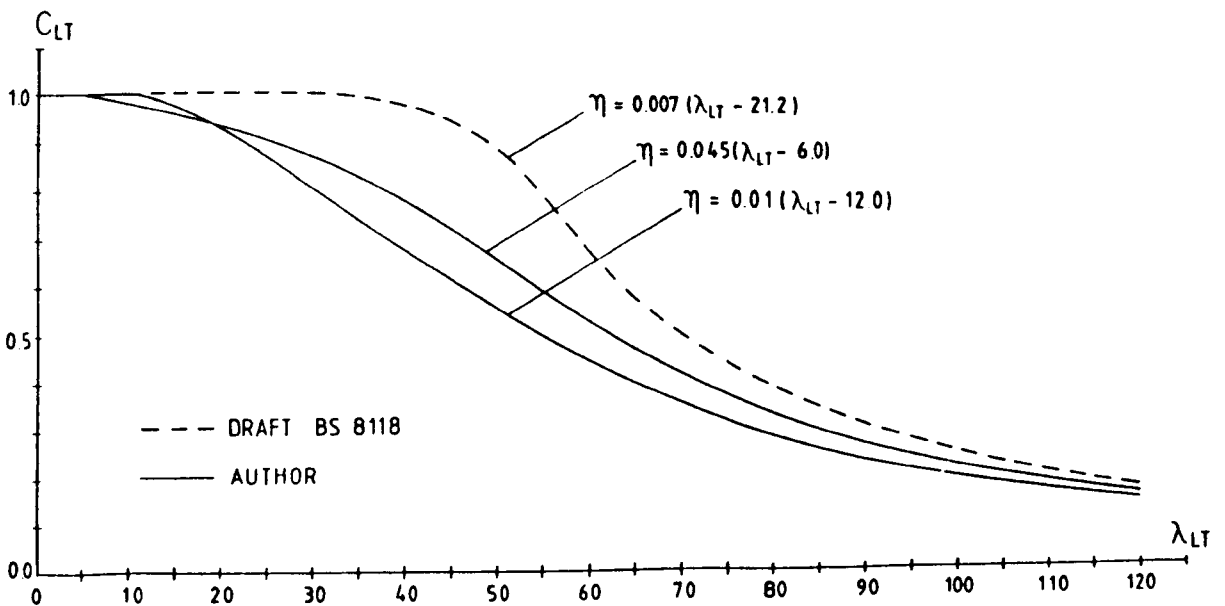
Figure 7.65 Suggested $C_{LT} - \lambda_{LT}$ Curves

Figure 7.64. Therefore, we can conclude that to divide the aluminium beams into two classes is sufficiently accurate in design. From Figures 7.62 to 7.64, it can be seen that the suggested design curves are sightly higher than the theoretical results as the slenderness is approaching the stocky range but much better predictions can be obtained for the intermediate and slender beams. The comparison between the $C_{LT} - \lambda_{LT}$ curves as suggested by the draft code BS 8118 and by the author is shown in Figure 7.65, it can be seen that the draft code is too optimistic for the lateral buckling strength of beams.

Finally, it is worthwhile to point out that the suggested design $C_{LT} - \lambda_{LT}$ curves by the author are based on the assumption that the maximum initial displacements are $\frac{L}{1000}$ in both the major and minor axis directions; and an initial twist of maximum 0.01 radian at mid-span (see Section 5.3). For the extruded sections, the initial imperfections are usually less than the above limits. But for the welded sections, the initial imperfections may be quite severe. From the parametric studies presented in Section 5.3.2.2 (see Figure 5.19), it is quite reasonable to assume that the value of C_{LT} be reduced by 20% if the beams fail to meet these limits. But for very stocky beams, $\lambda_{LT} < 5$ for $\frac{\sigma_{ult}}{\sigma_{0.2}} \leq 1.4$ and $\lambda_{LT} < 10$ for $\frac{\sigma_{ult}}{\sigma_{0.2}} > 1.4$, no reduction on the value of C_{LT} is necessary.

For the transversely welded beams, the draft BS 8118 can also lead to unsafe design, and the improvement will be discussed in Section 7.6.2.

7.5.3   Discussion on the Design of Aluminium Beam-columns

Since the lateral buckling strength of beams is over-estimated by the draft code, therefore, some discrepancy in results can be observed as the beams-columns are under relatively high end moments and low compression. But in general, the draft code can give safe results no matter whether the beam-columns are under in-plane failure; flexural-torsional failure or the beam-columns are under compression plus biaxial bending. Although the interaction equations (7.8) to (7.12) are based on the design principle of the steel code BS 5950, the comparison with theoretical results generally suggests these interaction equations as being suitable for the aluminium members. The main drawback is that the predictions tend to be very conservative for the stocky beam-columns with or without longitudinal welds.

7.6 Proposed Design Recommendations for Transversely Welded Members

For the transversely welded members, the draft BS 8118 will give unsafe design for most of the cases, so improvement in design is necessary. In the light of theoretical investigations, a more fundamental approach for the design of transversely welded aluminium members is proposed as a supplement to the new draft BS 8118. The proposed method is mainly to check whether the maximum stress within the reduced-strength zone (RSZ) due to the applied load is greater than the elastic limit stress, σ_e^*, of the RSZ material or not. If the maximum stress within the RSZ is greater than the elastic limit stress, σ_e^*, of the RSZ material, the aluminium member should be designed as if it contains wholly RSZ material, otherwise, the effect of RSZ softening can be neglected.

The elastic limit stress, σ_e^*, of the RSZ material can be obtained from equation (2.3) (see Section 2.2.5). The above approach is suitable for the design of transversely welded columns, beams or beam-columns.

7.6.1   Proposed Design Method for Transversely Welded Columns

The proposed design method for transversely welded columns is as follows:

1. If $P_c^* \leq P_e^*$, then the effect of RSZ softening can be neglected, and

$$P_e^* = \sigma_e^* A \qquad (7.16)$$

2. If $P_c^* > P_e^*$, then the location of the RSZ must be determined, and two cases can be classified.

   (a) If the RSZ is location near the two ends of the column and is within a distance of $0.25L$ measured from the supports, the column is classified as an end-welded column. We can design the columns as if non-welded but the maximum strength cannot be greater than

   $$\overline{P} = 1 - (1 - \omega)\frac{A^*}{A} \quad \text{(a cut-off line)}$$

   (b) If (a) is not satisfied, the column is classified as a centrally-welded column. The aluminium column should be designed as if it contains wholly RSZ material.

Moreover if the transversely welded column is also accompanied by longitudinal welding along the length of the member, the above approach is applied but the effect of RSZ softening within the cross-section due to longitudinal welds has to be taken into account in the value P_c^*.

7.6.2 Proposed Design Method for Transversely Welded Beams

The proposed design method for transversely welded beams is as follows:

1. If $M_{max}^* \leq M_e^*$ within the RSZ, the effect of local transverse welds can be neglected; and

$$M_e^* = \sigma_{0.2}^* Z \qquad (7.17)$$

   where $Z = Z_p$ if the sections are compact

   $Z_e < Z < Z_p$ if the sections are semi-compact

   $Z = Z_{eff}$ if the sections are slender

2. If $M_{max}^* > M_e^*$ within the RSZ, the transversely welded beam has to be designed as if contains wholly RSZ material.

Similar to transversely welded columns, if the transversely welded beam is also accompanied by longitudinal welding along the length of the member, the effect of RSZ softening within the cross-section due to longitudinal welds has to be taken into account in the value M_{max}^*.

7.6.3 Proposed Design Method for Transversely Welded Beam-columns

The proposed design method for transversely welded beam-columns is as follows:

1. If $\frac{P}{\frac{P_{ac}^*}{\gamma_m}} + \frac{M_x}{\frac{M_{ax}^*}{\gamma_m}} + \frac{M_y}{\frac{M_{ay}^*}{\gamma_m}} \leq \frac{\sigma_e^*}{\sigma_{0.2}^*}$ within the RSZ, then the effect of local transverse welds can be neglected. This condition usually is valid if the required section is over-estimated in the design.

2. If $\frac{P}{\frac{P_{ac}^*}{\gamma_m}} + \frac{M_x}{\frac{M_{ax}^*}{\gamma_m}} + \frac{M_y}{\frac{M_{ay}^*}{\gamma_m}} > \frac{\sigma_e^*}{\sigma_{0.2}^*}$ within the RSZ, the author would suggest that the values P_{sc}, P_{cx} and P_{cy} are based on the RSZ material (i.e. used P_{sc}^*, P_{cx}^* and P_{cy}^*) but the values M_{sx}, M_{sy} and M_{max} are obtained according to Section 7.6.2, i.e.

   (a) when $M_{max}^* \leq M_e^*$ within the RSZ,

   $$M_{sx} = M_{sx}$$
   $$M_{sy} = M_{sy}$$
   $$M_{max} = M_{max}$$

   (b) when $M_{max}^* > M_e^*$ within the RSZ,

   $$M_{sx} = M_{sx}^*$$
   $$M_{sy} = M_{sy}^*$$
   $$M_{max} = M_{max}^*$$

in which M_{sx}, M_{sy} and M_{max} are based on the mechanical properties of parent metal and $M_{sx}^*, M_{sy}^*, M_{max}^*$ are based on the mechanical properties of RSZ material.

The interaction equations (7.8) to (7.12) are also valid but the values M_{sx}, M_{sy}, M_{max} should be used according to condition (a) or (b).

7.7   Comments on Draft BS 8118

In designing an aluminium member which is fully affected by transverse welds, two approaches can be used:

1. The material properties are based on parent metal but with a reduction factor ω (0.5 for 6000 series alloy and 0.75 for 7000 series alloy) and a safety factor, $\gamma_m = 1.25$ on material strength.

2. The material properties are based on RSZ material with the entire member treated as a non-welded section. No reduction factor, ω, is used and the safety factor, $\gamma_m = 1.2$, is applied to material strength.

The first approach, is used in the draft BS 8118 although the second approach appears more rational and appropriate. The second approach, which is used by the authors, usually gives a higher but still safe design strength for aluminium members. Moreover, if the member having $\frac{A^*}{A} > 0.5$ within the cross-section, the author would recommend that the whole member should be designed as if it contains wholly RSZ material.

Form the previous theoretical and experimental investigations, it can be seen that the ultimate strength of welded aluminium members is essentially dependent on the mechanical properties of the RSZ material. However, except for those commonly used alloys, the draft BS 8118 cannot generally give good approximation on the mechanical properties of the RSZ material. If the RSZ material properties are uncertain, the author would suggest that the minimum values of the material properties should be used in design instead of

the mean values.

Generally the format of the new draft BS 8118 was clear and understandable although some corrections and additions are thought to be necessary and these have been outlined in previous sections.

7.8   Conclusions

The comparisons between the draft BS 8118 and theoretical results are presented in this chapter. The improvements on the design of aluminium members are also suggested. From the comparison, several important observations are arrived.

1. For the aluminium columns with or without longitudinal welds, the draft BS 8118 can generally give the design on the safe side. But for the aluminium columns having asymmetric cross-sections or having material properties $\frac{\sigma_{ult}}{\sigma_{0.2}} > 1.2$, the draft will tend to give very conservative results. For the transversely welded columns, the draft will lead to unsafe design in most of the cases.

2. For the aluminium beams, the draft code cannot give safe design because the lateral buckling reduction factor, C_{LT}, is not estimated correctly by the draft code. Much better estimates of C_{LT} can be obtained if two beam design curves are used instead of one. The accuracy of the two design beam curves suggested by the author have been discussed and demonstrated in Section 7.5.2.

3. The equivalent uniform moment factor, m, given by the draft code is also incorrect for the inelastic beams. Further research in this area, therefore, is necessary.

4. For the aluminium beam-columns, the draft code can generally give the design on the safe side. Therefore, the accuracy of the interaction equations as suggested by the draft BS 8118 can be supported by the present theoretical beam-column results.

References

[1] British Standards Institution, CP 118: 1969, "The Structural Use of Aluminium".

[2] British Standards Institution, Draft British Standard BS 8118, "Code of Practice for the Design of Aluminium Structures", 1985.

[3] Nethercot, D. A., Weston G., and Davison, J. B., "Comparative Study of Design Capacities of Aluminium Members Using the Draft BS 8118 and CP 118", Department of Civil and Structural Engineering, University of Sheffield.

[4] Brungraber, R. J. and Clark, J. W., "Strength of Welded Aluminium Columns", Transactions A.S.C.E., Vol. 27, Part II, 1962.

[5] Hong, G. M., "Buckling of Non-welded and welded Aluminium Columns", Ph.D Thesis, University of Cambridge, September 1986.

[6] British Standards Institution, BS 5950: Part I: 1985, "Structural Use of Steelwork in Building".

[7] Bulson, P. S., and Nethercot, D. A., "New British Code for the Design of Aluminium Structures", IABSE Colloquium, Stockholm, 1986.

[8] Nethercot, D. A., "Lateral Buckling - Supporting Case", BSI Committee for the Revision of CP 118, A/Paper 32, September 1981.

[9] Clark, J. W. and Jombock, J. R., "Lateral Buckling of I-beams subjected to Unequal End Moments", Journal of the Engineering Division, A.S.C.E., Vol. 83, No. EM3, July 1957.

[10] Trahair, N. S., "The Behaviour and Design of Steel Structures", Chapman and Hall, London, England, 1977.

CONCLUSIONS

8.1   General Summary of Present Study

The theoretical study of aluminium members with or without welds has been carried out and the reliability of the theoretical results has been verified through experiments conducted by the author or other researchers. Most of the theoretical results have been compared with the new draft BS 8118 so as to check its accuracy when used for the design of aluminium members. As a result of the comparison, some new proposals and design recommendations are suggested.

In the theoretical study, two finite element programs, INSTAF and BIAXIAL, were modified and used to simulate the special problems of aluminium structures. In both of the programs, the non-linear inelastic stress-strain properties of aluminium; the effect of longitudinal welds and/or local transverse welds and residual stresses were incorporated in the computer simulation. Program INSTAF was used to study the general in-plane behaviour of aluminium members. Since the in-plane behaviour of longitudinally welded members has been studied by Hong in 1983, therefore the parametric studies using program INSTAF were mainly confined to the general behaviour of transversely welded aluminium members and the theoretical results have been presented in Chapter 3. Program BIAXIAL was used to study the general flexural-torsional behaviour and the biaxially loaded aluminium members with or without longitudinal or local transverse welds. The parametric studies have been presented in Chapters 5 and 6. Using these programs numerous theoretical curves for columns, beams and beam-columns were generated in the parametric studies which mainly included:

1. the effect of initial out-of-straightness,

2. the effect of variation of material properties,

3. the effect of section geometry,

4. the general effect of local transverse welds,

5. the effect of heat-affected zone models,

6. the effect of symmetric or unsymmetric longitudinal welds,

7. the effect of residual stresses,

8. aluminium members with asymmetrical cross-sections,

9. the effect of loading path on biaxially loaded members.

In the experimental study, altogether 5 non-welded and 22 welded 7019 aluminium beams were tested. The aluminium beams were extruded rectangular box-section and the heat-affected zones were produced by welding two 7019 aluminium plates on the top and bottom flanges. The mechanical properties of parent metal and RSZ material were obtained by tensile test. The results of the beam tests were compared with the theoretical predictions obtained by program INSTAF using the measured material properties; and all the results have been presented in Chapter 4. There was very good agreement between the experimental and theoretical results for the non-welded and welded aluminium beams, therefore, the comparison strongly supported that the parametric studies and the background theory suggested by the author had very high reliability.

8.2   Conclusions

A number of specific conclusions, as well as some more general points, have
emerged as a result of the present study and these are summarised below.
When a particular subject area is indicated, further conclusions may be found
at the end of the relevant chapter.

8.2.1   Theoretical Studies

1. The stress-strain relationship for aluminium alloy proposed by
   Ramberg and Osgood has been confirmed as the most suitable rep-
   resentation of the behaviour of aluminium alloy tensile test spec-
   imens (see reference [1]). The knee factor, n , in the Ramberg-
   Osgood formula can best be expressed by $n = \frac{\ln 2}{\ln(\frac{\sigma_{0.2}}{\sigma_{0.1}})}$ (see equa-
   tion (A.24) in Section A.2.1). Since $\sigma_{0.1}$ is not usually quoted in
   specifications and design codes, and is therefore only likely to be
   available when tensile coupon tests have been performed, the pro-
   posal of Dwight [2] that the knee factor, n , be obtained from
   $n = \frac{4}{\ln(\frac{\sigma_{ult}}{\sigma_{0.2}})}$ (see equation (A.29) in Section A.2.1.4) represents a
   more convenient but only slightly less accurate approach.

2. Recommended values for the maximum tensile elongation for 6000
   series and 7000 series alloys for use in numerical work are 2.5%
   and 3.5% respectively. These would accord with a general value
   of $5\varepsilon_{\sigma_{0.2}}$ but full checks for other alloy types are required before
   this can be advanced.

3. The ultimate strength of transversely welded columns has been found to be principally controlled by two effects :

   (a) the basic reduction in squash load due to the presence of RSZ material

   (b) the effect on the stability ($P - \Delta$ effect) due to the presence of RSZ material

   When the RSZ is located within $0.25L$ of one or both ends, the reduction in strength may be safely approximated by considering only the reduction in squash load. At present the draft BS 8118 does not take this reduction in squash load into account. For RSZ within the middle $0.5L$ of the column, in addition to the reduction in squashing capacity of the column, the greater flexibility results in further reductions in load carrying capacity. The single most important influence on the strength of transversely welded columns is the properties of the fully heat-affected material, the presence of partially heat-affected material having negligible effect on the column's ultimate strength. A safe, although in some cases unnecessarily conservative, design approach consists of treating the whole column as if it was composed of RSZ material.

4. For transversely welded beams, the location of the RSZ material is the most important factor. Providing stresses within the RSZ remain below the σ_c^* value of equation (2.3), the beam may be designed as unwelded.

5. Special consideration should be paid to the effects of welded joints between members, since loss of fixity, leading to significant reduc-

tions in overall structural stability may result. Based on a limited study of some simple frames, the author suggests that those members affected by the presence of the welds at the joints should be designed as if containing wholly RSZ material. Since this will be conservative, further study is required to produce a better approach.

6. For longitudinally welded aluminium members, the reduction in ultimate strength is mainly due to the presence of RSZ within the cross-section. Irrespective of whether the longitudinal welds within the cross-section are symmetrically disposed or not, the presence of residual stresses causes a further reduction in ultimate strength of not more than 10%.

7. The ultimate strength of biaxially loaded beam-columns is load path dependent. For the studies conducted by the author, a maximum difference in ultimate load of 17% was obtained.

8.2.2 Tests on Aluminium Beams

1. For 7000 series aluminium alloy, the draft BS 8118 suggests a reduction in 0.2% proof stress for heat-affected material of 25%. From the tensile coupon tests carried out by the author, a figure of approximately 35% was obtained. This is in agreement with the findings of unpublished work at R.A.R.D.E.

2. In the beam tests, four of the beams (all of which were welded specimens) exhibited premature failure due to fracture. Whilst the reason for this loss of ductility is uncertain, it may well have been

caused by the development of microcracks within the partially heat-affected zone and/or severe localised residual strains in the HAZ generated after welding.

3. From the comparison between the theoretical and experimental load-deflection curves of the transversely welded beams within the range covered by the tests, generally good agreement was observed. Checks on the sensitivity of the numerical results to the exact set of input data used further confirmed that the strength of transversely welded members is principally dependent on the mechanical properties of the RSZ material.

8.2.3 Design of Aluminium Members Using Draft BS 8118

1. General findings on the comparisons between the author's results and design to the draft BS 8118 are summarised in Tables 8.1(a) and 8.1(b). Due to the limitation of the programs INSTAF and BIAXIAL, the effect of local buckling cannot be taken into account. In the comparisons between the theoretical results and draft BS 8118, this is therefore neglected in all cases.

2. In general, the draft BS 8118 tends to give very conservative results for aluminium members having asymmetric cross-sections. On the basis of the results presented herein for both columns (welded and unwelded) and laterally unrestrained beams, some modification would seem to be required.

3. For the transversely welded aluminium members, the draft BS 8118 will lead to unsafe design in most of the cases considered herein. Improvements to the design methods have been proposed in Section 7.6.

4. For columns, the reductions in design strength on passing through the different classes of column from A to H appear to be too great. Whilst the upper curves appear to be correctly positioned, design curve 5 undercuts even the lowest results and some upward revision of the design curves coupled with a re-allocation of classes would seem to be necessary.

5. For both non-welded and longitudinally welded beams, the lateral buckling reduction factor C_{LT} appears to be insufficient. Better estimates of C_{LT} can be observed if two beam design curves, as suggested in Section 7.5.2, are used thereby recognising the different forms of behaviour of low n and high n material.

6. For both non-welded and longitudinally welded beam-columns, the draft code generally gives designs on the safe side, although for stocky beam-columns, design will frequently be very conservative. In particular, the form of the various interaction equations would appear to be generally correct, where significant discrepancies arise between the author's numerical results and the predictions of the draft code they are normally due to the inaccuracies in the component formulae i.e. the denominators in the expressions for $\overline{P}$, $\overline{M}_x$ and $\overline{M}_y$.

	Non-welded	Longitudinally Welded	Transversely Welded
Columns	Safe design can be obtained	Safe design can be obtained (see reference [3])	Except for centrally-welded columns, the draft code generally gives unsafe design
Beams	Safe design can be obtained	Safe design can be obtained	The draft code potentially gives unsafe design, but safe design may be obtained depending on the location of RSZ and the applied moment pattern
Beam-columns	Safe design can be obtained	Safe design can be obtained	The draft code generally gives unsafe design

Table 8.1: (a) Comments on the Draft BS 8118 (Members under In-plane Flexural Buckling)

	Non-welded	Longitudinally Welded	Transversely Welded
Columns	Safe design can be obtained	Safe design can be obtained	Except for centrally-welded columns, the draft code generally gives unsafe design
Beams	Except for asymmetric sections, the draft code generally gives unsafe design	Except for asymmetric sections, the draft code generally gives unsafe design	The draft code generally gives unsafe design
Beam-columns under flexural-torsional buckling	Safe design can be obtained in most of the cases	Safe design can be obtained in most of the cases	The draft code generally gives unsafe design
Beam-columns under biaxial bending	Safe design can be obtained in most of the cases	Safe design can be obtained in most of the cases	The draft code generally gives unsafe design

Table 8.1: (b) Comments on the Draft BS 8118 (Members under Flexural-torsional Buckling and Biaxial Bending)

8.3 Further Work

The following areas deserve further investigation :

1. The improvement of the estimation of HAZ material properties.

2. The residual stress distribution due to the presence of local transverse welds especially in the cross-section partially affected by RSZ.

3. The ductility of partially affected zone material.

4. The improvement of Cambridge tendon force model which can incorporate asymmetrically distributed residual stresses and RSZ in symmetrical or asymmetrical sections.

5. Further investigation on flexural-torsional behaviour of asymmetrical non-welded and welded sections in general (e.g. equal and unequal angles)

6. The modification of equivalent uniform moment factor, m, in inelastic aluminium beams.

7. Further investigation on the effect of loading path on biaxially loaded aluminium beam-columns which includes the effect of warping restraint and torsion.

8. The general behaviour of biaxially loaded aluminium beam-columns having asymmetrical sections and with or without longitudinal and local transverse welds.

9. Experimental studies on flexural-torsional buckling of aluminium columns, beams and beam-columns with or without longitudinal and local transverse welds.

10. Experimental studies on biaxially loaded aluminium beam-columns with or without longitudinal and local transverse welds.

8.4 Application of Present Research Work

The propose of the present research work is to provide further up-to-date information for the rewriting of CP 118. However, the present research work can also apply to other metal structures having problems of similar sort of nature. Finally, all the results, presented in this thesis have been reported to the committee of B.S.I. for possible inclusion in the new code BS 8118.

References

[1] Mazzolani, F.M., "Aluminium Alloy Structures", Pitman.

[2] Dwight, J.B. and Mofflin, D.S., "Local Buckling of Aluminium - Preliminary Proposal", BSI Committee for the Revision of CP 118, A/Paper 50, March 1982.

[3] Hong, G.M., "Buckling of Non-welded and Welded Aluminium Columns", Ph.D Thesis, University of Cambridge, 1983.

VARIOUS PROPOSALS ON STRESS-STRAIN RELATIONSHIP OF ALUMINIUM

A.1   Stress-strain Relationships of Aluminium in Continuous Form of $\sigma = f(\varepsilon)$

Since it is very difficult to present stress-strain relationships of the form $\sigma = f(\varepsilon)$, which is based upon one mathematical expression, it is usually convenient to divide the function $\sigma = f(\varepsilon)$ into three separate regions. They can be defined in the following way:

Region 1: Elastic behaviour

Region 2: Inelastic behaviour

Region 3: Strain-hardening behaviour

In each region, the stress-strain relationship which represents the behaviour has to be found. To ensure continuity the three different regions have to produce coincident points at their limits.

A.1.1 Stress-strain Relationship Proposed by Baehre [1]

The dimensionless stress-strain relationship in the three different regions can be expressed as follows:

Region 1: Elastic behaviour

For $0 < \frac{\varepsilon}{\varepsilon_{0.2}} < \frac{\varepsilon_e}{\varepsilon_{0.2}}$ or $\frac{\varepsilon_{max}}{\varepsilon_{0.2}} \leq 0.5$,

$$\frac{\sigma}{\sigma_{0.2}} = \frac{\varepsilon}{\varepsilon_{0.2}}$$

(A.1)

Region 2: Inelastic behaviour

For $\frac{\varepsilon_e}{\varepsilon_{0.2}} < \frac{\varepsilon}{\varepsilon_{0.2}} \leq \frac{\varepsilon_{\sigma_{0.2}}}{\varepsilon_{0.2}}$ or $0.5 < \frac{\varepsilon_{max}}{\varepsilon_{0.2}} \leq 1.5$,

$$\frac{\sigma}{\sigma_{0.2}} = -0.2 + 1.85\left(\frac{\varepsilon}{\varepsilon_{0.2}}\right) - \left(\frac{\varepsilon}{\varepsilon_{0.2}}\right)^2 + 0.2\left(\frac{\varepsilon}{\varepsilon_{0.2}}\right)^3$$

(A.2)

Region 3: Strain-hardening behaviour

For $\frac{\varepsilon_{\sigma_{0.2}}}{\varepsilon_{0.2}} < \frac{\varepsilon}{\varepsilon_{0.2}} \leq \frac{\varepsilon_{ult}}{\varepsilon_{0.2}}$ or $1.5 < \frac{\varepsilon_{max}}{\varepsilon_{0.2}} \leq \frac{\varepsilon_{ult}}{\varepsilon_{0.2}}$,

$$\frac{\sigma}{\sigma_{0.2}} = \frac{\sigma_{ult}}{\sigma_{0.2}} - 1.5\left(\frac{\sigma_{ult}}{\sigma_{0.2}} - 1\right)\frac{\varepsilon_{0.2}}{\varepsilon}$$

(A.3)

Unless tension tests are carried out, the value ε_e cannot be obtained from any standard code of practice. Therefore, in practice, the three regions should be:

$$\frac{\sigma}{\sigma_{0.2}} = \frac{\sigma_{ult}}{\sigma_{0.2}} - 1.5 \left(\frac{\sigma_{ult}}{\sigma_{0.2}} - 1.0 \right) \frac{\varepsilon_{0.2}}{\varepsilon}$$
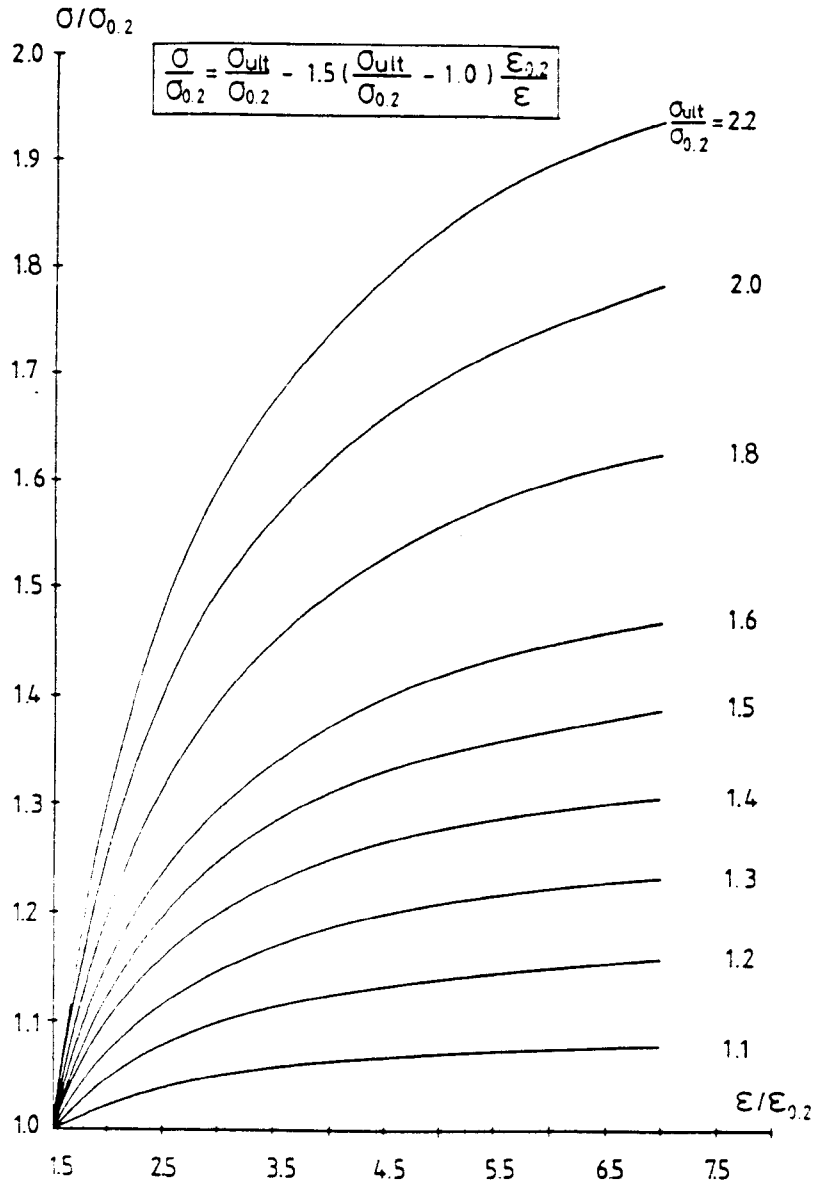
Figure A.1 Effect of Ratio $\frac{\sigma_{ult}}{\sigma_{0.2}}$ on $\frac{\sigma}{\sigma_{0.2}}$

Elastic region : $\frac{\varepsilon}{\varepsilon_{0.2}} \leq 0.5$

Inelastic region : $0.5 < \frac{\varepsilon}{\varepsilon_{0.2}} \leq 1.5$.

Strain-hardening region : $1.5 < \frac{\varepsilon}{\varepsilon_{0.2}} \leq \frac{\varepsilon_{ult}}{\varepsilon_{0.2}}$

This proposal, therefore, assumes that ε_e and $\varepsilon_{\sigma_{0.2}}$ are equal to $0.5\varepsilon_{0.2}$ and $1.5\varepsilon_{0.2}$ respectively. Moreover, in the strain-hardening region, the ratio $\frac{\sigma}{\sigma_{0.2}}$ is very sensitive to the ratio $\frac{\sigma_{ult}}{\sigma_{0.2}}$ (see Figure A.1).

A.1.2   Stress-strain Relationship Proposed by Mazzolani [1]

In the proposal suggested by Baehre, the elastic limit stress, σ_e, is not well-defined. Thus Mazzolani proposed that σ_e can be expressed by:

$$\sigma_e = \sigma_{0.2} \left[1 - \left(1 - \frac{\sigma_{0.1}}{\sigma_{0.2}} \right)^m \right] \tag{A.4}$$

where

$$m = 2.30 - 1.75 \left(\frac{\sigma_{0.2}}{\sigma_{0.1}} \right) \tag{A.5}$$

$$\varepsilon_e = \frac{\sigma_e}{E}$$

Using equations (A.4) and (A.5) to modify the proposal suggested by Baehre, greatly increases the accuracy. Moreover, Mazzolani also proposed the following non-dimensionalised stress-strain law by taking

$$\bar{\sigma} = \frac{\sigma}{\sigma_e} \tag{A.6}$$

and

$$\overline{\varepsilon} = \frac{\varepsilon}{\varepsilon_e} \tag{A.7}$$

The non-dimensionalised relations $\overline{\sigma} - \overline{\varepsilon}$ in the three regions are:

Region 1 : Elastic behaviour

For $0 < \overline{\sigma} < 1$; $0 < \overline{\varepsilon} < 1$

$$\overline{\sigma} = \overline{\varepsilon} \tag{A.8}$$

Region 2 : Inelastic behaviour

For $1 < \overline{\sigma} < \overline{\sigma}_1$; $1 < \overline{\varepsilon} < \overline{\varepsilon}_1$

$$\overline{\sigma} = \overline{\varepsilon} - \beta(\overline{\varepsilon} - 1)^{\alpha} \tag{A.9}$$

where

$$\overline{\sigma}_1 = \frac{\sigma_{0.2}}{\sigma_e}$$

$$= \left[1 - \left(1 - \frac{\sigma_{0.1}}{\sigma_{0.2}}\right)^m\right]^{-1} \tag{A.10}$$

$$\overline{\varepsilon}_1 = \frac{\varepsilon_{\sigma_{0.2}}}{\varepsilon_e}$$

$$= \left[1 + 0.002\frac{E}{\sigma_{0.2}}\right]\left[1 - \left(1 - \frac{\sigma_{0.1}}{\sigma_{0.2}}\right)^m\right]^{-1} \tag{A.11}$$

$$\varepsilon_{\sigma_{0.2}} = \frac{\sigma_{0.2}}{E} + 0.002 \tag{A.12}$$

and the semi-empirical coefficients α and β are given by:

$$\alpha = \frac{1 - \overline{\varepsilon}_1}{\overline{\sigma}_1 - \overline{\varepsilon}_1}\left[1 - \sigma_{0.2}\left(1 - \frac{\sigma_{0.1}}{\sigma_{0.2}}\right)\right] \tag{A.13}$$

$$\beta = \frac{\bar{\epsilon}_1 - \bar{\sigma}_1}{(\bar{\epsilon}_1 - 1)^\alpha} \qquad (A.14)$$

Region 3 : Strain-hardening behaviour

For $\bar{\sigma}_1 < \bar{\sigma} < \bar{\sigma}_{ult}$; $\bar{\epsilon} > \bar{\epsilon}_1$

$$\bar{\sigma} = \bar{\sigma}_{ult} - \psi \exp^{-\gamma(\bar{\epsilon} - \bar{\epsilon}_1)} \qquad (A.15)$$

where

$$\bar{\sigma}_{ult} = \bar{\sigma}_1 \left(\frac{\sigma_{0.2}}{\sigma_{0.1}}\right)^3 \qquad (A.16)$$

$$\psi = \bar{\sigma}_{ult} - \bar{\sigma}_1$$

$$= \bar{\sigma}_1 \left[\left(\frac{\sigma_{0.2}}{\sigma_{0.1}}\right)^3 - 1\right] \qquad (A.17)$$

$$\gamma = \frac{\sigma_{0.2}}{\psi} \left(1 - \frac{\sigma_{0.1}}{\sigma_{0.2}}\right) \qquad (A.18)$$

The units of $\sigma_{0.1}$ and $\sigma_{0.2}$ are in ton/cm^2.

The proposal suggested by Mazzolani can predict quite accurately within the limit $\epsilon_{\sigma_{0.2}}$ (i.e. region 1 and region 2), but is quite conservative at strains greater than $\epsilon_{\sigma_{0.2}}$. Moreover, this proposal is very complicated and difficult to apply to design work.

A.1.3   Stress-strain Relationship Proposed by Hong [2]

Hong suggested a linear-log curve to represent the stress-strain behaviour of aluminium alloy. The linear-log curve consisted of two parts; linear part (elastic) and logarithmic part (inelastic and strain-hardening).

In the linear part (elastic), for $\sigma \leq \sigma_e$,

$$\sigma = E\varepsilon$$

In the logarithmic part (inelastic and strain-hardening), for $\sigma > \sigma_e$,

$$\sigma = \alpha \ln (\varepsilon - \beta) + \gamma \qquad\qquad (A.19)$$

where α, β and γ are arbitrary constants.

The values of α, β and γ are determined by the following boundary conditions:

   (a) the curve passes through $(\varepsilon_{\sigma_{0.2}} , \sigma_{0.2})$

   (b) the curve passes through $(\varepsilon_{ult}, \sigma_{ult})$ and

   (c) $\frac{d\sigma}{d\varepsilon} |_{\varepsilon=\varepsilon_e} = E$

The actual location of the elastic limit point $(\varepsilon_e , \sigma_e)$ is fixed internally during the determination of the α, β and γ in equation (A.19). The linear-log equation can give very good agreement with the Ramberg-Osgood formula (see Section A.2.1) in all cases. The maximum difference between the two curves is less than 5% but trial and error is necessary during the the evaluation of the arbitrary constants.

A.1.4 Stress-strain Relationship Proposed by Frey [3]

A similar approach has been proposed by Frey to find the stress-strain curve of aluminium. This proposed equation, named a power law, also consists of two parts.

In the linear (elastic) part, for $\sigma \leq \sigma_e$,

$$\sigma = E\varepsilon$$

In the non-linear part (inelastic, strain-hardening), for $\sigma > \sigma_e$

$$\sigma = \sigma_e \left(\frac{q\,E\,\varepsilon}{\sigma_e} - q + 1 \right)^{\frac{1}{q}} \qquad (A.20)$$

and the tangent modulus,

$$E_t = E \left(\frac{\sigma_e}{\sigma} \right)^{q-1} \qquad (A.21)$$

Since this proposal is not well-developed, so it is impossible to link the parameter q to other material characteristics such as $\sigma_{0.2}, \sigma_{ult}$ etc. Nowadays, the only possible way to determine the parameter q is by assuming equation (A.20) passes through the point $(\varepsilon_{\sigma_{0.2}}, \sigma_{0.2})$, then using the trial and error method to determine the value of q. But using this assumption, the expression can only give good approximations when the stress is less than $\sigma_{0.2}$. When the stress is greater than $\sigma_{0.2}$, this proposal cannot represent the real behaviour of aluminium at all (see Section A.3).

Moreover, the value of σ_e is computed by

$$\sigma_e = \left(0.5 \times 10^{-3} \right)^{\frac{1}{n}} \sigma_{0.2} \qquad (A.22)$$
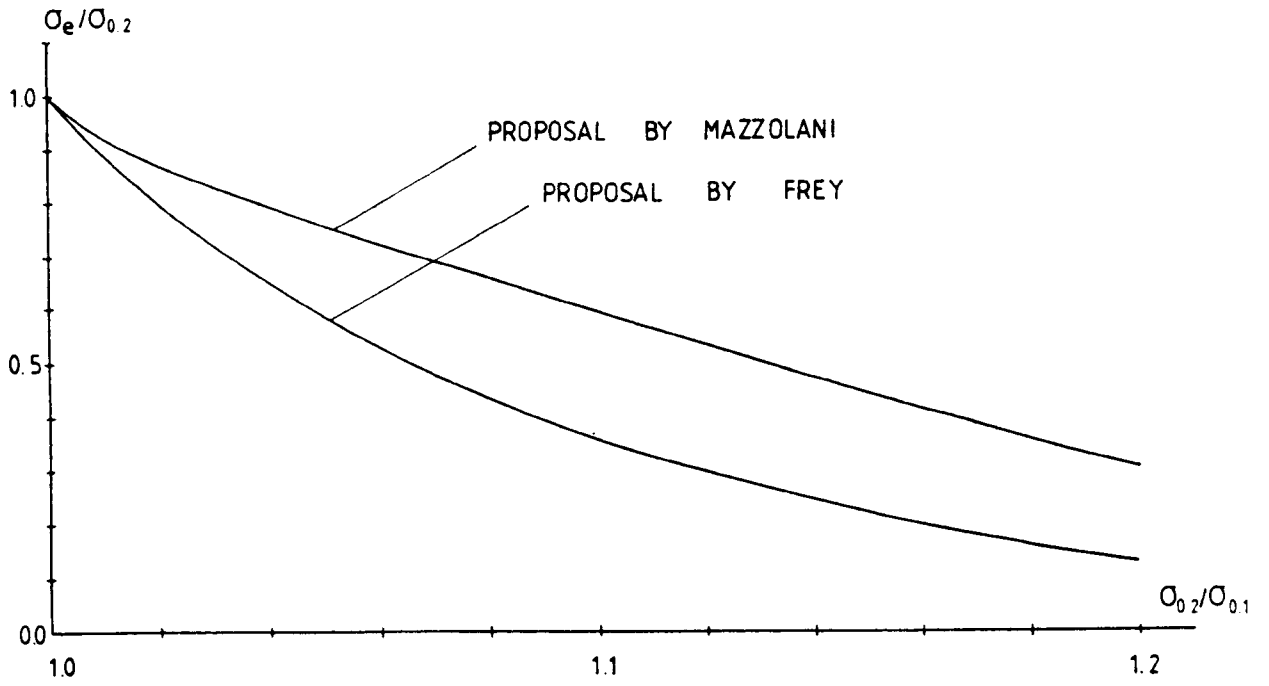
Figure A.2 Comparison between the Two Proposals on Elastic Limit Stress, σ_e

where n is the knee factor in the Ramberg-Osgood formula (see Section A.2.1). Referring to Section A.1.2, Mazzolani also suggested an expression to determine the elastic limit stress, σ_e (see equations (A.4) and (A.5)). If we compare the equations (A.4) and (A.22) as shown in Figure A.2, we can find that the suggestion by Frey is much more conservative than the proposal suggested by Mazzolani.

A.2   Stress-strain Relationships of Aluminium in Continuous Form of $\varepsilon = f(\sigma)$

A.2.1   Stress-strain Relationship Proposed by Ramberg and Osgood [1,2,4,5]

The most popular method of defining the stress-strain relationship for aluminium is the one suggested in 1943 by Ramberg and Osgood. The Ramberg-Osgood formula is usually expressed in the following form:

$$\varepsilon = \frac{\sigma}{E} + 0.002 \left(\frac{\sigma}{\sigma_{0.2}} \right)^n \qquad (A.23)$$

where E =   elastic modulus (N/mm^2)

       $\sigma_{0.2}$ =   0.2% proof stress (N/mm^2)

       n =   knee factor

The first term on the right hand side of the formula represents the elastic component of strain, and the second term represents the plastic component of strain. The Ramberg-Osgood formula can be easily defined by the three parameters $E, \sigma_{0.2}$ and n. Both E and $\sigma_{0.2}$ are commonly quoted in any standard code of practice (e.g. CP 118), but the knee factor, n, has to be deduced from other additional information. It can be shown that the knee factor, n, can be expressed by [1].

$$n = \frac{\ln 2}{\ln \left(\frac{\sigma_{0.2}}{\sigma_{0.1}} \right)} \qquad (A.24)$$

where $\frac{\sigma_{0.2}}{\sigma_{0.1}}$ is termed as the strain-hardening parameter.

Therefore, when if performing the tensile coupon test of any aluminium alloy,

the values $\sigma_{0.1}, \sigma_{0.2}$ and E can be determined. Hence, the Ramberg-Osgood formula, which passes through both the $\sigma_{0.1}$ point and $\sigma_{0.2}$ point, could be defined easily and the formula can give very good predictions of the experimental tensile coupon test results. Unfortunately in design, $\sigma_{0.1}$ is not usually quoted in specifications and design codes. Also, it is not possible to test each alloy used in design to obtain the value $\sigma_{0.1}$. Therefore, it is necessary to relate the knee factor, n, with an other parameter instead of $\sigma_{0.1}$. For this reason, several proposals are suggested and discussed below.

A.2.1.1 Determination of the Knee Factor Proposed by Steinhardt [1]

Steinhardt related the knee factor, n, to $\sigma_{0.2}$ and he proposed that

$$10 \ n = \sigma_{0.2} \tag{A.25}$$

The units of $\sigma_{0.2}$ are N/mm^2.

For non-heat-treated alloys, the values of $\sigma_{0.2}$ range between 100 and 150 N/mm^2. For heat-treated alloys, the values of $\sigma_{0.2}$ range between 200 and 400 N/mm^2. Therefore, the range of knee factors is between 10 and 40. This proposal is very simple and concise. It can also suggest a preliminary value of the knee factor during design or experimental works.

A.2.1.2 Determination of the Knee Factor Proposed by Mazzolani [1]

Mazzolani related the knee factor, n, to the 0.2% proof stress, $\sigma_{0.2}$; ultimate tensile stress, σ_{ult}; and the corresponding ultimate strain, ε_{ult}. He proposed the following approximate expression for the knee factor:

$$n = \frac{\ln 2}{\ln(1 + k\chi)} \qquad\qquad (A.26)$$

where

$$\chi \;=\; \frac{\sigma_{ult} - \sigma_{0.2}}{10 \; \varepsilon_{ult}} \frac{\sigma_{ult}}{\sigma_{0.2}} \quad (N/mm^2) \qquad\qquad (A.27)$$

$$k \;=\; 0.028 \quad (mm^2/N)$$

$$\varepsilon_{ult} \;=\; \text{ultimate strain in percentage}$$

Mazzolani has verified the above expression using the statistical results of testing carried out at Liege University. The values of $\sigma_{0.2}$, σ_{ult} and ε_{ult} are usually quoted in the specifications and design codes, so the above expression can be solved without any difficulties. From a detailed study carried out by the author, it was found that the knee factor, obtained from equation (A.26), is very sensitive to the ratio $\frac{\sigma_{ult}}{\sigma_{0.2}}$ and the ultimate strain, ε_{ult}. In general, the above proposal is on the conservative side (sometimes too conservative) and will give results on the safe side.

A.2.1.3   Determination of the Knee Factor Quoted by Hong [2]

Hong quoted an approximated expression for the knee factor, n, in his thesis which is similar to the expression suggested by Mazzolani. The expression is

$$n = \frac{\ln(5\,\varepsilon_{ult})}{\ln\left(\frac{\sigma_{ult}}{\sigma_{0.2}}\right)} \qquad (A.28)$$

where ε_{ult} is in percentage.

From the study by Hong, n is insensitive to ε_{ult} for high $\frac{\sigma_{ult}}{\sigma_{0.2}}$ ratio (≥ 1.3). For low $\frac{\sigma_{ult}}{\sigma_{0.2}}$ ratios (< 1.3), the author found that the value of n is much less sensitive than the proposal suggested by Mazzolani (equation (A.26)). The author has also compared both the Ramberg-Osgood curves with the knee factor, n, obtained from equations (A.26) and (A.28) respectively with the experimental results. This found that the Ramberg-Osgood curve using the n value quoted by Hong (equation (A.28)) can give more reliable and better predictions of the the actual behaviour of aluminium alloys.

A.2.1.4   Determination of the knee factor suggested by
Dwight [2,6]

From the study by Hong, the knee factor, n, is insensitive to ε_{ult} for high $\frac{\sigma_{ult}}{\sigma_{0.2}}$ ratios (i.e. in the low n range). Since the buckling strength of aluminium members is only sensitive to the low n range ($n < 15$), so the effect of the variation of ε_{ult} becomes less significant in practice and it is unnecessary to determine the knee factor, n, with great precision. Thus, Dwight has suggested that sufficient accuracy can be obtained by simplifying equation

(A.28) to

$$n = \frac{4}{\ln\left(\frac{\sigma_{ult}}{\sigma_{0.2}}\right)} \qquad (A.29)$$

This is equivalent to fixing a standard elongation of 11% in equation (A.28). Since the above formula only involves the ratio $\frac{\sigma_{ult}}{\sigma_{0.2}}$, so it is unnecessary to mention n in the code at all.

Alloy	$\sigma_{0.2}$ (N/mm^2)	σ_{ult} (N/mm^2)	ε_{ult} (%)	E (N/mm^2)	Knee Factor, n, Suggested by			
					Steinhardt	Mazzolani	Hong	Dwight
5083-M	130	280	11	68900	13.0	8.8	5.2	5.2
5083-M	125	275	13	68900	12.5	10.1	5.3	5.1
6061-TF	240	280	7	68900	24.0	37.5	23.1	25.9
6063-TF	160	185	7	65500	16.0	60.3	24.5	27.5
6063-TE	110	150	7	65500	11.0	32.1	11.5	12.9
6082-TF	255	295	7	68900	25.5	37.8	24.4	27.4
7020-TB	190	300	10	71700	19.0	14.6	8.6	8.8
7020-TF	280	340	8	71700	28.0	27.5	19.0	20.6

Table A.1 : Comparison between the Four Proposals for the
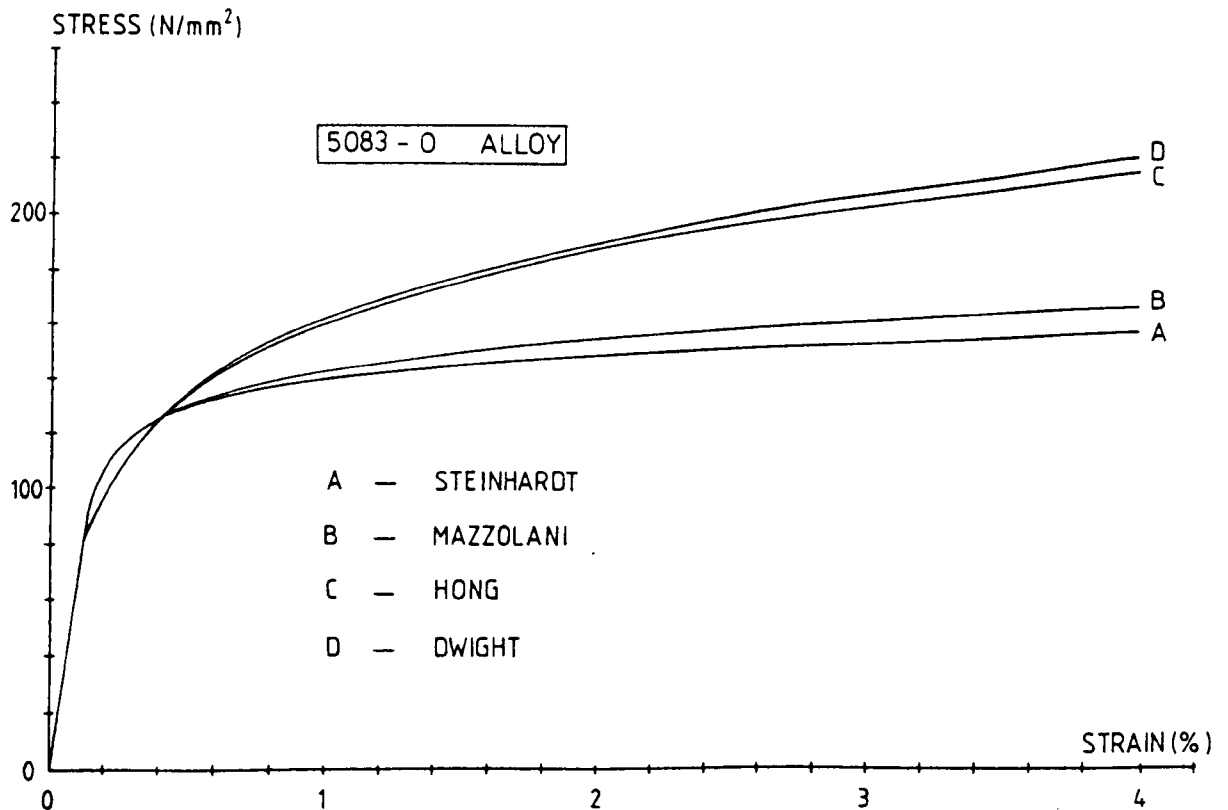Determination of Knee Factor

Figure A.3 Comparison between the Four Proposals to Determine the Knee
Factor, n

A.2.2   Comments to the Four Proposals for the Determination of Knee Factor, n

Using the values of the mechanical properties of the commonly used aluminium alloys as quoted in CP 118, the comparison between the four proposals for the determination of knee factor, n, are listed in Table A.1. It can be seen that the knee factor, n, suggested by Mazzolani is always higher than the knee factor quoted by Hong. Figure A.3 shows the comparison between the Ramberg-Osgood curves using the above four proposals. When compared with experimental results [1], the following conclusions are arrived:

1. The proposal suggested by Steinhardt is only a crude approximation, and very often, it cannot represent the actual behaviour of aluminium alloys. Therefore, this proposal is not recommended for analysis and design of aluminium structures.

2. The proposal suggested by Mazzolani is generally conservative in estimating the actual behaviour of aluminium alloy and gives designs on the safe side.

3. The expression quoted by Hong can give a better representation of the actual behaviour of aluminium alloy than the proposal suggested by Mazzolani.

4. Among the four proposals, the author would recommend Dwight's suggestion for the determination of the knee factor. It is because that proposal is quite concise but has sufficient accuracy and can eliminate the need to use the ultimate strain, ε_{ult}.
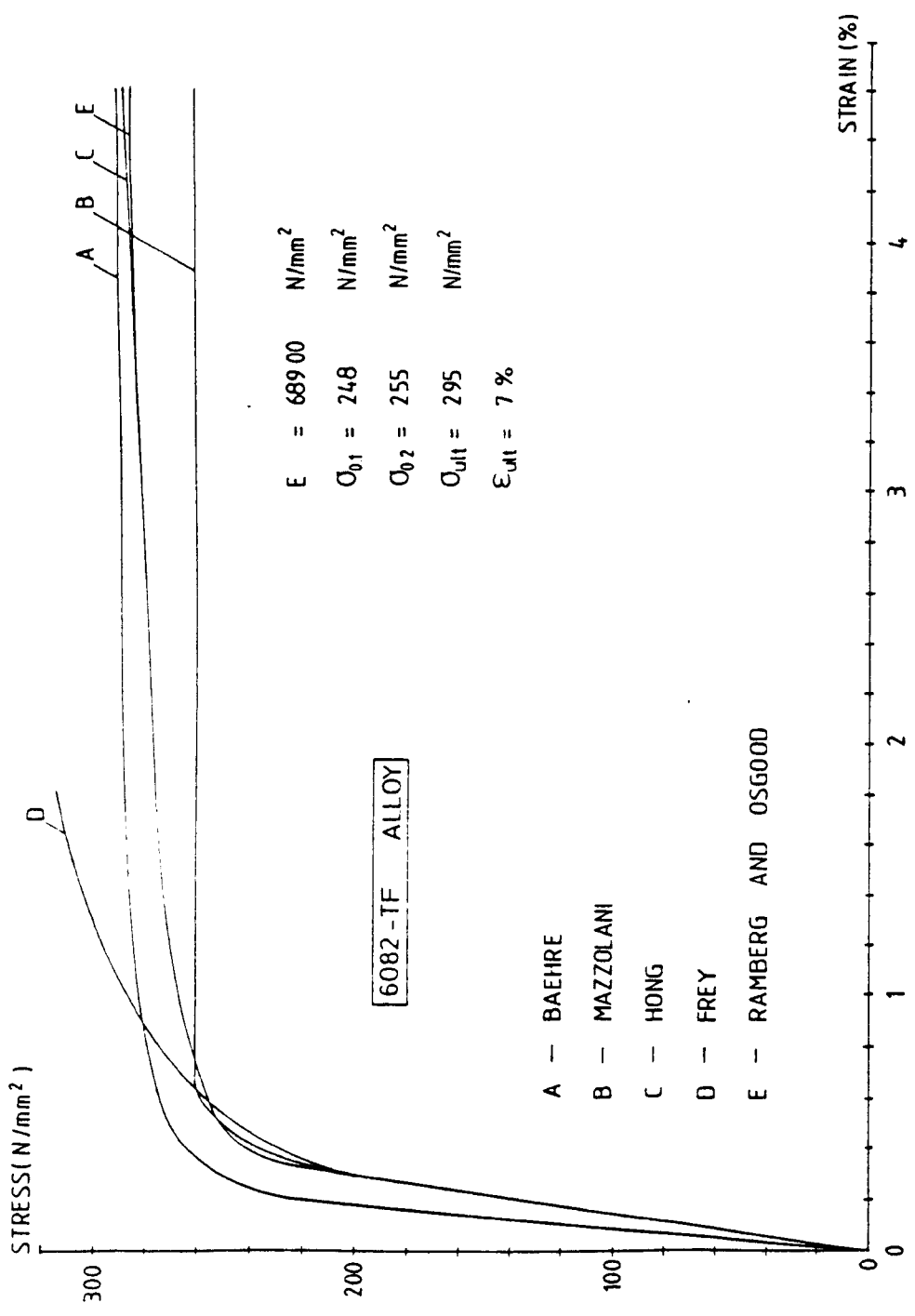
Figure A.4 Comparison between the Five Proposals to Determine the Stress-strain Relationships of Aluminium Alloy

A.3   Numerical Example for the Comparison between the Different Proposals on the Stress-strain Relationships of Aluminium Alloy

A numerical example as shown in Figure A.4 is used to demonstrate the stress-strain curves of aluminium alloy using the proposals mentioned in Sections A.1 and A.2. The 6082-TF alloy is chosen and the mechanical properties are:

$$E = 68900 \quad N/mm^2$$

$$\sigma_{0.1} = 248 \quad N/mm^2$$

$$\sigma_{0.2} = 255 \quad N/mm^2$$

$$\sigma_{ult} = 295 \quad N/mm^2$$

$$\varepsilon_{ult} = 7\%$$

The value of $\sigma_{0.1}$ is obtained by using equations (A.24) and (A.28) and the knee factor used in the Ramberg-Osgood formula is also evaluated by equation (A.28). From Figure A.4, we can find that Baehre's proposal is only a crude approximation, and is not recommended for use. Mazzolani's proposal is very complicated and tends to give very conservative results in the strain hardening region. The proposal suggested by Frey is not well-developed and is not recommended for use. Moreover, this proposal tends to overestimate the stress-strain relationship in the strain hardening region. The proposal suggested by Hong can give very good agreement with the Ramberg-Osgood

formula in all cases but trial and error is necessary. The Ramberg-Osgood formula is a well-known formula and is well-developed. The main drawback of the formula is that it is not explicit in stress (i.e. $\sigma = f(\varepsilon)$). This therefore, makes it unsuitable for computer computer simulation when the finite element method is used.

References

[1] Mazzolani, F. M., "Aluminium Alloy Structures", Pitman.

[2] Hong, G.M., "Buckling of Non-welded and Welded Aluminium Columns", Ph.D Thesis, University of Cambridge, 1983.

[3] Frey, F., Lemaire, E., de Ville de Goyet, V., Jetteur, P., and Studer, M., "Finel-G, Nonlinear Finite Element Analysis Program User Manual", University of Liege, IREM Internal Report 85/3, July 1985.

[4] Little, G. H., "Collapse Behaviour of Aluminium Plates", BSI Committee for the Revision of CP 118, A/Paper 27, March 1981.

[5] Ramberg, W. and Osgood, W. R., "Description Stress-strain Curves by Three Parameters", NACA Tech. Note 902, 1943.

[6] Dwight, J. B. and Mofflin, D. S., "Local Buckling of ~~Buckling of~~ Aluminium - Preliminary Proposal", BSI Committee for the Revision of CP 118, A/Paper 50, March 1982.
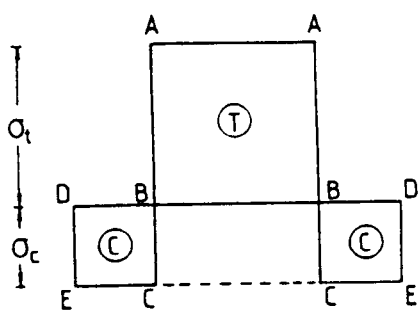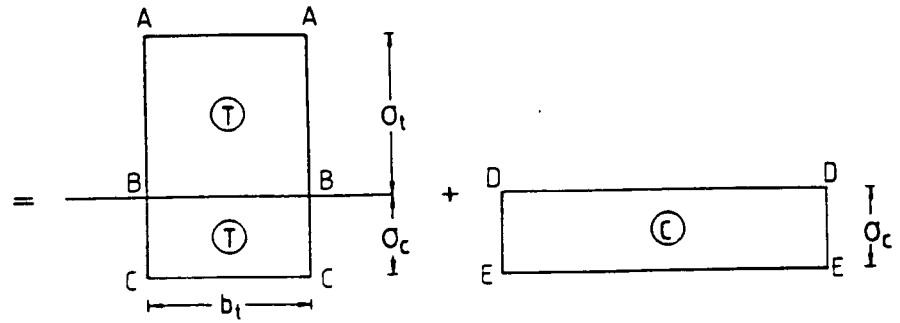
CAMBRIDGE RESIDUAL STRESS MODEL

Figure B.1 (a)   Figure B.1 (b)

SHRINKAGE FORCE $= \sigma_t \cdot b \cdot t$

TENDON   FORCE $= (\sigma_c + \sigma_t) \cdot b_t \cdot t \quad = \sigma_c \cdot b \cdot t$

Figure B.1 Tendon Force Model

B.1 Cambridge Residual Stress Model

The Cambridge model to determine residual stresses is based upon the definition of a conventional 'tendon force' which can be related to the shrinkage force F_s. This shrinkage force (area AABB of Figure B.1(a)) is a tension force which arises at welds and is caused by the greater resistance to elongation of fibres close to the weld, which experience higher temperatures, than those further from the weld.

In order to overcome the scatter in test data, the tendon force was introduced. This is insensitive to the width of the tension zone, plate dimension, material yield stress and actual stress pattern on the cross-section. The tendon force (area AACC of Figure B.1(b)) is resisted by the whole cross-section of the plate (area DDEE of Figure B.1(b)); and when divided by the total plate area, it gives the compressive stress on the whole plate, i.e.

$$F_t = \sigma_c \, b \, t \times 10^{-3} \quad (KN) \qquad (B.1)$$

$$= \sigma_c \, A \times 10^{-3} \quad (KN)$$

or

$$\sigma_c = \frac{F_t \times 10^{-3}}{A} \qquad (\text{ same as equation (2.11) })$$

From experiment,

$$F_t = k \left(\eta \frac{Q}{V} \right) \quad (KN) \qquad (B.2)$$

where k is a non-dimensional coefficient and $\left(\eta \frac{Q}{V} \right)$ is the effective welding heat input per unit length in *Joules/mm*.

Wong [1] has found that if MIG welding is used, the area of weld deposit, A_w, is given by:

$$A_w = 0.05 \left(\eta \frac{Q}{V} \right) \quad (mm^2) \tag{B.3}$$

From equations (B.2) and (B.3), a simpler equation is obtained:

$$F_t = 20 k A_w \tag{B.4}$$

Equation (B.4) is same as the equation (2.8), therefore, the rest of the information could be referred to Section 2.3.3.3.

References

[1] Wong, M. P., "Weld Shrinkage in Non-linear Materials", Ph.D Thesis, University of Cambridge, 1982.